Evolution of social interactions associated with matrix production in *Bacillus subtilis* biofilms

Dissertation

To Fulfill the

Requirements for the Degree of

„Doctor of Philosophy“ (PhD)

Submitted to the

Council of the Faculty of Biological Sciences

of the

Friedrich Schiller University Jena

by

M.Sc. Marivic Martin

born on 09.11.1978 in Manila, Philippines

Zugl.: Friedrich-Schiller-Universität Jena [2019]

Gutachter:

1) Prof. Dr. Ákos T. Kovács, Technical University Denmark (Kgs. Lyngby, Denmark)
2) PD Dr. Kerstin Voigt, Friedrich-Schiller-Universität Jena (Jena, Germany)
3) Prof. Dr. Martin Ackermann, Eawag ETH Zurich (Dübendorf, Switzerland)

Tag der Verteidigung: 20. Dez. 2019

To Victor and Mercy, for the gift of life and love, and for showing me the value of hardwork and dedication .

And to my Poong Maykapal, I give YOU back all the glory.

The more you read, the more things you'll know.
The more that you learn , the more places you'll go.

- Dr. Seuss

Table of Contents

Overview of Manuscripts

This cumulative dissertation comprises the following published and unpublished manuscripts.

Author abbreviations:
Marivic Martin (MM), Ákos T. Kovács (ATK), Anna Dragoš (AD), Theresa Hölscher (THö), Vaughn S. Cooper (VSC), Gergely Maróti (GM), Balázs Bálint (BB), Martin Westermann (MW), Nivedha Lakshmanan (NL), Balázs Horváth (BH), Carolina Falcón García (CFG), Oliver Lieleg (OL), Heiko T. Kiesewalter (HTK), Chih-Yu Hsu (CYH), Raimo Hartmann (RH), Tobias Wechsler (TW), Knut Drescher (KD), Nicola Stanley-Wall (NSW), Rolf Kümmerli (RK), Lara Kricks (LK), Patrick Pausch (PP), Thomas Heimerl (The), Gert Bange (GB), Daniel López (DL), Simon B. Otto (SBO), Daniel Schäfer (DS), Susanne Brix (SB)

- **Laboratory evolution of microbial interactions in bacterial biofilms.**

  Authors: Marivic Martin, Theresa Hölscher, Anna Dragoš, Vaughn S. Cooper, Ákos T. Kovács
  Publication in: Journal of Bacteriology (2016), 198(19):2564-2571, doi: 1128/JB.01018-15 (Mini-Review).
  Presented as: Chapter 1.

Conceived the paper	ATK (100%)
Wrote the manuscript	MM (25%), THö (25%), AD (20%), VSC (10%), ATK (20%)

- **Evolution of exploitative interactions during diversification in *Bacillus subtilis* biofilms.**

  Authors: Anna Dragoš, Nivedha Lakshmanan, Marivic Martin, Balázs Horváth, Gergely Maróti, Carolina Falcón García, Oliver Lieleg, Ákos T. Kovács
  Publication in: FEMS Microbiology Ecology (2018) 94: fix155, doi: 1093/femsec/fix155
  Presented as: Chapter 2.

Conceived the project	AD (50%), ATK (50%)
Designed the experiments	AD (45%), OL (10%), ATK (45%)
Constructed bacterial strains	AD (40%), NL (40%), MM (20%)
Performed the experiments	AD (35%), NL (50%), MM (15%)
Performed genome resequencing	GM (50%), BH (50%)
Performed and analysed biophysics experiments	AD (50%), CFG (25%), OL (25%)
Wrote the manuscript	AD (70%), MM (5%), CFG (5%), OL (5%), ATK (5%)

- ***De novo* evolved interference competition promotes the spread of biofilm defectors.**

  Authors: Marivic Martin, Anna Dragoš, Theresa Hölscher, Gergely Maróti, Balázs Bálint, Martin Westermann, Ákos T. Kovács
  Publication in: Nature Communications (2017), 8:15127, doi: 10.1038/ncomms15127.
  Presented as: Chapter 3.

Conceived the project	ATK (100%)
Designed the experiments	MM (25%), AD (25%), THö (25%), ATK (25%)
Constructed bacterial strains	MM (40%), AD (30%), THö (30%)
Performed the experiments	MM (40%), AD (30%), THö (30%)
Performed genome resequencing	GM (50%), BB (50%)
Performed electron microscopy	MW (100%)
Wrote the manuscript	MM (20%), AD (40%), THö (20%), ATK (20%)

- **Division of labor during biofilm matrix production.**

Authors: Anna Dragoš, Heiko T. Kiesewalter, Marivic Martin, Chih-Yu Hsu, Raimo Hartmann, Tobias Wechsler, Knut Drescher, Nicola Stanley-Wall, Rolf Kümmerli, Ákos T. Kovács
Publication in: Current Biology (2018), 28:1903-1913, doi: 10.1016/j.cub.2018.04.046
Presented as: Chapter 4.

Conceived the project	AD (75%), ATK (25%)
Designed the experiments	AD (70%), RK (10%), ATK (20%)
Constructed bacterial strains	AD (100%)
Performed the experiments	AD (70%), HTK (10%), MM (10%)
Performed modelling	TW (50%), RK (50%)
Performed microscopy analysis	RH (75%), KD (25%)
Performed flow cytometry	AD (35%), CYH (35%), NSW (30%)
Wrote the manuscript	AD (60%), RK (20%), ATK (20%)

- **Collapse of genetic division of labour and evolution of autonomy in pellicle biofilms.**

Authors: Anna Dragoš, Marivic Martin, Carolina Falcón García, Lara Kricks, Patrick Pausch, Thomas Heimerl, Balázs Bálint, Gergely Maróti, Gert Bange, Daniel López, Oliver Lieleg, Ákos T. Kovács
Publication in: Nature Microbiology (2018),3:1451-1460, doi:10.1038/s41564-018-0263-y
Presented as: Chapter 5.

Conceived the project	AD (50%), ATK (50%)
Designed the experiments	AD (80%), ATK (20%)
Constructed bacterial strains	AD (80%), MM (20%)
Performed the experiments	AD (70%), MM (10%), CFG (5%), LK (5%), PP (5%), THe (5%)
Performed genome resequencing	GM (50%), BB (50%)
Performed protein purification	PP (80%), GB (20%)
Performed electron microscopy	THe (100%)
Performed and analysed biophysics experiments	AD (50%), CFG (25%), OL (25%)
Performed and analysed Western analysis	LK (50%), DL (50%)
Wrote the manuscript	AD (80%), ATK (20%)

- **Cheater-mediated evolution shifts phenotypic heterogeneity in *Bacillus subtilis* biofilms.**

  Authors: Marivic Martin, Anna Dragoš, Simon B. Otto, Daniel Schäfer, Susanne Brix, Gergely Maróti, Ákos T. Kovács
  Submitted to: The ISME Journal, submission number: ISMEJ-19-00748A
  Preprint: bioRxiv (2019) 494716, doi: 10.1101/494716
  Presented as: Chapter 6.

Conceived the project	ATK (100%)
Designed the experiments	MM (50%), AD (25%), ATK (25%)
Constructed bacterial strains	MM (90%), SBO (10%)
Performed the experiments	MM (70%), AD (5%), SBO (20%), DS (5%)
Performed genome resequencing	GM (100%)
Provided equipment	SB (100%)
Wrote the manuscript	MM (50%), AD (30%), ATK (20%)

SUMMARY

Social interactions are ubiquitous in all life forms, even in the miniscule ecosphere of organisms. Numerous studies have demonstrated that microorganisms, due to their preference to a collective style of living, are good models to explore cooperative and competitive interactions. Recent findings showed that the communal matrix-bound surface-attached cells called biofilms serve as social arenas where a plethora of interactions exist. More significantly, in combination with evolution experiments, social interplays and how they developed in spatially structured settings could be investigated and monitored.

In *Bacillus subtilis* biofilms, the matrix components EPS and TasA serve as costly public goods that shape social interactions of cells within the biofilms. In this dissertation, different evolution experiments with multiple starting points involving clonal cells of matrix producers, co-cultures of matrix producers and non-producers, and two different kinds of matrix-deficient strains were performed to investigate intraspecies social synergies related to matrix formation in biofilms produced by *B. subtilis*. Various interdisciplinary approaches were further utilized to strengthen the experimental evolution set-ups using molecular biology methods, microscopic fluorescence techniques and quantitative analyses using biomechanical profiling, computational modelling and simulations.

This work highlights the complexity of social interactions in single species biofilms as influenced by evolution via diversification, division of labour and competitive interactions. Diversification in clonal populations occurs during evolution and facilitates interlace of cooperative and exploitative behaviours as affected by resource sharing. Division of labour during biofilm matrix production as a form cooperative trait in *B. subtilis* biofilms is optimal at a genotypic level than at phenotypic. However, this behaviour, although stable in both ecological and laboratory set-ups, is evolutionarily unstable as the evolution of autonomy further diminishes it by matrix mutants yielding novel biofilm qualities. Furthermore, the evolution of competitive behaviours demonstrates unpredicted adaptive events such as changes in mobile genetic elements via *de novo* evolved interference and shifts in phenotypic heterogeneity related to anti-cheating mechanisms.

Zusammenfassung

Soziale Interaktionen sind in allen Lebensformen gegenwärtig, sogar in der winzigen Ökosphäre von Organismen. Zahlreiche Studien haben demonstriert, dass Mikroorganismen durch den von ihnen präferierten kollektiven Lebensstil gute Modelle zur Untersuchung von kooperativen und wettbewerbsorientierten Interaktionen darstellen. Neuste Ergebnisse zeigten, dass die als Biofilm bezeichnete Matrix-gebundene und an Oberflächen angeheftete Zellen als soziale Arenen fungieren, in denen eine Fülle an Interaktionen existiert. Soziale Wechselwirkungen und ihre Entwicklung in räumlich strukturiertem Umfeld konnten maßgeblich in Kombination mit Evolutionsexperimenten erforscht und beobachtet werden.

In *Bacillus subtilis* Biofilmen dienen die Matrixkomponenten EPS und TasA als kostenintensive Allgemeingüter, die soziale Interaktionen der Zellen im Biofilm gestalten. In dieser Dissertation wurden verschiedene Evolutionsexperimente mit mehreren Startpunkten durchgeführt, um intraspezifische soziale Synergien in Zusammenhang mit der Matrixproduktion in Biofilmen von *B. subtilis* zu untersuchen. Diese beinhalteten klonale Zellen der Matrix-Produzenten, Co-Kulturen von Matrix-Produzenten und Nicht-Produzenten sowie zwei unterschiedliche Stämme mit defizienter Matrixproduktion. Verschiedene interdisziplinäre Set-ups mit biologischen Methoden, mikroskopischen Fluoreszenztechniken und quantitativen Analysen mittels biomechanischem Profiling und computergestütztem Modelling wurden genutzt um die experimentellen Evolutionsansätze zu stärken.

Diese Arbeit hebt die Komplexität von sozialen Interaktionen in Einzelspeziesbiofilmen hervor, welche durch Evolution via Diversifikation, Arbeitsteilung und wettbewerbsorientierten Interaktionen beeinflusst wird. Diversifikation in klonalen Populationen findet während der evolutionären Entwicklung statt und ermöglicht die von Ressourcenteilung beeinflusste Verknüpfung von kooperativem und ausbeuterischem Verhalten. Arbeitsteilung ist während der kooperativen Produktion der Matrix in *B. subtilis* Biofilmen optimaler auf einem genotypischen statt eines phänotypischen Levels. Allerdings ist dieses Verhalten trotz der Stabilität in ökologischen- und Laborexperimenten evolutionär instabil, da die Evolution der Autonomie sie zusätzlich durch Entstehung von Matrixmutanten mit neuen Biofilmeigenschaften verringert. Weiterhin demonstriert die Evolution von

wettbewerbsorientiertem Verhalten unvorhergesehene adaptive Ereignisse wie Veränderungen in mobilen genetischen Elementen via *de novo* evolvierter Interferenz und Verschiebungen der phänotypischen Heterogenität in Zusammenhang mit *anti-cheating* Mechanismen.

INTRODUCTION

Microbes prefer to exist in a collective lifestyle, and they are not alone in such a preference. In the animal kingdom, group behaviours such as flocks of birds, schools of fish, herds of mammals, and swarms of insects also exist [1]. Such is not surprising since living in a group provides advantages to individual members as compared to a single style of living. Collective living in microorganisms such as in biofilms involves group organization and cell-to-cell communication that consists of an array of social interactions. Biofilms represent the most widely represented microbial life form on Earth [2–5]. The earliest record of biofilm formation has been discovered from fossil records dated around 3.25 billion years ago[2]. Their persisting existence is attributed to their secured manner of growth that involves cell survival in stringent conditions and their ability to disengage and colonize new niche[2]. And due to their ubiquity and significant impact in health, industry, and natural environment[2,6,7], scientists have employed biofilms to broaden the scientific understanding on microbial social interactions [8–11], evolutionary adaptation and processes[12–20], antimicrobial resistance [21] and metabolic uptake [22], to name a few. In biofilms, individuals prosper from the divergence into various distinct traits involving metabolic activity[23], antimicrobial resistance [24–26], spore formation [27], and secretion of extracellular polymers [28]. However, these mentioned traits could undergo adaptation mechanisms based on the circumstances that occur during individual interactions within the group. It is therefore essential to understand how social interactions in biofilms evolve through time as this will help improve our scientific knowledge on how biofilms adapt by social interactions.

1. Sociomicrobiology

In 2005, the interlink of the two specialized fields in microbiology that study social phenomena in bacteria, namely, biofilm and quorum sensing, led to the introduction of the term "Sociomicrobiology"[29]. Bacterial cells in independent planktonic conditions enter a complex development path that organizes into surface-adhered multicellular communities known as biofilms[30]. These spatially arranged cells are bounded together by self-produced viscous matrix, mostly composed of extracellular DNAs, structural proteins and extracellular polysaccharides [31–33]. Although cells within biofilms are

physically in contact with each other due to their proximity, they need a cell-to-cell signalling network called quorum sensing, to organize themselves in the communities[32,34–39]. With the aid of low molecular weight molecules known as autoinducers, quorum sensing permits bacteria to shift between low-cell-density (LCD) and high-cell-density (HCD) gene expression programs which either favour asocial or social behaviours, respectively[29,37,40]. Additionally, bacterial surface movement is also regarded as another area of Sociomicrobiology wherein social interactions could be investigated based on collective motility[34,39,41–45].

Sociomicrobiology combines social evolution theory and microbiology to understand the evolutionary process of social interactions in microbial assemblies. A behaviour is considered social based on the effect it delivers to both the actor and recipient. Behavioural effects are classified as costly or beneficial based on the (a) long term effect of the action and (b) the absolute fitness consequence such as productivity based on offspring survival[46,47]. Fitness consequence is further organized into direct fitness (impact on the individual's reproduction) and indirect fitness benefits (effect on the propagation of related individuals)[46,48]. According to the Hamiltonian classification system introduced in 1964, social behaviours could be categorized into four possibilities based on natural selection[46,49]. Acts that provide benefit to the actor are termed mutualism and selfishness based on the benefits and costs they contribute to the recipient, respectively. While actions that are costly to the actor but offer profits or losses to the recipient are regarded as altruism and spite, respectively (Fig. 1). However, some conflicts arise on how to classify social behaviours based on the effect on the actor and recipient[10,47,50]. To simplify, the social interactions that I discuss here are based on the impact the recipient receives. Interactions that benefit the recipients (mutual benefit and altruism) are classified as cooperation while behaviours that are costly to the recipients (selfishness and spite) are categorized as competition.

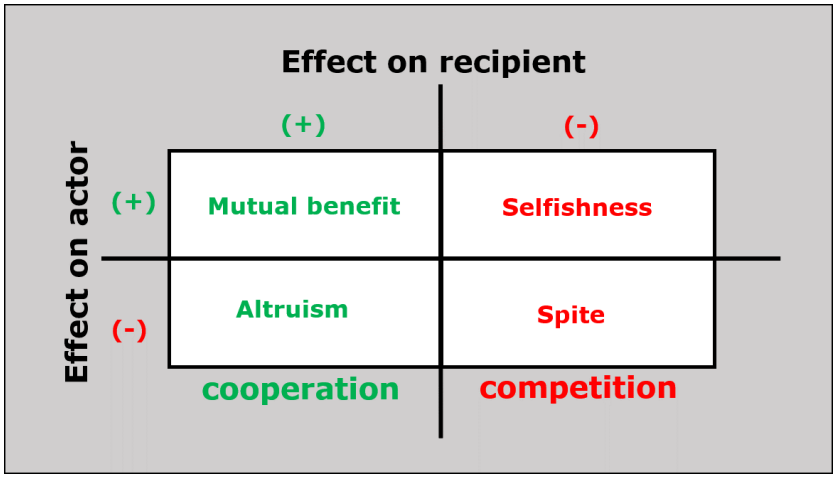

Figure 1. A classification scheme for social behaviours based on natural selection as introduced by W.D. Hamilton in 1964. (A modified version from West *et al.*, 2006 [47])

1.1 Public goods as a form of social behaviour

An essential element that shapes social interactions in microbes is the production of public goods. These are products that are manufactured by individuals for their utilization but also shared to neighbouring individuals (Fig. 2a[8])[7,46]. Such products are typically released into the environment through the cell membrane and play potential roles in social interplays among interacting individuals. To date, most social interaction studies both in planktonic and static cultures employ siderophores[51–60], extracellular digestive enzymes[61,62] and exopolysaccharides[63–66] (see also Chapters 2,3,4,5 and 6). However, there are a diverse variety of molecules produced by microbes which have potential roles as public goods that could be utilized to understand social interactions. As some of them were enumerated by West et al. based on their functions in previous studies[48] such as sucrose digesting enzyme[67,68], ß-lactamases[69], biosurfactants such as rhamnolipid and serrawettin produced by *Pseudomonas aeruginosa,* and *Serratia marcescens*, respectively[34,70], and surfactin by *B. subtilis*[71], shiga toxins[72,73], other forms of toxins[13] and virulence factors[74], quorum sensing signals[40], proteases[75,76], eDNAs as structural components in biofilms[32], antibiotics[77,78], and membrane vesicles[79,80].

The social nature of public goods production provides an efficient means to understand behaviours within a collective lifestyle. It facilitates the analysis of the problems in cooperation, which leads typically to competition since they are expensive products that offer benefits to all individuals, including those that do not produce it[10,48]. And in some cases, exploitation of public goods leads to the existence of cheaters that sometimes cause

the group to suffer such as in the case of the "the tragedy of the commons"[81](Fig. 2b)[10]. Cheaters are individuals who do not cooperate or cooperate less but benefits from those cells that produce a public good, leading to better competitive advantage to invade the population[10,47]. Although the evolutionary concept of cheating has been defined[82], the description mentioned above is commonly used in social evolution studies related to public goods production in microorganisms.

Social interplays between producers and non-producers of the so-called public goods usually are examined based on the fitness of the producer who carries the putative social behaviour and compared to the non-producer grown in monoculture and mixed-culture. Such is possible through phenotypic assessment related to the social behaviour[48,83] (see also Chapters 2,3,4,5 and 6) and the use of phenotypic or molecular marker [41,61,64,84,85] (see also Chapters 2,3,4,5 and 6). Public goods production provides direct fitness to the producers and indirect fitness to neighbouring individuals. Interestingly, due to the limiting factors encountered by cells within a biofilm, such as nutrients and niche, and the advantage of being in close proximities, cells can interact cooperatively or competitively with respect to the availability of the public goods.

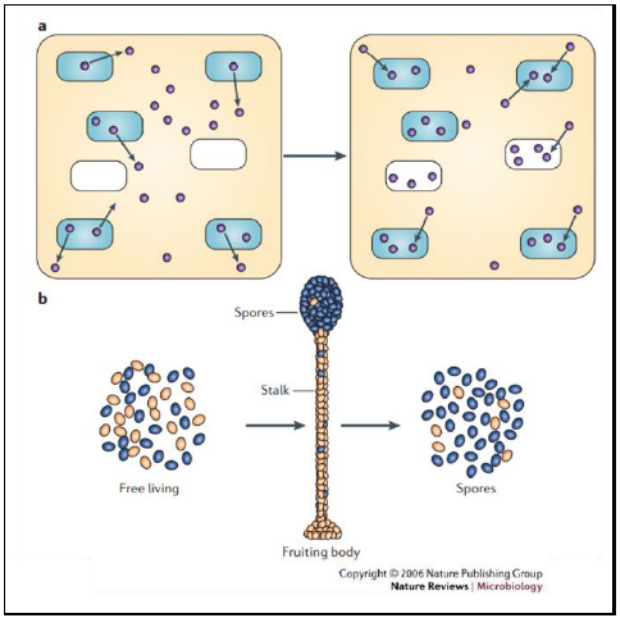

Figure 2. The problem of cooperation. a) "The tragedy of the commons"[81] occurs when cheaters (white oblongs) exploit the benefits the public goods (purple circles) produced by other cells (blue oblongs) without paying any cost. b) Altruistic sacrificial behaviour of *D. dictyostelium* happens when two lineages of cells cooperate to form a fruiting body, but one (orange lineage) would sacrifice by contributing more towards stalk formation while the other one (blue lineage) gains more fitness by providing less for stalk formation and more for spore production. (Figure adapted from West et al. 2006 [10])

1.2 Cooperative interactions

The theory of evolution introduced by Charles Darwin[86] is universally conceptualized as the "survival of the fittest", wherein the need to persist entails constant competition. However, in nature, cooperation is found to be very ubiquitous. It exists in numerous levels of biological systems such as cooperation of genes in genomes, chromosomes in eukaryotic cells, cells in multicellular entities, and humans in social communities[50]. Most recently cooperative behaviour in viruses has been reported as a form of surmounting inherent host immunity[87]. However, natural selection favours genes that support an individual's ability to survive and reproduce and therefore contradicts cooperative behaviour unless a specific mechanism is at work. In bacteria, the study of collaborative interactions offers an interdisciplinary interest to comprehend bacterial communities[52,88], clinical[89,90] and industrial relevance[91]. Studies on social interactions provide an understanding behind the dilemma of cooperation, where an individual performs a task that is costly to its fitness but confers fitness benefits to other individuals [46,47,49]. Generally, the problem of cooperation (Fig. 2)[10] is explained in theory behind the "the tragedy of the commons"[81] involving the production of public goods and why cooperative traits (altruism) include sacrificial benefits to the adjacent cells [10]. The latter is clearly illustrated in the fruiting body formation of the slime mould *Dictyostelium discoideum*[92] (Fig. 2b)[10], and in the bacterium, *Myxococcus xanthus*[43,93,94] wherein as a form of sacrifice, cells differentiate either as spores or non-viable stalk cells and non-spores, respectively.

Cooperation is a behaviour that provides positive effects in terms of fitness to the recipient[10]. However, some studies claim that cooperation requires a positive impact on the recipient and negative influence on the actor, commonly known as altruism[50] and not a positive effect on the recipient and actor known as mutualism. Here, I refer to cooperation based on the positive fitness effect it provides to the recipient, as explained by West et al.[10] wherein direct fitness benefits pertain to mutualistic behaviour and indirect fitness benefits for altruistic actions. Additionally, some studies argue that cooperation only occurs in intraspecific interactions. However, this argument has been refuted by cooperative studies dealing with interspecific interactions[95].

The sustainment of cooperation despite the prevalence of selfish motives in nature has led to the elucidation of this phenomenon in numerous ways[8,36,46,49,64,82,83,92,96–110]. The maintenance of cooperation could be explained in two ways based on direct or indirect

benefits the recipient receives (Fig. 3)[111]. The first explanation is that cooperation is maintained when the action provides direct benefits to the actor (mutualism) that outperforms the cost of the cooperative behaviour[99] or when it is enforced on a fixed or conditional basis[109,111]. The former pertains to cooperation via shared interest wherein the behaviour is selected when individuals have a common interest in working together[10,99] as observed in mixed-species biofilms of *Streptococcus oralis,* and *Actinomyces naeslundii*[112] and single species biofilms of *B. subtilis* demonstrated in Chapter 4. The latter type of cooperation occurs when individuals pursue their reproductive success by working together to boost the productivity of the group through enforcement either via conditional enforcement in the forms of rewards, punishment, sanctions and reciprocity or through fixed enforcement such as policing[109,113–115]. The second rationalization of cooperation is based on indirect fitness benefits, wherein the cooperative action (altruism) is aimed towards another individual who carries the cooperative trait[46,49]. Such as in the case of kin discrimination (cooperation towards relatives)[71,116,117], limited dispersal (spatial structure and proximity of neighbouring cells that are mostly related)[103,105,108] and "green beard" effect (a form of kin discrimination wherein an individual is recognised with the cooperative gene based on a phenotypic marker)[118,119].

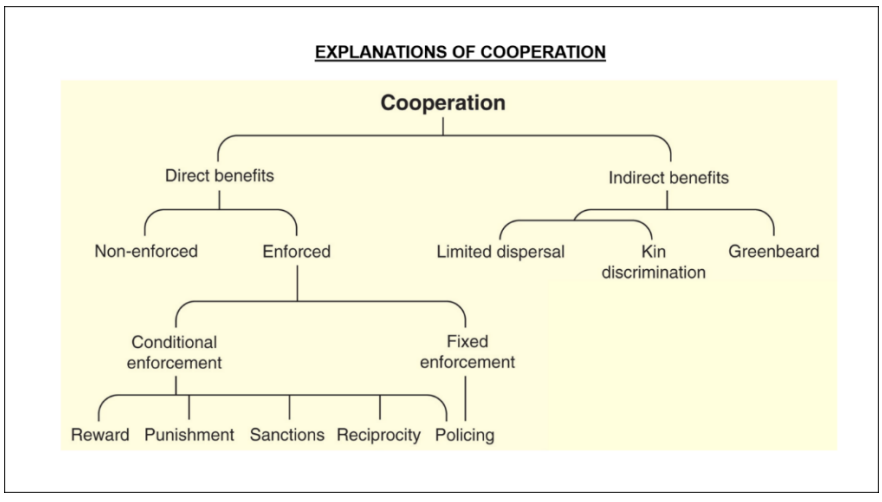

Figure 3. Classifications of the explanations of cooperation. Cooperation that provides direct benefits explains mutualism while indirect benefits explain altruism. Direct benefits could be classified into non-enforced or enforced and further categorised into conditional or fixed enforcement. Conditional enforcement involves reward, punishment, sanctions, and reciprocity, while fixed enforcement includes policing. Indirect benefits could be classified into limited dispersal or kin discrimination and green beard. (Adapted with modifications from West et al. 2007, 2007(1) [47,111]).

1.3 Competitive interactions

Competition is an indirect or direct interaction of individuals sharing the same resources that generally results in altered fitness[120]. In most cases, resources such as nutrients and space are limited and lead to an arms race to obtain better access to them[100]. Competition could be classified into three major forms such as interference competition, exploitation competition and apparent competition (Fig. 4)[120]. Furthermore, these behaviours could be characterized based on their direct or indirect occurrences between individuals; wherein interference competition entails a direct interaction while exploitation and apparent competitions occur indirectly[120,121]. According to Lang and Benbow, interference and exploitation competitions are regarded as real competitions as compared to the third form, which is ostensive. Apparent competition is an indirect rivalry of resources that involves unintended higher predation risk of the other individual to a common predator.[122] Interference competition occurs when individuals directly hinder the other individual from obtaining resources. Such could be via the injection of toxins like Type VI secretion system[123,124] or the use of biological weapons such as phages[125] (see also Chapter 3). Whereas, exploitation competition occurs when individuals indirectly compete for common resources such as food or niche, which later on result in decreased resource availability for other individuals[120,121]. Some examples of such are the competition for nutrient uptake[106,126,127], biofilm matrix components [64] (see Chapter 2, 3 and 6) and iron scavenging molecules [52,56,57,59,100]. Often, this exploitative behaviour is referred to as cheating, wherein an individual can benefit from the public goods that are produced by the other individual without having to pay the cost[9,10,48]. In some cases, exploitative behaviour of cheaters leads to the phenomenon called "the tragedy of the commons"[81] (Fig. 2a) wherein selfish interests become a detriment to the whole community. This occurrence was observed in evolutionary experiments on the collapse of mats formed in the air-liquid interface of *Pseudomonas fluorescens* [63] or the eventual collapse of the population in *B. subtilis* due the presence of cheaters (Chapter 6). Such a tragedy could be regarded as the result of competitive exclusion[128], wherein a better competitor outcompetes the inferior one.

In biofilms, most cases of competition are based on sharing limitation[96,129,130], biofilm spatial arrangement[64] or on a mother-daughter cell lineage-binding matrix component[65]. If resources are confined within the group, the competition will favour the most competitive individual with a greater share of benefits. However, the success of the

population and each is decreased due to the reduced overall productivity of the group. Therefore, specific defence mechanisms are developed by individual members to resist invasion or hitch-hiking strategies. In *Vibrio cholerae* biofilms, the anti-invasion approach of immotile and motile cells into the biofilm is through a secreted protein that strongly binds together cell lineages called RbmA[65]. Interestingly, inter-species competition could be used to modulate cooperation such as in the case of competition study between bacterium *Escherichia coli* and yeast *Saccharomyces cerevisiae*[101]. It is crucial to understand how competitive behaviours within biofilms could be prevented as it helps us understand pathogenicity in biofilms and how it could be infiltrated by antimicrobials such as in the case of biofilm weakening in *Salmonella enterica* serovar Typhimurium caused by non-matrix producers[130].

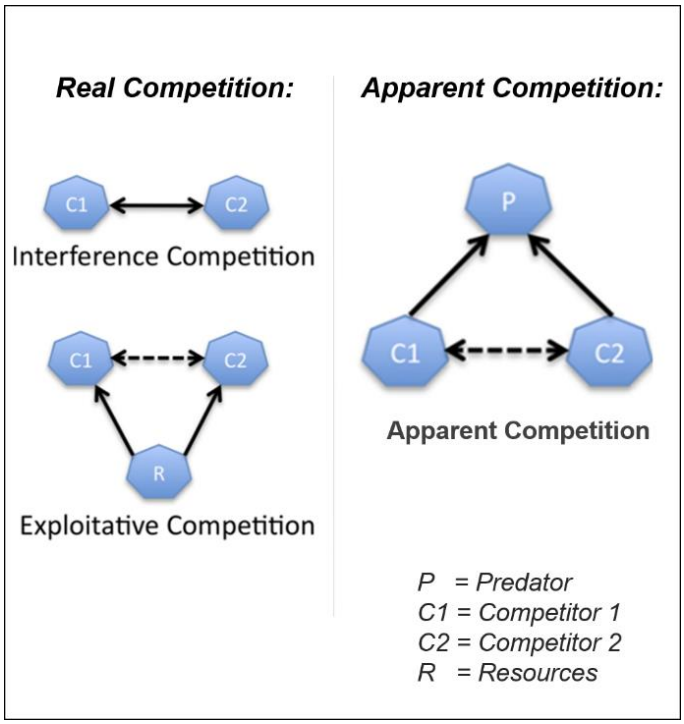

Figure 4. Classifications of competitive interactions. Schematic diagram of the three important types of competition based on two classes, namely real competition and apparent competition. Indirect interaction is represented by dashed lines, while direct interaction is indicated by solid lines. (Adapted with some modifications from Lang & Benbow, 2016 [120].)

2. Experimental evolution as a research tool

From the time Charles Darwin introduced the theory of natural selection[86], it has been established that microbes on Earth evolved and have been evolving for billions of years. And since evolutionary theories are guided and proven by observing patterns of phylogeny that manifests the previous evolution[131], the use of an alternative research framework to experimentally investigate evolutionary scheme in real time became apparent for scientists. Experimental evolution is defined as the analysis of evolutionary changes that transpire in experimental populations in response to certain factors and conditions as introduced by the investigator[131,132]. The utilization of microbes to support evolutionary theories and understand underlying evolutionary processes in microscale is a suitable opportunity to advance evolutionary perspectives further since microbes possess short generation time, they are easier to manipulate and grow into larger populations using controlled environments[131,133]. Moreover, travelling back in time is possible through the revival of stored frozen states of evolved and non-evolved strains, thus aiding scientists to compare different parameters between evolved and ancestor strains[14–17,20,63,134–137] (see also Chapters 1, 2, 3, 5 and 6).

Experimental evolution is occasionally referred to as "laboratory natural selection"[131] since most evolution studies are conducted in laboratories, except for those held in the fields[138–140]. Evolution experiments in the laboratory involve different population propagation techniques that are essential to understand genetic dynamics. There are three different ways to reproduce a population, namely single-cell bottlenecks, continuous culture and serial transfer[132]. Barrick *et al.* presented that each methodology is conducted depending on the intended type of evolution experiments needed, such as mutation accumulation experiments and adaptive evolution (Fig. 5)[132]. The single-cell bottleneck is a type of propagation that supports the accumulation of mutations through a repeated but random selection of single colony on culture plates. This scheme leads to population bottlenecks and eliminates genetic diversity resulting in the fixation of random genetic alterations regardless of their fitness influence. This type of evolution experiment is not suitable for biofilm evolution studies since it is focused on a single cell level. The other kind of evolution experiment, which is adaptive evolution is facilitated by two different population propagation methods, namely continuous culture and serial transfer. In continuous culture experiment, population propagation is achieved by a non-

stop inward flow of nutrients and outward flow of arbitrary individuals and wastes using a bioreactor with an open culture system. This set-up results in adaptive evolution and genetic diversity that preserves a steady volume. Such type of experimental set-up is commonly used in biofilm evolution studies employing flow chambers[61,141–146]. Another means of increasing populations is called serial transfer that is performed by subsequent re-inoculation into fresh media[14–16,18,20,134,136,147] (see Chapters 1, 2, 3, 5 and 6) and supports regrowth until nutrient depletion. It facilitates maintenance of sufficient genetic diversity on every transfer and ensues adaptive evolution. In another case, continuous population growth could also be achieved in such method by performing transfers prior to nutrient exhaustion. Interestingly, population bottlenecks also exist during adaptive evolution experiments as a result of selective sweeps, as demonstrated in Chapter 3.

In nature, microorganisms exist in groups and thus evolve in the company of other microbes. Therefore, experimental evolution using biofilms is a fitting scheme to study growth and interactions at a micro-scale level as it represents microorganisms present in spatially structured environment. Additionally, it helps in understanding the maintenance of cooperation despite the proliferation of selfish motives in the environment. The advantages of using biofilms over planktonic cultures as better models to study social interactions in an evolutionary perspective are extensively discussed in Chapter 1. Notably, it is vital to scrutinize if observations found in the evolution of biofilms in laboratory set-ups are pertinent to the evolution of biofilms in natural settings. Numerous experimental evolution studies performed in the laboratory demonstrated remarkable parallelism of laboratory-derived evolved strains with *in vivo* chronic infections isolates[14,142,143,146,148–150], thus proving that biofilm adaptations *in vitro* and biofilm-related persisting diseases could be influenced by the similar adaptive factors.[12]

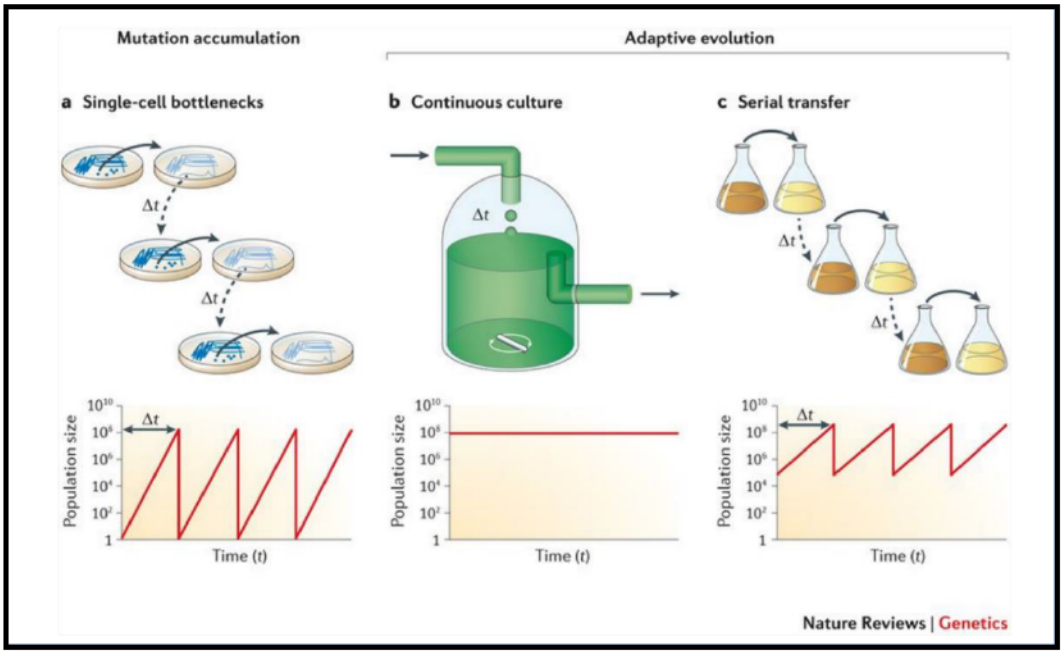

Figure 5. Types of evolution experiments. Three significant ways to propagate populations during evolution experiments include a) single-cell bottlenecks b) continuous culture and c) serial transfer. Top panels illustrate the mechanics of population propagation while bottom panels demonstrate changes in population size over time for each method (adapted from Barrick and Lenski, 2013)[132].

3. Phenotypic heterogeneity

In the bacterial world, phenotypic heterogeneity is a widely observed occurrence[151–153] wherein, within an isogenic population, a subpopulation of cells demonstrates expressions that are partially divergent from that of the rest [151,153–155]. It is a phenomenon in which non-genetic variations transpire in a genetically homogenous microenvironment[151,156]. In this context, the condition in which populations bifurcate into different co-existing type of cells is described as bistability[152,153,157,158]. Several studies have established occurrences of phenotypic heterogeneity and bistability traits associated with antibiotic resistance and the presence of persister cells[152,153,159], biofilm formation[157] (see also Chapter 4 and 6), DNA uptake[152,160], motility[152,161], surface colonization[162], sporulation[152,163], cannibalism[152] and quorum sensing-dependent processes[35,153]. Often, phenotypic heterogeneity is the result of genetic alterations, inherent stochasticity or environmental signals [154–156,162,164]. However, as pointed out and enumerated by Ackermann[151], phenotypic heterogeneity could also occur independent of genetic [165–167] or environmental[168] variations. Thus, certain mechanisms could still generate phenotypic heterogeneity without the presence of genetic and

environmental factors, such as in the case of stochasticity, cellular ageing and cell-to-cell contact via signal molecule mediation or through cell proximity[151].

Phenotypic heterogeneity is a biological trait that is variable, heritable for at least few generations and possesses a complex feature that is typically observed only when monitoring cells over a longer time scale or when comparing cells with another cell or subpopulations [151], such as in the case of biofilms wherein heterogeneity is highly pronounced in the early phase of development[35]. Furthermore, as it is shaped by natural selection, phenotypic heterogeneity can also evolve, as demonstrated by evolution in the laboratory based on experimental variable conditions that resulted in elevated levels of phenotypic heterogeneity [169,170]. Additionally, phenotypic heterogeneity associated with matrix production can also be altered during cheater-mediated experimental evolution in biofilms (Chapter 6).

It is presumed that the switching mechanism of bacteria to different cell types have evolved as a strategy for bacterial cells to be phenotypically adjusted to current or incoming unpredictable harsh conditions[152]. Phenotypic heterogeneity offers cells with higher chances of survival through increased bacterial fitness that allows individuals to persist in a continually changing environment[151–153]. From the vantage point of single cells, such behaviour confers altruism, while from the standpoint of a genome, it is a non-altruistic behaviour because they serve to increase the probability of survival in clonal populations where all cells are identical genotypically[152]. Significantly, phenotypic variation can lead to a division of labour[171] (see also Chapter 4), in which duties are distributed into several different subtasks and performed by specialised individuals, thus increasing the population growth rate and improving task performance[151]. Studies on phenotypic heterogeneity are essential as this complex trait has been associated with antibiotic resistance and persister cells[152,153]. At the same time, changes in the patterns of phenotypic diversity within a population can also be utilised to monitor the evolution of social interactions within genetically identical individuals that are enclosed in a spatially structured environment as demonstrated in Chapter 6.

4. Biofilm formation in *Bacillus subtilis*

The first Gram-positive bacterium to have its genome sequenced was *B. subtilis* [172,173] and ever since the discovery of its ability to form biofilm[27,174]; numerous studies proceeded to employ it as a model organism to study biofilm formation. Different strains of *B. subtilis* have been utilized, to name a few, are the predominantly studied undomesticated strain NCIB3610, the natural isolate PS216 from sandy soil in Slovenia [11,175,176] and the tryptophan auxotroph laboratory strain 168 from mutated Marburg strain [177]. Surprisingly, different 168 stocks from different laboratories exhibited varied biofilm capabilities in different nutrient set-ups [178], thus showing some complexities in metabolic dependencies of different strains. Nevertheless, the undomesticated strain NCIB3610 (Chapters 2,4 and 5) and domesticated strain 168 (Chapters 3 and 6) demonstrated well-developed biofilm using defined and complex media, respectively. Under laboratory conditions, biofilm models of *B. subtilis* exist in different forms (Fig. 6), such as on agar surfaces called colony biofilm [27,41,64,178–183], at the air-liquid interface known as pellicles [27,178–181,184,185] (see also Chapters 2, 3, 4, 5 and 6), and at the plant roots[116,178,186,187] (see also Chapter4). The primary model system used in this dissertation is the pellicle biofilm and in minority, the surface colony biofilm and plant root attachment.

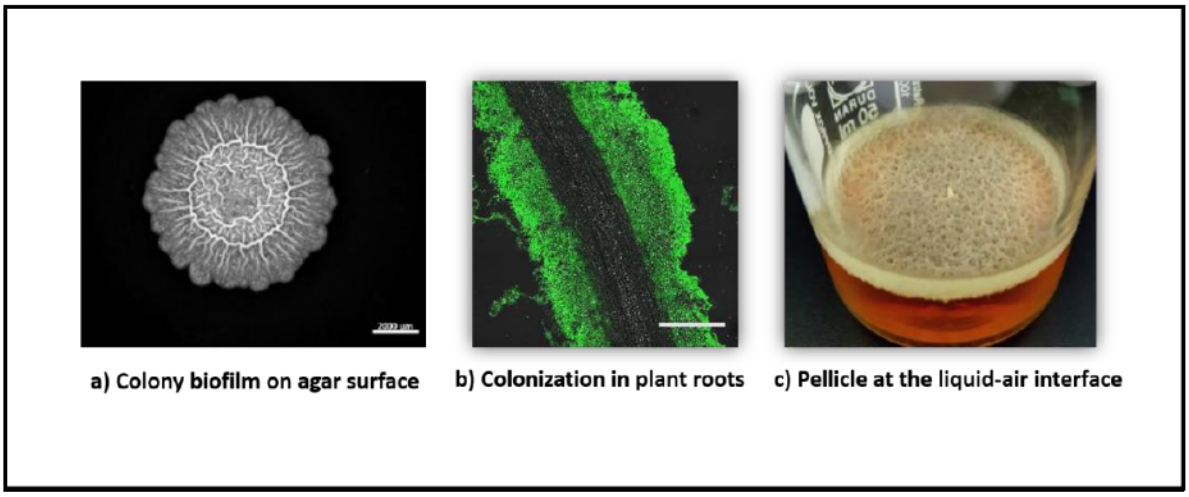

Figure 6. Biofilm formation in *B. subtilis*. Different types of biofilm models include a) biofilm on the surface of an agar culture plate b) attachment and colonization in roots such as *Arabidopsis thaliana* c) pellicle formed at the interface between liquid and air.

Biofilm formation in *B. subtilis*, specifically for pellicles (Fig. 7), starts when motile flagellated cells in the liquid medium swim towards the interface between the liquid and the air where the oxygen level is optimal. Once the cells reach the surface, cells differentiate into non-motile matrix-producing cells and cease to separate. Cells bundle up and commence forming chains that are enclosed by a self-produced matrix. In the maturation phase, the matrix-producing cells enter the sporulation stage where aerial protrusions are developed and become the preferential sites for sporulation [27]; however, sporulation is not an essential requisite in biofilm development [27,174].

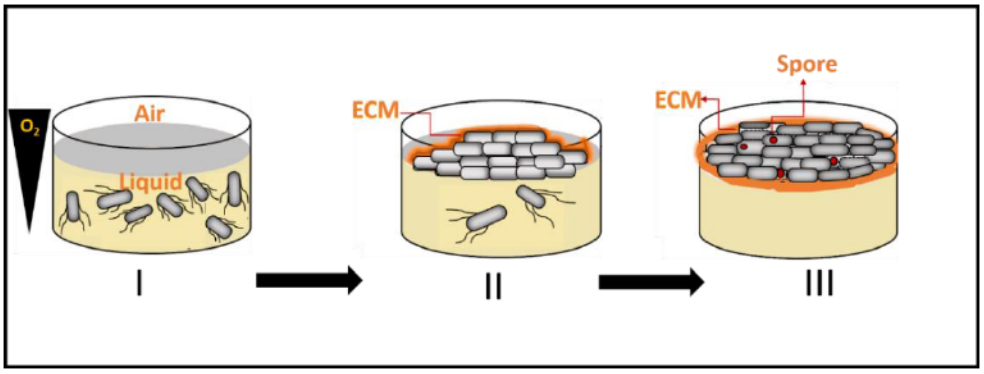

Fig 7. *B. subtilis* pellicle formation. I) Motile cells with flagella move towards the surface where oxygen is optimum. II) At the surface, cells become non-motile matrix producers that are enclosed by extracellular matrix (ECM). III) The cells within the pellicle mature and sporulate.

4.1 Regulatory pathway governing *B. subtilis* biofilm formation

The bacterium *B. subtilis* possesses a complex regulatory pathway related to matrix gene expression that starts with the entry of single motile planktonic cells to a sessile state known as a biofilm. This shift is affected by changes in the conditions of its natural habitat as signalled by different environmental cues[188] and is integrated by several subnetworks (I-IV) shown in Fig. 8 [189] that are involved in the activation or repression of matrix gene expression. Spo0A is the principal transcriptional regulator that controls the necessary genes relevant to biofilm formation[190] (Subnetwork I). An essential step to activate entry to biofilm development is through its activation via phosphorylation of a single aspartate residue [27,189]. The concentration of the phosphorylated Spo0A (from this on Spo0A~P) determines which differential gene regulation is to be facilitated and is determined by the activity of kinases KinA, KinB, KinC and KinD[189]. These kinases act either directly or

indirectly via direct activation of Spo0A or via phosphorylation, respectively [191]. Since Spo0A also controls sporulation genes, initial phosphorylation could involve intermediate levels of Spo0A~P concentration wherein biofilm genes will be expressed. However, once the Spo0A~P levels increase, its high accumulation will activate the sporulation genes. At the intermediate threshold level, Spo0A~P has two parallel pathways of anti-repression that are enabled to trigger transcription of operons essential for matrix expression, SinR and AbrB.

One of the regulatory pathways is regulated by the SinR master regulator that represses the operons responsible for the synthesis of the exopolysaccharide and protein components, e*psABCDEFGHIJKLMNO* and *tapA-sipW-tasA*, respectively. SinR is a transcription factor that serves as a principal regulator of biofilm development and authorizes the shift of solitary motile cells to clustered cells [192,193]. With the aid of the anti-repressor SinI, genes essential for matrix production are expressed.

Subnetwork II involves another regulation pathway that includes YwcC and SlrA (Fig 8)[189]. YwcC is a TetR type transcriptional repressor that represses *slrA* and the signal that relieves this repression is still not known [194,195]. SlrA as a paralogue of SinI, also binds and inactivates SinR[194]. However, unlike SinR, SlrA production occurs in almost all cells that results in transient elevation of matrix expression in the entire population, which signifies that this pathway could be involved in stress response mechanisms[194].

Another anti-repressor that binds to SinR is called SlrR[194], which is distinct from SinI as it is under the transcriptional repressor YwcC[194,195]. SlrR is a regulatory protein that is not only inhibited by SinR but also by AbrB[194–196]. It controls biofilm formation in two distinct ways: first, by forming a SinR-SlrR complex which results in derepression of the matrix gene operons e*psABCDEFGHIJKLMNO* and *tapA-sipW-tasA* and SlrR promoter[189]. Second, by repression of promoters of the flagellin genes (*hag*) and genes responsible for cell separation that encodes autolysin *lytABC* and *lytF* [158,197].

Moreover, its transcription is indirectly activated by the regulatory protein AbH[180] (Subnetwork III, Fig 8)[189]. AbH transcription is repressed by AbrB and controlled by different extracytoplasmic sigma factors, namely σ^M, σ^W and σ^X [184,198–203]. The latter mechanism is associated with cell wall stress and antibiotic resistance in biofilms [202–204] that is considered as Spo0A-independent system related to response to external

stimuli[189].

The other matrix gene repressor is AbrB[205–207] which could be controlled by Spo0A~P either by direct repression through the transcription of *abrB*[206,207] or via Spo0A~P anti-repression by means of AbrB anti-repressor, *abbA* [207]. Moreover, AbrB represses not only the *eps* operon and *tapA-sipW-tasA* but also the expression of regulatory proteins SlrR and AbH and hydrophobin BslA[205]. Subnetwork IV involves a pathway that facilitates the expression of the operons for BslA and PGA synthesis [189,208]. This network uses the DegS-DegU two-component system [183,208–211], wherein DegS phosphorylates the response regulator DegU. It is related to competence, motility, degradative enzymes[212], and colony biofilm formation associated with hydrophobicity protein BslA[183,209,210,213].

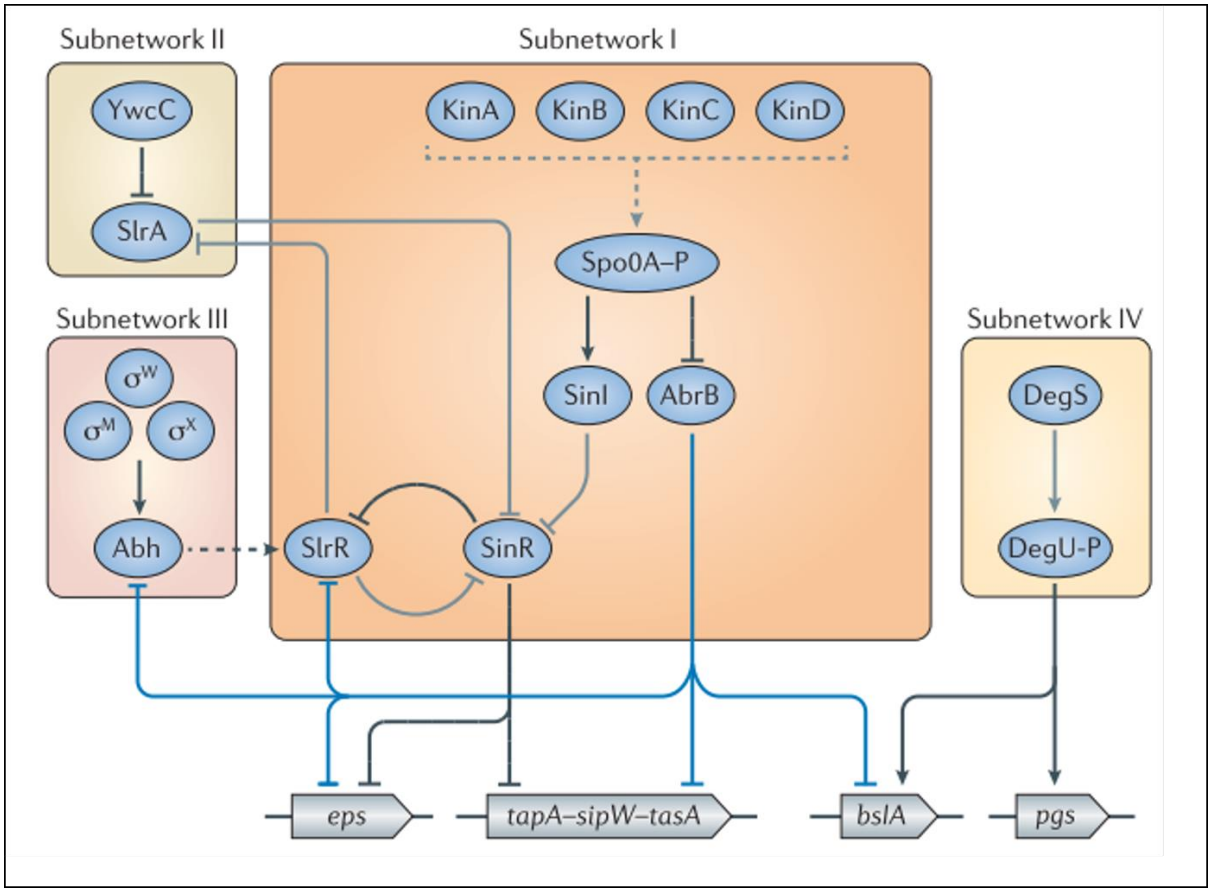

Figure 8. Schematic diagram of the regulatory network governing *B. subtilis* biofilm formation. Illustration of Subnetworks I-IV responsible for the activation and repression of the matrix genes expression based on environmental cues. Dark lines in grey and blue represent transcriptional regulation. Solid lines depict direct regulation, while dashed lines indicate indirect regulation (Adapted from Vlamakis et al. 2013 [189]).

4.2 Biofilm matrix components

During biofilm development, regulatory switch circuits responsible for the three main matrix components exopolysaccharide EPS, structural protein TasA and hydrophobin component BslA are activated. However, the work presented in this dissertation is primarily focused on EPS and TasA. Primarily, the absence of either TasA or EPS result to non-biofilm formation at the liquid air-interface (see Chapters 3, 4, 5 and 6). In the case of natural *B. subtilis* soil isolates, genes responsible for exopolysaccharide and surfactin production are related to the formation of a fruiting body structure that serves as preferential sites for sporulation[27]. In the case of pellicle development in *B. subtilis,* other factors such as movement and mobility appendages are essential but not primarily crucial for timely progression[185].

4.2.1 Structural protein TasA

In *B. subtilis*, protein components are important for a functional biofilm matrix. In particular, the proteinaceous element that is essential for matrix integrity in this Gram-positive plant-beneficial soil bacterium is comprised of a structural fibre called TasA [214]. Electron microscopy conducted by Romero *et al.* revealed that the protein assembly is composed of a fibre framework of 10-15 mm length and varying widths. It was first claimed to possess an amyloid-like fibre structure [214] that resembles the phenol soluble modulins (PSMs) in Gram-positive *Staphylococcus aureus* [215] and curli fibre in Gram-negative *Escherichia coli* [216]. Recent *in vitro* experiments with the use of X-ray fibre diffraction method confirmed previous claims that TasA is indeed of amyloid-like structure [217]. However, another study showed that TasA lacks the characteristic 'cross-β' architecture, thus could not be considered as an amyloid-like structure [218].

During biofilm formation, synthesis of TasA starts when the operon *tapA-sipW-tasA* controlled by master regulator SinR is derepressed by SinI [157,218,219] or repressed by AbrB[205–207]. The mature form of TasA is composed of 234 amino acid that is initially synthesized as 261 amino acid protein wherein 27 N terminal residue-encoding peptide is removed by SipW signal peptidase. Additionally, TasA protein fibres were reported to be fastened to the cell wall with the aid of another protein called TasA anchoring assembly protein (TapA) [220]. However, this accessory protein required for TasA polymerization and assembly has been recently reported to be not essential when TasA

is in fibre form [218], thus making the role of TapA in biofilm formation uncertain. Nevertheless, it is indisputable that TasA enacts a significant function in biofilm formation. Strains lacking *tasA* are not able to form proper biofilm at the air-liquid interface known as pellicles [214] (see Chapters 3, 4, 5 and 6) exhibit reduced wrinkly phenotype [182,214,220] and hindered hydrophobicity [213] suggesting that TasA portray a vital role in the structural component of *B. subtilis* biofilm matrix.

4.2.2 Exopolysaccharide (EPS)

Another predominant matrix component is the exopolysaccharide element EPS that is also repressed by SinR[27,192] or released from the repression by AbrB[205–207] . EPS is synthesized by the products of 15-gene operon *epsA-O*[27] (known as the *eps* operon) that encode biosynthetic mechanisms that produce EPS using nucleotide sugar substrates[193]. The EPS is comprised of glucose, galactose and N-acetylgalactosamine[221] and is seemingly the principal polysaccharide in biofilms cultured in the laboratory using MSgg medium[27,189,221,222] and culture medium for biofilm-plant root experiments[187]. While the polysaccharide levan is predominant in sucrose-rich medium[222]. Among the fifteen genes in the *eps* operon, only a few have been extensively studied[27,179,192,223–226]. EpsA and EpsB are reported to be both essential to biofilm formation[227–229], analogous to enzymes related to EPS chain length[230] and encode a putative transmembrane modulator protein and a putative protein tyrosine kinase, respectively[228,229]. EpsC is related to enzymes responsible for nucleotide sugar synthesis while EpsD, F, L and M are postulated as enzymes associated with glycosyl transferase[230]. EpsH, I, J and K encode proteins responsible for the synthesis of a conserved bacterial polysaccharide called poly-N-acetyl glucosamine (PNAG)[231] while EpsG is reported to be akin to proteins related to polymerization of EPS repeating units [230]. EpsE as a bifunctional protein is the most studied protein in the *eps* operon[226,227,230,232]. This protein is essential for EPS synthesis due to its glycosyltransferase activity and functions as a molecular clutch that inhibits motility [226,232]. This motility function serves as a reliable mechanism that saves energy by ensuring that flagella rotation stops when extracellular matrix production commences[161]. Moreover, flagellar inhibition due to transcription of EpsE also leads to increase in BslA transcription brought about by the elevated level of phosphorylated DegU.

4.2.3 Hydrophobin (BslA)

BslA is another component that plays an important role in biofilm matrix production in *B. subtilis*[213,233–235]. This small secreted protein aids in the assembly of the biofilm matrix together with the exopolysaccharide (EPS) and the protein component (TasA)[233]. Additionally, it is essential for biofilm complexity and hydrophobicity by acting as a surface active protein that configures a water-repellent layer in colony biofilms and a protein bundle similar to a raft below the buoyant pellicle[213,233]. Due to its conferred amphiphilic property, BslA is referred to as a bacterial hydrophobin that is analogous to the hydrophobic coat formed on surfaces of fungi[236]. Its role in liquid repellence suggests a potential contribution to increased protection of biofilms against antimicrobials[234].

REFERENCES

The following are the list of publications cited in the Introduction.

1. Sumpter, D. J. T. The principles of collective animal behaviour. *Philos. Trans. R. Soc. B Biol. Sci.* **361**, 5–22 (2006).

2. Hall-Stoodley, L., Costerton, J. W. & Stoodley, P. Bacterial biofilms: from the natural environment to infectious diseases. *Nat. Rev. Microbiol.* **2**, 95–108 (2004).

3. Costerton J, Lewandownski Z, Caldwell D, Korber D & Lappin-Scott H. Microbial Biofilms. *Annu Rev Microbiol* **49**, 711–745 (1995).

4. Flemming, H. C. & Wuertz, S. Bacteria and archaea on Earth and their abundance in biofilms. *Nat. Rev. Microbiol.* **17**, 247–260 (2019).

5. Flemming, H. C. *et al.* Biofilms: An emergent form of bacterial life. *Nature Reviews Microbiology* **14**, 563–575 (2016).

6. Nicolella, C., Van Loosdrecht, M. C. M. & Heijnen, J. J. Wastewater treatment with particulate biofilm reactors. *J. Biotechnol.* **80**, 1–33 (2000).

7. Costerton, J. W., Stewart, P. S. & Greenberg, E. P. Bacterial Biofilms: A Common Cause of. *Science* **284**, 1318–1322 (1999).

8. Nadell, C. D., Xavier, J. B. & Foster, K. R. The sociobiology of biofilms. *FEMS Microbiol. Rev.* **33**, 206–224 (2009).

9. Velicer, G. J. Social strife in the microbial world. *Trends Microbiol.* **11**, 330–337 (2003).

10. West, S. A., Griffin, A. S., Gardner, A. & Diggle, S. P. Social evolution theory for microorganisms. *Nat. Rev. Microbiol.* **4**, 597–607 (2006).

11. Dogsa, I., Oslizlo, A., Stefanic, P. & Mandic-mulec, I. Social Interactions and Biofilm Formation in Bacillus subtilis. *Food Technol. Biotechnol.* **52**, 149–157 (2014).

12. Steenackers, H. P., Parijs, I., Foster, K. R. & Vanderleyden, J. Experimental evolution in biofilm populations. *FEMS Microbiology Reviews* **40**, (2016).

13. Le Gac, M. & Doebeli, M. Environmental viscosity does not affect the evolution of cooperation during experimental evolution of colicigenic bacteria. *Evolution (N. Y).* **64**, 522–533 (2010).

14. Traverse, C. C., Mayo-smith, L. M., Poltak, S. R. & Cooper, V. S. Tangled bank of experimentally evolved Burkholderia biofims reflects selection during chronic infections. **110**, (2012).

15. Ellis, C. N. & Cooper, V. S. Experimental adaptation of Burkholderia cenocepacia to onion medium reduces host range. *Appl. Environ. Microbiol.* **76**, 2387–2396 (2010).

16. O'Rourke, D., FitzGerald, C. E., Traverse, C. C. & Cooper, V. S. There and back again: consequences of biofilm specialization under selection for dispersal. *Front. Genet.* **6**, (2015).

17. Ellis, C. N., Traverse, C. C., Mayo-Smith, L., Buskirk, S. W. & Cooper, V. S. Character displacement and the evolution of niche complementarity in a model biofilm

community. *Evolution (N. Y).* **69**, 283–293 (2015).

18. Cooper, V. S., Staples, R. K., Traverse, C. C. & Ellis, C. N. Parallel evolution of small colony variants in Burkholderia cenocepacia biofilms. *Genomics* **104**, 447–52 (2014).

19. Flynn, K. M. *et al.* Evolution of Ecological Diversity in Biofilms of Pseudomonas aeruginosa by Altered Cyclic Diguanylate Signaling. *J. Bacteriol.* **198**, 2608–2618 (2016).

20. Poltak, S. R. & Cooper, V. S. Ecological succession in long-term experimentally evolved biofilms produces synergistic communities. *ISME J.* **5**, 369–378 (2011).

21. Høiby, N., Bjarnsholt, T., Givskov, M., Molin, S. & Ciofu, O. Antibiotic resistance of bacteria in biofilms. *Int. J. Antimicrob. Agents* **35**, 322–332 (2010).

22. Rosenthal, A. Z. *et al.* Metabolic interactions between dynamic bacterial subpopulations. *Elife* **7**, 1–3 (2018).

23. Xu, K. D., Stewart, P. S., Xia, F., Huang, C. T. & McFeters, G. A. Spatial physiological heterogeneity in Pseudomonas aeruginosa biofilm is determined by oxygen availability. *Appl. Environ. Microbiol.* **64**, 4035–4039 (1998).

24. Balaban, N. Q., Merrin, J., Chait, R., Kowalik, L. & Leibler, S. Bacterial persistence as a phenotypic switch; Supplemental Materials. *Science* **305**, 1622–1625 (2004).

25. Hoiby, N., Bjarnsholt, T., Givskov, M., Molin, S. & Ciofu, O. Antibiotic resistance of bacterial biofilms. *Int. J. Antimicrob. Agents* **35**, 322–332 (2010).

26. Burmølle, M. *et al.* Biofilms in chronic infections - a matter of opportunity - monospecies biofilms in multispecies infections. *FEMS Immunol. Med. Microbiol.* **59**, 324–36 (2010).

27. Branda, S. S., González-Pastor, J. E., Ben-Yehuda, S., Losick, R. & Kolter, R. Fruiting body formation by Bacillus subtilis. *Proc. Natl. Acad. Sci. U. S. A.* **98**, 11621–6 (2001).

28. Vlamakis, H., Aguilar, C., Losick, R. & Kolter, R. Control of cell fate by the formation of an architecturally complex bacterial community. *Genes Dev.* **22**, 945–953 (2008).

29. Parsek, M. R. & Greenberg, E. P. Sociomicrobiology: The connections between quorum sensing and biofilms. *Trends Microbiol.* **13**, 27–33 (2005).

30. Kolter, R. & Watnick Paula. Biofilm, City of Microbes. *J. Bacteriol.* **182**, 2675–2679 (2000).

31. Abee, T., Kovács, A. T., Kuipers, O. P. & van der Veen, S. Biofilm formation and dispersal in Gram-positive bacteria. *Curr. Opin. Biotechnol.* **22**, 172–9 (2011).

32. Spoering, A. L. & Gilmore, M. S. Quorum sensing and DNA release in bacterial biofilms. *Curr. Opin. Microbiol.* **9**, 133–137 (2006).

33. Kolter, R. & Greenberg, E. P. The superficial life of microbes. *Nature* **441**, 300–302 (2006).

34. Daniels, R., Vanderleyden, J. & Michiels, J. Quorum sensing and swarming migration in bacteria. *FEMS Microbiol. Rev.* **28**, 261–289 (2004).

35. Cárcamo-Oyarce, G., Lumjiaktase, P., Kümmerli, R. & Eberl, L. Quorum sensing triggers the stochastic escape of individual cells from Pseudomonas putida biofilms. *Nat. Commun.* **6**, 5945 (2015).

36. Popat, R. *et al.* Quorum-sensing and cheating in bacterial biofilms. *Proc. Biol. Sci.* **279**, 4765–71 (2012).

37. Wai-Leung, N. & Bassler, B. Bacterial Quorum-Sensing Network Architectures. *Annu. Rev. Genet* **43**, 197–222 (2015).

38. Von Bodman, S. B., Willey, J. M. & Diggle, S. P. Cell-cell communication in bacteria: United we stand. *J. Bacteriol.* **190**, 4377–4391 (2008).

39. Greenberg, E. P. The new science of sociomicrobiology and the realm of synthetic and systems ecology. in *The Science and Applications of Synthetic and Systems Biology* (ed. Institute of Medicine) 213–222 (The National Academies Press, 2011).

40. Williams, P., Winzer, K., Chan, W. C. & Cámara, M. Look who's talking: Communication and quorum sensing in the bacterial world. *Philos. Trans. R. Soc. B Biol. Sci.* **362**, 1119–1134 (2007).

41. Hölscher, T. *et al.* Monitoring spatial segregation in surface colonizing microbial populations. *J. Vis. Exp.* **116**, e54752 (2016).

42. Gibbs, K. A. & Greenberg, E. P. Territoriality in Proteus: Advertisement and aggression. *Chem. Rev.* **111**, 188–194 (2011).

43. Velicer, G. J. & Yu, Y. N. Evolution of novel cooperative swarming in the bacterium Myxococcus xanthus. *Nature* **425**, 75–78 (2003).

44. Hölscher, T. Social interactions and regulatory pathways influencing Bacillus subtilis biofilm formation and motility. (2017).

45. Gibbs, K. A., Urbanowski, M. L. & E. Peter Greenberg. Genetic Determinants of Self Identity and Social Recognition in Bacteria. *Science* **321**, 256–259 (2008).

46. Hamilton, W. D. The genetical evolution of social behaviour. I. *J. Theor. Biol.* **7**, 1–16 (1964).

47. West, S. A., Griffin, A. S. & Gardner, A. Social semantics: Altruism, cooperation, mutualism, strong reciprocity and group selection. *J. Evol. Biol.* **20**, 415–432 (2007).

48. West, S. A., Diggle, S. P., Buckling, A., Gardner, A. & Griffin, A. S. The Social Lives of Microbes. *Annu. Rev. Ecol. Evol. Syst.* **38**, 53–77 (2007).

49. Hamilton, W. D. Selfish and Spiteful Behaviour in an Evolutionary Model. *Nature* **228**, 1218–1220 (1970).

50. Nowak, M. A. Five Rules for the Evolution of Cooperation. *Science* **314**, 1560–1563 (2006).

51. West, S. A. & Buckling, A. Cooperation, virulence and siderophore production in bacterial parasites. *Proc. R. Soc. London Ser B* **270**, 37–44 (2003).

52. Leinweber, A., Fredrik Inglis, R. & Kümmerli, R. Cheating fosters species co-

existence in well-mixed bacterial communities. *ISME J.* **11**, 1179–1188 (2017).

53. O'Brien, S., Luján, A. M., Paterson, S., Cant, M. A. & Buckling, A. Adaptation to public goods cheats in Pseudomonas aeruginosa. *Proc. R. Soc. B Biol. Sci.* **284**, (2017).

54. Cordero, O. X., Ventouras, L.-A., DeLong, E. F. & Polz, M. F. Public good dynamics drive evolution of iron acquisition strategies in natural bacterioplankton populations. *Proc. Natl. Acad. Sci.* **109**, 20059–20064 (2012).

55. Harrison, F. Dynamic social behaviour in a bacterium: Pseudomonas aeruginosa partially compensates for siderophore loss to cheats. *J. Evol. Biol.* **26**, 1370–1378 (2013).

56. Niehus, R., Picot, A., Oliveira, N. M., Mitri, S. & Foster, K. R. The evolution of siderophore production as a competitive trait. *Evolution (N. Y).* **71**, 1443–1455 (2017).

57. Butaite, E., Baumgartner, M., Wyder, S. & Kümmerli, R. Siderophore cheating and cheating resistance shape competition for iron in soil and freshwater Pseudomonas communities. *Nat. Commun.* **8**, (2017).

58. Luján, A. M., Gómez, P. & Buckling, A. Siderophore cooperation of the bacterium *Pseudomonas fluorescens* in soil. *Biol. Lett.* **11**, 20140934 (2015).

59. Kümmerli, R. *et al.* Co-evolutionary dynamics between public good producers and cheats in the bacterium Pseudomonas aeruginosa. *J. Evol. Biol.* **28**, 2264–2274 (2015).

60. Zhang, X.-X. & Rainey, P. B. Exploring the sociobiology of pyoverdin-producing Pseudomonas. *Evolution* **67**, 3161–74 (2013).

61. Drescher, K., Nadell, C. D., Stone, H. a., Wingreen, N. S. & Bassler, B. L. Solutions to the public goods dilemma in bacterial biofilms. *Curr. Biol.* **24**, 50–55 (2014).

62. Folse, H. J. & Allison, S. D. Cooperation, competition, and coalitions in enzyme-producing microbes: Social evolution and nutrient depolymerization rates. *Front. Microbiol.* **3**, 1–10 (2012).

63. Rainey, P. & Rainey, K. Evolution of cooperation and conflict in experimental bacterial populations. *Nature* **425**, 72–74 (2003).

64. van Gestel, J., Weissing, F. J., Kuipers, O. P. & Kovács, A. T. Density of founder cells affects spatial pattern formation and cooperation in Bacillus subtilis biofilms. *ISME J.* **8**, 2069–79 (2014).

65. Nadell, C. D., Drescher, K., Wingreen, N. S. & Bassler, B. L. Extracellular matrix structure governs invasion resistance in bacterial biofilms. *ISME J.* **9**, 1700–1709 (2015).

66. Davies, D. G. & Geesey, G. G. Regulation of the alginate biosynthesis gene algC in Pseudomonas aeruginosa during biofilm development in continuous culture. *Appl. Environ. Microbiol.* **61**, 860–867 (1995).

67. Greig, D. & Travisano, M. The Prisoner's Dilemma and polymorphism in yeast SUC genes. *Proc. R. Soc. B Biol. Sci.* **271**, 25–26 (2004).

68. Gore, J., Youk, H. & van Oudenaarden, A. Snowdrift game dynamics and facultative cheating in yeast. **459**, 253–256 (2009).

69. Ciofu, O., Beveridge, T. J., Kadurugamuwa, J. & Jan Walther-Rasmussen, N. H. Chromosomal β-lactamase is packaged into membrane vesicles and secreted from Pseudomonas aeruginosa. *J. Antimicrob. Chemother.* **45**, 9–13 (2000).

70. Daniels, R. *et al.* Quorum signal molecules as biosurfactants affecting swarming in Rhizobium etli. *Proc. Natl. Acad. Sci.* **103**, 14965–14970 (2006).

71. Lyons, N. A. & Kolter, R. Bacillus subtilis Protects Public Goods by Extending Kin Discrimination to Closely Related Species. *MBio* **8**, (2017).

72. O' Loughlin, E. V & Robins-browne, R. M. Effect of Shiga toxin and Shiga-like toxins on eukaryotic cells. *Microbes Infect.* **3**, 493–507 (2001).

73. Park, J. *et al.* Human Retinal Pigment Epithelial Cells. *Toxins (Basel).* **9**, 1–20 (2017).

74. Raymond, B., West, S. A., Griffin, A. S. & Bonsall, M. B. The Dynamics of Cooperative Bacterial Virulence in the Field. *Science* **337**, 85–88 (2012).

75. Hase, C. C. & Finkelstein, R. A. Bacterial Extracellular Zinc-Containing Metalloproteases. *Microbiol. Rev.* **57**, 823–837 (1993).

76. Schneider, J. S. & Glickman, M. S. Function of site-2 proteases in bacteria and bacterial pathogens. *Biochim. Biophys. Acta - Biomembr.* **1828**, 2808–2814 (2013).

77. Chuang, J. S., Rivoire, O. & Leibler, S. Simpson's Paradox in a Synthetic Microbial System. *Science* **323**, 272–276 (2009).

78. Lee, H. H., Molla, M. N., Cantor, C. R. & Collins, J. J. Bacterial charity work leads to population-wide resistance. *Nature* **467**, 82–85 (2010).

79. Schooling, S. R. & Beveridge, T. J. Membrane Vesicles : an Overlooked Component of the Matrices of Biofilms. *J. Bacteriol.* **188**, 5945–5957 (2006).

80. Tashiro, Y., Uchiyama, H. & Nomura, N. Multifunctional membrane vesicles in Pseudomonas aeruginosa. *Environ. Microbiol.* **14**, 1349–1362 (2012).

81. Hardin, G. The tragedy of the commons. *Science* **162**, 1243–1248 (1968).

82. Ghoul, M., Griffin, A. S. & West, S. A. Toward an evolutionary definition of cheating. *Evolution (N. Y).* **68**, 318–331 (2013).

83. Griffin, A. S., West, S. A. & Buckling, A. Cooperation and competition in pathogenic bacteria. *Nature* **430**, 1024–27 (2004).

84. van Gestel, J., Vlamakis, H. & Kolter, R. From Cell Differentiation to Cell Collectives: Bacillus subtilis Uses Division of Labor to Migrate. *PLoS Biol.* **13**, (2015).

85. Weigert, M. & Kümmerli, R. The physical boundaries of public goods cooperation between surface-attached bacterial cells. *Proc. R. Soc. B Biol. Sci.* **284**, (2017).

86. Darwin, C. *On the origin of species by means of natural selection, or the preservation of favoured races in the struggle for life.* (Murray, John, 1859).

87. Leeks, A. & West, S. Altruism in a virus. *Nat. Microbiol.* **4**, 910–911 (2019).

88. Jousset, A., Eisenhauer, N., Materne, E. & Scheu, S. Evolutionary history predicts the stability of cooperation in microbial communities. *Nat. Commun.* **4**, (2013).

89. Alizon, S. & Lion, S. Within-host parasite cooperation and the evolution of virulence. *Proc. R. Soc. B Biol. Sci.* **278**, 3738–3747 (2011).

90. Koehler, T., Buckling, A. & Delden, C. Van. Cooperation and virulence of clinical Pseudomonas aeruginosa populations. *Proc. Natl. Acad. Sci.* **106**, 6339–6344 (2009).

91. Bachmann, H., Bruggeman, F. J., Molenaar, D., Branco, F. & Teusink, B. Public goods and metabolic strategies. *Curr. Opin. Microbiol.* **31**, 109–115 (2016).

92. Strassmann, J. E., Zhu, Y. & Queller, D. C. Altruism and social cheating in the social amoeba Dictyostelium discoideum. *Nature* **408**, 965–967 (2000).

93. Velicer, G. J., Kroos, L. & Lenski, R. E. Developmental cheating in the social bacterium Myxococcus xanthus. *Nature* **404**, 598–601 (2000).

94. Velicer, G. J. & Vos, M. Sociobiology of the Myxobacteria. *Annu. Rev. Microbiol.* **63**, 599–623 (2009).

95. Coyte, K. Z. & Schluter, J. The ecology of the microbiome: Networks, competition, and stability. *Science* **350**, 663–666 (2015).

96. Xavier, J. B. & Foster, K. R. Cooperation and conflict in microbial biofilms. *Proc. Natl. Adac. Sci. USA* **104**, 876–881 (2007).

97. Foster, K. R. & Bell, T. Competition , Not Cooperation , Dominates Interactions among Culturable Microbial Species. *Curr. Biol.* **22**, 1845–1850 (2012).

98. Foster, K. R., Shaulsky, G., Strassmann, J. E., Queller, D. C. & Thompson, C. R. .-. Pleiotropy as a mechanism to stabilize cooperation. *Nature* **431**, 693–96 (2004).

99. Sachs, J., UG, M., TP, W. & JJ, B. The evolution of cooperation. *Q Rev Biol* **79**, 135–160 (2004).

100. Ghoul, M. & Mitri, S. The Ecology and Evolution of Microbial Competition. *Trends Microbiol.* **24**, 833–845 (2016).

101. Celiker, H. & Gore, J. Competition between species can stabilize public-goods cooperation within a species. *Mol. Syst. Biol.* **8**, 621 (2012).

102. Momeni, B., Waite, A. J. & Shou, W. Spatial self-organization favors heterotypic cooperation over cheating. *Elife.***2,** e00960 (2013).

103. Nadell, C. D., Drescher, K. & Foster, K. R. Spatial structure, cooperation and competition in biofilms. *Nat. Rev. Microbiol.* **14**, 589–600 (2016).

104. Drescher, K., Nadell, C. D., Stone, H. a, Wingreen, N. S. & Bassler, B. L. Solutions to the public goods dilemma in bacterial biofilms. *Curr. Biol.* **24**, 50–55 (2014).

105. Nadell, C. D., Foster, K. R. & Xavier, J. B. Emergence of spatial structure in cell groups and the evolution of cooperation. *PLoS Comput. Biol.* **6**, (2010).

106. Pfeiffer, T., Schuster, S. & Bonhoeffer, S. Cooperation and Competition in the Evolution of ATP-Producing Pathways. *Science* **292**, 504–508 (2001).

107. Tarnita, C. E. The ecology and evolution of social behavior in microbes. *J. Exp. Biol.* **220**, 18–24 (2017).

108. Kovács, Á. T. Impact of spatial distribution on the development of mutualism in microbes. *Front. Microbiol.* **5**, 1–5 (2014).

109. Steven Frank. Perspective: repression of competition and the evolution of cooperation. *Evolution (N. Y).* **57**, 693–705 (2003).

110. Oliveira, N. M., Niehus, R. & Foster, K. R. Evolutionary limits to cooperation in microbial communities. *Proc. Natl. Acad. Sci.* **111**, 17941–17946 (2014).

111. West, S. a, Griffin, A. S. & Gardner, A. Evolutionary Explanations for Cooperation. *Curr. Biol.* **17**, R661-72 (2007).

112. Palmer, J., Kazmerzak, K., Hansen, M. C. & Kolenbrander, P. E. Mutualism versus independence: Strategies of mixed-species oral biofilms in vitro using saliva as the sole nutrient source. *Infect. Immun.* **69**, 5794–5804 (2001).

113. West, S. A., Kiers, T. E., Pen, I. & Denison, R. F. Sanctions and mutualism stability when should less beneficial. *J Evol Biol* **15**, 830–837 (2002).

114. Frank, S. A. Mutual policing and repression of competition in the evolution of cooperative groups. *Nature* **377**, 520–522 (1995).

115. Kiers, T. E., Rousseau, R. A., Stuart A. West & R. Ford Denison. Host sanctions and the legume–rhizobium mutualism. *Nature* **425**, 78 (2003).

116. Stefanic, P., Kraigher, B., Lyons, N. A., Kolter, R. & Mandic-Mulec, I. Kin discrimination between sympatric Bacillus subtilis isolates. *Proc. Natl. Acad. Sci.* **112**, 14042–14047 (2015).

117. Lyons, N. A., Kraigher, B., Stefanic, P., Mandic-Mulec, I. & Roberto Kolter. A Combinatorial Kin Discrimination System in Bacillus subtilis. *Curr. Biol.* **26**, 733–742 (2016).

118. Queller, D. C., Ponte, E., Bozzaro, S. & Strassmann, J. E. Single-Gene Greenbeard Effects in the Social Amoeba Dictyostelium discoideum. *Science* **299**, 49–52 (2003).

119. Biernaskie, J. M., Gardner, A. & West, S. A. Multicoloured greenbeards, bacteriocin diversity and the rock-paper-scissors game. *J. Evol. Biol.* **26**, 2081–2094 (2013).

120. Lang, J. M. & Benbow, M. E. Species Interactions and Competition. *Nat. Educ. Knowl.* **4**, (2013).

121. Holomuzki, J. R., Feminella, J. W. & Power, M. E. Biotic interactions in freshwater benthic habitats. *J. North Am. Benthol. Soc.* **29**, 220–224 (2010).

122. Hatcher, M. J., Dick, J. T. A. & Dunn, A. M. How parasites affect interactions between competitors and predators. *Ecol. Lett.* **9**, 1253–1271 (2006).

123. Basler, M., Ho, B. T. & Mekalanos, J. J. Tit-for-tat: Type VI secretion system counterattack during bacterial cell-cell interactions. *Cell* **152**, 884–894 (2013).

124. Pukatzki, S. *et al.* Identification of a conserved bacterial protein secretion system in Vibrio cholerae using the Dictyostelium host model system. *Proc. Natl. Acad. Sci.*

103, 1528–1533 (2006).

125. Vasse, M., Torres-barcelo, C. & Hochberg, M. E. Phage selection for bacterial cheats leads to population decline. *Proc. R. Soc. B Biol. Sci.* **282**, (2015).

126. Maclean, R. C. & Gudelj, I. Resource competition and social conflict in experimental populations of yeast. **441**, 498–501 (2006).

127. Vulic, M. & Kolter, R. Evolutionary Cheating in Escherichia coli Stationary Phase Cultures. *Genetics* **158**, 519–526 (2001).

128. Hardin, G. The Competitive Exclusion Principle. *Science* **131**, 1292–1297 (1960).

129. Irie, Y. *et al.* The Pseudomonas aeruginosa PSL polysaccharide is a social but noncheatable trait in biofilms. *MBio* **8**, (2017).

130. Srinandan, C. S., Elango, M., Gnanadhas, D. P. & Chakravortty, D. Infiltration of matrix-non-producers weakens the salmonella biofilm and impairs its antimicrobial tolerance and pathogenicity. *Front. Microbiol.* **6**, 1–12 (2015).

131. Kawecki, T. *et al.* Experimental evolution. *Trends Ecol. Evol.* **27**, 547–560 (2012).

132. Barrick, J. E. & Lenski, R. E. Genome dynamics during experimental evolution. *Nat. Rev. Genet.* **14**, 827–839 (2013).

133. Elena, S. F. & Lenski, R. E. Evolution experiments with microorganisms: the dynamics and genetic bases of adaptation. *Nat. Rev. Genet.* **4**, 457–469 (2003).

134. Lenski, R. E., Rose, M. R., Simpson, S. C. & C., T. S. Long Term Experimental Evolution in E. coli I. Adaptation and Divergence During 2000 Generations. *Am. Nat.* **138**, 1315–1341 (1991).

135. Bennett, A.F. and Lenski, R. . Evolutionary adaptation to temperature. II. Thermal niches of experimental lines of Escherichia coli. *Evolution (N. Y).* 1–12 (1993).

136. Lenski, R. E. & Travisano, M. Dynamics of Adaptation and diversification: A 10,000-Generation Experiment with Bacterial Populations. *Proc. Natl. Acad. Sci. U. S. A.* **91**, 6808–6814 (1994).

137. Clarendon, M. J., Rainey, P. B. & Travisano, M. Adaptive radiation in a heterogeneous environment. *Nature* **32**, 69–72 (1998).

138. Reznick, D. A., Bryga, H. & Endlert, J. A. Experimentally induced life-history evolution in a natural population. *Nature* **346**, 357–359 (1990).

139. Ebert, D., Haag, C. & Kirkpatrick, M. A Selective Advantage to Immigrant Genes in a Daphnia Metapopulation. *Science* **295**, 485–489 (2002).

140. Zbinden, M., Haag, C. R. & Ebert, D. Experimental evolution of field populations of Daphnia magna in response to parasite treatment. *J. Evol. Biol.* **21**, 1068–1078 (2008).

141. Boles, B. R., Thoendel, M. & Singh, P. K. Self-generated diversity produces 'insurance effects' in biofilm communities. *Proc. Natl. Acad. Sci.* **101**, 16630–16635 (2004).

142. Kirisits, M. J., Prost, L. & Parsek, M. R. Characterization of Colony Morphology Variants Isolated from. *Am. Soc. Microbiol.* **71**, 4809–4821 (2005).

143. Penterman, J. *et al.* Rapid Evolution of Culture-Impaired Bacteria During Adaptation to Biofilm Growth. **6**, 293–300 (2014).

144. Koh, K. S. *et al.* Phenotypic diversification and adaptation of Serratia marcescens MG1 biofilm-derived morphotypes. *J. Bacteriol.* **189**, 119–130 (2007).

145. Yarwood, J. M., Paquette, K. M., Tikh, U. B., Volper, E. M. & Greenberg, E. P. Generation of virulence factor variants in Staphylococcus aureus biofilms. *J. Bacteriol.* **189**, 7961–7967 (2007).

146. Savage, V. J., Chopra, I. & O'Neill, A. J. Population Diversification in Staphylococcus aureus Biofilms May Promote Dissemination and Persistence. *PLoS One* **8**, (2013).

147. Cooper, V. S. & Lenski, R. E. The population genetics of ecological specialization in evolving Escherichia coli populations. *Nature* **407**, 736–739 (2000).

148. Smith, E. E. *et al.* Genetic adaptation by Pseudomonas aeruginosa to the airways of cystic fibrosis patients. *Proc. Natl. Acad. Sci.* **103**, 8487–8492 (2006).

149. Cramer, N. *et al.* Microevolution of the major common Pseudomonas aeruginosa clones C and PA14 in cystic fibrosis lungs. *Environ. Microbiol.* **13**, 1690–1704 (2011).

150. Lieberman, T. D. *et al.* Parallel bacterial evolution within multiple patients identifies candidate pathogenicity genes HHS Public Access Author manuscript. *Nat Genet* **43**, 1275–1280 (2012).

151. Ackermann, M. A functional perspective on phenotypic heterogeneity in microorganisms. *Nat. Rev. Microbiol.* **13**, 497–508 (2015).

152. Dubnau, D. & Losick, R. Bistability in bacteria. *Mol. Microbiol.* **61**, 564–72 (2006).

153. Grote, J., Krysciak, D. & Streit, W. R. Phenotypic Heterogeneity, a Phenomenon That May Explain Why Quorum Sensing Does Not Always Result in Truly Homogenous Cell Behavior. *Appl. Environ. Microbiol.* **81**, 5280–5289 (2015).

154. Avery, S. V. Microbial cell individuality and the underlying sources of heterogeneity. *Nat. Rev. Microbiol.* **4**, 577–587 (2006).

155. Stewart, P. S. & Franklin, M. J. Physiological heterogeneity in biofilms. *Nat. Rev. Microbiol.* **6**, 199–210 (2008).

156. Davidson, C. J. & Surette, M. G. Individuality in bacteria. *Annu. Rev. Genet.* **42**, 253–268 (2008).

157. Chai, Y., Chu, F., Kolter, R. & Losick, R. Bistability and biofilm Formation in Bacillus subtilis. *Mol Microbiol.* **67**, 254–263 (2008).

158. Chai, Y., Norman, T., Kolter, R. & Losick, R. Reversal of an epigenetic switch governing cell chaining in Bacillus subtilis by protein instability. *Mol. Microbiol.* **78**, 218–229 (2010).

159. Conlon, B. P. Staphylococcus aureus chronic and relapsing infections: Evidence of a role for persister cells: An investigation of persister cells, their formation and their role in S. aureus disease. *BioEssays* **36**, 991–996 (2014).

160. Hamoen, L. W., Venema, G. & Kuipers, O. P. Controlling competence in Bacillus subtilis: Shared use of regulators. *Microbiology* **149**, 9–17 (2003).

161. Lopez, D., Vlamakis, H. & Kolter, R. Generation of multiple cell types in Bacillus subtilis. *FEMS Microbiol. Rev.* **33**, 152–163 (2009).

162. van Gestel, J. & Nowak, M. A. Phenotypic Heterogeneity and the Evolution of Bacterial Life Cycles. *PLoS Comput. Biol.* **12**, 1–23 (2016).

163. Siebring, J. *et al.* Repeated triggering of sporulation in Bacillus subtilis selects against a protein that affects the timing of cell division. *ISME J.* **8**, 77–87 (2014).

164. Perkins, T. J. & Swain, P. S. Strategies for cellular decision-making. *Mol. Syst. Biol.* **5**, 1–15 (2009).

165. Michael B. Elowitz, Levine, A., Siggia, E. & Swan, P. Stochastic Gene Expression in a Single Cell. *Science* **297**, 1183–1187 (2002).

166. Blake, W. J. *et al.* Phenotypic Consequences of Promoter-Mediated Transcriptional Noise. *Mol. Cell* **24**, 853–865 (2006).

167. Gürol M. Süel, Kulkarni, R. P., Dworkin, J., Garcia-Ojalvo, J. & Elowitz, M. B. Tunability and Noise Dependence in Differentiation Dynamics. *Science* **315**, 1716–1719 (2007).

168. Freed, N. E. *et al.* A simple screen to identify promoters conferring high levels of phenotypic noise. *PLoS Genet.* **4**, 2–7 (2008).

169. New, A. M. *et al.* Different Levels of Catabolite Repression Optimize Growth in Stable and Variable Environments. *PLoS Biol.* **12**, 17–20 (2014).

170. Beaumont, H. J. E., Gallie, J., Kost, C., Ferguson, G. C. & Rainey, P. B. Experimental evolution of bet hedging. *Nature* **462**, 90–93 (2009).

171. Ackermann, M. *et al.* Self-destructive cooperation mediated by phenotypic noise. *Nature* **454**, 987–990 (2008).

172. Kunst, F. *et al.* The complete genome sequence of the Gram-positive bacterium Bacillus subtilis. *Nature* **390**, 249–256 (1997).

173. Barbe, V. *et al.* From a consortium sequence to a unified sequence : the Bacillus subtilis 168 reference genome a decade later. *Microbiology* **155**, 1758–1775 (2009).

174. Hamon, A. & Lazazzera, B. A. The sporulation transcription factor Spo0A is required for biofilm development in Bacillus subtilis. **42**, 1199–1209 (2001).

175. Stefanic, P. & Mandic-mulec, I. Social Interactions and Distribution of Bacillus subtilis Pherotypes at Microscale □. *J. Bacteriol.* **191**, 1756–1764 (2009).

176. Durrett, R. *et al.* Genome Sequence of the Bacillus subtilis Biofilm-Forming transformable Strain PS216. *Genome A* **1**, 2012–2013 (2013).

177. Burkholder, P. R. & Giles, N. H. Induced Biochemical Mutations in Bacillus subtilis. *Am. J. Bot.* **34**, 345–348 (1947).

178. Gallegos-Monterrosa, R., Mhatre, E. & Kovacs, Á. T. Specific Bacillus subtilis 168

variants form biofilms on nutrient-rich medium. *Microbiology* **162**, 1922–1932 (2016).

179. Nagórska, K., Ostrowski, A., Hinc, K., Holland, I. B. & Obuchowski, M. Importance of eps genes from Bacillus subtilis in biofilm formation and swarming. *J. Appl. Genet.* **51**, 369–381 (2010).

180. Murray, E. J., Strauch, M. a & Stanley-Wall, N. R. SigmaX is involved in controlling Bacillus subtilis biofilm architecture through the AbrB homologue Abh. *J. Bacteriol.* **191**, 6822–32 (2009).

181. Epstein, A. K., Pokroy, B., Seminara, A. & Aizenberg, J. Bacterial biofilm shows persistent resistance to liquid wetting and gas penetration. *Proc. Natl. Acad. Sci.* **108**, 995–1000 (2010).

182. Mhatre, E. *et al.* Presence of Calcium Lowers the Expansion of Bacillus subtilis Colony Biofilms. *Microorganisms* **5**, 7 (2017).

183. Verhamme, D. T., Murray, E. J. & Stanley-wall, N. R. DegU and Spo0A Jointly Control Transcription of Two Loci Required for Complex Colony Development by Bacillus subtilis. *J. Bacteriol.* **191**, 100–108 (2009).

184. Kobayashi, K. Bacillus subtilis Pellicle Formation Proceeds through Genetically Defined Morphological Changes. *J. Bacteriol.* **189**, 4920–4931 (2007).

185. Hölscher, T. *et al.* Motility, chemotaxis and aerotaxis contribute to competitiveness during bacterial pellicle biofilm development. *J. Mol. Biol.* **427**, 3695–3708 (2015).

186. Bais, H. P., Fall, R. & Vivanco, J. M. Biocontrol of Bacillus subtilis against Infection of Arabidopsis Roots by Pseudomonas syringae Is Facilitated by Biofilm Formation and Surfactin Production. *Am. Soc. Plant Biol.* **134**, 307–309 (2004).

187. Beauregard, P. B., Chai, Y., Vlamakis, H., Losick, R. & Kolter, R. Bacillus subtilis biofilm induction by plant polysaccharides. *Proc. Natl. Acad. Sci.* **110**, E1621–E1630 (2013).

188. Mhatre, E., Monterrosa, R. G. & Kovács, A. T. From environmental signals to regulators: modulation of biofilm development in Gram-positive bacteria. *J. Basic Microbiol.* **54**, 616–32 (2014).

189. Vlamakis, H., Chai, Y., Beauregard, P., Losick, R. & Kolter, R. Sticking together: Building a biofilm the Bacillus subtilis way. *Nat. Rev. Microbiol.* **11**, 157–168 (2013).

190. Kovács, Á. T. Bacterial differentiation via gradual activation of global regulators. *Current Genetics* **62**, 125–128 (2016).

191. Jiang, M., Shao, W., Perego, M. & Hoch, J. A. Multiple histidine kinases regulate entry into stationary phase and sporulation in Bacillus subtilis. *Mol. Microbiol.* **38**, 535–542 (2000).

192. Kearns, D. B., Chu, F., Branda, S. S., Kolter, R. & Losick, R. A master regulator for biofilm formation by Bacillus subtilis. *Mol. Microbiol.* **55**, 739–749 (2005).

193. Branda, S. S., Chu, F., Kearns, D. B., Losick, R. & Kolter, R. A major protein component of the Bacillus subtilis biofilm matrix. *Mol. Microbiol.* **59**, 1229–38 (2006).

194. Chai, Y., Kolter, R. & Losick, R. Paralogous antirepressors acting on the master regulator for biofilm formation in Bacillus subtilis. *Mol. Microbiol.* **74**, 876–887 (2009).

195. Kobayashi, K. SlrR / SlrA controls the initiation of biofilm formation in Bacillus subtilis. *Mol. Microbiol.* **69**, 1399–1410 (2008).

196. Chu, F. *et al.* A novel regulatory protein governing biofilm formation in Bacillus subtilis. *Mol. Microbiol.* **68**, 1117–1127 (2008).

197. Chai, Y., Norman, T., Kolter, R. & Losick, R. An epigenetic switch governing daughter cell separation in Bacillus subtilis. *Genes Dev.* **24**, 754–765 (2010).

198. Huang, X. & Helmann, J. D. Identification of Target Promoters for the Bacillus subtilis s X Factor using a Consensus-directed Search. *J. Mol. Biol.* **279**, 165–173 (1998).

199. Luo, Y., Asai, K., Sadaie, Y. & Helmann, J. D. Transcriptomic and phenotypic characterization of a Bacillus subtilis strain without extracytoplasmic function σ factors. *J. Bacteriol.* **192**, 5736–5745 (2010).

200. Mascher, T., Hachmann, A.-B. & Helmann, J. D. Regulatory Overlap and Functional Redundancy among Bacillus subtilis Extracytoplasmic Function σ Factors. *J. Bacteriol.* **189**, 6919–6927 (2007).

201. Helmann, J. D. The extracytoplasmic function (ECF) sigma factors. *Adv. Microbio Physiol* **46**, 47–110 (2002).

202. Helmann, J. D. Bacillus subtilis extracytoplasmic function (ECF) sigma factors and defense of the cell envelope. *Curr Opin Microbiol.* **30**, 122–132 (2016).

203. Luo, Y. & Helmann, J. D. Analysis of the role of Bacillus subtilis σ M in β-lactam resistance reveals an essential role for c-di-AMP in peptidoglycan homeostasis. *Molecular Microbiology* **83**, 623–639 (2012).

204. Cao, M. & Helmann, J. D. Regulation of the Bacillus subtilis bcrC bacitracin resistance gene by two extracytoplasmic function σ factors. *J. Bacteriol.* **184**, 6123–6129 (2002).

205. Strauch, M. A. *et al.* Abh and AbrB Control of Bacillus subtilis Antimicrobial Gene Expression. *J. Bacteriol.* **189**, 7720–7732 (2007).

206. Strauch, M., Webb, V., Spiegelman, G. & Hoch, J. A. The SpoOA protein of Bacillus subtilis is a repressor of the abrB gene. *Proc. Natl. Acad. Sci. U. S. A.* **87**, 1801–1805 (1990).

207. Banse, A. V, Chastanet, A., Rahn-lee, L., Hobbs, E. C. & Losick, R. Parallel pathways of repression and antirepression governing the transition to stationary phase in Bacillus subtilis. *Proc. Natl. Acad. Sci. U. S. A.* **105**, (2008).

208. Nicola R. Stanley & Lazazzera, B. A. Defining the genetic differences between wild and domestic strains of Bacillus subtilis that affect poly-γ-dl-glutamic acid production and biofilm formation.pdf. *Mol. Microbiol.* **57**, 1143–1158 (2005).

209. Kobayashi, K. Gradual activation of the response regulator DegU controls serial expression of genes for flagellum formation and biofilm formation in Bacillus

subtilis. *Mol. Microbiol.* **66**, 395–409 (2007).

210. Verhamme, D. T., Kiley, T. B. & Stanley-Wall, N. R. DegU co-ordinates multicellular behaviour exhibited by Bacillus subtilis. *Mol. Microbiol.* **65**, 554–568 (2007).

211. Molle, V. *et al.* The Spo0A regulon of Bacillus subtilis. *Mol. Biol. Evol.* **50**, 1683–1701 (2003).

212. Murray, E. J., Kiley, T. B. & Stanley-wall, N. R. A pivotal role for the response regulator DegU in controlling multicellular behaviour. *Microbiology* **155**, 1–8 (2009).

213. Kobayashi, K. & Iwano, M. BslA(YuaB) forms a hydrophobic layer on the surface of Bacillus subtilis biofilms. *Mol. Microbiol.* **85**, 51–66 (2012).

214. Romero, D., Aguilar, C., Losick, R. & Kolter, R. Amyloid fibers provide structural integrity to Bacillus subtilis biofilms. *Proc. Natl. Acad. Sci. U. S. A.* **107**, 2230–2234 (2010).

215. Schwartz, K., Syed, A. K., Stephenson, R. E., Rickard, A. H. & Boles, B. R. Functional amyloids composed of phenol soluble modulins stabilize Staphylococcus aureus biofilms. *PLoS Pathog.* **8**, (2012).

216. Epstein, E. A., Reizian, M. A. & Chapman, M. R. Spatial Clustering of the Curlin Secretion Lipoprotein Requires Curli Fiber Assembly. *J. Bacteriol.* **191**, 608–615 (2009).

217. Diehl, A. *et al.* Structural changes of TasA in biofilm formation of Bacillus subtilis. *Proc. Natl. Acad. Sci.* **115**, 3237–3242 (2018).

218. Erskine, E. *et al.* Formation of functional , non-amyloidogenic fibres by recombinant Bacillus subtilis TasA. **110**, 897–913 (2018).

219. Stöver, A. G. & Driks, A. Secretion, localization, and antibacterial activity of TasA, a Bacillus subtilis spore-associated protein. *J. Bacteriol.* **181**, 1664–1672 (1999).

220. Romero, D., Vlamakis, H., Losick, R. & Kolter, R. An Accessory Protein Required for Anchoring and Assembly of Amyloid Fibers in B. subtilis Biofilms. *Mol Microbiol.* **80**, 1155–1168 (2011).

221. Chai, Y., Beauregard, P. B., Vlamakis, H., Losick, R. & Kolter, R. Galactose Metabolism Plays a Crucial Role in Biofilm Formation by Bacillus subtilis. *MBio* **3**, (2012).

222. Dogsa, I., Brloznik, M., Stopar, D. & Mandic-Mulec, I. Exopolymer Diversity and the Role of Levan in Bacillus subtilis Biofilms. *PLoS One* **8**, 2–11 (2013).

223. Terra, R., Stanley-wall, N. R., Cao, G. & Lazazzera, B. A. Identification of Bacillus subtilis SipW as a Bifunctional Signal Peptidase That Controls Surface-Adhered Biofilm Formation. *J. Bacteriol.* **194**, 2781–2790 (2012).

224. Ren, D. *et al.* Gene Expression in Bacillus subtilis Surface Biofilms With and Without Sporulation and the Importance of yveR for Biofilm Maintenance. *Biotechnol. Bioeng* **86**, 344–364 (2004).

225. Nagorska, K., Hinc, K., Strauch, M. A. & Michał Obuchowski. Influence of the σB Stress Factor and yxaB, the Gene for a Putative Exopolysaccharide Synthase under

σB Control, on Biofilm Formation.pdf. *J. Bacteriol.* **190**, 3546–3556 (2008).

226. Blair, K. M., Turner, L., Winkelman, J. T., Berg, H. C. & Kearns, D. B. A Molecular Clutch Disables Flagella in the Bacillus subtilis Biofilm. *Science* **320**, 1636–1639 (2008).

227. Cairns, L. S., Hobley, L. & Stanley-wall, N. R. Biofilm formation by Bacillus subtilis : new insights into regulatory strategies and assembly mechanisms. *Mol. Microbiol.* **93**, 587–598 (2014).

228. Gerwig, J., Kiley, T. B., Gunka, K. & Stanley-wall, N. The protein tyrosine kinases EpsB and PtkA differentially affect biofilm formation in Bacillus subtilis. *microbiology* **160**, 682–691 (2014).

229. Elsholz, A. K. W., Wacker, S. A. & Losick, R. Self-regulation of exopolysaccharide production in Bacillus subtilis by a tyrosine kinase. *Genes Dev.* **28**, 1710–1720 (2014).

230. Lemon, K. P., Earl, A. M., Vlamakis, H. C., Aguilar, C. & Kolter, R. Biofilm Development with an Emphasis on Bacillus subtilis K. *Curr Top Microbiol Immunol* **322**, 1–16 (2008).

231. Roux, D. *et al.* Identification of Poly-N-acetyl Glucosamine as a Major Polysaccharide Component of the Bacillus Subtilis Biofilm Matrix. *J. Biol. Chem.* **290**, 19261–19272 (2015).

232. Guttenplan, S. B., Blair, K. M. & Kearns, D. B. The EpsE Flagellar Clutch Is Bifunctional and Synergizes with EPS Biosynthesis to Promote Bacillus subtilis Biofilm Formation. *PLoS Genet.* **6**, (2010).

233. Hobley, L. *et al.* BslA is a self-assembling bacterial hydrophobin that coats the Bacillus subtilis biofilm. *Proc. Natl. Acad. Sci. U. S. A.* **110**, 13600–5 (2013).

234. Kovács, Á. T., van Gestel, J. & Kuipers, O. P. The protective layer of biofilm: A repellent function for a new class of amphiphilic proteins. *Mol. Microbiol.* **85**, 8–11 (2012).

235. Hobley, L., Harkins, C., MacPhee, C. E. & Stanley-Wall, N. R. Giving structure to the biofilm matrix: An overview of individual strategies and emerging common themes. *FEMS Microbiol. Rev.* **39**, (2015).

236. Elliot, M. A. & Talbot, N. J. Building filaments in the air : aerial morphogenesis in bacteria and fungi. *Curr. Opin. Microbiol.* **7**, 594–601 (2004).

AIM AND OUTLINE OF THE DISSERTATION

This dissertation presents a cumulative work of research projects pertaining to social interactions in *Bacillus subtilis* biofilms performed for 3.5 years. This dissertation employs experimental evolution studies to understand the evolutionary interplay of social behaviours in relation to the formation of the biofilm matrix in *B. subtilis* pellicle biofilms.

It is comprised of six main chapters (Fig. 9) involving five published manuscripts and one that has been deposited on a preprint server and submitted for publication. As an introduction, I present several background information about Sociomicrobiology, microbial social interactions, experimental evolution and phenotypic heterogeneity. Furthermore, I introduce biofilm formation in *B. subtilis* with particular focus on the biofilm matrix components and its associated regulatory networks.

Chapter 1 provides a review of a set of experimental evolution studies from existing literature. It aims to demonstrate that biofilms are good models to employ in the examination of the origins of social interactions and how they evolve in time and space. In Chapter 2, clonal cells of *B. subtilis* biofilm was subjected to experimental evolution to examine the ability of a Gram-positive bacterium like *B. subtilis* to undergo diversification that was previously observed in Gram-negative bacteria (*Pseudomonas spp* and *Burkholderia cenocepacia*). Moreover, this chapter seeks to quantify the evolved biofilm traits that arise from diversification and to investigate the new mode of social interactions. Chapter 3 presents the long-term social dynamics of the co-cultures of matrix producer and non-matrix producer in pellicle biofilms. This chapter aims to understand how mobile genetic elements can unexpectedly emerge from adaptive events that alter the competition dynamics in biofilm formation. In Chapter 4, the division of labour between EPS -producers and TasA -producers in *B. subtilis* pellicle biofilms were examined. The objective is to investigate which type of division of labour between genetic and phenotypic level could provide optimal biofilm productivity. In Chapter 5, the evolutionary stability of the genetic division of labour between EPS-producing and TasA-producing cells conducted in Chapter 4 was further investigated by subjecting the co-culture into series of subsequent re-inoculation. In parallel, the solitary adaptation of partially deficient matrix producers was also challenged in order to understand the fate of cooperative behaviours and the emergence of new biofilm traits. In Chapter 6, the

evolution of pellicle-former (wild type) in the presence of cheaters (non-EPS producers) was performed in order to understand the influence of cheaters in the phenotypic heterogeneity and population dynamics of pellicles. In the last part of this dissertation, I present a general discussion and conclusion on how this dissertation provides novel findings that offer improved scientific footing on how social interactions within biofilms are shaped in the context of evolution.

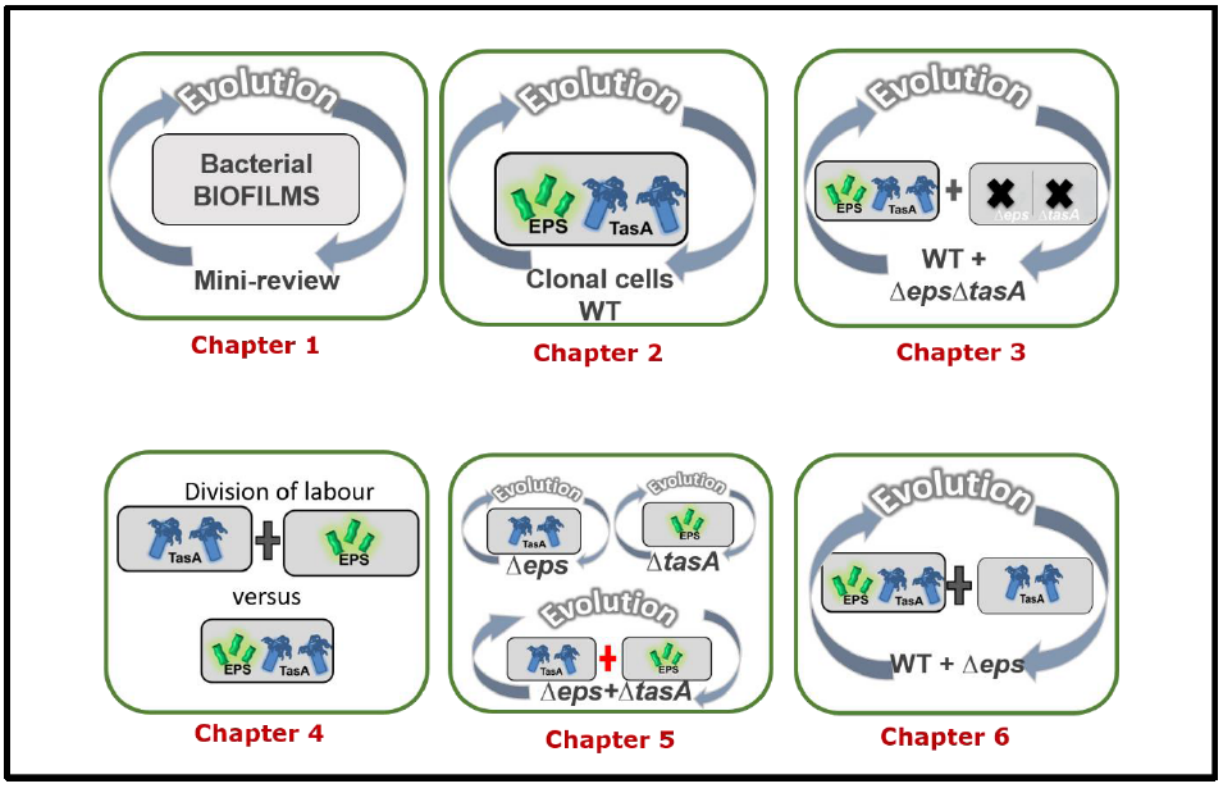

Figure 9. Summary of chapters. Simplified illustration of the six main chapters included in this dissertation.

MAIN CHAPTERS

Chapter 1

Laboratory evolution of microbial interactions in bacterial biofilms

Published in Journal of Bacteriology (2016)

AMERICAN SOCIETY FOR MICROBIOLOGY | Journal of Bacteriology

MEETING REVIEW

Laboratory Evolution of Microbial Interactions in Bacterial Biofilms

Marivic Martin,[a] Theresa Hölscher,[a] Anna Dragoš,[a] Vaughn S. Cooper,[b] Ákos T. Kovács[a]

Terrestrial Biofilms Group, Institute of Microbiology, Friedrich Schiller University Jena, Jena, Germany[a]; Department of Microbiology and Molecular Genetics, University of Pittsburgh, Pittsburgh, Pennsylvania, USA[b]

Microbial adaptation is conspicuous in essentially every environment, but the mechanisms of adaptive evolution are poorly understood. Studying evolution in the laboratory under controlled conditions can be a tractable approach, particularly when new, discernible phenotypes evolve rapidly. This is especially the case in the spatially structured environments of biofilms, which promote the occurrence and stability of new, heritable phenotypes. Further, diversity in biofilms can give rise to nascent social interactions among coexisting mutants and enable the study of the emerging field of sociomicrobiology. Here, we review findings from laboratory evolution experiments with either *Pseudomonas fluorescens* or *Burkholderia cenocepacia* in spatially structured environments that promote biofilm formation. In both systems, ecotypes with overlapping niches evolve and produce competitive or facilitative interactions that lead to novel community attributes, demonstrating the parallelism of adaptive processes captured in the lab.

Since the pioneering discoveries of Robert Koch, most bacteria generally have been studied in planktonic cultures, wherein cells grow dispersed from one another. Recently, the spatially structured environments (definitions of terminology are given in Table 1) of tightly packed bacterial biofilms have been recognized as more appropriate models to study microbial growth and interactions (1), because microbes may live more frequently in biofilms on inanimate or host surfaces (2) and the physiology of biofilm cells differs from that of planktonic cultures (3). The regulation of biofilm formation, persistence, and dispersal has been investigated at the molecular level for many years now, but much more remains to be discovered, particularly related to how biofilm cells interact when attached to one another (4, 5). The increasing interest in biofilm models has revealed the complexity of microbial social interactions (6). Since microbes, to some extent, share the structural components of biofilms (e.g., exopolysaccharides), the process of biofilm construction can be viewed as a form of cooperation, at least within a single lineage of cells (7–9). In addition, biofilm itself provides a structured environment that promotes other types of resource exchange among clonemates or metabolically interdependent strains (10–12). However, biofilm formation may also be triggered as a competitive or defensive response against other strains or species (13). In addition, the structured environment of biofilms creates gradients of nutrients that potentiate the competition for limiting resources, resulting in exploitative competition between cohabiting species (14).

Despite the increasing knowledge of the ecology (13, 15, 16), genetics (17–19), or physical mechanisms (20, 21) of biofilm development and the mechanisms that stabilize cooperation during biofilm formation (7, 9, 10, 22), we still know little about the long-term evolutionary dynamics within biofilm communities. It is unclear how social interactions shape biofilm evolution and how evolution in structured environments shift the balance between competition and mutualism. Long-term serial transfer experiments provide a key approach to fill this gap. Experimental evolution allows studying adaptation under controlled conditions and identification of the evolutionary forces and ecological processes that shape microbial cultures (23, 24). Today, the genomic changes of experimentally evolved bacteria can be easily explored using next-generation sequencing methods (25) that allow understanding of the molecular basis of evolutionary adaptation.

Here, by reviewing a set of experimental evolution studies, we demonstrate that biofilms are both good models to study the origins of social interactions and to examine how these interactions are shaped in time and space. We focus on the form and strength of interactions between microbial species, ecotypes, or early differentiated lineages cohabiting structured environments of biofilms. Based on the existing literature, we describe how such interactions influence the evolution of microbial communities. Importantly, evolutionary changes in microbial communities may be driven by a set of abiotic factors (e.g., fluctuations in the environment) or biotic components other than microbes (e.g., plant, animal, and human host or symbiont), which are not discussed in the paper. The study of evolutionary dynamics within biofilms and the origin of microbial interactions are significant for several reasons (26). First, biotic interactions among neighbors generate major selective forces that drive the development of many important traits of microbes, such as antibiotic resistance (27). Second, understanding how biofilms evolve can aid in predicting of evolutionary outcomes. Third, tracking molecular evolution in biofilms helps to unravel new regulatory pathways related to biofilm formation, persistence, or dispersal. Here, we present how recent advances in experimental evolution of biofilm systems fulfill this potential.

LABORATORY EVOLUTION OF COOPERATION AND INTERFERENCE IN STRUCTURED ENVIRONMENTS

A pioneering long-term evolution experiment with *Escherichia coli* started in 1988 by Richard Lenski provided direct evidence

Accepted manuscript posted online 4 April 2016

Citation Martin M, Hölscher T, Dragoš A, Cooper VS, Kovács ÁT. 2016. Laboratory evolution of microbial interactions in bacterial biofilms. J Bacteriol 198:2564–2571. doi:10.1128/JB.01018-15.

Editor: G. A. O'Toole, Geisel School of Medicine at Dartmouth

Address correspondence to Ákos T. Kovács, akos-tibor.kovacs@uni-jena.de.

M.M., T.H., and A.D. contributed equally to this article.

TABLE 1 Description of terms originating from ecology or evolutionary biology that are used in the text[a]

Term	Definition	Reference(s)
Competition	Negative interaction among organisms resulting from overlapping resource requirements or chemical warfare, which leads to reduced fitness of the interacting individuals	
Antagonism (parasitism, predation)	Interaction between two organisms in which one profits at the expense of the other (in terms of fitness); the behavior is a derived strategy	
Synergistic interaction/facilitation	Interaction that leads to an increased fitness of the interacting individuals relative to monocultures	35, 66, 72
Productivity	Increase in biomass or cell numbers over time that reflects the efficiency with which a given organism converts energy into biomass	
Niche complementation	When species inhabit functionally complementary niches or environments resulting in reduced competition	71, 73
Generalist	An ecotype that can tolerate a broad range of conditions (e.g., food sources, temperature stress, etc.)	69
Specialist	An ecotype that can tolerate a rather narrow range of conditions (e.g., food sources, temperature stress, etc.)	69
Ecotype	Organism that pursues a certain ecological strategy and differs in some fitness-relevant traits from other organisms	68
Morphotype	Different colony morphology	35, 69
Spatial structure/structured conditions	Environment with low degree of mixing	
Biotic interactions	Any ecological interactions that occurs between two living organisms; in contrast, interactions are termed abiotic when they involve nonliving elements, e.g., sunlight, temp, pH, etc.	
Social interactions	Interaction/behaviors in which the performance of two individuals influences each other's fitness positively or negatively; here, the definition of social interactions refers to microbes	74
Sociality	The ability and extent of a group or an individual to engage in social interactions	
Sociomicrobiology	Research field in which social interactions of microorganisms are investigated	
Cooperation	Costly behavior of one individual that increases the fitness of another individual and which has evolved for this purpose	74, 75
Public goods	Secreted compounds which are freely available for each member of the population, i.e., "public." These substances benefit the population or community yet do not have to be costly to produce	74

[a] The definitions explain the context of their usage in the text.

that microbes can be evolved in the lab and their phenotypic and genotypic changes can be tracked over time (28). Lenski's experiment is still in progress, reaching 64,000 generations in January 2016, and many similar studies have been performed by other researchers on different microbial species (not only bacteria but also yeasts, phages, or protists) covering basic scientific questions (29, 30) or even in directly applicative projects (31). While planktonic cultures offer a simple setup to study the evolution of bacteria (23, 28, 31, 32), several studies have shown that the selective pressures in unstructured conditions differ from those in biofilms (33–36). For example, homogeneous, well-mixed environments may select against "social" genotypes that secrete costly metabolites, so-called "public goods," and rather favor fast-reproducing selfish individuals (37). This is not surprising since mixing decreases the likelihood for such metabolites to be retained in the vicinity of the secretor and does not guarantee that the secretions will benefit its closest relatives or offspring cells (38), one of the core preconditions required for the evolution of sociality (39). Recent reports have shown that the situation differs dramatically in biofilms, where the secretors have the primary access to the substances produced, allowing the public good producers to easily outnumber the nonproducers (12, 22, 40, 41). It is therefore expected that structured environments would select for "social" adaptation strategies of microbes.

Experimental evolution studies provide evidence for the prediction that evolution in structured environments can favor adaptations to sociality (34, 35, 42–44). For example, Koch and colleagues demonstrated how the emergence of a strain with an increased level of cell-cell communication can eventually lead to evolution of antibiotic resistance to vancomycin, a last-resort antibiotic (27). Briefly, methicillin-resistant *Staphylococcus aureus* grown in a colony biofilm diversifies sequentially into mutants in which the first clones (named W) are selected due to increased cell-cell signaling, which triggered more surfactin and toxic bacteriocin secretion. Next, bacteriocin-resistant mutants that are also resistant to intermediate levels of vancomycin evolved in response to this new environment (27). Although overall diversification of *S. aureus* was driven by competition, the success of the W variant was due to an increased level of cooperation via the Agr quorum-sensing system that in addition triggered increased levels of bacteriocin secretion (27). This dynamic of evolved resistance depends on the structured environment that promotes both efficient cell-cell communication and intimate interactions between the strains. Bacteriocin producers trigger the appearance of a resistant variant in their vicinity due to local increased exposure to the toxic compound. Another study demonstrated that spontaneous mutants of *Pseudomonas fluorescens* with increased polysaccharide secretions (i.e., mucoid isolates) are able to use these secretions to position themselves on the oxygen-rich surface of the colony and dominate the population (45). The emergence of such mucoid isolates is not observed when the spatial structure of the colony is manually disturbed during development. Therefore,

spatial assortment not only promotes stability of cooperation in biofilms (22, 40) but also supports the evolution of novel public good producers that results in increased biofilm matrix production (34, 45). Spatial structure can also promote diversification into strong and weak secretors as shown in *Pseudomonas aeruginosa* colonies, where repetitive reinoculation of *P. aeruginosa* from the edge or the middle of colony biofilms resulted in clones with reduced or diversified matrix production levels, respectively (34). Structured environments can also support stable coexistence of cooperative and noncooperative strains, thereby promoting diversity within species (46).

In fact, environmental spatial structure is probably the major factor promoting diversity in the microbial world (47). Although spatial structure limits the number of possible interactions with nonrelatives and therefore promotes the evolution of public good production, it also facilitates intimate local interactions between neighboring species. Based on cocultivation studies of various natural isolates, interaction with nonrelatives seems to be dominated by competition (48, 49). Coevolution experiments document how such competition between two closely interacting species can progress into more exploitative interaction (50, 51). For example, an experimental community of *Pseudomonas putida* and *Acinetobacter* sp. was evolved and shown to produce an intimate and specialized association that results in more stable and more productive community than the ancestors. In the ancestral community, *P. putida* was dependent on *Acinetobacter* for benzoate that manifested in an exploitative interaction between the two strains (50). During coevolution, *P. putida* increased its stickiness due to mutations in a gene related to lipopolysaccharide synthesis. This enabled a more intimate relationship between the two species and more efficient exploitation of *Acinetobacter* by *P. putida*. Although coevolution resulted in a more exploitative interaction that was detrimental for one of the partners, the overall productivity of the community was doubled (50).

A similar pattern was recently observed by Kim and colleagues (52) where clonal populations of *P. fluorescens* rapidly diversified into morphotypes M (mucoid) and D (dry and wrinkly). The two morphotypes spread collectively faster than either of them in monoculture, which the authors describe as "division of labor." Microscopy analyses revealed that D dominates the spreading bulk of the colony sitting at the top of M. The authors proposed that the role of M is to reduce the tension of the solid surface, while D aids M by pushing it outward. Although D constitutes only 90% of the spreading colony and its interaction with M is exploitative, the performance of the whole community is improved as in the case of *P. putida* and *Acinetobacter*. Importantly, in contrast to the preassembled community of *P. putida* and *Acinetobacter*, the exploitative (and at the same time group beneficial) relationship between D and M evolved *de novo* from a monoclonal ancestor (52). In another study, new colony structures observed on agar medium were found to be indicative of altered biofilm formation or adaptation to a particular biofilm niche requirement (53). Studies on *P. fluorescens* microcosms revealed that certain morphotypes (e.g., the wrinkly morphotype) can be selected only under static conditions but not in shaking cultures (36). Similarly, the diversification of the Gram-positive *Bacillus subtilis* is also highly dependent on the condition used in experimental evolution (33). Namely, colony types with intermediate biofilm robustness dominated under static conditions, whereas those of marginal biofilm robustness (very high or very low) were much less common than shaking cultures (33). This result again highlights the impact of spatial structure on the outcome of laboratory evolution experiments.

EXPERIMENTALLY EVOLVED BIOFILMS OF *P. FLUORESCENS* AND *BURKHOLDERIA CENOCEPACIA*: MODELS OF BIOFILM DIVERSIFICATION

Below, we describe in greater detail studies of the laboratory evolution of *P. fluorescens* and *B. cenocepacia* in spatially structured biofilm environments, in which a mixture of ecological generalists and specialists evolve and coexist. The first project began in 1998 when Rainey and Travisano reported rapid diversification of *P. fluorescens* into 3 different colony types, preferentially inhabiting different niches of static liquid medium (surface, bottom, and the medium) (36). The story of *B. cenocepacia* began 13 years later, when the field of experimental evolution was already more advanced (e.g., the Lenski's evolution experiment had exceeded 50,000 generations). In 2011, Poltak and Cooper tracked the evolution of a *B. cenocepacia* community in a carefully designed microcosm equipped with floating beads that can be repeatedly colonized and decolonized by the evolving community. These two projects resulted in more than 30 research papers that vastly improved our understanding of ecological and molecular dynamics of adaptation in biofilms, making the two pioneering studies (35, 36) milestones in the field of experimental evolution. In the following sections, we examine each experimental design and findings separately, focusing mainly on the social interactions within the evolving microcosms.

EVOLUTION OF COOPERATION AND EXPLOITATION WITHIN AND BETWEEN ECOTYPES IN *P. FLUORESCENS* STATIC MICROCOSM

When *P. fluorescens* natural isolate SBW25 is incubated in unshaken glass vials ("static microcosms") in nutrient-rich medium, this strain rapidly diversifies into three main phenotypically and genotypically different variants (36). Each of these variants is specialized for a certain niche in the spatially structured microcosm and forms phenotypically distinct colonies when grown on agar plates (Fig. 1A). The ancestral smooth morphotype (S) grows predominantly in the liquid column of the microcosm, whereas the fuzzy spreader (F) forms aggregates at the bottom of the tube. The third colony variant is called the wrinkly spreader (W) and occupies the air-liquid interface where it forms a robust pellicle or biofilm (36, 44).

The diversification of the ancestral strain is greatly influenced by the oxygen gradient that is created by the ancestor itself shortly after inoculation of the microcosm (54). Close to the air-liquid interface, the oxygen level is high but decreases rapidly with increasing depth. This spatially heterogeneous environment therefore selects for specialist mutants that prevail under different levels of oxygen availability (54). Without such spatial heterogeneity, no morphologically different variants evolved, and this heterogeneous environment was also essential for maintenance of diversity (36). The W variant in particular is very successful in the spatially structured microcosm since it rapidly accounts for 30 to 50% of the whole population (36, 54) and achieves higher fitness than the S morphotype (53). This advantage and the rise of the W variant depends on its ability to access the elevated oxygen levels in the upper zone of the microcosm by forming a floating pellicle, while other variants grow slower in low-oxygen conditions (54).

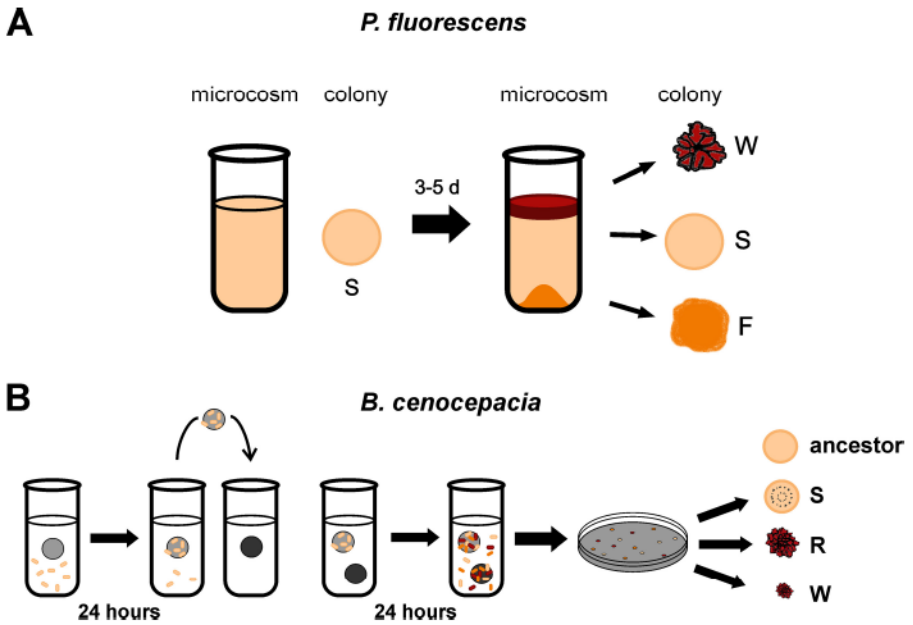

FIG 1 Experimental setup of biofilm evolution in the *P. fluorescens* microcosm (A) and the *B. cenocepacia* bead selection method (B). Biofilm populations in both setups reveal successive adaptive diversification into three ecotypes, namely, smooth or studded (S), fuzzy (F) or ruffled spreader (R), and wrinkly spreader (W). Note that the evolved smooth variant of *B. cenocepacia* is distinct from the ancestor exhibiting enhanced biofilm formation.

To form biofilms at the air-liquid interface, W mutants adapt by producing more cellulose polymers (53) that constitute the biofilm matrix and provide the robustness and structure necessary for a floating mat. It is important to note that in producing this cellulose pellicle, W mutants inherently become more cooperative by producing a public good, but similarly to other biofilm-based cooperative traits (22, 55), it is costly for the individuals to produce (53). Intriguingly, Rainey and Rainey (43) showed that noncooperators that were evolved in the presence of cooperators could invade biofilms formed by cooperating cells. These noncooperators showed an S-like morphology with no aggregation properties and their invasion caused biofilm collapse. Brockhurst et al. (42) also showed that the frequency of cooperators was higher when more resources were provided for the microcosm since relatively less energy was invested toward public good production. However, even under such conditions, competition might occur within the biofilm among different W variants.

Most studies addressing microbial cooperation describe noncooperators as "cheaters" or "free-loaders" and focus solely on their social exploitation. Yet, a study of Hammerschmidt et al. (56) used *P. fluorescens* to show that noncooperating cells carrying the S phenotype can function as colonists of new habitats. They reported that although S cells cause premature collapse of the biofilm mat formed by the W, they can also found a new microcosm where they diversify again and form W biofilms. Therefore, the relationship between W and S resembles the one between a vegetative cell and a spore, where only the latter can survive harsh conditions and give rise to new population, often at the cost of vegetative cells (57). The noncooperating S cells, therefore, could serve as new founders (germ line), allowing the reestablishment of the biofilm collective in another potential environment. This simple life cycle facilitated the maintenance of cooperative collectives. In addition, rapid switching between phenotypes (W and S variants) can be also interpreted as a bet-hedging mechanism that benefits simple organisms, like bacteria in fluctuating environments (58).

Genome sequencing of the *P. fluorescens* W variant revealed mutations in the diguanylate cyclases (DGCs) WspR, AwsR, and MwsR that catalyze the synthesis of cyclic diguanylate monophosphate (c-di-GMP) from GTP (59, 60). Initially, the impact of the *wsp* operon was understood only in the evolution of the W variant (53, 59, 61), while the influences of mutations in *aws* and *mws* genes were revealed only after additional evolutionary experiments (60). Specifically, when the static microcosm of *P. fluorescens* was allowed to adapt in a *wsp*-deficient background (using Δ*wspABCDEFR* as the ancestor), the *aws*-dependent circuit was discovered, resulting in a similar W variant. The third alternative circuit (*mws*), leading to the evolution of W, was discovered after evolvution of *P. fluorescens* that carried both Δ*wspABCDEFR* and Δ*awsXRO* alleles (60). These mutations in all three loci are mainly responsible for the increased c-di-GMP level that manifests in elevated cellulose production by the W variant (60, 62). Specifically, increased c-di-GMP is responsible for the activation of a membrane-bound enzyme complex responsible for cellulose synthesis that is encoded by the *wss* operon (53).

Initially, a screen of the W variant transposon library for loss of the wrinkly colony morphology supported the fact that the genes of this operon (*wssA-wssJ* and *wspR*) are crucial for the W variant (53). The operon encodes the DGC WspR and several proteins exhibiting similarity to known cellulose biosynthesis components and chemotaxis systems (53). Mutations in two genes of this operon, *wspE* and *wspF*, were also shown to be responsible for WS variant appearance. WspE represents a histidine kinase that activates WspR by phosphorylation, suggesting that certain mutations in WspE might lead to WspR overactivation (44, 60). WspF is thought to be involved in modulation of WspR activity, indicating that a mutation in the *wspF* gene might have effects similar to those in WspE (61). Later analysis of *wsp*-independent circuits

revealed the role of the *aws* locus in W variant formation. The authors discovered deletions in *awsX*, a negative regulator of diguanylate cyclase AwsR. They proposed that this new W variant resulted from overproduction of the acetylated cellulose through the *wss* pathway due to lack of AwsR regulation and increased synthesis of c-di-GMP (60). Another *wsp*- and *aws*-independent circuit resulting in the W phenotype was also related to increased activity of another diguanylate cyclase MwsR, which, in contrast to AwsR, was not caused by mutations in an extragenic negative regulator but by mutations in the *mwsR* gene itself (60). These experiments demonstrate that several pathways can lead to increased production of c-di-GMP and therefore elevated expression of the *wss* cellulose operon in certain members of the population that in turn increases overall fitness.

LONG-TERM EXPERIMENTAL EVOLUTION OF A COMPLETE BIOFILM LIFE CYCLE USING *B. CENOCEPACIA*

Evolution during the full life cycle of a biofilm, from attachment and maturation to dispersal, can be experimentally studied using a simple bead selection method (Fig. 1B) (35). Here, bacteria growing in a test tube must attach to a plastic bead to be transferred to a new tube with fresh medium each day. The new tube also contains a new bead; thus, a new biofilm must form on an uninhabited surface on a daily basis. Because tubes are incubated on a roller drum, established biofilms are continually subjected to shear forces that select for attachment, planktonic growth, and reattachment. Importantly, this cycle enables easy archiving of the evolving populations as well as precise reconstitution to study the ecological and evolutionary forces prevailing at that time (35), which renders the model especially suitable for long-term experimental evolution (LTEE). Additionally, LTEE can be paired with contemporary sequencing methods to identify the mutational mechanisms, enabling adaptation in the laboratory (25, 63, 64).

Adaptation under these conditions with minimal galactose growth medium has been studied for the opportunistic respiratory pathogen *B. cenocepacia*, but such an approach can be also applied for microbes in natural settings or during host infections (65). However, modifications of the bead-based experimental evolution setup, such as changes in the number of beads or in nutrient concentration, may allow the detailed study of social interactions (35), the degree of facilitation or competition among cells in the biofilm (66), and the predicted colonization and dispersal-dependent fitness (67).

With this novel approach, the biofilm population of *B. cenocepacia* revealed sequential adaptive diversification into three classes of heritable colony morphologies distinctive from that of the ancestor (35), similar to the diversification of *P. fluorescens* during biofilm establishment. The *B. cenocepacia* morphotypes were classified as studded or smooth (S), ruffled spreader (R), and wrinkly spreader (W) (35). Morphologically, the *B. cenocepacia* variants are similar to the experimentally evolved *P. fluorescens* colony types (36). As in *P. fluorescens*, these different *B. cenocepacia* morphotypes inhabit different niches in the test tube (35) and were therefore characterized as separate ecotypes (35, 68). The W variant, possessing strong adhesion to the bead and tube walls in monoculture, is an early colonist of the plastic bead. As the R frequency increases, the W variant declines in frequency. S cells, on the other hand, escalate steadily throughout the growth phase, suggesting that the early evolved S variant adheres to the later-evolved R and W variants, which are better surface colonizers. As S variants remain the dominant type in the community, their proportion decreases slightly prior to transfer as the frequencies of R and W variants escalate from their low initial occurrence (35).

Intriguingly, the three coevolved ecotypes in such biofilm community reach higher productivity than each one of them in monoculture or their expected productivity in the mix. This increased productivity is attributed to the prevailing facilitative effect of niche complementarity (35, 66), in which the ecotypes inhabit different spatial regions of the biofilm. Further synergy among these morphotypes was revealed in a cross-feeding assay demonstrating that the specialists (R and W variants) profit from metabolic by-products of other communal members but not from their own metabolites. This suggests the evolution of a resilient symbiotic food web wherein the generalist S variant achieves high biomass by superior growth but attaches preferentially to the biofilm produced by R and W cells, which in turn profit from secreted metabolites (35). Nonetheless, only the late S variant increased its productivity in the mix culture relative to that in its monoculture, while total productivities of R and W in the mix were reduced compared to those of their monocultures, although the per capita production of R and W increased (66). This indicates that although the competition in the late community was lessened both by facilitative effects (66) and via cross-feeding between R and W (35), it still affected the system.

The sequencing of evolved *B. cenocepacia* clones and populations revealed that the observed colony morphologies are the result of different mutations (69) that affect the regulation of the "stick-or-swim" decision (66, 67, 69). Surprisingly, biofilm specialists (R and W variants) recurrently evolved from generalist types (S variant) by adaptive mutations in the *wsp* locus homologous to the one first described in *P. fluorescens* (69). Sequencing of both population samples and clones revealed complex dynamics driving the evolution of the three ecotypes. Initially, cells that best attached to the plastic beads achieved high frequencies by way of mutations in genes related to the biofilm lifestyle regulator c-di-GMP. These mutations produced distinct colony morphologies and excluded the ancestor genotype. The independent occurrence of these adaptive changes in parallel populations suggests that changes in c-di-GMP production are sufficient for the adaptive niche partitioning because they generate ecotypes with different tendencies to attach or disperse (69). Subsequent mutations related to central metabolism and polysaccharide biosynthesis influenced the proliferation of the S variant and enhanced its competition against earlier mutants. Surprisingly, new *wsp* mutations evolving from S haplotypes gave rise to new R and W mutants, which invaded these more specialized biofilm niches. Interestingly, competition among ecotypes for limiting iron led to the remodelling of the entire community, as both S and W lineages independently acquired mutations in the promoter sequence of bacterioferritin and excluded all cells lacking either of these mutations (69).

A focused analysis on mutations evolved in replicate population B1 (one out of six independently evolving biofilm populations) determined the molecular basis of ecological differentiation of S, R, and W (69). In addition to the *wsp* mutations discussed above, at least eight independent mutations in the gene *yciR* (also known as *rpfR*) were discovered (69, 70). YciR harbors a PAS sensor domain that binds the quorum-sensing molecule *cis*-2-dodecenoic acid (BDSF) (70) as well as a diguanylate cyclase (GGDEF) and a phosphodiesterase (EAL) domain. YciR has been found in many bacterial species to function as a phosphodiesterase

that is responsible for degradation of c-di-GMP and the attenuation of biofilm development (66). A single mutation in *yciR* carried by the R ecotype resulted in its increased biofilm formation. Moreover, ecotype S carried a deletion of *yciR* along with 94 other neighboring genes (69). The different phenotypes of the *yciR* mutants imply that altering different domains can produce different ecological strategies that coordinate quorum sensing of BDSF with c-di-GMP metabolism and hence the stick-or-swim cell decision.

Meanwhile, analogous to the *P. fluorescens* system, the genetic causes of the wrinkly phenotype in *B. cenocepacia* are single missense mutations in either *wspA* or *wspE*, the products of which are involved in the biofilm signal transduction cascade related to c-di-GMP synthesis (71). Although the cognate diguanylate cyclase or phosphodiesterase in this bacterium is not yet known, subsequent evolution studies using W mutants as ancestors revealed a new two-component regulator (Bcen2424_1436) that could relate to the c-di-GMP response and explain this phenotype more generally. Further, growth of W mutants in planktonic culture generated strong selection to regain planktonic fitness, often favoring loss-of-function mutations in Wsp (67). Such mutations could limit subsequent evolution of the wrinkly biofilm in fluctuating environments (67).

CONCLUDING REMARKS

These laboratory experimental systems used spatially structured environments to demonstrate how microbial communities can evolve from clonal ancestors and generate complex ecological interactions. In both experimental setups (*P. fluorescens* static microcosms and *B. cenocepacia* biofilms on suspended beads), the spatially heterogeneous environment facilitated the evolution of distinct ecotypes. These systems allow for the study of adaptive diversification in real time and provide direct insights into evolutionary processes that used to be limited to theoretical models, like the positive feedback between niche construction and natural selection. Intriguingly, the diversified communities can be shaped by the range of social and ecological interactions, including antagonism (i.e., social exploitation of the W by S variants observed in *P. fluorescens*), niche complementation, or even synergistic interactions via cross-feeding as observed in *B. cenocepacia*. Finally, the interactions that arose between the ecotypes of the evolved community became a new factor determining biofilm productivity that could not be observed with an isogenic ancestor community. Importantly, parallel evolution experiments performed under unstructured conditions (planktonic cultures) in both species did not show diversification patterns similar to those of the structured environments in the biofilms (Fig. 2) (35, 36). In addition to the basic understanding of evolutionary processes, these studies provide insight into how microbes adapt at the molecular level. In both systems, wrinkly phenotypes emerged from mutations related to *wsp* genes, two-component transcriptional regulators, and polysaccharide production-associated genes. Understanding how opportunistic pathogens (e.g., *Burkholderia*) or beneficial root colonizers (e.g., *P. fluorescens*) undergo adaptive diversification in biofilms could illuminate the ecological forces that drive adaptation during chronic infections or plant biocontrol.

In the future, an experimental evolution approach using constructed microbial interactions might also provide a better understanding of the forces that govern assembly of natural mixed-species biofilms as well as how best to engineer stabile, synthetic microbial ecosystems. More broadly, laboratory evolution of biofilm populations can be an important asset in our understanding of ecoevolutionary dynamics within more complex communities of multicellular organisms that are less amenable to manipulation.

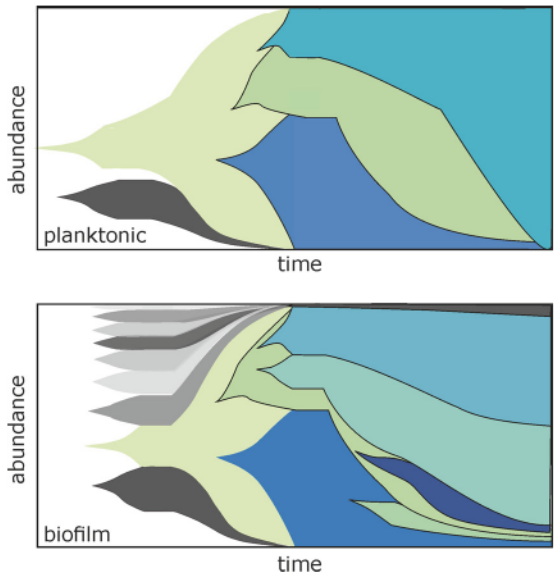

FIG 2 The population genetic dynamics of experimentally evolved bacterial populations differs between planktonic and biofilm cultures. Planktonic adaptation is frequently explained by few beneficial mutations that evolve sequentially on a haplotype that fixes and purges diversity. In contrast, biofilm adaptation involves the rise of multiple contending mutations in a spatially structured environment that preserves genetic diversity. This structure can also facilitate the evolution of ecological interactions that maintain diversity.

ACKNOWLEDGMENT

We thank Christian Kost for his valuable comments on the ecoevolutionary terms.

FUNDING INFORMATION

This work, including the efforts of Ákos T. Kovács, was funded by Marie Curie Career Integration Grant (PheHetBacBiofilm). This work, including the efforts of Vaughn S. Cooper, was funded by National Aeronautics and Space Administration (NASA) Astrobiology Institute (CAN-7 NNA15BB04A). This work, including the efforts of Theresa Hölscher, was funded by International Max Planck Research School. This work, including the efforts of Vaughn S. Cooper, was funded by HHS | National Institutes of Health (NIH) (R01GM110444). This work, including the efforts of Ákos T. Kovács, was funded by Deutsche Forschungsgemeinschaft (DFG) (KO4741/3-1). This work, including the efforts of Anna Dragoš, was funded by Alexander von Humboldt-Stiftung (Humboldt Foundation) (POL 1158809 STP-2).

This work, including the efforts of Ákos T. Kovács and Marivic Martin, was funded by Deutsche Forschungsgemeinschaft (DFG) (KO4741/2-1) within the priority program SPP1617. The funders had no role in study design, data collection and interpretation, or the decision to submit the work for publication.

REFERENCES

1. **Stewart PS, Franklin MJ.** 2008. Physiological heterogeneity in biofilms. Nat Rev Microbiol **6**:199–210. http://dx.doi.org/10.1038/nrmicro1838.
2. **Kolter R, Greenberg EP.** 2006. Microbial sciences: the superficial life of microbes. Nature **441**:300–302. http://dx.doi.org/10.1038/441300a.
3. **Mikkelsen H, Duck Z, Lilley KS, Welch M.** 2007. Interrelationships between colonies, biofilms, and planktonic cells of *Pseudomonas aeruginosa*. J Bacteriol **189**:2411–2416. http://dx.doi.org/10.1128/JB.01687-06.

4. **Davies D.** 2003. Understanding biofilm resistance to antibacterial agents. Nat Rev Drug Discov **2**:114–122. http://dx.doi.org/10.1038/nrd1008.
5. **McDougald D, Rice SA, Barraud N, Steinberg PD, Kjelleberg S.** 2012. Should we stay or should we go: mechanisms and ecological consequences for biofilm dispersal. Nat Rev Microbiol **10**:39–50. http://dx.doi.org/10.1038/nrmicro2695.
6. **Parsek MR, Greenberg EP.** 2005. Sociomicrobiology: the connections between quorum sensing and biofilms. Trends Microbiol **13**:27–33. http://dx.doi.org/10.1016/j.tim.2004.11.007.
7. **Boyle KE, Heilmann S, van Ditmarsch D, Xavier JB.** 2013. Exploiting social evolution in biofilms. Curr Opin Microbiol **16**:207–212. http://dx.doi.org/10.1016/j.mib.2013.01.003.
8. **Nadell CD, Xavier JB, Foster KR.** 2009. The sociobiology of biofilms. FEMS Microbiol Rev **33**:206–224. http://dx.doi.org/10.1111/j.1574-6976.2008.00150.x.
9. **Xavier JB, Foster KR.** 2007. Cooperation and conflict in microbial biofilms. Proc Natl Acad Sci U S A **104**:876–881. http://dx.doi.org/10.1073/pnas.0607651104.
10. **Kovács ÁT.** 2014. Impact of spatial distribution on the development of mutualism in microbes. Front Microbiol **5**:649. http://dx.doi.org/10.3389/fmicb.2014.00649.
11. **Mitri S, Xavier JB, Foster KR.** 2011. Social evolution in multispecies biofilms. Proc Natl Acad Sci U S A **108**(Suppl 2):10839–10846. http://dx.doi.org/10.1073/pnas.1100292108.
12. **Pande S, Kaftan F, Lang S, Svatos A, Germerodt S, Kost C.** 2016. Privatization of cooperative benefits stabilizes mutualistic cross-feeding interactions in spatially structured environments. ISME J **10**:1413−1423. http://dx.doi.org/10.1038/ismej.2015.212.
13. **Oliveira NM, Martinez-Garcia E, Xavier J, Durham WM, Kolter R, Kim W, Foster KR.** 2015. Biofilm formation as a response to ecological competition. PLoS Biol **13**:e1002191. http://dx.doi.org/10.1371/journal.pbio.1002191.
14. **Yamamoto K, Haruta S, Kato S, Ishii M, Igarashi Y.** 2010. Determinative factors of competitive advantage between aerobic bacteria for niches at the air-liquid interface. Microbes Environ **25**:317–320. http://dx.doi.org/10.1264/jsme2.ME10147.
15. **Davey ME, O'Toole GA.** 2000. Microbial biofilms: from ecology to molecular genetics. Microbiol Mol Biol Rev **64**:847–867. http://dx.doi.org/10.1128/MMBR.64.4.847-867.2000.
16. **Donlan RM.** 2002. Biofilms: microbial life on surfaces. Emerg Infect Dis **8**:881–890. http://dx.doi.org/10.3201/eid0809.020063.
17. **Fazli M, Almblad H, Rybtke ML, Givskov M, Eberl L, Tolker-Nielsen T.** 2014. Regulation of biofilm formation in *Pseudomonas* and *Burkholderia* species. Environ Microbiol **16**:1961–1981. http://dx.doi.org/10.1111/1462-2920.12448.
18. **Teschler JK, Zamorano-Sanchez D, Utada AS, Warner CJ, Wong GC, Linington RG, Yildiz FH.** 2015. Living in the matrix: assembly and control of *Vibrio cholerae* biofilms. Nat Rev Microbiol **13**:255–268. http://dx.doi.org/10.1038/nrmicro3433.
19. **Vlamakis H, Chai Y, Beauregard P, Losick R, Kolter R.** 2013. Sticking together: building a biofilm the *Bacillus subtilis* way. Nat Rev Microbiol **11**:157–168. http://dx.doi.org/10.1038/nrmicro2960.
20. **Asally M, Kittisopikul M, Rue P, Du Y, Hu Z, Cagatay T, Robinson AB, Lu H, Garcia-Ojalvo J, Suel GM.** 2012. Localized cell death focuses mechanical forces during 3D patterning in a biofilm. Proc Natl Acad Sci U S A **109**:18891–18896. http://dx.doi.org/10.1073/pnas.1212429109.
21. **Stewart PS.** 2014. Biophysics of biofilm infection. Pathog Dis **70**:212–218. http://dx.doi.org/10.1111/2049-632X.12118.
22. **van Gestel J, Weissing FJ, Kuipers OP, Kovács ÁT.** 2014. Density of founder cells affects spatial pattern formation and cooperation in *Bacillus subtilis* biofilms. ISME J **8**:2069–2079. http://dx.doi.org/10.1038/ismej.2014.52.
23. **Barrick JE, Lenski RE.** 2013. Genome dynamics during experimental evolution. Nat Rev Genet **14**:827–839. http://dx.doi.org/10.1038/nrg3564.
24. **Elena SF, Lenski RE.** 2003. Evolution experiments with microorganisms: the dynamics and genetic bases of adaptation. Nat Rev Genet **4**:457–469. http://dx.doi.org/10.1038/nrg1088.
25. **Brockhurst MA, Colegrave N, Rozen DE.** 2011. Next-generation sequencing as a tool to study microbial evolution. Mol Ecol **20**:972–980. http://dx.doi.org/10.1111/j.1365-294X.2010.04835.x.
26. **Steenackers HP, Parijs I, Foster KR, Vanderleyden J.** 2016. Experimental evolution in biofilm populations. FEMS Microbiol Rev **40**:373−397. http://dx.doi.org/10.1093/femsre/fuw002.
27. **Koch G, Yepes A, Forstner KU, Wermser C, Stengel ST, Modamio J, Ohlsen K, Foster KR, Lopez D.** 2014. Evolution of resistance to a last-resort antibiotic in *Staphylococcus aureus* via bacterial competition. Cell **158**:1060–1071. http://dx.doi.org/10.1016/j.cell.2014.06.046.
28. **Lenski RE, Rose MR, Simpson SC, Tadler SC.** 1991. Long-term experimental evolution in *Escherichia coli*. I. Adaptation and divergence during 2,000 generations. Am Nat **138**:1315–1341.
29. **Meyer JR, Dobias DT, Weitz JS, Barrick JE, Quick RT, Lenski RE.** 2012. Repeatability and contingency in the evolution of a key innovation in phage lambda. Science **335**:428–432. http://dx.doi.org/10.1126/science.1214449.
30. **terHorst CP.** 2011. Experimental evolution of protozoan traits in response to interspecific competition. J Evol Biol **24**:36–46. http://dx.doi.org/10.1111/j.1420-9101.2010.02140.x.
31. **Blaby IK, Lyons BJ, Wroclawska-Hughes E, Phillips GC, Pyle TP, Chamberlin SG, Benner SA, Lyons TJ, Crecy-Lagard V, Crecy E.** 2012. Experimental evolution of a facultative thermophile from a mesophilic ancestor. Appl Environ Microbiol **78**:144–155. http://dx.doi.org/10.1128/AEM.05773-11.
32. **Barrick JE, Yu DS, Yoon SH, Jeong H, Oh TK, Schneider D, Lenski RE, Kim JF.** 2009. Genome evolution and adaptation in a long-term experiment with *Escherichia coli*. Nature **461**:1243–1247. http://dx.doi.org/10.1038/nature08480.
33. **Leiman SA, Arboleda LC, Spina JS, McLoon AL.** 2014. SinR is a mutational target for fine-tuning biofilm formation in laboratory-evolved strains of *Bacillus subtilis*. BMC Microbiol **14**:301. http://dx.doi.org/10.1186/s12866-014-0301-8.
34. **Madsen JS, Lin YC, Squyres GR, Price-Whelan A, de Santiago Torio A, Song A, Cornell WC, Sorensen SJ, Xavier JB, Dietrich LE.** 2015. Facultative control of matrix production optimizes competitive fitness in *Pseudomonas aeruginosa* PA14 biofilm models. Appl Environ Microbiol **81**:8414–8426. http://dx.doi.org/10.1128/AEM.02628-15.
35. **Poltak SR, Cooper VS.** 2011. Ecological succession in long-term experimentally evolved biofilms produces synergistic communities. ISME J **5**:369–378. http://dx.doi.org/10.1038/ismej.2010.136.
36. **Rainey PB, Travisano M.** 1998. Adaptive radiation in a heterogeneous environment. Nature **394**:69–72. http://dx.doi.org/10.1038/27900.
37. **Ghoul M, Griffin AS, West SA.** 2014. Toward an evolutionary definition of cheating. Evolution **68**:318–331. http://dx.doi.org/10.1111/evo.12266.
38. **Wakano JY, Nowak MA, Hauert C.** 2009. Spatial dynamics of ecological public goods. Proc Natl Acad Sci U S A **106**:7910–7914. http://dx.doi.org/10.1073/pnas.0812644106.
39. **Hamilton WD.** 1964. The genetical evolution of social behaviour. II. J Theor Biol **7**:17–52. http://dx.doi.org/10.1016/0022-5193(64)90039-6.
40. **Drescher K, Nadell CD, Stone HA, Wingreen NS, Bassler BL.** 2014. Solutions to the public goods dilemma in bacterial biofilms. Curr Biol **24**:50–55. http://dx.doi.org/10.1016/j.cub.2013.10.030.
41. **Van Dyken JD, Müller MJ, Mack KM, Desai MM.** 2013. Spatial population expansion promotes the evolution of cooperation in an experimental Prisoner's Dilemma. Curr Biol **23**:919–923. http://dx.doi.org/10.1016/j.cub.2013.04.026.
42. **Brockhurst MA, Buckling A, Racey D, Gardner A.** 2008. Resource supply and the evolution of public-goods cooperation in bacteria. BMC Biol **6**:20. http://dx.doi.org/10.1186/1741-7007-6-20.
43. **Rainey PB, Rainey K.** 2003. Evolution of cooperation and conflict in experimental bacterial populations. Nature **425**:72–74. http://dx.doi.org/10.1038/nature01906.
44. **Spiers AJ.** 2014. A mechanistic explanation linking adaptive mutation, niche change, and fitness advantage for the wrinkly spreader. Int J Evol Biol **2014**:675432. http://dx.doi.org/10.1155/2014/675432.
45. **Kim W, Racimo F, Schluter J, Levy SB, Foster KR.** 2014. Importance of positioning for microbial evolution. Proc Natl Acad Sci U S A **111**:E1639−E1647. http://dx.doi.org/10.1073/pnas.1323632111.
46. **Hol FJ, Galajda P, Nagy K, Woolthuis RG, Dekker C, Keymer JE.** 2013. Spatial structure facilitates cooperation in a social dilemma: empirical evidence from a bacterial community. PLoS One **8**:e77042. http://dx.doi.org/10.1371/journal.pone.0077042.
47. **Kassen R.** 2002. The experimental evolution of specialists, generalists, and the maintenance of diversity. J Evol Biol **15**:173–190. http://dx.doi.org/10.1046/j.1420-9101.2002.00377.x.
48. **Abrudan MI, Smakman F, Grimbergen AJ, Westhoff S, Miller EL, van**

Wezel GP, Rozen DE. 2015. Socially mediated induction and suppression of antibiosis during bacterial coexistence. Proc Natl Acad Sci U S A **112:** 11054–11059. http://dx.doi.org/10.1073/pnas.1504076112.

49. **Foster KR, Bell T.** 2012. Competition, not cooperation, dominates interactions among culturable microbial species. Curr Biol **22:**1845–1850. http://dx.doi.org/10.1016/j.cub.2012.08.005.
50. **Hansen SK, Rainey PB, Haagensen JA, Molin S.** 2007. Evolution of species interactions in a biofilm community. Nature **445:**533–536. http://dx.doi.org/10.1038/nature05514.
51. **Kim HJ, Boedicker JQ, Choi JW, Ismagilov RF.** 2008. Defined spatial structure stabilizes a synthetic multispecies bacterial community. Proc Natl Acad Sci U S A **105:**18188–18193. http://dx.doi.org/10.1073/pnas.0807935105.
52. **Kim W, Levy SB, Foster KR.** 2016. Rapid radiation in bacteria leads to a division of labour. Nat Commun **7:**10508. http://dx.doi.org/10.1038/ncomms10508.
53. **Spiers AJ, Kahn SG, Bohannon J, Travisano M, Rainey PB.** 2002. Adaptive divergence in experimental populations of *Pseudomonas fluorescens*. I. Genetic and phenotypic bases of wrinkly spreader fitness. Genetics **161:**33–46.
54. **Koza A, Moshynets O, Otten W, Spiers AJ.** 2011. Environmental modification and niche construction: developing O_2 gradients drive the evolution of the Wrinkly Spreader. ISME J **5:**665–673. http://dx.doi.org/10.1038/ismej.2010.156.
55. **Nadell CD, Bassler BL.** 2011. A fitness trade-off between local competition and dispersal in *Vibrio cholerae* biofilms. Proc Natl Acad Sci U S A **108:**14181–14185. http://dx.doi.org/10.1073/pnas.1111147108.
56. **Hammerschmidt K, Rose CJ, Kerr B, Rainey PB.** 2014. Life cycles, fitness decoupling and the evolution of multicellularity. Nature **515:**75–79. http://dx.doi.org/10.1038/nature13884.
57. **Strassmann JE, Zhu Y, Queller DC.** 2000. Altruism and social cheating in the social amoeba *Dictyostelium discoideum*. Nature **408:**965–967. http://dx.doi.org/10.1038/35050087.
58. **Beaumont HJ, Gallie J, Kost C, Ferguson GC, Rainey PB.** 2009. Experimental evolution of bet hedging. Nature **462:**90–93. http://dx.doi.org/10.1038/nature08504.
59. **Goymer P, Kahn SG, Malone JG, Gehrig SM, Spiers AJ, Rainey PB.** 2006. Adaptive divergence in experimental populations of *Pseudomonas fluorescens*. II. Role of the GGDEF regulator WspR in evolution and development of the wrinkly spreader phenotype. Genetics **173:**515–526.
60. **McDonald MJ, Gehrig SM, Meintjes PL, Zhang XX, Rainey PB.** 2009. Adaptive divergence in experimental populations of *Pseudomonas fluorescens*. IV. Genetic constraints guide evolutionary trajectories in a parallel adaptive radiation. Genetics **183:**1041–1053.
61. **Bantinaki E, Kassen R, Knight CG, Robinson Z, Spiers AJ, Rainey PB.** 2007. Adaptive divergence in experimental populations of *Pseudomonas fluorescens*. III. Mutational origins of wrinkly spreader diversity. Genetics **176:**441–453.
62. **Malone JG, Williams R, Christen M, Jenal U, Spiers AJ, Rainey PB.** 2007. The structure-function relationship of WspR, a *Pseudomonas fluorescens* response regulator with a GGDEF output domain. Microbiology **153:**980–994. http://dx.doi.org/10.1099/mic.0.2006/002824-0.
63. **Adams J, Rosenzweig F.** 2014. Experimental microbial evolution: history and conceptual underpinnings. Genomics **104:**393–398. http://dx.doi.org/10.1016/j.ygeno.2014.10.004.
64. **Lang GI, Desai MM.** 2014. The spectrum of adaptive mutations in experimental evolution. Genomics **104:**412–416. http://dx.doi.org/10.1016/j.ygeno.2014.09.011.
65. **Andersen SB, Marvig RL, Molin S, Krogh Johansen H, Griffin AS.** 2015. Long-term social dynamics drive loss of function in pathogenic bacteria. Proc Natl Acad Sci U S A **112:**10756–10761. http://dx.doi.org/10.1073/pnas.1508324112.
66. **Ellis CN, Traverse CC, Mayo-Smith L, Buskirk SW, Cooper VS.** 2015. Character displacement and the evolution of niche complementarity in a model biofilm community. Evolution **69:**283–293. http://dx.doi.org/10.1111/evo.12581.
67. **O'Rourke D, FitzGerald CE, Traverse CC, Cooper VS.** 2015. There and back again: consequences of biofilm specialization under selection for dispersal. Front Genet **6:**18. http://dx.doi.org/10.3389/fgene.2015.00018.
68. **Cohan FM.** 2001. Bacterial species and speciation. Syst Biol **50:**513–524. http://dx.doi.org/10.1080/10635150118398.
69. **Traverse CC, Mayo-Smith LM, Poltak SR, Cooper VS.** 2013. Tangled bank of experimentally evolved *Burkholderia* biofilms reflects selection during chronic infections. Proc Natl Acad Sci U S A **110:**E250–259. http://dx.doi.org/10.1073/pnas.1207025110.
70. **Deng Y, Schmid N, Wang C, Wang J, Pessi G, Wu D, Lee J, Aguilar C, Ahrens CH, Chang C, Song H, Eberl L, Zhang LH.** 2012. Cis-2-dodecenoic acid receptor RpfR links quorum-sensing signal perception with regulation of virulence through cyclic dimeric guanosine monophosphate turnover. Proc Natl Acad Sci U S A **109:**15479–15484. http://dx.doi.org/10.1073/pnas.1205037109.
71. **Cooper VS, Staples RK, Traverse CC, Ellis CN.** 2014. Parallel evolution of small colony variants in *Burkholderia cenocepacia* biofilms. Genomics **104:**447–452. http://dx.doi.org/10.1016/j.ygeno.2014.09.007.
72. **Day T, Young KA.** 2004. Competitive and facilitative evolutionary diversification. Bioscience **54:**101–109. http://dx.doi.org/10.1641/0006-3568(2004)054[0101:CAFED]2.0.CO;2.
73. **Cordero OX, Polz MF.** 2014. Explaining microbial genomic diversity in light of evolutionary ecology. Nat Rev Microbiol **12:**263–273. http://dx.doi.org/10.1038/nrmicro3218.
74. **West SA, Griffin AS, Gardner A, Diggle SP.** 2006. Social evolution theory for microorganisms. Nat Rev Microbiol **4:**597–607. http://dx.doi.org/10.1038/nrmicro1461.
75. **Crespi BJ.** 2001. The evolution of social behavior in microorganisms. Trends Ecol Evol **16:**178–183. http://dx.doi.org/10.1016/S0169-5347(01)02115-2.

Chapter 2

Evolution of exploitative interactions during diversification in *Bacillus subtilis* biofilms

Published in FEMS Microbiology Ecology (2018)

FEMS Microbiology Ecology, 94, 2018, fix155

doi: 10.1093/femsec/fix155
Advance Access Publication Date: 8 November 2017
Research Article

RESEARCH ARTICLE

Evolution of exploitative interactions during diversification in *Bacillus subtilis* biofilms

Anna Dragoš[1,2], Nivedha Lakshmanan[2], Marivic Martin[1,2], Balázs Horváth[3], Gergely Maróti[4], Carolina Falcón García[5], Oliver Lieleg[5] and Ákos T. Kovács[1,2,*]

[1]Bacterial Interactions and Evolution Group, Department of Biotechnology and Biomedicine, Technical University of Denmark, Anker Engelunds Vej Building 301, Kgs Lyngby 2800, Denmark, [2]Terrestrial Biofilms Group, Institute of Microbiology, Friedrich Schiller University Jena, Neugasse 23, Jena 07743, Germany, [3]Seqomics Biotechnology Ltd, Vállalkozók útja 7, Mórahalom 6782, Hungary, [4]Institute of Plant Biology, Biological Research Centre, Hungarian Academy of Sciences, Temesvári krt. 62, Szeged 6726, Hungary and [5]Department of Mechanical Engineering and Munich School of Bioengineering, Technical University of Munich, Boltzmannstr. 11, Garching 85748, Germany

*Corresponding author: Bacterial Interactions and Evolution Group, Department of Biotechnology and Biomedicine, Technical University of Denmark, Anker Engelunds Vej Bgn 301, 2800 Kgs Lyngby, Denmark. Tel: +45 45 252527; Fax: +45 45 932809; E-mail: atkovacs@dtu.dk
One sentence summary: Evolution of *Bacillus subtilis* pellicle biofilms results in diversification into distinct colony variants that profoundly differ in biofilm-related features and in the social roles they play in mixed pellicles.
Editor: Rolf Kümmerli

ABSTRACT

Microbial biofilms are tightly packed, heterogeneous structures that serve as arenas for social interactions. Studies on Gram negative models reveal that during evolution in structured environments like biofilms, isogenic populations commonly diversify into phenotypically and genetically distinct variants. These variants can settle in alternative biofilm niches and develop new types of interactions that greatly influence population productivity. Here, we explore the evolutionary diversification of pellicle biofilms of the Gram positive, spore-forming bacterium *Bacillus subtilis*. We discovered that—similarly to other species—*B. subtilis* diversifies into distinct colony variants. These variants dramatically differ in biofilm formation abilities and expression of biofilm-related genes. In addition, using a quantitative approach, we reveal striking differences in surface complexity and hydrophobicity of the evolved colony types. Interestingly, one of the morphotypes completely lost the ability of independent biofilm formation and evolved to hitchhike with other morphotypes with improved biofilm forming abilities. Genome comparison suggests that major phenotypic transformations between the morphotypes can be triggered by subtle genetic differences. Our work demonstrates how positive complementarity effects and exploitative interactions intertwine during evolutionary diversification in biofilms.

Keywords: experimental evolution; morphotype; pellicle; social interactions; biofilm matrix; *Bacillus subtilis*

Received: 9 August 2017; **Accepted:** 7 November 2017

INTRODUCTION

Rapid evolution of microbes constitutes a tremendous challenge to modern medicine and, at the same time, a privilege for microbial ecology. Due to large population sizes coupled with short generation times, bacterial adaptation can be observed in a course of days or months, allowing for its experimental investigation (Kawecki *et al.* 2012; Rosenzweig and Sherlock 2014; Martin *et al.* 2016). Experimental evolution studies continuously deepen our understanding of microbial adaptation, revealing common evolutionary scenarios such as genome reduction (Nilsson *et al.* 2005) or genome rearrangements (Martin *et al.* 2017), hypermutability (Flynn *et al.* 2016; Tenaillon *et al.* 2016) or diversification (Rainey and Travisano 1998; Poltak and Cooper 2011; Traverse *et al.* 2013; Koch *et al.* 2014; Flynn *et al.* 2016; Kim, Levy and Foster 2016). The last one, where microbes diversify into distinct variants (typically referred to as morphotypes as they are identified based on distinct colony morphology) appears to be very common, especially in structured environments that offer alternative niches varying in nutrient and oxygen content (Martin *et al.* 2016; Steenackers *et al.* 2016). Biofilms, where microbes grow in tightly packed assemblies, represent an example of such an environment.

Evolutionary diversification tends to improve biofilm productivity as newly emerged variants specialize in occupying different niches thereby reducing competition (Rainey and Travisano 1998; Poltak and Cooper 2011; Ellis *et al.* 2015; Flynn *et al.* 2016). An excellent example derives from a comprehensive study of an opportunistic pathogen, *Burkholderia cenocepacia,* which was allowed to evolve in a form of submerged biofilm subsequently assembling on a polystyrene bead floating in the liquid medium (Poltak and Cooper 2011). *Burkholderia cenocepacia* diversified into three distinct morphotypes, the two of which preferentially attached to the polystyrene surface, whereas the third mostly resided on the top of the biofilm (Ellis *et al.* 2015). The productivity of this ecotype mix was elevated due to the so-called niche complementarity effect (Poltak and Cooper 2011; Ellis *et al.* 2015). Similar niche specialization was earlier observed in *Pseudomonas fluorescens* evolved in a static microcosm, where the population diversified into a 'Wrinkly' type colonizing the liquid–air interface, and 'Smooth' and 'Fuzzy' types residing at the bottom of the vessel or floating in the medium, respectively (Rainey and Travisano 1998).

Although evolutionary diversification is often associated with increased community productivity, interactions between the evolved variants can be complex and not necessarily positive. For example, *Pseudomonas aeruginosa* biofilms diversify into multiple variants differing in levels of key biofilm-stimulating messenger cyclic diguanosine monophosphate (c-di-GMP) (Flynn *et al.* 2016). These differences result in sequential surface colonization by the morphotypes, some of which remain in strong competition. In addition, subtle changes in c-di-GMP levels in one morphotype can dramatically shift the population structure, reducing the frequency of the c-di-GMP overproducer for the benefit of other variants (i.e. for the poor biofilm former) that, in turn, may decrease population productivity (Flynn *et al.* 2016). Analogous interplay takes place in *P. fluorescens* where the production of cellulose by a surface colonizer, the 'Wrinkly', creates an opportunity for exploitative invasion by the 'Smooth' that alone cannot colonize the surface (Hammerschmidt *et al.* 2014). Invasion and, as a consequence, premature pellicle collapse happens because the 'Wrinkly' variant secretes a costly extracellular product, an acetylated cellulose (Spiers *et al.* 2003), that becomes vulnerable to exploitation by the non-producer. The two morphotypes coexist since each has an advantage when present at low frequency (Rainey and Travisano 1998).

Altogether, experimental studies on adaptation in biofilms seem to share certain scenarios: variants with distinct colony morphology readily emerge; the derived morphotypes differ in biofilm formation capabilities (Rainey and Travisano 1998; Poltak and Cooper 2011; Traverse *et al.* 2013; Leiman *et al.* 2014; Flynn *et al.* 2016); these differences result in a new type of spatial arrangement that reduces niche overlap and improves population productivity (Rainey and Travisano 1998; Poltak and Cooper 2011; Ellis *et al.* 2015; Flynn *et al.* 2016; Kim, Levy and Foster 2016). While the evolution in biofilms of medically relevant Gram-negative microbes (*B. cenocepacia* and *Pseudomonas spp*) has been extensively studied, adaptive diversification in biofilms of Gram-positive bacteria has not received much attention. *Bacillus subtilis* is a wide spread, plant growth promoting spore-former, known from its ability to form complex pellicle biofilms at the liquid–air interface (Branda *et al.* 2001). Previous studies have already indicated that this bacterium readily diversifies into distinct colony types when cultivated under static or planktonic conditions (Leiman *et al.* 2014). Here, we explore the dynamics and ecological interactions during adaptive diversification in *B. subtilis* pellicle biofilms evolved in six parallel ecosystems.

When cultivated under static conditions, *B. subtilis* initially grows suspended, but increasing cell density results in decreasing oxygen concentration in bottom layers of the medium. Using aerotaxis, cells actively swim towards the liquid–air interface and colonize it in a form of densely packed pellicle (Hölscher *et al.* 2015). Pellicle formation requires secretion of extracellular matrix (ECM) comprising mainly exopolysaccharide EPS, fiber protein TasA and a hydrophobin called BslA. Lack of EPS or TasA prevents pellicle formation, but these matrix components can be shared by producers with the non-producers (Romero *et al.* 2011; van Gestel, Vlamakis and Kolter 2015; Martin *et al.* 2017). In contrast to rather slimy pellicles of *P. fluorescence* or *P. aeruginosa*, biofilms of *B. subtilis* yield a rigid and highly hydrophobic mat (Vlamakis *et al.* 2013; Arnaouteli, MacPhee and Stanley-Wall 2016). The non-wetting properties of those biofilms and pellicles are due to the ECM, with a major role of BslA (Kobayashi and Iwano 2012). The hydrophobicity of *B. subtilis* biofilms can be associated with the level of surface complexity (Werb *et al.* 2017). Comparable properties are observed for both colony and pellicle biofilms, and the ability to form wrinkly pellicles correlates with the ability to develop complex colonies (Romero *et al.* 2011; Shemesh and Chai 2013).

In this study, we ask whether, likewise Gram-negative species, *B. subtilis* can undergo reproducible evolutionary diversification, whether this diversification will involve easily quantifiable biofilm-related traits and finally, whether it will result in new types of social interactions.

MATERIALS AND METHODS

Strains and cultivation conditions

Table S1, Supporting Information describes the strains used in this study and construction of their mutant derivatives. Strains were maintained in Lysogeny broth (LB) medium (LB-Lennox, Carl Roth; 10 g/L tryptone, 5 g/L yeast extract and 5 g/L NaCl), while MSgg medium was used for biofilm induction (Branda *et al.* 2001).

Experimental evolution and productivity assays

Experimental evolution was performed using the natural competent derivative of the undomesticated *B. subtilis* NCBI 3610, DK1042 strain (Konkol, Blair and Kearns 2013) grown in MSgg medium statically in a 24-well plate at 30°C for 48 h in six parallel replicates. Mature pellicles were gently harvested from the surface of the liquid medium using a plastic inoculating loop. First, the edge of the pellicle was gently pierced to partially detach the biofilm from the wall of the plastic well. Second, the pellicle was collected by rapidly moving the loop clockwise, constantly keeping the loop at the liquid–air interface and touching the wall/edge of the pellicle. This allowed harvesting of the entire biofilm, leaving the conditioned medium clear (optical density at 600 nm∼0). The material was then transferred to 2 mL Eppendorf tube containing 1 mL of 0.9% NaCl and 100 μL of glass sand and vortexed vigorously for 60 s. This allowed efficient disruption of the material into single cells and small clumps, without the need for sonication that would highly increase the risk of contamination. Finally, the disrupted culture was reinoculated after 100 × dilution. After the 5th, 10th, 14th, 19th, 24th, 29th and 35th pellicle transfers, colony forming units (CFU)/mL in the pellicles described here as pellicle productivity were monitored and frozen (−80°C) stocks were preserved.

Single isolates representing the four different morphotypes were isolated from population 1. Productivity assays in mixed cultures containing different morphotypes were performed by mixing certain ratios of 100-fold diluted LB-pregrown cultures that were then incubated under pellicle forming conditions for 48 h. Prior each CFU assay, pellicles were sonicated according to a protocol optimized in our laboratory (Martin *et al.* 2017). Expected productivity was calculated by multiplying the frequency of a given morphotype in the initial inoculum by its productivity in monoculture (Poltak and Cooper 2011).

Colony morphology assay

Colony morphologies were examined on LB and MSgg medium with 1.5% agar. The plates were dried under laminar airflow conditions for 20 min after solidifying. 2 μL of the overnight grown cultures were spotted on the plate, and the lids were closed once the spotted culture had dried. The plates were incubated at 30°C for 48 h.

Profilometric analysis

The surface profiles of colonies were obtained using a NanoFocus μsurf light profilometer (NanoFocus AG, Oberhausen, Germany). Randomly selected spots within colony center and colony periphery were scanned using 20× magnification resulting in images covering an 800 × 722 μm area. Missing data points were interpolated, and the scanned area was then evaluated with the software μsoft (Version 6.0, NanoFocus AG, Oberhausen, Germany) to obtain the developed interfacial area ratio (*Sdr* value). This metrological parameter determines the level of surface complexity (Werb *et al.* 2017), whereas $Sdr = 0$ in the case of perfectly flat surfaces, the *Sdr* values are high for surfaces containing multiple grooves and valleys.

Wetting

To test the wetting behavior of colonies, a 10 μL water droplet was placed onto the colony center (and the colony periphery if the colony was large enough), and an image of the droplet was captured using a horizontal camera setup. Contact angles were extracted from these images using the 'drop snake' plug-in in the software ImageJ.

Spent media complementation assay

The supernatants (SN) were obtained from the ancestor strain and the Smooth strain grown under static conditions at 30°C. The SNs were sterilized using Milipore filters (0.2μm pore size) and mixed in 1:1 ratio with 2× MSgg resulting in MSgg + ancestor SN and MSgg + Smooth SN, respectively. Next the pellicle formation of the Smooth in the presence of MSgg + ancestor SN was compared with the negative control, MSgg + Smooth SN.

Microscopy/confocal laser scanning microscopy

Bright field images of whole pellicles and colonies were obtained with an Axio Zoom V16 stereomicroscope (Carl Zeiss, Germany) equipped with a Zeiss CL 9000 LED light source and an AxioCam MRm monochrome camera (Carl Zeiss, Germany). For single-cell level epifluorescence measurements, pellicles were harvested into 1.5 mL Eppendorf tubes containing 500 μL sterile MSgg base medium, vortexed for 90 s, mildly sonicated at 10% amplitude for 12 s with 1 s pause (Soniprep 150). 5 μL of sonicated cells was spotted on microscope slide covered with 0.8% agarose, covered with clean cover slip and examined under the fluorescence microscope (Olympus Bx51; 100× FASE Oil Objective; 98 ms exposure time). Images were captured using the bright light and fluorescence light using the GFP filter. This procedure was done on two separate days with two biological replicates per day.

The pellicles were also analyzed using a confocal laser scanning microscope (LSM 780 equipped with an argon laser, Carl Zeiss, Germany) and Plan-Apochromat/1.4 Oil DIC M27 63× objective. Fluorescent reporter excitation was performed at 488 nm for green fluorescence and at 564 nm for red fluorescence, while the emitted fluorescence was recorded at 484–536 nm and 567–654 nm for GFP and mKate, respectively. To generate pellicle images, Z-stack series with 1 μm steps were acquired. Zen 2012 Software (Carl Zeiss, Germany) was used for both stereomicroscopy and confocal laser scanning microscopy (CLSM) image visualization.

Genome resequencing and genome analysis

Genomic DNA of selected isolated strains was extracted using the EURx Bacterial and Yeast Genomic DNA Kit from cultures grown for 16 h. Paired-end fragment reads (2 × 150 nucleotides) were generated using an Illumina NextSeq sequencer. Primary data analysis (base-calling) was carried out with 'bcl2fastq' software (v2.17.1.14, Illumina). All further analysis steps were done in CLC Genomics Workbench Tool 9.5.1. Reads were quality-trimmed using an error probability of 0.05 (Q13) as the threshold. In addition, the first ten bases of each read were removed. Reads that displayed ≥80% similarity to the reference over ≥80% of their read lengths were used in mapping. Non-specific reads were randomly placed to one of their possible genomic locations. Quality-based SNP and small In/Del variant calling was carried out requiring ≥8× read coverage with ≥25% variant frequency. Only variants supported by good quality bases (Q ≥ 20) were taken into account and only when they were supported by evidence from both DNA strands. Data on mutation frequencies for each strain sequenced in the study are provided in Table S2, Supporting Information.

RESULTS

Evolution of pellicle biofilms of *B. subtilis* involves rapid diversification into four distinct morphotypes

To examine whether evolutionary diversification can be observed in *B. subtilis* NCBI 3610 pellicle biofilms, we allowed six parallel pellicle populations to evolve for over ca. 200 generations (see methods). Pellicles were visually accessed after each subsequent transfer, and their productivities (total cell number/mL) were assessed every 5th transfer. All pellicles appeared robust throughout the experiment preserving a thick and wrinkly structure similar to the ancestral strain. The productivity assay suggested that, with certain exceptions (e.g. #35), CFU/mL of all biofilm populations increased gradually thorough the evolution experiment (Fig. 1A). The significant increase in productivity was confirmed by regression analysis when considering all replicates regardless of the timeframe analyzed (0–24# or 0–35#) (Table S3, Supporting Information). When looking at individual ecosystems, the statistical significance could only be confirmed for replicate 4 (0–24#; $P < 0.02$), while replicate 6 served as an outlier with dramatic productivity drop at 35#, resulting in its lower final as compared to initial productivity (0–35#; $P < 0.99$). On the same line, correlation analysis revealed strong synchrony in productivity changes across all populations, except for the population 6, which exhibited the lowest values of Pearson's correlation coefficient when compared to all remaining populations (Table S4, Supporting Information).

In all six populations, four distinct colony types (morphotypes) could easily be detected in CFU assay. A representative example from each morphotype was isolated from population 1 and stored as pure culture stock for further studies. To better assess differences between the morphotypes, a colony spotting assay was performed (see methods) on two alternative media types: rich LB medium (Fig. 1B) and minimal biofilm-promoting MSgg medium (Branda *et al.* 2001) (Fig. S1A, Supporting Information). Inspired by the striking difference in the appearance of the morphotypes on LB medium, we introduced the following names: Wrinkly—displaying an increased complexity in the colony center; Rough—similar to the ancestor; Spreader—showing dramatically increased colony expansion and Smooth—exhibiting a very flat surface similar to certain biofilm mutants (Romero *et al.* 2010) (Fig. 1B).

To determine the final frequencies of these morphotypes in six parallel evolved populations, small fractions of the corresponding −80°C stocks were serially diluted and plated on LB-agar. The frequency of the Wrinkly morphotype was similar in all populations ranging from 8% in population 6 up to 17% in population 5 (Fig. 1C) (Table S5, Supporting Information). The Rough derivative was the most abundant morphotype in all populations with the highest relative abundance in populations 2 and 4 (76% and 77%, respectively) and least dominant in population 6 (47%). The Spreader showed a maximum of 10% in population 6, while it was barely detected in population 2 (0.2%). Finally, the Smooth variant showed the highest frequency in populations 6 and 1 accounting for 35% and 31% of the pellicles, respectively (Fig. 1C). Statistical analysis revealed that in these two populations the frequency of Smooth was significantly higher than in populations 2–5 (Table S5, Supporting Information). High frequency of Smooth in populations 1 and 6 was coupled with a lower frequency of Rough morphotype in these populations (Fig. 1C, Table S5, Supporting Information).

We were next interested in the evolutionary history of diversification in pellicles. To assess the subsequent emergence of the detected four morphotypes during the experimental evolution, frozen pellicle stocks of population 1 from seven chronological time -points (i.e. from every 5th transfer) were re-examined. All colonies obtained from the 5th transfer resembled the Rough morphotype; however, it is important to note that the ancestor and the Rough variant are very similar (Fig. 1D). The Wrinkly variant was first observed in the 10th transfer and its frequency remained relatively constant until the 35th transfer. The Spreader and Smooth variants both emerged around the 19th pellicle. Whereas the frequency of the Spreader variant remained very stable throughout the evolution, the frequency of the Smooth morphotype was oscillating: it dropped to nearly zero in the 24th pellicle but it recovered to over 30% at later evolutionary time points (Fig. 1D). Interestingly, the frequency of the Smooth variant inversely matched with the productivity pattern throughout the evolutionary history of population 1 (Fig. 1A): transfers where the productivity dropped displayed an increase in the frequency of the Smooth morphotype (Fig. 1D) (linear regression analysis gave negative slope with $r^2 = 0.32$; $P < 0.06$). Similarly, population 6 had the lowest final productivity, but the highest frequency of the Smooth morphotype (Fig. 1C) (negative slope with $r^2 = 0.26$; $P < 0.03$).

Evolved morphotypes develop colonies with distinct surface complexity and hydrophobicity

Next, we attempted to quantitatively describe differences between the observed morphotypes and examine the microscopic surface profiles of the pellicle colonies. Surface profilometry was performed for all morphotypes and the ancestor, both on LB and MSgg medium (Fig. 2; Fig. S1, Supporting Information). Although the results were affected by the media type, certain pronounced differences between the morphotypes were media independent. The Smooth variant showed a lack of surface complexity on both media types that was reflected by a *Sdr* value of practically 0 (see methods). On MSgg medium, the Ancestor and Rough morphotypes showed the highest surface complexity that was about 4-fold higher as compared to the colonies of the Wrinkly and Spreader variants (Fig. 2A and B). On LB medium, all morphotypes depicted lower surface complexity as compared to the ancestor, with higher *Sdr* values for the Wrinkly and Rough derivatives (Fig. S1B, Supporting Information).

Analyses of surface profiles of expanding colony edges showed that, when cultivated on MSgg medium, only the Spreader variant exhibited lower surface complexity at the edge than the ancestor; in contrast, on LB, all strains showed lower *Sdr* values on the edge as compared to the ancestor (Fig. S2, Supporting Information).

As previous studies suggested that the complexity of the biofilm surface might directly correlate with its hydrophobicity (Werb *et al.* 2017), we additionally performed wetting studies using the four morphotypes (see methods). In line with those previous results, the Smooth variant was lacking typical biofilm hydrophobicity and acted completely hydrophilic on both LB and MSgg media (Fig. 2A and C; Fig. S1, Supporting Information). When grown on Msgg medium, the Rough morphotype showed a non-wetting behavior similar to the ancestor, but not on LB; here, the Wrinkly and Rough variants both showed hydrophilic properties (Fig. 2A and C; Fig. S1, Supporting Information). Interestingly, while the Spreader morphotype was generally hydrophilic, its expanding edge showed highly hydrophobic properties outperforming those of the ancestor strain (Fig. S1C, Supporting Information).

Overall, these studies revealed that evolutionary diversification led to clear and measurable differences in the colony

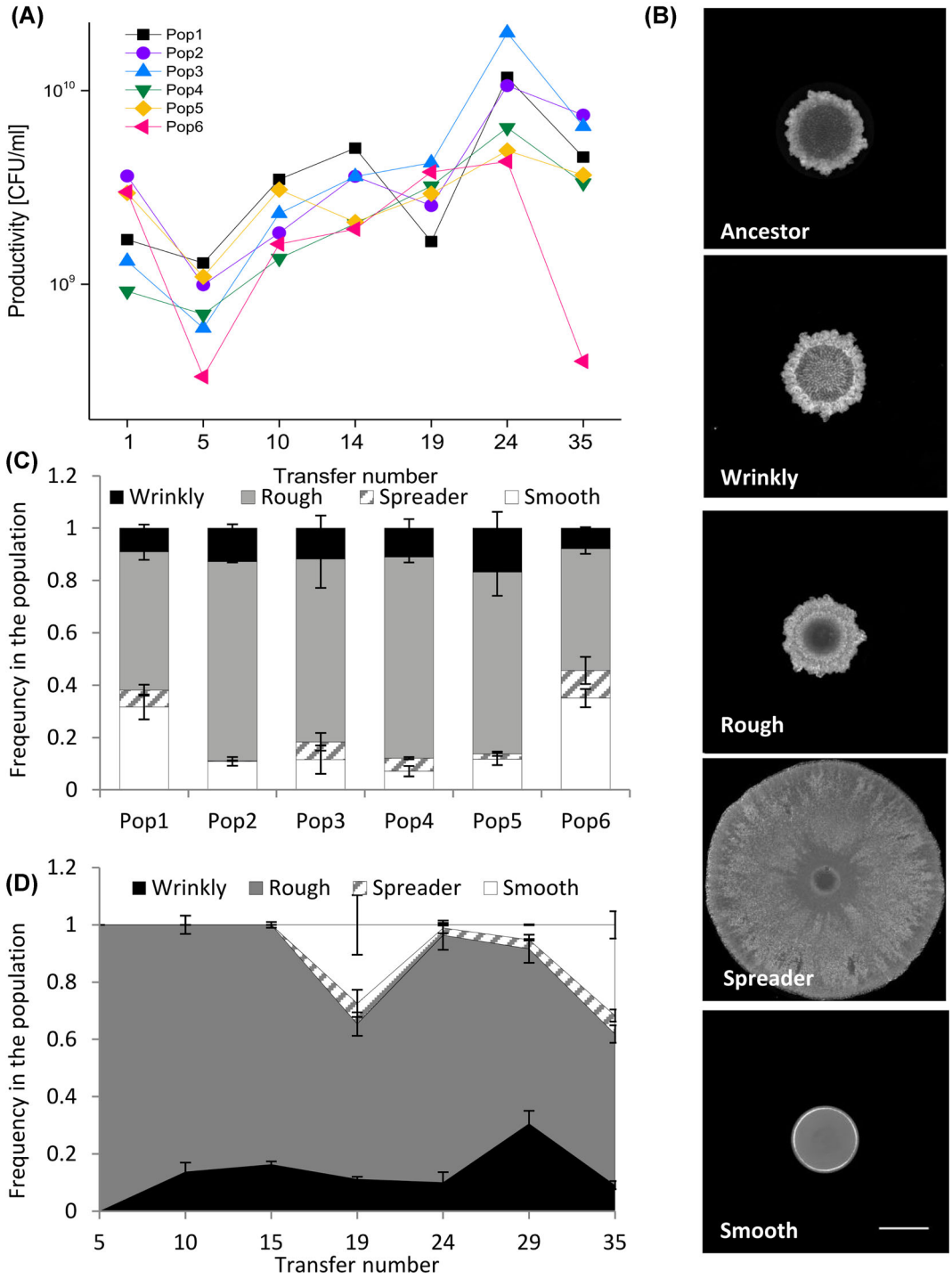

Figure 1. Productivity changes and diversification in *B. subtilis* pellicles. **(A)** Biofilm productivities were systematically monitored (as CFU/ml) during ongoing evolution experiment. Productivities were assessed every 5th or 4th transfer, with an exception of the two final time points, where sampling gap was larger (11 transfers). **(B)** Distinct colony morphologies of the evolved variants were especially pronounced on solid LB medium. The ancestor *B. subtilis* NCBI 3610 and four morphotypes isolated from population 1 and were spotted on LB agar (1.5%) and imaged after 48 h of incubation at 30°C. The names (Wrinkly, Rough, Spreader and Smooth) were assigned arbitrarily, based on colony appearance. Scale bar represents 5 mm. **(C)** Final (35th transfer) relative frequencies of different morphotypes (Wrinkly, Rough, Spreader and Smooth) in all six parallel evolved populations (for each population n = 3). Data represent the mean and error bars represent standard error. **(D)** Relative frequencies of different morphotypes in subsequent evolutionary time points in population 1 (n = 3). For panel C and D, data represent the mean and error bars represent standard error.

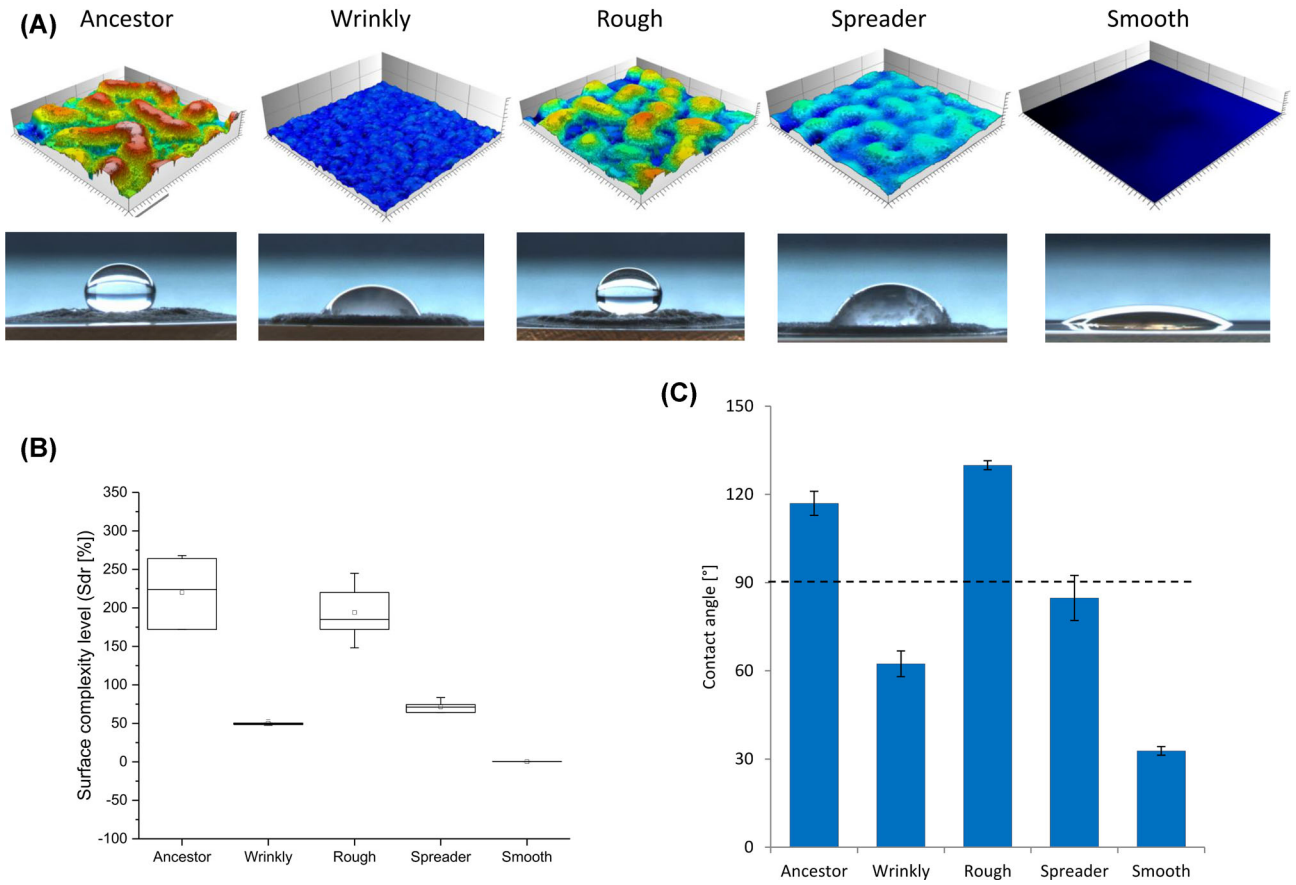

Figure 2. Quantitative characterization of colony features displayed by the evolved morphotypes on biofilm-promoting MSgg medium. **(A)** Surface topologies of colony center of the ancestor and evolved morphotypes were acquired using light profilometry. 3D images of the surface topology were generated using the software μsurf (see methods) showing topological features with a standard color scale-where dark blue represents the lowest and white represents the highest features. Colonies were grown for 48 h at 30°C. Scale bar represents 200 μm. Below: image of 10 μL water droplet spotted at the corresponding colony center. **(B)** Developed interfacial area *Sdr* calculated for colony center based on surface topology (some samples n = 6, while others n = 5). Boxes represent Q1–Q3, lines represent the median, and bars span from max to min. **(C)** Contact angles calculated for water spotted in colony center (n = 3). Dashed line represents contractual hydrophobicity cutoff, separating the hydrophilic (below the line) from hydrophobic (above) surfaces. Data points represent mean and error bars represent standard error.

surface properties with correspondingly different wetting properties.

Morphotypes display distinct levels of matrix gene expression

Since previous experiments revealed dramatic differences in colony surface complexity and wetting behavior, we further hypothesized that these differences could be linked to different levels of ECM production by the morphotypes (Kobayashi and Iwano 2012; Kesel *et al.* 2016). In order to test this, the matrix-genes reporters P_{tapA}-*gfp* and P_{eps}-*gfp* were introduced into the four morphotypes and the ancestor strain, and changes in matrix genes expression were determined (Fig. 3A; Figs S3 and S4, Supporting Information). Fluorescence images of colonies developed by P_{tapA}-*gfp* and P_{eps}-*gfp* labeled strains suggested the lowest expression of both matrix genes in the Smooth variant, moderate expression (comparable to the ancestor) in the Spreader variant and increased expression in the case of the Rough and Wrinkly variants (Figs S3 and S4, Supporting Information). To confirm this observation, the P_{tapA}-*gfp* fluorescence was quantified during planktonic growth in all morphotypes and the ancestor (Fig. 3A). As expected, the Wrinkly and Rough morphotypes showed dramatic increase in *tapA* expression as compared to the ancestor. The detected fluorescence level from the P_{tapA}-*gfp* construct in the Spreader variant was also increased. Finally, the Smooth variant showed decreased P_{tapA}-*gfp* fluorescence as compared to the ancestor indicating lower levels of matrix genes expression (Fig. 3A). We also compared the expression of *tapA* in the ancestor and evolved morphotypes at single-cell level (Fig. S5, Supporting Information). While Wrinkly, Rough and Spreader preserved phenotypic heterogeneity pattern of matrix genes expression similar to the ancestor, *tapA* expressing cells could barely be detected in the Smooth population (Fig. S5, Supporting Information).

As expected based on colony morphology and low levels of matrix genes expression, the Smooth morphotype was not able to form a pellicle biofilm when cultivated solitarily (Fig. 3B). Pellicles formed by the Wrinkly variant resembled the ancestral pellicle, but those formed by the Rough and Spreader variants showed a less wrinkled and shinier surface as compared to the ancestor (Fig. 3B). Pellicles formed by the mix of all four morphotypes showed a typical wrinkly structure with a matte surface

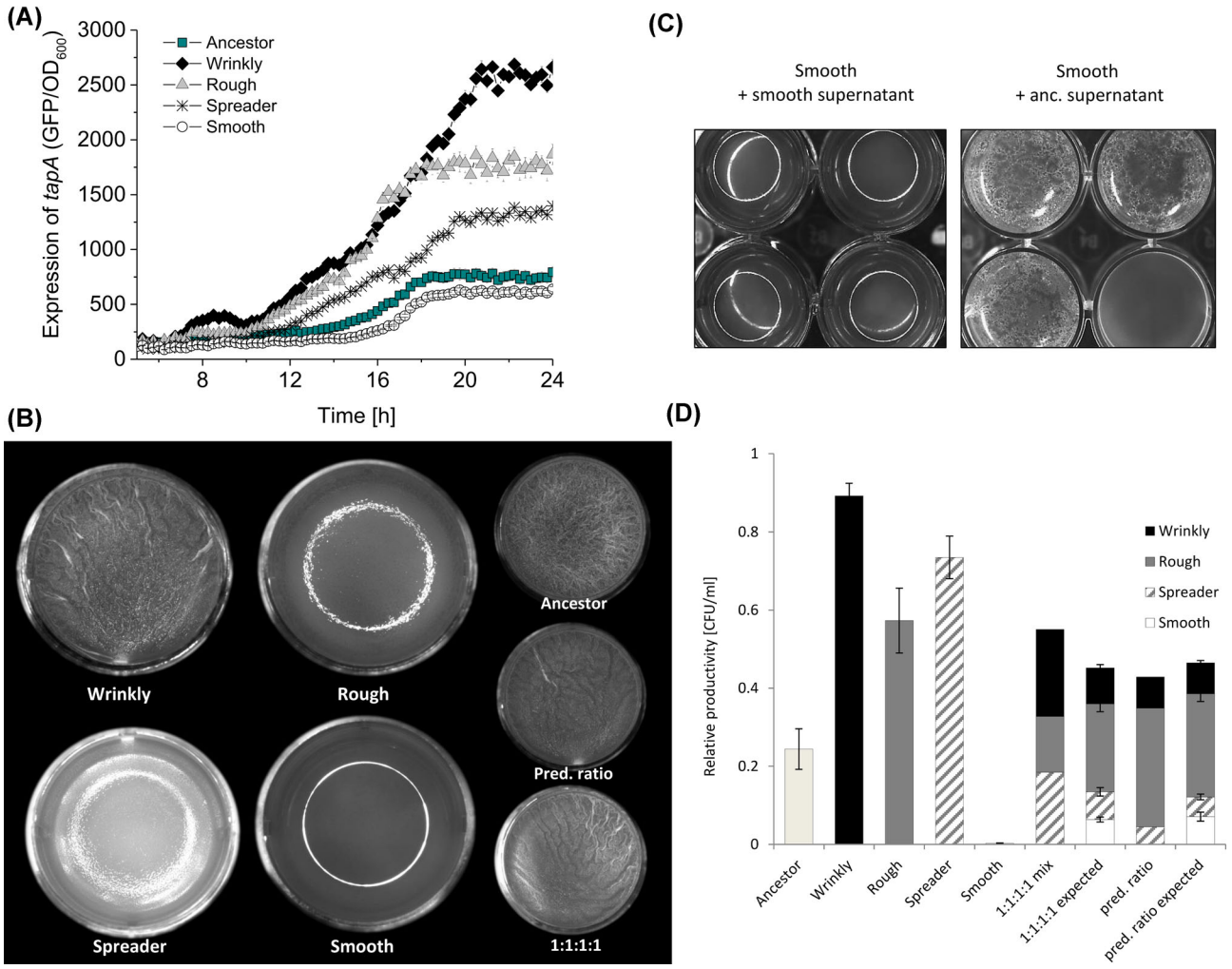

Figure 3. Biofilm genes expression and pellicle productivities in monocultures and in the mix. **(A)** Expression of *tapA* gene in the ancestor and all four morphotypes was compared using corresponding strains carrying P_{tapA}-*gfp* reporter fusion. The experiment was terminated after 24 h due to clumping of cells that interferes with reliable OD and fluorescence signal reads (n = 8). Data points represent mean and error bars represent standard error. **(B)** Pellicle morphology developed by the ancestor, all morphotypes grown in monocultures and two types of morphotype mixes: equal frequencies of morphotypes in initial inoculum (1:1:1:1); predicted frequencies of morphotypes in initial inoculum (0.9: 5.3:0.6:3.2) that are matching their original ratios in evolved pellicle (see Fig. 1B,C). Pellicle were grown for 48 h at 30°C. **(C)** Effect of the spent media produced by the ancestor on pellicle formation by the Smooth morphotype. Four wells were imaged to represent the biological variation of the assay. Well diameter is 1.5 cm. **(D)** Productivities of the ancestor, Wrinkly, Rough, Spreader and Smooth morphotypes, grown in monoculture and in mixes. Expected productivity was calculated as the product of the proportion of each morphotype in the initial population and its yield (CFU per mL) in monoculture (Loreau and Hector 2001; Poltak and Cooper 2011). Observed productivity is the total yield of the mixed community in the experimental environment (for monocultures n = 9; for mixes n = 12). Data points represent mean and error bars represent standard error.

similar to the ancestor, regardless whether the initial ratio was 1:1:1:1 or the derivatives were mixed according to ratios established in the last stage of evolution, i.e. pellicle 35 (Fig. 3B).

Since the Smooth morphotype could not develop a pellicle but was detectable in the mixed population (Fig. 1), we tested whether biofilm formation by the Smooth variant can be complemented by the supernatant produced by the pellicle-forming ancestor that secretes a functional ECM. Although a robust pellicle could not be completely restored, the Smooth morphotype displayed improved surface colonization when grown in the presence of the ancestors spent medium (Fig. 3C), but not when its own supernatant was applied. Therefore, the Smooth variant can benefit from extracellular substances released by other non-defective strains and thereby co-colonize the liquid–air interface.

Non-matrix producing morphotype exploits matrix-producing variants

Finally, we inspected the impact of diversity on individual and group performance by the morphotypes by comparing the productivity of monoculture pellicles with the mixed pellicles in addition to determining the frequency of each morphotype in the mix (as previously implemented by Poltak and Cooper 2011). All morphotypes except the Smooth variant performed significantly better than the ancestor. The Rough and the Spreader morphotypes displayed over 2- or 3-fold higher productivity, respectively, while the Wrinkly variant showed the highest productivity (Fig. 3D). The effect of diversity was assessed using two types of mixes with alternative inoculation strategies: (A) using equal initial frequencies of all morphotypes (1:1:1:1) or

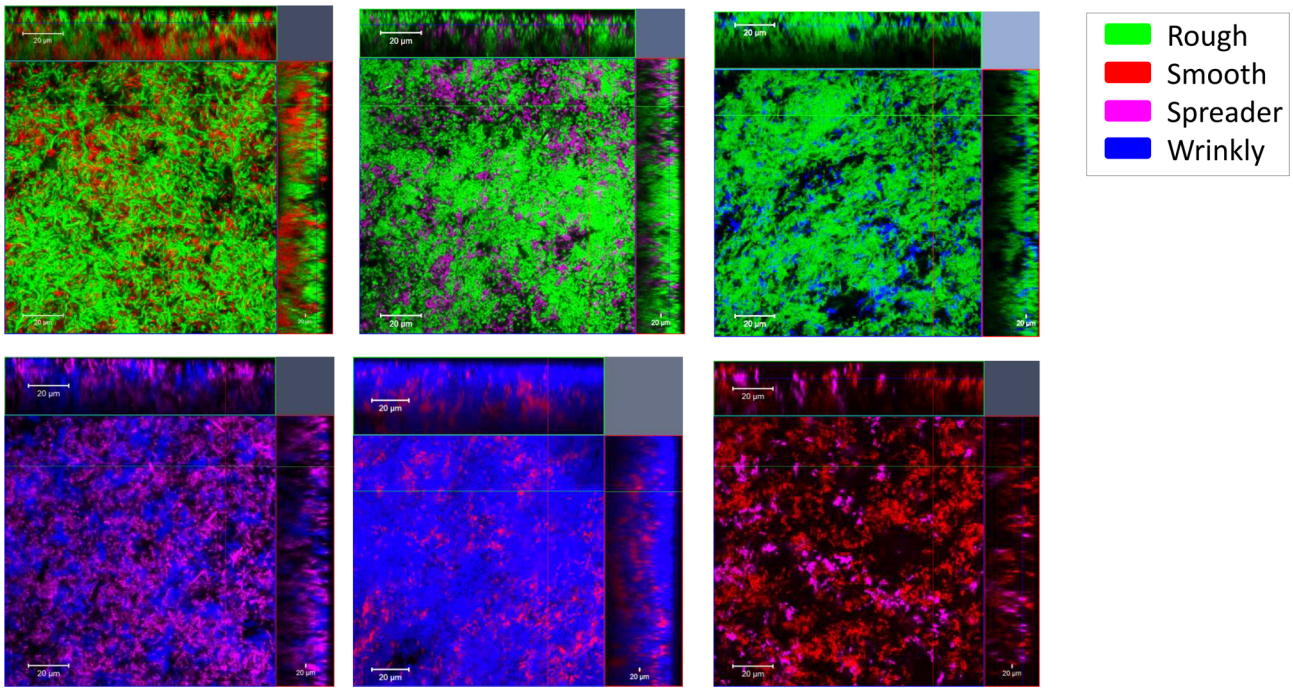

Figure 4. Spatial assortment of morphotypes in pellicle. Confocal microscopy images of pellicle biofilms formed by the mix of four morphotypes were taken. Each time only two selected morphotypes were labeled with constitutive fluorescent reporters and could be visualized in the pellicle. Morphotypes were mixed in ratios 0.9:5.3:0.6:3.2 and pellicles were allowed to form for 48 h at 30°C. To simplify image comparison, each morphotype was artificially labeled with the same assigned color (regardless on actual fluorescent marker used) across all images: Rough—green, Smooth—red, Spreader—purple, Wrinkly—blue. The actual mixed cultures were as follows: $Rough_{mKate}$ + $Smooth_{GFP}$ (+Wrinkly and Spreader unlabeled), $Rough_{GFP}$ + $Spreader_{mKate}$ (+Wrinkly and Smooth unlabeled), $Rough_{GFP}$ + $Wrinkly_{mKate}$ (+Spreader and Smooth unlabeled), $Spreader_{GFP}$ + $Wrinkly_{mKate}$ (+Rough and Smooth unlabeled), $Smooth_{GFP}$ + $Wrinkly_{mKate}$ (+Rough and Spreader unlabeled), $Smooth_{GFP}$ + $Spreader_{mKate}$ (+Rough and Wrinkly unlabeled).

(B) inoculating with frequencies observed in the evolved pellicle (i.e. Wrinkly 9%, Rough 53%, Spreader 6%, and Smooth 32%). The expected productivities in the mix were calculated as a product of their initial frequencies in the mix and the monoculture yield (as previously defined in Poltak and Cooper 2011). First, we discovered that the Wrinkly, Rough and Spreader monoculture yields were higher than the yields of the mixes (Fig. 3C). Interestingly, the net biodiversity effect on the yield was dependent on the inoculation strategy. Specifically, in mix A, the observed yield of the mix was lower than the predicted productivity indicating interference effects. The productivity changes of the Wrinkly, Rough and Spreader variants in the mix were moderate (0.41-fold, 1.57-fold and 0.39-fold, respectively), but the productivity of biofilm-defective Smooth showed a dramatic 98.2-fold increase (Fig. 3D). In mix B (containing altered frequencies), the individual productivity changes of the Wrinkly, Rough and Spreader variants were minimal (0.99-fold, 0.87-fold and 1.15-fold, respectively), while the amplified abundance of the Smooth variant was slightly reduced to 86.6-fold (Fig. 3D), overall resulting in a slightly positive effect on biodiversity and community yield. The calculated effects of selection and complementarity revealed negative selection effects in both mixes (A: −13.4, B: −14.82), balanced by positive complementary effects (A: 13.3, B: 14.86), and resulting in slightly positive net effects in mix B.

It is interesting to note that the final frequencies of the morphotypes in mix A and B were nearly identical despite the differences in the initial inocula. We hypothesized that the robust structure of the community can be governed by certain assortment patterns of the morphotypes in the pellicle. To test whether morphotypes are non-randomly distributed in the pellicles, we fluorescently labeled all morphotypes and evaluated the assortment of each morphotype in a pairwise assay (Fig. 4; Fig. S5, Supporting Information). CLSM analysis revealed that the Smooth variant was mostly localized at the bottom layer of the pellicle probably attaching to the matrix-producing strains (Fig. 4; Fig. S5, Supporting Information). Both the Spreader and the Wrinkly variants were present across the whole intersection of the pellicle, although at lower frequencies as compared to the Rough variant (which is in line with cell count results, see Fig. 3D) (Fig. 4; Fig. S5, Supporting Information). Although technical limitations did not allow us to visualize all morphotypes in the pellicle simultaneously, the pairwise analysis suggests that the Rough, Wrinkly and Spreader variants share the same niche, while the Smooth variant is mostly localized in the lower, medium proximal sections of the pellicle (Fig. 4; Fig. S5, Supporting Information).

Diversification involves mutations related to biofilm regulation, motility and anaerobic respiration pathways

To understand the genetic bases of diversification and interactions between the morphotypes, the genomes of the Wrinkly, Rough, Spreader and Smooth variants isolated from population 1 were sequenced. In addition, six randomly picked isolates from other parallel populations were selected for sequencing (Table 1). The genome of the ancestor was also re-sequenced to screen for single SNPs that could emerge before the evolution experiment during standard stock preparation.

Colony morphology analysis later revealed that the additional strains 2A, 2B and 3C represented the Wrinkly morphotypes, while 1B, 4B and 6C represented the Rough morphotypes (Fig. 6A, Supporting Information). All isolates contained over 400

Table 1 List of mutations detected in genomes of sequenced morphotypes. NC stands for non-coding, Fs denotes frame shift, while *indicates missing amino acid. Total number of mutations: 58; non-coding regions—11; rRNA—5; synonymous substitutions—5; non-synonymous substitutions—22 (blue); frame shifts—15 (red).

Wrinkly				Rough				Spreader	Smooth	Position	Gene	Mutation	Function of gene product
1	2A	2B	3C	1	1B	4B	6C						
√		√	√	√	√	√	√	√	√	1968190	*ppsD*	5844A > T	Plipastin synthesis
√				√	√	√	√	√		3917048	*qoxA*	Val66Leu	Respiration
	√									3917073		171C > G	
√	√	√		√	√	√	√			1112769	*hemAT*	Leu140Pro	Chemotactic movement towards oxygen
			√							1112779		Phe137Leu	
			√	√	√	√	√			1591893	*murG*	Lys363*	Biosynthesis of peptidoglycan precursor
		√	√			√				361201	*nirB*	Gly363Ala	Nitrate reduction
√		√	√				√			392313	*srfAA*	Asn1678Lys	Surfactin synthesis
√				√		√				385447		Ile2983Asn	
√	√				√	√		√		1968046	*pyrP*	806insT	Uracil transport
√	√				√					1619096		Pro271fs	
√							√			2402234	*gdhA*	282G > A	Glu/Leu/Phe/Val dehydrogenase
						√				4076083	*iolF*	Cys355fs	D-chiro-inositol uptake
			√							4076094		Gln351fs	
			√							4076085		Cys355fs	
			√							1470935	*kinA*	Gly548fs	Phosphorylation of Spo0F, initiation of sporulation
√	√	√								1470941		Ile549Thr	
√	√	√								2007297	*yogA*	Leu199Met	Unknown function
√	√	√								43671	*coaX*	Asp214fs	Biosynthesis of Coenzyme A
√										1195323	*argC*	Ile341fs	Biosynthesis of arginine
√										1195326		Thr342fs	
		√								1464366	*mcpC*	Leu489*	Chemotaxis towards Aminoacids
			√							1472011	*patA*	Ala98_Gln99insArg	Lysine/peptidoglycan biosynthesis
	√									2002073	*iseA*	Ala87Glu	Unknown function
			√							2076516	*yobO*	Ala378Thr	Unknown function
		√								3895285	*ywdH*	Ser4fs	Unknown function
				√			√			4103061	*yxaL*	40fs	Unknown function
					√					494175	*gsiB*	150G > A	Response to water deficits
							√			699075	*purK*	Ala226fs	Purine biosynthesis
				√						1078223	*escB*	Arg260Trp	Exoprotein transport
						√				1713474	*cheA*	Ile467fs	Chemotactic signal modulator
				√						1729544	*polC*	Pro1051Leu	DNA replication
						√				1730647		Arg1421insLeuAsp	
				√						2980723	*citZ*	Ala187Val	TCA cycle
							√			3716482	*cotG*	Arg54Lys	Spore resistance
							√			3858320	*ywgA*	Ile58Asn	Unknown function
							√			4103063	*yxaL*	Gln39fs	Unknown function
							√			646792	*Rex*	Gly64Arg	Regulation of fermentation and anaerobic respiration
								√	√	646634		Ala11Glu	
							√			692497	*guaA*	Asp148fs	Biosynthesis of GMP
								√		692504		Thr151fs	
								√	√	1702110	*fliY*	Leu59Phe	Flagellar protein, role in motility and chemotaxis
√	√					√		√	√	95368	*rRNA*		Ribosome formation
√	√	√	√	√	√	√	√	√		946071			
		√	√			√	√	√		3176962			
	√						√			947097			
	√									3176965			
√	√	√	√		√	√	√	√	√	945900	NC	A > T	
√	√	√	√		√	√	√	√	√	945906		A > T	
					√					84148		C > A	
								√		84208		C > A	
			√							496153		CAGCG_del	
			√							1334245		CG_del	
√	√	√	√	√	√	√		√		1353334		G_ins	
		√	√							1609430		CTTG_del	
									√	3528923		A > G	
								√	√	3761423		C_del	
									√	4103056		A_del	

mutations of which 386 were overlapping and were therefore not subjected to further analysis, since they probably were linked to general adaptation to laboratory conditions or specifically to the medium. Fifty eight non-overlapping mutations were detected in total, most of which resulted in amino-acid substitution or a frame shift (22 and 15, respectively). Remaining mutations were found in non-coding regions (11), rRNA (5) or resulted in synonymous substitutions (5). Certain mutations detected in non-coding regions (NC) and rRNA reproduced across representatives of different morphotypes, suggesting their early occurrence in evolution (Table 1). On the other hand, certain NC mutations were unique for the Smooth (2) or Spreader (1), and could indicate an unknown regulatory role of those regions (Table 1). The most common mutation (detected in seven out of eight sequenced isolates) was synonymous substitution in *ppsD* gene that could be a part of codon optimization process. Remaining mutations detected in coding regions could be divided into six categories: mutations detected in Wrinkly, Rough and Spreader strains, mutations detected in both, Wrinkly and Rough strains, mutations present solely in the Wrinkly strain, mutations exclusive to the Rough strain, mutations shared between the Smooth and the Spreader strain, and finally a single mutation present only in the Spreader strain (Table 1). There were two mutations that were placed in the first category: Val66Leu substitution in the product of *qoxA* gene encoding for quinol oxidase, and a synonymous substitution in *pyrP* (Table 1).

All Rough and all Wrinkly strains contained a substitution in HemAT, a soluble chemotactic receptor playing a crucial role in pellicle formation (Hölscher *et al*. 2015). The substitution was either Phe137Leu in case of Wrinkly 3C or Leu140Pro in other Wrinkly and Rough representatives (Table 1). Certain genes like *srfAA, pyrP* or *iolF,* encoding for surfactin synthetase, uracil permease and D-chiro-inositol transport protein, respectively, were reproducibly mutated in different Wrinkly/Rough strains but at different positions (Table 1).

All Wrinkly isolates shared a mutation in the *kinA* gene that is directly linked to the matrix master regulator Spo0A (Stephenson and Hoch 2002). In addition, all but one Wrinkly representative had non-synonymous substitution in *yogA* (unknown function) and frame shift mutation in *coaX* involved in Coenzyme A biosynthesis (Table 1). Mutations unique for the Rough group were rather scattered through different strains, but non-synonymous substitution in *polC* encoding for DNA polymerase III were found in two different strains at different positions of this gene (Table 1).

Both the Spreader and the Smooth strain exhibited a substitution in the *rex* gene that may play a role in their adaptation to the limited oxygen availability in the bottom layers of the pellicle. Interestingly, they also shared a substitution in the flagella-related gene *fliY*, but the Spreader strain additionally carries a frame shift mutation in the GMP-synthesis gene *guaA*. We examined the effects of *rex* and *guaA* deletion on pellicle and colony morphology, but neither resulted in a phenotype that would resemble that of Spreader or Smooth pellicles (Fig. S6B, Supporting Information) indicating that at least two different SNPs are needed to recreate the evolved morphotypes (assuming no effects of SNPs present in non-coding regions). The mutation pattern (Table 1) and the simultaneous emergence of Spreader and Smooth morphotypes during the evolution suggest that the Smooth variant could be the ancestral form of the Spreader variant. The Wrinkly morphotype likely evolved from the Rough variant, since it emerged after the Rough morphotype (Fig. 1C) and it contained mutations that overlap with those found in the Rough variant in addition to subsequent SNPs.

DISCUSSION

Several studies have already proved that diversification is a rapid, general and significant process in microbial evolution. Our work fills the gap of equivalent knowledge on a non-pathogenic and biotechnologically relevant Gram-positive model. We reveal, that diversification pattern during *B. subtilis* pellicle evolution with respect to colony types that emerge from a common ancestor, reproduced in all parallel ecosystems. Although the detailed evolutionary history was examined only in one out of six parallel populations, the synchrony in productivity changes throughout the evolutionary time and similarities in the final frequencies of morphotypes across all six populations point towards strong parallelism of evolutionary events occurring in independent pellicles. We employed a novel quantitative approach to describe the evolved morphotypes and to confirm that they were different from each other and from their common ancestor. Surface profilometry combined with wetting studies were especially helpful in the case of early morphotypes (Rough or Wrinkly), whereas they still resembled the ancestral colony in terms of macro-scale morphology, remarkable differences in microstructure and hydrophobicity were revealed. Recent work indicated that subtle differences in colony microstructure could be of profound importance for colony wetting behavior (Arnaouteli *et al*. 2017; Werb *et al*. 2017) and, consequently, for its resistance to antimicrobials (Arnaouteli *et al*. 2017). However, recent findings clearly show that complex surface topology is not sufficient to maintain non-wetting behavior of *B. subtilis* colonies (Arnaouteli *et al*. 2017). To a certain extent, the measured surface complexity/hydrophobicity levels were positively correlated with the levels of matrix genes expression, but this correlation was not perfect. For instance, the Wrinkly variant showed a strongly increased expression of the *tapA* operon and yet a decreased surface complexity and hydrophobicity as compared to the ancestor. This is in line with a recent survey of domesticated *B. subtilis* 168 variants where the authors also found a certain mismatch between the colony surface complexity (at macroscale) and the level of biofilm-genes expression (Gallegos-Monterrosa, Mhatre and Kovács 2016). As a complex colony structure is affected by localized cell death (Asally *et al*. 2012), changes in cell viability in evolved morphotypes could potentially balance the effects of increased EPS production levels.

Similar to previous studies, *B. subtilis* evolved into variants with improved biofilm productivities (Rough, Wrinkly and Spreader); however, a quantitative analysis revealed that some of them lost the important surface properties of the ancestor (Wrinkly and Spreader), presumably pointing towards quantity vs. quality trade-offs. Remarkably, one of the morphotypes (Smooth) completely lost the ability to form a pellicle, and it could only reside in such biofilms encompassing also the other variants. Moreover, the evolved non-producer (Smooth) was the only morphotype gaining a strong individual benefit from being a part of the mixed population regardless of its initial frequency in the inoculum. The minor complementarity effects that were estimated when comparing the expected vs. obtained mix productivity *in toto* may derive from the fact that the Smooth variant mostly resides in the bottom layers of the pellicle. This might reduce its competition with the biofilm-forming morphotypes due to restricted oxygen availability. The interaction between *B. subtilis* Smooth and other variants resembles the interplay between 'Smooth' and 'Wrinkly' morphotypes of *P. fluorescens* (Rainey and Travisano 1998), with the particular difference that, here, the 'defector' evolves *de novo*. We believe that the success of the Smooth variant could depend on early

adaptive events in the population, specifically the rise of Rough and Wrinkly variants that both showed a tremendous increase in EPS production. Still, the diversity within matrix-producers (in this case Spreader, Rough and Wrinkly) can actually limit the spread of matrix-non-producers (Brockhurst *et al.* 2006).

Such non-producers were not identified in evolving *B. cenocepacia* or *P. aeruginosa* biofilms. Possibly, submerged biofilms of *B. cenocepacia* or *P. aeruginosa* may strongly select for attachment and stratification of individual cells (Xavier and Foster 2007), while in floating biofilms of *B. subtilis* and *P. fluorescens*, cells can partially rely on medium diluted EPS.

Although we did not unravel the molecular evolution pattern, certain mutations discovered in given morphotypes represent promising targets for future studies. For example, Rough and Wrinkly carried a Leu140Pro or Phe137Leu substitutions in HemAT, which is a key oxygen receptor important for pellicle formation (Hölscher *et al.* 2015). Since Phe137 is directly at heme-biding side and a substitution to Leu very likely alters the function of the receptor. Similar is the case for Leu140, part of the α-helix and only three amino acids away from the heme-binding side, where a non-conserved substitution to Proline likely influences the function of the receptor. Non-synonymous substitutions in *srfAA* detected in certain Wrinkly and Rough isolates could alter the function of surfactin synthetase (especially the non-conserved Ile2983Asn detected in Wrinkly 1, Rough 1 and 4B) what could influence the amounts of produced surfactin. As surfactin is believed to affect matrix genes expression as a paracrine signaling molecule (López *et al.* 2009), it might have an impact the *eps/tapA* expression levels in those morphotypes.

Both Smooth and Spreader strains share mutations in the *rex* and *fliY* gene, which could indicate their adaptation to the oxygen-poor bottom layers of biofilms and changes in motility, respectively. In addition, another substitution in *rex* was also found in Rough 6C and other genes linked to anaerobic respiration (*nirB*) or chemotaxis (*mcpC, cheA*) were also altered in selected Wrinkly and Rough isolates (Table 1).

Interestingly, all but two NC mutations present in the Smooth overlap with the Spreader that contains three additional unique mutations only one of which (Thr151 fs in *guaA*) is positioned in a coding region. Presumably, supplementing Smooth genetic background with a *guaA* mutation might result in secondary effects that transform the Smooth into a Spreader phenotype. As c-di-GMP plays an important role in motility arrest (Chen *et al.* 2012a), mutation in GMP synthetize GuaA probably reduces the level of c-di-GMP possibly enhancing motility.

It is difficult to point towards the mutations that are responsible for Rough and Wrinkly morphotype. Rough 1B carries the lowest amount of mutations where only *qoxA* (related to respiration), *hemAT*, *murG* (peptidoglycan synthesis) and *pyrP* were identified to carry non-synonymous substitutions/frame shifts. Unless Rough resulted from changes in unknown regulatory elements, those four genes could be potential targets of molecular evolution. Morphogenesis of Wrinkly could require additional changes in *kinA*.

Variations in biofilm formation within laboratory *B. subtilis* strains are commonly associated with the domestication problem, that occurs during cultivation of a bacterium in rich LB medium (McLoon *et al.* 2011; Leiman *et al.* 2014; Gallegos-Monterrosa, Mhatre and Kovács 2016). Indeed, biofilm-altered variants of *B. subtilis* could be experimentally evolved in static and liquid LB, mostly carrying mutations in the biofilm regulator *sinR* (Leiman *et al.* 2014). Here, we showed that biofilm non-producers readily evolve also in minimal medium under biofilm selective conditions indicating they can also be part of a normal eco-evolutionary process, rather than just a product of domestication. We still know relatively little about the natural diversity of biofilm formation within *B. subtilis*. Such information would be of great importance taking into account biocontrol properties of the species which rely on biofilm formation capability (Chen *et al.* 2012b).

We here showed that evolution in pellicle biofilms may give rise to variants with variable biofilm phenotypes including biofilm non-producers that rely on 'upgraded' pellicle formers. Our work reveals that, in addition to positive niche opportunities, spatially structured environments provide a platform where positive interactions intertwine with exploitation.

SUPPLEMENTARY DATA

Supplementary data are available at *FEMSEC* online.

FUNDING

This work was supported by Alexander von Humboldt foundation fellowship to A.D., a Semester Abroad Program to N.L., a Consejo Nacional de Ciencia y Tecnología (CONACyT) fellowship to C.F.G., the Deutsche Forschungsgemeinschaft (DFG) through project B11 in the framework of SFB863 granted to O.L. and a Start-up grant from the Technical University of Denmark to Á.T.K.

Conflicts of interest. None declared.

REFERENCES

Arnaouteli S, Ferreira AS, Schor M *et al.* Bifunctionality of a biofilm matrix protein controlled by redox state. *P Natl Acad Sci* 2017;**114**:E6184–91.

Arnaouteli S, MacPhee CE, Stanley-Wall NR. Just in case it rains: building a hydrophobic biofilm the *Bacillus subtilis* way. *Curr Opin Microbiol* 2016;**34**:7–12.

Asally M, Kittisopikul M, Rue P *et al.* Localized cell death focuses mechanical forces during 3D patterning in a biofilm. *Proc Natl Acad Sci USA* 2012;**109**:18891–6.

Branda SS, Gonzalez-Pastor JE, Ben-Yehuda S *et al.* Fruiting body formation by *Bacillus subtilis*. *P Natl Acad Sci USA* 2001;**98**:11621–6.

Brockhurst MA, Hochberg ME, Bell T *et al.* Character displacement promotes cooperation in bacterial biofilms. *Curr Biol* 2006;**16**:2030–4.

Chen Y, Chai Y, Guo JH *et al.* Evidence for cyclic di-GMP-mediated signaling in *Bacillus subtilis*. *J Bacteriol* 2012a;**194**:5080–90.

Chen Y, Yan F, Chai Y *et al.* Biocontrol of tomato wilt disease by *Bacillus subtilis* isolates from natural environments depends on conserved genes mediating biofilm formation. *Environ Microbiol* 2012b;**15**:848–64.

Ellis CN, Traverse CC, Mayo-Smith L *et al.* Character displacement and the evolution of niche complementarity in a model biofilm community. *Evolution (N Y)* 2015;**69**:283–93.

Flynn KM, Dowell G, Johnson TM *et al.* Evolution of ecological diversity in biofilms of *Pseudomonas aeruginosa* by altered cyclic diguanylate signaling. *J Bacteriol* 2016;**198**:2608–18.

Gallegos-Monterrosa R, Mhatre E, Kovács AT. Specific *Bacillus subtilis* 168 variants form biofilms on nutrient-rich medium. *Microbiology* 2016;**162**:1922–32.

van Gestel J, Vlamakis H, Kolter R. From cell differentiation to cell collectives: *Bacillus subtilis* uses division of labor to migrate. *PLoS Biol* 2015;**13**:e1002141.

Hammerschmidt K, Rose CJ, Kerr B *et al*. Life cycles, fitness decoupling and the evolution of multicellularity. *Nature* 2014;**515**:75–9.

Hölscher T, Bartels B, Lin YC *et al*. Motility, chemotaxis and aerotaxis contribute to competitiveness during bacterial pellicle biofilm development. *J Mol Biol* 2015;**427**:3695–708.

Kawecki TJ, Lenski RE, Ebert D *et al*. Experimental evolution. *Trends Ecol Evol* 2012;**27**:547–60.

Kesel S, Grumbein S, Gumperlein I *et al*. Direct comparison of physical properties of *Bacillus subtilis* NCIB 3610 and B-1 biofilms. *Appl Env Microbiol* 2016;**82**:2424–32.

Kim W, Levy SB, Foster KR. Rapid radiation in bacteria leads to a division of labour. *Nat Commun* 2016;**7**:10508.

Kobayashi K, Iwano M. BslA(YuaB) forms a hydrophobic layer on the surface of *Bacillus subtilis* biofilms. *Mol Microbiol* 2012;**85**:51–66.

Koch G, Yepes A, Forstner KU *et al*. Evolution of resistance to a last-resort antibiotic in Staphylococcus aureus via bacterial competition. *Cell* 2014;**158**:1060–71.

Konkol MA, Blair KM, Kearns DB. Plasmid-encoded ComI inhibits competence in the ancestral 3610 strain of *Bacillus subtilis*. *J Bacteriol* 2013;**195**:4085–93.

Leiman SA, Arboleda LC, Spina JS *et al*. SinR is a mutational target for fine-tuning biofilm formation in laboratory-evolved strains of *Bacillus subtilis*. *BMC Microbiol* 2014;**14**:301.

López D, Vlamakis H, Losick R *et al*. Paracrine signaling in a bacterium. *Genes Dev* 2009;**23**:1631–8.

Loreau M, Hector A. Partitioning selection and complementarity in biodiversity experiments. *Nature* 2001;**412**:72–6.

Martin M, Dragoš A, Hölscher T *et al*. *De novo* evolved interference competition promotes the spread of biofilm defectors. *Nat Commun* 2017;**8**:15127.

Martin M, Hölscher T, Dragoš A *et al*. Laboratory evolution of microbial interactions in bacterial biofilms. *J Bacteriol* 2016;**198**:2564–71.

McLoon AL, Guttenplan SB, Kearns DB *et al*. Tracing the domestication of a biofilm-forming bacterium. *J Bacteriol* 2011;**193**:2027–34.

Nilsson AI, Koskiniemi S, Eriksson S *et al*. Bacterial genome size reduction by experimental evolution. *P Natl Acad Sci USA* 2005;**102**:12112–6.

Poltak SR, Cooper VS. Ecological succession in long-term experimentally evolved biofilms produces synergistic communities. *ISME J* 2011;**5**:369–78.

Rainey PB, Travisano M. Adaptive radiation in a heterogeneous environment. *Nature* 1998;**394**:69–72.

Romero D, Aguilar C, Losick R *et al*. Amyloid fibers provide structural integrity to *Bacillus subtilis* biofilms. *P Natl Acad Sci USA* 2010;**107**:2230–4.

Romero D, Vlamakis H, Losick R *et al*. An accessory protein required for anchoring and assembly of amyloid fibres in *B. subtilis* biofilms. *Mol Microbiol* 2011;**80**:1155–68.

Rosenzweig F, Sherlock G. Experimental evolution: prospects and challenges. *Genomics* 2014;**104**:v–vi.

Shemesh M, Chai Y. A combination of glycerol and manganese promotes biofilm formation in *Bacillus subtilis* via histidine kinase KinD signaling. *J Bacteriol* 2013;**195**:2747–54.

Spiers AJ, Bohannon J, Gehrig SM *et al*. Biofilm formation at the air-liquid interface by the *Pseudomonas fluorescens* SBW25 wrinkly spreader requires an acetylated form of cellulose. *Mol Microbiol* 2003;**50**:15–27.

Steenackers HP, Parijs I, Foster KR *et al*. Experimental evolution in biofilm populations. *FEMS Microbiol Rev* 2016;**40**:373–97.

Stephenson K, Hoch JA. Evolution of signalling in the sporulation phosphorelay. *Mol Microbiol* 2002;**46**:297–304.

Tenaillon O, Barrick JE, Ribeck N *et al*. Tempo and mode of genome evolution in a 50,000-generation experiment. *Nature* 2016;**536**:165–70.

Traverse CC, Mayo-Smith LM, Poltak SR *et al*. Tangled bank of experimentally evolved *Burkholderia* biofilms reflects selection during chronic infections. *P Natl Acad Sci USA* 2013;**110**:E250–9.

Vlamakis H, Chai Y, Beauregard P *et al*. Sticking together: building a biofilm the *Bacillus subtilis* way. *Nat Rev Microbiol* 2013;**11**:157–68.

Werb M, Garcia CF, Bach NC *et al*. Surface topology affects wetting behavior of *Bacillus subtilis* biofilms. *NPJ Biofilms Microbiomes* 2017;**3**:11.

Xavier JB, Foster KR. Cooperation and conflict in microbial biofilms. *Proc Natl Acad Sci* 2007;**104**:876–81.

Chapter 3

De novo evolved interference competition promotes the spread of biofilm defectors

Published in Nature Communications (2017)

nature COMMUNICATIONS

ARTICLE

Received 5 Oct 2016 | Accepted 2 Mar 2017 | Published 2 May 2017

DOI: 10.1038/ncomms15127 OPEN

De novo evolved interference competition promotes the spread of biofilm defectors

Marivic Martin[1,*], Anna Dragoš[1,*], Theresa Hölscher[1,*], Gergely Maróti[2], Balázs Bálint[3], Martin Westermann[4] & Ákos T. Kovács[1]

Biofilms are social entities where bacteria live in tightly packed agglomerations, surrounded by self-secreted exopolymers. Since production of exopolymers is costly and potentially exploitable by non-producers, mechanisms that prevent invasion of non-producing mutants are hypothesized. Here we study long-term dynamics and evolution in *Bacillus subtilis* biofilm populations consisting of wild-type (WT) matrix producers and mutant non-producers. We show that non-producers initially fail to incorporate into biofilms formed by the WT cells, resulting in 100-fold lower final frequency compared to the WT. However, this is modulated in a long-term scenario, as non-producers evolve the ability to better incorporate into biofilms, thereby slightly decreasing the productivity of the whole population. Detailed molecular analysis reveals that the unexpected shift in the initially stable biofilm is coupled with newly evolved phage-mediated interference competition. Our work therefore demonstrates how collective behaviour can be disrupted as a result of rapid adaptation through mobile genetic elements.

[1] Terrestrial Biofilms Group, Institute of Microbiology, Friedrich Schiller University Jena, Jena 07743, Germany. [2] Institute of Biochemistry, Biological Research Centre, Hungarian Academy of Sciences, Szeged 6726, Hungary. [3] Seqomics Biotechnology Ltd., Mórahalom 6782, Hungary. [4] Electron Microscopy Center, Jena University Hospital, Jena 07743, Germany. * These authors contributed equally to this work. Correspondence and requests for materials should be addressed to Á.T.K. (email: atkovacs@dtu.dk).

Biofilms, consisting of densely packed single- or multi-species communities embedded in self-produced slimy polymers, represent the most common microbial life form[1–3]. Several recent studies have shown that the spatial structure of biofilms has a major impact on competition and cooperation among microbes and drives evolutionary changes within microbial communities (reviewed in refs 4,5). One particularly well-studied example used static cultures of *Pseudomonas fluorescens*, where an oxygen gradient led to the emergence of a new wrinkly (W) phenotype that secretes polysaccharides and forms a biofilm at the air–liquid interface[6,7]. Interestingly, biofilms formed by W undergo a premature collapse caused by the incorporation of another phenotype into the biofilm without sharing the metabolic costs of exopolymer production[8]. This scenario of biofilm collapse reflects the phenomenon known as 'tragedy of the commons', which happens due to invasion by non-cooperators and depletion of an overly-exploited resource (in this case the exopolymer)[9].

How often the 'tragedy of the commons' happens in other biofilm communities remains an open question in sociomicrobiology. Several studies suggest that exopolymer production cannot easily be exploited by non-producing defectors[10,11]. Such robustness of cooperation-based biofilm formation is often explained by limited sharing of matrix components[10–12], the low costs of polymer production[11], the spatial assortment of cells in biofilms[13] or even the intrinsic nature of certain matrix components that are exclusively shared between mother and daughter cells[14]. Although the key principles of certain non-producer exclusion mechanisms are becoming clear, competition experiments involving producers and non-producers are usually conducted over short timescales[11–14], leaving a window of opportunity for unexpected evolutionary scenarios[15]. Data from various bacterial models suggest that defectors can leave a fingerprint on the evolution of social strains and promote the evolution of novel cheating-suppression mechanisms[16]. These can be linked to lowering the cost of cooperation by the wild-type (WT) cells[17]. Selection can also work to the advantage of the non-producers, which can evolve better exploitation skills[15,17]. In extreme cases, cooperators can be *de novo* selected from the population of cheats[18]. In general, long-term scenarios in socially heterogeneous populations of microbes are still very difficult to predict.

In this manuscript, we study the long-term social dynamics of co-cultures comprising matrix producer and non-producer strains using the widespread soil bacterium *Bacillus subtilis*. *B. subtilis* forms thick, robust structures at the air-liquid interface (pellicle) facilitated by two crucial secreted compounds: an exopolysaccharide, Eps (encoded by *epsA-O*), and a protein component, TasA (encoded by *tapA-sipW-tasA*). In a standing culture, driven by oxygen limitation, matrix-producing strains form pellicles[19]. Strains lacking either one or both matrix components cannot form robust biofilms at the air–liquid interface and they barely colonize the liquid surface[20]. Moreover, strains producing only one of the components are able to complement each other and form a WT-like pellicle[20]. This strongly suggests that both matrix components secreted by producers are freely shared with non-producers and could therefore be exploited by non-producing mutants.

Here we show that on a short timescale, *B. subtilis* matrix non-producers have a tremendous disadvantage in co-culture with the WT. We further demonstrate how unexpected adaptive events involving mobile genetic elements can shift the social dynamics in the population and reduce biofilm formation.

Results

Biofilm non-producers are outcompeted from mixed pellicles. A positive result in a complementation assay of *B. subtilis* Δ*eps* and Δ*tasA* biofilm mutants suggests that both key biofilm components, Eps and TasA, can be shared (Fig. 1a)[20]. We therefore predicted that the double mutant Δ*eps*–Δ*tasA*, which cannot form a pellicle in monoculture[20], would still be able to incorporate into the pellicle when co-cultured with the WT. To test our hypothesis, we mixed WT and Δ*eps*–Δ*tasA* strains in a 1:1 ratio and allowed the pellicle to form (see Methods). The final ratio of the WT to the Δ*eps*–Δ*tasA* strain was assessed by two alternative methods: antibiotic marker based colony forming unit (c.f.u.) counts (Fig. 1a) and fluorescence microscopy (here, GFP and mKATE2 producing WT and Δ*eps*–Δ*tasA* mutants were used, respectively, or we used the same strains with swapped fluorescent markers; Fig. 1b,c). Surprisingly both c.f.u. assay and microscopy indicated a dramatic advantage of the WT over

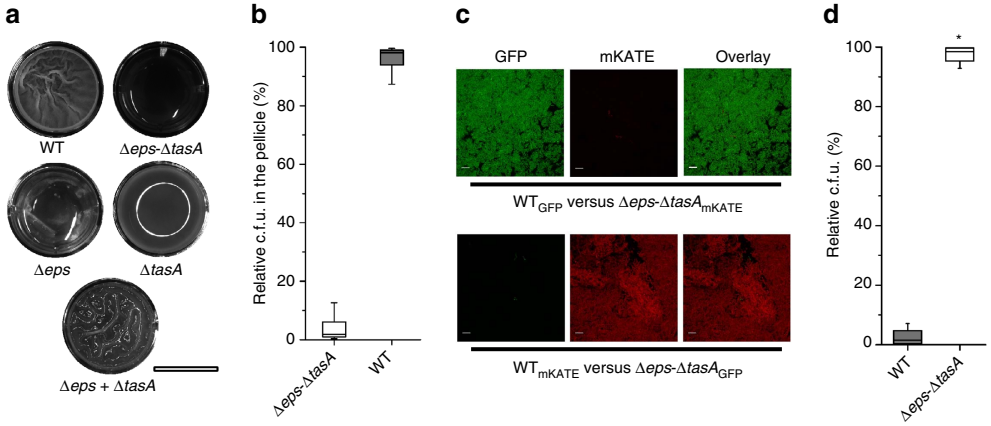

Figure 1 | Matrix non-producer strain does not incorporate into the wild-type pellicle. (**a**) Pellicle biofilms of wild-type (WT) *Bacillus subtilis* 168 and its mutant derivatives were recorded using an Axio Zoom microscope equipped with a black and white camera. Scale bar, 1 cm. The reflection of the light source can be observed in the Δ*tasA* culture. (**b**) Pellicle competition assay between Δ*eps*–Δ*tasA* and WT ($n=25$). (**c**) Confocal microscopy images of pellicle biofilm from culture initially consisting of a 1:1 ratio of WT and Δ*eps*–Δ*tasA* (upper) and cells with swapped fluorescence protein labels (lower). Scale bars, 10 μm. (**d**) Planktonic culture competition assay between Δ*eps*–Δ*tasA* and WT ($n=25$). Boxes represent Q1–Q3, lines represent the median, and bars span from max to min. The experiments were independently repeated at least three times. * indicates that the relative c.f.u. is significantly higher than the relative c.f.u. of Δ*eps*–Δ*tasA* ancestor in the pellicle (in panel **b**).

Δ*eps*–Δ*tasA*; the latter was almost completely outcompeted from the pellicle formed by the WT (Fig. 1a–c).

The incorporation success of Δ*eps*–Δ*tasA* into the pellicle was positively dependent on its initial frequency (Pearson's correlation coefficient $r = 0.74$; Supplementary Fig. 1A). Specifically, the mutant showed increased pellicle incorporation, up to $23 \pm 1.9\%$, which also correlated with decline in total c.f.u. of the pellicle, but only when its initial proportion was $>50\%$, while at initial frequencies $<50\%$, the pellicle incorporation ranged from 0.11 to 5% (Supplementary Fig. 1A).

To understand if the availability of nutrients influenced the ability of non-producers to incorporate into the pellicle, the competition assay was repeated using a medium in which the broth and other components were doubled ($4 \times$ SG, see Methods). It was observed that the Δ*eps*–Δ*tasA* strain could incorporate better in richer medium (Supplementary Fig. 1B). Using $2 \times$ SG, the incorporation ability of the Δ*eps*–Δ*tasA* strain was 2% (mean; $n = 5$; s.d. = 1.37), while in $4 \times$ SG medium pellicle incorporation increased to 6.72% (mean; $n = 5$; s.d. = 3.40). Importantly, the starting ratios in these competition assays were identical (46.72% Δ*eps*–Δ*tasA*; mean; $n = 5$; s.d. = 14.4), therefore, the possibility of the initial frequency influencing these results could be excluded.

Finally, to ensure that the above result was caused by a mechanism that is specific to biofilm conditions and not simply caused by a growth defect of the Δ*eps*–Δ*tasA* strain, WT versus Δ*eps*–Δ*tasA* competition experiments were also performed in planktonic cultures where oxygen distribution is more homogenous and no fitness benefits from biofilm formation are to be expected[11,13,21]. In planktonic culture, Δ*eps*–Δ*tasA* had a strong fitness advantage over the WT (Fig. 1d) that is likely due to the release of the mutant from the metabolic costs of Eps and TasA production[13], as also indicated by its higher growth rate in planktonic culture conditions (Supplementary Fig. 1C). We therefore concluded that a specific mechanism prevents incorporation of the Δ*eps*–Δ*tasA* mutant into *B. subtilis* pellicles.

The ratio of non-producers increases during co-evolution. For the investigation of long-term dynamics in *B. subtilis* WT and Δ*eps*–Δ*tasA* mutant co-culture over time, a serial transfer experiment was conducted in conditions promoting pellicle formation (see Methods). During the evolution experiment, two transfer methods were applied: in transfer method A, the disrupted biofilm suspension was used directly for the inoculation of fresh medium; in transfer method B the disrupted biofilm suspension was heat-treated, thereby selecting only spores for the inoculation (for detailed description see Methods). Method B was chosen to select for individuals that successfully went through the entire biofilm life cycle.

The ratio of WT to the Δ*eps*–Δ*tasA* mutant was monitored by selective plating of frozen stocks prepared at different timepoints from the experiment, from the 2nd up to the final (10th) transfer. Despite the initial incorporation failure of Δ*eps*–Δ*tasA* into the pellicle (Fig. 1a–c), its representation in certain populations of transfer method B was observed to increase dramatically over longer timescales. Remarkably, in parallel populations where transfer method B was applied (that is, selection for spores), the fraction of the Δ*eps*–Δ*tasA* mutant was considerably higher after the 10th transfer than at the start of the experimental evolution in all but two replicates (Fig. 2b). Importantly, with several exceptions (in replicates 2 that remained relatively stable WT:Δ*eps*–Δ*tasA* ratio over time and replicate 4 that showed an outlying outburst of Δ*eps*–Δ*tasA* at passage 8), the percentage of the Δ*eps*–Δ*tasA* mutant was increased in each successive passage of these populations (Fig. 2b). The values rose to $>30\%$ in general and to a maximum of around 80% after the 10th transfer of replicate 5. Also, in one out of five parallel populations that were transferred by method A, the fraction of Δ*eps*–Δ*tasA* was slightly higher after the 10th transfer compared to that at the beginning of the evolution experiment (Fig. 2a).

Non-producers evolve to better incorporate into the pellicle. To further investigate the evolutionary phenomena involved in improved performance of Δ*eps*–Δ*tasA* in the evolved biofilm population, single clones of both the WT and Δ*eps*–Δ*tasA* mutant were isolated from three randomly chosen populations after the 10th transfer where an increase of Δ*eps*–Δ*tasA* in the pellicle was observed (replicates 3, 4 and 5 from transfer method B) (Fig. 2b). All evolved populations and single clones that were further analysed (or genetically modified) in this study are listed in Supplementary Table 2. For clarity, we refer to evolved matrix producers (WT strains) as eMP and to the evolved matrix non-producers (Δ*eps*–Δ*tasA*) as eNMP.

First, to understand which of the co-cultured strains evolved to facilitate better incorporation of the mutant into the pellicle, a series of pellicle competition assays were performed. Competition assays revealed that all but one tested eNMP strains from populations B410m and B510m, and one isolate from population B310m, could increase their fraction within the pellicles as compared to their ancestor when co-cultured with the ancestor WT (Fig. 3a,b). This result was confirmed by both c.f.u. assay (Fig. 3a) and fluorescence microscopy (Fig. 3b). Moreover, the ancestor Δ*eps*–Δ*tasA* performed even worse when co-cultured with the eMP strains compared to its performance against the WT ancestor (Fig. 3). Therefore, the eMPs completely suppressed the ancestral Δ*eps*–Δ*tasA*.

The performance of three selected eMP and eNMP representatives (one from each evolved population) against the WT ancestor was additionally determined by calculating the selection rate coefficient. All eMPs showed a positive selection rate and their relative c.f.u. in the pellicle was significantly higher that 50% (Supplementary Fig. 3). However, the ancestor Δ*eps*–Δ*tasA* and eNMPs had negative selection rates, which indicates poor performance during competition with the ancestor WT. Nevertheless, the ancestor Δ*eps*–Δ*tasA* strain showed the poorest performance (selection rate value of -3.36) and all the eNMPs, B310mA, B410mB and B510mC, revealed improved performance compared to the ancestor mutant strain, with selection rate values of -2.59, -1.14 and -2.25, respectively.

Finally, the eNMPs were challenged with the eMPs selected from the corresponding populations (that is, B310mA versus B310wtA or B410mB versus B410wtB). We noticed that the eNMPs from population B310m exhibited a slight decrease in pellicle incorporation compared to their pellicle incorporation when in competition with the ancestor WT (Fig. 3). Overall the eMPs performed better at suppressing the eNMPs as compared to the WT ancestor, however, certain eNMPs from populations B410m and B510m still displayed significantly improved incorporation whether competing against the evolved or ancestor WT (Fig. 3). On the basis of these competition assays, we conclude that evolutionary changes in the Δ*eps*–Δ*tasA* mutant, rather than the WT, resulted in the improved performance of the non-producers in mixed pellicles.

It was further revealed that the incorporation success of the eNMPs did not depend on their initial frequency. Competition assays with different starting ratios of the WT ancestor to each of the eNMPs (B310mA, B410mB and B510mC) revealed that the eNMPs exhibited higher levels of pellicle incorporation regardless of their starting frequency (Supplementary Fig. 1D–F). B310mA, B410mB and B510mC showed an average pellicle incorporation percentage of

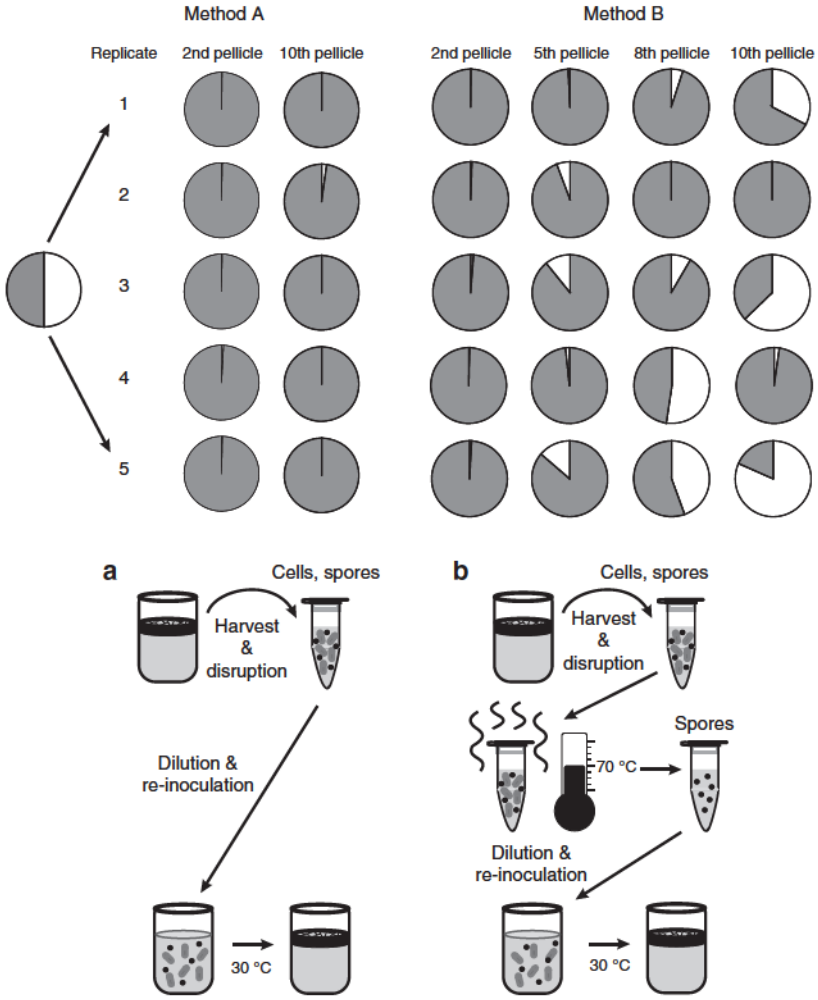

Figure 2 | Fraction of WT and Δ*eps*-Δ*tasA* strains changes during pellicle serial transfer. In transfer method (**a**), the pellicle was harvested, disrupted (see Methods) and the suspension of spores and cells was directly used for inoculation of new medium. After harvest and disruption, the cells in transfer method (**b**) were heat-treated at 70 °C for 15 min to eliminate all vegetative cells. The resulting spore suspension was used to inoculate new medium and was incubated for 2–3 days to allow for pellicle formation. For transfer method (**b**), the gradual change of wild-type (grey) and Δ*eps*-Δ*tasA* (white) ratio during the evolution experiment is also presented. The ratio was followed during evolution experiments using the disrupted pellicle suspension directly. In addition, the ratio was redetermined from frozen glycerol stocks for the second, eighth and tenth pellicles.

9.13% (Pearson's correlation coefficient $r=0.17$), 18% ($r=0.22$) and 27% ($r=0.16$), respectively (Supplementary Fig. 1D–F).

Further experiments also revealed that, in contrast to the ancestor mutant (Supplementary Fig. 1B), the incorporation percentage of the eNMP B310mA was not affected by doubling the concentration of resources in the medium (Supplementary Fig. 1B); the incorporation of the evolved B310mA was $9.54\% \pm 3.04\%$ in $2\times$SG medium and $9.88\% \pm 2.04\%$ in $4\times$SG. These results suggest that the incorporation efficiency of the eNMPs might be driven by a different mechanism from that in the ancestor Δ*eps*–Δ*tasA*.

Incorporation of eNMPs decreases biofilm productivity. A productivity assay was performed to understand the effect of increased incorporation of the eNMPs on the biofilm productivity and to compare the productivity of the eMPs relative to the ancestor WT. Productivity was measured by weighing the whole biomass of the pellicle and is represented as relative productivity compared with the ancestor WT (that is, ancestor WT productivity = 1).

As expected, the productivity of the mixed pellicle consisting of the WT ancestor and mutant ancestor was very similar to the productivity of the WT ancestor grown alone, indicating that the presence of the ancestor Δ*eps*–Δ*tasA* did not affect the biofilm productivity (Fig. 4). This result agrees with our results showing that ancestor Δ*eps*–Δ*tasA* was almost completely outcompeted from the pellicle (Fig. 1a–c). In contrast, the productivity of pellicles containing both the ancestor WT and the eNMPs was lower than the productivity of the monoculture WT (productivity values <1), indicating that the population was negatively affected overall when eNMPs were present (Fig. 4). Interestingly, the eMPs in monocultures (B310wtA, B410wtB and B510wtC) had higher productivity than the WT ancestor (Fig. 4; Supplementary Fig. 4A). Finally, we examined the productivities of the evolved pairs with common evolutionary histories (B310wtA + B310mA; B410wtB + B410mB; and B510wtC + B510mC). For all three pairs, the productivity of the mixed pellicles was lower than the productivity of the ancestor WT; however, these differences were statistically significant only for the pairs B410wtB + B410mB and B510wtC + B510mC (Fig. 4). Nevertheless, in all combinations, the eNMP + eMP productivities were significantly lower than the corresponding eMP productivity, indicating reproducible

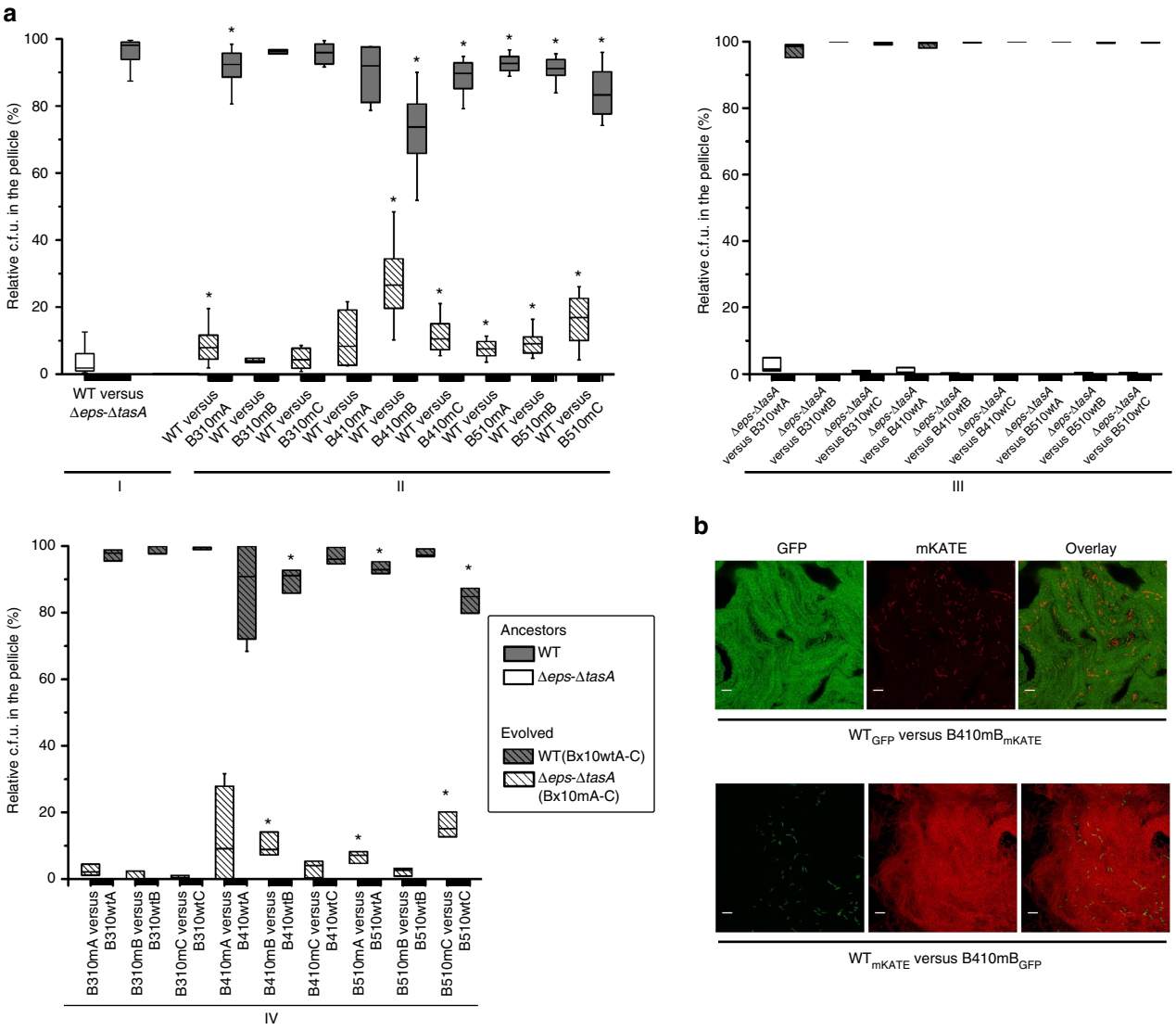

Figure 3 | Pellicle competition assay. (**a**) WT ancestor and Δ*eps*-Δ*tasA* mutant ancestor (I); and WT ancestor and eNMP strains 310mA, 310mB, 310mC, 410 mA, 410mB, 410mC and 510mA, 510mB, 510mC (II). On a separate panel (above right): pellicle competition assay between WT ancestor and Δ*eps*-Δ*tasA* mutant ancestor, eMP strains (three isolates per population, as in **a**) and Δ*eps*-Δ*tasA* mutant ancestor (III). On a panel below: pellicle competition assay between WT ancestor and Δ*eps*-Δ*tasA* mutant ancestor, eMP strains and eNMP strains sharing evolutionary history (IV). Boxes represent Q1–Q3, lines represent the median, and bars span from max to min. Each competition assay was replicated in parallel with the ancestor WT versus Δ*eps*-Δ*tasA* combination at least twice. * in sections II and IV indicate that the relative c.f.u. are significantly different from the relative c.f.u. of WT versus Δ*eps*-Δ*tasA* ancestor competition. (**b**) Confocal microscopy images of pellicle biofilms (left) including swapped fluorescence marker proteins (right). Scale bars, 10 μm.

negative effects of the eNMPs on the productivity of the entire evolved population (Fig. 4). In addition, the pellicles formed by the populations from sequential evolutionary timepoints showed overall decreases in productivity in evolutionary time (Supplementary Fig. 4B), presumably caused by the increasing frequency of eNMPs in pellicles (Fig. 2b).

These results show that although matrix producers evolved a higher productivity, higher incorporation of the coevolved matrix non-producers into the pellicle eventually decreased the overall population productivity.

eMPs and eNMPs contain multiple SNPs in prophage elements. To understand the genetic basis of the observed evolutionary dynamics, the genomes of three eMP and three eNMP populations separated from the 10th transfer of method B cultures (replicates 3, 4 and 5), where the frequency of non-producers was observed to increase during evolution (either gradually or periodically), were subjected to high-throughput sequencing (Supplementary Table 2). The genomes of corresponding three single isolates of eMPs (B310wtA, B410wtB and B510wtC) and three eNMPs (B310mA, B410mB and B510mC) from those populations were also sequenced. In addition, the genomes of the WT ancestor and the Δ*eps*–Δ*tasA* ancestor were resequenced to screen for any single SNPs that emerged before the evolution experiment during standard stock preparation and laboratory procedures. The sequencing of six populations (eMPs B310wt, B410wt and B510wt and eNMPs B310m, B410m and B510m) and six single isolates (B310wtA, B410wtB, B510wtC, B310mA, B410mB and B510mC) revealed multiple single-nucleotide polymorphisms (SNPs) exclusively accumulated in three distinct sites on the chromosome compared to the ancestors: two prophage-like regions previously described as prophage-like element 5 and prophage-like element 6 (ref. 22), and the SPβ prophage region (Supplementary Data 1; Fig. 5a,b). In population B310 there were 617 SNPs, while in populations B410 and B510 the number of SNPs exceeded 1000. More than

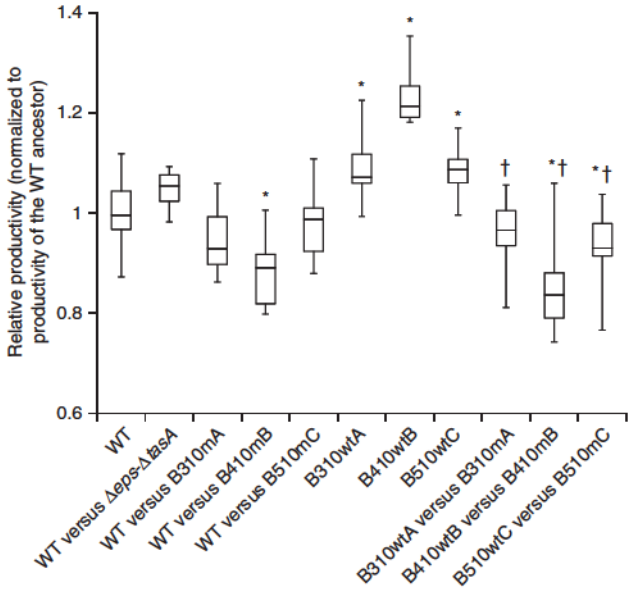

Figure 4 | Productivity assay based on biofilm biomass. Productivity of Δ*eps*-Δ*tasA* ancestor and eNMPs B310mA, B410mB and B510mC, respectively, in co-cultures with WT ancestor, monocultures of eMPs B310wtA, B410wtB and B510wtC, and co-cultures of eNMPs with corresponding eMPs compared to the WT ancestor ($n=10$; *t*-Student; two-tail $P<0.05$). Boxes represent Q1–Q3, lines represent the median, and bars span from max to min. Each WT versus co-culture/eMP comparison was replicated at least twice. *—productivities significantly different from the WT ancestor. †—productivities significantly lower from the corresponding eMP cultures.

50% of SNPs detected in single isolates overlapped with SNPs found in the corresponding populations (Supplementary Data 1; Fig. 6a,b).

Further analysis of the sequenced genomes revealed that there was also a large parallel mutational overlap between the evolutionarily unrelated populations and single isolates (regardless of WT or Δ*eps*–Δ*tasA* background; Supplementary Data 1; Fig. 6a,b). For visual representation of this overlap we produced a windowed-average identity score for the alignment of the entire 134 kbp SPβ region of the evolved strains/populations to the ancestral SPβ (Supplementary Fig. 5A). A global analysis of SNPs from all six single isolates showed that the majority of SNPs represented synonymous substitutions (58%), 17% were non-synonymous but evolutionarily conserved (that is, similar; Blosum62 matrix score$\geq$1), 9% were evolutionarily non-conserved and non-synonymous (Blosum62 matrix score$\leq$0), and the remaining 16% of the substitutions were located in non-coding regions (Supplementary Fig. 5B). We also compared the distributions of SNPs in the eMPs and eNMPs by analysing the functions of affected genes. We observed that eMPs accumulated more SNPs than the corresponding eNMPs, especially in genes related to the toxin production and secretion (Supplementary Data 1; Supplementary Fig. 5D,E). However, most of the affected genes belonged to the unknown function category.

More detailed analyses of the sequencing data on the evolved strains suggested duplications of certain genome fragments and genome rearrangements compared to the ancestors. Duplications were indicated by the increased sequencing coverage within the SNP-containing regions (Supplementary Fig. 6A) and the striking pattern of SNP frequencies (Supplementary Data 1; Supplementary Fig. 6B), which was confirmed by PCR and Sanger sequencing of the particularly highly-mutated SPβ fragment (2,178,034–2,179,407) from the genomic DNA of B310mA and B310wtA (Supplementary Fig. 6*C*). Interestingly, the PCR product obtained from B310mA gave a clear chromatogram with all SNPs present, whereas B310wtA showed a heterogeneous chromatogram with double peaks in the positions of SNPs, one peak coming from an ancestor-like base and the other from the evolved-like base (Supplementary Fig. 6C). In addition, the SPβ fragments could still be amplified by PCR even after deletion of the original SPβ region from the chromosomes of B410mB and B510mC (Supplementary Fig. 6D–F). The identification of genome rearrangements was made after *de novo* assembly of sequencing reads into contigs (Fig. 6c). All of the predicted rearrangements involved sequences belonging to prophage-like elements 5 and 6 and various SPβ fragments, and included the exact regions where multiple SNPs accumulated (Fig. 6c). The presence of two randomly selected rearrangements (contig type 1 and type 4) was confirmed by PCR to occur exclusively in the evolved strains; it did not occur in the ancestor WT or ancestor Δ*eps*–Δ*tasA* (Supplementary Fig. 6G). Altogether, we conclude that the emergence of multiple SNPs in all evolved strains (both eMPs and eNMPs) was linked to duplications and rearrangements within prophage elements in the *B. subtilis* genome. It is important to note that the mutation frequencies of the ancestor and the evolved strains were similar, as confirmed using fluctuation assays (Supplementary Fig. 5C). The obtained mutation frequencies were comparable to previously reported data for other *B. subtilis* strains[23], suggesting that the ancestor strains used here were not hypermutators. Moreover, when the same ancestor strain was evolved for ~350 generations in emulsion droplets, 60 SNPs and short deletions were identified (Eisha Mhatre and Á.T. Kovács, unpublished data).

Hybrid SPβ prophage shows lytic activity towards the ancestors. Rearrangements involving SPβ prophage regions have previously been described as a result of the hybridization of SPβ with another *B. subtilis* phage, phi3T (ref. 24). A hybrid form of SPβ can undergo spontaneous excision from the chromosome to form a pseudolysogen, or it can enter a lytic cycle leading to active phage-particle release[24]. To verify whether the eMPs and eNMPs in the present study spontaneously released phage particles into the medium, phages were precipitated from the supernatants of cultures of selected evolved strains and of the WT ancestor (as a negative control) and visualized by transmission electron microscopy.

No phage particles could be detected in the precipitate obtained from the WT ancestor, which was in line with previous findings[25]. When the WT ancestor was grown in the presence of the prophage-inducing agent mitomycin C, PBSX-like phage particles were detected in its supernatant, which again reproduced previous results[26] (Supplementary Fig. 7A). However, even in the absence of mitomycin C, the evolved strains B410mB and B410wtB released two types of phage particles—PBSX-like particles with a small head and a rigid tail (assignment based on ref. 26), and SPβ-like particles with a big head and a longer, flexible tail (assignment based on an image provided by Vladimir Lazarevic, Hôpitaux Universitaires de Genève, Switzerland, personal communication; Fig. 7a; Supplementary Fig. 7A). The addition of mitomycin C to B410mB and B410wtB cultures resulted in a dramatic increase in the number of SPβ-like phage particles in the culture supernatants (Supplementary Fig. 7A). SPβ-like particles could not be detected in the supernatant of B310mA$^{SP\beta\ -}$ cultures, but were still present in B410mB$^{SP\beta\ -}$ cultures, which corresponded well with the results of molecular analysis, which indicated successful deletion of SPβ from strain B310mA$^{SP\beta\ -}$ but not from B410mB$^{SP\beta\ -}$ (Supplementary Figs 6D–F and 7A).

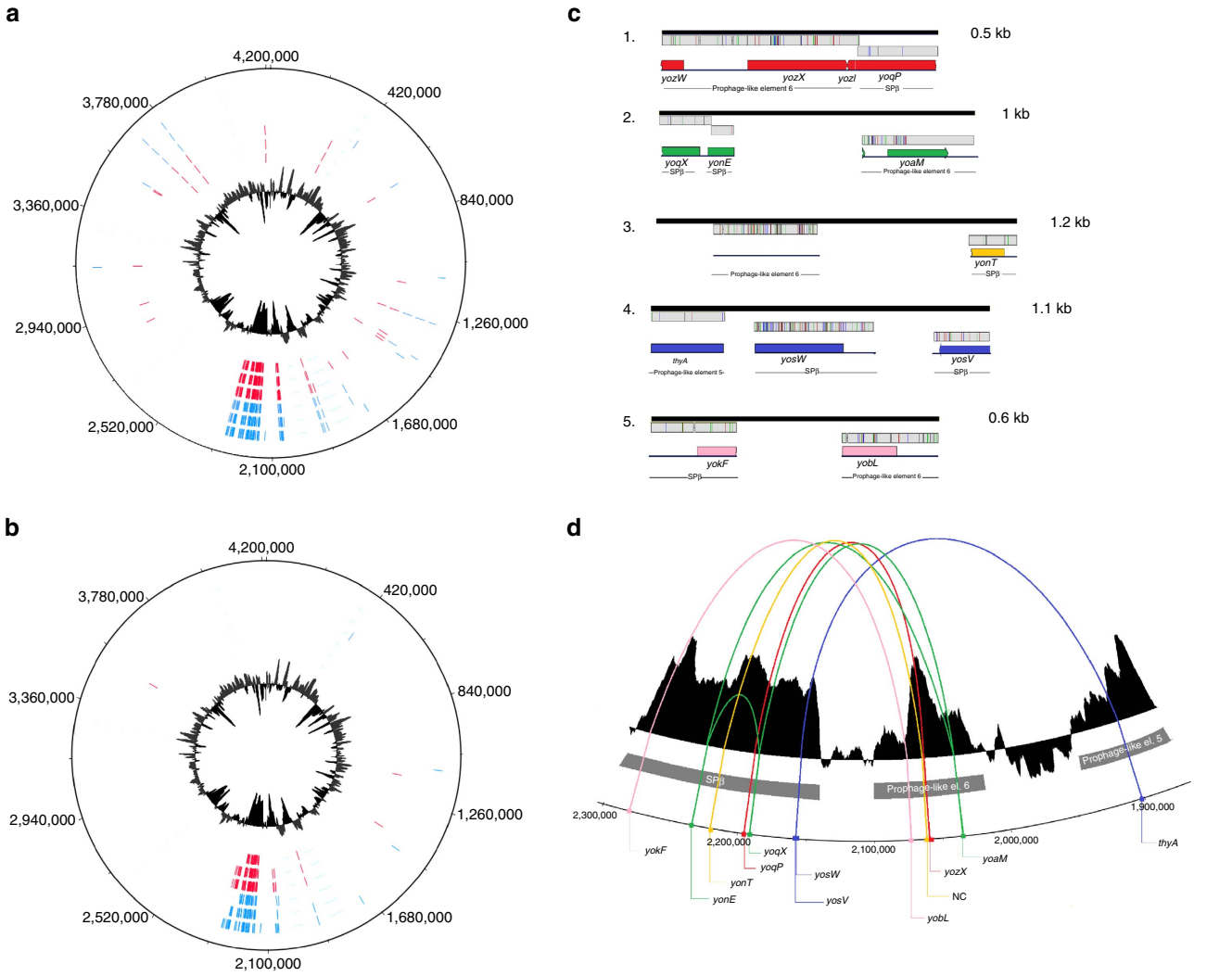

Figure 5 | Multiple SNPs and genome rearrangements are detected in the evolved strains. Genome wide distribution of SNP loci across the evolved *B. subtilis* populations (**a**) and single isolates (**b**) generated using the DNAPlotter tool[56]. (**a**) SNPs from six populations are presented on separate tracks; starting from the outside and moving towards the inside: B310wt, B410wt, B510wt (all shown in blue), B310m, B410m, and B510m (all shown in red). (**b**) SNPs in six isolates are presented on separate tracks; starting from the outside and moving towards the inside: B310wtA, B410wtB, B510wtC (all shown in blue), B310mA, B410mB, and B510mC (all shown in red). Internal black circles represent GC profiles. (**c**) Genome rearrangements predicted for the evolved strains based on bioinformatics analysis of the sequencing data. Black lines represent *de novo* assembled contigs with their sizes indicated on the right, grey boxes show aligned fragments of the reference genome (GenBank accession number AL009126), and stripes show SNP positions. Visualization was performed using Geneious software[57]. Corresponding genes (or non-coding regions) in the reference *B. subtilis* genome are shown below the alignment with different coloration used for each type of rearrangement. (**d**) DNA plotter graphical representation of predicted genome rearrangements (zoom view on the SPβ and prophage-like element 6 and 5 regions). The black histogram represents the GC profile, where three clusters of low-GC content directly correspond to SPβ, prophage-like element 6 and prophage-like element 5. Distantly located genes that participated in rearrangements and became neighbours in the evolved strains are connected by arched lines (different colour used for each rearrangement) and are additionally marked with dots of the same colour. The coloration used for each rearrangement type corresponds to that in **c**.

Next, the lytic activity of the SPβ particles released by the evolved strains was tested against the ancestor strains. A series of plaque assays were performed where each strain served both as a supernatant donor and as potential prey. Neither of the ancestor strains (WT or Δ*eps*–Δ*tasA*) showed lytic activity when serving as the supernatant donor, but they were both susceptible to the lytic activity of almost all supernatants of the evolved strains (Fig. 6b, Supplementary Fig. 7B). Strain B310mA$^{SP\beta-}$ performed exactly the same as the ancestors, showing no lytic activity but displaying susceptibility to all supernatants, including that of B310mA (from which it was derived; Fig. 6b; Supplementary Fig. 7B). Despite the fact that all evolved strains showed lytic activity and immunity, they could be differentiated into strong (for example, B410mB) and moderate levels (for example, B510wtC) (Fig. 6b; Supplementary Fig. 7B). The lytic activity of the supernatants of all evolved populations was assessed, including all five populations from transfer method A and all five populations from transfer method B (Fig. 2). Strong lytic activity towards the ancestor WT strain was found exclusively in populations that showed an increased incorporation of non-producers into the pellicle following the evolution experiment, specifically population 2 from transfer method A, and populations 1, 3, 4 and 5 from transfer method B (Supplementary Fig. 7C). Further, populations that did not show increased incorporation of non-producers and lacked lytic activity towards the ancestor strains did not contain multiple SNPs within the SPβ regions, as confirmed by Sanger sequencing of the 2,178,034–2,179,407 genomic fragment.

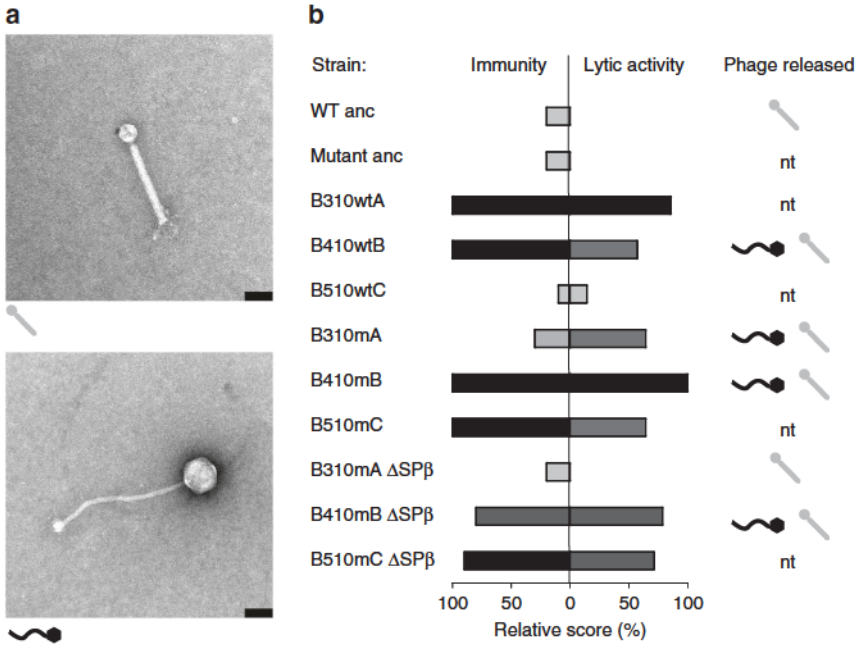

Figure 6 | Lytic phage activity appears in the evolved strains. (**a**) Electron micrographs of phage particles purified from *B. subtilis* supernatants. Upper image shows PBSX-like phage particle released by the ancestor WT only in the presence of mitomycin C, and by all evolved strains in the absence of mitomycin C. The lower image shows SPβ-like phage particle spontaneously released by all evolved strains tested, but not by the ancestor WT or by B310mA$^{SPβ-}$. Scale bars, 70 nm. (**b**) Results of plaque assays performed with the ancestor WT, ancestor Δ*eps*-Δ*tasA* and all the evolved strains, where each strain served both as a supernatant donor and as a potential host. Each strain was given 1 immunity point when resistant to a given supernatant (excluding its own supernatant), and a number of lytic activity points when showing lytic activity towards a given host (excluding itself), depending on the strength of lytic activity. Specifically, the number of points was equal to a maximal log dilution factor where lytic activity was still present (for example, a lytic activity that can still be detected in a conditioned medium diluted to 10^{-3} but not 10^{-4} is denoted with 3 points). Obtained immunity and lytic activity scores were then divided by the maximum value of each and are presented as relative percentages. Darkness of the bars is proportional to immunity/lytic activity scores values. High immunity/lytic activity scores correlated with presence of SPβ-like particles (black in the right-hand column) isolated from the culture medium of those strains. 'nt' indicates media were not tested by transmission electron microscopy. The experiment was independently replicated four times.

Spontaneous phage release by the evolved strains and their lytic activity towards the ancestors suggested that higher incorporation of the eNMPs into pellicles may be the result of newly evolved interference competition. We therefore examined whether the ancestor mutant could acquire the evolved-like phenotype with higher incorporation pellicle properties through a single-phage transduction step. For the infection assay, a 1:1 mixture of the WT and Δ*eps*–Δ*tasA* ancestors was introduced into standard 2 × SG medium supplemented with phage precipitate obtained from B410mB where the presence of SPβ-like phage particles was detected. After a single growth cycle, three colonies of the WT and three colonies of Δ*eps*–Δ*tasA* were isolated and their acquired lytic activity towards the ancestor strains was assessed. Finally, pellicle competition assays were performed using the WT ancestor and the three Δ*eps*–Δ*tasA* strains isolated from the infected population (ImA, ImB and ImC). As expected, the phage-infected strains behaved similarly to the evolved mutants, showing >4-fold (in the case of ImA) and >2.5-fold (ImB and ImC) increased incorporation rates into the pellicle compared with the ancestor mutant (Fig. 7).

Phage release facilitates higher pellicle inclusion of eNMPs. Finally, we asked whether the presence of an identical active phage variant in both producers and non-producers is sufficient to explain the higher incorporation of the eNMPs into pellicles. This was first tested by assaying the infected mutants (ImA, ImB and ImC) with the infected WT strains (Supplementary Fig. 8). No increased pellicle incorporation of the mutants was observed, indicating that higher incorporation of the mutants cannot be explained by a general increase of phage activity in the entire population (Supplementary Fig. 8), but is due instead to subtle differences within phage elements of evolved non-producers and producers.

This was further confirmed by a fitness assay that involved Δ*eps*–Δ*tasA* and WT strains with an isogenic evolved background. Isogenic evolved WT and mutant strains were obtained simply by introducing the Δ*eps*–Δ*tasA* deletions into eMPs. Genome resequencing confirmed that the obtained Δ*eps*–Δ*tasA* strains still contained the genetic background of corresponding eMPs (Supplementary Data 1). When the eMPs B310wtA, B410wtB and B510wtC were competed against their direct derivatives B310wtA$^{Δeps–ΔtasA}$, B410wtB$^{Δeps–ΔtasA}$, and B510wtC$^{Δeps–ΔtasA}$, respectively, a very low pellicle incorporation percentage of the mutants was observed, which was comparable to the performance of the ancestor Δ*eps*–Δ*tasA* against the ancestor WT (Supplementary Fig. 8). As expected, competition assays with the WT ancestor revealed that the transformants had comparable incorporation probabilities to the eNMPs (Fig. 7). These results indicated that although producers and non-producers showed very similar general adaptation patterns involving major changes in mobile genetic elements, some of these changes were specific to the evolved non-producers, resulting in their improved incorporation into pellicles, most likely through an advantage in interference competition.

Discussion

Stability of cooperative interactions can determine the performance of microbes in most medically and biotechnologically relevant situations[27–32]. In recent years, understanding of microbial group behaviours and the mechanisms that prevent

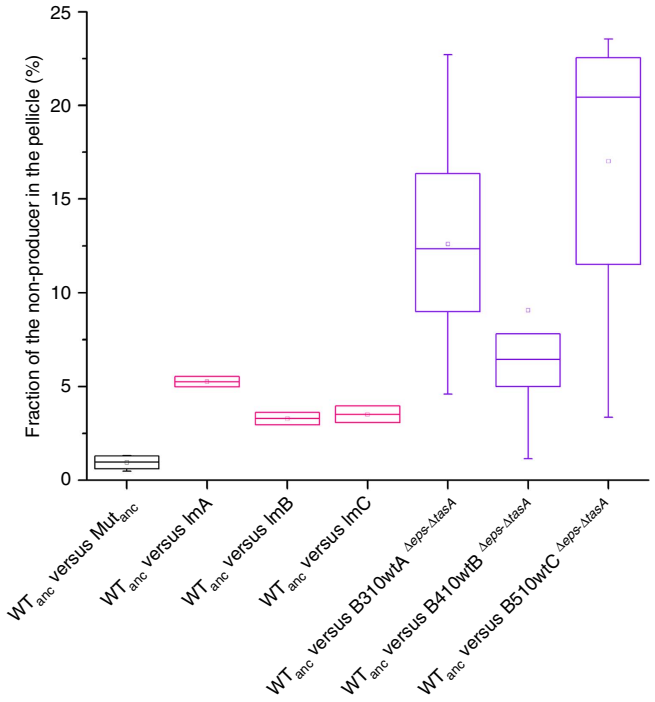

Figure 7 | Evolved mutants and ancestor mutants hosting the evolved phage have increased incorporations into the pellicle. Competition assay between the WT ancestor and Δ*eps*-Δ*tasA* ancestor (control) ($n=7$); between the WT ancestor and three single colonies obtained after transduction of the Δ*eps*-Δ*tasA* ancestor with phage particles released by eNMP B410mB ($n=2$); and between the WT ancestor and eMPs (B310wtA, B410wtB, and B510wtC) with deleted *eps* and *tasA* ($n=10$; $n=10$; $n=7$, respectively). Boxes represent Q1-Q3, lines represent the median, and bars span from max to min. Each competition assay in parallel with the ancestor WT versus Δ*eps*-Δ*tasA* was replicated at least twice.

spreading of non-cooperative mutants has become one of the key aims of sociomicrobiology. Long timescale evolutionary experiments have already demonstrated the evolutionary plasticity of social interactions in various bacterial models[18,33,34]. Here we describe a scenario where a biofilm matrix non-producer that is initially eliminated from the population increases its performance over longer timescales and evolves the ability to better incorporate into the biofilm. The evolution of improved invasion of biofilms by non-producers was previously observed by Zhang *et al.*[15]. They excluded the possibility of general adaptation being responsible for the changed social dynamics in biofilms since the evolved producer did not increase its performance towards the ancestor producer. In the present work, an increased selection coefficient and improved productivity of the evolved WT could be observed in monocultures; the same, unfortunately, could not be tested for the evolved mutants because of their inability to form pellicles in monocultures. We therefore hypothesize that the evolved increased-biofilm-incorporation-ability of the mutant was a side effect of extremely fast general adaptation of both producer and non-producers driven by mobile genetic elements. Interestingly, the improved incorporation of the non-producers into biofilms was not reproduced when both WT and non-producer strains had identical evolved genetic backgrounds (that of the evolved WT strains). This means that although the general adaptation pattern in the entire population was very similar, the non-producers are evolutionarily ahead of the producers and carry certain specific changes that allow their improved performance in incorporation into biofilms formed by the evolved WT strains. We believe those specific differences are hidden within prophage elements of the evolved strains, and they could be revealed by *de novo* sequencing in the future.

In the ancestral population, the matrix non-producers (Δ*eps*–Δ*tasA*, which do not secrete two key matrix components Eps and TasA) can hardly incorporate into pellicle biofilms formed by the WT. This result was rather unexpected for two reasons: first, previous work demonstrated that both Eps and TasA are shared with non-producing strains[20], and, second, the production of at least one of those compounds (Eps) was proven to be costly and exploitable[13]. Although we did not study the competition mechanism in detail, a positive correlation between fitness, initial Δ*eps*–Δ*tasA* frequency and resource availability suggests that in the ancestral population the growth of Δ*eps*–Δ*tasA* is not only limited by the lack of oxygen, but also by carbon resources. We speculate that this is caused by a delay in surface co-colonization of Δ*eps*–Δ*tasA*, because the producer can partially privatize the matrix components. Since the WT is released from oxygen-limitation first, it can quickly deplete the remaining carbon resources, preventing further growth of the mutant. This model, however, awaits further studies.

The pellicle incorporation mechanism of evolved Δ*eps*–Δ*tasA* does not depend on resource concentration or on the initial frequency of the mutant in the co-culture. It is likely that new antagonistic interactions involving infection and lysis of the ancestor WT by the evolved mutant delay surface colonization by the WT, giving the mutant a prolonged window of opportunity for co-colonization. A similar mechanism could play a role in the competition between the evolved mutant and the evolved WT, since the evolved WT strains spontaneously release phages into the medium and show a delay in pellicle formation.

How did the new lytic properties evolve? We believe that multiple rearrangements in the genomes of the evolved strains, combined with series of SNPs in regions that were rearranged, resulted in new lytic properties of the normally inactive domesticated SPβ prophage. Since this scenario was more likely to occur on sporulation treatment (that is, treatment method B), we suspect that the multiple heat-treatments involved in this treatment might have promoted phage activation[35] or even rearrangements of phage elements in the genome[36]. The accumulation of multiple SNPs and rearrangements resembles the previously reported evolutionary response of the *Streptococcus thermophilus* phage to the host's CRISPR system[37], however, no CRISPR/Cas has yet been identified in *B. subtilis*. Alternatively, rapid diversification within prophage regions combined with lytic induction may be a universal adaptive pattern of bacteria to a biofilm lifestyle, as it was previously also observed during experimental evolution of *Pseudomonas aeruginosa* biofilms[38]. Our work also demonstrates how such newly evolved phage warfare shifts social dynamics in the bacterial population in favour of biofilm non-producers. The dynamics of host-phage interactions is long studied in various experimental systems[39]. It was previously observed that lytic phages can shift the balance in competitive interactions by reducing the frequency of a winning partner[40], or impair biofilm formation ability as a trade-off for phage immunity[41]. We hypothesize that in the case of the *B. subtilis* pellicles, the disadvantage of matrix producers could originate from the degeneration of toxin/secretion-related genes in the evolved wild-types that in turn became less efficient competitors than the evolved mutants.

The improved fitness of the evolved WT strain in monoculture could be a direct result of the evolved spontaneous phage release. Normally, the excision of the SPβ prophage from the *B. subtilis* chromosome takes place before sporulation and allows reconstitution of the *spsM* gene involved in spore polysaccharide

biosynthesis[42]. Sanchez-Vizuete *et al.*[43] demonstrated that removal of SPβ from the chromosome permanently restores *spsM*, resulting in increased biofilm thickness. We presume that frequent spontaneous excision of SPβ, or even pseudolysogeny (as demonstrated in ref. 24) in the evolved WT strains, could positively contribute to the biofilm productivity through *spsM* reconstitution. Excision of prophage from the host chromosome was recently linked to improved biofilm formation by *Shewanella oneidensis* facing cold stress[44]. Such a phage excision benefited the host through gene inactivation rather than reconstitution (as observed in ref. 43). Similar genetic switches triggered by prophage excision were also described in several other species (reviewed in ref. 45).

The *B. subtilis* SPβ prophage carries a bacteriocin-immunity system[46], several putative toxin–antitoxin systems[47] and cell wall hydrolases[48]. Several SPβ segments of >250 nucleotides exhibit >90% identity with *B. subtilis* chromosomal regions[25] promoting recombination events, especially in naturally competent strains. Not surprisingly, recent reports strongly indicate a key role of phage elements in rapid evolution of kin recognition mechanisms and antagonistic interactions between closely related, sympatric *B. subtilis* strains[49,50]. Accumulation of SNPs in the SPβ region was also observed in the evolution experiments of Overkamp *et al.*[51], where *B. subtilis* was kept in zero-growth conditions for 42 days. Among hundreds of SNPs discovered by Overkamp *et al.*[51], 80% overlapped with the SNPs reported in this study. In addition, most of the SNPs detected were synonymous and evolutionarily conserved, suggesting selection against loss of function. Recent reports show that even non-synonymous mutations can positively contribute to fitness[52,53]. This again suggests that mutations or rearrangements within phage elements can be a very important evolutionary force in *B. subtilis*, with a major impact on social interactions. Recently, the profound impact of prophages on the evolution of a pathogenic bacterium was experimentally demonstrated in *P. aeruginosa* biofilms[54], where the presence of phages resulted in strong selection against phage recognition elements (type IV pilus), at the same time enhancing parallel evolution[54]. Similar selective pressure could emerge after fast evolution of active SPβ variants in *B. subtilis* biofilms, resulting in striking parallelism in evolved populations of both WT and Δ*eps*–Δ*tasA* bacteria.

Our work demonstrates how social dynamics in an initially very robust biofilm can be shifted by unexpected evolutionary events. We show that an adaptive genotype that is quickly tailored by mobile genetic elements can easily spread through horizontal gene transfer. The same adaptive path, although beneficial for the producer, became maladaptive in a mixed population where producers coexisted with non-producers.

Methods

Strains and cultivation conditions. Supplementary Table 1 describes strains used in this study and construction of their mutant derivatives. Strain *B. subtilis* 168 hymKATE P_{tapA}-yfp was obtained by transforming the laboratory strain, *B. subtilis* 168, with genomic DNA from DL821 and selecting for MLS resistance. Subsequently, the created strain was transformed with genomic DNA from 168 hymKate and selecting on chloramphenicol resistance and for the loss of amylase activity. The Δ*eps* and Δ*tasA* strains were obtained by transforming the 168 strains with genomic DNA isolated from DL1032 and specifically selecting for tetracycline or kanamycin resistance, respectively. The double mutant Δ*eps*–Δ*tasA* was obtained by transforming 168 Δ*eps* with genomic DNA from DL1032 and selecting on the kanamycin marker. The Δ*eps*–Δ*tasA* hyGFP and Δ*eps*–Δ*tasA* hymKate strains were obtained by transforming the Δ*eps*–Δ*tasA* strain with genomic DNA obtained from 168 hyGFP and 168 hymKate, respectively. Deletion of *epsA-O* and *tasA* genes were confirmed with PCR using oligos described in Supplementary Table 3. Strains were maintained in LB medium (Lennox broth; Carl Roth, Germany), while 2 × SG medium was used for biofilm induction[55].

Experimental evolution and competition assays. Experimental evolution was performed using co-cultures of fluorescently labelled but otherwise WT and Δ*eps*–Δ*tasA* strains grown in 2 ml 2 × SG medium statically in a 24-well plate at 30 °C for 2–3 days. For transfer method A, the mature pellicles were harvested, mildly disrupted, and reinoculated after 100 × dilution. For transfer method B, the pellicles were additionally heat-treated after disruption and diluted × 20 during reinoculation. The sporulation frequency in the conditions applied in the evolution experiment was about 20% (Supplementary Fig. 2). To maintain similar selection bottlenecks in the two transfer methods, a fivefold lower dilution factor was used in transfer method B.

After the 2nd, 8th and 10th pellicle transfers, frozen stocks were preserved. Evolved populations or single isolates were isolated by selecting with appropriate antibiotics. Competition experiments were performed by mixing certain ratios of 100-fold diluted LB-pregrown cultures which were then incubated in static pellicle forming conditions for 3 days or in agitated planktonic cultures for 16 h. The numbers of c.f.u. of the inocula and the final cultures were determined on LB-agar plates containing selective antibiotics, incubated overnight at 37 °C. Prior the c.f.u. assays, pellicles were sonicated according to a protocol optimized in our laboratory (2 cycles each containing 12 × 1 s pulses at 20% amplitude with 1 s pause between the pulses), that ensured efficient disruption of biofilm clumps (as verified by microscopy) and therefore accurate total cell counts in the pellicles.

Microscopy. Bright field images of whole pellicles were obtained with an Axio Zoom V16 stereomicroscope (Carl Zeiss, Jena, Germany) equipped with a Zeiss CL 9000 LED light source and an AxioCam MRm monochrome camera (Carl Zeiss). The pellicles were also analysed using a confocal laser scanning microscope (LSM 780 equipped with an argon laser, Carl Zeiss) and Plan-Apochromat/1.4 Oil DIC M27 × 63 objective. Fluorescent reporter excitation was performed with the argon laser at 488 nm and the emitted fluorescence was recorded at 484–536 nm and 567–654 nm for GFP and mKate, respectively. To generate pellicle images, Z-stack series with 1 μm steps were acquired. Zen 2012 Software (Carl Zeiss) was used for both stereomicroscopy and CLSM image visualization.

Productivity assay. For productivity assays, pellicles were inoculated into 4 ml of 2 × SG medium placed in 35 mm-diameter Petri dishes and incubated for 3 days at 30 °C. Next, the medium fraction was removed, and pellicles were dried at 55 °C for 3 h. The dry biomass was determined on an analytical balance.

Fluctuation assay. To determine the mutation rate, single colonies were picked from LB-agar medium and cultivated for 18 h in LB broth at 37 °C. After 100-times dilution in 2 × SG medium, cultures ($n = 10$ for each strain) were subsequently cultivated for 18 h with vigorous shaking, and dilution series were plated on LB-agar medium to assay the frequency of streptomycin (50 μg ml^{-1}) resistant c.f.u. after 18–24 h at 37 °C.

Genome resequencing and genome analysis. Genomic DNA of selected populations or isolated strains was isolated using the EURex Bacterial and Yeast Genomic DNA Kit from cultures grown for 18 h. For the evolved population, single-end fragment reads were sequenced using a Life Technologies SOLiD 5500xl sequencer. Base-calling was carried out with the software provided by the supplier. All other downstream analysis steps were done in CLC Genomics Workbench Tool 7.0.4. Reads were length-filtered, keeping only ≥50 nucleotide long fragments. Mapping used only those reads that displayed ≥80% similarity to the reference genome (GenBank accession number AL009126) over ≥60% of the read length (meaning an alignment of ≥30 nucleotides having ≥24 identical matches). Non-specific reads were randomly placed to one of their possible genomic locations. Quality-based SNP and small in/del variant calling was carried out requiring ≥10 × read coverage with ≥20% variant frequency. Only variants suggested by good quality bases (Q≥20) were taken into account. Furthermore, mutations had to be supported by evidence from both DNA strands.

For single isolate strains, paired-end fragment reads (2 × 250 nucleotides) were generated using an Illumina MiSeq sequencer. Primary data analysis (base-calling) was carried out with MiSeq Reporter software (Illumina). All further analysis steps were done in CLC Genomics Workbench Tool 8.0.2. Reads were quality-trimmed using an error probability of 0.05 (Q13) as the threshold. Reads that displayed ≥80% similarity to the reference genome (GenBank accession number AL009126) over ≥80% of their read lengths were used in mapping. Non-specific reads were randomly placed to one of their possible genomic locations. Quality-based SNP and small In/Del variant calling was carried out requiring ≥40 × read coverage with ≥20% variant frequency. Only variants supported by good quality bases (Q≥20) were taken into account and only if they were supported by evidence from both DNA strands. Selected genomic regions were validated by Sanger sequencing (GATC Biotech, Konstanz, Germany) using oligos listed in Supplementary Table 3.

Transmission electron microscopy analysis. Selected bacterial strains were grown overnight in LB medium at 37 °C with shaking at 200 r.p.m. In the case of mitomycin-C-treated cultures, mitomycin C was added in late exponential phase to a final concentration of 0.5 μg ml^{-1}. Culture supernatants were collected, mixed at a 1:4 ratio with PEG-8000 solution (PEG-8000 20%, 2 M NaCl), incubated on ice for at least 90 min and finally centrifuged (20 min, 7,600 r.p.m.) to obtain

precipitate. The pellet was resuspended in 10% of the original supernatant volume in TBS solution (50 mM Tris-HCl, 150 mM NaCl, pH 7), incubated on ice for 90 min and centrifuged (20 min, 7600 r.p.m.). Supernatant was carefully transferred to clean Eppendorf tubes. Purified samples (100 µl) were adsorbed onto duplicate 400 mesh carbon-coated Cu grids (Quantifoil, Großlöbichau, Germany) for 2 min. Before use, the carbon grids were hydrophilized by 30 s of electric glow discharging. The grids were washed twice in distilled water and stained for 30 s with 1% uranyl acetate. Virus morphologies were examined using a Zeiss CEM 902A transmission electron microscope (Carl Zeiss AG, Oberkochen, Germany). At least 20 images were taken per sample at different magnifications using a 1k FastScan CCD-Camera (camera and software from TVIPS, Munich, Germany).

Statistical analyses. Statistical differences between two experimental groups were identified using two-tailed Student's *t*-tests assuming equal variance. Variances in the two main types of datasets (c.f.u. counts in competition assays and weight of biomass) were similar across different samples. One data point with a value greater than the mean plus 3 times the s.d. was removed from the dataset of $n>10$ as an outlier. Normal distributions within the two main data types (biomass and c.f.u.) were confirmed by Kolmogorov–Smirnov ($P>0.05$). No statistical methods were used to predetermine sample size and the experiments were not randomized.

Data availability. The genome resequencing data are available in Supplementary Data 1. The authors declare that all other relevant data supporting the findings of the study are available within the article and its Supplementary Information files, or from the corresponding author upon request.

References

1. Costerton, J. W., Lewandowski, Z., Caldwell, D. E., Korber, D. R. & Lappin-Scott, H. M. Microbial biofilms. *Annu. Rev. Microbiol.* **49,** 711–745 (1995).
2. Hall-Stoodley, L., Costerton, J. W. & Stoodley, P. Bacterial biofilms: from the natural environment to infectious diseases. *Nat. Rev. Microbiol.* **2,** 95–108 (2004).
3. Røder, H. L., Sørensen, S. J. & Burmølle, M. Studying bacterial multispecies biofilms: where to start? *Trends Microbiol.* **24,** 503–513 (2016).
4. Martin, M., Hölscher, T., Dragos, A., Cooper, V. S. & Kovács, Á. T. Laboratory evolution of microbial interactions in bacterial biofilms. *J. Bacteriol.* **198,** 2564–2571 (2016).
5. Steenackers, H. P., Parijs, I., Foster, K. R. & Vanderleyden, J. Experimental evolution in biofilm populations. *FEMS Microbiol. Rev.* **40,** 373–397 (2016).
6. Rainey, P. B. & Travisano, M. Adaptive radiation in a heterogeneous environment. *Nature* **394,** 69–72 (1998).
7. Udall, Y. C., Deeni, Y., Hapca, S. M., Raikes, D. & Spiers, A. J. The evolution of biofilm-forming Wrinkly Spreaders in static microcosms and drip-fed columns selects for subtle differences in wrinkleality and fitness. *FEMS. Microbiol. Ecol.* **91,** fiv057 (2015).
8. Hammerschmidt, K., Rose, C. J., Kerr, B. & Rainey, P. B. Life cycles, fitness decoupling and the evolution of multicellularity. *Nature* **515,** 75–79 (2014).
9. Hardin, G. The tragedy of the commons. The population problem has no technical solution; it requires a fundamental extension in morality. *Science* **162,** 1243–1248 (1968).
10. Xavier, J. B. & Foster, K. R. Cooperation and conflict in microbial biofilms. *Proc. Natl Acad. Sci. USA* **104,** 876–881 (2007).
11. Irie, Y. *et al.* The *Pseudomonas aeruginosa* PSL polysaccharide is a social but non-cheatable trait in biofilms. Preprint at *bioRxiv* http://dx.doi.org/10.1101/049783 (2016).
12. Srinandan, C. S., Elango, M., Gnanadhas, D. P. & Chakravortty, D. Infiltration of matrix-non-producers weakens the *Salmonella* biofilm and impairs its antimicrobial tolerance and pathogenicity. *Front. Microbiol.* **6,** 1468 (2015).
13. van Gestel, J., Weissing, F. J., Kuipers, O. P. & Kovács, Á. T. Density of founder cells affects spatial pattern formation and cooperation in *Bacillus subtilis* biofilms. *ISME J.* **8,** 2069–2079 (2014).
14. Nadell, C. D., Drescher, K., Wingreen, N. S. & Bassler, B. L. Extracellular matrix structure governs invasion resistance in bacterial biofilms. *ISME J.* **9,** 1700–1709 (2015).
15. Zhang, Q. G., Buckling, A., Ellis, R. J. & Godfray, H. C. Coevolution between cooperators and cheats in a microbial system. *Evolution* **63,** 2248–2256 (2009).
16. Manhes, P. & Velicer, G. J. Experimental evolution of selfish policing in social bacteria. *Proc. Natl Acad. Sci. USA* **108,** 8357–8362 (2011).
17. Kümmerli, R. *et al.* Co-evolutionary dynamics between public good producers and cheats in the bacterium *Pseudomonas aeruginosa*. *J. Evol. Biol.* **28,** 2264–2274 (2015).
18. Fiegna, F., Yu, Y. T., Kadam, S. V. & Velicer, G. J. Evolution of an obligate social cheater to a superior cooperator. *Nature* **441,** 310–314 (2006).
19. Hölscher, T. *et al.* Motility, chemotaxis and aerotaxis contribute to competitiveness during bacterial pellicle biofilm development. *J. Mol. Biol.* **427,** 3695–3708 (2015).
20. Branda, S. S., Chu, F., Kearns, D. B., Losick, R. & Kolter, R. A major protein component of the *Bacillus subtilis* biofilm matrix. *Mol. Microbiol.* **59,** 1229–1238 (2006).
21. Madsen, J. S. *et al.* Facultative control of matrix production optimizes competitive fitness in *Pseudomonas aeruginosa* PA14 biofilm models. *Appl. Environ. Microbiol.* **81,** 8414–8426 (2015).
22. Kunst, F. *et al.* The complete genome sequence of the gram-positive bacterium *Bacillus subtilis*. *Nature* **390,** 249–256 (1997).
23. Viret, J. F. & Alonso, J. C. A new mutator strain of *Bacillus subtilis*. *Mol. Gen. Genet.* **208,** 353–356 (1987).
24. Spancake, G. A., Hemphill, H. E. & Fink, P. S. Genome organization of SPbeta c2 bacteriophage carrying the *thyP3* gene. *J. Bacteriol.* **157,** 428–434 (1984).
25. Lazarevic, V. *et al.* Nucleotide sequence of the *Bacillus subtilis* temperate bacteriophage SPβc2. *Microbiology* **145,** 1055–1067 (1999).
26. Okamoto, K. *et al.* Properties of the defective phage of *Bacillus subtilis*. *J. Mol. Biol.* **34,** 413–428 (1968).
27. Inglis, R. F., Gardner, A., Cornelis, P. & Buckling, A. Spite and virulence in the bacterium *Pseudomonas aeruginosa*. *Proc. Natl Acad. Sci. USA* **106,** 5703–5707 (2009).
28. Itoh, T. *et al.* Cooperative degradation of chitin by extracellular and cell surface-expressed chitinases from *Paenibacillus* sp. strain FPU-7. *Appl. Environ. Microbiol.* **79,** 7482–7490 (2013).
29. Katsuyama, C. *et al.* Complementary cooperation between two syntrophic bacteria in pesticide degradation. *J. Theor. Biol.* **256,** 644–654 (2009).
30. Li, Y. H. & Tian, X. Quorum sensing and bacterial social interactions in biofilms. *Sensors (Basel)* **12,** 2519–2538 (2012).
31. Pollitt, E. J., West, S. A., Crusz, S. A., Burton-Chellew, M. N. & Diggle, S. P. Cooperation, quorum sensing, and evolution of virulence in *Staphylococcus aureus*. *Infect. Immun.* **82,** 1045–1051 (2014).
32. Raymond, B., West, S. A., Griffin, A. S. & Bonsall, M. B. The dynamics of cooperative bacterial virulence in the field. *Science* **337,** 85–88 (2012).
33. Andersen, S. B., Marvig, R. L., Molin, S., Krogh Johansen, H. & Griffin, A. S. Long-term social dynamics drive loss of function in pathogenic bacteria. *Proc. Natl Acad. Sci. USA* **112,** 10756–10761 (2015).
34. Velicer, G. J., Kroos, L. & Lenski, R. E. Loss of social behaviors by *Myxococcus xanthus* during evolution in an unstructured habitat. *Proc. Natl Acad. Sci. USA* **95,** 12376–12380 (1998).
35. Siegel, E. C. & Marmur, J. Temperature-sensitive induction of bacteriophage in *Bacillus subtilis* 168. *J. Virol.* **4,** 610–618 (1969).
36. Kawamura, F., Saito, H. & Ikeda, Y. A method for construction of specialized transducing phage rho 11 of *Bacillus subtilis*. *Gene* **5,** 87–91 (1979).
37. Paez-Espino, D. *et al.* CRISPR immunity drives rapid phage genome evolution in *Streptococcus thermophilus*. *MBio* **6,** e00262-15 (2015).
38. McElroy, K. E. *et al.* Strain-specific parallel evolution drives short-term diversification during *Pseudomonas aeruginosa* biofilm formation. *Proc. Natl Acad. Sci. USA* **111,** E1419–E1427 (2014).
39. Lenski, R. E. & Levin, B. R. Constraints on the coevolution of bacteria and virulent phage: a model, some experiments, and predictions for natural communities. *Am. Nat.* **125,** 585–602 (1985).
40. Brockhurst, M. A., Fenton, A., Roulston, B. & Rainey, P. B. The impact of phages on interspecific competition in experimental populations of bacteria. *BMC. Ecol.* **6,** 19 (2006).
41. Brockhurst, M. A., Buckling, A. & Rainey, P. B. The effect of a bacteriophage on diversification of the opportunistic bacterial pathogen, *Pseudomonas aeruginosa*. *Proc. Biol. Sci.* **272,** 1385–1391 (2005).
42. Abe, K. *et al.* Developmentally-regulated excision of the SPbeta prophage reconstitutes a gene required for spore envelope maturation in *Bacillus subtilis*. *PLoS Genet.* **10,** e1004636 (2014).
43. Sanchez-Vizuete, P. *et al.* Identification of *ypqP* as a new *Bacillus subtilis* biofilm determinant that mediates the protection of *Staphylococcus aureus* against antimicrobial agents in mixed-species communities. *Appl. Environ. Microbiol.* **81,** 109–118 (2015).
44. Zeng, G. *et al.* Cold adaptation regulated by cryptic prophage excision in *Shewanella oneidensis*. *ISME J.* **10,** 2787–2800 (2016).
45. Feiner, R. *et al.* A new perspective on lysogeny: prophages as active regulatory switches of bacteria. *Nat. Rev. Microbiol.* **13,** 641–650 (2015).
46. Dubois, J. Y. *et al.* Immunity to the bacteriocin sublancin 168 Is determined by the SunI (YolF) protein of *Bacillus subtilis*. *Antimicrob. Agents Chemother.* **53,** 651–661 (2009).
47. Jahn, N., Preis, H., Wiedemann, C. & Brantl, S. BsrG/SR4 from *Bacillus subtilis* - the first temperature-dependent type I toxin-antitoxin system. *Mol. Microbiol.* **83,** 579–598 (2012).
48. Sudiarta, I. P., Fukushima, T. & Sekiguchi, J. *Bacillus subtilis* CwlP of the SPβ prophage has two novel peptidoglycan hydrolase domains, muramidase and cross-linkage digesting D-endopeptidase. *J. Biol. Chem.* **285,** 41232–41243 (2010).
49. Lyons, N. A., Kraigher, B., Stefanic, P., Mandic-Mulec, I. & Kolter, R. A combinatorial Kin discrimination system in *Bacillus subtilis*. *Curr. Biol.* **26,** 733–742 (2016).

50. Stefanic, P., Kraigher, B., Lyons, N. A., Kolter, R. & Mandic-Mulec, I. Kin discrimination between sympatric *Bacillus subtilis* isolates. *Proc. Natl Acad. Sci. USA* **112**, 14042–14047 (2015).
51. Overkamp, W. *et al.* Physiological and cell morphology adaptation of *Bacillus subtilis* at near-zero specific growth rates: a transcriptome analysis. *Environ. Microbiol.* **17**, 346–363 (2015).
52. Agashe, D. *et al.* Large-effect beneficial synonymous mutations mediate rapid and parallel adaptation in a bacterium. *Mol. Biol. Evol.* **33**, 1542–1553 (2016).
53. Bailey, S. F., Hinz, A. & Kassen, R. Adaptive synonymous mutations in an experimentally evolved *Pseudomonas fluorescens* population. *Nat. Commun.* **5**, 4076 (2014).
54. Davies, E. V. *et al.* Temperate phages both mediate and drive adaptive evolution in pathogen biofilms. *Proc. Natl Acad. Sci. USA* **113**, 8266–8271 (2016).
55. Kobayashi, K. *Bacillus subtilis* pellicle formation proceeds through genetically defined morphological changes. *J. Bacteriol.* **189**, 4920–4931 (2007).
56. Carver, T., Thomson, N., Bleasby, A., Berriman, M. & Parkhill, J. DNAPlotter: circular and linear interactive genome visualization. *Bioinformatics* **25**, 119–120 (2009).
57. Kearse, M. *et al.* Geneious Basic: an integrated and extendable desktop software platform for the organization and analysis of sequence data. *Bioinformatics* **28**, 1647–1649 (2012).

Acknowledgements

We are grateful to Christian Kost and Michael Brockhurst for helpful discussions. *B. subtilis* strain SPmini was kindly provided by Prof Tsutomu Sato (Research Center of Micro-Nano Technology, Hosei University). This work was funded by grant KO4741/2-1 from the Deutsche Forschungsgemeinschaft (DFG) within the priority program SPP1617 and a Startup Fund from Jena School for Microbial Communications (JSMC). MG was supported by GINOP-2.3.2-15-2016-00011 (EU Structural Funds). T.H. and A.D. were supported by International Max Planck Research School and Alexander von Humboldt foundation fellowships, respectively.

Author contributions

A.T.K. conceived the project; M.M., A.D., T.H., and A.T.K. designed the research; M.M., A.D. and T.H. performed the research; M.M., A.D. and T.H. analysed the data; M.W. performed the electron microscopy; G.M. and B.B. performed and analysed genome resequencing; and M.M., A.D., T.H., and A.T.K. wrote the paper.

Additional information

Supplementary Information accompanies this paper at http://www.nature.com/naturecommunications

Competing interests: The authors declare no competing financial interests.

Reprints and permission information is available online at http://npg.nature.com/reprintsandpermissions/

How to cite this article: Martin, M. *et al. De novo* evolved interference competition promotes the spread of biofilm defectors. *Nat. Commun.* **8**, 15127 doi: 10.1038/ncomms15127 (2017).

Publisher's note: Springer Nature remains neutral with regard to jurisdictional claims in published maps and institutional affiliations.

Chapter 4

Division of labor during biofilm matrix production

Published in Current Biology (2018)

Article

Current Biology

Division of Labor during Biofilm Matrix Production

Graphical Abstract

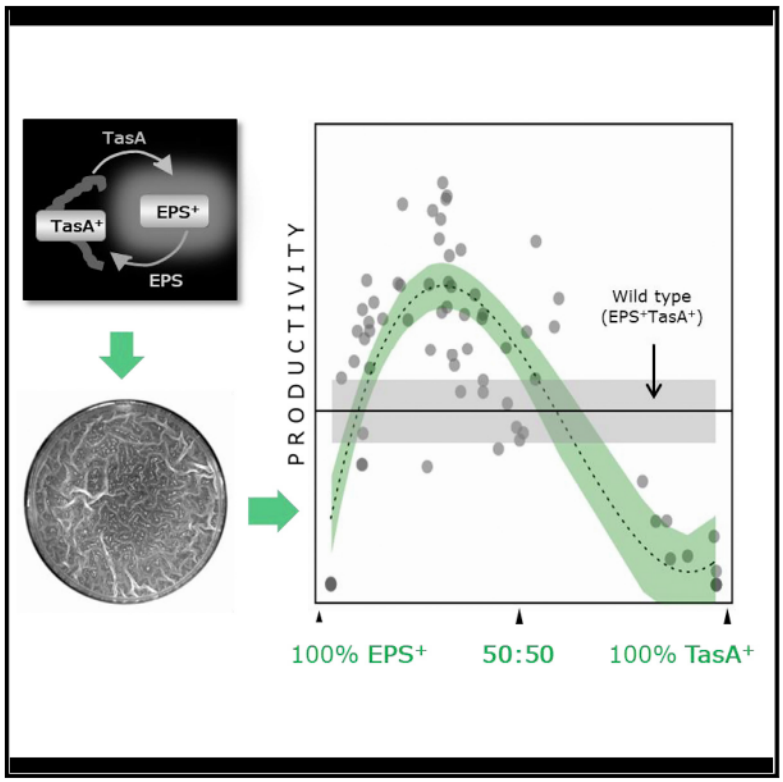

Authors

Anna Dragoš, Heiko Kiesewalter, Marivic Martin, ..., Nicola Stanley-Wall, Rolf Kümmerli, Ákos T. Kovács

Correspondence

atkovacs@dtu.dk

In Brief

Microbes that live predominantly in complex biofilms often cooperate with each other by performing complementary tasks. Dragoš et al. use a plant-colonizing *Bacillus subtilis* model and combine experimental and computational approaches to demonstrate and rationalize benefits arising from genetic division of labor during biofilm matrix production.

Highlights

- Matrix components EPS and TasA are costly public goods in *B. subtilis* biofilms
- Genetic division of labor using Δ*eps* and Δ*tasA* fosters maximal biofilm productivity
- Δ*eps* and Δ*tasA* cooperation is evolutionarily stable in laboratory and ecological setups
- Costly metabolic coupling of public goods favors genetic division of labor

Dragoš et al., 2018, Current Biology *28*, 1–11
June 18, 2018
https://doi.org/10.1016/j.cub.2018.04.046

CellPress

Please cite this article in press as: Dragoš et al., Division of Labor during Biofilm Matrix Production, Current Biology (2018), https://doi.org/10.1016/j.cub.2018.04.046

Division of Labor during Biofilm Matrix Production

Anna Dragoš,[1,2,8] Heiko Kiesewalter,[1,9] Marivic Martin,[1,2,10] Chih-Yu Hsu,[3] Raimo Hartmann,[4] Tobias Wechsler,[5] Carsten Eriksen,[6] Susanne Brix,[6] Knut Drescher,[4,7,11] Nicola Stanley-Wall,[3,12] Rolf Kümmerli,[5,13] and Ákos T. Kovács[1,2,14,15,*]

[1]Bacterial Interactions and Evolution Group, Department of Biotechnology and Biomedicine, Technical University of Denmark, Kgs Lyngby 2800, Denmark
[2]Terrestrial Biofilms Group, Institute of Microbiology, Friedrich Schiller University Jena, Jena 07743, Germany
[3]School of Life Sciences, University of Dundee, Dundee DD1 5EH, UK
[4]Max Planck Institute for Terrestrial Microbiology, Marburg 35043, Germany
[5]Department of Plant and Microbial Biology, University of Zürich, Zürich 8057, Switzerland
[6]Disease Systems Immunology Group, Department of Biotechnology and Biomedicine, Technical University of Denmark, Kgs Lyngby 2800, Denmark
[7]Department of Physics, Philipps University, Marburg 35037, Germany
[8]Twitter: @anna_dragos
[9]Twitter: @h_kiesewalter
[10]Twitter: @martinmavs
[11]Twitter: @knutdrescher
[12]Twitter: @bacteriacities
[13]Twitter: @rolfsmicrobes
[14]Twitter: @evolvedbiofilm
[15]Lead Contact
*Correspondence: atkovacs@dtu.dk
https://doi.org/10.1016/j.cub.2018.04.046

SUMMARY

Organisms as simple as bacteria can engage in complex collective actions, such as group motility and fruiting body formation. Some of these actions involve a division of labor, where phenotypically specialized clonal subpopulations or genetically distinct lineages cooperate with each other by performing complementary tasks. Here, we combine experimental and computational approaches to investigate potential benefits arising from division of labor during biofilm matrix production. We show that both phenotypic and genetic strategies for a division of labor can promote collective biofilm formation in the soil bacterium *Bacillus subtilis*. In this species, biofilm matrix consists of two major components, exopolysaccharides (EPSs) and TasA. We observed that clonal groups of *B. subtilis* phenotypically segregate into three subpopulations composed of matrix non-producers, EPS producers, and generalists, which produce both EPSs and TasA. This incomplete phenotypic specialization was outperformed by a genetic division of labor, where two mutants, engineered as specialists, complemented each other by exchanging EPSs and TasA. The relative fitness of the two mutants displayed a negative frequency dependence both *in vitro* and on plant roots, with strain frequency reaching a stable equilibrium at 30% TasA producers, corresponding exactly to the population composition where group productivity is maximized. Using individual-based modeling, we show that asymmetries in strain ratio can arise due to differences in the relative benefits that matrix compounds generate for the collective and that genetic division of labor can be favored when it breaks metabolic constraints associated with the simultaneous production of two matrix components.

INTRODUCTION

Microbes can act collectively in groups, and thereby substantially influence their local environment to their own benefit. Such beneficial collective actions include the secretion of nutrient-degrading enzymes [1], iron-scavenging siderophores [2], biosurfactants for group motility [3], and structural components for biofilm formation [4, 5]. In certain cases, cooperation even involves a division of labor, where subpopulations of cells specialize to perform different tasks [6, 7]. Division of labor requires three basic conditions: individuals must exhibit different phenotypes (task allocation), the interaction between phenotypes must be cooperative, and all individuals must gain an inclusive fitness benefit from the interaction [8]. The allocation of tasks can be achieved either at the phenotypic or at the genotypic level. In the phenotypic specialization scenario, each individual carries genetic machineries for all tasks, but differences in gene expression result in tasks allocation [9]. In the genotypic specialization scenario, individuals carry only the genetic machinery for their own specialist task [9].

Both types of division of labor have been proposed to occur in microbes. For instance, during sliding colony expansion *Bacillus subtilis* cells phenotypically differentiate into surfactant producers and matrix producers where the role of the first is to

reduce surface tension, while the latter allows expanding colony "arms" to form and explore new territories [7]. Given the high relatedness between cells, specialization is likely beneficial for the group as a whole [8], with individuals gaining an inclusive fitness benefit from helping their clone mates [10–12]. However, division of labor has recently also been documented between genetically different strains or species [13, 14].Cooperative division of labor based on genetic differentiation seems to evolve both frequently and reproducibly [14, 15], lending support for the so-called Black Queen hypothesis, which depicts the microbial world as a network of interdependencies between species [16].

While our understanding of division of labor in microbes deepens [7, 13, 14], it has remained unclear what the advantages and disadvantages of the phenotypically versus genetically determined division of labor are, and which form yields higher fitness returns for the specialists and the community as a whole. When considering division of labor based on the exchange of two beneficial public goods, a phenotypic specialization could offer advantages because cells producing the two public goods will naturally be close to one another due to binary cell division. Close spatial proximity is essential for efficient public good sharing [17], yet might be compromised with genetically determined division of labor, as spatial separation of partners can readily occur and the switching of specialization states is not possible [18]. Conversely, genetically determined division of labor might offer advantages because it allows a complete decoupling of traits at the metabolic level. Specifically, the expression of two alternative synthetic pathways (both bearing a metabolic burden) can be terminally allocated into two different genetic lineages [19]. Finally, it has been argued that in contrast to phenotypic differentiation, terminal genetic divergence bears risks of conflicts such as social exploitation because relatedness between interacting partners is reduced, potentially leading to diverging interests between partners [18].

Here, we focus on identifying the costs and benefits associated with different division of labor strategies for biofilm formation in the common soil and plant-colonizing bacterium *B. subtilis*, in terms of individual and collective productivity. Biofilms represent the most common lifestyle of bacteria, where cells are in close proximity to one another, embedded in extracellular matrix (ECM) [20]. There is ample opportunity for division of labor over matrix construction, because ECM usually consists of multiple secreted compounds that form a mesh of complex exopolysaccharides (EPSs) and structural proteins, sometimes accompanied by extracellular DNA (eDNA). While the presence of eDNA can be the consequence of cell death [21], the production of matrix EPSs and proteins tends to be triggered by cooperative signaling [22], cues released by competitors [23], or specific nutrient components [24, 25]. As the synthesis of large polymers is metabolically costly, tight regulation of matrix gene expression is often in place, and it has been suggested that the overall metabolic costs for the community may be reduced by assigning matrix production only to a subpopulation of cells [26]. Here, we propose an alternative scenario involving division of labor, where subgroups of individuals within a biofilm each specialize (either phenotypically or genetically) in the production of a different matrix component, which are then shared at the level of the group.

Our model system involves *B. subtilis* forming robust, wrinkly pellicle biofilms that reside at the oxygen-rich liquid-air interface [27]. Increasing cell density of the planktonic cells results in a decreasing oxygen concentration in the bottom layers of the static medium. Aerotaxis of *B. subtilis* leads to an accumulation of cells near the liquid-air interface and eventually a colonization of the surface in a form of a densely packed pellicle biofilm. During pellicle development transcription of the matrix-related operons *epsA-O* and *tapA-sipW-tasA* is derepressed [26, 28–30] eventually allowing synthesis of the biofilm EPS, and the structural protein TasA [31, 32]. Mutants lacking either EPSs or TasA cannot establish pellicle biofilms individually, but they can complement each other in co-culture, indicating that both matrix components are necessary for pellicle biofilms and that they are shared [31, 33, 34].

Using a mixture of fitness assays, single-cell gene expression analyses and mathematical modeling, we show that the two matrix components EPSs and TasA are indeed costly to produce. We further found that cells within a biofilm phenotypically differentiate into three distinct subpopulations consisting of cells producing either both of the matrix components, EPSs alone, or none of the two components. We then demonstrate that in terms of group productivity, genetic division of labor for matrix construction can be superior to the phenotypic differentiation strategy present in the wild-type. Specifically, biofilm productivity was maximized at an intermediate mixing ratio of mutants deficient for either EPSs or TasA, both in pellicle biofilms grown in the laboratory, and in biofilms grown on plant hosts. Crucially, the Δ*eps*: Δ*tasA* proportion at which biofilm productivity maximization occurred represents a stable equilibrium.

RESULTS

The Matrix Components EPSs and TasA Serve as Costly Public Goods

Components of bacterial ECM are often large, complex polymers, which can potentially bear significant metabolic production costs [1, 35]. To demonstrate the costs associated with the production of EPSs and TasA in our *B. subtilis* strain (NCBI 3610), we competed the non-producing mutants Δ*eps* and Δ*tasA* against the wild-type (WT) under conditions where matrix is synthesized but not required for survival [36], which is up to 16 hr of growth, prior to surface colonization (Video S1; see STAR Methods). We confirmed that in the pre-pellicle phase the WT, Δ*eps*, and Δ*tasA* strains first grow exponentially before reaching the early stationary phase (Figure S1A). While strains expressed the corresponding matrix components (Figures S1B–S1D assays based on fluorescent transcriptional reporters P_{eps}-*gfp* and P_{tapA}-*gfp*), the expression patterns slightly varied between the WT and the mutants. The expression of P_{tapA} in Δ*eps* and P_{eps} in Δ*tasA* was slightly stronger and weaker, respectively, with shift toward more homogeneous expression in both mutants (Figure S1C). Under these conditions, our growth competition fitness assay revealed significant costs for both matrix components (Figure 1A). The fact that Δ*eps* had significantly higher relative fitness than Δ*tasA* in pairwise competition against the WT suggests that EPS synthesis bears a higher cost than TasA production under these conditions (Figure 1A).

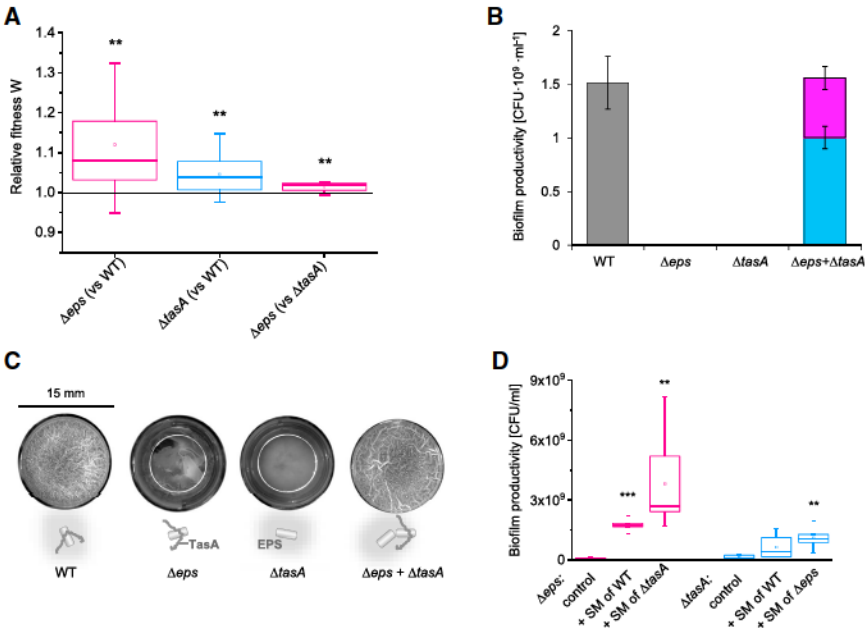

Figure 1. Costs and Benefits of Matrix Components EPSs and TasA

(A) To estimate the metabolic costs of EPS and TasA production the matrix-deficient strains Δ*eps* and Δ*tasA* were competed against the WT and against each other under conditions where matrix components are produced but not required (see STAR Methods). Relative fitness (W) was calculated for Δ*eps* (when competed against WT), Δ*tasA* (when competed against WT), and Δ*eps* (when competed against Δ*tasA*). Relative fitness W significantly larger than 1 indicates an advantage of a given strain in a given pairwise competition. For Δ*eps* versus WT, n = 13, p < 003; for Δ*tasA* versus WT, n = 13, p < 008; for Δ*tasA* versus WT, n = 8, p < 007 (**p < 0.01, ***p < 0.001).

(B) Productivity of the WT, Δ*eps*, Δ*tasA*, and Δ*eps*+Δ*tasA* co-culture (50:50 ratio) measured as colony-forming units (CFUs) per milliliter. Data points represent mean and error bars represent SE obtained from biological triplicates.

(C) Bright-field images of pellicle morphology developed by the WT, matrix-deficient mutants in monocultures, and by the Δ*eps*+Δ*tasA* co-culture (50:50 ratio). The cartoons below represent public goods produced by each culture.

(D) To confirm that EPSs and TasA can be shared and thereby serve as public goods, the matrix-deficient strains Δ*eps* and Δ*tasA* were allowed to form pellicles in presence of spent media (SM) obtained from the WT or from the complementary mutant (n = 4–6). Pellicle productivity (CFU/mL) reached in presence of those SMs was compared with the productivity of the control (a strain exposed to its own SM): for Δ*eps* + SM of WT $p < 5 \times 10^{-7}$; Δ*eps* + SM of Δ*tasA* p < 0.008; Δ*tasA* + SM of WT p < ; Δ*tasA* + SM of Δ*eps* SM p < 0.001 (**p < 0.01). Boxes represent Q1–Q3 (quartiles), lines represent the median, and bars span from max to min. To better distinguish between the matrix-deficient mutants, data for Δ*eps* and Δ*tasA* are presented in pink and blue, respectively.

See also Figures S1 and S2 and Video S1.

Next, we examined sharing of the two components. We began with complementation assays mixing the two mutants (Δ*eps* and Δ*tasA* single-deletion mutants) in 1:1 ratios. In line with previous reports [31, 33, 34], we found that the mutants could not establish pellicles when grown in monocultures but complemented each other when co-cultured, indicating that EPSs and TasA can be shared (Figures 1B and 1C). Since TasA was previously depicted as a cell-associated amyloid fiber, anchored through the accessory protein TapA to the cell [33], we performed additional experiments to confirm cross-complementation. Specifically, we added conditioned media from the EPS and TasA producers to growing cultures of the Δ*eps* and Δ*tasA*, respectively, and quantified their surface colonization ability. We observed that the conditioned medium from the WT or the complementary mutant significantly improved pellicle formation as compared to the control, with the effect being more pronounced for the Δ*eps* than the Δ*tasA* mutant (Figure 1D). This result suggests that the spent medium obtained from the WT and Δ*tasA* contained freely released EPSs, which could complement the Δ*eps* strain. Similarly, WT and Δ*eps* released a portion of TasA into the medium that could partially complement the Δ*tasA* phenotype.

As the above results (Figure 1D) suggest that the matrix components EPS and TasA differ in the extent to which they are shared, pointing toward stronger privatization of TasA, we hypothesized that efficient mixing of EPS producers and TasA producers is necessary for successful complementation. To test the role of mixing, we took advantage of a previously observed motility effect on cell assortment in pellicle biofilms [37]: cells lacking a functional flagellum (Δ*hag*) are less efficient in swimming to the top of the liquid, which likely results in very low number of founder cells carrying the Δ*hag* mutation (compared to WT) in the pellicle. As a result, pellicles formed by two isogenic Δ*hag* strains labeled with different fluorophores contain large clusters of cells of the same lineage, indicating limited genotype mixing [37]. As expected, the efficiency of complementation between EPS and TasA producers was negatively affected in the Δ*hag* genetic background as compared to the control with functional flagella (Figure S2A). Finally, the spatial assortment of cells in the pellicles formed by mixtures of Δ*eps* and Δ*tasA* and pellicles formed by the WT were compared using a density correlation function quantification method (see STAR Methods), to assess the spatial effects of genetic division of labor (Figures S2B–S2D). The level of spatial strain mixing was slightly higher in pellicles formed by mixtures of Δ*eps* and Δ*tasA* (regardless of the fluorescence reporter combination) as compared to pellicles formed by the WT (Figures S2C and S2D).

Altogether, these results confirm that both matrix components EPSs and TasA can be shared and that robust pellicle biofilm formation depends on the efficient exchange of these compounds.

WT Cells Exhibit Phenotypic Heterogeneity in the Expression of Matrix Components

As EPSs and TasA are costly to produce (Figure 1A) and can both be shared between the producers and non-producers (Figures 1B–1D), we hypothesized that phenotypic differentiation into EPS producers and TasA producers could occur and form the basis of a division of labor in WT *B. subtilis* populations during

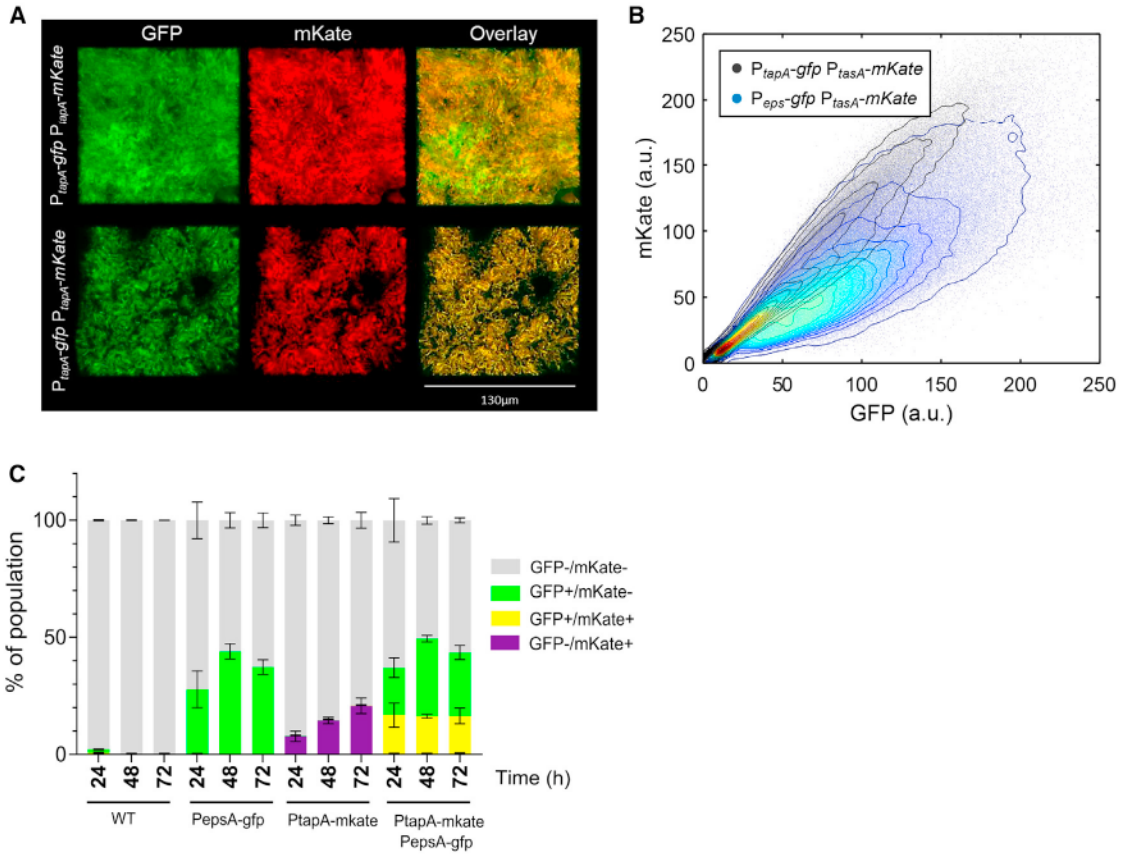

Figure 2. Native Phenotypic Heterogeneity in the Expression of Matrix Components

(A) Pellicles formed by the double-labeled strain carrying the P_{eps}-*gfp* P_{tapA}-*mKate* reporters and the strain carrying the P_{tapA}-*gfp* P_{tapA}-*mKate* reporters (control) were visualized using a confocal microscope to compare the distribution of fluorescence signal from different fluorescence reporters (GFP, mKate).

(B) Volumes in GFP and mKate fluorescence channels (obtained by manual thresholding) were merged and dissected into cubes, and the average intensities in the GFP and mKate channels for all cubes were plotted (see STAR Methods). The maximum density is normalized to 1 and the contour lines correspond to 0.05 decrease in density.

(C) The following strains: NCIB3610, NRS2242 (carrying P_{eps}-*gfp*), NRS3913 (carrying P_{tapA}-*mKate*), and NRS5832 (carrying P_{eps}-*gfp* and P_{tapA}-*mKate*) were allowed to form pellicles and were then analyzed using flow cytometry. Bar chart (mean ± SD) represents fraction of OFF cells, cells expressing *eps-gfp*, *tapA-mKate*, and cells expressing both reporters (n = 3).

See also Figure S3.

pellicle formation. To test for phenotypic heterogeneity of *eps* and *tasA* expression at the single-cell level, we used a reporter strain carrying a promoter fusion of the *eps* promoter to *gfp* (P_{eps}-*gfp*) and an analogous reporter for the *tapA* promoter based on *mKate* (P_{tapA}-*mKate*) at two distinct genomic loci (see STAR Methods; Table S1). As a control, we used the P_{tapA}-*gfp* P_{tapA}-*mKate* strain (see STAR Methods; Table S1) for which no phenotypic heterogeneity and a linear correlation between the two fluorescence channels was expected. Fluorescent images of mature pellicles of the WT P_{eps}-*gfp* P_{tapA}-*mKate* strain and the control WT P_{tapA}-*gfp* P_{tapA}-*mKate* strain were captured using confocal laser scanning microscopy (CLSM). While the control strain showed a clear spatial correlation between GFP and mKate fluorescence intensities, this was not the case for the WT P_{eps}-*gfp* P_{tapA}-*mKate* strain (Figure 2A). Specifically, large bright clusters of strong GFP signal could be observed in locations in which there was reduced mKate fluorescence, suggesting the presence of a subpopulation that is partially specialized for EPS production (Figure 2A). We further performed quantitative analyses of the fluorescent images by artificially dissecting the images into small cubes and quantifying the GFP- and mKate-signal intensities in each cube (see STAR Methods). This allowed us to examine whether GFP and mKate fluorescence intensities linearly correlate in space. Such linear correlation was expected from the control strain (WT P_{tapA}-*gfp* P_{tapA}-*mKate*) and could be the case for the P_{eps}-*gfp* P_{tapA}-*mKate* strain if *eps* and *tasA* were expressed by the same population of cells. The analysis confirmed that, for biofilms made by the P_{tapA}-*gfp* P_{tapA}-*mKate* strain, signal intensities from GFP and mKate channels showed strong linear correlation in space, this correlation was much weaker in case of the P_{eps}-*gfp* P_{tapA}-*mKate* strain (Figures 2B and S3A).

The above experiment suggests that matrix-expressing subpopulations of WT *B. subtilis* exhibit a certain degree of phenotypic differentiation into cells that produce mostly EPSs and cells that produce both EPSs and TasA (generalists). To confirm this pattern, we analyzed single cells extracted from pellicles using fluorescence-guided flow cytometry (FC). FC analyses were

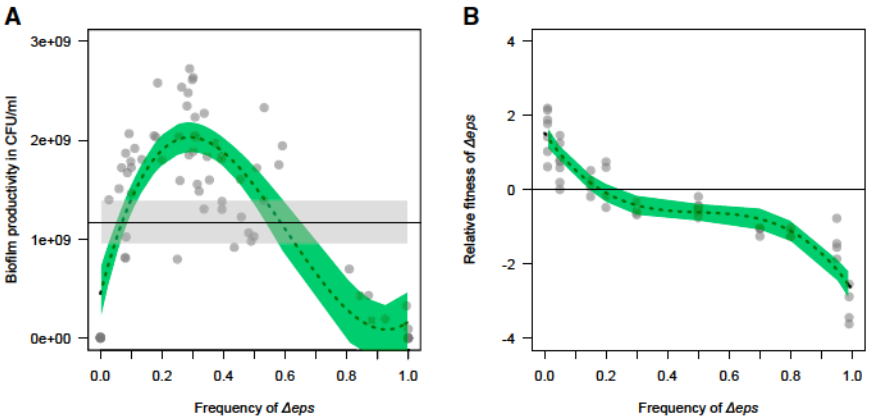

Figure 3. Productivity and Fitness in Pellicles with Genetic Division of Labor

(A) Productivities of Δ*eps*+Δ*tasA* biofilms (CFU/mL) measured for different mixing ratios and compared to average productivity reached by the WT (black horizontal line with gray shaded 95% confidence interval [CI]). The dashed line and green shaded 95% CI represent a cubic fit to the fitness data ($F_{3, 68} = 54.9$, $R^2 = 0.695$, $p < 0.0001$). (B) The relative fitness of Δ*eps* in competition with Δ*tasA* followed a negative-frequency-dependent trajectory, best described by a cubic fit (dashed line with 95% CI: $F_{3,46} = 94.7$, $R^2 = 0.852$, $p < 0.0001$).

performed at 3 time points during pellicle development (24, 48, and 72 hr) and included controls with strains carrying single reporter fusions (see STAR Methods; Table S1). These analyses revealed the presence of 3 distinct subpopulations of cells: (1) matrix-OFF cells where fluorescence signals from both the P_{eps} and P_{tapA} promoters were below the detection thresholds; (2) matrix-ON cells where there was a positive linear correlation of the signals from the P_{eps} and P_{tapA} promoters: (3) EPS-ON cells, containing a fluorescent signal from P_{eps}, but not from P_{tapA} (Figures 2C and S3B). Differences in relative frequencies of P_{eps}-*gfp* and P_{tapA}-*mKate* ON cells were not due to the use of different fluorescent reporters, as evidenced by our FC control experiments where strains carrying either a P_{tapA}-*gfp* or a P_{tapA}-*mKate* reporter construct showed identical frequencies of ON cells (Figures S3C and S3D). Thus, our FC experiments confirmed that the expression of the two major matrix promoters P_{eps} and P_{tapA} is not perfectly correlated, which likely translates into phenotypic diversity at the level of EPS and TasA production in WT *B. subtilis* pellicles.

Genetic Division of Labor Yields Higher Biofilm Productivity than Phenotypic Differentiation

Although the above data indicate that WT cells differentiate into EPS producers, generalists, and non-producers during pellicle biofilm formation, this pattern does not resemble the canonical principle of division of labor where distinct subpopulations of cells are expected to either commit completely to TasA or EPS production. The incomplete specialization could be due to regulatory constraints. For instance, it is known that the *epsA-O* and *tapA-sipW-tasA* operons share multiple regulators, suggesting that some level of parallel expression (either on or off) at the single-cell level is expected [38, 39].

We thus wondered whether an incomplete specialization represents a beneficial strategy or whether it can be outperformed by a genetically determined specialization, where cells are ultimately constrained in the production of either TasA or EPSs. To address this question, we studied the division of labor between Δ*tasA* as the exclusive EPS producer and Δ*eps* as the exclusive TasA producer. In a first experiment, we mixed the exclusive EPS and TasA producers at different ratios and examined the productivities of pellicles (Figure 3A). We found that pellicle productivity varied in response to strain frequency and peaked at a strain ratio of approximately 30% Δ*eps*: 70% Δ*tasA* (Figure 3A). Interestingly, the group productivity of mixtures close to this optimal ratio was significantly higher than the WT productivity, indicating that the genetic division of labor over matrix construction outperforms the native phenotypic differentiation observed in the WT (Figure 3A).

Genetic Division of Labor Is Evolutionarily Stable in Pellicles and on Plant Roots

We next asked whether such genetic division of labor, which yields the highest fitness returns at a strain ratio of approximately 30:70, represents a stable equilibrium or simply a transient phenomenon. To test this possibility, we competed the Δ*eps* strain against the Δ*tasA* strain across a range of frequencies (1%–99%), over the full cycle of pellicle growth (from inoculation until formation of robust, wrinkly pellicle after 48 hr). These competitions revealed that the relative fitness of Δ*eps* followed a negative frequency-dependent pattern: Δ*eps* outcompeted Δ*tasA* when rare but lost the competition when common (Figure 3B). Strikingly, the two strains showed equal competitiveness at starting frequencies between 20% and 30% Δ*eps*, thus exactly at the strain ratio where biofilm productivity is maximized. These findings strongly suggest that, regardless of the metabolic cost imbalance between the two matrix components, stable coexistence of the EPS and TasA producers is favored in the pellicle, with strain frequency evolving toward the optimum in terms of biofilm biomass productivity (Figures 1A and 3B).

To test whether stable genetic division of labor could also manifest in a relevant ecological environment, we repeated several key experiments using plant root associated biofilms. Specifically, we subjected the roots of *Arabidopsis thaliana* seedlings to colonization by the WT, or a mixture of Δ*eps* and Δ*tasA* strains at a 50:50 ratio, or monocultures of the two mutants (see STAR Methods). Each strain carried a constitutive fluorescent reporter to allow biofilm visualization by CLSM (see STAR Methods; Table S1). In line with previous studies [40], both the WT and the mixture of Δ*eps* and Δ*tasA* strains were able to produce thick biofilms on the roots, which was not the case for the Δ*eps* and Δ*tasA* mutants grown in monocultures on the plant root (Figures 4A and 4B). Analogous to the pellicles, we found that the productivity of root biofilms was significantly higher for the Δ*eps* + Δ*tasA* mixture as compared to the WT. Next, we estimated the relative frequencies of Δ*eps* and

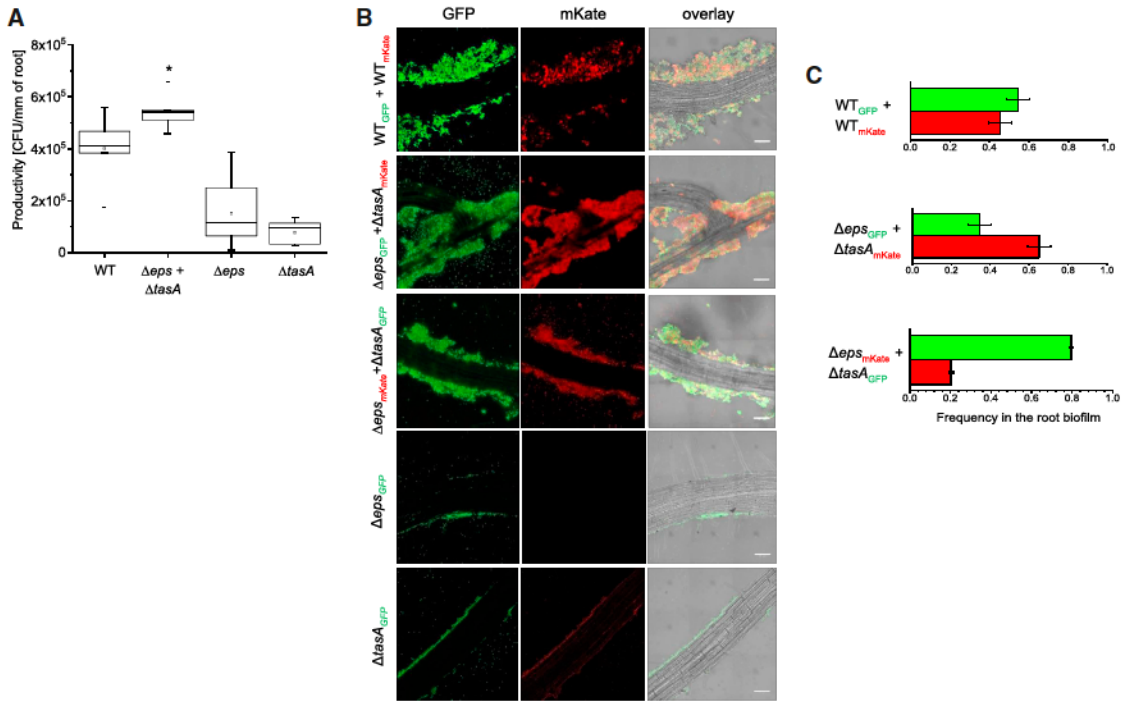

Figure 4. Genetic Division of Labor on Plant Roots

(A) *Arabidopsis thaliana* roots were colonized by the WT and Δ*eps*+Δ*tasA* mix, and the mutants in monocultures and biofilm productivities were measured as CFUs per millimeter of root (for WT and co-culture, n = 6; for Δ*eps* and Δ*tasA*, n = 11) (see STAR Methods). The productivity reached by the Δ*eps*+Δ*tasA* mixture was compared with productivity of the WT ($p < 0.04$).

(B) *A. thaliana* roots were colonized by mixed cultures of WT_{GFP}+WT_{mKate}, Δeps_{GFP}+$\Delta tasA_{mKate}$, Δeps_{mKate}+$\Delta tasA_{GFP}$, and the mutants in monocultures (Δeps_{GFP} and $\Delta tasA_{GFP}$) and visualized using CLSM. Scale bar represents 10 μm.

(C) Frequencies of each strain in the root-associated biofilm were determined based on image analysis (see STAR Methods). Bars represent average (n = 3–5) and error bars represent SE.

Δ*tasA* mutants in the mixed biofilm on the root, based on total pixel volumes (see STAR Methods), and found that the mutant frequency settled at the optimal ratio of 20% and 30% Δ*eps* (Figures 4B and 4C). In contrast, the frequency remained close to 0.5:0.5 in our control mixtures of two WT strains labeled with different fluorescent reporters (Figures 4B and 4C). Altogether, our experiments demonstrate that the genetically hard-wired division of labor between EPS and TasA producers provides fitness benefits not only in pellicles, but also on plant roots.

Simulating Pellicle Formation to Understand the Drivers of Genetic Division of Labor

To better understand the conditions required for genetic division of labor to evolve between EPS- and TasA-producing specialists, we used an individual-based modeling platform, specifically developed to simulate microbial interactions [41]. The platform consists of a two-dimensional toroidal surface, where bacterial cells are modeled as discs. Bacteria are seeded in low numbers to their *in silico* habitat and are then allowed to consume resources, grow, divide, disperse, and produce public goods according to specified parameters for 10,000 time steps (see STAR Methods for fitness equations). The system keeps track of both bacterial strains and their public goods over time and space, and closely recovers patterns of real pellicle formation (Figure S4).

First, we examined the performance of a WT strain, which simultaneously produces two complementary public goods, representing EPSs and TasA. Simulations started with eight cells placed in the center of the landscape to mimic the early phase of pellicle formation. Cells grew and divided at a basic rate (μ). Cells additionally produced diffusible public goods at a constant rate. Public goods diffuse randomly and can decay or generate fitness benefits for receiver cells. While each public good generates a benefit on its own, synergistic benefits accrue to cells that encounter the two complementary public goods within a certain time frame. Using this setup, we found that WT biofilm productivity peaked with lower public good diffusion *d* (Figure S5A), indicating that reduced diffusion minimizes the loss and improves sharing of public goods. Since our experimental data suggest that TasA and EPSs differ in the level of sharing, and thus in the relative benefit these goods can generate for the group, we varied this parameter in our model but found that it did not affect the productivity of WT pellicles (Figure S5B). We then implemented metabolic constraints (via the factor *f*, defined in Equation 1 in the STAR Methods) in the WT to account for the possibility that the simultaneous production of two public goods exceeds the sum of each individual public good ($f > 1$) [19]. We observed that biofilm productivity sharply declined with increased levels of constraints (Figure S5C).

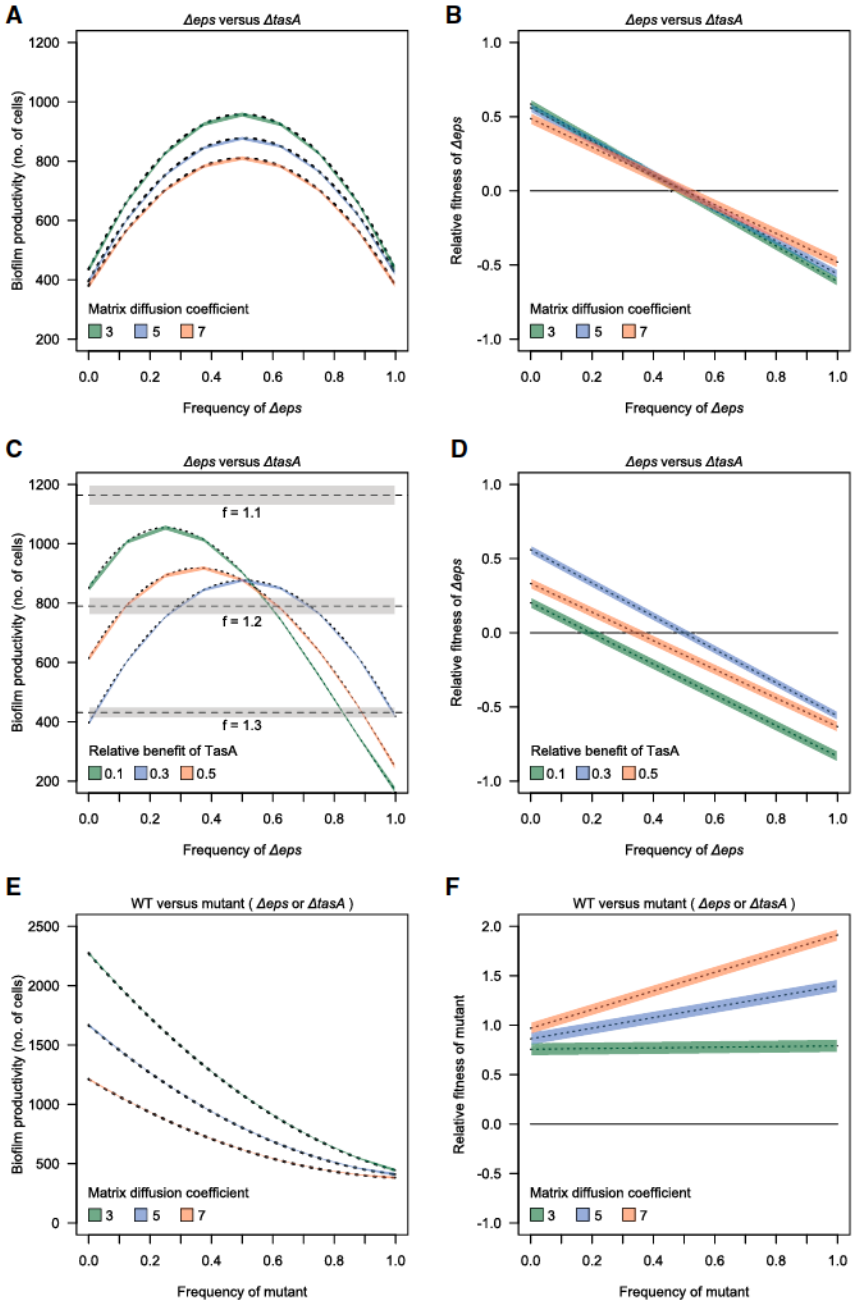

Figure 5. Individual-Based Simulations Identify Drivers of Genetic Division of Labor

We simulated biofilm formation of the mutants Δ*eps* (producing TasA) and Δ*tasA* (producing EPSs) when grown in co-culture. Biofilms were initiated with eight cells, with Δ*eps* frequency varying between 0 and 1, in steps of 0.125. Cells produced diffusible matrix components (either TasA or EPSs) and grew according to their fitness functions. After 10,000 time steps, we measured the absolute productivity of the biofilm (no. of cells) and the relative fitness of the competing strains within biofilms. Fitness trajectories are shown as the best fit from linear models across 50 simulations for each condition (±95% CI).

(A and B) Variation in biofilm productivity (A) and relative fitness of mutants (B) as a function of strain frequency and the matrix diffusion coefficient, under conditions where both matrix components generate equal benefits.

(C and D) Variation in biofilm productivity (C) and relative fitness of mutants (D) as a function of strain frequency and different relative benefits of the two matrix components (diffusion coefficient $d = 5$). Dashed lines and gray shaded area in (D) depict mean ± 95% CI productivities of WT biofilms across a range of metabolic constraints (f) accruing in the WT for simultaneously producing two public goods.

(E and F) Biofilm productivity (E) and relative fitness (F) of a mutant growing together with the WT, respectively, as a function of strain frequency and the matrix diffusion coefficient, under conditions where both matrix components generate equal benefits.

See also Figures S4 and S5.

Next, we considered different levels of phenotypic heterogeneity in the WT by starting simulations with different ratios of specialist and non-specialist cells (Figures S5D–S5F). We found that any level of phenotypic heterogeneity outperformed uniform trait expression at the beginning of pellicle formation (Figure S5D). Conversely, the most beneficial strategies in more mature pellicles were either complete specialization or no specialization at all (Figures S5E and S5F). We hypothesize that no specialization performs well because it allows efficient public good sharing at higher cell densities, and complete specialization is beneficial because it breaks metabolic constraints. In contrast, any intermediate form of phenotypic heterogeneity suffers from reduced sharing and sustained metabolic constraints and should thus be selected against. This finding might explain why the *B. subtilis* WT strain showed relatively low levels of phenotypic heterogeneity.

We then asked whether two genetically fixed mutants, producing either one or the other public good (i.e., mimicking Δ*eps* and Δ*tasA* mutants) can complement each other. Similar to our empirical observations, we found successful complementation between the two specialist strains, with pellicle productivity peaking at intermediate mixing ratios (Figure 5A). Moreover, the relative fitness of the Δ*eps* strain exhibited negative-frequency dependence (Figure 5B), and the point of fitness equilibrium occurred exactly at the productivity peak of the group. Next, we implemented the experimental observation that TasA yields lower benefits than EPSs. We again observed successful complementation, but pellicle productivity reached higher levels and peaks shifted to lower frequencies of the Δ*eps* strain, in the case of a greater benefit imbalance between the two public goods (Figure 5C). The relative fitness of the Δ*eps* strain again followed a negative-frequency dependence with the point of intersection being exactly at the pellicle productivity peak

(Figure 5D). To examine whether the reciprocal symmetric exchange of public goods is the reason for why strain equilibrium frequency coincides with maximal group productivity, we simulated a scenario of asymmetrical public good exchange between a strain producing both public goods and a strain producing a single public good (Figures 5E and 5F). For this scenario, we found that the relationship between strain equilibrium and maximal group productivity breaks: the strain producing only one public good experienced relative fitness advantages at all strain frequencies, driving strain frequency away from maximal group fitness.

Finally, we asked whether genetic division of labor between the Δ*eps* and Δ*tasA* strains can outperform the WT strategy, as observed in our empirical experiments. However, in the absence of any metabolic constraints ($f = 1$), the WT pellicle productivity was 1,714 ± 39 cells (mean ± SE, with intermediate diffusion $d = 5$), and thus by far higher than productivity in any of the complementation scenarios (Figure 5). Conversely, when the WT faces metabolic constraints, we found a parameter space ($f > 1.1$), in which pellicle productivity of complementing strains exceeds WT performance (Figure 5C).

Taken together, our simulations recover the key features of our experimental system and suggest that the reciprocal symmetrical exchange of public goods under conditions of relatively low diffusion together with the decoupling of metabolic constraints are the preconditions required for the evolution of stable genetic division of labor over biofilm matrix production.

DISCUSSION

Despite their unicellular simplicity, microbes can coordinate complex behaviors as a group. Some of these multicellular behaviors involve division of labor between phenotypically distinct subpopulations [7, 42], or even different genetic lineages [14]. Here, we deployed a combination of experiments and simulations to directly compare these two alternative cooperative strategies. By focusing on the production of two biofilm matrix components in *B. subtilis*, we found evidence for significant, yet incomplete phenotypic specialization in matrix production among clonal cells of the WT strain. However, this strategy of phenotypic specialization was outperformed by genetic division of labor, where strains, engineered as strict specialists, settled on an equilibrium ratio that maximized biofilm productivity. Our individual-based modeling approach captures the experimental system and reveals that metabolic decoupling of two costly traits can be the key to success for genetic specialization.

While we demonstrate that *B. subtilis* WT displays partial phenotypic differentiation at the level of matrix production, we might ask why this form of specialization is not more pronounced, especially in the context of the reported fitness benefits that can accrue from complete genetic specialization (Figure 3A). One explanation might be that the *epsA-O* and *tapA-sipW-tasA* operons share multiple regulators, such that some level of parallel expression is inevitable [38, 39, 43, 44]. Still, there could be certain mechanisms in place to decouple EPS and TasA production, for example, a positive feedback where EPSs prevent autophosphorylation of the EpsAB kinase, allowing activation of the EpsE glycosyl-transferase, thereby promoting EPS synthesis [45]. It was also proposed that the major matrix repressor SinR, acts differently on P_{eps} and P_{tapA} promoters. Specifically, in the case of P_{eps} it directly competes with an activator RemA for the binding site upstream of the promoter, thereby serving as an anti-activator, while in case of P_{tapA} it binds simultaneously with RemA, probably serving as a repressor [44]. The opposing relationship between SinR and RemA may lead to an outburst of *epsA-O* expression in a subpopulation of cells, while *tapA-sipW-tasA* remains under tighter control of SinR. While these regulatory mechanisms could allow for some heterogeneity in gene expression, complete specialization seems impossible. Another possibility is that such complete specialization with 30:70 frequencies of TasA producers and EPS producers does not always reflect an optimal solution. Biofilm formation is only one out of multiple cooperative survival strategies of *B. subtilis* and each strategy might require different optimal ratios of generalists and specialists. For instance, the presence of generalists that can produce both EPSs and TasA may be favored during social spreading on solid surfaces, where both components are important [7], but where the diffusion of these public goods is reduced compared with pellicle growth conditions.

Our findings on successful genetic division of labor between specialized strains, producing either EPSs or TasA, show that strain frequency settles as a stable frequency of approximately 70:30. Our model suggests that the dominance of EPS producers in biofilms may be driven by a higher relative benefit of EPSs compared with TasA. In addition, the altered matrix gene expression patterns in Δ*eps* (overproducing TasA) and Δ*tasA* (reduced EPS production) suggest that a higher proportion of Δ*tasA* might be required for stable pellicle production. Perhaps the two matrix components engage in an interaction that alters their biochemical properties. One possibility is that, upon interaction with EPSs, TasA becomes less soluble and vice versa. This could explain a decreased complementation efficiency of Δ*eps* and Δ*tasA* strains by the spent media obtained from the WT (Figure 1D). Recent work suggests that the structural functionality of TasA fibers may directly depend on the presence of EPSs in the extracellular environment [46].

The 70:30 population structure is stable in typical laboratory setup (pellicle biofilms) and in plant root-associated biofilms. Although the genetic division of labor arose as the winning strategy, our study also points toward the canonical problem associated with fixed cooperation strategies: limited mixing of strains prevents efficient genetic division of labor [18]. Specifically, we found that the complementation between EPS and TasA producers was ineffective in experiments with flagellum-deficient strains, which exhibit a decreased level of mixing, thereby reducing public good sharing and the formation of robust pellicle biofilms. Mathematical models ([47], our model) suggest that complementation is most efficient when strain mixing is high, but the diffusion of public goods is reduced, conditions that foster efficient public good exchange between neighbors and prevent losses due to diffusion. A further complication is that the goods to be exchanged might often vary in their diffusion properties. Our assays, for instance, suggest that the diffusion and sharing of TasA is rather limited compared to EPSs. We argue that such low diffusion rates must be compensated by an increased spatial mixing of the cooperation partners. Therefore, in opposition to "xenophobic" mechanisms employed by

microbes to avoid strangers [48–50], "xenophilic" strategies might be crucial for genetic division of labor.

In conclusion, our study offers major insights into the evolution of division of labor. First, it shows that genetic specialization can be superior over phenotypic division of labor because it enables to break metabolic and regulatory constraints prevailing in organisms that remain totipotent. Second, sophisticated genetic division of labor can occur in simple organisms such as bacteria. Finally, genetic division of labor, based on the reciprocal exchange of public goods, could represent an evolutionary stable strategy, with strain frequency evolving toward an equilibrium that maximizes group productivity. Important to consider is whether *de novo* mutations may occur in the long term and disturb the observed equilibrium. For instance, a double-mutant Δ*eps*Δ*tasA*, which is deficient in both matrix components could exploit the complementing partners and derail the genetic division of labor. Future studies will need to experimentally test whether the reported cases of genetic division of labor are evolutionary stable in the long run.

STAR★METHODS

Detailed methods are provided in the online version of this paper and include the following:

- KEY RESOURCES TABLE
- CONTACT FOR REAGENT AND RESOURCE SHARING
- EXPERIMENTAL MODEL AND SUBJECT DETAILS
  - Strain construction
- METHOD DETAILS
  - Pellicle formation and productivity assays
  - Fitness assays
  - Spent media complementation assay
  - Microscopy/confocal laser scanning microscopy
  - Sample fixing and flow cytometry
  - Root colonization assay/root biofilms productivity
  - Images of plant roots
  - Modeling
- QUANTIFICATION AND STATISTICAL ANALYSIS
  - Relative fitness
  - Strain frequencies on plant roots
  - Density correlation
  - Statistical analysis

SUPPLEMENTAL INFORMATION

Supplemental Information includes five figures, three tables, and one video and can be found with this article online at https://doi.org/10.1016/j.cub.2018.04.046.

ACKNOWLEDGMENTS

This work was funded by the Deutsche Forschungsgemeinschaft (DFG) to Á.T.K. (KO4741/2.1) within the Priority Program SPP1617. A.D. was supported by fellowships from Alexander von Humboldt Foundation in Germany and H.C. Ørsted Cofund (EcoEvoVirBac) in Denmark. R.K. was funded by the Swiss National Science Foundation (grant no. PP00P3_165835) and the European Research Council (ERC-CoG no. 681295). This work was further supported by BBSRC grant code BB/P0001335 to N.S.-W., a scholarship from BeautyHsiao Biotech. to C.-Y.H., the European Research Council (ERC-StG no. 716734) and the Human Frontier Science Program (CDA00084/2015-C) to K.D., and a start-up grant from the Technical University of Denmark to Á.T.K. Work in the laboratory of Á.T.K. is partly supported by the Danish National Research Foundation (DNRF137) for the Center for Microbial Secondary Metabolites. We acknowledge the help of Dr. Rosemary Clarke for assistance with flow cytometry performed at the University of Dundee.

AUTHOR CONTRIBUTIONS

A.D. and Á.T.K. conceived the project, A.D., H.K., M.M., C.-Y.H., and C.E. performed experiments, R.H. and K.D. analyzed quantitatively the CLSM imaging data, C.-Y.H., N.S.-W., C.E., and S.B. analyzed the flow cytometry results, and T.W. and R.K. performed modeling and analyzed the simulations. A.D., R.K., and Á.T.K. wrote and corrected the manuscript. All authors contributed critically to the drafts and gave final approval for publication.

DECLARATION OF INTERESTS

The authors declare no competing interests.

Received: January 1, 2018
Revised: March 13, 2018
Accepted: April 13, 2018
Published: June 7, 2018

REFERENCES

1. Drescher, K., Nadell, C.D., Stone, H.A., Wingreen, N.S., and Bassler, B.L. (2014). Solutions to the public goods dilemma in bacterial biofilms. Curr. Biol. *24*, 50–55.
2. Harrison, F., and Buckling, A. (2009). Siderophore production and biofilm formation as linked social traits. ISME J. *3*, 632–634.
3. Pollak, S., Omer-Bendori, S., Even-Tov, E., Lipsman, V., Bareia, T., Ben-Zion, I., and Eldar, A. (2016). Facultative cheating supports the coexistence of diverse quorum-sensing alleles. Proc. Natl. Acad. Sci. USA *113*, 2152–2157.
4. Boyle, K.E., Heilmann, S., van Ditmarsch, D., and Xavier, J.B. (2013). Exploiting social evolution in biofilms. Curr. Opin. Microbiol. *16*, 207–212.
5. Dragoš, A., and Kovács, Á.T. (2017). The peculiar functions of the bacterial extracellular matrix. Trends Microbiol. *25*, 257–266.
6. Strassmann, J.E., and Queller, D.C. (2011). Evolution of cooperation and control of cheating in a social microbe. Proc. Natl. Acad. Sci. USA *108* (*Suppl 2*), 10855–10862.
7. van Gestel, J., Vlamakis, H., and Kolter, R. (2015). From cell differentiation to cell collectives: *Bacillus subtilis* uses division of labor to migrate. PLoS Biol. *13*, e1002141.
8. West, S.A., and Cooper, G.A. (2016). Division of labour in microorganisms: An evolutionary perspective. Nat. Rev. Microbiol. *14*, 716–723.
9. Wahl, L.M. (2002). The division of labor: Genotypic versus phenotypic specialization. Am. Nat. *160*, 135–145.
10. Hamilton, W.D. (1964). The genetical evolution of social behaviour. I. J. Theor. Biol. *7*, 1–16.
11. Ackerman, J.M., and Kenrick, D.T. (2008). The costs of benefits: Help-refusals highlight key trade-offs of social life. Pers. Soc. Psychol. Rev. *12*, 118–140.
12. Refardt, D., Bergmiller, T., and Kümmerli, R. (2013). Altruism can evolve when relatedness is low: Evidence from bacteria committing suicide upon phage infection. Proc. Biol. Sci. *280*, 20123035.
13. D'Souza, G., and Kost, C. (2016). Experimental evolution of metabolic dependency in bacteria. PLoS Genet. *12*, e1006364.
14. Kim, W., Levy, S.B., and Foster, K.R. (2016). Rapid radiation in bacteria leads to a division of labour. Nat. Commun. *7*, 10508.
15. Germerodt, S., Bohl, K., Lück, A., Pande, S., Schröter, A., Kaleta, C., Schuster, S., and Kost, C. (2016). Pervasive selection for cooperative cross-feeding in bacterial communities. PLoS Comput. Biol. *12*, e1004986.

16. Morris, J.J., Lenski, R.E., and Zinser, E.R. (2012). The Black Queen Hypothesis: Evolution of dependencies through adaptive gene loss. MBio. Published online May 2, 2012. https://doi.org/10.1128/mBio.00036-12.
17. Weigert, M., and Kümmerli, R. (2017). The physical boundaries of public goods cooperation between surface-attached bacterial cells. Proc. Biol. Sci. *284*, 20170631.
18. Oliveira, N.M., Niehus, R., and Foster, K.R. (2014). Evolutionary limits to cooperation in microbial communities. Proc. Natl. Acad. Sci. USA *111*, 17941–17946.
19. Rueffler, C., Hermisson, J., and Wagner, G.P. (2012). Evolution of functional specialization and division of labor. Proc. Natl. Acad. Sci. USA *109*, E326–E335.
20. Nadell, C.D., Xavier, J.B., and Foster, K.R. (2009). The sociobiology of biofilms. FEMS Microbiol. Rev. *33*, 206–224.
21. Jakubovics, N.S., Shields, R.C., Rajarajan, N., and Burgess, J.G. (2013). Life after death: The critical role of extracellular DNA in microbial biofilms. Lett. Appl. Microbiol. *57*, 467–475.
22. Waters, C.M., Lu, W., Rabinowitz, J.D., and Bassler, B.L. (2008). Quorum sensing controls biofilm formation in *Vibrio cholerae* through modulation of cyclic di-GMP levels and repression of *vpsT*. J. Bacteriol. *190*, 2527–2536.
23. Oliveira, N.M., Martinez-Garcia, E., Xavier, J., Durham, W.M., Kolter, R., Kim, W., and Foster, K.R. (2015). Biofilm formation as a response to ecological competition. PLoS Biol. *13*, e1002191.
24. Shemesh, M., and Chai, Y. (2013). A combination of glycerol and manganese promotes biofilm formation in *Bacillus subtilis* via histidine kinase KinD signaling. J. Bacteriol. *195*, 2747–2754.
25. Marsden, A.E., Grudzinski, K., Ondrey, J.M., DeLoney-Marino, C.R., and Visick, K.L. (2017). Impact of salt and nutrient content on biofilm formation by *Vibrio fischeri*. PLoS ONE *12*, e0169521.
26. Chai, Y., Chu, F., Kolter, R., and Losick, R. (2008). Bistability and biofilm formation in *Bacillus subtilis*. Mol. Microbiol. *67*, 254–263.
27. Branda, S.S., González-Pastor, J.E., Ben-Yehuda, S., Losick, R., and Kolter, R. (2001). Fruiting body formation by *Bacillus subtilis*. Proc. Natl. Acad. Sci. USA *98*, 11621–11626.
28. Kobayashi, K. (2008). SlrR/SlrA controls the initiation of biofilm formation in *Bacillus subtilis*. Mol. Microbiol. *69*, 1399–1410.
29. Cozy, L.M., Phillips, A.M., Calvo, R.A., Bate, A.R., Hsueh, Y.-H., Bonneau, R., Eichenberger, P., and Kearns, D.B. (2012). SlrA/SinR/SlrR inhibits motility gene expression upstream of a hypersensitive and hysteretic switch at the level of σ(D) in *Bacillus subtilis*. Mol. Microbiol. *83*, 1210–1228.
30. Kearns, D.B. (2013). You get what you select for: Better swarming through more flagella. Trends Microbiol. *21*, 508–509.
31. Branda, S.S., Chu, F., Kearns, D.B., Losick, R., and Kolter, R. (2006). A major protein component of the *Bacillus subtilis* biofilm matrix. Mol. Microbiol. *59*, 1229–1238.
32. Romero, D., Vlamakis, H., Losick, R., and Kolter, R. (2011). An accessory protein required for anchoring and assembly of amyloid fibres in *B. subtilis* biofilms. Mol. Microbiol. *80*, 1155–1168.
33. Romero, D., Aguilar, C., Losick, R., and Kolter, R. (2010). Amyloid fibers provide structural integrity to *Bacillus subtilis* biofilms. Proc. Natl. Acad. Sci. USA *107*, 2230–2234.
34. Martin, M., Dragoš, A., Hölscher, T., Maróti, G., Bálint, B., Westermann, M., and Kovács, Á.T. (2017). *De novo* evolved interference competition promotes the spread of biofilm defectors. Nat. Commun. *8*, 15127.
35. van Gestel, J., Weissing, F.J., Kuipers, O.P., and Kovács, Á.T. (2014). Density of founder cells affects spatial pattern formation and cooperation in *Bacillus subtilis* biofilms. ISME J. *8*, 2069–2079.
36. West, S.A., Griffin, A.S., Gardner, A., and Diggle, S.P. (2006). Social evolution theory for microorganisms. Nat. Rev. Microbiol. *4*, 597–607.
37. Hölscher, T., Bartels, B., Lin, Y.C., Gallegos-Monterrosa, R., Price-Whelan, A., Kolter, R., Dietrich, L.E.P., and Kovács, Á.T. (2015). Motility, chemotaxis and aerotaxis contribute to competitiveness during bacterial pellicle biofilm development. J. Mol. Biol. *427*, 3695–3708.
38. López, D., Vlamakis, H., and Kolter, R. (2009). Generation of multiple cell types in *Bacillus subtilis*. FEMS Microbiol. Rev. *33*, 152–163.
39. Diethmaier, C., Pietack, N., Gunka, K., Wrede, C., Lehnik-Habrink, M., Herzberg, C., Hübner, S., and Stülke, J. (2011). A novel factor controlling bistability in *Bacillus subtilis*: The YmdB protein affects flagellin expression and biofilm formation. J. Bacteriol. *193*, 5997–6007.
40. Beauregard, P.B., Chai, Y., Vlamakis, H., Losick, R., and Kolter, R. (2013). *Bacillus subtilis* biofilm induction by plant polysaccharides. Proc. Natl. Acad. Sci. USA *110*, E1621–E1630.
41. Dobay, A., Bagheri, H.C., Messina, A., Kümmerli, R., and Rankin, D.J. (2014). Interaction effects of cell diffusion, cell density and public goods properties on the evolution of cooperation in digital microbes. J. Evol. Biol. *27*, 1869–1877.
42. Mohri, K., Kiyota, Y., Kuwayama, H., and Urushihara, H. (2013). Temporal and non-permanent division of labor during sorocarp formation in the social amoeba *Acytostelium subglobosum*. Dev. Biol. *375*, 202–209.
43. López, D., and Kolter, R. (2010). Extracellular signals that define distinct and coexisting cell fates in *Bacillus subtilis*. FEMS Microbiol. Rev. *34*, 134–149.
44. Winkelman, J.T., Bree, A.C., Bate, A.R., Eichenberger, P., Gourse, R.L., and Kearns, D.B. (2013). RemA is a DNA-binding protein that activates biofilm matrix gene expression in *Bacillus subtilis*. Mol. Microbiol. *88*, 984–997.
45. Elsholz, A.K.W., Wacker, S.A., and Losick, R. (2014). Self-regulation of exopolysaccharide production in *Bacillus subtilis* by a tyrosine kinase. Genes Dev. *28*, 1710–1720.
46. Erskine, E., Morris, R., Schor, M., Earl, C., Gillespie, R.M.C., Bromley, K., Sukhodub, T., Clark, L., Fyfe, P., Serpell, L., et al. (2017). Formation of functional, non-amyloidogenic fibres by recombinant Bacillus subtilis TasA. bioRxiv.
47. Allen, B., Gore, J., and Nowak, M.A. (2013). Spatial dilemmas of diffusible public goods. eLife *2*, e01169.
48. Alteri, C.J., Himpsl, S.D., Pickens, S.R., Lindner, J.R., Zora, J.S., Miller, J.E., Arno, P.D., Straight, S.W., and Mobley, H.L.T. (2013). Multicellular bacteria deploy the type VI secretion system to preemptively strike neighboring cells. PLoS Pathog. *9*, e1003608.
49. Štefanič, P., Kraigher, B., Lyons, N.A., Kolter, R., and Mandić-Mulec, I. (2015). Kin discrimination between sympatric *Bacillus subtilis* isolates. Proc. Natl. Acad. Sci. USA *112*, 14042–14047.
50. Lyons, N.A., Kraigher, B., Štefanič, P., Mandić-Mulec, I., and Kolter, R. (2016). A combinatorial kin discrimination system in *Bacillus subtilis*. Curr. Biol. *26*, 733–742.
51. Rubinstein, S.M., Kolodkin-Gal, I., McLoon, A., Chai, L., Kolter, R., Losick, R., and Weitz, D.A. (2012). Osmotic pressure can regulate matrix gene expression in *Bacillus subtilis*. Mol. Microbiol. *86*, 426–436.
52. Shemesh, M., Kolter, R., and Losick, R. (2010). The biocide chlorine dioxide stimulates biofilm formation in *Bacillus subtilis* by activation of the histidine kinase KinC. J. Bacteriol. *192*, 6352–6356.
53. Konkol, M.A., Blair, K.M., and Kearns, D.B. (2013). Plasmid-encoded ComI inhibits competence in the ancestral 3610 strain of *Bacillus subtilis*. J. Bacteriol. *195*, 4085–4093.
54. Mhatre, E., Sundaram, A., Hölscher, T., Mühlstädt, M., Bossert, J., and Kovács, Á.T. (2017). Presence of calcium lowers the expansion of *Bacillus subtilis* colony biofilms. Microorganisms *5*, 7.
55. Murray, E.J., Strauch, M.A., and Stanley-Wall, N.R. (2009). SigmaX is involved in controlling Bacillus subtilis biofilm architecture through the AbrB homologue Abh. J. Bacteriol. *191*, 6822–6832.

56. Verhamme, D.T., Murray, E.J., and Stanley-Wall, N.R. (2009). DegU and Spo0A jointly control transcription of two loci required for complex colony development by *Bacillus subtilis*. J. Bacteriol. *191*, 100–108.

57. Dragoš, A., Lakshmanan, N., Martin, M., Horváth, B., Maróti, G., Falcón García, C., Lieleg, O., and Kovács, Á.T. (2017). Evolution of exploitative interactions during diversification in *Bacillus subtilis* biofilms. FEMS Microbiol. Ecol. *93*, fix155.

58. Hölscher, T., Dragoš, A., Gallegos-Monterrosa, R., Martin, M., Mhatre, E., Richter, A., and Kovács, Á.T. (2016). Monitoring spatial segregation in surface colonizing microbial populations. J. Vis. Exp. *116*, e54752.

STAR★METHODS

KEY RESOURCES TABLE

Reagent or Resource	Source	Identifier
Chemicals		
Lysogeny broth (LB), Lennox	Carl Roth GmbH	Catalog # X964.1
Agar-Agar	Carl Roth GmbH	Catalog # 5210.3
Potassium Hydrogen Phosphate	Carl Roth GmbH	Catalog # P749.1
Potassium Dihydrogen Phosphate	Carl Roth GmbH	Catalog # 3904.2
L-Glutamic acid Monopotassium salt monohydrate	Alfa Aesar	Catalog # 17232
Magnesium chloride hexahydrate	Carl Roth GmbH	Catalog # 2189.1
Potassium chloride	Carl Roth GmbH	Catalog # 6781.3
Calcium chloride	Carl Roth GmbH	Catalog # 5239.2
Manganese(II) chloride	Carl Roth GmbH	Catalog # T881.3
Iron(III) chloride	Carl Roth GmbH	Catalog # P742.1
Zinc chloride	Carl Roth GmbH	Catalog # T887.1
Ammonium chloride	Carl Roth GmbH	Catalog # K298.2
Thiamin	Carl Roth GmbH	Catalog # T911.1
MOPS	Carl Roth GmbH	Catalog # 6979.4
Glycerol	Carl Roth GmbH	Catalog # 7533.1
Murashige and Skoog medium (MS)	Sigma Aldrich	Catalog # M5519
Sodium hypochlorite	Carl Roth GmbH	Catalog # 9062.3
Tetracycline hydrochloride	Carl Roth GmbH	Catalog # 0237.1
Spectinomycin dihydrochloride	Alfa Aesar	Catalog # J61820
Glucose	Fisher Scientific	Catalog # G/0500/61
EDTA	VWR	Catalog # 20302.260
Tris	VWR	Catalog # 103157P
HCl	VWR	Catalog # 20252.335
Experimental Models: Organisms/Strains		
Bacillus subtilis NCBI 3610 *comI*^{Q12l}	[51]	Strain DK1042
Bacillus subtilis NCBI 3610 *comI*^{Q12l} derivatives (listed in Table S1).	This study	N/A
Arabidopsis thaliana Col-0	Greenhouse of Max Plank Institute for Chemical Ecology, Jena	N/A
Recombinant DNA		
pmKATErrnB	[35]	GenBank: KF245454; https://www.ncbi.nlm.nih.gov/nuccore/KF245454
pTB848	This study	N/A
pTB849	This study	N/A
pTB498	This study	N/A
pNW725	This study	N/A
Sequence-Based Reagents		
Primers used in this study are listed in Table S2.	This study	N/A
Software and Algorithms		
ImageJ	[52]	https://imagej.nih.gov/ij/
OriginPro 2015G	OriginLab, Northampton, MA	http://www.originlab.com/

CONTACT FOR REAGENT AND RESOURCE SHARING

Further information and requests for resources and reagents should be directed to and will be fulfilled by the Lead Contact, Ákos T. Kovács (atkovacs@dtu.dk).

EXPERIMENTAL MODEL AND SUBJECT DETAILS

All bacterial strains used in this study derived from *Bacillus subtilis* NCBI 3610 *comI*^{Q12I} strain [53]. Strains were maintained in LB medium (Lysogeny broth (Lennox); Carl Roth, Germany), while MSgg medium was used for pellicle formation assay [27]. The MSgg medium was prepared as follows: MSgg base was prepared by weighting 0.026 g KH_2PO_4, 0.061 g K_2HPO_4, 2.09 g MOPS and 0.04 g $MgCl_2x6H_2O$ per 100ml of dH2O and adjusting the pH to 7.0 using KOH. The MSgg base was autoclaved, cooled down to RT and supplemented with 0.1ml of 0.7 M $CaCl_2$, 0.1ml of 100mM $MnCl_2$, 0.1ml of 50mM $FeCl_3$, 0.1ml of 1mM $ZnCl_2$, 0.1ml of 2mM thiamine, 0.57ml of 86% glycerol and 10 mL of 5% K-glutamate.

Strain construction

All strains that were used in this study or that were used solely as gDNA donors are listed in Table S1. To obtain TB601 and TB863, the NCBI 3610 *comI*^{Q12I} was transformed with gDNA isolated from DL1032 selecting for Tet-resistant colonies or Km-resistant colonies, respectively.

TB524.1 and TB525.2 were obtained by transforming TB601 with gDNA isolated from TB500.1 and TB501.1, respectively. TB538.1 and TB539.1 were obtained by transforming TB602 with gDNA isolated from TB500.1 and TB501.1, respectively. To obtain TB864 and TB865, NCBI 3610 *comI*^{Q12I} was first transformed with gDNA from 168hymKate and then with gDNA isolated from NRS2242 and NRS3913, respectively. To obtain Anc Kate P_{eps}-GFP, strain TB602 was first transformed with gDNA from 168hymKate and then with gDNA from NRS2242. To obtain Anc Kate P_{tapA}-GFP, strain TB 601 was first transformed with gDNA from 168hymKate and then with gDNA from NRS2394. In order to construct pTB848 and pTB849, the *eps* and *tapA* promoters were amplified using oTB172-oTB173 and oTB174-oTB175 primers pairs, respectively (see Table S2), the PCR products were digested with EcoRI and *Nhe*I, and cloned into the corresponding sites of vector pmKATErrnB. To obtain strains TB961 and TB962, first NCBI 3610 *comI*^{Q12I} was transformed with gDNA from NRS2242, and the obtained strain (TB373) was transformed with plasmids pTB848 and pTB849, respectively. TB960 was constructed by transforming NCBI 3610 *comI*^{Q12I} with gDNA from NRS3913 and the obtained strain (TB363) was subsequently transformed with pTB849 plasmid. To construct plasmid pTB498 harboring a constitutively expressed mKATE2 gene, the $P_{hyperspank}$-mKATE2 fragment was PCR amplified with primers oTH1 and oTH2 from plasmid phy-mKATE2 [35], digested with *Xba*I and EcoRI, ligated into plasmid pWK-Sp as described in [54]. Resulting plasmids were verified by sequencing and transformed into *B. subtilis* NCBI 3610 *comI*^{Q12I}, resulting in TB539.

Plasmid pNW725 was used to construct strain NRS3913. This was generated through amplification of the *mKate2* coding region from plasmid pTMN387 using primers NSW1026 and NSW1027 (see Table S2) and ligation into plasmid pNW600 using *HinD*III and BamHI. Plasmid pNW600 carries the P*tapA* promoter region [55], and therefore plasmid pNW725 has the *mKate2* coding region under the control of the *tapA* promoter region. Plasmid pNW725 was integrated into the chromosome of *B. subtilis* NCIB3610 at the *amyE* locus. Strain NRS5832 was generated by phage transduction of the P*epsA-gfp* reporter fusion from strain NRS2242 into NRS3913 as the recipient. Phage transduction was performed using SSP1 phage as previously described [56].

METHOD DETAILS

Pellicle formation and productivity assays

To obtain pellicle biofilms, bacteria were routinely growth in static liquid MSgg medium at 30°C for 48 hours, using 1% inoculum from overnight cultures. Productivities where accessed by examining colony forming units (CFUs) in mature pellicles. Prior each CFU assays, pellicles were sonicated according to a protocol optimized in our laboratory that allows proper disruption of biofilms without affecting cell viability [34, 57]. To access relative frequencies of Δ*eps* and Δ*tasA* strains, the cocultures were plated on selective antibiotics tetracycline (10μg/ml) and spectinomycin (100μg/ml), respectively.

Fitness assays

Since the expression of *epsA-O* and *tapA-sipW-tasA* operons strongly depend on cultivation conditions and media composition [24, 40, 51, 54, 56], we performed the competition experiment for the fitness costs of EPS and TasA production under the same conditions that were later used for the assays that involved pellicles. Strains of interest were premixed at 1:1 ratios based on their OD_{600} values and the mixture was inoculated into MSgg medium at 1%. Cultures were grown under static conditions at 30°C. CFU assays (using selective antibiotics for the Δ*eps* and Δ*tasA* strains) were performed immediately after inoculation and after 16 hours of growth. The growth curves obtained at the initial stage of pellicle formation were performed under standard pellicle growth conditions in 96-well plates. The optical densities and GFP-fluorescence were monitored using an infinite F200PRO plate reader (TECAN Group Ltd, Männedorf, Switzerland).

Spent media complementation assay

The supernatants were obtained from the WT, Δ*eps* and Δ*tasA* strains grown under static conditions in MSgg medium at 30°C for 48 hours. Cells were pelleted by centrifugation (5min, 8000 rpm), the supernatants were sterilized using Millipore filters (0.2μm pore size), and mixed in 1:1 ratio with 2 times' concentrated MSgg medium. Surface colonization of the Δ*eps* and Δ*tasA* in presence of conditioned media from the WT or complementary mutant strains were compared with the negative controls where the mutants grew in presence of their own conditioned media.

Microscopy/confocal laser scanning microscopy

Bright field images of whole pellicles and colonies were obtained with an Axio Zoom V16 stereomicroscope (Carl Zeiss, Jena, Germany) equipped with a Zeiss CL 9000 LED light source and an AxioCam MRm monochrome camera (Carl Zeiss). For time-lapse experiment, cultures were grown in 24-well plates (1.5 cm diameter per well), incubated in INUL-MS2-F1 incubator (Tokai Hit, Shizuoka, Japan) at 30°C and images were recorded every 15 min. The detailed description of the fluorescence time lapse microscope has been previously published [58]. The pellicles were also analyzed using a confocal laser scanning microscope (LSM 780 equipped with an argon laser, Carl Zeiss) and Plan-Apochromat/1.4 Oil DIC M27 63 × objective. Fluorescent reporter excitation was performed with the argon laser at 488 nm and the emitted fluorescence was recorded at 484–536 nm and 567–654 nm for GFP and mKate, respectively. To generate pellicle images, Z stack series with 1 μm steps were acquired. Zen 2012 Software (Carl Zeiss) was used for both stereomicroscopy and CLSM (confocal laser scanning microscopy) image visualization.

Sample fixing and flow cytometry

Pellicles were harvested at 24, 48, and 72 h into sterile 2 mL screw cap tubes, followed by centrifugation at 17000'g for 10 min. GTA buffer (50 mM glucose, 10 mM EDTA pH 8.0, and 20 mM Tris-HCl pH 8.0) was added into 24-well plates to harvest the cells remained in wells and pooled with cell pellet from previous step. Pooled cell pellets were then pumped through 23G needles 6 times to disperse pellicles. Dispersed samples were pelleted down and fixed by incubation with 4% paraformaldehyde for 7 min at room temperature. Fixed samples were washed with GTA, and subjected to mild sonication prior flow cytometry. Flow cytometry (LSRFortessa, BD biosciences) were operated by FACS facility in School of Life Sciences, University of Dundee. For initial experiments comparing the expression of matrix genes in the WT and the biofilm mutants flow cytometry (BD Facscanto II, BD biosciences) was performed at Disease Systems Immunology Group, DTU Bioengineering.

Root colonization assay/root biofilms productivity

Colonization of *Arabidopsis thaliana* roots was performed according to modified protocol from [40]. *Arabidopsis* ecotype Col-0 seeds were surface sterilized using 2% (v/v) sodium hypochlorite solution as follows: seeds were incubated in 2% (v/v) sodium hypochlorite with mixing on an orbital shaker for 20 min and then washed five times with sterile distilled water. The seeds were placed on pre-dried MS agar plates (Murashige and Skoog basal salts mixture; Sigma) (2.2 g l^{-1}) in an arrangement approximately 20 seeds per plate at a minimum distance of 1 cm. Seeds were germinated and grown on agar plates containing MS medium. After 3 days of incubation at 4°C, plates were placed at an angle of 65° in a plant chamber (21°C, 16h light per day). After 6 days, homogeneous seedlings ranging 0.8-1.2cm in length were selected for root colonization assay. Seedlings were transferred into 48-well plates containing 270μl of MSNg medium [40] per well. The MSN medium was prepared as follows: the base was prepared by weighting 0.026 g KH_2PO_4, 0.061 g K_2HPO_4, 2.09 g MOPS and 0.04 g $MgCl_2x6H_2O$ per 100ml of dH2O and adjusting the pH to 7.0. The base was autoclaved, cooled down to RT and supplemented with 0.1ml of 0.7 M $CaCl_2$, 0.05ml of 100mM $MnCl_2$, 0.1ml of 1mM $ZnCl_2$, 0.1ml of 2mM thiamine, NH_4Cl to final 0.2% and glycerol to final 0.05%. The MSNg medium was supplemented with 30μl of exponentially growing bacterial culture diluted to OD_{650} = 0.2. The sealed plates were incubated at rotary shaker at 28°C for 18h at 90 rpm After the incubation, plants were washed 3 times with MSNg to remove non-attaching cells and then transferred to a glass slide for imaging using CLSM. To access root biofilm productivities, the roots were transferred into Eppendorf tubes, subjected to standard sonication protocol and the CFU assays were performed for obtained cell suspensions. To extract CFU/mm of root, the obtain CFU values were divided by total length of a corresponding root.

Images of plant roots

For biofilm roots visualization, the GFP and mKate images were converted into 3D projections, contrast was enhanced using normalized function and green and red lookup tables were applied for GFP and mKate channels, respectively. Overlay images were obtained in ZEN software and further processed using ImageJ as follows: Brightness and contrast were adjusted, the root and biofilm area was manually selected and the background was lightened and smoothed using 'adjust brightness' and 'smooth' functions, respectively.

Modeling

We performed individual-based simulations, using the platform developed previously [41]. Microbial simulations occur on a two-dimensional toroidal surface with connected edges (i.e., there are no boundaries). The surface of the torus is 10,000 μm^2 (100 × 100 μm). Bacteria are modeled as discs with an initial radius of 0.5 μm. Bacteria can consume resources, grow at a basic growth rate (μ = 1) and divide when reaching the threshold radius of 1 μm. In our simulations, we assumed that resources are not limited. Bacteria further produce beneficial public goods at a cost *c* per molecule and at constant rate of 1 molecule/s. Public goods diffuse randomly according to the diffusion coefficient *d* (μm^2/s) and following a Gaussian random walk. Public goods can decay with

a certain probability p, with p increasing exponentially with time following the exponential function $p = 1 - e^{-w\Delta t/\partial}$, where Δt is the age of the molecule, w the stiffness of the decay and ∂ the durability of the molecule. A public good can generate a benefit b to the cell that takes it up, which occurs when the cell and the public good physically overlap on the landscape. Bacteria can randomly disperse, too, defined by the diffusion coefficient D ($\mu m^2/s$). Because we aimed to model bacterial performance in biofilms, where cell dispersal is relatively low, we set $D = 0.01\ \mu m^2/s$. Important to note is that neither bacteria nor public goods are bound to a grid, but move on a continuous landscape (following an off-lattice model with double-precision numbers). This mimics natural bacterial behavior as close as possible. One practical complication of this approach is that cells overlap with each other following diffusion. To cope with this issue, we applied an overlap correction after each time step following the procedure described in [41].

Using this setup, we simulated the performance of a wild-type (WT) strain, producing two public goods representing EPS and TasA, and two strains (PG1 and PG2) producing only one of the two public goods. We arbitrarily considered PG1 = TasA producer and PG2 = EPS producer. The growth of the three strains is defined by the following recursive functions:

$$G_{WT}(t+1) = \left[\mu - f(c_1 + c_2) + b_1 \sum pg1 + b_2 \sum pg2 + b_3 \left(\sum pg1 + R_{pg1}\right)\left(\sum pg2 + R_{pg2}\right)\right] G_{WT}(t) \quad (1)$$

$$G_{PG1}(t+1) = \left[\mu - c_1 + b_1 \sum pg1 + b_2 \sum pg2 + b_3 \left(\sum pg1 + R_{pg1}\right)\left(\sum pg2 + R_{pg2}\right)\right] G_{PG1}(t) \quad (2)$$

$$G_{PG2}(t+1) = \left[\mu - c_2 + b_1 \sum pg1 + b_2 \sum pg2 + b_3 \left(\sum pg1 + R_{pg1}\right)\left(\sum pg2 + R_{pg2}\right)\right] G_{PG2}(t), \quad (3)$$

where G is the radius increase per time step t, μ is the basic growth rate, c_1 and c_2 are the costs of producing the respective public goods, and f is the metabolic constraint factor, whereby $f > 1$ if the simultaneous production of both public goods is costlier than producing either of the public goods alone. Furthermore, while b_1 and b_2 are the benefits accruing when a respective public good is taken up multiplied by the total number of public goods consumed ($\sum$pg1 and $\sum$pg2) per time step, b_3 is the synergistic benefit accruing for all the complementary public goods taken up within a certain period of time (R_{pg1} and R_{pg2}, respectively). We arbitrarily chose five time steps for R_{pg1} and R_{pg2}.

For all simulations, we seeded our in-silico landscape with eight cells placed in the center of the landscape to mimic the early phase of pellicle formation. Cells then started to produce public goods, grew and divided defined by their growth function. We let bacteria grow for 10,000 time steps in 50 independent replicates for each parameter combination. We examined three growth treatments, which included the WT strain in monoculture, the two complementary strains PG1 and PG2 in monocultures, and the two complementary strains PG1 and PG2 in mixed cultures. In the mixed cultures, we varied the starting frequency of the two strains from 1:7 (PG1 to PG2) to 7:1. For all simulations, we extracted the absolute productivity of the biofilm and the relative fitness of the competing strains within biofilms. To assess the role of public good diffusion on biofilm productivity and relative strain fitness, we varied public good diffusion from 3 to 7 $\mu m^2/s$ in steps of 0.5 $\mu m^2/s$. To take into account that the public goods TasA and EPS might generate different benefits we varied the b_1/b_2 ratio from 1/9 to 1/1. Finally, we examined the effect of metabolic constraints on WT fitness by varying f from 1 to 1.3. All parameters together with the specific values used are given in the Table S3.

QUANTIFICATION AND STATISTICAL ANALYSIS

Relative fitness

Relative fitness W_A for strain A in competition with strain B was calculated as follows:

$$W_A = \left[\ln\left(CFU_{A\_16h}/CFU_{A\_start}\right)\right] / \left[\ln\left(CFU_{B\_16h}/CFU_{B\_start}\right)\right]$$

All replicates where one strain occurred to strongly dominate in the initial inoculum (exceeding initial 0.8 frequency) were removed from the dataset.

Strain frequencies on plant roots

Ratios of the Δ*eps*^{GFP} and ΔtasA^{mKate} (and control with swapped fluorescent reporters) in root biofilms were estimated from the ratios of white pixel volumes measured on corresponding fluorescent images. Images were analyzed using ImageJ software. First, the root and biofilm area it was manually selected on the white-light image. For each channel, the stacks were converted into binary images and threshold was set up to > 0 value. Next, the root+biofilm selection was activated on the processed stacks and total pixel volumes for each channel were extracted using 'stacks statistics' function.

Density correlation

The corresponding image stacks were dissected into cubes of 10 px side length. For each channel, the biovolume per cube was obtained. For all cubes containing biovolume in either of the two fluorescence channels (designated ch1 and ch2) the total biovolume in ch1 and ch2 within a sphere of a given radius (1 - 5 μm) was summed up, multiplied and normalized by the total volume of the sphere.

The resulting value ranges from 0 (no correlation, no biomass in one of the channels) over 0.25 (50% of biomass in ch1, 50% of biomass in ch2) to 1 (cube is completely filled in both channels = 100% overlap).

Statistical analysis

For relative fitness assay, statistical differences from W = 1 were identified using one-sample Student's t test. In case of productivity measurements statistical differences between two experimental groups were identified using two-tailed Student's t tests assuming equal variance. Variances in the two main types of datasets (relative fitness, productivity) were similar across different samples. No statistical methods were used to predetermine sample size and the experiments were not randomized. All relevant data are available from the authors.

Chapter 5

Collapse of genetic division of labour and evolution of autonomy in pellicle biofilms

Published in Nature Microbiology (2018)

nature microbiology

ARTICLES

https://doi.org/10.1038/s41564-018-0263-y

Collapse of genetic division of labour and evolution of autonomy in pellicle biofilms

Anna Dragoš[1,2], Marivic Martin[1,2], Carolina Falcón Garcia[3], Lara Kricks[4], Patrick Pausch[5], Thomas Heimerl[6], Balázs Bálint[7,9], Gergely Maróti[8], Gert Bange[5], Daniel López[4], Oliver Lieleg[3] and Ákos T. Kovács[1,2*]

Closely related microorganisms often cooperate, but the prevalence and stability of cooperation between different genotypes remain debatable. Here, we track the evolution of pellicle biofilms formed through genetic division of labour and ask whether partially deficient partners can evolve autonomy. Pellicles of *Bacillus subtilis* rely on an extracellular matrix composed of exopolysaccharide (EPS) and the fibre protein TasA. In monocultures, Δ*eps* and Δ*tasA* mutants fail to form pellicles, but, facilitated by cooperation, they succeed in co-culture. Interestingly, cooperation collapses on an evolutionary timescale and Δ*tasA* gradually outcompetes its partner Δ*eps*. Pellicle formation can evolve independently from division of labour in Δ*eps* and Δ*tasA* monocultures, by selection acting on the residual matrix component, TasA or EPS, respectively. Using a set of interdisciplinary tools, we unravel that the TasA producer (Δ*eps*) evolves via an unconventional but reproducible substitution in TasA that modulates the biochemical properties of the protein. Conversely, the EPS producer (Δ*tasA*) undergoes genetically variable adaptations, all leading to enhanced EPS secretion and biofilms with different biomechanical properties. Finally, we revisit the collapse of division of labour between Δ*eps* and Δ*tasA* in light of a strong frequency versus exploitability trade-off that manifested in the solitarily evolving partners. We propose that such trade-off differences may represent an additional barrier to evolution of division of labour between genetically distinct microorganisms.

Cooperation among microorganisms is indisputable, but the mechanism of partner selection remains under discussion. According to the fundamental theory of kin selection, cooperation should predominantly occur within closely related groups, in which the chances that a beneficiary carries the same cooperative gene are maximized[1]. Nevertheless, it has been documented that individuals of low genetic relatedness can help each other, as long as they share a locus encoding for cooperation or a mechanism exists that allows discrimination against non-cooperators[2–5]. Cooperation may also take place via division of labour between (sub)populations of cells carrying or expressing different cooperative loci[6–8]. Benefits from allocation of cooperative tasks between different subpopulations or even genetically different strains have been demonstrated both experimentally[8–10] and by modelling[11,12]. Although in phenotypic division of labour task allocation is achieved by differences in gene expression, in the genetic division of labour, individuals carry only the genetic machinery for their own specialist task[13].

Moreover, spontaneous deletions[14] potentially leading to cooperative metabolic exchange[15], and even spontaneous evolution of genetic division of labour[10], have been experimentally documented. Nevertheless, some models predict that cooperative trading between genetically 'reduced' partners is evolutionarily unstable owing to risks of partner separation or social cheating[16,17].

Recent studies that directly tested the long-term stability of cooperation revealed that the evolutionary fate of social interactions can be unpredictable[18,19]. In the long-term presence of cheaters, cooperation may be reduced[20,21] or rewired towards another type of public good[20]. In particular cases, typically constrained defectors can spread as a side effect of evolutionary awakening of mobile genetic elements[19]. Finally, co-operators can de novo evolve from defectors, sometimes exhibiting high resistance against exploitation[22], whereas being highly vulnerable to invasions by cheaters in other cases[23]. Altogether, social evolution is a very dynamic process in which exploiters easily evolve[24]; their presence modulates the evolution of cooperators[20,21], which, even if extinct, may revive from defectors[22]. In light of such complexity, without direct experimental examination, the long-term evolutionary fate of cooperation within or beyond single genetic lineages is difficult to predict.

Here, we experimentally challenged the long-term evolutionary stability of genetic division of labour and explored the solitary adaptation of partially defective partners. The study was performed using a simple model system in which two *Bacillus subtilis* strains, when co-inoculated, benefit from division of labour in extracellular matrix construction by exchanging key matrix components: exopolysaccharide (EPS) and an amyloid protein, TasA[24]. These components form an extracellular matrix that allows *B. subtilis* to establish pellicle biofilms at the oxygen-rich liquid–air interface[25]. Pellicles emerge when *B. subtilis* grows in undisturbed liquid medium and encounters oxygen limitation[25]. Mutants lacking either EPS (Δ*eps*) or TasA (Δ*tasA*) cannot establish pellicle biofilms, but they can

[1]Bacterial Interactions and Evolution Group, Department of Biotechnology and Biomedicine, Technical University of Denmark, Kgs Lyngby, Denmark. [2]Terrestrial Biofilms Group, Institute of Microbiology, Friedrich Schiller University Jena, Jena, Germany. [3]Department of Mechanical Engineering and Munich School of Bioengineering, Technical University of Munich, Garching, Germany. [4]National Centre for Biotechnology (CNB), Spanish Research Council (CSIC), Madrid, Spain. [5]Faculty of Chemistry & LOEWE Center for Synthetic Microbiology, Philipps-University Marburg, Marburg, Germany. [6]Cell Biology & Electron Microscopy, LOEWE Center for Synthetic Microbiology, Philipps-University Marburg, Marburg, Germany. [7]Seqomics Biotechnology Ltd, Mórahalom, Hungary. [8]Institute of Plant Biology, Biological Research Centre, Hungarian Academy of Sciences, Szeged, Hungary. [9]Present address: Synthetic and Systems Biology Unit, Institute of Biochemistry, Biological Research Centre, Hungarian Academy of Sciences, Szeged, Hungary. *e-mail: atkovacs@dtu.dk

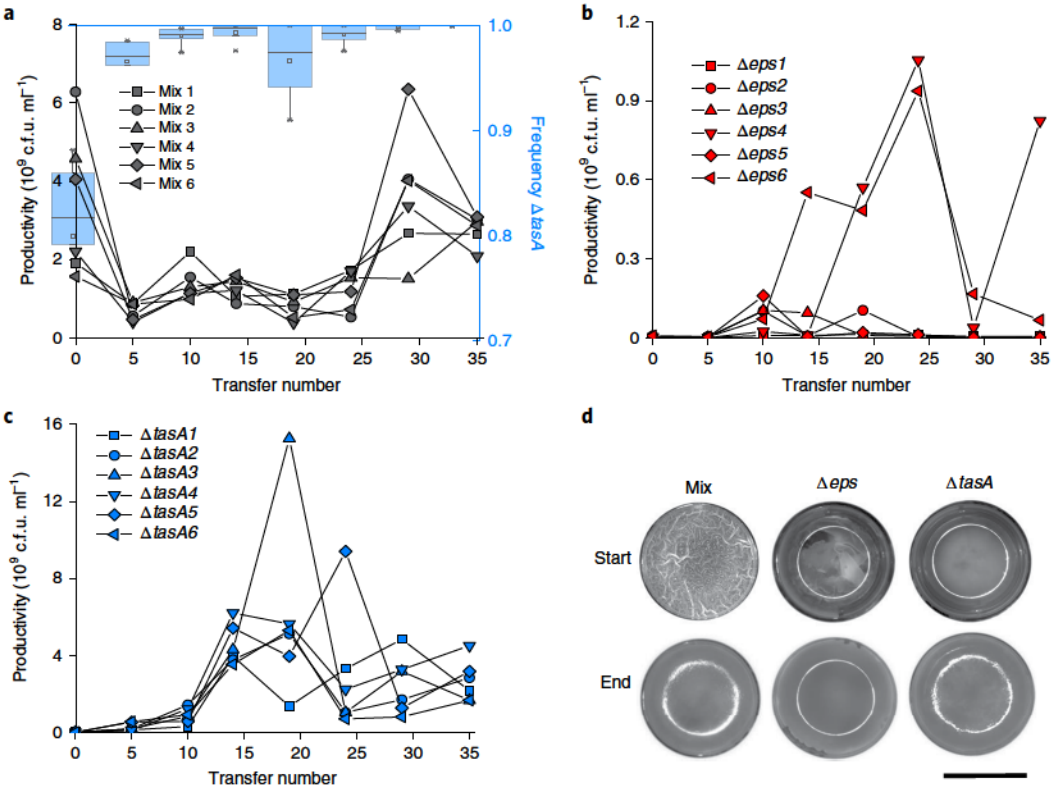

Fig. 1 | Changes in pellicle productivity and morphology during evolution. a, Biofilm productivities of six parallel Δ*eps*+Δ*tasA* co-cultures were systematically monitored (as c.f.u. ml^{-1}) during ongoing evolution experiments. Productivities were assessed every fourth or fifth transfer. Relative frequencies of Δ*eps* and Δ*tasA* in the mixtures were assessed by plating the co-cultures onto media containing an appropriate antibiotic. Relative frequencies of the Δ*tasA* strain at each evolutionary time point (pulled from six parallel co-cultures) are shown as blue box plots. Boxes represent the first quartile and the third quartile, the lines represent the median and the bars span from the maximum to the minimum values ($n=6$). **b**, Productivities of surface-colonizing Δ*eps* evolved in six parallel monocultures were systematically monitored as in **a**. **c**, Productivities of surface-colonizing Δ*tasA* evolved in six parallel monocultures were systematically monitored as in **a** and **b**. **d**, Pellicle morphology developed by the Δ*eps*+Δ*tasA* mix, and Δ*eps* and Δ*tasA* monocultures at the start and at the end of the evolution experiment. Pellicles were cultivated in a 24-well plate (well diameter, 15 mm). Scale bar, 10 mm. Morphology was tested in more than ten independent experiments with similar results.

complement each other in co-culture[19,26,27]. Previous studies suggest that such division of labour pays off and should be stable over evolutionary timescales[8]. Here, we directly challenge this hypothesis using an experimental evolution approach, hoping to reveal co-adaptation mechanisms of cooperating partners. Our work reveals an unexpected scenario regarding the fate of cooperation and striking adaptive trajectories followed by solitarily evolving partners.

Results

Collapse of division of labour and evolution of autonomy in *B. subtilis* pellicles. Our initial goal was to study co-adaptation of partners Δ*eps* and Δ*tasA* that are involved in the genetic division of labour, which seems to be an evolutionarily stable and more productive strategy for biofilm formation compared to that employed by the isogenic wild-type (WT) bacteria[8]. In addition, the Δ*eps* and Δ*tasA* strains were allowed to adapt in monocultures (see Methods).

In line with previous findings[8], the first pellicles formed by the mixtures showed very high productivity compared to the initial pellicles formed by solitary-grown Δ*eps* and Δ*tasA* (Fig. 1a–c, transfer 0; Fig. 1d). In addition, although inoculated at a 1/1 ratio, the pellicles consisted of a Δ*eps* minority and a Δ*tasA* majority, a mixture that was previously identified as an evolutionarily stable optimum[8].

Surprisingly, the productivities in all the mixed cultures dropped by transfer 5 and remained low until transfer 24, rising again after transfer 29 or 35 (Fig. 1a). It was evident that the rapid decrease in pellicle productivities coincided with an increase in the frequency of Δ*tasA* cells in the co-cultures and the permanent domination of this strain through the experiment, even at the late evolutionary time points during which productivities were rising again, indicating that, after a depression, the mutant adapted to colonize the interface without the help of the Δ*eps* strain (Fig. 1). Ultimately, the Δ*eps* strain showed complete extinction in four out of six initially mixed parallel populations. An identical scenario was observed when experimental evolution was repeated from fresh culture stocks: a decrease in overall productivity and an increase in Δ*tasA* frequency (Supplementary Fig. 1a).

In monocultures, both mutants evolved mechanisms that allowed colonization of the liquid–air interface independently (Fig. 1b–d). Nevertheless the 'success rate' of the adaptive process seemed to differ between the mutants as only two out of six parallel populations of Δ*eps* showed improvement, in contrast to increased air–medium colonization by all populations of Δ*tasA* (Fig. 1b–d). For both Δ*eps* and Δ*tasA*, the final pellicles lacked the typical 'wrinkled' surface complexity that can be observed for the WT pellicles or the initial mix of mutants (Fig. 1d). However, a densely packed mat on the liquid surface could easily be observed on the macroscale (Fig. 1d), as well as at the single-cell level (Supplementary Fig. 1b; see Methods). Specifically, cells of the evolved Δ*eps* seemed tightly packed, and the evolved Δ*tasA* pellicle appeared as a loosely connected mesh of cells and intracellular space (Supplementary Fig. 1b). Importantly,

the phenotype and final productivities of evolved Δ*tasA* were nearly identical regardless of its evolutionary history (initiated in co-culture versus in monoculture). Nevertheless, the evolution of independence by Δ*tasA* was delayed when it started in co-culture with Δ*eps* (Fig. 1a,c,d).

'Alter' strategy: EPS-independent pellicle formation involves modification of the TasA protein. As a next step, we aimed to untangle the molecular mechanisms that allowed the Δ*eps* mutants to colonize the liquid–air interface. We selected three representative single clones from monoculture population 4 and population 6 (which we named e4A, e4B and e4C and e6A, e6B and e6C, respectively) that showed pellicle development, as well as two representatives of non-pellicle formers coming from population 3 (e3A) and population 5 (e5A), for whole-genome sequencing. All adapted strains, but none of the non-pellicle-forming negative controls was found to contain single-nucleotide polymorphisms (SNPs) in the *tasA* locus (Supplementary Dataset 1). Strikingly, these SNPs were distinct in population 4 and population 6, but they resulted in a substitution of an amino acid to cysteine in both cases, specifically Y124C in population 4 and G183C in population 6 (Supplementary Dataset 1).

As TasA is a putative amyloid fibre protein[27–29], and cysteine plays important roles in protein oligomerization (reviewed in ref. [29]), the introduction of this amino acid into TasA could have dramatic effects on its amyloidogenesis. Moreover, a comparison of TasA proteins across different Firmicutes (the phylum to which *Bacillus* belongs) revealed a conservative lack of cysteines in this protein, whereas positions Y124 and G183 that were replaced by cysteines in the evolved Δ*eps* are located in the most conserved regions of TasA (Supplementary Fig. 2).

To test whether a single substitution in TasA can restore pellicle formation in the absence of EPS, we introduced $tasA_{Y124C}$ and $tasA_{G183C}$ into the ectopic *amyE* locus of the Δ*eps*Δ*tasA* double mutant, so that the original *tasA* was replaced by the cysteine-containing variants, resulting in Δ*eps*Δ*tasA*_$tasA_{Y124C}$ and Δ*eps*Δ*tasA*_$tasA_{G183C}$ strains (see Methods). Both substitutions completely restored the dense biofilm mat for strains Δ*eps*Δ*tasA*_$tasA_{Y124C}$ and Δ*eps*Δ*tasA*_$tasA_{G183C}$ in an isopropyl β-D-1-thiogalactopyranoside (IPTG)-dependent manner (Fig. 2a and Supplementary Fig. 3), but not in the control strain Δ*eps*Δ*tasA*_$tasA_{anc}$ in which the native *tasA* was inserted into the *amyE* locus (Fig. 2a). This result was supported by quantitative measurements of pellicle productivity, in which the Δ*eps* ancestor (Δeps_{anc}) and Δ*eps*Δ*tasA*_$tasA_{anc}$ performed poorly, whereas the evolved (e4A and e6A) or the complemented (Δ*eps*Δ*tasA*_$tasA_{Y124C}$ and Δ*eps*Δ*tasA*_$tasA_{G183C}$) strains carrying cysteine-containing TasA showed tremendous and comparable improvement (Fig. 2b). Moreover, the relative fitness of Δ*eps*Δ*tasA*_$tasA_{Y124C}$ and Δ*eps*Δ*tasA*_$tasA_{G183C}$ was higher than that of Δeps_{anc} (Fig. 2c), whereas the Δ*eps*Δ*tasA*_$tasA_{anc}$ control strain did not show increased fitness when competed with Δeps_{anc} (Fig. 2c). Altogether, these results indicated that substitutions of certain residues in TasA to cysteine allow pellicle formation in the absence of EPS (Fig. 2c).

TasA evolves different biochemical properties and different amyloid fibre morphology. How does the presence of cysteine change the properties of TasA? First, we asked whether it results in different biochemical properties of TasA that modulate oligomerization of the protein. To answer this question, we performed electrophoresis under native conditions combined with immunoblotting to detect the TasA protein (see Methods). The native TasA (detected in Δeps_{anc} and Δ*eps*Δ*tasA*_$tasA_{anc}$) formed oligomers of ~900 kDa, whereas the oligomers formed by the evolved variants showed both a smaller band (~800 kDa) and a smear at around 1,000–1,100 kDa (Supplementary Fig. 4b). It is highly unlikely that these results, or the results of the complementation assays (Fig. 2), were affected by differences in the production levels of ancestral and evolved TasA variants, as SDS–polyacrylamide gel electrophoresis (PAGE) combined with immunoblotting showed nearly identical band intensities for $TasA_{anc}$ (produced by Δeps_{anc} or Δ*eps*Δ*tasA*_$tasA_{anc}$ strains) and for the cysteine-containing variants (produced by the evolved or complemented strains) (Supplementary Fig. 4a).

Does the difference in oligomerization manifest in amyloid fibre formation by TasA? To explore this, we purified and visualized the fibres using transmission electron microscopy (see Methods; Supplementary Fig. 4c). All TasA variants showed formation of fibrous structures (Fig. 3) similar to those observed previously[27]. However, although native TasA showed a dense mesh of less organized, relatively thin fibres, the cysteine-containing variants assembled into thicker fibres that were formed by multiple, parallel-arranged thin fibres (Fig. 3 and Supplementary Fig. 4d). For $TasA_{anc}$, we observed bundles up to a fibre width of 20 nm. For the evolved TasA variants, we observed bundle widths up to 40 nm and 120 nm for $TasA_{Y124C}$ and $TasA_{G183C}$, respectively (Supplementary Fig. 4d). Based on the obtained electron micrographs, we speculate that the biochemical properties of the evolved, cysteine-containing TasA variant might be altered, which seems to influence filament architecture. However, more detailed studies are required to determine the exact structural properties of the evolved TasA protein and its filaments (for example, by NMR and X-ray scattering)[30].

Cysteine-containing TasA probably interacts with other components of the extracellular matrix. The above results suggested that cysteine-containing TasA can result in a dramatic fitness advantage (Fig. 2); thus, the conserved absence of this amino acid from native TasA proteins present in Firmicutes seemed puzzling (Supplementary Fig. 2). To explore this contradiction, we examined the effects of Y124C and G183C substitutions in TasA in the WT *B. subtilis* background, in which the EPS component is still present, $tasA_{anc}$, $tasA_{Y124C}$ and $tasA_{G183C}$ were introduced into the *amyE* locus of the Δ*tasA* ancestor. Surprisingly, the presence of cysteine-containing TasA hindered biofilm productivity, hydrophobicity and surface spreading (Supplementary Figs. 5 and 6 and Supplementary Result 1).

Recently, it was shown that the main biofilm hydrophobin, BslA, carries a conserved CXXC motif on its carboxy-terminal tail, which is crucial for protein oligomerization and therefore the hydrophobicity of *B. subtilis* biofilms[31]. Further experiments suggest that the putative TasA–BslA interaction might interfere with proper biofilm maturation in the EPS-producing background (Supplementary Fig. 5d and Supplementary Results 2).

'Make more' strategy: TasA-independent pellicle formation involves overexpression of *epsA–O*. Whole-genome sequencing of selected Δ*tasA* single isolates revealed multiple mutations that could potentially improve its fitness, but we could not identify one common locus that was changed in all isolates during improved surface colonization (Supplementary Dataset 1). Interestingly, despite strong genetic diversity, all of the evolved surface colonizers produced very similar, remarkably slimy pellicles (Fig. 1d and Supplementary Fig. 7a), which strongly differed in texture from mats of the WT or evolved Δ*eps* derivatives (see Fig. 1d for the evolved Δ*eps* pellicle structures and Supplementary Fig. 5b for the WT pellicle structures). Indeed, the rheology studies performed on selected evolved Δ*tasA* isolates (Mt1a evolved from co-culture mix 1 and t5A isolated from monoculture population 5), WT and evolved Δ*eps* revealed that the elastic moduli obtained for the WT and evolved Δ*eps* isolates (e4A and e6A) were 2–3 log higher than those obtained for the evolved Δ*tasA* strains, indicating low stiffness of the latter. In addition, the higher loss factor values obtained for the evolved Δ*tasA* compared to the WT and evolved Δ*eps*

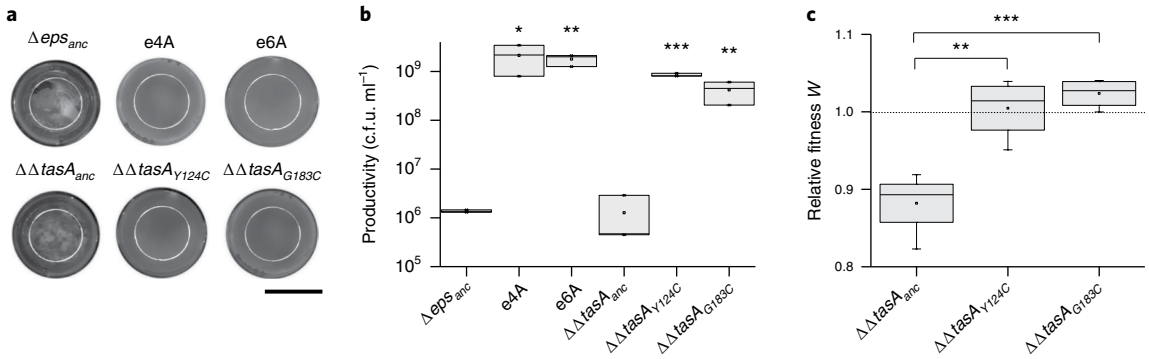

Fig. 2 | Complementation assay to recreate the evolved Δ*eps* phenotype. a, Pellicle morphology developed by Δeps_{anc} and two isolates, e4A and e6A, that showed improved surface-colonizing properties and were randomly selected from the evolved populations Δ*eps*4 and Δ*eps*6. $\Delta\Delta tasA_{anc}$, Δ*eps* $\Delta tasA\_tasA_{anc}$; $\Delta\Delta tasA_{Y124C}$, Δ*eps* $\Delta tasA\_tasA_{Y124C}$; $\Delta\Delta tasA_{G183C}$, Δ*eps* $\Delta tasA\_tasA_{G183C}$. Pellicles were cultivated in a 24-well plate (well diameter, 15 mm). Scale bar, 10 mm. A similar result was obtained in more than five independent experiments. **b**, Productivities of surface-colonizing Δeps_{anc}, e4A, e6A, Δ*eps* $\Delta tasA\_tasA_{anc}$, Δ*eps* $\Delta tasA\_tasA_{Y124C}$ and Δ*eps* $\Delta tasA\_tasA_{G183C}$ were recorded as c.f.u. ml^{-1} ($n = 3$ biologically independent samples). The asterisks indicate significant differences from Δeps_{anc} ($^{*}P < 0.05$; $^{**}P < 0.01$; $^{***}P < 0.001$; *t*-test, two tailed). **c**, Fitness of Δ*eps* $\Delta tasA\_tasA_{anc}$, Δ*eps* $\Delta tasA\_tasA_{Y124C}$ and Δ*eps* $\Delta tasA\_tasA_{G183C}$ when challenged with Δeps_{anc} in pellicle biofilm-forming conditions ($n = 4$ biologically independent samples). The asterisks indicate significant differences ($^{**}P < 0.01$; $^{***}P < 0.001$; *t*-test, two tailed). Boxes represent the first quartile and the third quartile, lines represent the median and the bars span from the maximum to the minimum value (**b**,**c**). For morphology (**a**), productivity (**b**) and fitness (**c**) studies, the complemented strains were grown in the presence of 0.2 mM IPTG to induce the expression of introduced *tasA* variants. Horizontal dashed line indicates value of 1.0 (no effects of complementation on fitness).

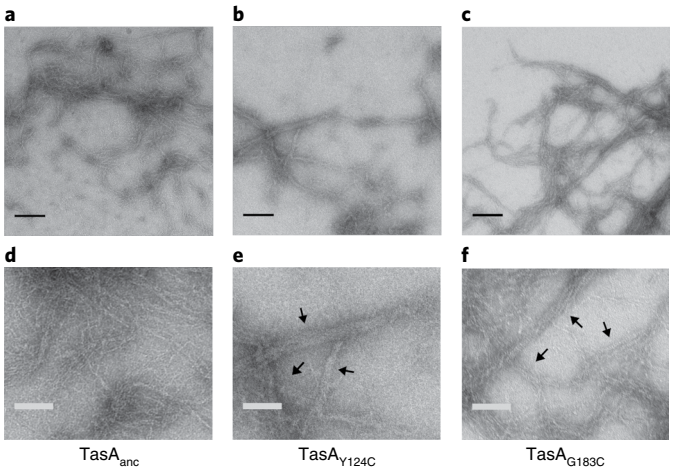

Fig. 3 | Fibre formation by native ΔSP-TasA and its cysteine-containing derivatives. a–**f**, Transmission electron microscopy images of fibres formed by $\Delta SP\text{-}TasA_{anc}$ (native TasA) (**a**,**d**), $\Delta SP\text{-}TasA_{Y124C}$ (**b**,**e**) and $\Delta SP\text{-}TasA_{G183C}$ (**c**,**f**) on carbon-coated electron microscopy grids. Scale bars, 0.2 µm (**a**–**c**) and 0.1 µm (**d**–**f**). The arrows (**e**,**f**) indicate filaments of stiff parallel arrangement that were typically formed by cysteine-containing ΔSP-TasA variants. Expression, purification and electron microscopy analyses of the TasA variants were performed in parallel to ensure comparability. Similar results were obtained for ten different micrographs obtained per sample.

isolates indicated increased viscosity of the evolved Δ*tasA* pellicles (Fig. 4a and Supplementary Fig. 7b).

Slimy surfaces of bacterial colonies, similar to that observed for the evolved Δ*tasA* pellicles, might be associated with an increased production of EPS[32]. To test this possibility, we compared the amounts of EPS produced per dry biomass in WT, $\Delta tasA_{anc}$, Δ*tasA* overexpressing *epsA–O* (which encodes EPS) from an IPTG-inducible $P_{hyperspank}$ promoter ($\Delta tasA_{hyEPS}$), Δ*eps* (used as a negative control) and selected evolved strains (see Methods; Supplementary Fig. 7c). The results pointed towards an increased production of EPS by the evolved strains (Supplementary Fig. 7c). In the next step, a P_{eps}-*gfp* (green fluorescent protein) promoter fusion was introduced into randomly selected evolved Δ*tasA* isolates, and their *epsA–O* expression levels were compared with the $\Delta tasA_{anc}$ under planktonic conditions in the biofilm-promoting MSgg medium. All examined evolved strains showed a higher GFP signal than $\Delta tasA_{anc}$ (Fig. 4b). The same result was evident from assaying *epsA–O* expression in biofilm colonies (with one exception, strain t6B, which also showed the lowest GFP signal among the evolved Δ*tasA* strains in the quantitative assay) (Supplementary Fig. 8a). We presume that one of the possible SNPs resulting in overproduction of EPS could be a mutation in the *ptpZ* gene (Fig. 4c,d, Supplementary Table 1, Supplementary Fig. 8b and Supplementary Results 3). Finally, we examined pellicle formation of $\Delta tasA_{hyEPS}$ in both the presence and the absence of IPTG. As expected, in the presence of IPTG, $\Delta tasA_{hyEPS}$ produced a comparable slimy pellicle phenotype, with identical biophysical properties and pellicle productivity, to the evolved Δ*tasA* strains (Fig. 4c,d and Supplementary Fig. 7b).

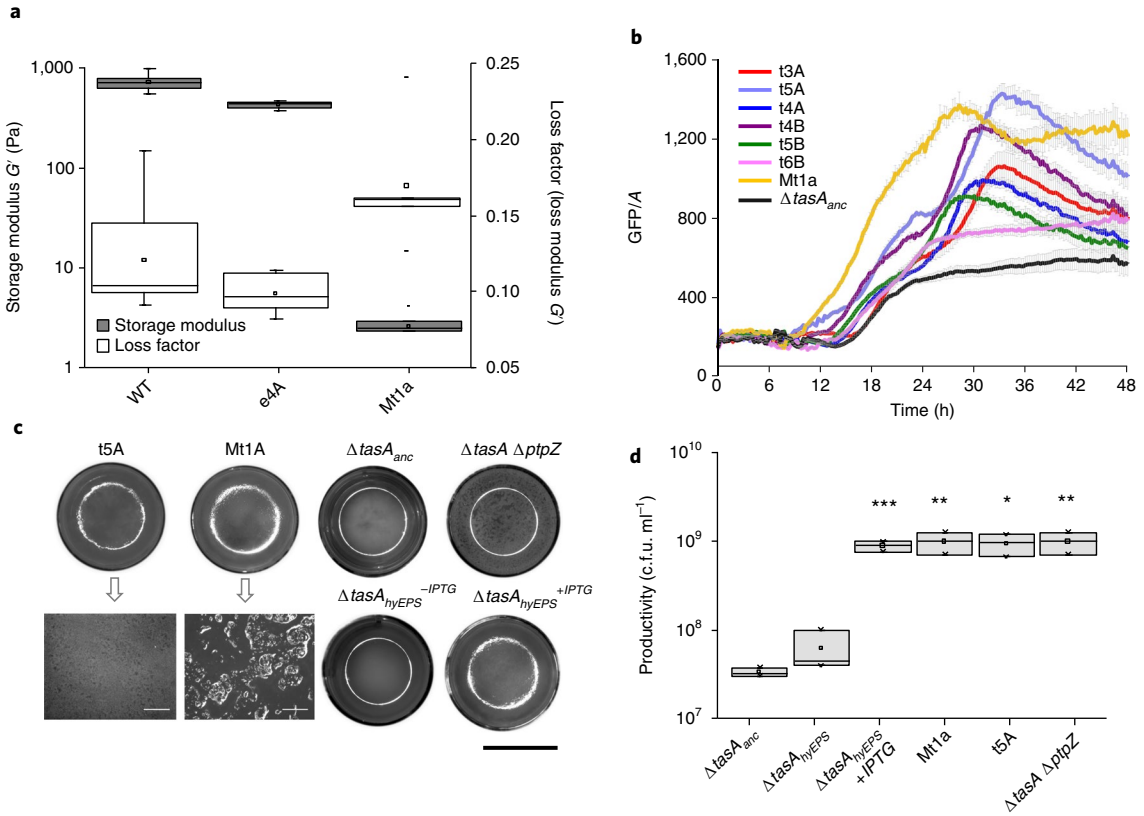

Fig. 4 | Investigation and recreation of the evolved Δ*tasA* phenotype. a, Viscoelastic properties of pellicles developed by WT (WT *B. subtilis* strain NCBI 3610), e4A and Mt1A (which is a Δ*tasA* isolate that shows improved surface-colonizing properties selected from the evolved population mix 1) were compared. The storage modulus (G′) and loss factors (G″/G′) of WT and e4A are similar, whereas Mt1A exhibits lower G′ and loss factor, indicating more pronounced viscous properties of Mt1A pellicles than those of WT and e4A. Boxes represent the first quartile and the third quartile, lines represent the median and the bars span from the maximum to the minimum value (for WT, $n=9$; e4A, $n=6$; Mt1A, $n=5$ biologically independent samples). **b**, Expression of the *eps* gene in the Δ$tasA_{anc}$ strain and seven randomly selected evolved isolates that showed improved surface-colonizing properties was compared using corresponding strains carrying a P_{eps}-*gfp* reporter fusion ($n=8$ biologically independent samples). Data points represent the mean and the error bars represent the standard error. **c**, Pellicle morphology developed by two evolved Δ*tasA* isolates: t5A and Mt1A (Δ$tasA_{anc}$ and Δ*tasA* Δ*ptpZ*). In the bottom panel, zoom images of the surfaces of the t5A and Mt1a pellicles are shown. Pellicle morphology of Δ$tasA_{hyEPS}$ (a Δ*tasA* strain with a native *eps* promoter replaced with an IPTG-inducible promoter) grown without IPTG and Δ$tasA_{hyEPS}$ grown with 0.2 mM IPTG. Pellicles were cultivated in a 24-well plate (well diameter, 15 mm). White scale bars, 500 µm; black scale bar, 10 mm. A similar result was obtained in two independent experiments. **d**, Productivities of surface-colonizing Δ$tasA_{anc}$, Δ$tasA_{hyEPS}$ (no IPTG), Δ$tasA_{hyEPS}$ (with 0.2 mM IPTG), t5A, Mt1A and Δ*tasA* Δ*ptpZ* were assessed as c.f.u. ml^{-1} ($n=3$ biologically independent samples). Boxes represent the first quartile and the third quartile, lines represent the median and the bars span from the maximum to the minimum value. The asterisks indicate significant differences compared to Δ$tasA_{anc}$ (*$P<0.05$; **$P<0.01$; ***$P<0.001$; *t*-test, two tailed).

This result confirmed that, in analogy to Δ*eps*, the adaptation of Δ*tasA* involved the remaining matrix component EPS. However, here, the improvement could simply be achieved through overproduction. Interestingly, some of the evolved Δ*eps* isolates also showed increased levels of *tasA* expression (Supplementary Fig. 8c), but simple overexpression of ancestral *tasA* (using the strain Δ*eps* ΔtasA_$tasA_{anc}$ at high IPTG concentrations) did not translate into improved pellicle formation (Fig. 2b).

The adaptive strategy of the EPS producer and the TasA producer is associated with low and high exploitability levels, respectively. Next, we asked what the implications of the two adaptive strategies ('alter' for Δ*eps* and 'make more' for Δ*tasA*) were on population dynamics of the evolved lineages and on subsequent changes in relative fitness during evolution (see Methods).

The structures of the evolved Δ*eps* populations exhibited an 'all-or-nothing' pattern, in which either all isolates within the population behaved like the ancestor or nearly all of them showed robust pellicle development (Fig. 5a). Conversely, all examined populations of Δ*tasA* exhibited high diversity with respect to the ability to form pellicles (Fig. 5c). The results of this large-scale, but purely qualitative, screen were supported by smaller-scale quantitative assays that confirmed low and high phenotypic diversity within the evolved Δ*eps* and evolved Δ*tasA* populations, respectively (Supplementary Fig. 9). Relative fitness analysis highlighted further differences between the adaptive patterns of Δ*eps* and Δ*tasA* populations; namely, populations of Δ*eps* from subsequent evolutionary time points showed, in general terms, a steady increase in relative fitness compared to the ancestor (Fig. 5b and Supplementary Fig. 10a). By contrast, although populations of Δ*tasA* from early evolutionary time points showed an increase in relative fitness, the advantage diminished in later populations, as the ancestor was able to hitchhike with the improved pellicle formers, possibly exploiting the EPS secreted by the evolved population (Fig. 5d and Supplementary Fig. 10b). These results point towards exploitability differences between the evolved Δ*eps* and Δ*tasA* strains: although hitchhiking of poorly performing isolates within the evolved Δ*eps* populations is limited, it seems prevalent in the case of the evolved Δ*tasA* populations.

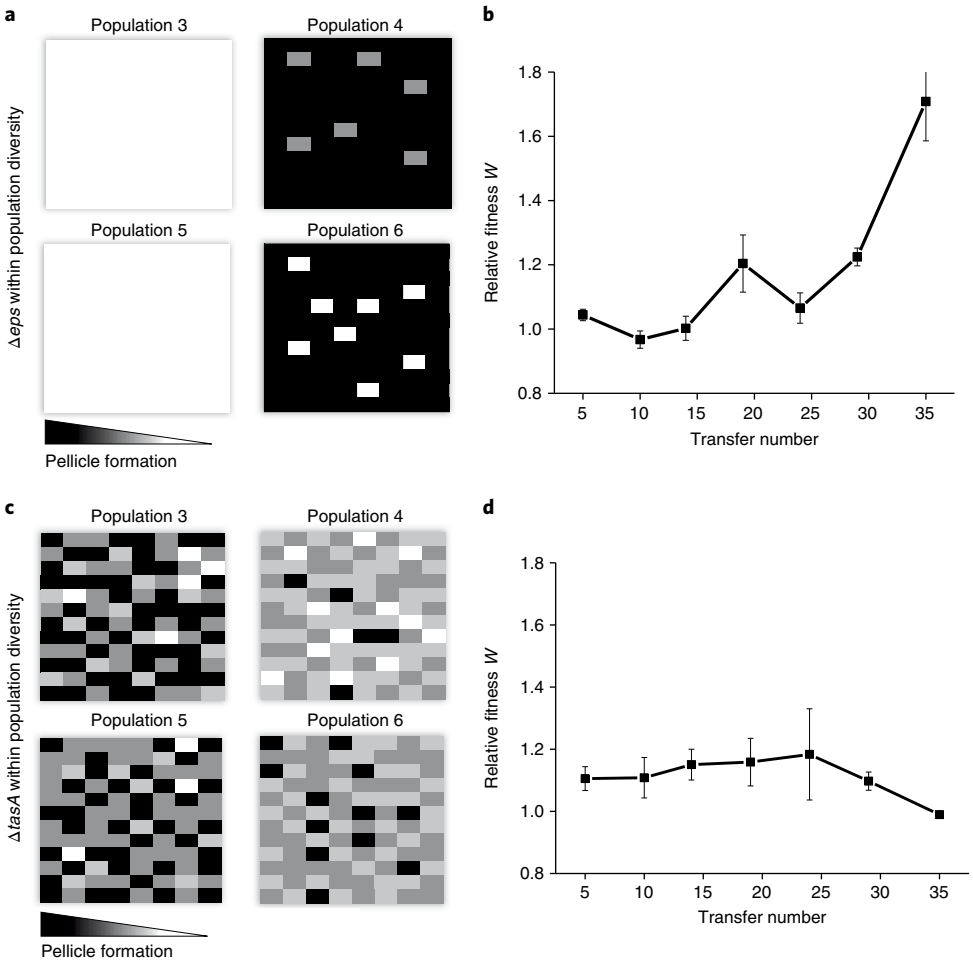

Fig. 5 | Population structure and fitness of the evolved Δ*eps* and Δ*tasA* populations. a, Four independently evolved Δ*eps* populations (Δ*eps*3, Δ*eps*4, Δ*eps*5 and Δ*eps*6) were examined for diversity at the productivity level within the population. Specifically, 96 randomly selected isolates from each population were allowed to form pellicles that were then scored according to their performance: 0 (ancestor-like residual pellicle) to 3 (strong pellicle (as for e4A or e6A)). Each population is graphically represented by a square made of 96 cubes. The colours of the cubes correspond to the performance of the isolates: score = 0, white; 1, light grey; 2, dark grey; 3, black. **b**, Changes in fitness in the Δ*eps*4 population through evolutionary time points when challenged with Δeps_{anc} in pellicle biofilm-forming conditions ($n = 4$ biologically independent samples). Data points represent the mean and the error bars represent the standard error. **c**, Four independently evolved Δ*tasA* populations (Δ*tasA*3, Δ*tasA*4, Δ*tasA*5 and Δ*tasA*6) were examined for diversity at the productivity level within the population, as described in **a**. The results are represented graphically as described in **a**. **d**, Changes in fitness in the Δ*tasA*4 population through evolutionary time points when challenged with $\Delta tasA_{anc}$ in pellicle biofilm-forming conditions ($n = 4$ biologically independent samples). Data points represent the mean and the error bars represent the standard error.

Disparity in the adaptive potential of cooperating partners may predestine the cooperation to collapse. As both Δ*eps* and Δ*tasA* strains could adapt in monocultures, delivering pellicles of comparable productivities, we further wondered why cooperation between the Δ*eps*-mutant and the Δ*tasA*-mutant strains collapsed. Specifically, we were interested in the link between the frequency increase of Δ*tasA* and the overall productivity loss that consistently happened at the beginning of coevolution (Fig. 1a). Thus, the productivity of the Δ*eps* and Δ*tasA* mix was assessed in three alternative scenarios: (1) Δ*tasA* adapts before Δ*eps*; (2) Δ*eps* adapts before Δ*tasA*; or (3) both strains adapt at the same time. To artificially simulate such scenarios, the productivities of mixed pellicles formed by (1) Δeps_{anc} + evolved Δ*tasA*, (2) evolved Δ*eps* + $\Delta tasA_{anc}$ and (3) evolved Δ*eps* + evolved Δ*tasA* were compared to the productivity of the ancestral mix. Nearly all Δeps_{anc} + evolved Δ*tasA* mixes developed pellicles with lower productivity than the ancestral mix, whereas evolved Δ*eps* + $\Delta tasA_{anc}$ mixes tended to perform better than or similar to the ancestors (Fig. 6). Thus, the performance of the mix was negatively affected when Δ*tasA*, but not Δ*eps*, was preadapted to pellicle growth conditions, but improved with the opposite combination (Fig. 6). In addition, the absence of a cysteine-containing TasA variant in $\Delta eps_{evolved}$ had a negative effect on its relative frequency in co-culture with $\Delta tasA_{evolved}$ (Supplementary Fig. 10d).

As previous results suggest that EPS is exploitable[8] and that evolved Δ*tasA* strains serve as EPS overproducers, we directly assessed how EPS overproduction by Δ*tasA* (in the absence of other adaptive mutations) would influence growth dynamics in pellicles. Interestingly, overproduction of EPS by Δ*tasA* had positive effects on the total productivity and it improved the productivity of the Δ*eps* strain in the mix. This suggests that the cooperation collapse was due to other mutations occurring in the evolved Δ*tasA* (Supplementary Fig. 10c). To test whether, during early stages of coevolution, the Δ*tasA* was able to accumulate or fix more SNPs than Δ*eps*, the Δ*eps* and Δ*tasA* populations obtained from transfers 5, 15 and 25 were subjected to resequencing. Unexpectedly, nearly all of the mutations previously identified for coevolved Δ*eps* and Δ*tasA* were already present in all populations from transfer 5 at nearly 90% frequency (Supplementary Dataset 1).

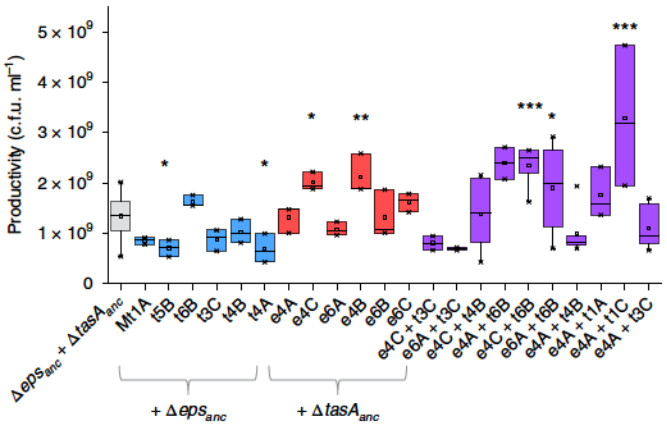

Fig. 6 | Effects of Δ*eps* or Δ*tasA* evolutionary advantage on the productivity of mixed pellicles. Productivities of pellicles formed by Δ*eps*$_{anc}$ + Δ*tasA*$_{anc}$, Δ*eps*$_{anc}$ + Δ*tasA*$_{evolved}$, Δ*eps*$_{evolved}$ + Δ*tasA*$_{anc}$ and Δ*eps*$_{evolved}$ + Δ*tasA*$_{evolved}$ were compared. Six evolved Δ*eps* and Δ*tasA* isolates were incorporated into the analysis. Boxes represent the first quartile and the third quartile, lines represent the median and the bars span from the maximum to the minimum value (for Δ*eps*$_{anc}$ + Δ*tasA*$_{anc}$ co-culture: $n = 22$; for e4C + t4B, e4C + t6B, e6A + t6B, e4A + t4B and e4A + t3C: $n = 6$; for e4C + t3C, e6A + t3C and e4A + t6B: $n = 2$; for other co-cultures: $n = 3$ biologically independent samples). The asterisks indicate significant differences from the ancestral mix (*$P < 0.05$; **$P < 0.01$; ***$P < 0.001$; *t*-test, two tailed).

Finally, we assessed whether, in contrast to the ancestor, the evolved Δ*eps* and Δ*tasA* can coexist on an evolutionary timescale. Interestingly, several of the evolved Δ*tasA* + evolved Δ*eps* combinations showed higher pellicle productivities than the ancestral mix (Fig. 6) and, in general, the frequencies were shifted towards Δ*eps* abundance compared to the ancestral mix (Supplementary Fig. 10d). Indeed, we have also observed that preadaptation of Δ*eps* and Δ*tasA* to independent surface colonization facilitated their long-term coexistence (Supplementary Fig. 11).

The above results indicate that the evolutionary advantage of Δ*tasA* results in diminishing frequencies of Δ*eps* in the mix, preventing its adaptation and leading to collapse of the division of labour. Such a scenario, although suboptimal for both partners, is likely to occur (Supplementary Fig. 11).

Discussion

The prevalence of cooperation beyond isogenic populations of microorganisms remains controversial. Here, using an experimental evolution approach, we challenged the long-term stability of genetic division of labour during pellicle biofilm formation. Although both partially defective strains gained significant net benefits from coexistence, the pervasive dominance of one partner (Δ*tasA*) repeatedly triggered the collapse of cooperation. Specifically, the overabundance of an EPS producer (Δ*tasA*) and the diminished frequency of a TasA producer (Δ*eps*) led to an imbalance in extracellular matrix composition and therefore low pellicle productivity, resulting in populations mimicking the composition of solitary Δ*tasA* lineages. Interestingly, the productivities of the Δ*tasA* lineages from the originally mixed populations were delayed compared to monoculture-initiated populations that lacked the cooperation–collapse history. Thus, in addition to being unstable, cooperation also inferred long-term negative consequences for both members of the original population, leading to extinction of Δ*eps* and slowing down the adaptation of Δ*tasA*.

Recently, spontaneous emergence of 'genetic division of labour' was observed during adaptive radiation of *Pseudomonas aeruginosa*[10]. As the evolved variants differed only in the levels of the biofilm messenger cyclic di-GMP, they could undergo reciprocal reversions, potentially rescuing cooperation from a collapse caused by the dominance of the more abundant partner. On the contrary, in our approach, division of labour was highly sensitive to disturbances in the relative frequencies of the two partners. Strikingly, experimental[10,14] and computational[11] studies suggest that mutually beneficial interactions can frequently evolve and provide fitness benefits to the whole population[9,10]. However, not all mutually beneficial behaviours account for cooperation[33], which as such may rarely be maintained beyond genetic lineages[16,34,35].

Our work indicates that, when defectors take over the population, alternative survival strategies might evolve, demonstrating that cooperation collapse does not lead to evolutionary dead-end and population extinction. Although newly evolved mechanisms of pellicle formation were based on the remaining matrix components, TasA or EPS, respectively, they differed in frequency of occurrence, strategy and vulnerability to exploitation.

The EPS-producing Δ*tasA* evolved through a more 'feasible' strategy, which we termed 'make more', as it simply involved overproduction of EPS. Similar adaptive strategies were previously observed in several unrelated species, including *Pseudomonas fluorescens* or *P. aeruginosa* that evolved to overproduce cellulose[36] or alginate[32], respectively. Matrix overproduction not only allows niche expansion[10,32,36] but also helps to cope with stress caused by predators[37] or the immune system of a host[38]. As secreted EPSs are products of several enzymes controlled by numerous regulators, many genes serve as potential targets for the acquisition of mutation(s) that could lead to increased EPS synthesis. Nevertheless, previous studies and our work[23,24,39] point towards the vulnerability of such a strategy to social exploitation, indicating that it may represent a feasible but possibly also unstable evolutionary solution.

Our results also reveal another adaptive pattern in the absence of EPS, based on a single amino acid substitution in the protein matrix component TasA. In contrast to the 'make more' strategy observed in the case of the EPS producer, the TasA producer employed the 'alter' approach, which, although less likely to occur, is evolutionarily more stable. Molecular studies revealed interesting properties of cysteine-containing TasA: an altered oligomerization pattern that might translate into assembly of initially smaller fibres into strengthened parallel fibres that provide a robust chassis for cells lacking EPS. However, these larger fibres might generate a porous biofilm, as revealed by wetting studies using WT strains carrying TasA$_{Y124C}$ or TasA$_{G183C}$ in the presence of EPS. Alternatively, loss of non-wetting behaviour could be explained by interactions with BslA (especially in the case of the TasA$_{Y124C}$ derivative). Lack of a positive effect on fitness combined with biofilm porosity probably explains the persistent lack of cysteines in TasA proteins of other Bacilli.

Cysteine-containing TasA might exist in EPS-deficient strains, but such may be vastly undersampled owing to atypical colony morphology[24,25,27].

Importantly, in addition to matrix-related mutations, other adaptive mutations could contribute to the productivity of the evolved strains. For instance, numerous mutations were detected that could modify motility (*fliY and fliG*) in some of the evolved Δ*eps* strains, and anaerobic respiration (*rex*), chemotaxis (*mcpC* and *cheA*) or aerotaxis (*hemAT*) in the evolved Δ*tasA* strains (Supplementary Dataset 1).

There are important questions remaining as to the underlying evolutionary dynamics in the Δ*eps*+Δ*tasA* co-culture system. Still, evolutionary success of the solitary-grown defectors allowed deeper understanding of their failure as a cooperative community. Specifically, early evolutionary events resulted in dominance of Δ*tasA* in co-cultures, quickly reducing the prevalence of Δ*eps*, minimizing the feasibility of substitutions in TasA. Paradoxically, if Δ*eps* was evolutionarily ahead of Δ*tasA*, or both partners evolved in concordance, the community productivity might be superior. This is potentially caused by the higher exploitability of EPS than of TasA[8]; thus, a lower frequency of the EPS producer could still offer sufficient quantities of this matrix component for the whole population (especially in the case of evolved strains that overproduce EPS).

Although cooperation between different strains or lineages might be common during adaptive diversification or co-evolution of different strains or species, our work reveals possible vulnerabilities of this phenomenon and alternative, cooperation-independent solutions.

Methods

Strains and cultivation conditions. Supplementary Table 1 describes the strains used in this study and Supplementary Table 2 lists all of the strains from which genomic DNA was obtained to construct the strains needed. Plasmids and oligonucleotides used for cloning purposes to construct some of the strains used here are listed in Supplementary Table 3 and Supplementary Table 4, respectively. Strains were maintained in LB medium (LB-Lennox, Carl Roth; 10 g l^{-1} tryptone, 5 g l^{-1} yeast extract and 5 g l^{-1} NaCl), whereas MSgg medium was used for pellicle biofilm induction[25].

Experimental evolution and productivity assays. All of the strains used in this study originated from naturally competent derivatives of the undomesticated *B. subtilis* NCBI 3610 DK1042 strain[40]. Pellicles of *B. subtilis* can be constructed through the interaction of two partially deficient mutants, Δ*eps* and Δ*tasA*, that exchange matrix components with each other[8,19,27]. The 1/1 initial ratio of Δ*eps* + Δ*tasA* mixtures was adjusted based on absorbance values at 600 nm of corresponding overnight cultures. Pellicles (or residual pellicles in the case of Δ*eps* and Δ*tasA* monocultures) were grown in MSgg medium statically in a 24-well plate at 30 °C for 48 h in 6 parallel replicates. Experimental evolution was performed as previously described[24]. Specifically, six parallel co-cultures of Δ*eps* and Δ*tasA* mixed in an initial ratio of 1/1 were subjected to experimental evolution for 35 transfers, representing approximately 250 generations. Pellicles were monitored qualitatively at every transfer, and the relative frequencies of the mutants and pellicle productivities (that is, colony-forming unit (c.f.u.) ml^{-1}) were quantified every five transfers. Mature pellicles were gently harvested from the surface of the MSgg medium using a plastic inoculating loop, transferred to 2-ml Eppendorf tubes containing 1 ml of 0.9% NaCl and 100 µl glass sand, and vigorously vortexed for 1 min. This approach allowed effective disruption of the material into single cells and small clumps without a requirement for sonication (which would increase the risk of contamination). Finally, the populations were reinoculated after 100× dilution. In the case of the monoculture mutants, the thin layer of cells colonizing the liquid–air interface was carefully harvested, mildly disrupted and reinoculated using a proportionally lower dilution factor, to avoid strong bottleneck effects. After the 5th, 10th, 14th, 19th, 24th, 29th and 35th pellicle transfers, Δ*eps* and Δ*tasA* frequencies (in the case of mixed pellicles) and c.f.u. ml^{-1}, described here as pellicle productivity, were monitored, and deep frozen (−80 °C) stocks were preserved. Before each c.f.u. assay, pellicles were sonicated according to a protocol optimized in our laboratory[19].

Population structure and relative fitness assay. To examine population structure in the evolved Δ*eps* and Δ*tasA* populations, four final populations (from transfer 35) of solitary-evolved Δ*eps* and Δ*tasA* were selected and 96 randomly picked isolates per population were screened for performance. The ability of the isolates to make pellicles was qualitatively evaluated and scored from 0 (performs like the ancestor, no pellicle) to 3 (forms a strong pellicle).

For the relative fitness assay, strains or populations of interest were premixed at a 1/1 ratio based on their absorbance values at 600 nm and the mixture was inoculated in MSgg medium at 1%. The ancestral strains (Δ*eps* or Δ*tasA*) that were used for the fitness assays carried an *amyE*::P_{cc}-*lacZ* fusion allowing easy assessment of their relative frequencies on LB-agar plates containing X-Gal (5-bromo-4-chloro-3-indolyl β-D-galactopyranoside) substrate (40 µg ml^{-1}). Ancestral strains and populations from different evolutionary time points were allowed to compete for 48 h at 30 °C in standard pellicle growth conditions. After that time, the pellicles were carefully harvested from the liquid surface, mildly sonicated and subjected to the c.f.u. assay. For the relative fitness assays performed for $\Delta\Delta tasA_{ane}$, $\Delta\Delta tasA_{Y124C}$ and $\Delta\Delta tasA_{G183C}$, the MSgg medium was supplemented with 0.2 mM IPTG. Relative fitness W_A for strain A in competition with strain B was calculated as:

$$W_A = [\ln(\text{c.f.u.}_{A\_16\,h}/\text{c.f.u.}_{A\_start})] \;/\; [\ln(\text{c.f.u.}_{B\_16\,h}/\text{c.f.u.}_{B\_start})]$$

Western blotting. Strains were grown in MSgg medium and *tasA* was induced with 0.2 mM IPTG. Cultures were incubated in 24-well plates for 48 h at 30 °C. To induce expression of *tasA*, MSgg medium was supplemented with 0.2 mM IPTG. Biofilms were dispersed by sonication for two pulses of 10 s each. Total protein amount was determined with Bradford reagent (Bio-Rad) and samples were normalized. Samples were resolved on 12% SDS–PAGE and proteins were transferred to a polyvinylidene fluoride (PVDF) membrane using wet blotting. Non-specific binding sites were blocked with 10% skimmed milk in TBST (Tris-buffered saline and 0.1% Tween 20) for 1 h at room temperature, followed by incubation with TasA antibody overnight at 4 °C (the antibody was kindly provided by K. Turgay, Leibniz Universität Hannover, Hannover, Germany) diluted 1:10,000 in TBST. The membrane was washed three times with TBST for 10 min each before and after incubation with the secondary antibody goat anti-rabbit IgG (diluted 1:20,000 in TBST; Bio-Rad) for 1 h at room temperature. The signal was developed with Clarity Western ECL Substrate (Bio-Rad) and detected with the Chemi Doc Touch Imaging System (Bio-Rad).

Blue-native PAGE. Preparation of cell lysates was performed as stated above. Normalized protein samples were loaded on a 3–12% Bis-Tris gel (Invitrogen). Electrophoresis was performed according to the manufacturer's instructions and proteins were transferred to a PVDF membrane. The membrane was incubated for 15 min in 8% acetic acid, rinsed with water, air dried and incubated in methanol for 1 min. The membrane was rinsed with water and a picture of the membrane was taken to record protein standard positions. The detection of TasA was performed as described above.

Expression and purification of TasA. His-tagged WT TasA, $TasA_{Y124C}$ and $TasA_{G183C}$, lacking the amino-terminal signal peptide (ΔSP), were heterologously overexpressed in *Escherichia coli* and successfully purified by Ni-NTA affinity chromatography (Supplementary Fig. 4c) to visualize the corresponding amyloid fibres using transmission electron microscopy. Cloning of TasA is described in Supplementary Table 3. Transformed *E. coli* BL21 (DE3) cells (Novagen) were inoculated into 100 ml LB medium supplemented with lactose (12.5 g l^{-1}) and kanamycin (50 mg l^{-1}). Cells were incubated at 30 °C overnight with vigorous shaking (180 r.p.m.). Cells were harvested by centrifugation (3,500*g* for 20 min at 4 °C) and resuspended in 30 ml buffer A (20 mM HEPES-Na, pH 8.0, 250 mM NaCl, 20 mM KCl, 20 mM $MgCl_2$ and 40 mM imidazole) before lysis in a M-110L Microfluidizer (Microfluidics). The lysate was cleared at 47,850*g* for 20 min at 4 °C and the supernatant was transferred to a 50-ml Falcon tube; 300 µl washed Ni-NTA bead slurry (Ni-Sepharose 6 Fast Flow; GE Healthcare) was added and incubated on ice for 20 min on a shaking platform at 50 r.p.m. Ni-NTA beads with bound TasA and TasA polymers were subsequently separated from the soluble fraction by centrifugation at 3,200*g* for 5 min at 4 °C, transferred into a 1.5-ml tube and washed three times with 1 ml buffer A. Proteins were eluted in 500 µl buffer B (20 mM HEPES-Na, pH 8.0, 250 mM NaCl, 20 mM KCl, 20 mM $MgCl_2$ and 500 mM imidazole) and dialysed overnight at 4 °C in buffer C (20 mM Tris-Na, pH 7.4, and 100 mM NaCl). Protein concentrations were determined as 1 µM for $TasA_{anc}$ and $TasA_{Y124C}$ and 0.5 µM for $TasA_{G183C}$, by measuring the absorption at 280 nm using a NanoDrop Lite Spectrophotometer (Thermo Scientific). For visual and quantitative analysis of transmission electron micrographs, the regions where TasA filaments and bundles were located and where the staining and carbon coating was of good quality were selected.

Transmission electron microscopy analysis. Carbon-coated copper grids (400 mesh) were hydrophilized by glow discharge (PELCO easiGlow, Ted Pella). Protein suspensions (5 µl) with a concentration of 0.5 µM or 1 µM were applied onto the hydrophilized grids and stained with 2% uranyl acetate after a short washing step with double-distilled water. Samples were analysed with a JEOL JEM-2100 transmission electron microscope using an acceleration voltage of 120 kV. For image acquisition, a F214 FastScan CCD camera (TVIPS) was used.

Rheological characterization. Rheological measurements were performed using a commercial shear rheometer (MCR 302; Anton Paar)[42]. To produce enough biofilm material, pellicles were grown in Petri dishes of 60-mm diameter for 48 h at 30 °C and three mature pellicles were pooled to produce a single biological replicate. Frequency spectra from 0.1 Hz to 10 Hz were obtained at 21 °C using plate–plate geometry (PP25 measuring head; Anton Paar) and a measuring gap of 250–400 µm (depending on the amount of material obtained from pooling pellicles). Small torques (~1 µN m^{-1}) were applied to guarantee a linear material response. A pairwise significance analysis was performed. The *P* values obtained are given in Supplementary Table 5.

EPS precipitation. Strains were cultivated in MSgg medium at 30 °C for 48 h with shaking at 225 r.p.m. Biomass was separated from the supernatant by centrifugation (for 10 min at 12,000*g*). Biomass was dried (48 h at 55 °C) and weighed. Supernatants were mixed with three volumes of cold 96% ethanol and precipitated for 24 h at 4 °C. The precipitate was collected by centrifugation (for 10 min at 7,500*g*) and resuspended in 0.4% NaCl solution (0.1% of the initial supernatant volume). The suspension was again mixed with three volumes of cold 96% ethanol and allowed to precipitate for 24 h at 4 °C. After this second precipitation round, in all samples but Δ*eps*, EPS could be observed as a white gel floating at the ethanol–air interface[41]. The gel was carefully collected using a syringe, transferred to a fresh Eppendorf tube and pelleted down (for 1 min at 12,000*g*). The pellet was dried (for 48 h at 55 °C) and weighed. Dry EPS mass was normalized to total dry biomass.

Microscopy and confocal laser scanning microscopy. Bright-field and fluorescence images of whole pellicles and colonies were obtained with an Axio Zoom V16 stereomicroscope (Carl Zeiss) equipped with a ×0.5 Plan Apo objective, two LED cold-light sources (one for fluorescence detection and one for the visible light), a HE 38 filter set for GFP (excitation at 470/40 nm and emission at 525/50 nm), a 63 HE filter set for red fluorescent protein (excitation at 572/25 nm and emission at 629/62 nm) and an AxioCam MRm monochrome camera (Carl Zeiss). The pellicles were also analysed using a confocal laser scanning microscope (LSM 780 equipped with an argon laser; Carl Zeiss) and a Plan-Apochromat/1.4 Oil DIC M27 ×63 objective. Fluorescent reporter excitation was performed at 488 nm for green fluorescence and at 564 nm for red fluorescence, while the emitted fluorescence was recorded at 484–536 nm and 567–654 nm for GFP and mKate, respectively. To generate pellicle images, Z-stack series with 1-µm steps were acquired. Zen 2012 software (Carl Zeiss) was used for both stereomicroscopy and confocal laser scanning microscopy image visualization.

Genome resequencing and genome analysis. Genomic DNA of selected isolated strains was extracted using the EURex Bacterial and Yeast Genomic DNA Kit from cultures grown for 16 h. Paired-end fragment reads (2×150 nucleotides) were generated using an Illumina NextSeq sequencer. Primary data analysis (base calling) was carried out with 'bcl2fastq' software (v.2.17.1.14, Illumina). All further analysis steps were done in CLC Genomics Workbench Tool 9.5.1. Reads were quality trimmed using an error probability of 0.05 (Q13) as the threshold. In addition, the first ten bases of each read were removed. Only those reads were used in the mapping that displayed an alignment longer than 80% of the read length while showing at least 80% sequence identity against the reference genome. Non-specific reads were randomly placed to one of their possible genomic locations. Quality-based SNP and small insertion/deletion variant calling was carried out, requiring ≥8× read coverage with ≥25% variant frequency. Only variants supported by good-quality bases (Q ≥ 20) were considered and only when they were supported by evidence from both DNA strands. The genome of the WT ancestor was also resequenced to subtract the mutations that could have been present before the evolution experiment. Data on the average coverage for each strain sequenced in this study are provided in Supplementary Table 5.

Statistical analyses. Statistical differences between two experimental groups were identified using two-tailed Student's *t*-tests assuming equal variance. Variances in the two main types of data sets (c.f.u. counts in competition assays and weight of biomass) were similar across different samples and their normal distribution was confirmed using the Kolmogorov–Smirnov test ($P > 0.05$). No data points were removed from the data set before analyses. No statistical methods were used to predetermine sample size and the experiments were not randomized.

Data availability

All data sets generated and analysed during this study are available from the corresponding author on request.

Received: 9 January 2018; Accepted: 5 September 2018;
Published online: 8 October 2018

References

1. Hamilton, W. D. The genetical evolution of social behaviour. I. *J. Theor. Biol.* **7**, 1–16 (1964).
2. Queller, D. C., Ponte, E., Bozzaro, S. & Strassmann, J. E. Single-gene greenbeard effects in the social amoeba *Dictyostelium discoideum*. *Science* **299**, 105–106 (2003).
3. Gibbs, K. A. & Greenberg, E. P. Territoriality in *Proteus*: advertisement and aggression. *Chem. Rev.* **111**, 188–194 (2011).
4. Kiers, T. E., Rousseau, R. A., West, S. A. & Denison, R. F. Host sanctions and the legume–rhizobium mutualism. *Nature* **425**, 78–81 (2003).
5. West, S. A., Griffin, A. S. & Gardner, A. Evolutionary explanations for cooperation. *Curr. Biol.* **17**, R661–R672 (2007).
6. Zhang, Z., Claessen, D. & Rozen, D. E. Understanding microbial divisions of labor. *Front. Microbiol.* **7**, 2070 (2016).
7. van Gestel, J., Vlamakis, H. & Kolter, R. From cell differentiation to cell collectives: *Bacillus subtilis* uses division of labor to migrate. *PLoS Biol.* **13**, e1002141 (2015).
8. Dragoš, A. et al. Division of labor during biofilm matrix production. *Curr. Biol.* **28**, 1903–1913 (2018).
9. Pande, S. & Kost, C. Bacterial unculturability and the formation of intercellular metabolic networks. *Trends Microbiol.* **25**, 349–361 (2017).
10. Kim, W., Levy, S. B. & Foster, K. R. Rapid radiation in bacteria leads to a division of labour. *Nat. Commun.* **7**, 10508 (2016).
11. Germerodt, S. et al. Pervasive selection for cooperative cross-feeding in bacterial communities. *PLoS Comput. Biol.* **12**, e1004986 (2016).
12. Lowery, N. V., McNally, L., Ratcliff, W. C. & Brown, S. P. Division of labor, bet hedging, and the evolution of mixed biofilm investment strategies. *mBio* **8**, e00672-17 (2017).
13. Wahl, L. M. The division of labor: genotypic versus phenotypic specialization. *Am. Nat.* **160**, 135–145 (2002).
14. D'Souza, G. & Kost, C. Experimental evolution of metabolic dependency in bacteria. *PLoS Genet.* **12**, e1006364 (2016).
15. Morris, J. J., Lenski, R. E. & Zinser, E. R. The Black Queen Hypothesis: evolution of dependencies through adaptive gene loss. *mBio* **3**, e00036-12 (2012).
16. Oliveira, N. M., Niehus, R. & Foster, K. R. Evolutionary limits to cooperation in microbial communities. *Proc. Natl Acad. Sci. USA* **111**, 17941–17946 (2014).
17. Cooper, G. A. & West, S. A. Division of labour and the evolution of extreme specialization. *Nat. Ecol. Evol.* **2**, 1161–1167 (2018).
18. Waite, A. J. & Shou, W. Adaptation to a new environment allows cooperators to purge cheaters stochastically. *Proc. Natl Acad. Sci. USA* **109**, 19079–19086 (2012).
19. Martin, M. et al. De novo evolved interference competition promotes the spread of biofilm defectors. *Nat. Commun.* **8**, 15127 (2017).
20. O'Brien, S., Luján, A. M., Paterson, S., Cant, M. A. & Buckling, A. Adaptation to public goods cheats in *Pseudomonas aeruginosa*. *Proc. Biol. Sci.* **284**, 20171089 (2017).
21. Kümmerli, R. et al. Co-evolutionary dynamics between public good producers and cheats in the bacterium *Pseudomonas aeruginosa*. *J. Evol. Biol.* **28**, 2264–2274 (2015).
22. Fiegna, F., Yu, Y.-T. N., Kadam, S. V. & Velicer, G. J. Evolution of an obligate social cheater to a superior cooperator. *Nature* **441**, 310–314 (2006).
23. Hammerschmidt, K., Rose, C. J., Kerr, B. & Rainey, P. B. Life cycles, fitness decoupling and the evolution of multicellularity. *Nature* **515**, 75–79 (2014).
24. Dragoš, A. et al. Evolution of exploitative interactions during diversification in *Bacillus subtilis* biofilms. *FEMS Microbiol. Ecol.* **94**, fix155 (2018).
25. Branda, S. S., Gonzalez-Pastor, J. E., Ben-Yehuda, S., Losick, R. & Kolter, R. Fruiting body formation by *Bacillus subtilis*. *Proc. Natl Acad. Sci. USA* **98**, 11621–11626 (2001).
26. Branda, S. S., Chu, F., Kearns, D. B., Losick, R. & Kolter, R. A major protein component of the *Bacillus subtilis* biofilm matrix. *Mol. Microbiol.* **59**, 1229–1238 (2006).
27. Romero, D., Vlamakis, H., Losick, R. & Kolter, R. An accessory protein required for anchoring and assembly of amyloid fibres in *B. subtilis* biofilms. *Mol. Microbiol.* **80**, 1155–1168 (2011).
28. Romero, D., Aguilar, C., Losick, R. & Kolter, R. Amyloid fibers provide structural integrity to *Bacillus subtilis* biofilms. *Proc. Natl Acad. Sci. USA* **107**, 2230–2234 (2010).
29. Dragoš, A., Kovács, Á. T. & Claessen, D. The role of functional amyloids in multicellular growth and development of Gram-positive bacteria. *Biomolecules* **7**, E60 (2017)..
30. Diehl, A. et al. Structural changes of TasA in biofilm formation of *Bacillus subtilis*. *Proc. Natl Acad. Sci. USA* **115**, 3237–3242 (2018).
31. Arnaouteli, S. et al. Bifunctionality of a biofilm matrix protein controlled by redox state. *Proc. Natl Acad. Sci. USA* **114**, E6184–E6191 (2017).
32. Kim, W., Racimo, F., Schluter, J., Levy, S. B. & Foster, K. R. Importance of positioning for microbial evolution. *Proc. Natl Acad. Sci. USA* **111**, E1639–E1647 (2014).
33. West, S. A., Griffin, A. S. & Gardner, A. Social semantics: altruism, cooperation, mutualism, strong reciprocity and group selection. *J. Evol. Biol.* **20**, 415–432 (2007).
34. Foster, K. R. & Bell, T. Competition, not cooperation, dominates interactions among culturable microbial species. *Curr. Biol.* **22**, 1845–1850 (2012).
35. Abrudan, M. I. et al. Socially mediated induction and suppression of antibiosis during bacterial coexistence. *Proc. Natl Acad. Sci. USA* **112**, 11054–11059 (2015).

36. Rainey, P. B. & Rainey, K. Evolution of cooperation and conflict in experimental bacterial populations. *Nature* **425**, 72–74 (2003).
37. Scanlan, P. D. & Buckling, A. Co-evolution with lytic phage selects for the mucoid phenotype of *Pseudomonas fluorescens* SBW25. *ISME J.* **6**, 1148–1158 (2012).
38. Miskinyte, M. et al. The genetic basis of *Escherichia coli* pathoadaptation to macrophages. *PLoS Pathog.* **9**, e1003802 (2013).
39. Rainey, P. B. & Travisano, M. Adaptive radiation in a heterogeneous environment. *Nature* **394**, 69–72 (1998).
40. Konkol, M. A., Blair, K. M. & Kearns, D. B. Plasmid-encoded ComI inhibits competence in the ancestral 3610 strain of *Bacillus subtilis*. *J. Bacteriol.* **195**, 4085–4093 (2013).
41. Borkar, S. G. *Laboratory Techniques in Plant Bacteriology* (CRC Press, Boca Raton, 2017).
42. Werb, M. et al. Surface topology affects wetting behavior of *Bacillus subtilis* biofilms. *NPJ Biofilms Microbiomes* **3**, 11 (2017).

Acknowledgements

We thank S. West for his comments on our manuscript. This work was funded by the Deutsche Forschungsgemeinschaft (DFG) to Á.T.K. (KO4741/2.1) within the Priority Program SPP1617. A.D. and C.F.G. were supported by fellowships from the Alexander von Humboldt Foundation and Consejo Nacional de Ciencia y Tecnología (CONACyT), respectively. The research leading to these results has received funding from the European Union's Horizon 2020 research and innovation programme under the Marie Sklodowska-Curie grant agreement no. 713683 (COFUNDfellowsDTU). This work was also supported by the DFG through project B11 in the framework of SFB863 granted to O.L., and a start-up grant from the Technical University of Denmark to Á.T.K.

Authors contributions

A.D. and Á.T.K. conceived the project. A.D., M.M., C.F.G., L.K., P.P. and T.H. performed the experiments. B.B. performed the next-generation sequencing data analysis. G.M., G.B., D.L. and O.L. contributed with the methods, analysed the data and supervised the experiments. A.D. and Á.T.K. wrote the manuscript, with all authors contributing to the final version.

Competing interests

The authors declare no competing interests.

Additional information

Supplementary information is available for this paper at https://doi.org/10.1038/s41564-018-0263-y.

Reprints and permissions information is available at www.nature.com/reprints.

Correspondence and requests for materials should be addressed to Á.T.K.

Publisher's note: Springer Nature remains neutral with regard to jurisdictional claims in published maps and institutional affiliations.

Chapter 6

Cheater-mediated evolution shifts phenotypic heterogeneity in *Bacillus subtilis* biofilms

Submitted to The ISME Journal (2019)

Deposited in bioRxiv (2019)

Cheater-mediated evolution shifts phenotypic heterogeneity in *Bacillus subtilis* biofilms

Marivic Martin[1,2], Anna Dragoš[1], Simon B. Otto[1], Daniel Schäfer[2], Susanne Brix[3], Gergely Maróti[4], and Ákos T. Kovács[1,2]

[1] Bacterial Interactions and Evolution Group, Department of Biotechnology and Biomedicine, Technical University of Denmark, Kongens Lyngby, 2800, Denmark
[2] Terrestrial Biofilms Group, Friedrich Schiller University Jena, Jena, 07743, Germany
[3] Disease Systems Immunology Group, Department of Biotechnology and Biomedicine, Technical University of Denmark, Kongens Lyngby, 2800, Denmark
[4] Institute of Plant Biology, Biological Research Center of the Hungarian Academy of Sciences, Szeged, 6726, Hungary

Corresponding Author: Ákos T. Kovács; atkovacs@dtu.dk

Running title: Evolution of phenotypic heterogeneity in biofilms

Keywords: *Bacillus subtilis*, biofilm, phenotypic heterogeneity, experimental evolution, exopolysaccharide

ABSTRACT

Biofilms are closely packed cells held and shielded by extracellular matrix composed of structural proteins and exopolysaccharides (EPS). As matrix components are costly to produce and shared within the population, EPS-deficient cells can act as cheaters by gaining benefits from the cooperative nature of EPS producers. Remarkably, genetically programmed EPS producers can also exhibit phenotypic heterogeneity at single cell level. For instance, mature biofilms of *Bacillus subtilis* contain cells in an 'ON' state, expressing extracellular matrix genes, as well as cells in an 'OFF' state. Previous studies have shown that spatial structure of biofilms limits the spread of cheaters, but the long-term influence of cheating on biofilm evolution is not well understood. In addition, the influence of cheats on phenotypic heterogeneity pattern within matrix-producers, was never examined. Here, we examine the influence of EPS non-producers (cheaters) on phenotypic heterogeneity of matrix production within the populations of EPS producers (cooperators). We discovered that cheater-mediated evolution in pellicles leads to a transient shift in phenotypic heterogeneity pattern of cooperators, resulting in larger numbers of cells sustaining very high *eps* expression as depicted by hyper ON phenotype. Although, hyper ON strategy seems adaptive in presence of cheats, allowing favorable positioning of the WT in pellicles, it is soon substituted by hyper OFF phenotype and/or soon after by population collapse. This study provides additional insights on how biofilms adapt and respond to stress caused by exploitation in long-term scenario.

INTRODUCTION

Cooperative interactions are prevalent for all life forms [1], even for simple microbes that often exist in communities of matrix bound surface-attached cells called biofilms [2–6]. However, when costly products such as siderophores [7, 8], extracellular polymeric substances [9, 10], digestive enzymes [11], and signaling molecules [12, 13] are secreted and shared, cooperative behavior becomes susceptible to cheating [2, 14–16], where mutants defective in cooperation can still benefit from cooperative community members [4, 5, 17]. It has been shown that spatially structured biofilms, where interactions with clonemates are common and diffusion of public goods is limited, may serve as natural defense against cheating [18–20]. However, long time scale studies have recently reported that biofilm defectors can spontaneously emerge and spread in biofilms by exploiting other matrix-proficient lineages [21–24]. In fact, a pioneering microbial

evolution study on *Pseudomonas fluorescens* has already pointed towards dynamic evolutionary interplay between cooperation and exploitation in a biofilm mat [25], where emergence of cellulose overproducer (Wrinkly) allowed mat formation, but also created an opportunity for exploitation by non-producers (Smooth), eventually leading to so called 'tragedy of the commons' [4, 26, 27].

Taken together, biofilms are a suitable model to understand social interactions in an evolutionary time scale [23, 28–31]. Modelling and empirical data confirm that mutualism (beneficial to both actor and recipient) and altruism (beneficial to recipient but not to actor) play crucial roles in biofilm enhancement [32] but at the same time can lead to biofilm destabilization [25]. Can cooperators evolve tactics to evade exploitation and in turn, can cheats utilize evolution to enhance their selfish actions?

Recent studies showed that in well-mixed environment, cooperators adapt to cheats by reducing cooperation [14, 15, 33]. Such reduction could be achieved by various strategies, for instance decrease in motility [15], down regulation or minimal production in public goods [14, 15, 33], up-regulation of other alternative public goods [14], or bi-stable expression in virulence gene [2]. Interestingly, populations of cooperators often exhibit phenotypic heterogeneity at the single cell level [34, 35]. Therefore, an alternative and simple mechanism to modulate levels of cooperation in a population would be through changes in phenotypic heterogeneity pattern. However, the long-term effects of cheats on costly goods' expression at individual cell level have never been examined. Understanding how heterogeneity of gene expression within the population is affected in the presence of cheats would provide better insight on microbial adaptation and stress response mechanisms.

Here, we address this question using pellicle biofilm model of *Bacillus subtilis* [36, 37]. Pellicle formation in *B. subtilis* involves, amongst others, aerotaxis driven motility and subsequent matrix production [38]. Aerotaxis is important for oxygen sensing to aid cells reach the surface, while matrix formation is significant to sustain cells to adhere to the surface and to each other. Exopolysaccharide (EPS) is a costly public good in *Bacillus subtilis* biofilms [10, 18, 39] and is heterogeneously expressed during biofilm formation with approximately 40% of cells exhibiting the ON state [39, 40]. We aimed to investigate the cheat-dependent alteration related to phenotypic heterogeneity in *eps* expression by the producer.

We reveal that cheating mitigation by the EPS producers involves a shift in phenotypic heterogeneity towards increased frequency of *eps*-expressing cells, which is achieved by a loss-of-function mutation in a single regulatory gene. We also demonstrate that although 'hyper ON' phenotype helps to reduce cheating, it is rapidly replaced by hyper OFF strategy. Our study uncovers an alternative anti-cheating mechanism based on changes in phenotypic heterogeneity and highlights meandering trajectories prior cooperation collapse.

MATERIALS AND METHODS

Bacterial strains and culture conditions

Strain *B. subtilis* 168 $P_{hyperspank}$-mKATE P_{eps}-GFP (TB869) was obtained by transforming the laboratory strain, *B. subtilis* 168 $P_{hyperspank}$-mKATE (TB49) [10, 18], with genomic DNA from NRS2243 (*sacA*::P_{epsA}-*gfp*(Km)*hag*::cat) and selecting for Km resistance. The Δ*rsiX* strain with fluorescence reporters (TB959) was obtained by transforming TB869 with genomic DNA isolated from BKE23090 (168 *trpC*2 Δ*rsiX*::erm) [41]. Strains were maintained in LB medium (Lysogeny Broth (Lennox), Carl Roth, Germany), while 2×SG medium was used for biofilm induction [10]. The Δ*eps* strains (TB608) was created previously [10].

Experimental evolution

Eight biological replicates of the co-cultures of 1:1 ratio of *B. subtilis* TB869 and TB608 were grown in 48-well plate containing 1ml 2×SG medium at 30°C for two days. Pellicles were harvested into Eppendorf tubes containing 500 µl sterile 2×SG medium and 100 µl of sterile glass sand, vortexed for 90 seconds, 10 µl fraction was transferred into 1ml 2×SG medium of a 48 well plate and incubated at 30°C static condition for two days. This cycle was continuously repeated 35 times. As control, four biological replicates of mono-cultures of *B. subtilis* TB869 were evolved using the same transfer method. Every 5^{th} transfer cycle, harvested cultures were mixed with 15% glycerol and stored at –80°C.

Population ratio assay

At every 5^{th} transfer, pellicle biofilm productivities and relative frequencies of mutants and WT were qualitatively assessed (colony forming units (CFU)/ml) using LB agar containing selective antibiotics. LB agar plates were incubated at 37°C for 16 h and

colonies were counted. Three single clones of WT and of *Δeps* per population per timepoint were isolated from plates and stored at –80°C in the presence of 15% glycerol.

Quantitative assessment of hyper ON and hyper OFF populations

Ninety-five single isolates of ancestor or evolved TB869 strains obtained from the population per timepoint were allowed to form pellicles in 96-well PCR plate containing 100µl 2×SG medium. After incubation at 30°C for 24 h, the plate was vortexed for 90 seconds, bath sonicated (mini ultrasonic bath, Carl Roth, Germany) for 5 min and fluorescence was recorded using TECAN Infinite F200 PRO microplate reader (excitation at 485/20 nm and emission at 535/10 nm for GFP; excitation at 590/20 nm and emission at 635/35 nm for RFP; using manual gain of 35 and 50 for GFP and RFP, respectively). Hyper ON and hyper OFF phenotypes were categorized based on cut off value of the WT ancestor mean ± 1SD. GFP intensity values above 134 arbitrary units (AU) were considered as hyper ON and values below 70 AU were categorized as hyper OFF.

Pellicle competition assay/Fitness assay

Competition assays were performed as previously described [10]. Specifically, strains of interest were premixed at 1:1 ratio based on their OD_{600} values and the mixture was inoculated into 2×SG medium at 1%. Cultures were grown for 48h under static conditions at 30°C and their relative frequencies were accessed using CFU counts (and selective antibiotics).

Stereomicroscopy to assess competition of WT and Δ*rsiX* against Δ*eps*

Fluorescent images of pellicles were obtained with an Axio Zoom V16 stereomicroscope (Carl Zeiss, Jena, Germany) equipped with a Zeiss CL 9000 LED light source and an AxioCam MRm monochrome camera (Carl Zeiss) and HE eGFP (excitation at 470/40 nm and emission at 525/50 nm), and HE mRFP (excitation at 572/25 nm and emission at 629/62 nm) filter sets. Images were taken at 3.5× and 55× magnifications. The exposure times for green and red fluorescence were set up to maximal possible values before reaching overexposure, using range indicator function. Zeiss software was used to obtain overlaid, artificially colored images of both fluorescence channels.

Qualitative assessment of Hyper ONs and Hyper OFFs via microscopy

Single clones of evolved WT (TB869) obtained from population ratio assay were allowed to form 1-day old pellicle. Harvested pellicles were subjected to microscopic analysis using an Axio Observer 780 Laser Scanning Confocal Microscope (Carl Zeiss) equipped with a Plan-Apochromat 63×/1.4 Oil DIC M27 objective, an argon laser for stimulation of fluorescence (excitation at 488 for green fluorescence and 561 nm for red fluorescence, with emission at 528/26 nm and 630/32 nm respectively). Zen 2012 Software (Carl Zeiss) and FIJI Image J Software [42] were used for image recording and processing, respectively.

Flow cytometry and data analysis

Frozen stocks of evolved populations were transferred onto LB-agar plates containing kanamycin (5µg/ml) to select solely for WT colonies. The plates were incubated overnight at 37°C, followed by inoculation of 10 randomly selected single colonies into 2×SG medium. After 24h-incubation at 30°C, the pellicles were harvested, sonicated and diluted accordingly. Flow cytometry was performed using BD FACSCanto II (BD Biosciences). To obtained average distribution of *eps* expression within populations, data obtained for all single isolates were subjected to binning using identical bin size. Next, a mean count for each bin by averaging individual counts within this bin obtained for single isolates, resulting in mean distribution of single cell level *eps* expression per population.

Genome re-sequencing and genome analysis

Genomic DNA of single clones from selected evolved populations were isolated using Bacterial and Yeast Genomic DNA kit (EURx) directly from –80°C stocks grown in LB medium for 5 h at 37°C with shaking at 220 rpm. For population sequencing analysis, approx. 100 colonies belonging to the evolved populations were harvested into 2ml LB broth and incubated at 37°C shaking at 220 rpm for 2-3 h. Re-sequencing was performed on an Illumina NextSeq instrument using V2 sequencing chemistry (2x150 nt). Base-calling was carried out with "bcl2fastq" software (v.2.17.1.14, Illumina). Paired-end reads were further analyzed in CLC Genomics Workbench Tool 9.5.1. Reads were quality-trimmed using an error probability of 0.05 (Q13) as the threshold. Reads that displayed ≥80% similarity to the reference over ≥80% of their read lengths were used in mapping.

Quality-based SNP and small In/Del variant calling was carried out requiring ≥10× read coverage with ≥25% variant frequency. Only variants supported by good quality bases (Q ≥ 30) on both strands were considered. Gene functions (product names) in *SI Appendix* Datasets were reported based on SubtiWiki [43].

RESULTS

'Hyper ON' matrix producers emerge during evolution with cheats

Exopolysaccharide EPS is one of the major components of *B. subtilis* biofilm matrix and mutants deficient in EPS production (Δ*eps*) are not able to form pellicle biofilms (Supplementary Fig. 1). In line with previous results [10, 18, 39], we confirmed that the Δ*eps* can take advantage of EPS-producing wild type (WT) and incorporate into the pellicle biofilm, resulting in lower productivity of the WT (Supplementary Fig. 1b) and reduced surface complexity of the pellicle (Supplementary Fig. 1a).

We were further interested if such social cheating could leave a phenotypic or genetic fingerprint in the population of the wild type *B. subtilis*. Previous studies have shown that cooperators can adapt to presence of cheats for example by decreasing the amount of released public goods and therefore minimizing cheating opportunities [2, 14, 15]. As *B. subtilis* exhibits phenotypic heterogeneity in *eps* matrix gene expression [39, 40] (Supplementary Fig. 2), we investigated how such heterogeneous expression is influenced by the presence of cheats in an evolutionary perspective.

To address this question, we co-cultured the EPS producers (wild type- WT) and cheating strain (Δ*eps*) for 10 biofilm growth cycles (~60 generations) (see methods). Based on previous studies [44, 45], we assumed that this evolutionary timeframe will be sufficient for evolution of adaptive mechanisms in the WT in response to social cheating, at the same time preventing the diversification of the WT into a biofilm-deficient morphotype, which can be observed on longer evolutionary timescales [44].

During 10-cycle co-cultivation of WT and Δ*eps* strain, we observed a general trend of declining pellicle productivity accompanied by an increasing ratio of EPS non-producers in biofilms across all parallel populations (Fig. 1), indicating that the WT strain was constantly exposed to social cheating throughout the experiment.

Using confocal laser scanning microscopy, qualitative assessment of randomly selected isolates revealed that early populations of the EPS producers (5-10 transfer) which co-evolved with cheats exhibited a so called hyper ON phenotype, where the fraction of *eps* expressing cells was largely increased as compared to the ancestral strain (Fig. 1a, Supplementary Fig. 2). On the contrary, evolution in the absence of Δ*eps* mostly resulted in hyper OFF phenotype, with larger amounts of cells that do not express *eps* (Fig. 2a, Supplementary Fig. 2). To obtain a quantitative insight into the single-cell level expression of *eps* in the evolved WT populations, we performed flow cytometry measurements of P_{eps}-GFP harboring strain in pellicles formed by 10 randomly selected isolates per population (Fig. 2b, Supplementary Fig. 3, Supplementary Fig. 4). Although single isolates notably varied in their P_{eps}-GFP signal distributions (Supplementary Fig. 3), we spotted a general trend within the populations, that was in line with the microscopy results (Fig. 2b, Supplementary Fig. 4). Specifically, on average, the isolates from WT populations that co-evolved with Δ*eps,* were showing an increase in phenotypic heterogeneity, with a shift towards higher expression of *eps*, when compared with the ancestor (Fig. 2b, Supplementary Fig. 3). On the other hand, isolates that evolved without Δ*eps*, showed a substantial increase in OFF subpopulation (Fig. 2b, Supplementary Fig. 4). As flow cytometry revealed large within-population variations of *eps* expression, we additionally screened 95 single isolates per population for average P_{eps}-GFP intensity (see methods) (Supplementary Fig. 5).

The results revealed major changes in distribution of P_{eps}-GFP intensity across the evolved and co-evolved WT populations as compared to the WT ancestor (Supplementary Fig. 5). Specifically, for all WTs evolved alone, the distributions narrowed and dramatically shifted to the left, so that the clear majority of isolates matched the hyper OFF category across the entire evolutionary time (Supplementary Fig. 5). On the contrary, in some co-evolved WT populations (population 3, 5 and 7) the distributions widened at the 10^{th} transfer, resulting in increased frequency of hyper ON isolates (Supplementary Fig. 5).

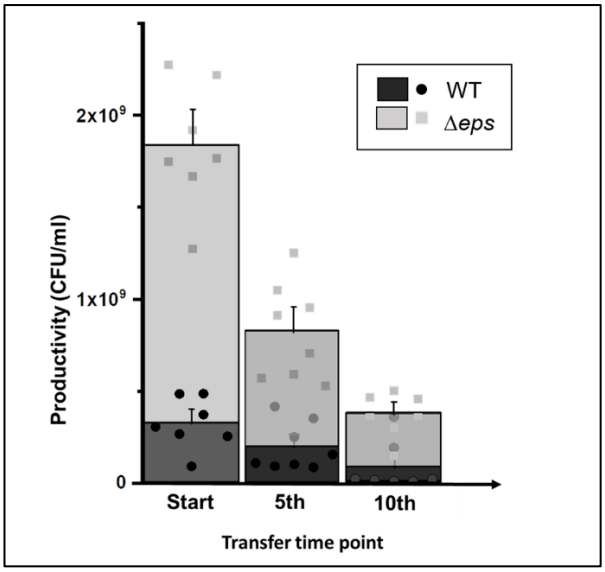

Fig. 1 Pellicle productivity. Total colony forming unit per ml of WT and Δ*eps* in 48 h old pellicles non-evolved (Start) (n=9), after experimental evolution at 5th (n=8 populations) and 10th transfer (n=7 populations). One population after 10th transfer was unable to form pellicle attributed to WT being totally outnumbered by Δ*eps*. Dots represent data obtained for all individual populations, while columns represent averages. Error bars correspond to standard error.

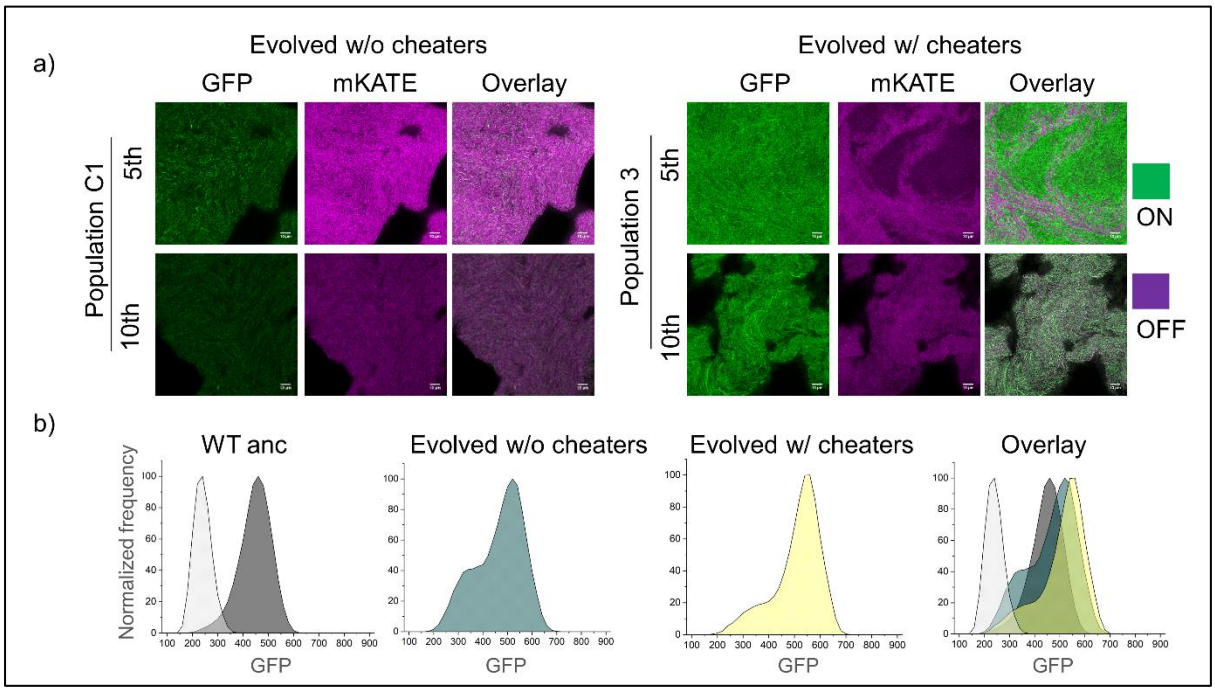

Fig. 2 Evolved WT biofilms in the presence of cheaters shows altered *eps* expression. **a** Qualitative assessment of *eps* gene expression based on confocal laser scanning microscopy of pellicles formed by single clones of WT evolved without cheaters belonging to population C1 (5th and 10th) and WT evolved with cheaters belonging to population 3 (5th and 10th transfer). Cells constitutively expressing mKATE (OFF cells) are represented in magenta and *eps* expressing cells (ON cells) are shown in green. Scale bar = 10 µm. **b** Flow cytometry analysis showing average distributions of fluorescence intensities of cells belonging to WT ancestor (dark grey), WT evolved without cheaters (blue), WT evolved with cheaters (yellow), and overlay of all 3 in comparison to WT non-labelled (light grey).

Mutations in *rsiX* lead to Hyper ON phenotype

To unravel the genetic basis of the hyper ON phenotype that evolved in presence of cheats, several single isolates from the evolved populations were subjected to genome resequencing (for details see methods). The comparative analysis of sequencing data revealed that the WT isolates that co-evolved with cheats and exhibited the hyper ON phenotype, shared mutations in *rsiX* gene (Supplementary Dataset 1). The *rsiX* gene encodes for an anti-sigma factor that controls the activity of extracellular cytoplasmic function (ECF) sigma factor X which is involved in cationic antimicrobial peptide resistance important for cell envelope stress response [46]. Detected mutations resulted either in substitution of Valine 106 to Alanine or frameshift mutations in Serine 104 or Isoleucine 347 that could lead to change or loss of anti-SigX function. Indeed, we were able to recreate the evolved hyper ON phenotype in the pellicle solely by deleting the *rsiX* gene in the WT ancestor (Fig. 3a and b). Interestingly, a different type of frameshift mutation in Lysine 200 was found in one population of evolved WT alone but this population demonstrated a hyper OFF phenotype (Fig. 2a), suggesting that only certain types of mutations in *rsiX* lead to the increase in number of *eps* expressing cells in the population or additional mutations have antagonistic effects in this isolate.

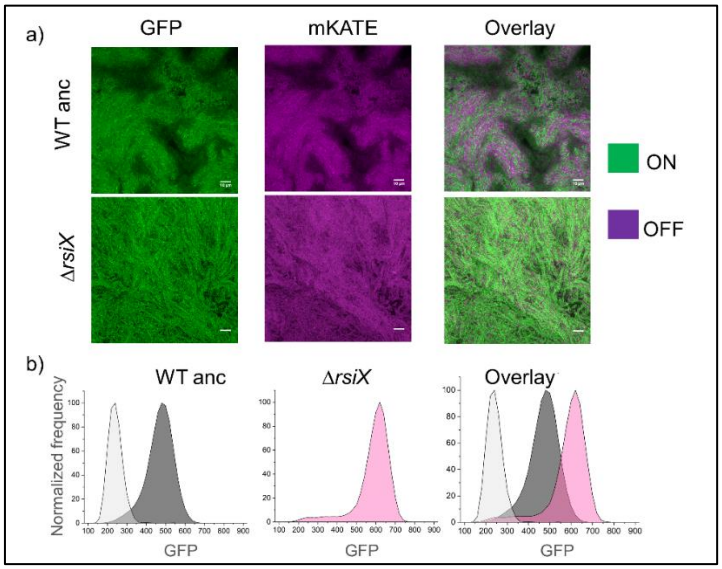

Fig. 3 Deletion of *rsiX* results in increased *eps* expression in pellicles. **a** Qualitative assessment of *eps* gene expression based on confocal laser scanning microscopy of pellicles formed by Δ*rsiX* (TB959) showing Hyper ON phenotype in contrast to WT ancestor (TB869). Cells constitutively expressing mKATE (OFF) are shown in magenta and *eps*- expressing cells (ON) are represented in green. Scale bar 10µm. **b** Flow cytometry results showing average distribution of fluorescence intensities of WT cells (dark grey), Δ*rsiX* cells (TB959) (pink) and overlay of the 2 in comparison to WT non-labelled (light grey).

Mutation in *rsiX* contributes to competitive advantage of producer strains against cheats

As mutation in *rsiX* resulted in hyper ON phenotype that may be linked to elevated secretion of EPS, we hypothesized that Δ*rsiX* producers could support the spread of cheats. To better understand how ancestor WT and Δ*rsiX* interact with Δ*eps,* we cultivated the Δ*eps* in presence of EPS-containing supernatants obtained from the WT and Δ*rsiX* (Supplementary Fig. 6). Both supernatants could partially restore pellicle formation by Δ*eps* resulting in similar productivities of Δ*eps,* thereby not supporting our hypothesis on improved performance of the mutant in presence of hyper ON Δ*rsiX* strain.

In order to determine the effect of *rsiX* deletion on fitness of the WT in presence of cheats, we performed a series of competition assays*.* Apparently, the Δ*rsiX* showed two-fold increase in relative frequency (40%) (Fig. 4, Supplementary Fig. 7) when competed against the Δ*eps*, as compared to the WT ancestor (20%). Additionally, the significant fitness improvement of the WT strain evolved with cheats was already observed in 5th transfer and 10th transfer, mutually with an early occurrence of hyper ON phenotype in those populations. This was not the case for the WT evolved alone at 5th transfer (20%) (Fig. 4a, Supplementary Fig. 7). These results suggest that the early improvement in competitive strategies against cheats are caused by the *rsiX* mutation associated with hyper ON phenotype.

It is worth to mention that we could not detect any significant fitness costs or benefits linked to *rsiX* deletion in pairwise competition between Δ*rsiX* and WT in the liquid medium (Supplementary Fig. 8; relative fitness of Δ*rsiX* = 1.00 ±0.02 S.D.). Furthermore, we did not observe significant differences in productivities of WT and the hyper ON Δ*rsiX* mutant, when grown in monoculture pellicles (Supplementary Fig. 9), suggesting that positive effect of *rsiX* mutation only manifests in presence of cheats. Similarly, different relative frequencies of Δ*eps* in pellicles formed by the ancestor or evolved matrix producers, did not result in different productivities of mixed pellicles (Supplementary Fig. 9). These results suggest that hyper ON phenotypes are vested on the increase in *eps*-expressing cells or limiting the spread of cheats but do not result in an increase in total yield.

It was previously demonstrated that increased matrix production can allow favorable positioning of a bacterial strain in the biofilm, thereby providing fitness advantage [47].

To test whether hyper ON phenotype can allow better positioning of the Δ*rsiX* in presence of Δ*eps,* we visualized 48 h grown pellicles formed by Δ*rsiX*:Δ*eps* and WT:Δ*eps* mixtures inoculated at 1:1 initial frequencies (Fig. 5, Supplementary Fig. 10). While WT and Δ*eps* were 'well-mixed' with both strains present on the oxygen-rich surface of the pellicle, the Δ*rsiX* strain clearly dominated over the Δ*eps* occupying majority of the biofilm surface and marginalizing the Δ*eps* into small clusters (Fig. 5, Supplementary Fig. 10). Therefore, deletion of *rsiX* that results in hyper-ON phenotype, provides fitness advantage over biofilm cheats, most likely by allowing favorable positioning of the matrix producers in the biofilm.

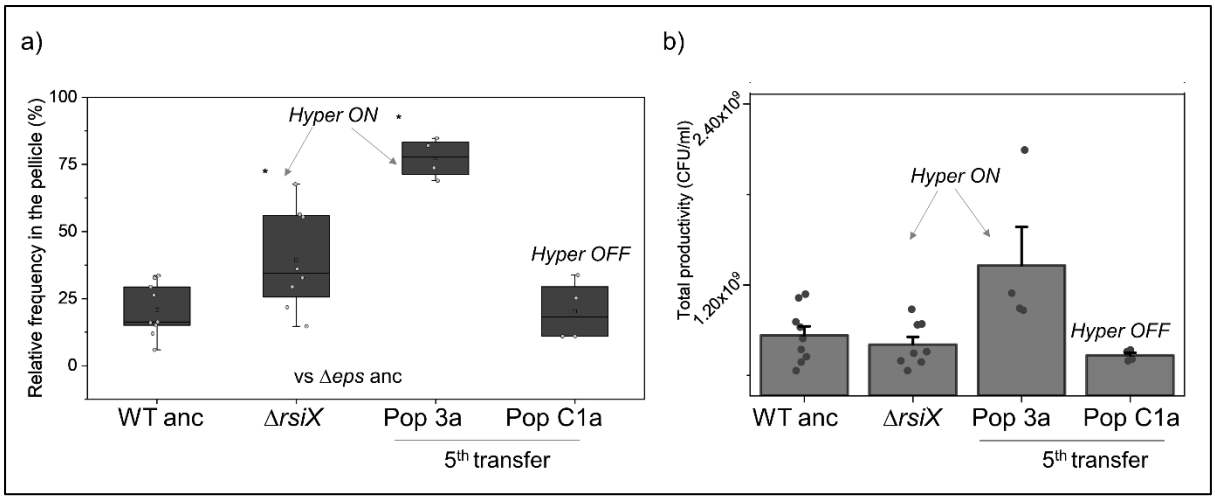

Fig. 4 a Pellicle competition assay of single clones belonging to producer populations (WT ancestor (n=9), Δ*rsiX* (n=8), evolved with (n=4) and without cheaters (n=4)) against Δ*eps* ancestor. **b** Productivity assay based on total CFU/ml of pellicles of co-cultures of Δ*eps* ancestor and single clones belonging to producer populations (WT ancestor (n=9), Δ*rsiX* (n=8), evolved with (n=4) and without cheaters (n=4)). Mean is represented in square within the box plots; median is denoted by horizontal line inside the boxes; whiskers represent the min and max; Error bars in bar graph are based on Standard error; single dots represent the individual data points (n); asterisk (*) represents the significant difference from the WT ancestor ANOVA (P value 0.05).

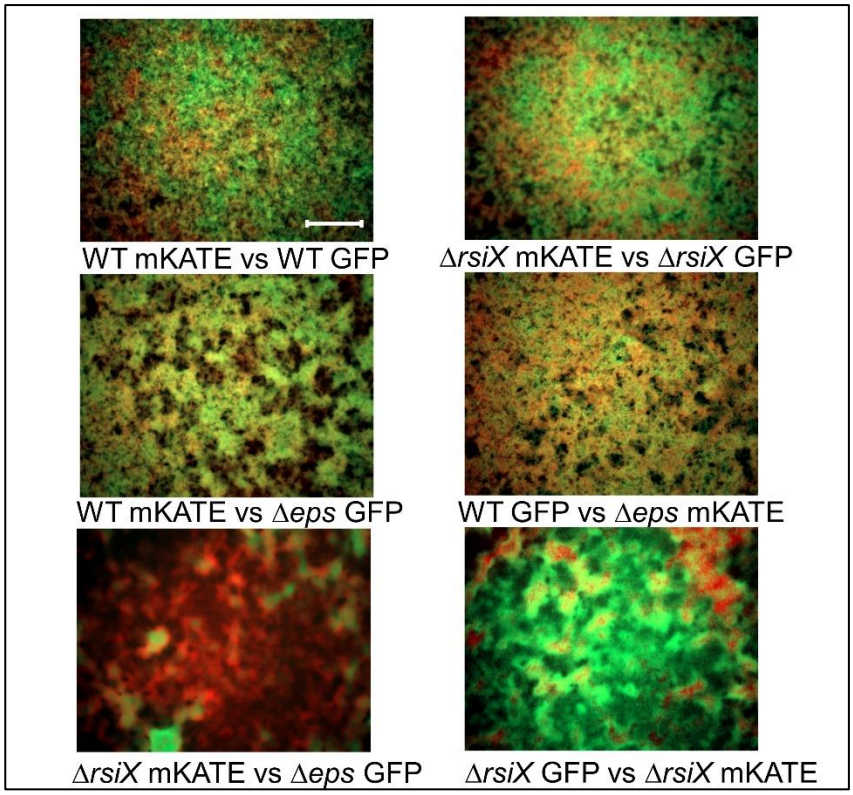

Fig. 5 Competition assay between fluorescently WT vs Δ*eps* and Δ*rsiX* vs Δ*eps*. Strains labelled with constitutively expressed GFP and mKate proteins, were inoculated in 1:1 initial frequency, pellicles were cultivated for 48h at 30^0C and visualized using stereomicroscope. Upper panels represent controls (two isogenic WT or Δ*rsiX* strains labelled with different fluorescent markers), middle panel represents pellicles formed by WT vs Δ*eps* and bottom panels represent pellicles formed by Δ*rsiX* vs Δ*eps,* each in two alternative combinations of fluorescent markers. Scale bar corresponds to 500 μm.

Hyper ON phenotype serves as a transient adaptive response to cheating

As the evolved WT isolates carrying point mutation in *rsiX* as well as the recreated Δ*rsiX* mutant (in ancestral genetic background) performed better in competition with Δ*eps* as compared to the WT ancestor, we reasoned that loss-of-function mutation in *rsiX* together with an associated hyper ON phenotype, might be an efficient evolutionary strategy against social cheating. Surprisingly however, prolonged evolution experiment eventually led to so called 'tragedy of the commons' as the Δ*eps* mutant took over in 6 out of 8 populations, completely abolishing the pellicle formation (Fig. 6 and Supplementary Fig. 11).

We next investigated changes in phenotypic heterogeneity pattern in late (transfer 15 onwards) co-evolved WT populations, similarly, as performed before for the early populations (see Supplementary Fig. 5). Specifically, we measured an average P_{eps}-GFP intensity in 95 randomly selected single isolates per population. Interestingly, in contrast

to the early co-evolved WT carrying hyper ON phenotype, the results for late co-evolved populations revealed a strong shift towards low *eps* expression levels already in transfer 15 (Supplementary Fig. 12) and consistent for later evolutionary time points. The CLSM analysis on selected single isolates confirmed that the hyper ON phenotype observed until transfer 10 was now replaced by 'Hyper OFF' phenotype, which also developed in the control WT populations evolved in the absence of Δ*eps* (Supplementary Fig. 12).

To investigate the genetics behind this phenomenon all evolved WT populations from the last evolutionary time point (or the last time point prior the collapse) were re-sequenced. Curiously, both WT populations which resisted the invasion of Δ*eps* (population 5 and 8), but neither of the 'defeated' WT populations, carried mutations in *yvrG* gene (Supplementary Fig. 11, Supplementary Dataset 2) encoding for two-component histidine kinase involved in cell wall process. Finally, the *rsiX* mutation was not detected neither in the last populations before the collapse, with an exemption of population 7 with 1% hyper ON phenotype (Supplementary Fig. 11, Supplementary Dataset 1), nor at the last transfer point for the non-collapse, implying that this mutation was lost in parallel with the loss of hyper ON phenotype in the late populations.

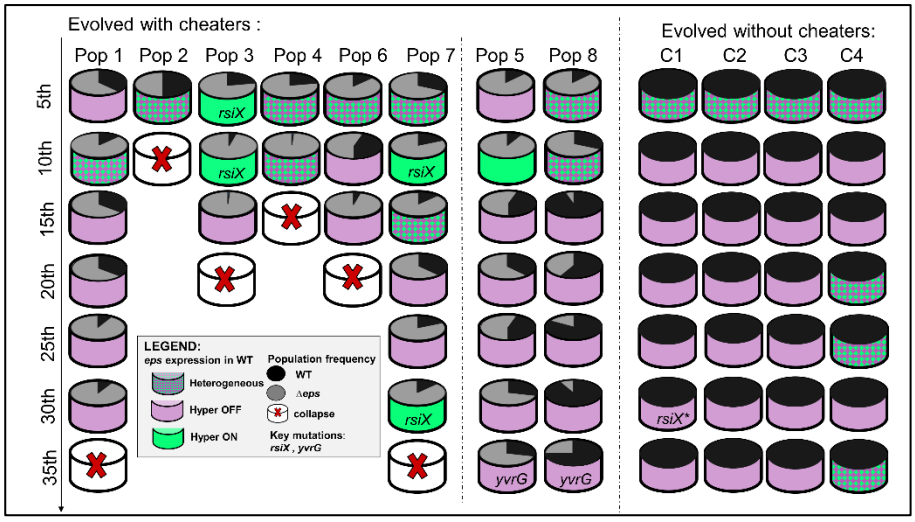

Fig. 6 Summary figure shows the population dynamics based on producer and cheater frequency per population from 5th transfer to 35th transfers for populations evolved with cheaters with collapse (Pop 1, 2, 3, 4, 6 and 7) and without collapse (Pop 5 and 8) and populations evolved without cheaters (C1, C2, C3, C4) with indications of phenotypes based on hyper ON, hyper OFF or heterogenous *eps*-expression. Key mutations on single clone level of evolved WT and evolved Δ*eps* or population level are specified. The **rsiX* mutation differs from mutation observed in strains evolved with cheaters.

DISCUSSION

Studies on evolution of cooperative behavior is important to understand how social behaviors are shaped in longer time scale. Moreover, exploring long term consequences of exposure to cheating allows to better understand how cooperation prevails in nature where environmental stress and exploitation exist inherently. Previous evolution studies on cheater-cooperator interactions in spatially structured environment showed cheater mitigation via minimization of the cooperative trait [2, 14, 15]. On the contrary, here we show that cooperators initially respond to cheating by intensifying the cooperative behaviors through shift in phenotypic heterogeneity pattern towards hyper ON phenotype, where, in contrast to the ancestral strain, nearly all members of the population express the operon involved in EPS production (Fig. 6). Further molecular analysis of the hyper ON isolates strongly suggests that this phenotype is triggered by loss-of-function mutation in *rsiX* gene. The product of *rsiX* represses the activity of ECF sigma factor, SigX that is involved in cell envelope stress response against cationic antimicrobial peptides [48]. Importantly, SigX has been previously shown to induce expression of *epsA-O* in *B. subtilis* via a complex regulatory pathway involving Abh and SlrR [49], explaining the observed enhanced in *eps* gene expression in *rsiX* mutant. Another example of matrix overproduction via ECF adaptation was also reported in Gram-negative bacterium *Pseudomonas aeruginosa* where mutations in another ECF called AlgT led to alginate overproduction and increased resistance to antimicrobials [50]. Therefore, adaptive boosts in matrix production through modulation of ECF is not exclusive for *B. subtilis* but seems to occur also in medically relevant Gram-negative pathogens like *P. aeruginosa*.

In contrast to previous studies that addressed long term cheating on diffusible siderophores, we explored evolutionary interplay between biofilm producers and non-producers in structured environment. Our results support previous observations on evolution of specific cheating-resisting mechanisms in co-operators, pointing towards ubiquity of this phenomenon. In addition, our work brings up two major findings 1) matrix producers can adapt to matrix non-producers by shifting phenotypic heterogeneity towards increased number of matrix-overexpressing cells 2) hyper ON phenotype is associated with favorable positioning of the matrix producers in the biofilm in presence of cheats, thereby limiting their numbers 3) hyper ON anti-cheating strategy is a short-term solution, which can either be replaced by another, yet unknown strategy

linked to hyper OFF phenotype, or followed by tragedy of the commons. As recently demonstrated, alternative EPS-independent biofilm formation strategies can emerge by single amino acid change is TasA [45]. It remains to be discovered whether shifts in phenotypic heterogeneity in response to long term cheating is general phenomenon that applies to different types of public goods.

Acknowledgements

This work was funded by the Deutsche Forschungsgemeinschaft (DFG) to Á.T.K. (KO4741/2.1) within the Priority Program SPP1617. M.M. was supported a FEMS Research and Training Grant (FEMS-RG-2017-0054). This project has received funding from the European Union's Horizon 2020 research and innovation programme under the Marie Skłodowska-Curie grant agreement No 713683 (H.C. Ørsted COFUND to A.D.). Work in the laboratory of Á.T.K. is partly supported by the Danish National Research Foundation (DNRF137) for the Center for Microbial Secondary Metabolites.

Competing Interests

The authors declare that there are no competing financial interests in relation to the work described.

Authors contributions

Á.T.K. conceived the project, M.M., A.D., S.B. and D.S. performed the experiments. G.M contributed with methods. M.M., A.D. and Á.T.K. wrote the manuscript, with all authors contributing to the final version.

REFERENCES

1. Bourke A. Principals of social evolution: Oxford series in ecology and evolution. 2011. Oxford University Press, Oxford, UK.
2. Diard M, Garcia V, Maier L, Remus-Emsermann MNP, Regoes RR, Ackermann M, et al. Stabilization of cooperative virulence by the expression of an avirulent phenotype. *Nature* 2013; 494:353–356.
3. Nadell CD, Xavier JB, Foster KR. The sociobiology of biofilms. *FEMS Microbiol Rev* 2009; 33:206–224.
4. West SA, Diggle SP, Buckling A, Gardner A, Griffin AS. The social lives of microbes. *Annu Rev Ecol Evol Syst* 2007; 38:53–77.
5. West S a., Griffin AS, Gardner A. Evolutionary explanations for cooperation. *Curr Biol* 2007; 17:661–672.
6. Xavier J, Foster KR. Cooperation and conflict in microbial biofilms. *Proc Natl Adac Sci U S A* 2007; 104:876–881.
7. Luján AM, Gómez P, Buckling A. Siderophore cooperation of the bacterium Pseudomonas fluorescens in soil. *Biol Lett* 2015; 11:20140934.
8. Weigert M, Kümmerli R. The physical boundaries of public goods cooperation between surface-attached bacterial cells. *Proc R Soc B Biol Sci* 2017; 284:20170631.
9. Dragoš A, Kovács ÁT. The peculiar functions of the bacterial extracellular matrix. *Trends Microbiol* 2017; 25:257–266.
10. Martin M, Dragoš A, Hölscher T, Maróti G, Bálint B, Westermann M, et al. *De novo* evolved interference competition promotes the spread of biofilm defectors. *Nat Commun* 2017; 8:15127.
11. Folse HJ, Allison SD. Cooperation, competition, and coalitions in enzyme-producing microbes: Social evolution and nutrient depolymerization rates. *Front Microbiol* 2012; 3:338.
12. Popat R, Crusz SA, Messina M, Williams P, West SA, Diggle SP. Quorum-sensing and cheating in bacterial biofilms. *Proc R Soc B Biol Sci* 2012; 279:4765–4771.
13. Dogsa I, Oslizlo A, Stefanic P, Mandic-mulec I. Social interactions and biofilm formation in *Bacillus subtilis*. *Food Technol Biotechnol* 2014; 52:149–157.
14. O'Brien S, Luján AM, Paterson S, Cant MA, Buckling A. Adaptation to public goods cheats in *Pseudomonas aeruginosa*. *Proc R Soc B Biol Sci* 2017; 284:20171089.
15. Kümmerli R, Santorelli LA, Granato ET, Dumas Z, Dobay A, Griffin AS, et al. Co-evolutionary dynamics between public good producers and cheats in the bacterium *Pseudomonas aeruginosa*. *J Evol Biol* 2015; 28:2264–2274.
16. Harrison F. Dynamic social behaviour in a bacterium: *Pseudomonas aeruginosa* partially compensates for siderophore loss to cheats. *J Evol Biol* 2013; 26:1370–1378.
17. Hamilton WD. The genetical evolution of social behaviour. I. *J Theor Biol* 1964; 7:1–16.
18. van Gestel J, Weissing FJ, Kuipers OP, Kovács ÁT. Density of founder cells affects spatial pattern formation and cooperation in *Bacillus subtilis* biofilms. *ISME J* 2014; 8:2069–2079.
19. Nadell CD, Foster KR, Xavier JB. Emergence of spatial structure in cell groups and the evolution of cooperation. *PLoS Comput Biol* 2010; 6:e1000716.
20. Momeni B, Waite AJ, Shou W. Spatial self-organization favors heterotypic cooperation over cheating. *Elife* 2013; 2:e00960.
21. Dragoš A, Lakshmanan N, Martin M, Horváth B, Maróti G, García CF, et al. Evolution of exploitative interactions during diversification in *Bacillus subtilis* biofilms. *FEMS*

Microbiol Ecol 2018; 94:fix155.
22. Ellis CN, Traverse CC, Mayo-Smith L, Buskirk SW, Cooper VS. Character displacement and the evolution of niche complementarity in a model biofilm community. *Evolution (N Y)* 2015; 69:283–293.
23. Poltak SR, Cooper VS. Ecological succession in long-term experimentally evolved biofilms produces synergistic communities. *ISME J* 2011; 5:369–378.
24. Goymer P, Kahn SG, Malone JG, Gehrig SM, Spiers AJ, Rainey PB. Adaptive divergence in experimental populations of *Pseudomonas fluorescens*. II. Role of the GGDEF regulator WspR in evolution and development of the wrinkly spreader phenotype. *Genetics* 2006; 173:515–526.
25. Rainey PB, Rainey K. Evolution of cooperation and conflict in experimental bacterial populations. *Nature* 2003; 425:72–74.
26. West SA, Griffin AS, Gardner A, Diggle SP. Social evolution theory for microorganisms. *Nat Rev Microbiol* 2006; 4:597–607.
27. Hardin G. The tragedy of the commons. *Science (80-)* 1968; 162:1243–1248.
28. Martin M, Hölscher T, Dragoš A, Cooper VS, Kovács ÁT. Laboratory evolution of microbial interactions in bacterial biofilms. *J Bacteriol* 2016; 198:2564–2571.
29. Traverse CC, Mayo-Smith LM, Poltak SR, Cooper VS. Tangled bank of experimentally evolved *Burkholderia* biofilms reflects selection during chronic infections. *Proc Natl Acad Sci U S A* 2013; 110:E250-9.
30. Madsen JS, Lin YC, Squyres GR, Price-Whelan A, Torio A de S, Song A, et al. Facultative control of matrix production optimizes competitive fitness in *Pseudomonas aeruginosa* PA14 biofilm models. *Appl Environ Microbiol* 2015; 81:8414–8426.
31. Rainey PB, Travisano M. Adaptive radiation in a heterogeneous environment. *Nature* 1998; 394:69–72.
32. Kreft JU. Biofilms promote altruism. *Microbiology* 2004; 150:2751–2760.
33. Lyons NA, Kolter R. A single mutation in *rapP* induces cheating to prevent cheating in *Bacillus subtilis* by minimizing public good production. *Commun Biol* 2018; 1:133.
34. Veening JW, Igoshin OA, Eijlander RT, Nijland R, Hamoen LW, Kuipers OP. Transient heterogeneity in extracellular protease production by *Bacillus subtilis*. *Mol Syst Biol* 2008; 4:1–15.
35. Davidson FA, Seon-Yi C, Stanley-Wall NR. Selective heterogeneity in exoprotease production by *Bacillus subtilis*. *PLoS One* 2012; 7:e38574.
36. Kovács ÁT. *Bacillus subtilis*. *Trends Microbiol* 2019; in press:doi: 10.1016/j.tim.2019.03.008.
37. Kovács ÁT, Dragoš A. Evolved Biofilm: review on the experimental evolution studies of *Bacillus subtilis* pellicles. *J Mol Biol* 2019; in press:doi:10.1016/j.jmb.2019.02.005.
38. Hölscher T, Bartels B, Lin Y-C, Gallegos-Monterrosa R, Price-Whelan A, Kolter R, et al. Motility, chemotaxis and aerotaxis contribute to competitiveness during bacterial pellicle biofilm development. *J Mol Biol* 2015; 427:3695–3708.
39. Dragoš A, Kiesewalter H, Martin M, Hsu C-Y, Hartmann R, Wechsler T, et al. Division of labor during biofilm matrix production. *Curr Biol* 2018; 28:1903–1913.
40. Chai Y, Chu F, Kolter R, Losick R. Bistability and biofilm Formation in *Bacillus subtilis*. *Mol Microbiol* 2008; 67:254–263.
41. Koo BM, Kritikos G, Farelli JD, Todor H, Tong K, Kimsey H, et al. Construction and analysis of two genome-scale deletion libraries for *Bacillus subtilis*. *Cell Syst* 2017;

4:291-305.e7.
42. Rueden CT, Schindelin J, Hiner MC, DeZonia BE, Walter AE, Arena ET, et al. ImageJ2: ImageJ for the next generation of scientific image data. *BMC Bioinformatics* 2017; 18:529.
43. Zhu B, Stülke J. SubtiWiki in 2018: From genes and proteins to functional network annotation of the model organism *Bacillus subtilis*. *Nucleic Acids Res* 2018; 46:D743–D748.
44. Dragos A, Lakshmanan N, Martin M, Horvath B, Maroti G, Falcon Garcia C, et al. Evolution of exploitative interactions during diversification in *Bacillus subtilis* biofilms. *FEMS Microbiol Ecol* 2018; 94:1–28.
45. Dragoš A, Martin M, Garcia CF, Kricks L, Pausch P, Heimerl T, et al. Collapse of genetic division of labour and evolution of autonomy in pellicle biofilms. *Nat Microbiol* 2018; 3:1451–1460.
46. Helmann JD. *Bacillus subtilis* extracytoplasmic function (ECF) sigma factors and defense of the cell envelope. *Curr Opin Microbiol* 2016; 30:122–132.
47. Kim W, Racimo F, Schluter J, Levy SB, Foster KR. Importance of positioning for microbial evolution. *Proc Natl Acad Sci U S A* 2014; 111:E1639-1647.
48. Cao M, Helmann JD. The *Bacillus subtilis* extracytoplasmic-function σX factor regulates modification of the cell envelope and resistance to cationic antimicrobial peptides. *J Bacteriol* 2004; 186:1136–1146.
49. Murray EJ, Strauch M a, Stanley-Wall NR. SigmaX is involved in controlling *Bacillus subtilis* biofilm architecture through the AbrB homologue Abh. *J Bacteriol* 2009; 191:6822–6832.
50. Hentzer M, Teitzel GM, Balzer GJ, Heydorn A, Molin S, Givskov M, et al. Alginate overproduction affects *Pseudomonas aeruginosa* biofilm structure and function. *J Bacteriol* 2001; 183:5395–401.

GENERAL DISCUSSION

1. Public goods EPS and TasA as effective tools to examine the evolutionary social interactions in *B. subtilis* biofilms

The biofilm matrix components, EPS and TasA, of *B. subtilis* contributes not only to the structural integrity of the spatial structure but also fosters cooperation[1]. However, they are also prone to exploitation and competition due to the metabolic burden they carry as public goods. As previously mentioned in the introduction, public goods are secreted substances that are freely available to other individuals and profits the whole population[2] (see also Chapter 1). Outside the context of biofilm development, the role of these components, have been enumerated (reviewed in [3,4]). In addition to those features, their roles as public goods offer a high impact in examining social behaviours in spatial structures in the context of evolution, as they could evolve to continuously remain freely shared or become more privatized (Chapters 2, 3, 4, 5 and 6).

Since both EPS and TasA components are essential in the formation of pellicle biofilms, different schemes of evolutionary social interaction set-ups are employed in this dissertation to understand how these public goods are shared by producers in a spatially structured environment. The initial evolutionary points used in this study involve social interplays within clonal cells (Chapter 2), between producers and non-producers (WT and Δ*eps*Δ*tasA* in Chapter 3; WT and Δ*eps* in Chapter 6) and between two types of matrix producers (Δ*eps* and Δ*tasA* in Chapters 4 and 5). These evolution models foster either cooperative behaviours (Chapter 2 and 4) or evolution of microbial interactions in biofilms (reviewed in Chapter 1) such as exploitation by cheaters (Chapter 2 and 6) or competitive behaviours by defectors (Chapter 3) or development of cooperation-independent alternatives (Chapter 5).

The use of EPS and TasA to investigate social interaction is an appropriate model since the extent to which these expensive goods are shared, and the cost and benefits to individuals (direct or indirect fitness) and group (inclusive fitness) could be measured using different methods and scenarios. The overall benefit (fitness) acquired by the group could be quantified via biofilm productivity assay through dried biomass weight as performed in Chapter 3 or through total colony forming unit per ml (CFU/ml) as

employed in Chapters 2, 4, 5 and 6. While the extent of cost carried by each could be measured through relative fitness assay as utilized in Chapters 2, 3, 4, 5 and 6.

Importantly, the difference in the extent to which these goods are shared or privatized could also be monitored through cross-complementation assay wherein spent medium of interacting strains were supplemented on the other strain as shown in Chapters 2, 3, 4, 5 and 6. Additionally, the intensity and gene expression levels could be tracked by insertion of molecular marker wherein the promoter locus is tagged with reporter fusion (P*tapA* for TasA and P*eps* for EPS)[5], to monitor gene expression and phenotypic heterogeneity through fluorescence microscopy easily. Additionally, genetic variations in matrix production could lead to altered biofilm structural properties and efficiently assessed using biomechanical analyses [6–8] of hydrophobicity and surface topography (Chapter 2 and Chapter 5).

2. The costly metabolic pairing of EPS and TasA yields cooperative traits

Phenotypic heterogeneity is one of the prominent characteristics of biofilms[9] that also plays a role in social interactions[10]. It allows individuals to persist and survive in spite of the harsh environmental shifts that eventually lead to the division of labour [10]. Division of labour in *B. subtilis* biofilms is shown in Chapter 4 based on task allocation, cooperation and inclusive fitness gain of individuals. Exponentially growing *B. subtilis* demonstrated a metabolic specialisation in clonal bacterial population [11]. Seemingly, this also occurs in biofilms concerning matrix production. In *B. subtilis* biofilms, not all cells are dedicated to matrix production[12], and as confirmed in Chapter 4, the phenotypic task allocation in clonal biofilms is grouped into matrix non-producers, EPS producers and most commonly EPS and TasA-formers. However, it is surpassed by the genetic division of labour of two engineered specialists producing the TasA and the EPS, as demonstrated in Chapter 4. Division of labour occurs when cooperative individuals specialize in specific tasks and are favoured by natural selection when specialization facilitates efficiency benefits[13]. In the evolution study performed in Chapter 4, genetic task allocation resulted in maximal productivity in comparison to the phenotypic division of labour. Why is a genotypic division of labour much favourable than the phenotypic task allocation? It is evident that the genotypic division of labour saves cost since individual task allocation is based on

their genetic machinery rather than differentiation in gene expression (Chapter 4). This finding provides improved insights on how cooperation is more favourable based on genotypic specialization in spatial structures. Specifically, such advantage is caused by balanced mutual exchange of commodities based on low distribution and certain metabolic restrictions (reviewed in [14]). And since optimal matrix ratio of 30% EPS and 70% TasA production is also observed in plant root colonization, this shows that *B. subtilis* could be optimized in terms of ecological importance such as better crop yield.

Moreover, this platform demonstrates how cooperative traits based on fitness gain through task allocation occurs in biofilm systems. However, such phenomenon when subjected to experimental evolutionary scheme that mimics the changing environment in natural setting, the aforementioned genetic task allocation collapses through time. The difference in their exploitability, with EPS being more shareable and the protein component TasA being more privatized, led to the alterity of their abilities to maintain cooperation thus, leading to one of them to dominate the population. As it is in Charles Darwin's theory of evolution[15], the ones that survive seemingly are individuals that have best adapted to the condition. These led to a thought-provoking query of how an engineered matrix mutant (EPS producer) survives better than the other (TasA producer). As the data are shown in Chapter 5, evolution of individuality perishes cooperative traits. However, such tragedy seemingly is not a hurdle to the scientific knowledge of evolution of cooperative traits. The obvious reasons will be discussed further in the discussion section 3.2.

3. Evolution of social interactions in *B. subtilis* biofilms

Social interactions in *B. subtilis* is a prolific occurrence[16–18], interestingly so, it also observed in *B. subtilis* biofilms[1] such as in the case of cooperative interactions via division of labour of matrix components in clonal cells of *B. subtilis* (Chapter 4). However, it is not well established if these social relations would change, diminish or persist through time. Evolutionary adaptation is influenced by different biotic or abiotic factors that lead to new traits beneficial to an individual or to the community. As mentioned in Chapter 1, experimental evolution in biofilms yields unique community attributes that would shape social synergy. Experimental evolution in pellicle biofilms using different starting points

of clonal cells (Chapter 2), matrix producer versus non-producer (Chapter 3 and 6), and solitary scheme of two types of matrix producers (Chapter 5) provides insights on how social interactions are shaped in a prolonged time scale.

3.1. Diversification leads to complex social interplay

Morphotypic diversity, including phenotypic and genotypic heterogeneity, is widely observed in biofilm evolution experiments as compared to planktonic experimental set-ups (Chapter 1)[19]. First descriptions of morphotype diversification in biofilm evolution were detailed in 1994 and 1998 in *Comomonas* sp by Korona *et al.* and *Pseudomonas fluorescens* static microcosms by Rainey and Travisano, respectively. The latter experiment delved into the evolutionary dynamics on morphology diversification that led to the emergence of three prevailing morphology types that reproducibly existed on a consistent sequence. From then on, several other experimental evolution studies followed [20–28] and revealed similar striking observations that involved predictable order and time-dependent occurrences of morphology variants such as in the cases of *Serratia marcescens*[29], *Streptococcus pneumoniae* [30] *Staphylococcus aureus*[25,31] and *Burkholderia cenocepacia*[23,24]. The sequence and timing dependency is plausibly due to either epistasis, wherein the fitness and adaptation consequence on genetic modifications is reliant on the mutations in other genes, or niche construction, wherein the effect of environment alterations rendered by prior variants influenced the nature of the succeeding variants[19].

Most evolutionary diversification studies have been done using Gram-negative species except for the medically relevant pathogen *S. aureus* [25,31,32]. Experimental evolution on a non-pathogenic Gram-positive bacterium renders another evolutionary perspective in an ecological setting such as in the case of the plant root colonizer *B. subtilis*. As shown in Chapter 2, the spatial structures in the pellicle biofilms of *B. subtilis* are also a favourable environment for morphotypic divergence, wherein the diversified community could be influenced by numerous social and ecological interplays. As in the case of the emergence of morphotypes W (Wrinkly), S (Smooth or studded), Fuzzy (F) and Ruffled spreader (R) in the experimental evolution set-up of *P. fluorescens* [33] and bead selection method of *B. cenocepacia* [23], pellicle evolution scheme in *B. subtilis* likewise revealed a variety of

morphotypes called Wrinkly, Rough, Spreader and Smooth (Chapter 2). Genetic analyses of these morphotypes revealed two genetic lineages wherein wrinkly evolved from rough and smooth from the spreader. These morphotypes co-exist by inhabiting different niches within the biofilms, thus preventing competition and rendering an improvement in biofilm productivity similarly observed in previous studies [23,33–35].

Interestingly, they also exhibited unique quantifiable differences based on surface topography and non-wettability. Previous studies have linked biofilm surface properties with hydrophobicity alongside with biofilm matrix production [6,7,14,36–39], which also supported the observed distinction in surface structure and hydrophobic properties of the morphotypes. Understanding the different wetting properties of evolved biofilm structures is vital to fathom how they adapt to dry and humid conditions. Moreover, additional insights on surface structure related to hydrophobicity and matrix production play a crucial role in finding effective ways to eradicate biofilms through mechanical or chemical force, such as the use of antibacterial agents.

Evolutionary diversification, although first classified through morphological differences in colony structure, could also be further analysed using different properties. Aside from the previously mentioned physical property based on surface structure and hydrophobicity, biofilm formation through matrix gene expression could also be utilized to differentiate one morphotype from the other (Chapter 2). Additionally, it also helps in comprehending the social interplay within evolved strains based on public good availability. Colony structures are linked to different biofilm-associated characteristics such as in the case of the wrinkly phenotype isolated from the evolution studies of *P. fluorescens* and *B. cenocepacia* showing increased cluster formation, improved attachment and higher productivity based on biomass [20,23,33]. This is also true in the case of the observed distinctions in matrix gene expression profiles based on pellicle formation abilities of the morphotypes isolated from the evolution experiment in *B. subtilis* detailed in Chapter 2. Wrinkly isolate has the highest matrix gene expression, followed by rough and spreader strains. The least is the smooth morphotype that is comparably lower than the ancestor. Evidently, due to low matrix gene expression, the smooth morphotype isolate is unable to form a pellicle. However, the presence of such phenotype increases the productivity (based on the total number of the colony- forming

units) of the whole population thus implying exploitation of the cooperative behaviours rendered by the other morphotypes to the smooth.

Additionally, when supernatant coming from the ancestor strain is supplemented to the smooth variant, the ability to form pellicle is restored, suggesting an exploitative interaction. However, since co-culturing of the four morphotypes reveal that the smooth variant is located at the bottom layer of the pellicle, its exploitative behaviour could be modulated due to poor oxygen availability. Positioning is an important basis for competition in biofilms [40], and since smooth variant is at a disadvantage, exploitation restraint occurs, which is then evident in the increased productivity of the population.

Social interactions during evolutionary diversification reveal positive interaction based on niche construction opportunities. Alteration in the environment brought about by genotypic variants creates new niches that known as niche construction[23,34,41]. Diversification provides ecological prospects based on vacant niches due to the spatial structure, and nutrient gradient involve in biofilms. Such empty niches are often not utilized by existing genotypes/phenotypes until novel ones arise. These niches provide a harmonious relationship among genotypes as they occupy a niche that is complementary to their specialized needs. However, gradients of stress factors, such as oxygen gradient in pellicles, could also result in competitive interactions resulting in exploitative behaviours. Competition is driven by positioning[40], which is also highly modulated in niche construction.

Thus, diversification is not exclusive to pathogenic Gram-negatives and Gram-positives but also occurs in non-pathogenic Gram-positive bacterium, as represented by *B. subtilis.* More importantly, it offers complex social interactions involving a crisscross of positive and exploitative behaviours — a positive interaction based on cooperation via shared interest as evident in the increased group fitness and a negative interaction via exploitation caused by nascent evolved non-producers taking advantage of the cooperative behaviour of the evolved producers.

3.2. Evolution of individuality diminishes cooperation via novel biofilm traits

Since the pioneering evolutionary experiment of Richard Lenski with *E. coli* in 1988 [42], numerous studies have established the role of evolution in the rapid development of new

traits in microorganisms. As in the case of microbial communities, the ability to sense threats from different environmental cues and be protected by biofilm matrix offers experimental evolution studies an excellent system to study the emergence of new biofilm lifestyle. Such as shown in biofilm evolution study in *P. aeruginosa* [33,43] and *B. subtilis* demonstrated in Chapter 5, wherein a type of task allocation collapses through time due to a much favourable adaptive skill which leads to new traits of improved surface colonization. Investigation of temporal properties of adaptive matrix autonomy as performed in Chapter 5 led to the understanding that the collapse of cooperation in biofilms is due to the disparity of the individual adaptation skills of EPS and TasA producers. Cells that are deficient in *eps* and those that do not harbour *tasA* genes are innately unable to form pellicles solitarily but are able to evolve into new biofilm traits that allow pellicle formation.

EPS producers evolve to a new lifestyle of elevated expression of *eps* through various transcriptional regulatory pathways yielding into improved transcription. An overabundance of such adaptive routes leads to the overproduction of EPS that facilitates surface colonization without the aid of the other matrix component TasA. This suggests that new biofilm lifestyle could evolve even in the absence of the other matrix component. Additionally, it demonstrates how evolution could reshape a known lifestyle into a new mode of living. And since EPS provides cells within the biofilms robust protection against external assaults, the evolution of unique ways of delivering copious protection signifies that biofilm resistance is a much more complicated problem.

Moreover, aside from its structural role, EPS in *B. subtilis* plays a signalling role similar to Psl polysaccharide in *P. aeruginosa*[44]. As a signalling molecule, interaction with membrane and kinase components EpsA and EpsB, respectively, promotes autophosphorylation of EpsA/EpsB tyrosine kinases[45] that inhibits EPS production but simultaneously activates phosphorylation of other substrates of the EPS biosynthetic, such as glucosyltransferase (EpsE) pathways that leads to EPS synthesis[46]. An evolved trait of EPS overproduction could influence EPS' role as a signalling molecule. Particularly so, since it was investigated by Elsholz *et al.* that addition of purified EPS revives phosphorylation in a dose-dependent approach[3]. Furthermore, EPS has a vital role in the root colonization of *Arabidopsis thaliana* [47] (see also Chapter 4). As previously mentioned, in comparison to TasA, EPS is highly exploitable. Thus an evolved lifestyle of EPS

overproduction would result in a much more complex social interplay aside from improved surface colonization, particularly in dealing with antibiotic resistance in biofilms and in plant-root colonization.

Another output of the evolution of individual matrix mutants is the evolution of TasA producer as presented in Chapter 5. Evolved TasA-formers harbour substitution of certain amino acids to cysteine that yielded a tremendous effect on amyloid structural properties such as thicker fibres and elevated oligomerization. Interestingly, this evolved trait that confers altered properties could only be observed in the absence of an EPS component, as pellicle formation would result to weakened water repellency due to modified interaction with another matrix component BslA [37]. Moreover, to date, there has been no cysteine existing in any of the TasA protein sequence coded in the sequenced genomes. Thus, it is seemingly selected against in nature, possibly due to the decrease in repellency.

TasA aside from being one of the key structural components of the biofilm matrix in *B. subtilis* is critical in root-related biofilm formation[47] (see also Chapter 4), and therefore, an altered form of TasA brought about by evolution might lead to a better or poorer plant root interactions. As such, evolved biofilm trait has not been examined yet to exist in a natural setting. Moreover, TasA confers antimicrobial properties when overexpressed in *E. coli* [48] and anti-fungal effect in *Fusarium culmorum*[49], however, it is yet to be known if a different amyloid fibre structure of TasA would also affect such inhibiting efficacy. Presence of cysteine in TasA interestingly poses new questions on possible effects on TasA's known properties and features. Although it was reported in amyloids associated with plant pathogens, such as harpins, that absence of cysteine in amyloids promotes better functionality[50], it is still interesting to investigate what other new functions a cysteine-containing TasA could offer.

3.3. Evolution of competitive interactions leads to shifts in mobile genetic elements and phenotypic heterogeneity

In *B. subtilis* biofilms, competitive interactions could evolve in systems that involve different shifts such as mobile genetic changes that are employed as a biological weapon (Chapter 3) or shift in phenotypic heterogeneity related to matrix gene expression

utilized as an anti-cheating mechanism (Chapter 6). Furthermore, the presence of cheaters leads to the competitive exclusion that facilitates the collapse of the population, commonly referred to as "The tragedy of the commons"[51] (Chapter 6). In another case, the presence of non-producers that are excluded from the community could foster an evolutionary event that leads to interference competition that provides an improved advantage to the evolved competing strain (Chapter 3).

3.3.1. Evolved competitive interference triggers phage release

Deficiency in both matrix components EPS and TasA tenders a tremendous disadvantage when it comes to pellicle formation (Chapter 3). Since both mentioned matrix components are essential in biofilm pellicle formation[52], they play a vital role in the evolutionary interplay between matrix producer and non-producer (Chapter 3). Moreover, proper positioning provides a significant function during pellicle formation[53] and competitive advantage[40]. In contrast to motility, chemo- and aerotaxis mutants that have a slight disadvantage due to delayed pellicle formation [53], the matrix mutants are more impaired since they are not able to stick to the surface and are at the bottom of the pellicle where oxygen is not accessible, and the carbon source is depleted. However, molecular adaptation strategies during evolution involving mobile genetic shifts rendered an increase in competitive advantage via phage mediation. Bacterial viruses, also known as phages, have been used as an important tool to understand bacterial evolution[54–59] since their independent discoveries in 1915 and 1917 by Fredrick Twort and Felix D'Herelle, respectively [60,61]. Moreover, they are able to degrade the extracellular polysaccharide matrix in biofilms by producing polysaccharide depolymerases [62–64]. The novel finding on the activation of phages into the lytic cycle in *B. subtilis* biofilm proves that social dynamics based on competitive interactions could be altered within the confines of adaptive evolutionary occurrences. Aside from those mentioned in Chapter 3, it is also plausible that non-matrix producing strain harbouring phages through adaptive strategy is able to gain advantage through the phage's ability to disintegrate the biofilm matrix enclosure produced by the producer cells and provide space for non-matrix producers in the biofilm. Although, it is worth mentioning that the effect of the *B. subtilis* released phages on the matrix are yet to be known. Phages have been studied to be effective in eradicating biofilms formed by pathogens such as the

Gram-positive bacterium *Streptococcus suis* [65]and Gram-negative bacteria such as *E. coli*, *Proteus mirabilis* and *Klebsiella pneumoniae* [66,67]. In 2016, temperate phages were shown to effectively facilitate adaptive evolution in host-pathogen interactions in cystic fibrosis-causing opportunistic pathogen *P. aeruginosa* [57]. These studies show the importance of phages and its role in evolution and advances knowledge in clinical studies. Although *B. subtilis* is a non-pathogenic bacterium, it has great relevance in the medical setting. It was employed to heal dysentery during World War II[68], and its EPS secretion has probiotic properties against enteric diseases and inflammations. The ability of *B. subtilis* to utilize phages during evolutionary adaptation caused by competitive interactions provides ecological relevance to understand better how it interacts in the soil where other numerous microorganisms compete for niches. Such as in the case of the interaction between *B. subtilis* with another plant-beneficial bacterium *Pseudomonas chlororaphis,* wherein their co-existence depends on extracellular matrix and Type VI Secretion system, respectively [69]. It is interesting to confirm the important role of matrix components in the social interactions using two different plant bacteria both *in vitro* and in plants as recently studied by Molina-Santiago *et.al*. More so, it is thought-provoking to know how such interaction could evolve through time and if phages will also play a role in such interplay just as how it happened in the evolution of matrix and non-matrix producers in Chapter 3.

3.3.2. Evolved anti-cheating mechanism alters heterogeneity pattern in response to exploitative interactions

Strategies have evolved through a cooperative system that renders avoidance of conflicts (reviewed in [70]; [1,71–73]). In Chapter 6, another mechanism that involves evolution with cheaters offers a different perspective. In contrast to the disadvantage in full non-producers (*eps* and *tasA* mutants) shown in Chapter 3, the presence of one of the matrix components offers a different social interplay. Absence of EPS provides a cheating phenomenon where TasA producer is able to benefit from the EPS produced by the other strain, in this case, the WT (co-operator). As previously mentioned, biofilms are highly characterized by phenotypic heterogeneity, which can be caused by genetic alterations, various environmental factors and intrinsic stochasticity[74]. In *B. subtilis*, heterogeneity within bacterial populations is observed in matrix production (Chapters 4, 5, 6, and [12]),

sporulation [75–77], competence [78–80] and motility [81]. In chapter 6, the effect of the presence of cheaters in the heterogeneous matrix gene expression within clonal populations in *B. subtilis* has been explored on a long-time scale. This novel approach demonstrates how cheating behaviour influences gene expression within the producer population and how biofilms respond to stress and exploitation. Since the extracellular matrix in *B. subtilis* provides protection against invasion of another plant bacterium [69], it is not surprising that higher *eps* expression within the subpopulation of cooperators has been observed in an evolution set-up between matrix producer (co-operator) and *eps* mutant (cheater). This is further supported by genetic shifts in the *rsiX* region of the producer strain (co-operator cells). The *rsiX* gene, formerly known as *ypuN* [82], is a member of regulons YvrHb, SigA and SigX[83]. As a downstream gene of extracytoplasmic function (ECF) sigma factor X ($\boldsymbol{\sigma}^X$), it controls the activity of $\boldsymbol{\sigma}^X$ and functions as anti- $\boldsymbol{\sigma}^X$ [82,83], thus, specific alterations in *rsiX* could render activation of $\boldsymbol{\sigma}^X$. ECF sigma factors actuates genes that confers resistance and protection against bacterial cell envelope threats such as antibiotics[84]. *B. subtilis* carries seven ECF sigma factors, wherein four of them, namely $\boldsymbol{\sigma}^X$, $\boldsymbol{\sigma}^M$, $\boldsymbol{\sigma}^W$ and $\boldsymbol{\sigma}^V$ have been well characterized. $\boldsymbol{\sigma}^X$ has the ability to confer protection against nisin and other cationic antimicrobial peptides by modifying cell surface properties [85,86]. Additionally, it has a protective function that overlaps in certain cases with another ECF sigma factor $\boldsymbol{\sigma}^M$, wherein it plays a secondary role of resistance to ß-lactam antibiotics[87].

Taking all these into consideration, *B. subtilis* is likewise a useful model organism to study cell envelope stress response. And since bacterial cell envelope is the primary line of protection against environmental stress, biofilm studies using *B. subtilis* offers a good combination in the investigation of stress response mechanisms within biofilms. In relation to the findings in Chapter 6, it is possible to assume that the stress offered by the presence of cheaters (*eps* mutants) provides a potential representation of antibiotic stress response in biofilms. It is relevant to mention that although the reported anti-cheating mechanism (e.g. shift towards higher *eps* expression amongst the *eps* expressing cells within the subpopulation) is transient and is then replaced by other mechanisms that involve minimization of *eps* expression (hyper OFF phenotype) and/or population tragedy. These findings suggest that response to stress and exploitations within biofilm subpopulation exists in various ways and could also mimic another system in the environment which that is related or unrelated to antibiotic resistance. Whichever

system it mirrors, be it in the medical or ecological settings, it provides an improved knowledge on how evolution shapes competitive interactions.

4. The significance of cheaters in the evolution of social interactions

Most studies have been done focusing on the role of cooperation wherein the cooperative framework is about the tragedy of cooperation due to the presence of the "bad guys" known as cheaters[88]. Even in Chapter 6, the presence of cheaters demonstrated the downfall of the population due to the exploitation of the matrix component. However, it is also possible that cooperation is not always the end of the line. As pointed out by Tarnita[88], cooperation and cheating could form a temporary phase to make way for new interactions and behaviours as shown in the evolution studies in *P. fluorescens*[33,43,89,90], *M. xanthus*[91,92] and possibly in *B. subtilis* (Chapter 6).

In the case of *P. fluorescens*, cheaters function as an integral part in propagating an integrated life cycle that interchanges between two states of phenotypes (wrinkly and smooth) without the aid of any genetic alterations[89]. This type of cheater occurrence is termed as propagules, wherein a smooth phenotype ensures the survival and dispersal of the wrinkly phenotype [43]. This shows that although the scenario led to a tragedy wherein cheaters outnumbered the wrinkly phenotype and caused it to perish, cheaters are able to reintroduce the wrinkly phenotype through spontaneous mutation. Thus, demonstrating that cheaters could successfully preserve a phenotypic life cycle.

Novel traits commonly arise from the evolution of cooperation or from the evolution of individuality shown in Chapter 5. However, in the case of *M. xanthus*, presence of cheaters could also result in the emergence of novel social traits. The obligate cheater, although it triggered the collapse of cooperation, resulted in genetic shifts related to new social traits bearing independent attributes [91]. The same is true with *B. subtilis*. As shown in Chapter 6, the presence of cheaters led to the emergence of a new phenotype (hyper ON) that confers mutations related to the altered stress response. It has been shown that genetic mutations in *rsiX* provide a higher tolerance to cationic antimicrobial peptides such as nisin[86].

Moreover, one of the important functions of EPS is to provide protection from environmental stress[3]. The new phenotype (hyper ON) harbours higher expression

intensity of *eps* matrix gene within the cell population, which corresponds to possible elevated protection against antimicrobials. Similar to *P. fluorescens* and *M. xanthus*, presence of cheaters in *B. subtilis* pellicles also resulted in population collapse. However, this tragedy seemingly resulted in a positive effect of the new trait related to antimicrobial resistance. These further confirms the perspective introduced by Tarnita that evolutionary social interactions between cheaters and co-operators do not always necessary culminate into a tragedy but rather a transient stage that bridges a disaster into a transformed social feature.

CONCLUDING REMARKS AND OUTLOOK

The work presented in this dissertation provides an added understanding of the relevant role of biofilm matrix components EPS and TasA as public goods that offer an effective means to investigate intraspecies interactions in *B. subtilis* biofilms. More significantly, in combination with experimental evolution, this system provides an efficient tool to examine and assess how interactions in the spatially structured environment become adaptive, maintained, diminished and/or eventually developed into novel biofilms traits. Additionally, this work offers additional knowledge on the extent of protection provided by the biofilm matrix within the population. Genetic division of labour between matrix components imparts beneficial rewards to the population, *in vitro* and in plants. Although such cooperative interaction is evolutionary unstable, the evolution of individuality reveals novel traits and the discovery of unexplored evolutionary routes.

Evolutionary diversification, although offers interactions within clonal cells, also yields exploitative traits such as spontaneous occurrences of matrix deficient cells. Moreover, laboratory evolution in the presence of cheaters provokes overexpression of matrix gene *eps* used as one of the anti-cheating mechanisms. Thus, could possibly mimic antibiotic resistance mechanisms in biofilms. Additionally, experimental evolution between producers and non-producers provides better insights on evolved strategies that individuals utilize to survive, such as the use of biological weapons. In a different circumstance, the release of phages through evolved interference competition demonstrates how cells within the biofilm could be a target of infiltration. Thus, offering an appealing promise of phage therapy as a possible option for the antimicrobial stratagem.

In natural settings, most microorganisms exist in multispecies communities. The work revealed in this dissertation has been done in single-species biofilms. However, it is noteworthy to mention that in most cases, multispecies infection in pathogenic biofilms is characterized by minimal bacterial diversification and governed by mono-species biofilms[93]. Thus, the findings in this study provide a stable platform to understand the complexities of evolution in clinical settings. Furthermore, evolution studies in single species biofilms could assist in forthcoming multispecies evolutionary investigations. Additionally, antibiotic resistance related to clinical biofilms has been a significant problem. Improved understanding of the evolutionary mechanisms used by biofilms as

stress response caused by exploitation offers advanced scientific footing on improved biofilm control strategies related to antimicrobial defection.

On another note, since *B. subtilis* is a plant growth promoting bacterium, findings in this work offer improved strategies in an ecological set-up. Better bacterial growth yield or growth rate could be investigated to examine how such could influence plant growth and yield qualities. Although the evolutionary work performed in this dissertation mostly involved the use of pellicle, and a small part, the use of plant colonization as biofilm models, it is still reliable to state that pellicle formation could also be a good representation of soil environment based on nutrient and oxygen supplies wherein the gradients could be similar.

Moreover, the observations established in this work offers not only better evolutionary perspectives applicable to biofilms or bacteria but also to viruses. Recent studies showed that cooperation via altruistic behaviours facilitates the viruses in overcoming the innate host immunity similarly as how animals behave altruistically [94]. It is also plausible to observe a resemblance with the realized cooperative traits in biofilms. In the same way, as cancer cells and bacterial populations are similar in terms of being established by ancestors that propagate into more massive clusters [95], cheating mechanisms in biofilms could also be utilized to investigate social interactions involved in the proliferation of cancer cells.

Biofilms offer a complex but effective system of understanding microbial interactions with the use of costly public goods that are shareable and exploitable. Several other biofilm properties that could also undergo evolutionary social interplays have not been explored, such as the other matrix components BslA. Synergistic relationship among TasA, EPS and BslA (previously known as YuaB) has been previously studied[96], and it could be expected that this social affinity could also evolve in time resulting to the emergence of unique hydrophobic property. Also, it is noteworthy to consider the evolutionary effect of quorum sensing (QS) in matrix production. Since matrix producers respond to QS signals at a higher level, which could result in matrix privatization [97], it is possible to investigate the evolutionary perspective of such interplay through the use of synthetic quorum system. Moreover, previous studies in *Pseudomonas aeruginosa* demonstrated that anti-quorum sensing inhibitors[98] as anti-biofilm strategies could be a better alternative to the increasing resistance of biofilms to traditional antibiotics.

Evolution studies could be employed to challenge the inhibitory efficacy of anti-quorum sensing system as an antibiofilm strategy.

Furthermore, other social behaviours that are divergent to biofilm lifestyles such as motility are altered after biofilm laboratory evolution. In most cases, experimental evolution in the presence of matrix deficient strains or of matrix mutants yields motility-related mutations, such as chemo / aero-taxis genes *hemAT* and *cheA* (Chapters 3, 5, 6). It is interesting to investigate how a known biofilm lifestyle with an advantageous biofilm trait such as oxygen-sensing-dependent movement [53] could undergo modifications via adaptive pathways and still could provide an improved advantage.

Significant findings revealed in this dissertation provides an enhanced understanding of the evolution of social interactions using biofilms as excellent models. However, it is a complex topic that requires further investigation as these conclusions open more scientific questions to explore with regards to the evolutionary aspects of Sociomicrobiology.

REFERENCES

List of published papers cited in the general discussion and concluding remarks:

1. van Gestel, J., Weissing, F. J., Kuipers, O. P. & Kovács, A. T. Density of founder cells affects spatial pattern formation and cooperation in Bacillus subtilis biofilms. *ISME J.* **8**, 2069–79 (2014).
2. West, S. A., Griffin, A. S., Gardner, A. & Diggle, S. P. Social evolution theory for microorganisms. *Nat. Rev. Microbiol.* **4**, 597–607 (2006).
3. Dragoš, A. & Kovács, Á. T. The Peculiar Functions of the Bacterial Extracellular Matrix. *Trends Microbiol.* **25**, 257–266 (2017).
4. Dragoš, A., Kovács, Á. T. & Claessen, D. The role of functional amyloids in multicellular growth and development of gram-positive bacteria. *Biomolecules* **7**, 1–13 (2017).
5. Hölscher, T. *et al.* Monitoring spatial segregation in surface colonizing microbial populations. *J. Vis. Exp.* **116**, e54752 (2016).
6. Falcón García, C. *et al.* Topographical alterations render bacterial biofilms susceptible to chemical and mechanical stress. *Biomater. Sci.* **7**, 220–232 (2019).
7. Werb, M. *et al.* Surface topology affects wetting behavior of Bacillus subtilis biofilms. *npj Biofilms Microbiomes* **3**, (2017).
8. Kesel, S. *et al.* Direct comparison of physical properties of Bacillus subtilis NCIB 3610 and B-1 biofilms. *Appl. Environ. Microbiol.* **82**, (2016).
9. van Gestel, J. & Nowak, M. A. Phenotypic Heterogeneity and the Evolution of Bacterial Life Cycles. *PLoS Comput. Biol.* **12**, 1–23 (2016).
10. Ackermann, M. A functional perspective on phenotypic heterogeneity in microorganisms. *Nat. Rev. Microbiol.* **13**, 497–508 (2015).
11. Rosenthal, A. Z. *et al.* Metabolic interactions between dynamic bacterial subpopulations. *Elife* **7**, 1–3 (2018).
12. Vlamakis, H., Aguilar, C., Losick, R. & Kolter, R. Control of cell fate by the formation of an architecturally complex bacterial community. *Genes Dev.* **22**, 945–953 (2008).
13. West, S. A., Fisher, R. M., Gardner, A. & Kiers, E. T. Major evolutionary transitions in individuality. *Proc. Natl. Acad. Sci.* **112**, 10112–10119 (2015).
14. Kovács, Á. T. & Dragoš, A. Evolved Biofilm: Review on the Experimental Evolution Studies of Bacillus subtilis Pellicles. *J. Mol. Biol.* 16–18 (2019). doi:10.1016/j.jmb.2019.02.005
15. Darwin, C. *On the origin of species by means of natural selection, or the preservation of favoured races in the struggle for life.* (Murray, John, 1859).
16. Dogsa, I., Oslizlo, A., Stefanic, P. & Mandic-mulec, I. Social Interactions and Biofilm Formation in Bacillus subtilis. *Food Technol. Biotechnol.* **52**, 149–157 (2014).
17. van Gestel, J., Vlamakis, H. & Kolter, R. From Cell Differentiation to Cell Collectives: Bacillus subtilis Uses Division of Labor to Migrate. *PLoS Biol.* **13**, (2015).

18. Hölscher, T. Social interactions and regulatory pathways influencing Bacillus subtilis biofilm formation and motility. (2017).

19. Steenackers, H. P., Parijs, I., Foster, K. R. & Vanderleyden, J. Experimental evolution in biofilm populations. *FEMS Microbiology Reviews* **40**, (2016).

20. Boles, B. R., Thoendel, M. & Singh, P. K. Self-generated diversity produces 'insurance effects' in biofilm communities. *Proc. Natl. Acad. Sci.* **101**, 16630–16635 (2004).

21. Smith, E. E. *et al.* Genetic adaptation by Pseudomonas aeruginosa to the airways of cystic fibrosis patients. *Proc. Natl. Acad. Sci.* **103**, 8487–8492 (2006).

22. Cramer, N. *et al.* Microevolution of the major common Pseudomonas aeruginosa clones C and PA14 in cystic fibrosis lungs. *Environ. Microbiol.* **13**, 1690–1704 (2011).

23. Poltak, S. R. & Cooper, V. S. Ecological succession in long-term experimentally evolved biofilms produces synergistic communities. *ISME J.* **5**, 369–378 (2011).

24. Traverse, C. C., Mayo-smith, L. M., Poltak, S. R. & Cooper, V. S. Tangled bank of experimentally evolved Burkholderia biofims reflects selection during chronic infections. **110**, (2012).

25. Savage, V. J., Chopra, I. & O'Neill, A. J. Population Diversification in Staphylococcus aureus Biofilms May Promote Dissemination and Persistence. *PLoS One* **8**, (2013).

26. Penterman, J. *et al.* Rapid Evolution of Culture-Impaired Bacteria During Adaptation to Biofilm Growth. **6**, 293–300 (2014).

27. Gómez, P. & Buckling, A. Real-time microbial adaptive diversification in soil. *Ecol. Lett.* **16**, 650–655 (2013).

28. Kim, W., Levy, S. B. & Foster, K. R. Rapid radiation in bacteria leads to a division of labour. *Nat. Commun.* **7**, 1–10 (2016).

29. Koh, K. S. *et al.* Phenotypic diversification and adaptation of Serratia marcescens MG1 biofilm-derived morphotypes. *J. Bacteriol.* **189**, 119–130 (2007).

30. Allegrucci, M. & Sauer, K. Characterization of colony morphology variants isolated from Streptococcus pneumoniae biofilms. *J. Bacteriol.* **189**, 2030–2038 (2007).

31. Koch, G. *et al.* Evolution of resistance to a last-resort antibiotic in Staphyloccocus aureus via bacterial competition. *Cell* **158**, 1060–1071 (2015).

32. Yarwood, J. M., Paquette, K. M., Tikh, U. B., Volper, E. M. & Greenberg, E. P. Generation of virulence factor variants in Staphylococcus aureus biofilms. *J. Bacteriol.* **189**, 7961–7967 (2007).

33. Rainey, P. B. & Travisano, M. Adaptive radiation in a heterogeneous environment. *Nature* **394**, 69–72 (1998).

34. Ellis, C. N., Traverse, C. C., Mayo-Smith, L., Buskirk, S. W. & Cooper, V. S. Character displacement and the evolution of niche complementarity in a model biofilm community. *Evolution (N. Y).* **69**, 283–293 (2015).

35. Flynn, K. M. *et al.* Evolution of Ecological Diversity in Biofilms of Pseudomonas

aeruginosa by Altered Cyclic Diguanylate Signaling. *J. Bacteriol.* **198**, 2608–2618 (2016).

36. Epstein, A. K., Pokroy, B., Seminara, A. & Aizenberg, J. Bacterial biofilm shows persistent resistance to liquid wetting and gas penetration. *Proc. Natl. Acad. Sci.* **108**, 995–1000 (2010).

37. Kobayashi, K. & Iwano, M. BslA(YuaB) forms a hydrophobic layer on the surface of Bacillus subtilis biofilms. *Mol. Microbiol.* **85**, 51–66 (2012).

38. Kovács, Á. T., van Gestel, J. & Kuipers, O. P. The protective layer of biofilm: A repellent function for a new class of amphiphilic proteins. *Mol. Microbiol.* **85**, 8–11 (2012).

39. Hobley, L. *et al.* BslA is a self-assembling bacterial hydrophobin that coats the Bacillus subtilis biofilm. *Proc. Natl. Acad. Sci. U. S. A.* **110**, 13600–5 (2013).

40. Kim, W., Racimo, F., Schluter, J., Levy, S. B. & Foster, K. R. Importance of positioning for microbial evolution. *Proc. Natl. Acad. Sci. U. S. A.* **111**, E1639-47 (2014).

41. O'Rourke, D., FitzGerald, C. E., Traverse, C. C. & Cooper, V. S. There and back again: consequences of biofilm specialization under selection for dispersal. *Front. Genet.* **6**, (2015).

42. Lenski, R. E., Rose, M. R., Simpson, S. C. & C., T. S. Long Term Experimental Evolution in E. coli I. Adaptation and Divergence During 2000 Generations. *Am. Nat.* **138**, 1315–1341 (1991).

43. Rainey, P. & Rainey, K. Evolution of cooperation and conflict in experimental bacterial populations. *Nature* **425**, 72–74 (2003).

44. Irie, Y. *et al.* Self-produced exopolysaccharide is a signal that stimulates biofilm formation in Pseudomonas aeruginosa. *Proc. Natl. Acad. Sci.* **109**, 20632–20636 (2012).

45. Gerwig, J., Kiley, T. B., Gunka, K. & Stanley-wall, N. The protein tyrosine kinases EpsB and PtkA differentially affect biofilm formation in Bacillus subtilis. *microbiology* **160**, 682–691 (2014).

46. Elsholz, A. K. W., Wacker, S. A. & Losick, R. Self-regulation of exopolysaccharide production in Bacillus subtilis by a tyrosine kinase. *Genes Dev.* **28**, 1710–1720 (2014).

47. Beauregard, P. B., Chai, Y., Vlamakis, H., Losick, R. & Kolter, R. Bacillus subtilis biofilm induction by plant polysaccharides. *Proc. Natl. Acad. Sci.* **110**, E1621–E1630 (2013).

48. Stöver, A. G. & Driks, A. Control of Synthesis and Secretion of the Bacillus subtilis Protein YqxM These include : Control of Synthesis and Secretion of the Bacillus subtilis Protein YqxM. *J. Bacteriol* **181**, 1–6 (1999).

49. Khezri, M., Jouzani, G. S. & Ahmadzadeh, M. Fusarium culmorum affects expression of biofilm formation key genes in Bacillus subtilis. *Brazilian J. Microbiol.* **47**, 47–54 (2016).

50. Choi, M.-S., Kim, W., Lee, C. & Oh, C.-S. Harpins, Multifunctional Proteins Secreted

by Gram-Negative Plant-Pathogenic Bacteria. *Mol. Plant-Microbe Interact.* **26**, 1115–1122 (2013).

51. Hardin, G. The tragedy of the commons. *Science* **162**, 1243–1248 (1968).

52. Branda, S. S., González-Pastor, J. E., Ben-Yehuda, S., Losick, R. & Kolter, R. Fruiting body formation by Bacillus subtilis. *Proc. Natl. Acad. Sci. U. S. A.* **98**, 11621–6 (2001).

53. Hölscher, T. *et al.* Motility, chemotaxis and aerotaxis contribute to competitiveness during bacterial pellicle biofilm development. *J. Mol. Biol.* **427**, 3695–3708 (2015).

54. Feiner, R. *et al.* A new perspective on lysogeny: Prophages as active regulatory switches of bacteria. *Nat. Rev. Microbiol.* **13**, 641–650 (2015).

55. Labrie, S. J., Samson, J. E. & Moineau, S. Bacteriophage resistance mechanisms. *Nat. Rev. Microbiol.* **8**, 317–327 (2010).

56. Bobay, L.-M., Touchon, M. & Rocha, E. P. C. Pervasive domestication of defective prophages by bacteria. *Proc. Natl. Acad. Sci.* **111**, 12127–12132 (2014).

57. Davies, E. V. *et al.* Temperate phages both mediate and drive adaptive evolution in pathogen biofilms. *Proc. Natl. Acad. Sci.* **113**, 8266–8271 (2016).

58. Stern, A. & Sorek, R. The phage-host arms-race: Shaping the evolution of microbes. *BioEssays* **33**, 43–51 (2011).

59. Pawluk, A., Bondy-Denomy, J., Cheung, V. H. W., Maxwell, K. L. & Davidson, A. R. A New Group of Phage Anti-CRISPR Genes Inhibits the Type I-E CRISPR-Cas System of Pseudomonas aeruginosa. *MBio* **5**, 1–7 (2014).

60. Twort, F. W. an Investigation on the Nature of Ultra-Microscopic Viruses. *Lancet* **186**, 1241–1243 (1915).

61. Felix D'Herelle. On an invisible microbe antagonistic toward dysenteric bacilli: brief note by Mr. F. D'Herelle, presented by Mr. Roux. *Res. Microbiol.* **158**, 553–554 (2007).

62. Harper, D. *et al.* Bacteriophages and Biofilms. *Antibiotics* **3**, 270–284 (2014).

63. Donlan, R. M. Preventing biofilms of clinically relevant organisms using bacteriophage. *Trends Microbiol.* **17**, 66–72 (2009).

64. Yan, J., Mao, J. & Xie, J. Bacteriophage polysaccharide depolymerases and biomedical applications. *BioDrugs* **28**, 265–274 (2014).

65. Meng, X. *et al.* Application of a Bacteriophage Lysin To Disrupt Biofilms Formed by the Animal Pathogen Streptococcus suis. *Appl. Environ. Microbiol.* **77**, 8272–8279 (2011).

66. Carson, L., Gorman, S. P. & Gilmore, B. F. The use of lytic bacteriophages in the prevention and eradication of biofilms of Proteus mirabilis and Escherichia coli. *FEMS Immunol. Med. Microbiol.* **59**, 447–455 (2010).

67. Chibeu, A. *et al.* Bacteriophages with the ability to degrade uropathogenic Escherichia Coli biofilms. *Viruses* **4**, 471–487 (2012).

68. Kovács, Á. T. Bacillus subtilis. *Trends Microbiol.* 246–248 (2013).

doi:10.1016/B978-0-12-374984-0.00125-X

69. Molina-santiago, C. *et al.* The extracellular matrix protects Bacillus subtilis colonies from Pseudomonas invasion and modulates. *Nat. Commun.* **10**, (2019).

70. Travisano, M. & Velicer, G. J. Strategies of microbial cheater control. *Trends Microbiol.* **12**, 72–78 (2004).

71. Diard, M. *et al.* Stabilization of cooperative virulence by the expression of an avirulent phenotype. *Nature* **494**, 353–356 (2013).

72. O'Brien, S., Luján, A. M., Paterson, S., Cant, M. A. & Buckling, A. Adaptation to public goods cheats in Pseudomonas aeruginosa. *Proc. R. Soc. B Biol. Sci.* **284**, (2017).

73. Kümmerli, R. *et al.* Co-evolutionary dynamics between public good producers and cheats in the bacterium Pseudomonas aeruginosa. *J. Evol. Biol.* **28**, 2264–2274 (2015).

74. Kovács, Á. T. Bacterial differentiation via gradual activation of global regulators. *Current Genetics* **62**, 125–128 (2016).

75. Chung, J. D., Stephanopoulos, G., Ireton, K. & Grossman, A. D. Gene expression in single cells of Bacillus subtilis: Evidence that a threshold mechanism controls the initiation of sporulation. *J. Bacteriol.* **176**, 1977–1984 (1994).

76. Gonzalez-Pastor, J. E., Hobbs, E. C. & Losick, R. Cannibalism by Sporulating Bacteria. *Science* **301**, 510–513 (2003).

77. Fujita, M. & Losick, R. High- and Low-Threshold Genes in the Spo0A Regulon of. *Society* **187**, 1357–1368 (2005).

78. Hadden, C. & Nester, E. W. Purification of competent cells in the Bacillus subtilis transformation system. *J. Bacteriol.* **95**, 876–885 (1968).

79. Haseltine-Cahn, F. & Fox, M. S. Fractionation of transformable bacteria from competent cultures of Bacillus subtilis on renografin gradients. *J. Bacteriol.* **95**, 867–875 (1968).

80. Haijema, B. J., Hahn, J., Haynes, J. & Dubnau, D. A ComGA-dependent checkpoint limits growth during the escape from competence. *Mol. Microbiol.* **40**, 52–64 (2001).

81. Kearns, D. B. & Losick, R. Cell population heterogeneity during growth of Bacillus subtilis. **24**, 3083–3094 (2005).

82. Brutsche, S. & Braun, V. SigX of Bacillus subtilis replaces the ECF sigma factor FecI of Escherichia coli and is inhibited by RsiX. *Mol. Gen. Genet.* **256**, 416–425 (1997).

83. Zhu, B. & Stülke, J. SubtiWiki in 2018: From genes and proteins to functional network annotation of the model organism Bacillus subtilis. *Nucleic Acids Res.* **46**, D743–D748 (2018).

84. Helmann, J. D. Bacillus subtilis extracytoplasmic function (ECF) sigma factors and defense of the cell envelope. *Curr Opin Microbiol.* **30**, 122–132 (2016).

85. Cao, M. & Helmann, J. D. Regulation of the Bacillus subtilis bcrC bacitracin

resistance gene by two extracytoplasmic function σ factors. *J. Bacteriol.* **184**, 6123–6129 (2002).

86. Cao, M. & Helmann, J. D. The Bacillus subtilis Extracytoplasmic-Function σX Factor Regulates Modification of the Cell Envelope and Resistance to Cationic Antimicrobial Peptides. *J. Bacteriol.* **186**, 1136–1146 (2004).

87. Luo, Y. & Helmann, J. D. Analysis of the role of Bacillus subtilis σ M in β-lactam resistance reveals an essential role for c-di-AMP in peptidoglycan homeostasis. *Molecular Microbiology* **83**, 623–639 (2012).

88. Tarnita, C. E. The ecology and evolution of social behavior in microbes. *J. Exp. Biol.* **220**, 18–24 (2017).

89. Hammerschmidt, K., Rose, C. J., Kerr, B. & Rainey, P. B. Life cycles, fitness decoupling and the evolution of multicellularity. *Nature* **515**, 75–79 (2014).

90. Rainey, P. B. & Kerr, B. Cheats as first propagules: A new hypothesis for the evolution of individuality during the transition from single cells to multicellularity. *BioEssays* **32**, 872–880 (2010).

91. Fiegna, F., Yu, Y. T. N., Kadam, S. V. & Velicer, G. J. Evolution of an obligate social cheater to a superior cooperator. *Nature* **441**, 310–314 (2006).

92. Velicer, G. J. & Vos, M. Sociobiology of the Myxobacteria. *Annu. Rev. Microbiol.* **63**, 599–623 (2009).

93. Burmølle, M., Ren, D., Bjarnsholt, T. & Sørensen, S. J. Interactions in multispecies biofilms: do they actually matter? *Trends Microbiol.* **22**, 84–91 (2014).

94. Leeks, A. & West, S. Altruism in a virus. *Nat. Microbiol.* **4**, 910–911 (2019).

95. Nadell, C. D., Foster, K. R. & Xavier, J. B. Emergence of spatial structure in cell groups and the evolution of cooperation. *PLoS Comput. Biol.* **6**, (2010).

96. Ostrowski, A., Mehert, A., Prescott, A., Kiley, T. B. & Stanley-wall, N. R. YuaB Functions Synergistically with the Exopolysaccharide and TasA Amyloid Fibers To Allow Biofilm Formation by Bacillus subtilis. *J. Bacteriol.* **193**, 4821–4831 (2011).

97. Zhang, F., Kwan, A., Xu, A. & Süel, G. M. A synthetic quorum sensing system reveals a potential private benefit for public good production in a biofilm. *PLoS One* **10**, 15–19 (2015).

98. Rice, S. A. *et al.* Inhibition of quorum sensing in Pseudomonas aeruginosa biofilm bacteria by a halogenated furanone compound. *Microbiology* **148**, 87–102 (2002).

Supporting information for Chapter 2

Evolution of exploitative interactions during diversification in *Bacillus subtilis* biofilms

Published in FEMS Microbiology Ecology (2018)

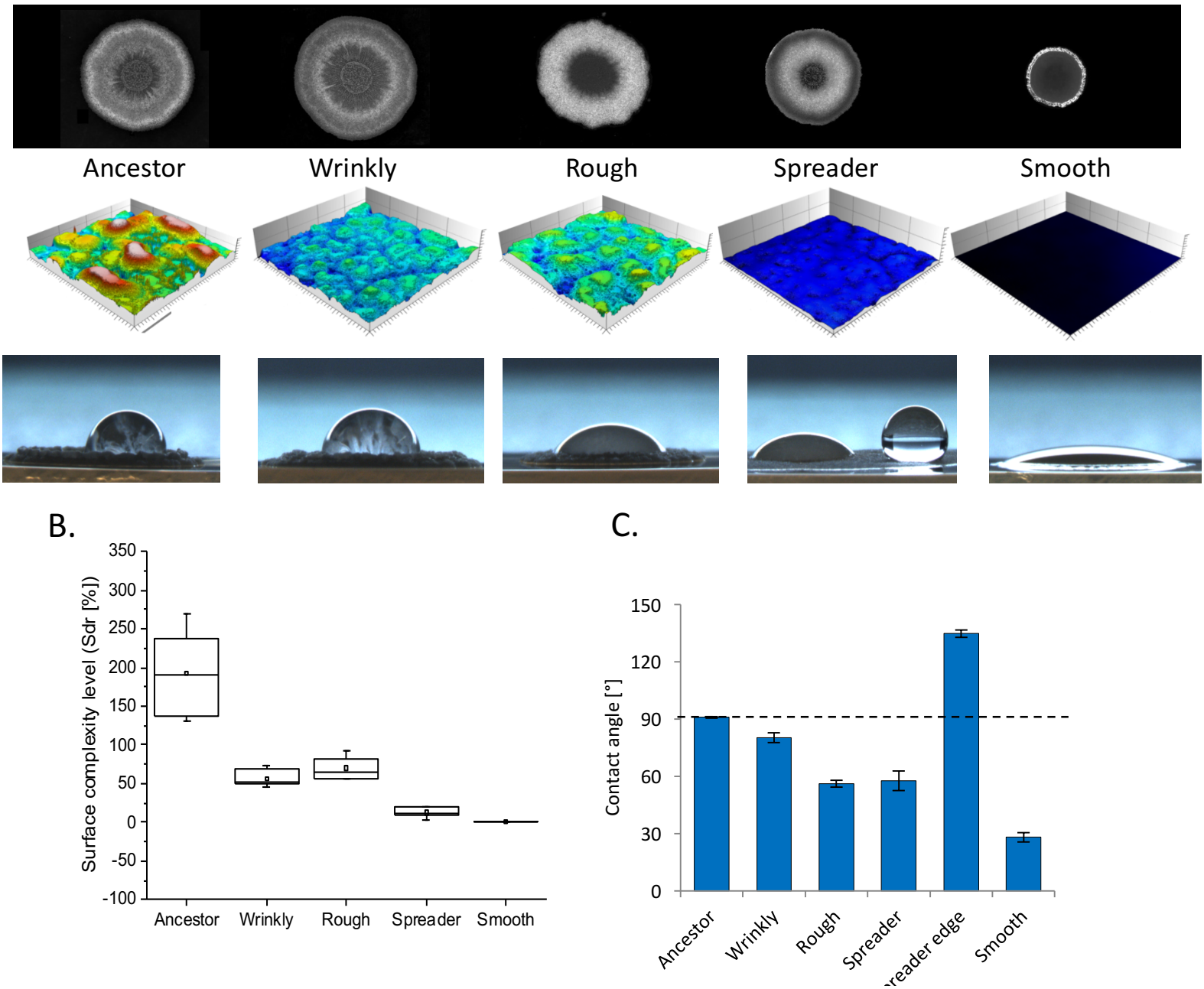

Supplementary Figure S1. Morphotypes morphology on MSgg and quantitative characterization of their colony features displayed on rich LB medium. **(A)** Colony morphologies of the ancestor and four distinct morphotypes spotted on MSgg medium (1.5% agar) are shown above. Middle, the surface topologies of the colonies developed on LB medium. Surface topologies of the ancestor and evolved morphotypes were acquired using light profilometry. 3D images of the surface topology were generated using the software µsurf (see methods) showing topological features with a standard color scale- where dark blue represents the lowest and white represents the highest features. Colonies were grown for 48h at 30°C. Scale bar represents 200µm. Below, image of 10µl water droplet spotted in the center, or colony periphery in case of the Spreader morphotype. **(B)** Developed interfacial area *Sdr* calculated for colony center of the ancestor and four morphotypes (n=6 or n=5) for colonies grown on LB medium. Boxes represent Q1–Q3, lines represent the median, small squares represent the mean and bars span from max to min. **(C)** Contact angles of water spotted in the colony center, or colony periphery in case of the Spreader (n=3) for colonies grown on LB medium. Dashed line represents contractual hydrophobicity cut-off, separating the surfaces on hydrophilic (below the line) and hydrophobic (above). Data points represent mean and error bars represent standard error.

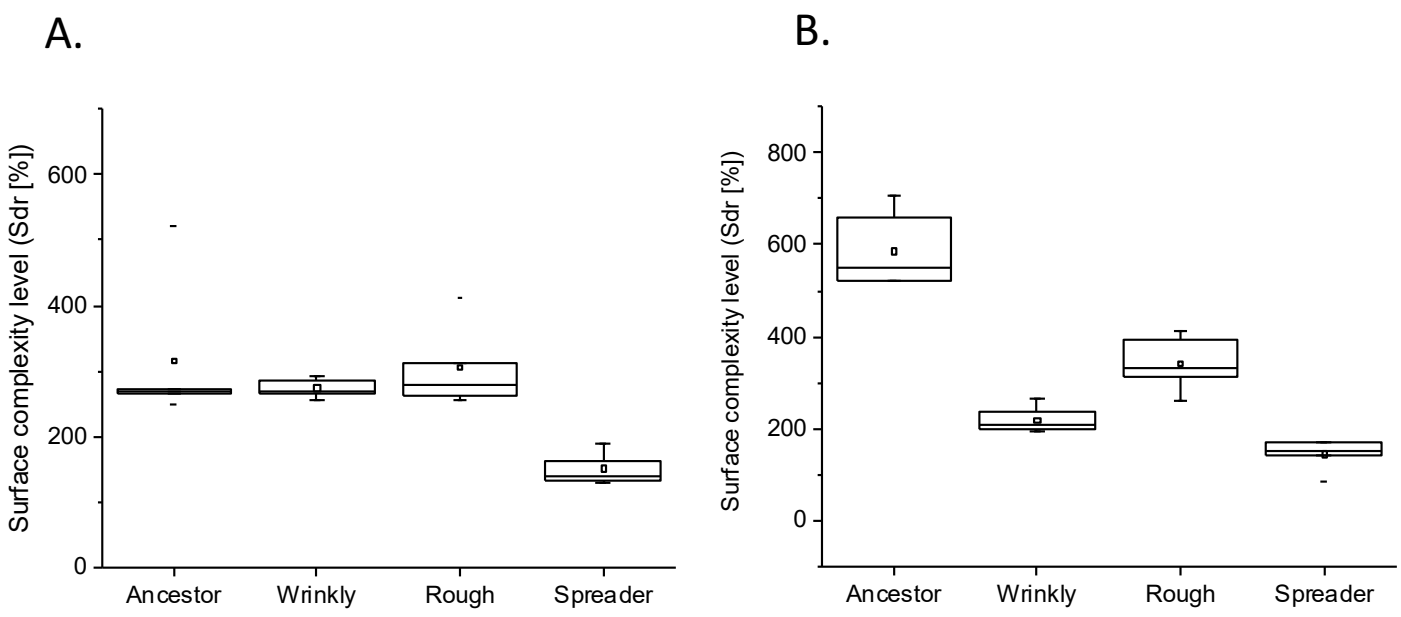

Supplementary Figure S2. Characterization of colony surface profiles at colony periphery. **(A)** Developed interfacial area *Sdr* calculated for colony periphery for colonies developed on MSgg medium (n=6 or n=5). **(B)** Developed interfacial area *Sdr* calculated for colony periphery for colonies developed on LB medium (n=6). Boxes represent Q1–Q3, lines represent the median, small squares represent the mean and bars span from max to min.

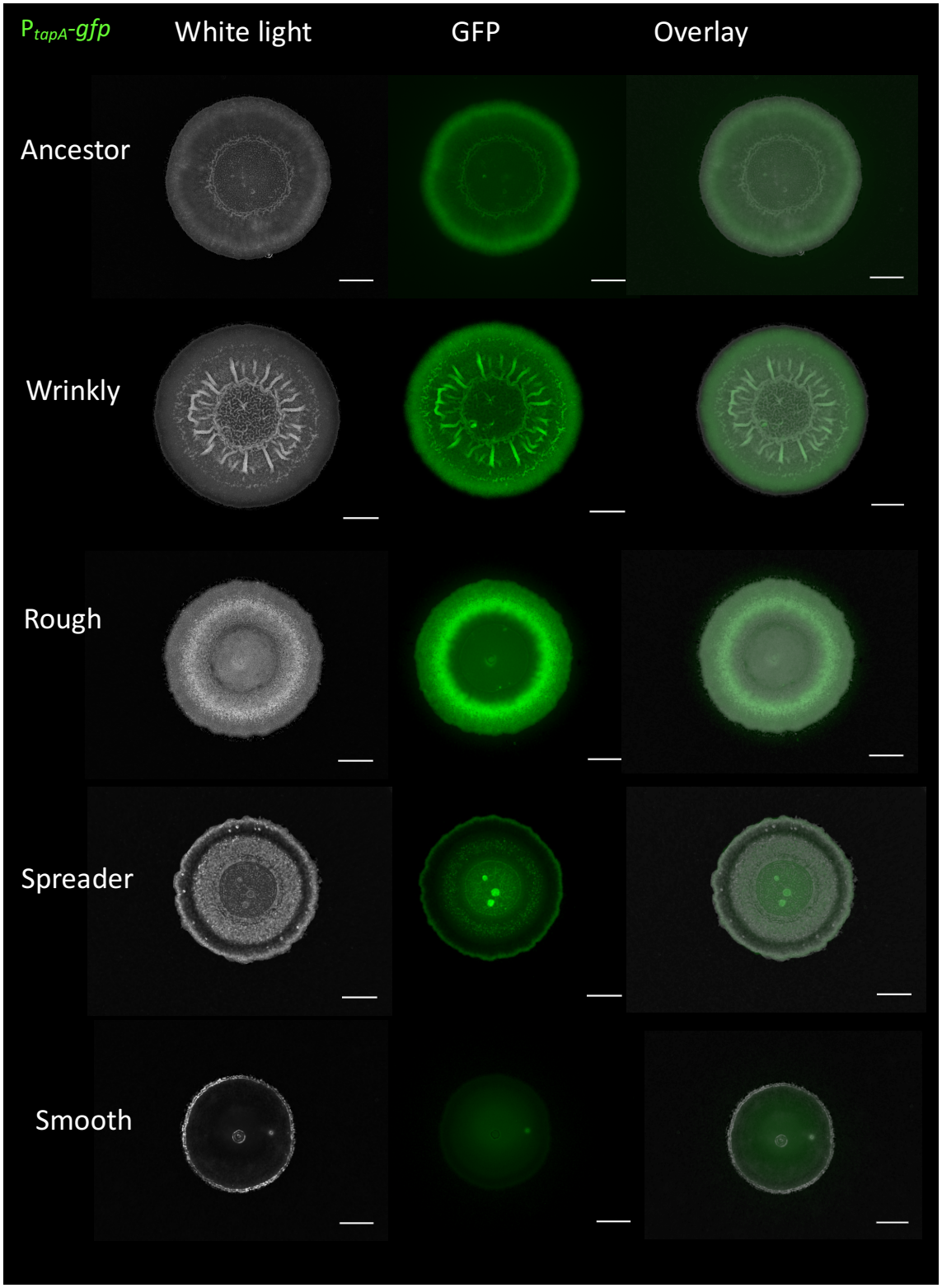

Supplementary Figure S3. Qualitative comparison of matrix-genes expression by different morphotypes. Expression of *eps* was monitored in the ancestor and all morphotypes in colonies developed on MSgg using P_{tapA}-*gfp* reporter fusion. Scale bar represents 2mm.

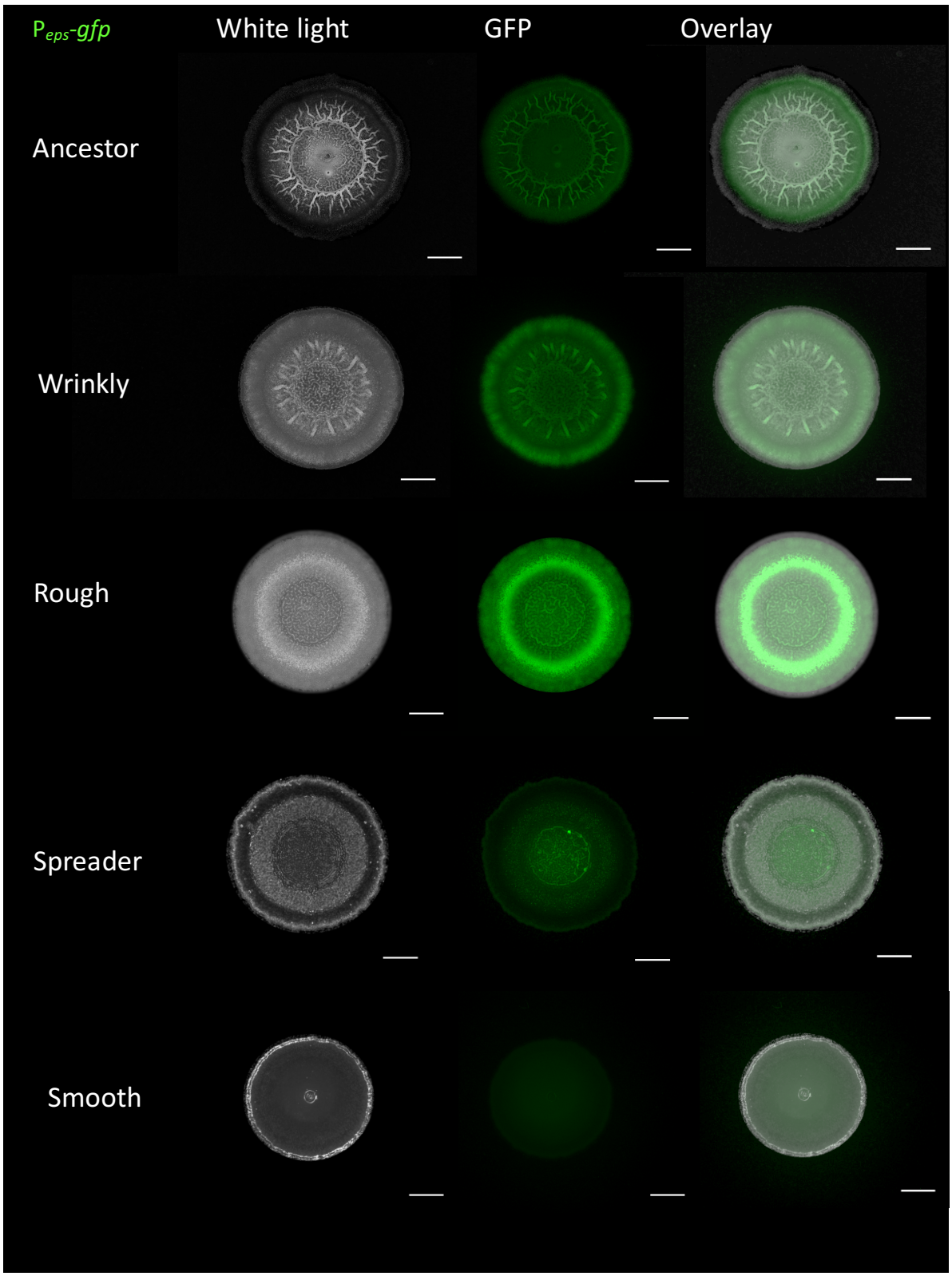

Supplementary Figure S4. Qualitative comparison of matrix-genes expression by different morphotypes. Expression of *tapA* was monitored in the ancestor and all morphotypes in colonies developed on MSgg using P_{eps}-*gfp* reporter fusion. Scale bar represents 2mm.

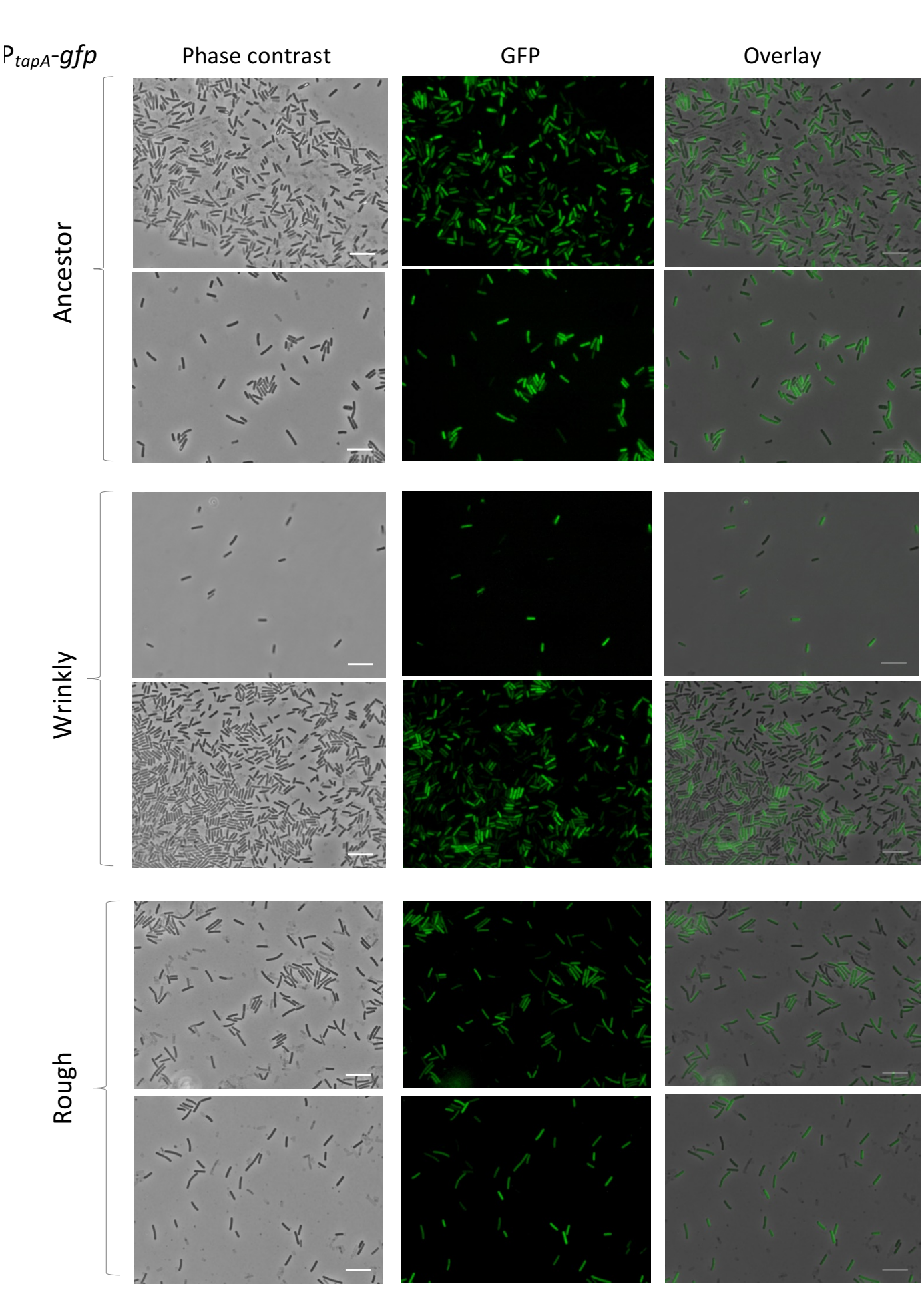
P_{tapA}-*gfp*
Phase contrast
GFP
Overlay
Ancestor
Wrinkly
Rough

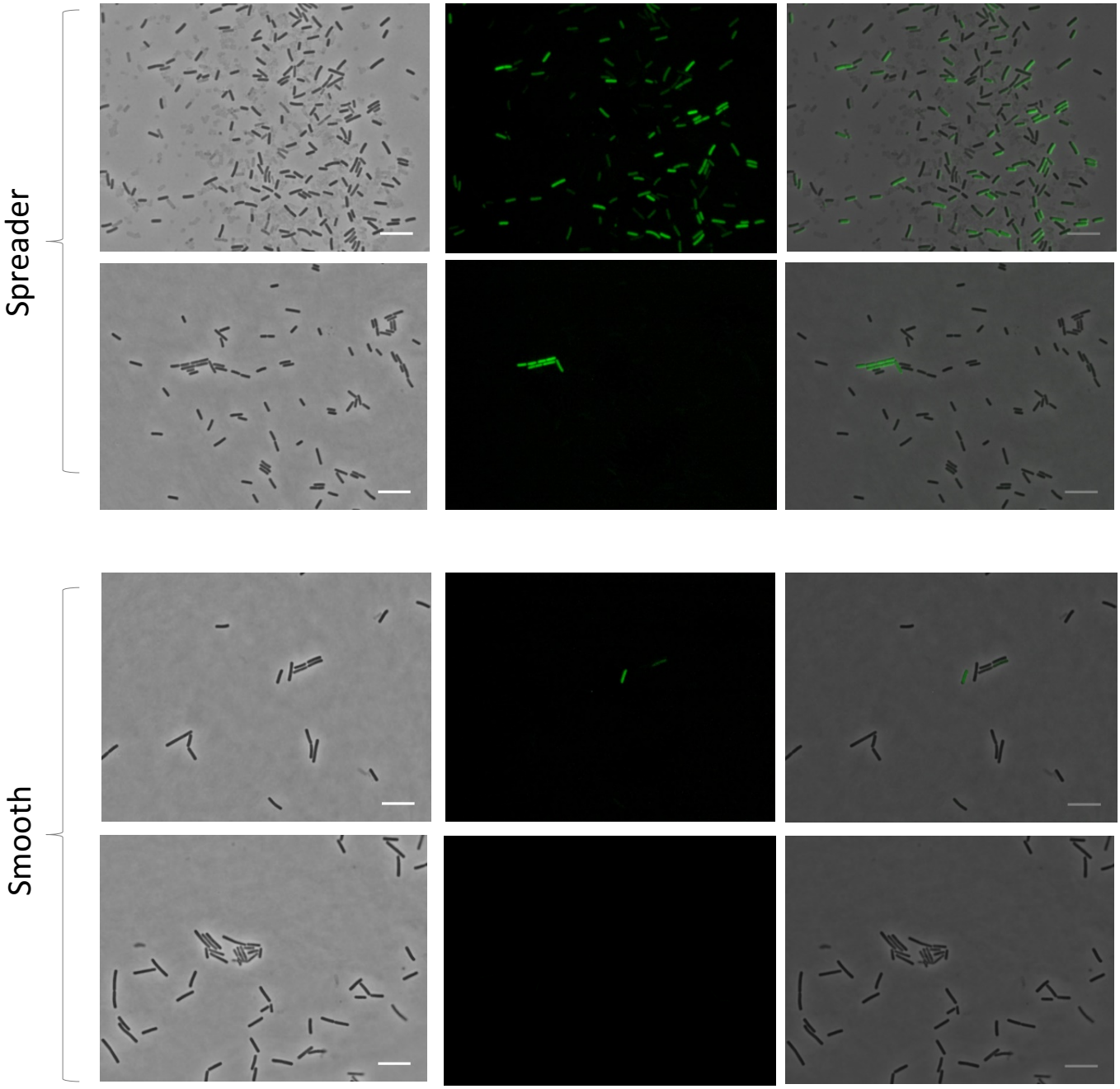

Supplemenatary Figure S5. Single-cell level expression of *tapA* in the ancestor and evolved morphotypes. The expression of P_{tapA}-*gfp* at single cell level was compared using epifluorescence. Pellicles were grown in MSgg medium at 30°C for 24 hours, harvested and disrupted to single-cell level by sonication. Time point 24h was selected, based on spectrofluorimetric analysis, as showing high differences in P*tapA* expression among morphotypes (Fig. 3A). Images taken from two independent biological replicates are presented for each morphotype. Scale bar corresponds to 10µm.

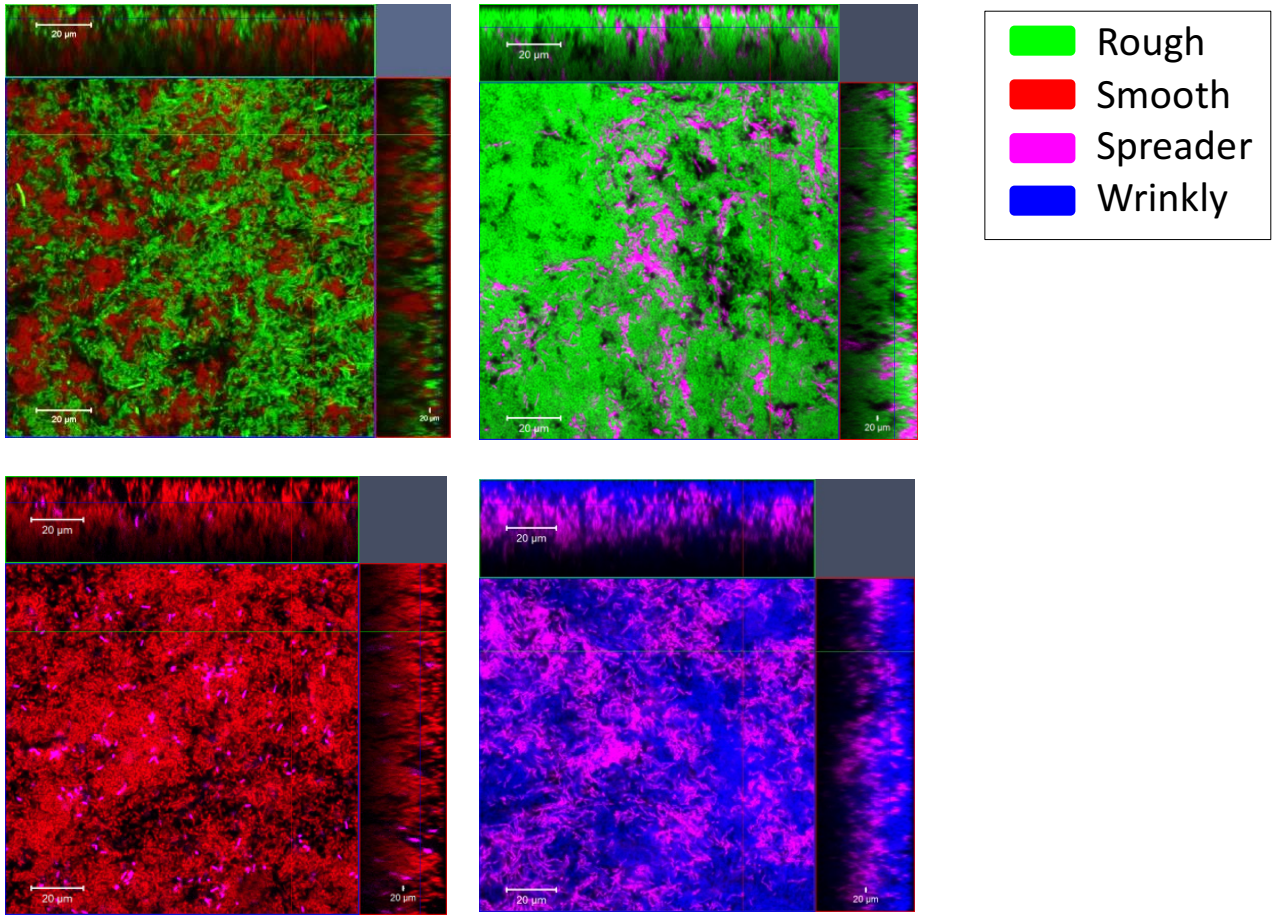

Supplementary Figure S6. Control experiments with swapped fluorescent markers for estimating the spatial assortment of morphotypes in the pellicles. Confocal microscopy images of pellicle biofilms formed by the mix of four morphotypes were taken. Each time only 2 selected morphotypes were labelled with constitutive fluorescent reporters and could be visualized in the pellicle. Morphotypes were mixed in ratios 0.9: 5.3:0.6:3.2 ratios and pellicle were allowed to form for 48h at 30°C. To simplify image comparison, each morphotype was artificially labelled with the same assigned color (regardless on actual fluorescent marker used) across all images: Rough – green, Smooth – red, Spreader – purple, Wrinkly - blue. The actual mixed cultures were: $Rough_{GFP}$ + $Smooth_{mKate}$ (+Wrinkly and Spreader unlabeled), $Rough_{mKate}$ + $Spreader_{GFP}$ (+Wrinkly and Smooth unlabeled), $Smooth_{mKate}$ + $Spreader_{GFP}$ (+Rough and Wrinkly unlabeled), $Spreader_{mKate}$ + $Wrinkly_{GFP}$ (+Rough and Smooth unlabeled).

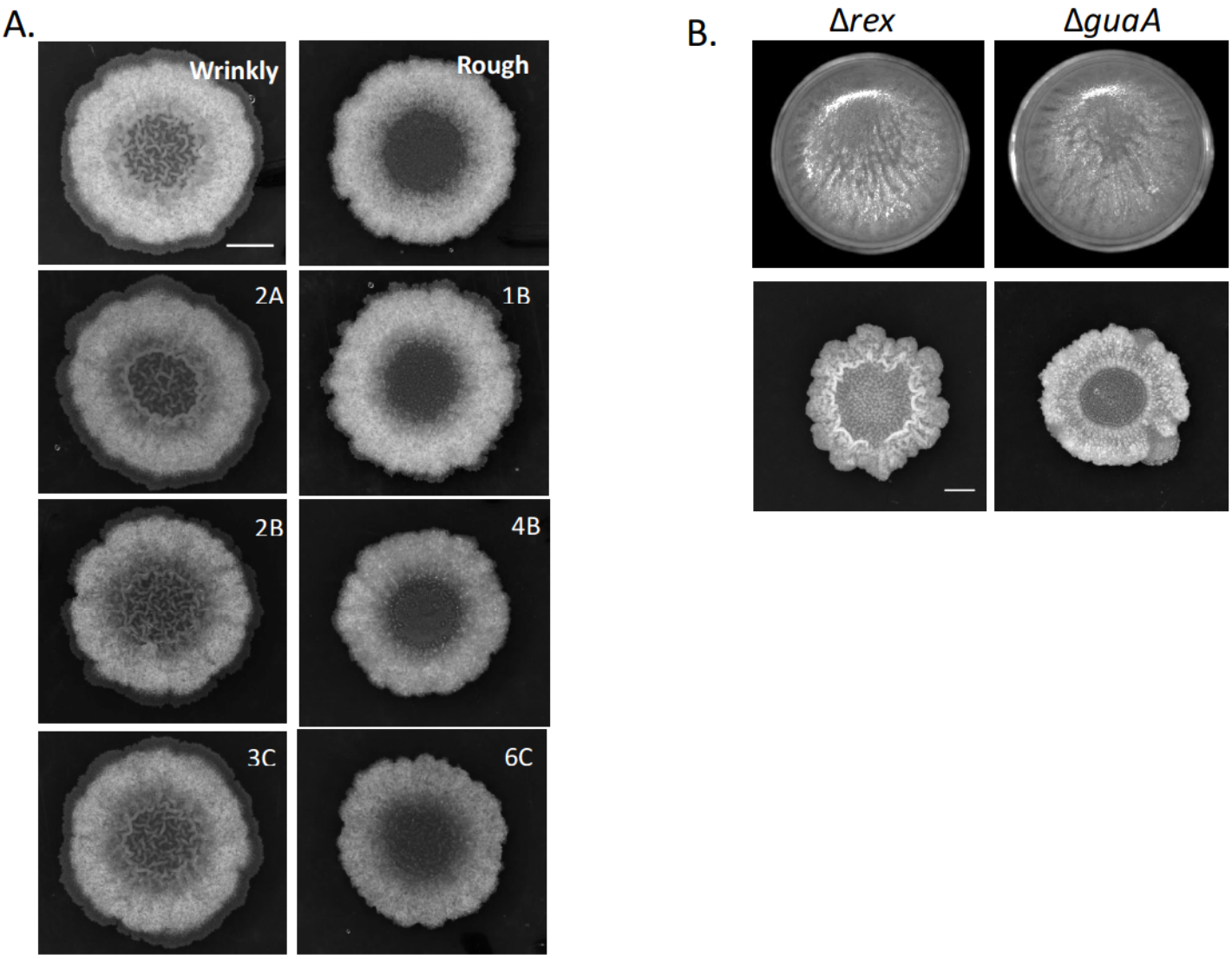

Supplementary Figure S7. Exploring molecular evolution pattern during diversification. **(A)** Morphologies of randomly picked colonies from populations 2-6 were evaluated and assigned to Wrinkly or Rough category based on similarity to those morphotypes from population 1. Isolates were subjected to whole- genome sequencing together with all morphotypes from population 1. Scale bar represents 2 mm. **(B)** Pellicle and colony morphologies of the ancestor strain carrying *rex* and *guaA* knockout strains. Pellicles and colonies were grown for 48h at 30°C. Well diameter is 1.5 cm. Scale bar represents 1 mm.

Strain name	Genotype	Reference
DK1042	NCIB 3610 *comI*^{Q12I}	Konkol, Blair and Kearns 2013
NRS2243	3610 *sacI::*P$_{eps}$-*gfp* (Km^{R})	Murray, Strauch and Stanley-Wall 2009
NRS2394	3610 *sacI::*P$_{tapA}$-*gfp* (Km^{R})	Murray, Strauch and Stanley-Wall 2009
BKE12280	168 *rex::mls*	Koo *et al.* 2017
BKE06360	168 *guaA::mls*	Koo *et al.* 2017
168 hyGFP	168 *amyE*::P$_{hyperspank}$-GFP (Cm^{R})	van Gestel *et al.* 2014
168 hymKate	168 *amyE*::P$_{hyperspank}$-mKATE2 (Cm^{R})	van Gestel *et al.* 2014
DTUB18	comI Rough *sacI::*P$_{eps}$-*gfp* (Km^{R})	This work
DTUB19	3610 *comI*^{Q12I} Wrinkly *sacI::*P$_{eps}$-*gfp* (Km^{R})	This work
DTUB20	3610 *comI*^{Q12I} Spreader *sacI::*P$_{eps}$-*gfp* (Km^{R})	This work
DTUB21	3610 *comI*^{Q12I} Smooth *sacI::*P$_{eps}$-*gfp* (Km^{R})	This work
DTUB22	3610 *comI*^{Q12I} Rough *sacI::*P$_{tapA}$-*gfp* (Km^{R})	This work
DTUB23	3610 *comI*^{Q12I} Wrinkly *sacI::*P$_{tapA}$-*gfp* (Km^{R})	This work
DTUB24	3610 *comI*^{Q12I} Spreader *sacI::*P$_{tapA}$-*gfp* (Km^{R})	This work
DTUB25	3610 *comI*^{Q12I} Smooth *sacI::*P$_{tapA}$-*gfp* (Km^{R})	This work
DTUB10	3610 *comI*^{Q12I} Rough *amyE*::P$_{hyperspank}$-*gfp* (Cm^{R})	This work
DTUB11	3610 *comI*^{Q12I} Wrinkly *amyE*::P$_{hyperspank}$-*gfp* (Cm^{R})	This work
DTUB12	3610 *comI*^{Q12I} Spreader *amyE*::P$_{hyperspank}$-*gfp* (Cm^{R})	This work
DTUB13	3610 *comI*^{Q12I} Smooth *amyE*::P$_{hyperspank}$-*gfp* (Cm^{R})	This work
DTUB14	3610 *comI*^{Q12I} Rough *amyE*::P$_{hyperspank}$-*mKATE2* (Cm^{R})	This work
DTUB15	3610 *comI*^{Q12I} Wrinkly *amyE*::P$_{hyperspank}$-*mKATE2* (Cm^{R})	This work
DTUB16	3610 *comI*^{Q12I} Spreader *amyE*::P$_{hyperspank}$-*mKATE2* (Cm^{R})	This work
DTUB17	3610 *comI*^{Q12I} Smooth *amyE*::P$_{hyperspank}$-*mKATE2* (Cm^{R})	This work
TB963	3610 *comI*^{Q12I} *rex::mls*	This work
TB964	3610 *comI*^{Q12I} *guaA::mls*	This work

Supplementary Table S1. Strains that were used in this study. NCIB 3610 *comI*^{Q12I} served as an ancestral strain in evolution experiment. Strains carrying fluorescent fusions were used as a source of genomic DNA to transform the evolved colony types. Strains DTU18-21 were obtained by transforming the evolved morphotypes with gDNA obtained from NRS2243. Strains DTU22-25 were obtained by transforming the evolved morphotypes with gDNA obtained from NRS2394. Strains DTUB10-B13 were obtained by transforming the evolved morphotypes with gDNA obtained from 168hyGFP. Strains DTUB14-B17 were obtained by transforming the evolved morphotypes with gDNA obtained from 168hymKate. Strains lacking *rex* and *guaA* were used as a source of gDNA to transform the ancestral strain in order to test for phenotypic effects of those mutations. TB963 and TB964 were obtained by transforming the DK1042 with gDNA obtained from BKE12280 and BKE06360, respectively.

REFERENCES

van Gestel J, Weissing FJ, Kuipers OP *et al.* Density of founder cells affects spatial pattern formation and cooperation in *Bacillus subtilis* biofilms. *ISME J* 2014;**8**:2069–2079.

Konkol MA, Blair KM, Kearns DB. Plasmid-encoded ComI inhibits competence in the ancestral 3610 Strain of *Bacillus subtilis*. *J Bacteriol* 2013;**195**:4085–4093.

Koo B-M, Kritikos G, Farelli JD *et al.* Construction and analysis of two genome-scale deletion libraries for *Bacillus subtilis*. *Cell Syst* 2017;**4**:291–305.

Murray EJ, Strauch MA, Stanley-Wall NR. SigmaX is involved in controlling *Bacillus subtilis* biofilm architecture through the AbrB homologue Abh. *J Bacteriol* 2009;**191**:6822-6832.

Strain	Av. Coverage	Av. Freq. of mutation [%]	mutations with freq.<50% [%]
Ancestor	174.05	97.4	0.05
Wrinkly 1	150.14	92.3	0.06
Wrinkly 2A	145.22	92.4	0.06
Wrinkly 2B	360.2	93.2	0.06
Wrinkly 3C	552.05	92.5	0.07
Rough 1	214.88	93.9	0.006
Rough 1B	131.66	92.8	0.05
Rough 4B	305.72	92.8	0.06
Rough 6C	218.4	91.8	0.07
Spreader	172.54	93.1	0.06
Smooth	156.4	93.8	0.037

Supplementary Table S2. Sequencing statistics. The table lists following parameters: Average coverage per genome obtained for each strain that was sequenced in the study; Average frequency of detected mutation (SNP or InDel) per genome (with 25% of variant calling frequency); Percent of detected mutations with frequency lower than 50%.

Population	r^2 (0-24#)	p-value (0-24#)	r^2 (0-24#)	p-value (0-35#)
1	0.51	0.11	0.27	0.24
2	0.41	0.17	0.48	0.09
3	0.61	0.07	0.34	0.17
4	**0.79**	**0.02**	0.52	0.07
5	0.37	0.20	0.35	0.16
6	0.38	0.19	0.00	0.99
All populations	**0.35**	**0.0001**	**0.24**	**0.0009**

Supplementary Table S3. Regression analysis of productivity changes during evolution. Changes of productivity thorough an evolutionary time for each population separately and together for all populations were statistically accessed using regression analysis. The analysis was performed with and without the final time point 35# where productivity dropped for all populations. R-squared (r^2) values correspond to proportion of variation explained by linear model. Statistically significant results ($p<0.05$) are highlighted in green.

	Pop 1	Pop 2	Pop 3	Pop 4	Pop 5	Pop 6
Pop 1	1					
Pop 2	0.87	1				
Pop 3	0.95	0.91	1			
Pop 4	0.87	0.88	0.96	1		
Pop 5	0.75	0.86	0.82	0.83	1	
Pop 6	0.43	0.37	0.55	0.57	0.57	1

Supplementary Table S4. Synchrony in productivity changes across evolutionary time in all 6 independently evolved populations accessed using correlation test. Pair-wise comparison was performed for all possible combinations and the obtained values of Pearson's correlation coefficients r were presented in the table. In most cases (with an exception of Population 6) r values are very high ($r>0.8$) indicating synchronous productivity changes across the populations.

Single Factor ANOVA			
	F	*p-value*	*F critical*
Smooth	**11.5**	**0.0003**	**3.11**
Rough	4.27	0.02	3.11
Wrinkly	0.75	0.60	3.11
Spreader	1.83	0.18	3.11

Student's t test - Smooth%						
	Pop 1	Pop 2	Pop 3	Pop 4	Pop 5	Pop 6
Pop 1						
Pop 2	**0.01**					
Pop 3	**0.05**	0.91				
Pop 4	**0.009**	0.22	0.48			
Pop 5	**0.02**	0.77	0.98	0.20		
Pop 6	0.59	**0.003**	**0.02**	**0.002**	**0.005**	

Student's t test - Rough%						
	Pop 1	Pop 2	Pop 3	Pop 4	Pop 5	Pop 6
Pop 1						
Pop 2	**0.002**					
Pop 3	0.21	0.60				
Pop 4	**0.003**	0.78	0.57			
Pop 5	0.16	0.50	0.97	0.47		
Pop 6	0.16	**0.0001**	0.11	**0.0004**	0.07	

Supplementary Table S5. Differences in distribution of 4 morphotypes (Wrinkly, Rough, Spreader and Smooth) across 6 independently evolved populations at final #35 evolutionary timepoint. According to Benferroni adjusted p-value for the above single factor ANOVA (N=15; adjusted p-value<0.003), we detect statistically significant differences between the populations with respect to percent of Smooth morphotype. Student's t test further revealed that Population 1 and 6 were significantly differed from other populations in percentage of Smooth morphotype ($p<0.05$). Consistently, the Populations 1 and 6 showed the lowest p-values when percentage of Rough morphotype was compared with other populations.

Supporting information for Chapter 3

De novo evolved interference competition promotes the spread of biofilm defectors

Published in Nature Communications (2017)

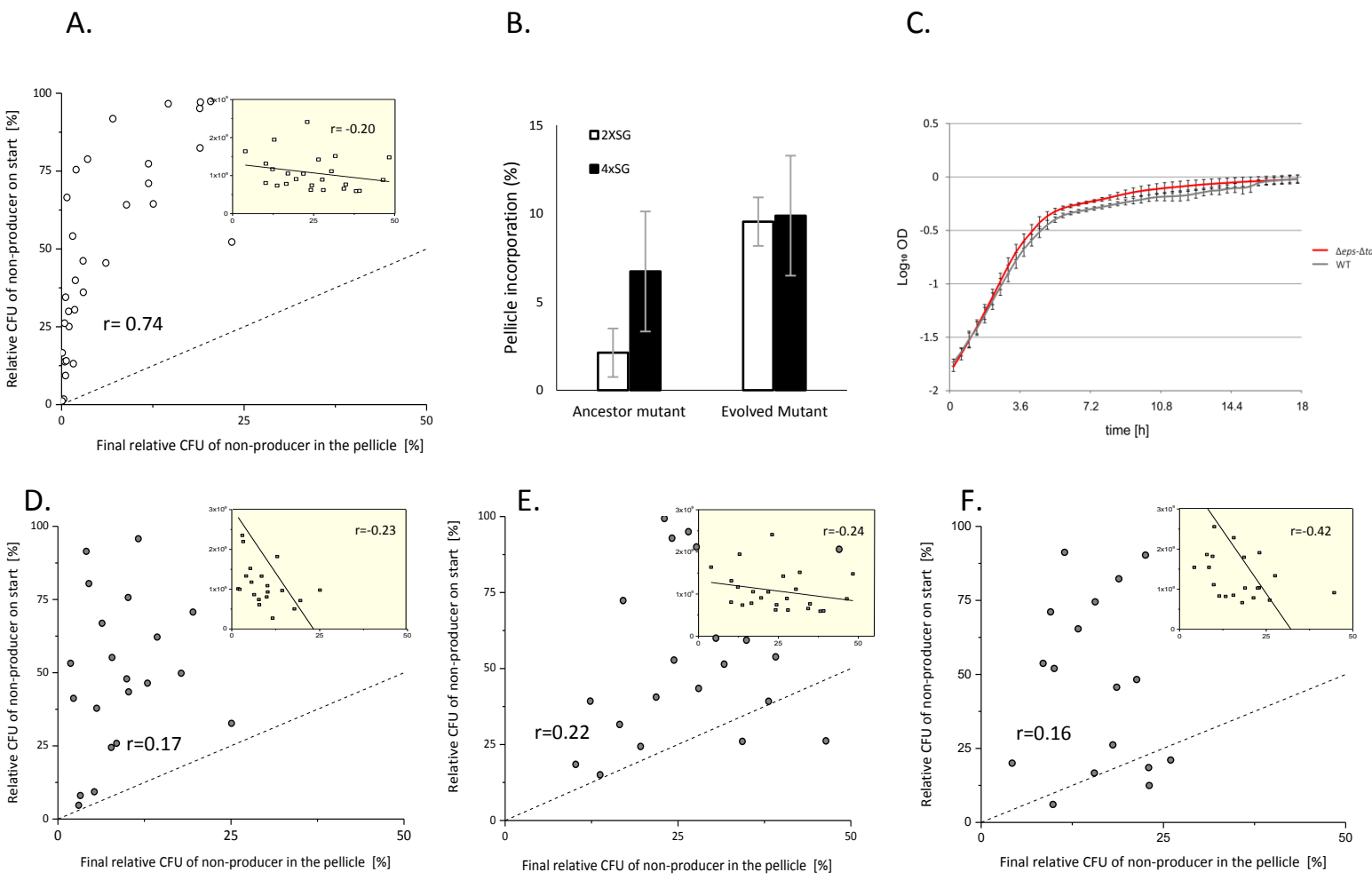

Supplementary Figure 1. Pellicle competition assays at different starting ratio of the producer and non-producer. A. Pellicle competition assay of *B. subtilis* wild type against the non-producer *Δeps-ΔtasA* at different starting (%) ratio (n=28; r=0.74). The incorporation of the non-producer *Δeps-ΔtasA* into the pellicle is dependent on its initial frequency. Dashed line represents 1.0 slope. Total CFU in the pellcle for each final relative CFU on the non-producer were plotted in the upper-right corner. **B.** Pellicle competition assay of *B. subtilis* wild type against the non-producer Δ*eps*-Δ*tasA* (left: ancestor, right: evolved) at different nutrient concentrations (n=5): 2xSG medium (standard nutrient concentration) and 4xSG medium (doubled nutrient concentration). Starting ratios were set to 50%. Pellicle incorporation of the ancestor non-producer Δ*eps*-Δ*tasA* escalates as the nutrient concentration increases. On the contrary, nutrient concentration has no effect on incorporation of the eNMP into the pellicle. Values represent the mean and error bars s.d.m. **C.** Growth curve of the *B. subtilis* 168 wild-type and Δ*eps*-Δ*tasA* mutant. OD^{595} was measured every 15 min using a TECAN Infinite F200 PRO microplate reader. The experiment was conducted in 2xSG medium at 30°C (n=9). Central values represent the mean and error bars s.d.m. Calculated growth rates [OD/h] for the WT and Δ*eps*-Δ*tasA* were μ=0.65 and μ=0.71, respectively, indicating a faster growth of the mutant strain; *t*-Student, two-tail $p < 0.05$. **D-F.** Pellicle incorporation of evolved non-producers at different starting (%) ratios. The incorporation success of the evolved non-producers B310mA (n=21; r=0.17) (**D**), B410mB (n=21; r=0.22) (**E**) and B510mC (n=18; r=0.16) (**F**) does not depend on their initial frequency. Dashed lines represent 1.0 slopes. Total CFU in the pellcle for each final relative CFU on the non-producer were plotted in the upper-right corner in each graph. Each experiment was performed at least twice.

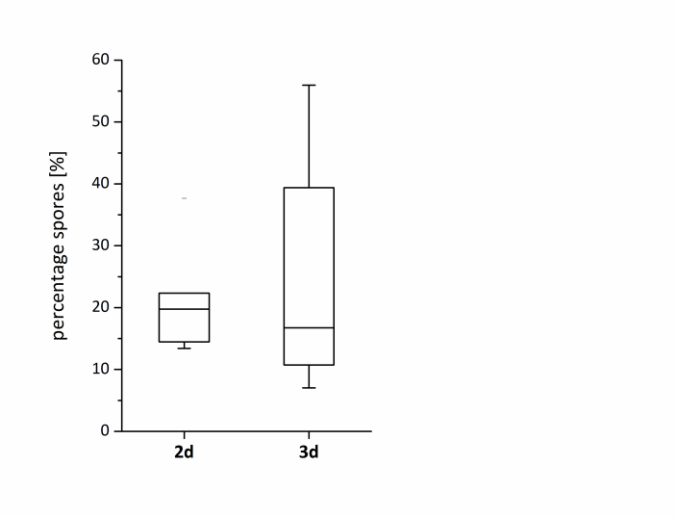

Supplementary Figure 2. Sporulation frequency in *B. subtilis* 168 pellicle. Sporulation frequency in *B. subtilis* 168 pellicle was determined after 2 and 3 days by comparing the total CFU (vegetative cells+spores) with the CFU after 20 min of incubation at 80°C (where only the spores survive) (n=7). Boxes represent Q1-Q3, lines represent the median and bars span from max to min. The experiment performed twice.

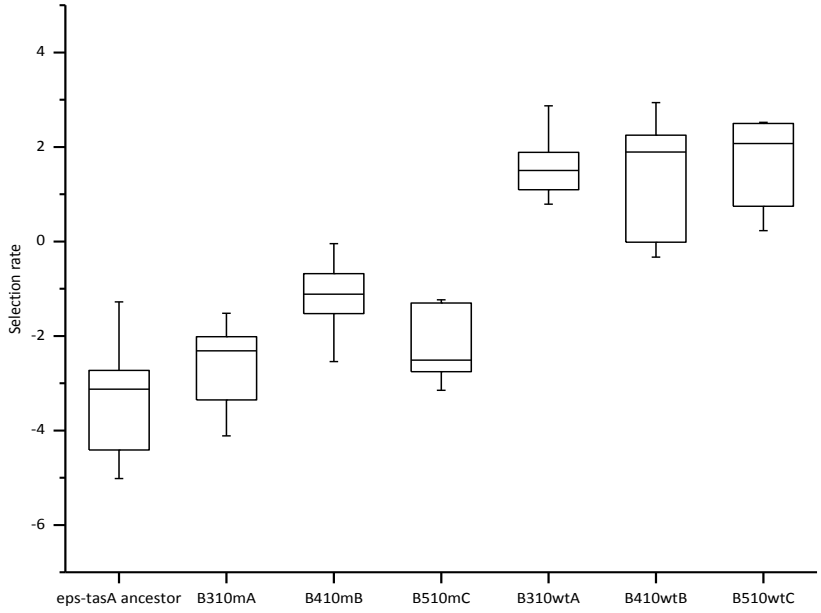

Supplementary Figure 3. Improved selection rate of evolved non-producers and producers against the wild type ancestor. Performance of selected strains against the wild type ancestor in pellicle competition assay was examined and the selection rate for each strain was calculated. The initial ratios of the strains in competition assays were in the range from 35% to 70% (n = 6-12). Boxes represent Q1-Q3, lines represent the median and bars span from max to min. Each *Δeps-ΔtasA* vs eMP/eNMP comparison was performed at least twice. The incorporation of the eMPs B310wtA, B410wtB and B510wtC into pellicles were 73.2 ±6.4(%), 67.8 ±8.8(%) and 82.0 ±2.9(%), respectively.

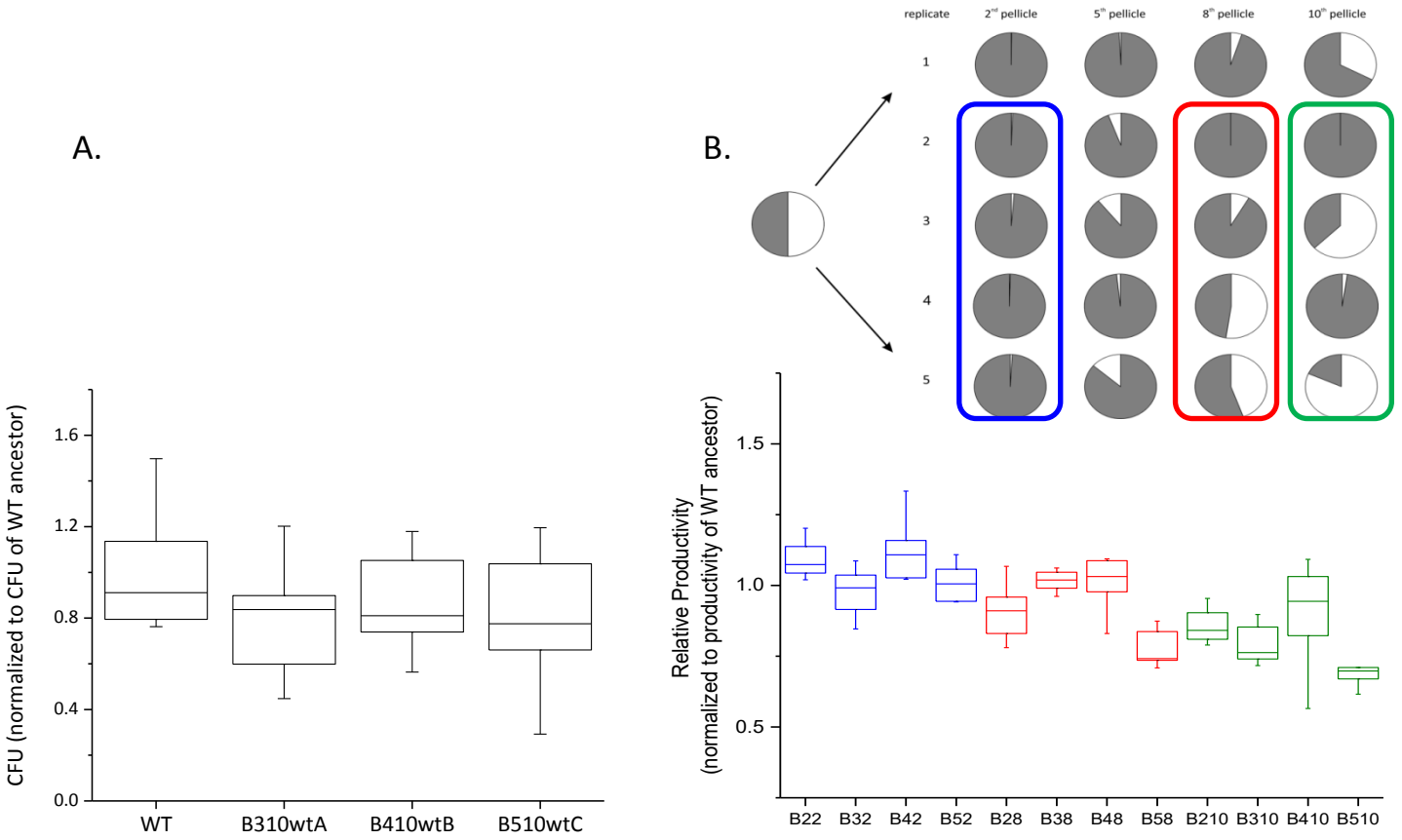

Supplementary Figure 4. Viable cell counts and productivity changes in the evolved pellicles. A. Total cell count of pellicles of evolved WT strains, B310wtA, B410wtB, B510wtC (n=10) normalized to the CFU of WT ancestor showing no significant difference compared to WT ancestor. We did not observe increased viable cell numbers in the eMP, as was the case for the overall biomass. We hypothesize that increased frequency of cell lysis, linked to spontaneous lytic induction in the eMP, may lead to release of various substances that contribute to the extracellular matrix and overall biomass. **B.** Productivity estimates of pellicle population mixes of WT and Δ*eps*-Δ*tasA* in replicates 2, 3, 4 and 5 at different time points (2nd, 8th, and 10th transfer) (n=10); Boxes represent Q1-Q3, lines represent the median and bars span from max to min. The experiments were performed twice.

A.

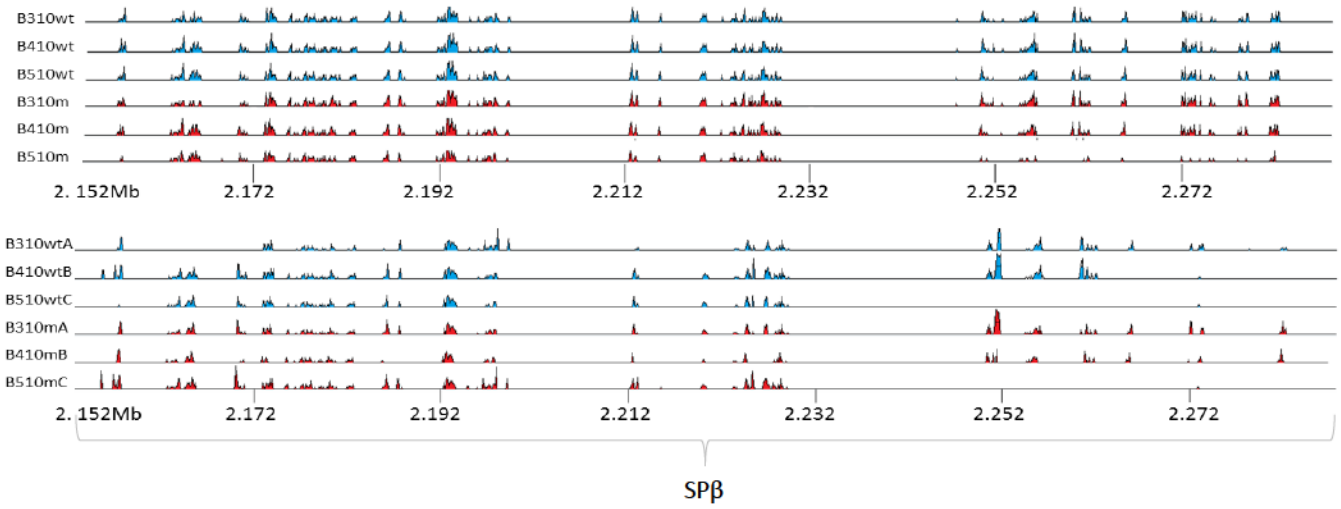

B.

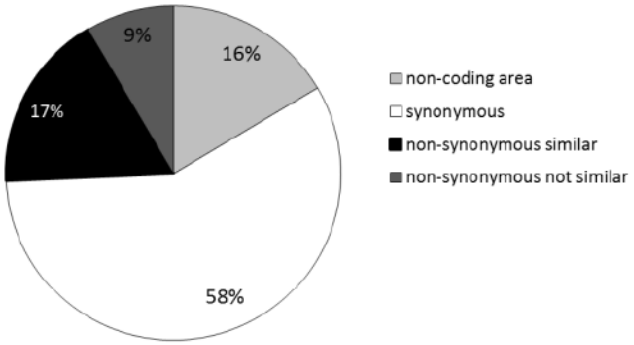

C.

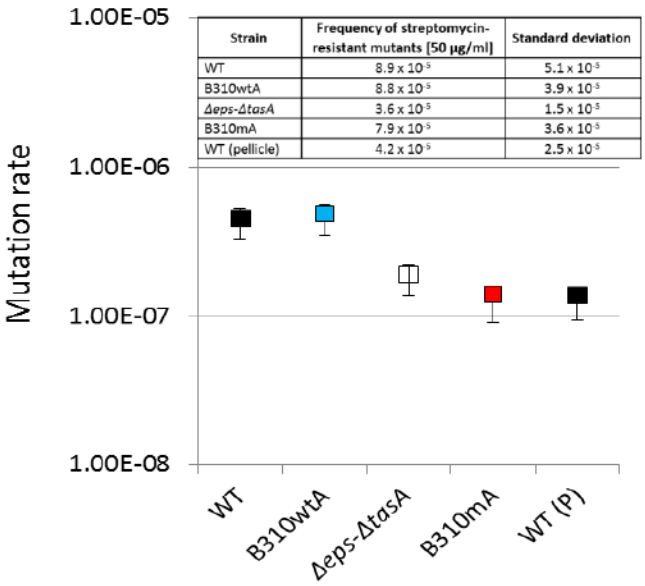

Strain	Frequency of streptomycin-resistant mutants [50 µg/ml]	Standard deviation
WT	8.9×10^{-5}	5.1×10^{-5}
B310wtA	8.8×10^{-5}	3.9×10^{-5}
Δeps-ΔtasA	3.6×10^{-5}	1.5×10^{-5}
B310mA	7.9×10^{-5}	3.6×10^{-5}
WT (pellicle)	4.2×10^{-5}	2.5×10^{-5}

D.

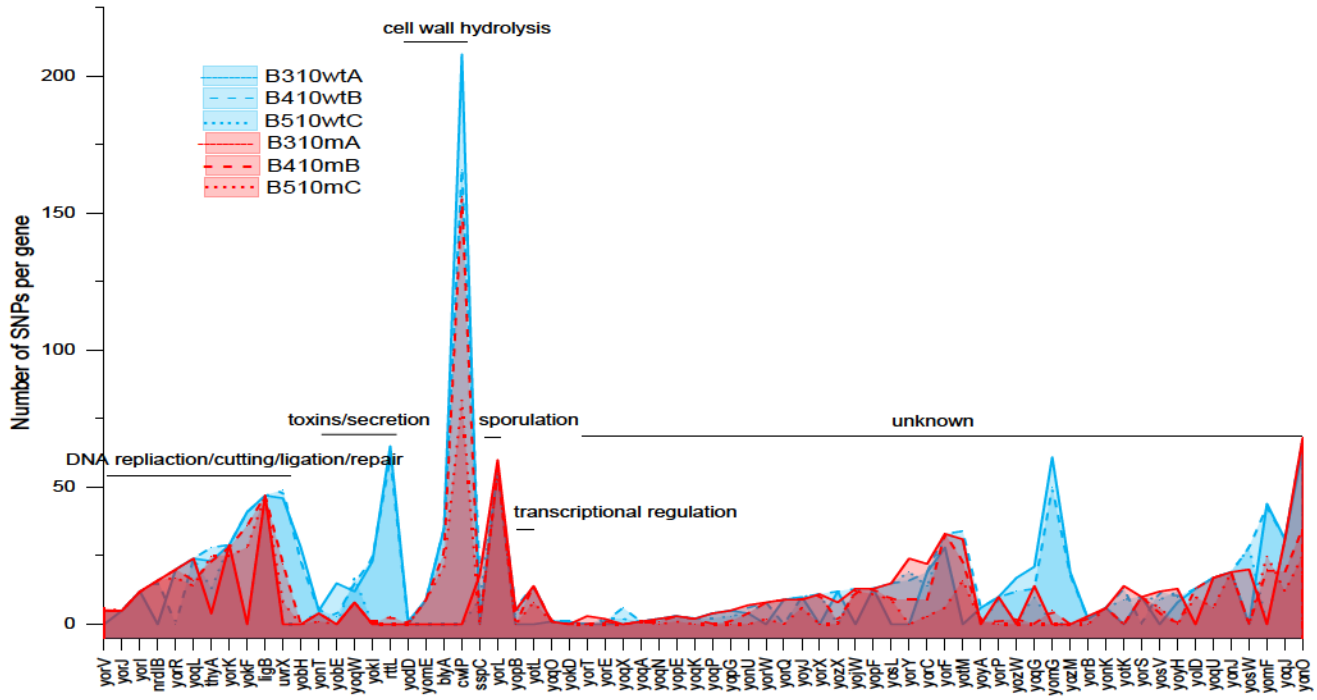

E.

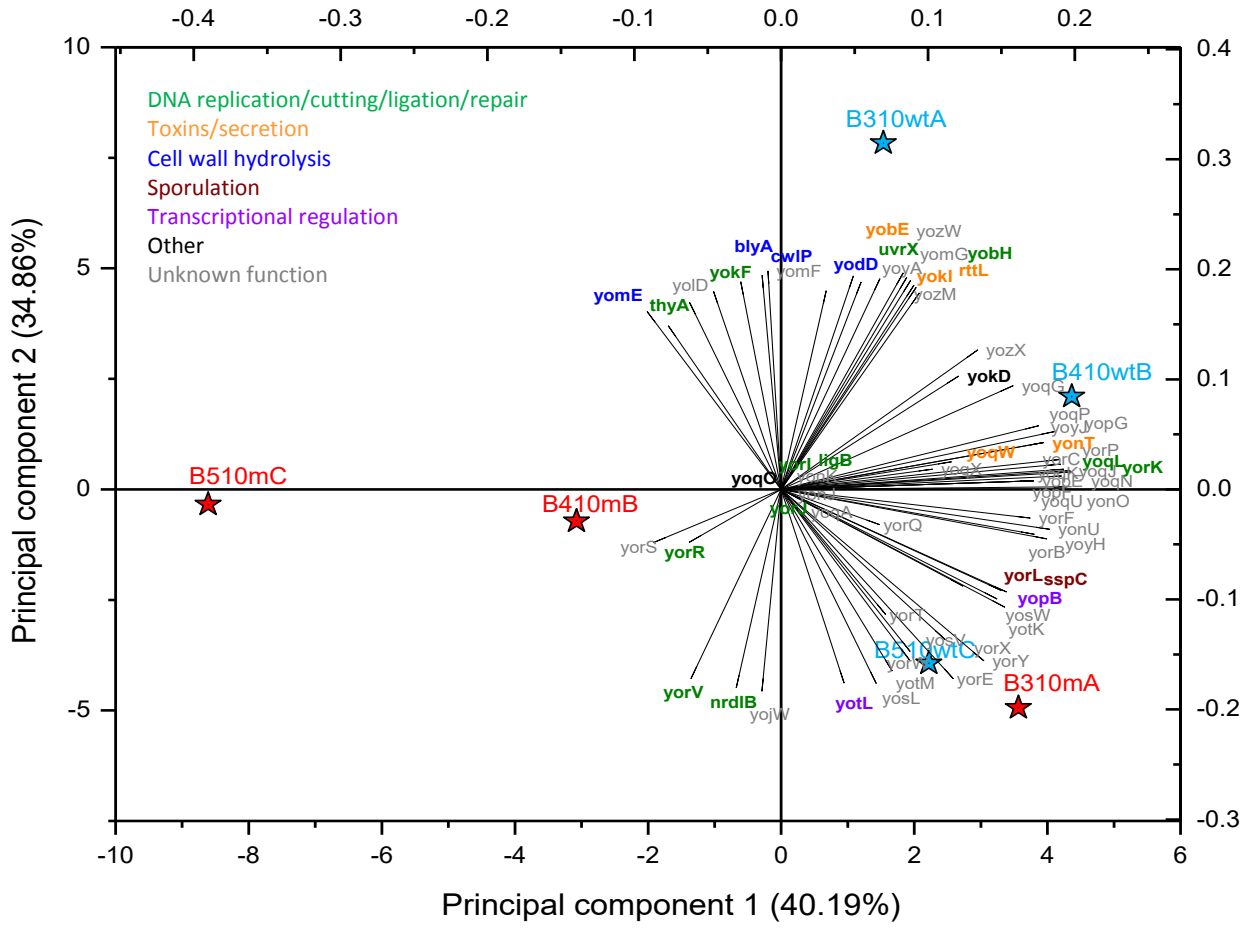

Supplementary Figure 5. Comparisons of SNPs patterns and mutation rates in the eMP and eNMP strains. A. The SPβ prophage regions of 6 evolved populations (the above panel) and corresponding single isolates (the below panel) were aligned with the SPβ sequence of the ancestor strain using VISTA tools (http://genome.lbl.gov/vista/index.shtml, 54). Peaks represent non-conserved regions based on scores for each base pair in the genomic interval of 100-bp and conservation identity 70%. A region is considered conserved if the conservation over this region is greater/equal to 70% and has minimum length of 100-bp. **B.** Percent distribution of different SNPs types detected in 6 evolved single isolates. Non-synonymous similar substitutions had Blosum62 matrix score ≥1. Non-synonymous not similar substitutions had Blosum62 matrix score ≤ 0. **C.** Fluctuation assay (n=10) was done to determine the frequency of streptomycin-resistant mutants in Δ*eps*-Δ*tasA* ancestor, evolved mutant B410mB, evolved WT B310wtA and WT ancestor strains in liquid and in pellicle (P). Analysis was conducted using LB agar medium without and with 50µg/ml streptomycin. Results show overlapping frequency rate of evolved strains with the ancestor wild type. Mutation rate estimates was determined using bz-rates web based tool (http://www.lcqb.upmc.fr/bzrates). Data points represent the mean and bars span from lower to upper CI (95%). **D.** Linear plots showing the number of SNPs per each mutated gene (genes are sorted according to their functional group) for eMPs (shown in blue) and eNMPs (shown in red). **E.** PCA biplot containing the mutated genes of eMPs (B310wtA, B410wtB and B510wtC) and eNMPs (B310mA, B410mB and B510mC) strains in two

dimensions using their projections onto the first two principal components. All mutated genes are represented on the plot using their weights for the components. The genes are color-coded by functional category. The scales shown on x and y axis are for the strains; the scales shown above the plot and on the right are for genes.

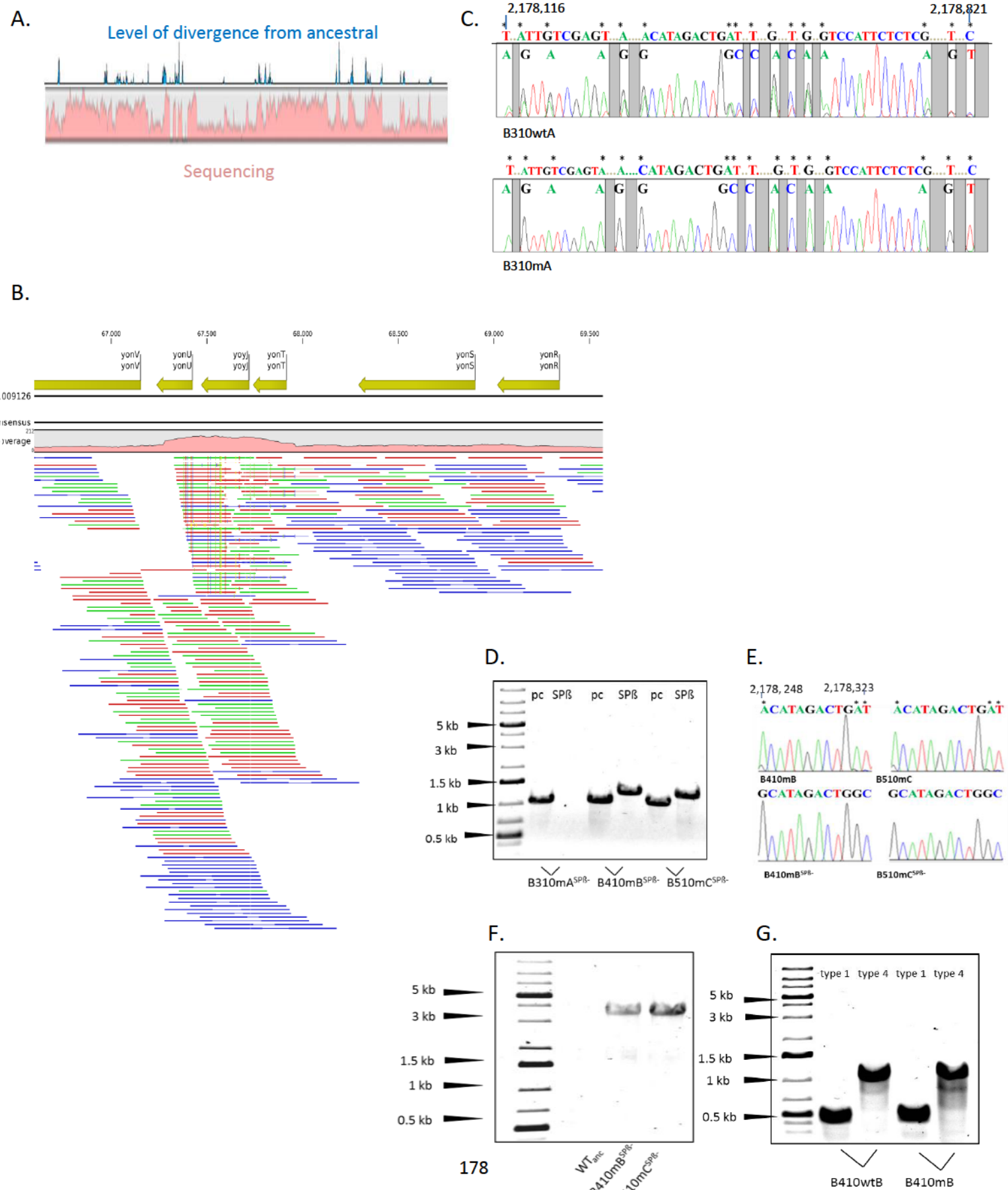

Supplementary Figure 6. Detailed molecular analysis confirm presence of genome rearrangements in the evolved strains. A. Alignment of Vista curve (54) showing regions of SNPs accumulation within the evolved SPβ sequence (see also S5A) (blue) and the sequencing coverage curve (pink) indicates duplications of mutated SPβ fragments. **B.** Sequence reads obtained for the evolved *B. subtilis* strains that are mapped to reference genome. Color coding: green-reads mapped based on the FWD strand; red-reads mapped based on the REV strand; blue–paired reads. Mismatch SNPs are marked as vertical stripes. Two types of reads were identified: reference-matching reads without SNPs and reads with SNPs. **C.** Selected SPβ fragment was amplified by PCR using B310wtA and B310mA gDNA and re-sequenced by Sanger method. Product obtained from B310wtA showed double peaks on the sequencing chromatogram at the positions of SNPs detected by high-throughput sequencing. The double peaks correlated with ~50% SNPs frequency in SPβ region, confirming presence of two types of SPβ fragments in the B310wtA, but not in the B310mA. **D.** Presence of a selected SPβ fragment was confirmed by PCR using primer pair oTB86F/oTB87R (for oligo sequences, see Supplementary Table 3) in the strains B410mB ΔSPβ and B510mC ΔSPβ but not in the B310mA ΔSPβ. Pc= positive control, amplified fragment outside SPβ. **E.** Comparison of Sanger sequencing chromatograms obtained for selected SPβ fragments before and after SPβ deletion in B410mB and B510mC strains. After deletion of SPβ PCR product could still be obtained (see Fig. S6D), but it produced clear sequencing result with single peaks at the SNPs positions containing solely the evolved sequence. **F.** Knockout of SPβ prophage region in strains B410mB ΔSPβ and B510mC ΔSPβ was confirmed by PCR using primers oAD1F/oAD2R. **G.** Presence of predicted genome rearrangements (see Fig. 5CD) of type 1 and type 4 was confirmed in the evolved strains and not in the ancestor strains using primer pairs AD4F/oAD5R and oAD6F/oAD7R, respectively.

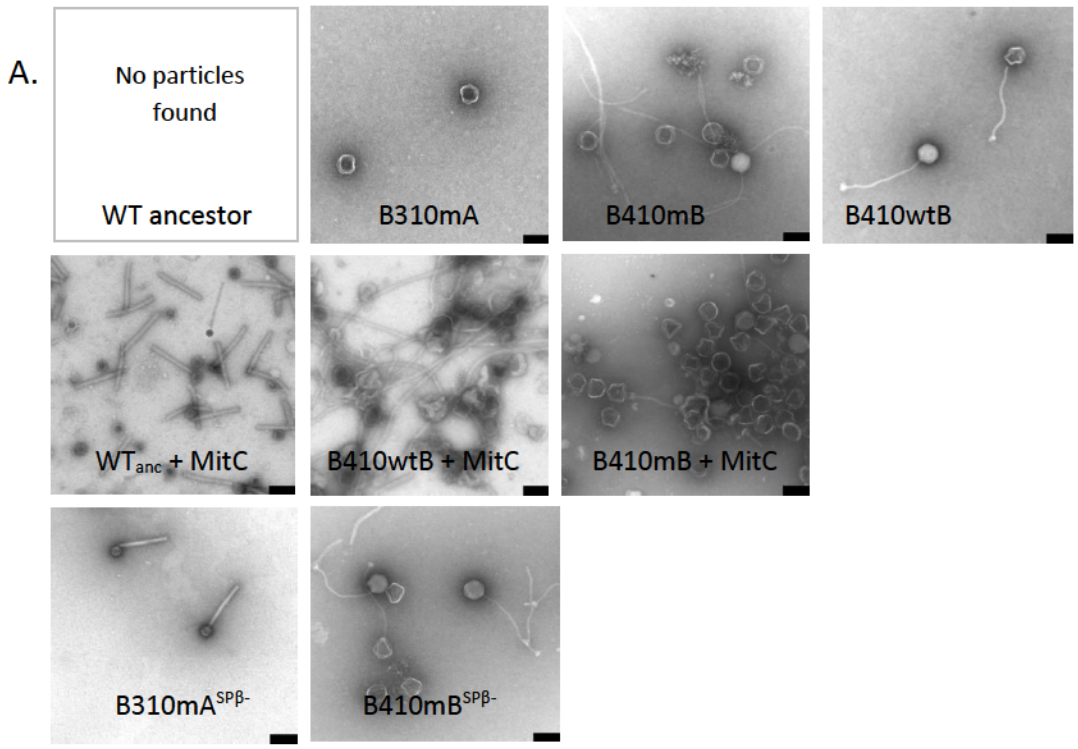

B.

Lawn / Supernatant donor

	WT anc	Mut anc	B310wtA	B410wtB	B510wtC	B310mA	B410mB	B510mC	B310mA SPβ-	B310mA SPβ-	B310mA SPβ-
WT anc			++	++		+++	++++	+++		++++	+++
Mut anc			++	+		++	+++	++		+++	+++
B310wtA											
B410wtB											
B510wtC			+	+		+	+	+		+	+
B310mA											
B410mB											
B510mC											
B310mA SPβ-			+++++	++++	++	+++	++++	+++		+++	+++
B310mA SPβ-			++				+				
B310mA SPβ-											

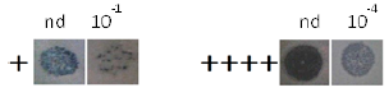

C.

Lawn / Supernatant donor

	B110	B210	B310	B410	B510	A110	A210	A310	A410	A510
WT anc	++++	+	++++	++++	++++		++++			

Supplementary Figure 7. Evolved strains spontaneously release SPbeta-like phage that is lytic towards the ancestral strains. A. Electron micrographs of phage particles purified from *B. subtilis* supernatants. No phage particles were spontaneously released by the WT ancestor strain. All evolved strains tested spontaneously released SPβ-like phage particles and treatment with Mitomycin C dramatically increased the number of those particles. WT ancestor incubated with Mitomycin C and the evolved B310mA ΔSPβ produced solely PBSX-like phage particles. Scale bar equals 100 nm. **B.** Results of the plaque assays performed with the ancestor WT, ancestor Δ*eps*-Δ*tasA* and all the evolved strains, where each strain served both as a supernatant donor and as a potential host. To better access lytic activity of the strains, their supernatants were diluted using saline solution and scored as shown on the scale below. Blank cell in the table translates into lack of lytic activity towards given host even if non-diluted supernatant was applied on the loan. **C.** Lytic activity of all evolved populations (transfer method A and transfer method B) against the WT ancestor was tested. All populations that showed increase of Δ*eps*-Δ*tasA* ratio (see Fig. 2) thorough the evolutionary time showed lytic activity towards the WT ancestor.

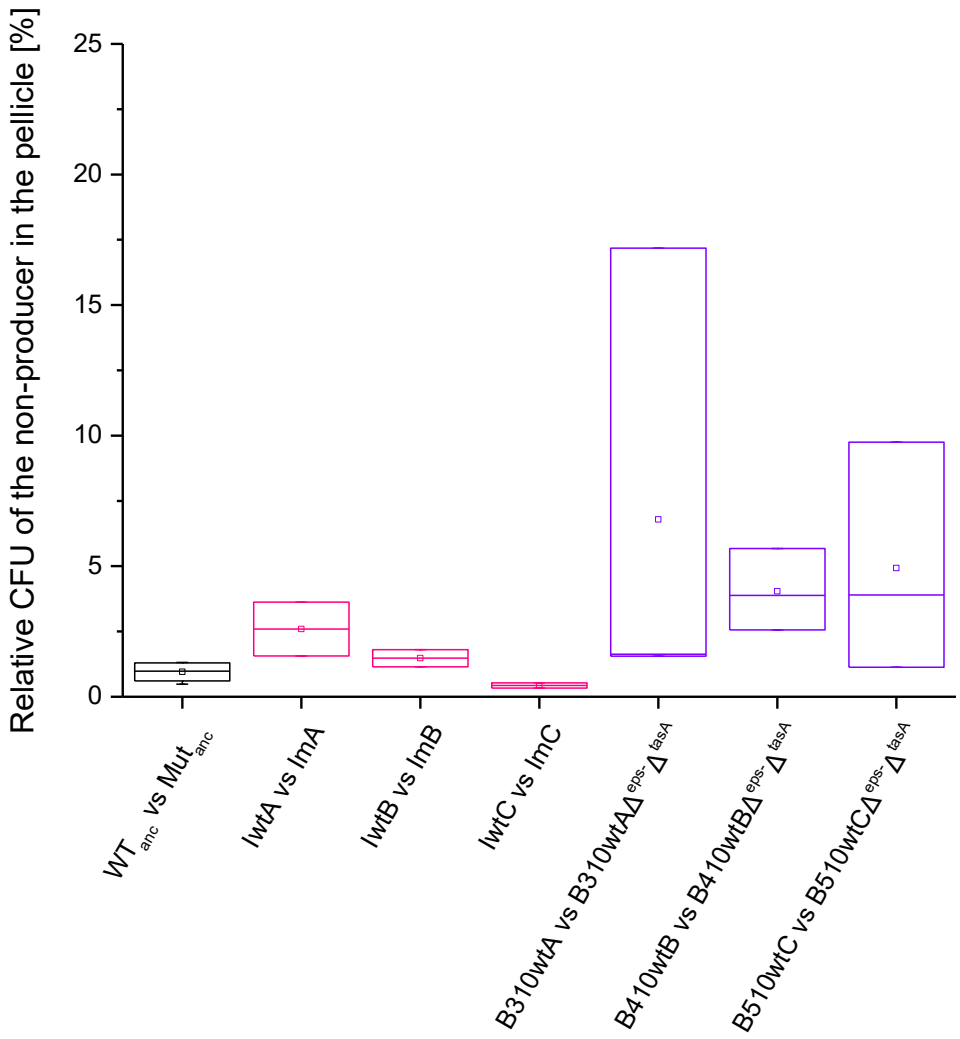

Supplementary Figure 8. When producers and non-producers carry the same evolved genetic background, improved incorporation of non-producers is not observed. Pellicle competition assay performed for 3 randomly selected WT and Δ*eps*-Δ*tasA* colonies after the infection assay (n=2) (columns 2-4). In addition, pellicle competition assays between WT evolved strains and their corresponding strains with Δ*eps*-Δ*tasA* markers (n=3) were performed (columns 5-7). Boxes represent Q1-Q3 and lines represent median values. Results show that the infected mutant strains cannot increase their performance when competed against infected WT strains. The same is true for the evolved WT strains with deleted *eps* and *tasA* that behave comparably as the ancestor Δ*eps*-Δ*tasA* mutant when competed with WT (first column). The experiments were performed twice.

Supplementary Table 1. Strains used in this study

Strain name	Genotype	Reference
168	Δ*trpC*	[1]
DL821	NCIB 3610 *lacA::*P_{tapA}*:yfp* (Mls^R)	[2]
DL1032	NCIB 3610 Δ*epsA-O*::Tet^R Δ*tasA*::Km^R *amyE::*P_{srfAA}*-lacZ*	[2]
168 hymKATE P_{tapA}*-yfp*	Δ*trpC amyE:* $P_{hyperspank}$*-mKATE* (Cm^R) *lacA::*P_{tapA}*:yfp* (Mls^R)	this work
Δ*eps*-Δ*tasA*	Δ*trpC* Δ*epsA-O*::Tet^R Δ*tasA*::Km^R	this work
Δ*eps*	Δ*trpC* Δ*epsA-O*::Tet^R	this work
Δ*tasA*	Δ*trpC* Δ*tasA*::Km^R	this work
168 hyGFP	Δ*trpC amyE*::$P_{hyperspank}$-GFP (Cm^R)	[3]
168 hymKate	Δ*trpC amyE*::$P_{hyperspank}$--mKATE2 (Cm^R)	[3]
Δ*eps*-Δ*tasA* hyGFP	Δ*trpC* Δ*epsA-O*::Tet^R Δ*tasA*::Km^R *amyE:*$P_{hyperspank}$*-GFP* (Cm^R)	this work
Δ*eps*-Δ*tasA* hymKate	Δ*trpC* Δ*epsA-O*::Tet^R Δ*tasA*::Km^R *amyE:*$P_{hyperspank}$*-mKATE* (Cm^R)	this work

Supplementary Table 2. Evolved populations and single isolates obtained in the study and used for further analyses.

Co-culture name	Population	Single isolate	Strains derived from single isolates
B310	B310wt	B310wtA	B310wtA GFP
			B310wtA mKate
			B310wtA Δ*eps*Δ*tasA*
		B310mB	
		B310mC	
	B310m	B310mA	B310mA GFP
			B310mA mKate
			B310mA ΔSPß
		B310mB	
		B310mC	
B410	B410wt	B410wtB	B410wtB GFP
			B410wtB mKate
			B410wtB Δ*eps*Δ*tasA*
		B410wtA	
		B410wtC	
	B410m	B410mB	B410mB GFP
			B410mB mKate
			B410mB ΔSPß
		B410mA	
		B410mC	
B510	B510wt	B510wtC	B510wtC GFP
			B510wtC mKate
			B510wtC Δ*eps*Δ*tasA*
		B510wtA	
		B510wtB	
	B510m	B510mC	B510mC GFP
			B510mC mKate
			B510mC ΔSPß
		B510mA	
		B510mB	

Supplementary Table 3. Primers used in this study

Primer	Experimental purpose	Sequence
oAD1F	confirm SPbeta deletion from the original position in the chromosome	ATCTGGACTGGCACCTTATGGATACC
oAD2R	confirm SPbeta deletion from the original positions in the chromosome	CTGCTCTGGAAAGGAAGGCAGAGTAA
oTB86F	check for additional copy of SPbeta, examine Sanger chromatogram	CACGCTTGTCTCCAAACC
oTB87R	check for additional copy of SPbeta, examine Sanger chromatogram	GATTGGCCATAACAGACC
oAD4F	confirm SPbeta rearrangement type 1	CTAAGGAGAGATAGGGCAT
oAD5R	confirm SPbeta rearrangement type 1	TGGTTTGAAGGCCATCACA
oAD6F	confirm SPbeta rearrangement type 4	CGATTTCAGCTGCCAAATCC
oAD7R	confirm SPbeta rearrangement type 4	CAGGAAAACTGGTCAGAAAC
oTB74	confirm *eps* deletion	GGGAAGTGCAGTAAATTAG
oTB75	confirm *eps* deletion	GAAACGGATTCAGCATTTAG
oTB73	confirm *tasA* deletion	GATCAGCAGCGCCATTAGAG
oTB72	confirm *tasA* deletion	CATGGCATGCGCCTGAGCAGAGGCACTAAC

Supplementary References:

1 Kovács, Á. T. & Kuipers, O. P. Rok regulates *yuaB* expression during architecturally complex colony development of *Bacillus subtilis* 168. *J Bacteriol* **193,** 998-1002 (2011).
2 López, D., Vlamakis, H., Losick, R. & Kolter, R. Paracrine signaling in a bacterium. *Genes Dev* **23,** 1631-1638 (2009).
3 van Gestel, J., Weissing, F. J., Kuipers, O. P. & Kovács, Á. T. Density of founder cells affects spatial pattern formation and cooperation in *Bacillus subtilis* biofilms. *ISME J* **8,** 2069-2079 (2014).

Supplementary data set can be found at https://www.nature.com/articles/ncomms15127#supplementary-information

Supporting information for Chapter 4

Division of labor during biofilm matrix production

Published in Current Biology (2018)

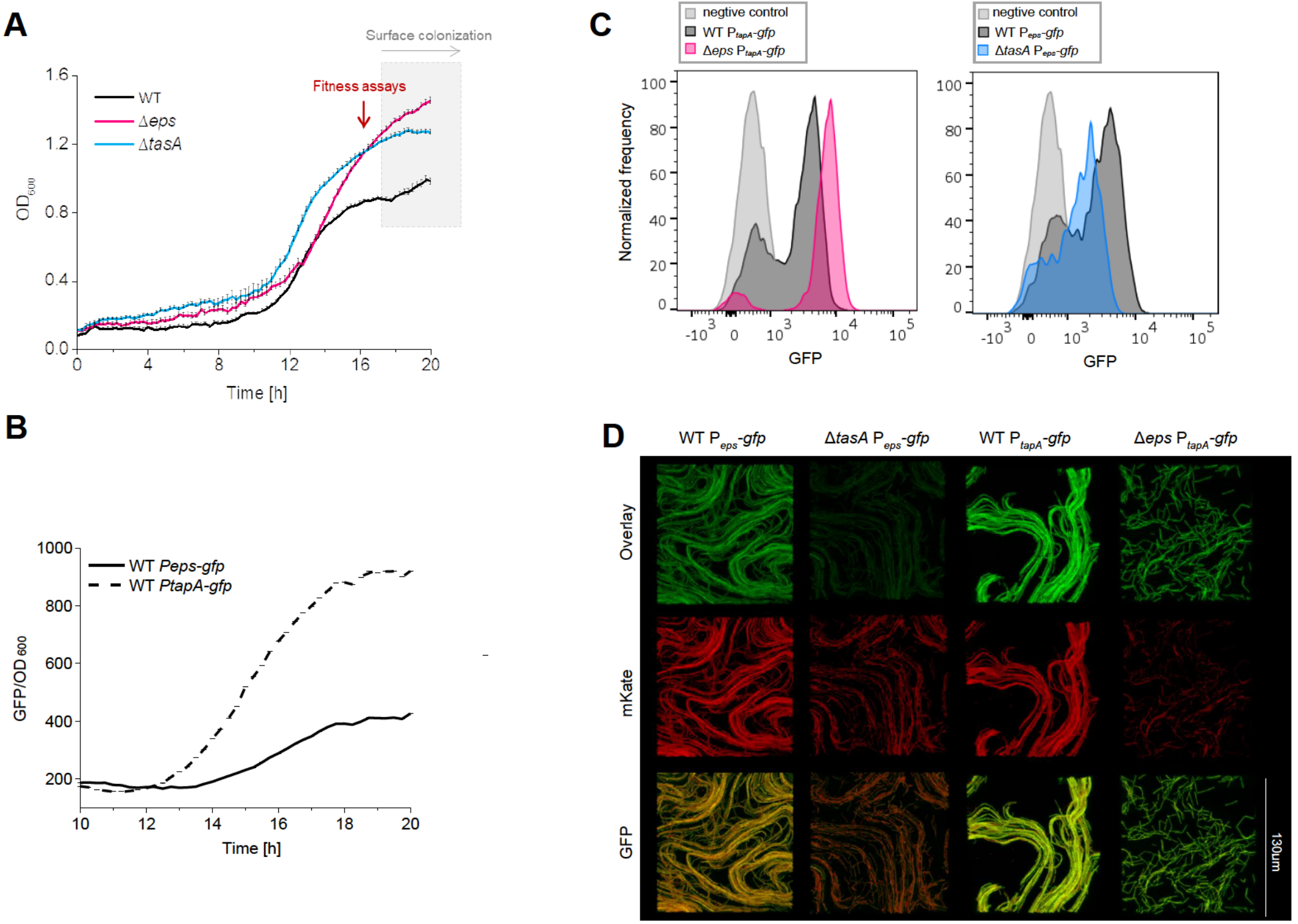
A
Surface colonization
Fitness assays
WT
Δeps
ΔtasA
OD600
Time [h]
B
WT Peps-gfp
WT PtapA-gfp
GFP/OD 600
Time [h]
C
negtive control
WT PtapA-gfp
Δeps PtapA-gfp
negtive control
WT Peps-gfp
ΔtasA Peps-gfp
Normalized frequency
GFP
GFP
D
WT Peps-gfp
ΔtasA Peps-gfp
WT PtapA-gfp
Δeps PtapA-gfp
Overlay
mKate
GFP
130um

Figure S1. Growth and matrix gene expression in the WT, Δ*eps* and Δ*tasA*. Related to Figure 1. (A) Planktonic growth of the WT and matrix-deficient mutants Δ*eps* and Δ*tasA* were monitored for 20 h. Red arrow represents the time point selected as suitable for the fitness assays. Grey area corresponds to surface colonization phase where matrix components EPS and TasA become beneficial for the cells and when OD reads become less reliable due to cell clumping (see Video S1). **(B)** Expression dynamics of *eps* and *tasA* were monitored in the WT using the P_{eps}-*gfp* and WT P_{tasA}-*gfp* reporter strains. It is important to note that the P_{tapA}-*gfp* reporter construct produced significantly stronger signal than the P_{eps}-*gfp*. Such differences can be due to actual differences in promoter strength or different efficiencies of promoter fusions. For panel A and B: data points represent an average (n=8) and error bars represent standard error. **(C)** Histograms of flow cytometric measurements for P_{eps}-*gfp* and PtapA-*gfp* in the WT and corresponding biofilm mutants. Y-axis shows normalized cell count and X-axis shows GFP fluorescence in arbitrary units. Negative control represents GFP expression in non-*gfp*-labelled WT strain. Representative images are shown for each strain (n=5). **(D)** Comparative analysis of CLSM images of Δ*eps* P_{tapA}-*gfp*, WT P_{tapA}-*gfp*, Δ*tasA* P_{eps}-*gfp* and WT P_{eps}-*gfp*, to evaluate the expression of remaining matrix genes (from P_{tapA} and P_{eps} promoters, respectively) by matrix-deficient strains. All strains used in this experiment constitutively expressed *mKate*. Width of each confocal image corresponds to 130 μm.

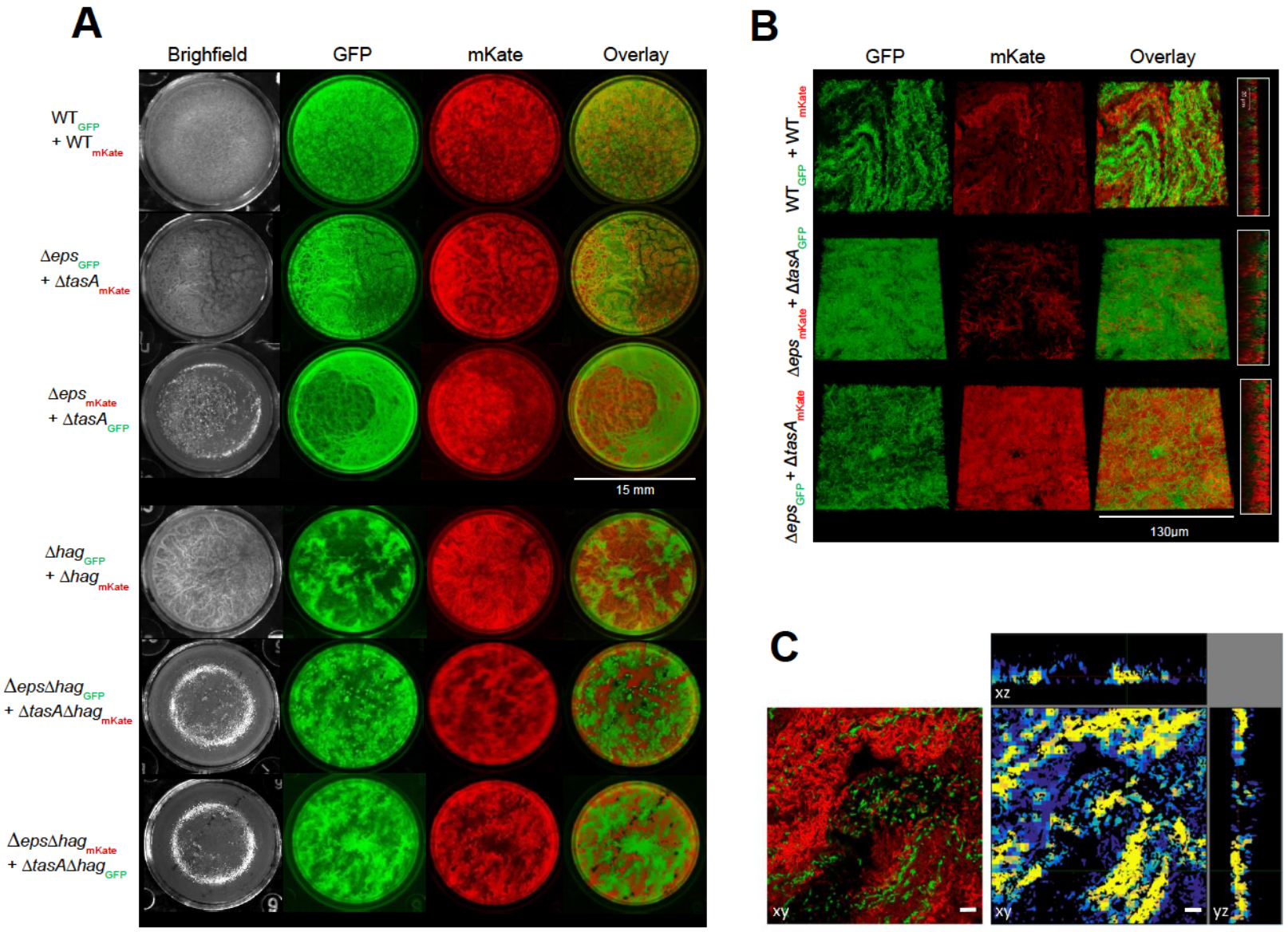
A
Brighfield
GFP
mKate
Overlay
WT GFP + WT mKate
ΔepsGFP + ΔtasAmKate
ΔepsmKate + ΔtasAGFP
ΔhagGFP + ΔhagmKate
ΔepsΔhagGFP + ΔtasAΔhagmKate
ΔepsΔhagmKate + ΔtasAΔhagGFP
15 mm
B
GFP
mKate
Overlay
WT mKate + WT GFP
ΔepsmKate + ΔtasAGFP
ΔepsGFP + ΔtasAmKate
130µm
C
xz
xy
xy
yz

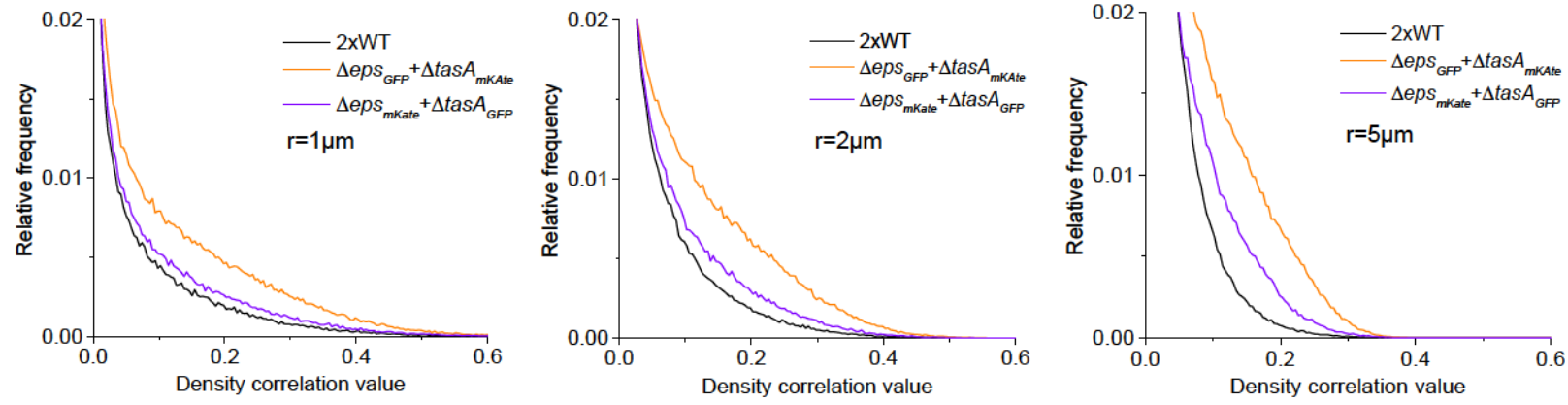
D
Relative frequency
Density correlation value
2xWT
ΔepsGFP+ΔtasAmKAte
ΔepsmKate+ΔtasAGFP
r=1µm
r=2µm
r=5µm
0.00
0.01
0.02
0.0
0.2
0.4
0.6

Figure S2. Role of motility and mixing in complementation assay. Related to Figure 1. (A) Three upper rows: matrix-proficient strains (WTs) and complementary mutant strains Δ*eps*+Δ*tasA* labelled with different constitutive fluorescent reporters were mixed in 50:50 ratios and allowed to form pellicles. Three bottom rows: the same experiment was performed in flagellum-deficient background (Δ*hag*). Assortment of strains in co-cultures was assessed after 48h (mature pellicles) using a fluorescence stereomicroscope. **(B)** Pellicles formed by WT strain mixtures with different fluorescent reporters (labeled 2xWT in the figure) and Δ*eps*+Δ*tasA* mixtures labelled with different constitutive fluorescent reporters were visualized using CLSM. **(C)** Visual representation of density correlation function applied in (D); Left: example pellicle image of WT_{GFP}+WT_{mKate} obtained using CLSM; right: density correlation map for the same image with r = 2 μm. Blue: low density in either GFP or mKate channel. Yellow: high density in both channels. Scale bar represents 10μm. **(D)** Distribution of density correlation (2-class thresholding) for different ranges (see Methods) was compared for pellicles formed by matrix-proficient strains (WTs) and complementary mutants Δ*eps*+Δ*tasA*.

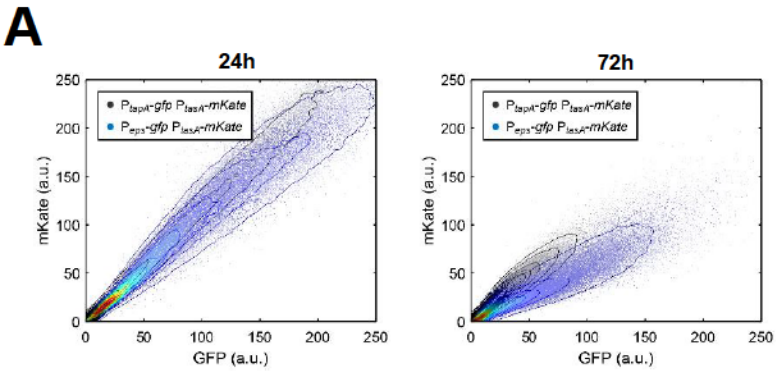
A
24h
72h
mKate (a.u.)
GFP (a.u.)

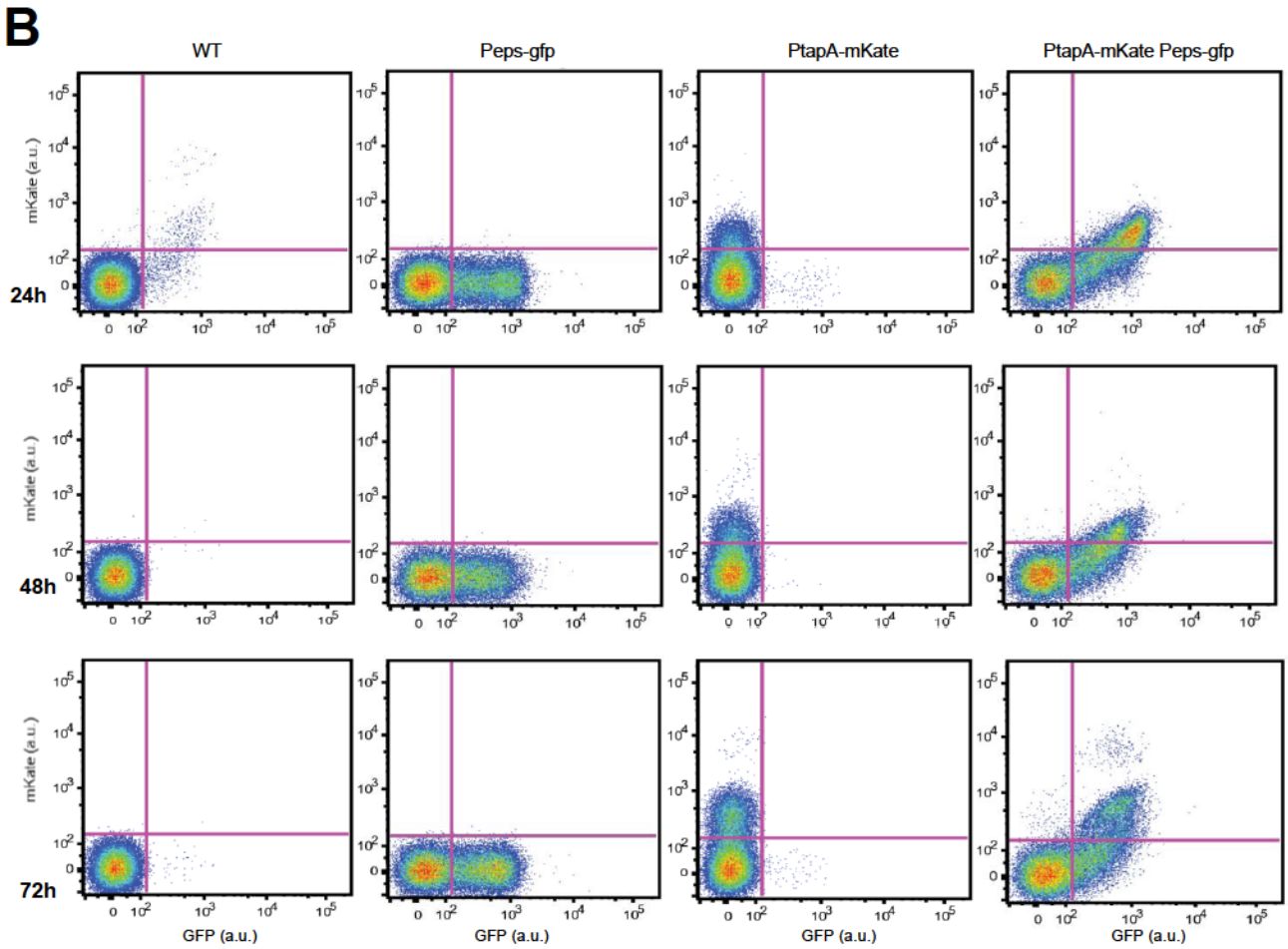
B
WT
Peps-gfp
PtapA-mKate
PtapA-mKate Peps-gfp
24h
48h
72h
mKate (a.u.)
GFP (a.u.)

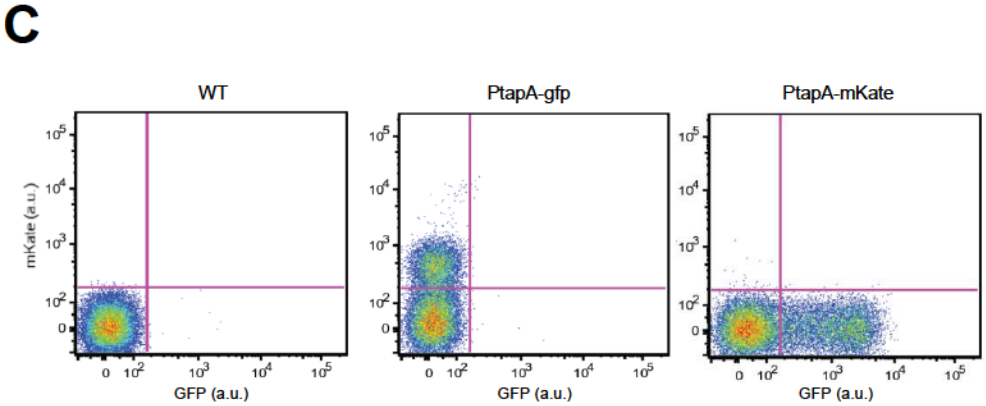
C
WT
PtapA-gfp
PtapA-mKate
mKate (a.u.)
GFP (a.u.)

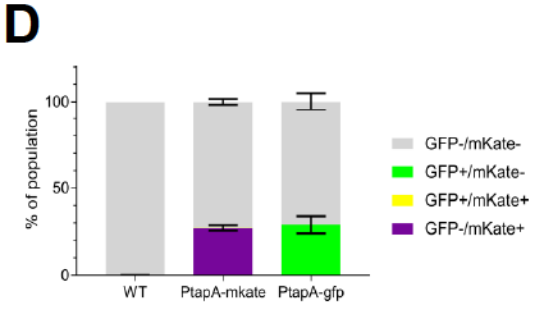
D
% of population
GFP-/mKate-
GFP+/mKate-
GFP+/mKate+
GFP-/mKate+
WT
PtapA-mkate
PtapA-gfp

Figure S3. Native phenotypic heterogeneity in the expression of matrix components accessed at different time points. Related to Figure 2. (A) Volumes in GFP and mKate channels (obtained by manual thresholding) were merged, dissected into cubes and the average intensities in GFP and mKate for all cubes are plotted (see methods). The pellicles were sampled after 24h and 72h. The maximum density is normalized to 1 and the contour lines correspond to 0.05 decrease in density. **(B)** Pellicles formed by NCIB3610, NRS2242 (P_{eps}-*gfp*), NRS3913 (P_{tasA}-*mKate*) and NRS5832 (P_{eps}-*gfp* P_{tasA}-*mKate*) were sampled after 24h, 48h and 72h and analysed by flow cytometry. GFP (X-axis) and mKate (Y-axis) intensity were shown and threshold for fluorescent expression were set based on the cell distribution of NCIB3610. **(C)** Cell fluorescence distribution of NCIB3610, NRS3913 (P_{tasA}-*mKate*), and NRS2394 (P_{tasA}-*gfp*) obtained via flow cytometry. Pellicles were grown for 48 h. **(D)** Corresponding bar chart (mean±SD) representing the fractions of ON and OFF cells in the pellicles analyzed in (C) (n=2).

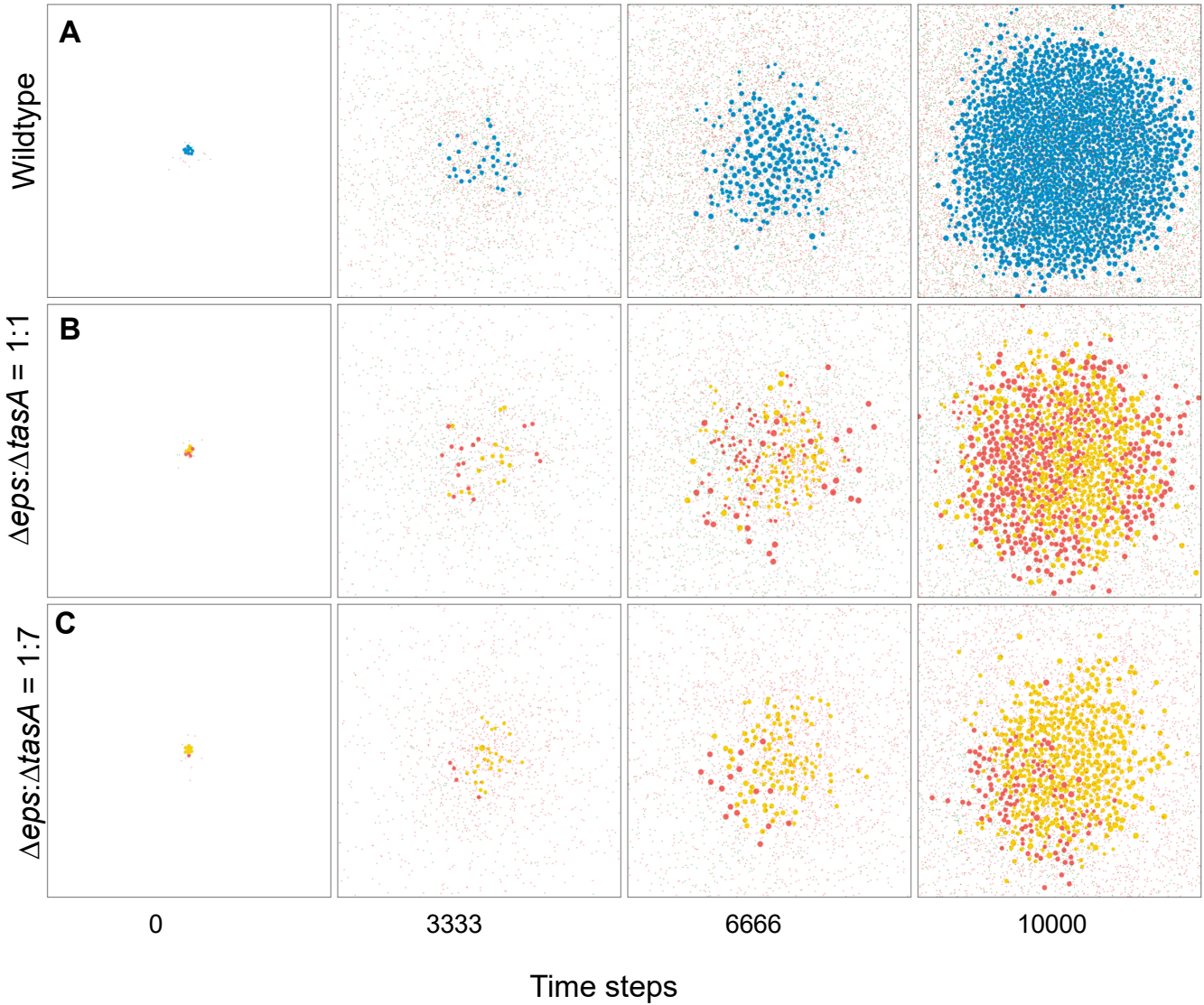
A
Wildtype
B
Δeps:ΔtasA = 1:1
C
Δeps:ΔtasA = 1:7
0
3333
6666
10000
Time steps

Figure S4. Illustrative examples of simulated pellicle formation. Related to Figure 5. (A) Wildtype bacteria (blue discs), simultaneously producing the two complementary public goods TasA and EPS (depicted by the tiny colored dots) grows to high cell densities and forms circular pellicles. **(B)** Co-culture of the two specialized mutants Δ*eps* (red discs, producing TasA) and Δ*tasA* (yellow discs, producing EPS) can complement each other by exchanging public goods. However, cell density is lower at the end of the simulation compared to the wildtype since these examples assume that there are no metabolic constraints of producing two public goods in the wildtype. **(C)** Inefficient complementation between the two mutants at a non-optimal strain ratio leads to low cell density in the pellicle. These examples further demonstrate that a high proportion of public goods is lost by diffusion, especially at low cell densities (i.e. early time points). Parameter settings were: public good diffusion d = 5, metabolic constraints f = 1, benefits $b_1 = b_2 = b_3 = 0.0005$.

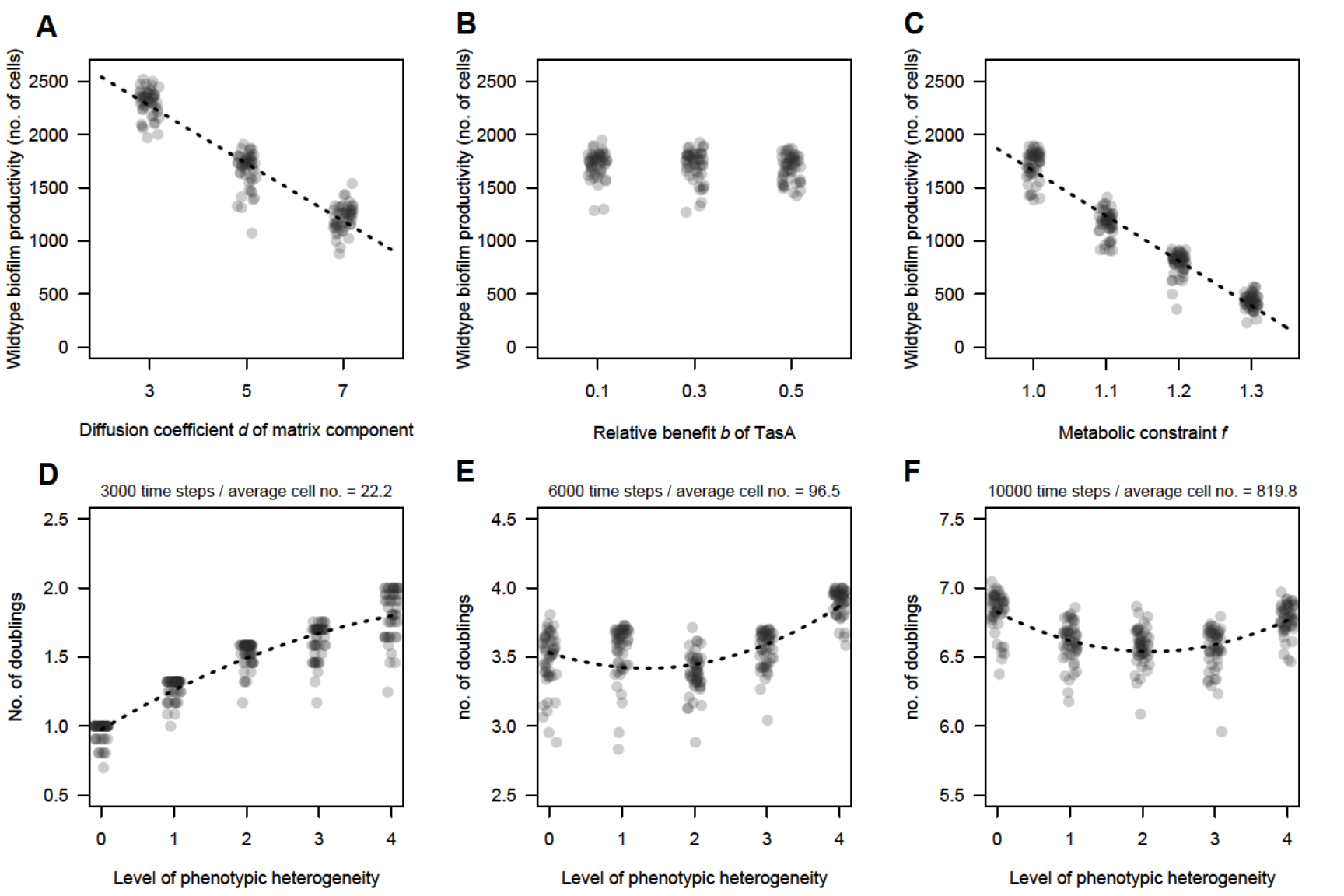
A
Wildtype biofilm productivity (no. of cells)
2500
2000
1500
1000
500
0
3
5
7
Diffusion coefficient d of matrix component
B
Wildtype biofilm productivity (no. of cells)
2500
2000
1500
1000
500
0
0.1
0.3
0.5
Relative benefit b of TasA
C
Wildtype biofilm productivity (no. of cells)
2500
2000
1500
1000
500
0
1.0
1.1
1.2
1.3
Metabolic constraint f
D
3000 time steps / average cell no. = 22.2
No. of doublings
2.5
2.0
1.5
1.0
0.5
0
1
2
3
4
Level of phenotypic heterogeneity
E
6000 time steps / average cell no. = 96.5
no. of doublings
4.5
4.0
3.5
3.0
2.5
0
1
2
3
4
Level of phenotypic heterogeneity
F
10000 time steps / average cell no. = 819.8
no. of doublings
7.5
7.0
6.5
6.0
5.5
0
1
2
3
4
Level of phenotypic heterogeneity

Figure S5. Variables affecting *in-silico* biofilm productivity of the wild type strain. Related to Figure 5. (A) - **(C)** Simulated biofilm formation of the wild type strain, simultaneously producing TasA and EPS. Biofilms were initiated with eight cells, each producing the two matrix components at the same rate and growing according to their fitness function (see STAR methods). Panels show endpoint productivity of the biofilms after 10,000 time steps, under conditions, where the diffusion coefficient *d* of the matrix components **(A)**, the relative benefit *b* of the two matrix components **(B)**, or the strength of metabolic constraints *f* for simultaneously producing two matrix components **(C**) were varied. Panels **(D)** - **(F)** show the number of cell doublings for different time intervals and for different levels of phenotypic heterogeneity. All simulations started with 8 cells. The metabolic constraint value was set to $f = 1.16$. With this value, unspecialized and completely specialized groups perform equally well across the entire growth cycle. It thus allows to compare how intermediate levels of specialization compare relative to these two extremes. The implemented levels of phenotypic heterogeneity were: 0 = 8 unspecialized cells; 1 = 6 unspecialized cells + 1 TasA specialist + 1 EPS specialist; 2 = 4 unspecialized cells + 2 TasA specialists + 2 EPS specialists; 3 = 2 unspecialized cells + 3 TasA specialists + 3 EPS specialists; 4 = 4 TasA specialists + 4 EPS specialists. Dashed lines indicate trend lines of the best significant fit to the data. If not indicated otherwise, parameter settings were $d = 5$, $f = 1$, $b_1 = b_2 = b_3 = 0.0005$.

Strain name	Genotype	Reference
DL1032	*eps*::*tet, tasA*::*Km, amyE*::P_{srfAA}-*lacZ (ery)*	[S1]
NCIB3610	*Prototroph*	NSW laboratory
TB601	3610 *comI*^{Q12l} *eps*::*tet*	This work
TB602	3610 *comI*^{Q12l} *tasA*::*spec*	[S2]
TB863	3610 *comI*^{Q12l} *tasA*::*kan*	This work
TB500	3610 *comI*^{Q12l} *amyE*::$P_{hyperspank}$-GFP (Spec^R)	[S2]
TB501	3610 *comI*^{Q12l} *amyE*::$P_{hyperspank}$-mKate (Spec^R)	This work
TB524	3610 *comI*^{Q12l} *eps*::*tet amyE*::$P_{hyperspank}$-GFP (Spec^R)	This work
TB525	3610 *comI*^{Q12l} *eps*::*tet amyE*::$P_{hyperspank}$-mKate (Spec^R)	This work
TB538	3610 *comI*^{Q12l} *tasA*::*kan amyE*::$P_{hyperspank}$-GFP (Spec^R)	This work
TB539	3610 *comI*^{Q12l} *tasA*::*kan amyE*::$P_{hyperspank}$-mKate (Spec^R)	This work
168hymKate	168 *amyE*::$P_{hyperspank}$-mKATE2 (Cm^R)	[S3]
TB864	3610 *comI*^{Q12l} *amyE*::$P_{hyperspank}$-mKate (Cm^R) *sacI*::P_{eps}-*gfp* (Km^R)	This work
TB865	3610 *comI*^{Q12l} *amyE*::$P_{hyperspank}$-mKate (Cm^R) *sacI*::P_{tapA}-*gfp* (Km^R)	This work
Anc Kate P_{eps}-GFP	3610 *comI*^{Q12l} *tasA*::*spec* amyE::$P_{hyperspank}$-mKate (Cm^R) *sacI*::P_{eps}-*gfp* (Km^R)	This work
Anc Kate P_{tapA}-GFP	3610 *comI*^{Q12l} *eps*::*tet* amyE::$P_{hyperspank}$-mKate (Cm^R) *sacI*::P_{tapA}-*gfp* (Km^R)	This work
TB960	3610 *comI*^{Q12l} *amyE*::P_{tapA}-*mKate* (Cm^R) *sacI*::P_{eps}-*gfp* (Km^R)	This work
TB961	3610 *comI*^{Q12l} *amyE*::P_{eps}-*mKate* (Cm^R) *sacI*::P_{tapA}-*gfp* (Km^R)	This work
TB962	3610 *comI*^{Q12l} *amyE*::P_{tapA}-*mKate* (Cm^R) *sacI*::P_{tapA}-*gfp* (Km^R)	This work
NRS2394	3610 *sacA*::P_{tapA}-*gfp* (Km^R)	[S4]
NRS3913	3610 *amyE*::P_{tapA}-*mKate2* (Cm^R)	This work
NRS2242	3610 *sacI*::P_{eps}-*gfp* (Km^R)	[S4]
NRS5832	3610 *sacI*::P_{eps}-*gfp* (Km^R) *amyE*::P_{tapA}-*mKate2* (Cm^R)	This work

Table S1. Bacterial strains used during experiments or as a source of genomic DNA. Related to STAR Methods.

Primer	Experimental purpose	Sequence
oTB172	Cloning *eps* promoter into pmKATErrnB	CACGAATTCCAACAGCCAGCTGATTAATAG
oTB173	Cloning *eps* promoter into pmKATErrnB	CTGAGCTAGCCATTTCCTCTCCTCCTTCCCGCGGCTGGCTTC
oTB174	Cloning *tapA* promoter into pmKATErrnB	CACGAATTCCCTTCCCTCAGAGTTAAATG
oTB175	Cloning *tapA* promoter into pmKATErrnB	CTGAGCTAGCCATTTCCTCTCCTCCTGTAAAACACTGTAAC
oTH1	Cloning $P_{hyperspank}$-mKate into pWK-Sp	GCATCTAGAGTTGCTCGCGGGTAAATGTG
oTH2	Cloning $P_{hyperspank}$-mKate into pWK-Sp	CGAGAATTCATCCAGAAGCCTTGCATATC
NSW1026	Amplification *mKate2* from plasmid pTMN387	GTACAAGCTTAAGGAGGAACTACTATGGATTCAATAGAAAAGGTAAG
NSW1027	Amplification *mKate2* from plasmid pTMN387	GTACGGATCCTTATCTGTGCCCCAGTTTGCT

Table S2. Primers used in this study. Related to STAR Methods.

Parameter	Description	Value(s)
μ	basic growth rate	1
D	cell diffusion	0.01
d	public good diffusion	3 - 7 $\mu m^2/s$
ω	stiffness of decay function	0.1
δ	public good durability	500 s
c_1	cost of public good 1 (TasA)	0.0005 per molecule
c_2	cost of public good 2 (EPS)	0.0005 per molecule
f	metabolic constraint factor	1 - 1.3
b_1	benefit of public good 1 (TasA)	0.0001 - 0.0009
b_2	benefit of public good 2 (EPS)	0.0001 - 0.0009
b_3	synergistic benefit	0.0005

Table S3. Parameters and specific values used in modeling. Related to STAR Methods.

Supplemental references

S1. López, D., Vlamakis, H., Losick, R., and Kolter, R. (2009). Paracrine signaling in a bacterium. Genes Dev. *23*, 1631–8.

S2. Mhatre, E., Sundaram, A., Hölscher, T., Mühlstädt, M., Bossert, J., and Kovács, Á.T. (2017). Presence of calcium lowers the expansion of *Bacillus subtilis* colony biofilms. Microorganisms *5*, 7.

S3. van Gestel, J., Weissing, F.J., Kuipers, O.P., and Kovács, Á.T. (2014). Density of founder cells affects spatial pattern formation and cooperation in Bacillus subtilis biofilms. ISME J. *8*, 2069–79.

S4. Murray, E.J., Strauch, M.A., and Stanley-Wall, N.R. (2009). X Is involved in controlling *Bacillus subtilis* biofilm architecture through the AbrB homologue Abh. J. Bacteriol. *191*, 6822–6832.

Supplementary video S1 can be found at:
https://www.sciencedirect.com/science/article/pii/S096098221830518 9?via%3Dihub#mmc2

Supporting information for Chapter 5

Collapse of genetic division of labour and evolution of autonomy in pellicle biofilms

Published in Nature Microbiology (2018)

nature microbiology

SUPPLEMENTARY INFORMATION

https://doi.org/10.1038/s41564-018-0263-y

In the format provided by the authors and unedited.

Collapse of genetic division of labour and evolution of autonomy in pellicle biofilms

Anna Dragoš[1,2], Marivic Martin[1,2], Carolina Falcón García[3], Lara Kricks[4], Patrick Pausch[5], Thomas Heimerl[6], Balázs Bálint[7,9], Gergely Maróti[8], Gert Bange[5], Daniel López[4], Oliver Lieleg[3] and Ákos T. Kovács[1,2]*

[1]Bacterial Interactions and Evolution Group, Department of Biotechnology and Biomedicine, Technical University of Denmark, Kgs Lyngby, Denmark. [2]Terrestrial Biofilms Group, Institute of Microbiology, Friedrich Schiller University Jena, Jena, Germany. [3]Department of Mechanical Engineering and Munich School of Bioengineering, Technical University of Munich, Garching, Germany. [4]National Centre for Biotechnology (CNB), Spanish Research Council (CSIC), Madrid, Spain. [5]Faculty of Chemistry & LOEWE Center for Synthetic Microbiology, Philipps-University Marburg, Marburg, Germany. [6]Cell Biology & Electron Microscopy, LOEWE Center for Synthetic Microbiology, Philipps-University Marburg, Marburg, Germany. [7]Seqomics Biotechnology Ltd, Mórahalom, Hungary. [8]Institute of Plant Biology, Biological Research Centre, Hungarian Academy of Sciences, Szeged, Hungary. [9]Present address: Synthetic and Systems Biology Unit, Institute of Biochemistry, Biological Research Centre, Hungarian Academy of Sciences, Szeged, Hungary. *e-mail: atkovacs@dtu.dk

Supplementary Table 1 | The strains used in this study.

Strain name	Genotype	Reference
DK1042	Naturally competent derivative of the undomesticated NCIB 3610 containing *comI*^{Q12I} allele	1¹
TB601	3610 *comI*^{Q12I} *eps::tet*	[2]
TB602	3610 *comI*^{Q12I} *tasA::spec*	[3]
TB857	3610 *comI*^{Q12I} *tasA::kan, eps::tet, amyE::*$P_{hyperspank}$-*tasA*$_{anc}$ (Spec^R)	This work
TB859	3610 *comI*^{Q12I} *tasA::kan, eps::tet, amyE::*$P_{hyperspank}$-*tasA*$_{Y124C}$ (Spec^R)	This work
TB861	3610 *comI*^{Q12I} *tasA::kan, eps::tet, amyE::*$P_{hyperspank}$-*tasA*$_{G183C}$ (Spec^R)	This work
TB906	3610 *comI*^{Q12I} *tasA::kan, amyE::*$P_{hyperspank}$-*tasA*$_{anc}$ (Spec^R)	This work
TB907	3610 *comI*^{Q12I} *tasA::kan, amyE::*$P_{hyperspank}$-*tasA*$_{Y124C}$ (Spec^R)	This work
TB908	3610 *comI*^{Q12I} *tasA::kan, amyE::*$P_{hyperspank}$-*tasA*$_{G183C}$ (Spec^R)	This work
TB966	3610 *comI*^{Q12I} e4A *eps::tet, bslA::kan*	This work
TB967	3610 *comI*^{Q12I} e6A *eps::tet, bslA::kan*	This work
TB868	3610 *comI*^{Q12I} *tasA::kan, Pspach-hy-epsA-O* (Cm^R)	This work
Anc Kate P_{eps}-GFP	3610 *comI*^{Q12I} *tasA::spec*, *amyE::*$P_{hyperspank}$-mKate2 (Cm^R), *sacI::*P_{eps}-*gfp* (Km^R)	This work
Anc Kate P_{tapA}-GFP	3610 *comI*^{Q12I} *eps::tet, amyE::*$P_{hyperspank}$-mKate2 (Cm^R), *sacI::*P_{eps}-*gfp* (Km^R)	This work
TB905	3610 *comI*^{Q12I} *tasA::spec*, *ptpZ::mls, amyE::*$P_{hyperspank}$-mKate2 (Cm^R), *sacI::*P_{eps}-*gfp* (Km^R)	This work
t3A Kate P_{eps}-GFP	3610 *comI*^{Q12I} t3A *tasA::spec*, *amyE::*$P_{hyperspank}$-mKate2 (Cm^R), *sacI::Peps-gfp* (Km^R)	This work
t5A Kate P_{eps}-GFP	3610 *comI*^{Q12I} t5A *tasA::spec*, *amyE::*$P_{hyperspank}$-mKate2 (Cm^R), *sacI::*P_{eps}-*gfp* (Km^R)	This work
t4A Kate P_{eps}-GFP	3610 *comI*^{Q12I} t4A *tasA::*spec, amyE::$P_{hyperspank}$-mKate2 (Cm^R), *sacI::*P_{eps}-*gfp* (Km^R)	This work
t4B Kate P_{eps}-GFP	3610 *comI*^{Q12I} t4B *tasA::spec*, *amyE::*$P_{hyperspank}$-mKate2 (Cm^R), *sacI::*P_{eps}-*gfp* (Km^R)	This work
t5B Kate P_{eps}-GFP	3610 *comI*^{Q12I} t5B *tasA::spec*, *amyE::*$P_{hyperspank}$-mKate2 (Cm^R), *sacI::*P_{eps}-*gfp* (Km^R)	This work
t6B Kate P_{eps}-GFP	3610 *comI*^{Q12I} t6B *tasA::spec*, *amyE::*$P_{hyperspank}$-mKate2 (Cm^R), *sacI::*P_{eps}-*gfp* (Km^R)	This work
Mt1a Kate P_{eps}-GFP	3610 *comI*^{Q12I} Mt1a *tasA::spec*, *amyE::*$P_{hyperspank}$-mKate2 (Cm^R), *sacI::*P_{eps}-*gfp* (Km^R)	This work
Anc Kate P_{tapA}-GFP	3610 *comI*^{Q12I} *eps::tet*, *amyE::*$P_{hyperspank}$-mKate2 (Cm^R), *sacI::*P_{tapA}-*gfp* (Km^R)	This work
e3A Kate P_{tapA}-GFP	3610 *comI*^{Q12I} e3A *eps::tet*, *amyE::*$P_{hyperspank}$-mKate2 (Cm^R), *sacI::*P_{tapA}-*gfp* (Km^R)	This work
e4A Kate P_{tapA}-GFP	3610 *comI*^{Q12I} e4A *eps::tet*, *amyE::*$P_{hyperspank}$-mKate2 (Cm^R), *sacI::*P_{tapA}-*gfp* (Km^R)	This work
e4B Kate P_{tapA}-GFP	3610 *comI*^{Q12I} e4B *eps::tet*, *amyE::*$P_{hyperspank}$-mKate2 (Cm^R), *sacI::*P_{tapA}-*gfp* (Km^R)	This work
e4C Kate	3610 *comI*^{Q12I} e4C *eps::tet*, *amyE::*$P_{hyperspank}$-mKate2 (Cm^R), *sacI::*P_{tapA}-*gfp*	This work

P_{tapA}-GFP	(Km^R)	
e6A Kate P_{tapA}-GFP	3610 *comI*^{Q12I} e6A *eps::tet*, *amyE::*$P_{hyperspank}$-mKate2 (Cm^R), *sacI::*P_{tapA}-*gfp* (Km^R)	This work
e6C Kate P_{tapA}-GFP	3610 *comI*^{Q12I} e6B *eps::tet*, *amyE::*$P_{hyperspank}$-mKate2 (Cm^R), *sacI::*P_{tapA}-*gfp* (Km^R)	This work
e4A_$tasA_{anc}$	3610 *comI*^{Q12I} e4A *eps::tet*, *tasA::kan, amyE::*$P_{hyperspank}$-$tasA_{anc}$ ($Spec^R$)	This work
e4C_$tasA_{anc}$	3610 *comI*^{Q12I} e4C *eps::tet*, *tasA::kan, amyE::*$P_{hyperspank}$-$tasA_{anc}$ ($Spec^R$)	This work
TB500.1	3610 *comI*^{Q12I} *amyE::*$P_{hyperspank}$-GFP (Cm^R)	This work
e4A GFP	3610 *comI*^{Q12I} e4A *eps::tet*, *amyE*::$P_{hyperspank}$-GFP (Cm^R)	This work
t6B mKate	3610 *comI*^{Q12I} t6B *tasA::spec*, *amyE*::$P_{hyperspank}$-mKate2 (Cm^R)	This work
TB790	3610 *comI*^{Q12I} *eps::tet, amyE::*P_{ctc}-*lacZ* ($Spec^R$)	This work
TB851	3610 *comI*^{Q12I} *tasA::kan, amyE::*P_{ctc}-*lacZ* ($Spec^R$)	This work

To obtain TB601, the transformable NCBI 3610 derivative DK1042 was transformed with gDNA isolated from DL1032 (Table S2) selecting for Tet-resistant colonies. To obtain TB857, TB859 and TB861 first the Δ*eps*Δ*tasA* double mutant was constructed by transforming TB601 with gDNA from DL1032 and selecting for Km-resistant colonies. Then the plasmids pDR111_$tasA_{anc}$, pDR111_$tasA_{Y124C}$ and pDR111_$tasA_{G183C}$ (Table S3) were introduced into the Δ*eps*Δ*tasA*, selecting for transformants that carried triple antibiotic resistance (Tet, Km and Spec) and were negative in Lugol test indicating double integration of the vector into *amyE* locus, ultimately resulting in TB857, TB859 and TB861, respectively. The TB906, TB907 and TB908 were obtained by transforming TB602 with gDNA isolated from TB857, TB859 and TB861, respectively. The strains 966 and 967 were obtained by transforming the evolved isolates e4A and e6A with gDNA from NRS2097 (Table S2) and selecting for Km and Tet resistance. To obtain TB868, first the NCBI 3610 was transformed with gDNA from DL1032 selecting for Km-resistant colonies, therefore resulting in Δ*tasA* (Km^R) and next this strain was transformed with gDNA from NRS1685 (Table S2). The Anc Kate P_{epsA}-GFP and its evolved derivatives [(t3A/t5A/t4A/t4B/t5B/t6B) Kate P_{epsA}-GFP] were constructed by first transforming the TB602 or the evolved isolate with gDNA from 168 hymKate (Table S2) and next with gDNA from NRS2243 (Table S2). Analogically the Anc Kate P_{tapA}-GFP and its evolved derivatives [(e3A/e4A/e4B/e4C/e6A/e6C) Kate P_{tapA}-GFP] were constructed by first transforming the TB601 or the evolved isolate with gDNA from 168 hymKate (Table S2) and next with gDNA from NRS2394 (Table S2). To obtain TB500.1 and e4A GFP strains, DK1042 and e4A were transformed with gDNA from 168 hyGFP, respectively. Strain t6B mKate was obtained by transforming t6B with gDNA from 168 hymKate. In order to obtain TB790 and TB851, strains TB601 and TB602 were transformed with gDNA from JH642 P*ctc-lacZ*, respectively (Table S2). Strains e4A_$tasA_{anc}$ and e4C_$tasA_{anc}$ were obtained by first transforming the strains with gDNA from DL1032 and selecting for Km-resistant colonies, and by introducing the gDNA from TB906 and selecting for Spec-resistant colonies in another transformation step.
For clarity, the following abbreviations were used for the indicated strains: TB601 - Δeps_{anc}; TB602 - Δ$tasA_{anc}$; TB857 - ΔΔ$tasA_{anc}$; TB859 - ΔΔ$tasA_{Y124C}$; TB861 - ΔΔ$tasA_{G183C}$; TB906 - Δ*tasA*_$tasA_{anc}$; TB907 - Δ*tasA*_$tasA_{Y124C}$; TB908 - Δ*tasA*_$tasA_{G183C}$; TB966 - e4A Δ*bslA*; TB967 - e6A Δ*bslA*; TB905 - Δ*tasA*Δ*ptpZ*; TB868 - Δ$tasA_{hyEPS.}$

References

1. Konkol, M. A., Blair, K. M. & Kearns, D. B. Plasmid-encoded ComI inhibits competence in the ancestral 3610 strain of *Bacillus subtilis*. *J. Bacteriol.* **195,** 4085–4093 (2013).

2. Dragoš, A. *et al.* Division of labor during biofilm matrix production. *Curr. Biol.* **28,** 1903–1913.e5 (2018).

3. Mhatre, E., Sundaram, A., Hölscher, T., Mühlstädt, M., Bossert, J. & Kovács, Á. T. Presence of calcium lowers the expansion of *Bacillus subtilis* colony biofilms. *Microorganisms* **5,** 7 (2017).

Supplementary Table 2 | The strains that were used as gDNA donors

Strain name	Genotype	Reference
DL1032	*eps:tet, tasA:Km, amyE::*P_{srfAA}*-lacZ (ery)*	[1]
168 hyGFP	*amyE::*$P_{hyperspank}$*-gfp* (Cm^R)	[2]
168 hymKate	*amyE::*$P_{hyperspank}$*-mKate2* (Cm^R)	[2]
NRS2243	3610 *sacI::*P_{eps}*-gfp* (Km^R)	3²²
NRS2394	3610 *sacI::*P_{tapA}*-gfp* (Km^R)	[3]
BKE36240	*ptpZ::mls*	[4]
JH642 ctc-lacZ	*amyE::*P_{ctc}*-lacZ* ($Spec^R$)	[5]
NRS2097	*bslA::kan*	[6]
NRS1685	3610 *epsA::pBL584* ($P_{spach-hy}$-epsA-O) (Cm^R)	[6]

References

1. López, D., Vlamakis, H., Losick, R. & Kolter, R. Paracrine signaling in a bacterium. *Genes Dev.* **23,** 1631-1638 (2009).

2. van Gestel, J., Weissing, F. J., Kuipers, O. P. & Kovács, Á. T. Density of founder cells affects spatial pattern formation and cooperation in *Bacillus subtilis* biofilms. *ISME J.* **8,** 2069-2079 (2014).

3. Murray, E. J., Strauch, M. A. & Stanley-Wall, N. R. SigmaX is involved in controlling *Bacillus subtilis* biofilm architecture through the AbrB homologue Abh. *J. Bacteriol.* **191,** 6822-6832 (2009).

4. Koo, B. M. et al. Construction and analysis of two genome-scale deletion libraries for *Bacillus subtilis*. *Cell Syst.* **4,** 291-305.e7 (2017).

5. Boylan, S. A., Rutherford, A., Thomas, S. M. & Price, C. W. Activation of *Bacillus subtilis* transcription factor σ^B by a regulatory pathway responsive to stationary-phase signals. *J. Bacteriol.* **174,** 3695-3706 (1992).

6. Verhamme, D. T., Murray, E. J. & Stanley-Wall, N. R. DegU and Spo0A jointly control transcription of two loci required for complex colony development by *Bacillus subtilis*. *J. Bacteriol.* **191,** 100-108 (2009).

Supplementary Table 3 | Plasmids used in this study

Plasmid	Bacterial host	Experimental purpose
pDR111_*tasA*$_{anc}$	*E. coli* MC1000	Complementation of *B. subtilis* ΔΔ*tasA*$_{anc}$ with native TasA
pDR111_*tasA*$_{Y124C}$	*E. coli* MC1000	Complementation of *B. subtilis* ΔΔ*tasA*$_{anc}$ with TasA^{Y124C}
pDR111_*tasA*$_{G183C}$	*E. coli* MC1000	Complementation of *B. subtilis* ΔΔ*tasA*$_{anc}$ with TasA^{G183C}
pET24d_His-ΔSP-TasA	*E. coli* BL21(DE3)	Expression of TasA with His-tag on N-term
pET24d_His-ΔSP-TasA_Y124C	*E. coli* BL21(DE3)	Expression of TasA^{Y124C} with His-tag on N-term
pET24d_His-ΔSP-TasA_G183C	*E. coli* BL21(DE3)	Expression of TasA^{G183C} with His-tag on N-term
pET24d_ΔSP-TasA-His	*E. coli* BL21(DE3)	Expression of TasA with His-tag on C-term
pET24d_ΔSP-TasA-His_Y124C	*E. coli* BL21(DE3)	Expression of TasA^{Y124C} with His-tag on C-term
pET24d_ΔSP-TasA-His_G183C	*E. coli* BL21(DE3)	Expression of TasA^{G183C} with His-tag on C-term

To obtain pDR111_*tasA*$_{anc}$, pDR111_*tasA*$_{Y124C}$ and pDR111_*tasA*$_{G183C}$ the native *tasA* gene, and modified *tasA* variants from e4A and e6A strains were cloned into the pDR111 vector: *tasA* from TB601, e4A and e6A were amplified using oTB71 and oTB72 primers (Table S4), the obtained PCR products and the pDR111 were digested with *Sph*I and *Sal*I, ligated overnight and transformed into *E. coli* MC1000 selecting for Spec-resistant colonies. The pET24d plasmids were obtained as follows: *tasA*, lacking the N-terminal signal peptide coding region (aa 1-27), was amplified from *B. subtilis* 168 gDNA using primers BsTasA-Nco-6H-28-F and BsTasA-BamHI-R (see Table S4) for the N-terminally His-tagged and primers BsTasA-Nco-28-F and BsTasA-6H-BamHI-R (see Table S4) for the C-terminally His tagged construct. This resulted in pET24d_His-ΔSP-TasA and pET24d_ΔSP-TasA-His plasmids, respectively. The PCR fragments were subsequently mutagenized in a two-step fusion PCR using mutagenesis primers BsTasA-Y124C-F and BsTasA-Y124C-R (Table S4) to introduce TasAY124C mutation (resulting in pET24d_His-ΔSP-TasA_Y124C and pET24d_ΔSP-TasA-His_Y124C) and primers BsTasA-G183C-F and BsTasA-G183C-R (Table S4) to introduce TasAG183C (resulting in pET24d_His-ΔSP-TasA_G183C and pET24d_ΔSP-TasA-His_G183C). Gene fragments were digested with *Nco*I and *Bam*HI and ligated into pET24d.

Supplementary Table 4 | Primers used in this study

Primer	Experimental purpose	Sequence (5' to 3')
oTB71	cloning of tasA for complementation assays	CACGGTCGACATAAAAGGGGAGCTTACCATGGG
oTB72	cloning of tasA for complementation assays	CATGGCATGCGCCTGAGCAGAGGCACTAAC
BsTasA-Nco-6H-28-F	cloning of *tasA* for expression in *E. coli* – N-term His tag	TTAACCATGGCCCACCATCACCATCACCATGCAT TTAACGACATTAAATC
BsTasA-BamHI-R	cloning of *tasA* for expression in *E. coli* – N-term His tag	TATAGGATCCTTAATTTTTATCCTCGC
BsTasA-Nco-28-F	cloning of *tasA* for expression in *E. coli* – C-term His tag	TTAACCATGGCATTTAACGACATTAAATC
BsTasA-6H-BamHI-R	cloning of *tasA* for expression in *E. coli* – C-term His tag	TATAGGATCCTTAATGGTGATGGTGATGGTGATT TTTATCCTCGCTATGCGC
BsTasA-Y124C-F	*tasA* mutagenesis	GCAATGGCTGCCCGAAAAAC
BsTasA-Y124C-R	*tasA* mutagenesis	GTTTTTCGGGCAGCCATTGC
BsTasA-G183C-F	*tasA* mutagenesis	GAATATGATTGTGTTCCAAAAAC
BsTasA-G183C-R	*tasA* mutagenesis	GTTTTTGGAACACAATCATATTC

Supplementary Table 5 | Average coverage per genome obtained for each strain that was sequenced in the study.

Strain	Av. Coverage
Ancestor WT	174.05
e4A	283.36
e4B	222.3
e4C	200.81
e6A	714.75
e6B	640.65
e6C	348.98
e3A	200.38
e5A	434.55
Me3C	166.56
Me4A	181.13
t3C	263.71
t4A	239.05
t4B	1013.01
t5B	253.18
t6B	474.62
t6C	214.88
t3A	209.82
t5A	262.83
Mt4C	274.65
Mt3C	193.58
Mt4B	282.6
Mt3B	442.38
Mt5B	278.38
Mt5C	247.06
Mt1A	190.04
Mt1B	253.75

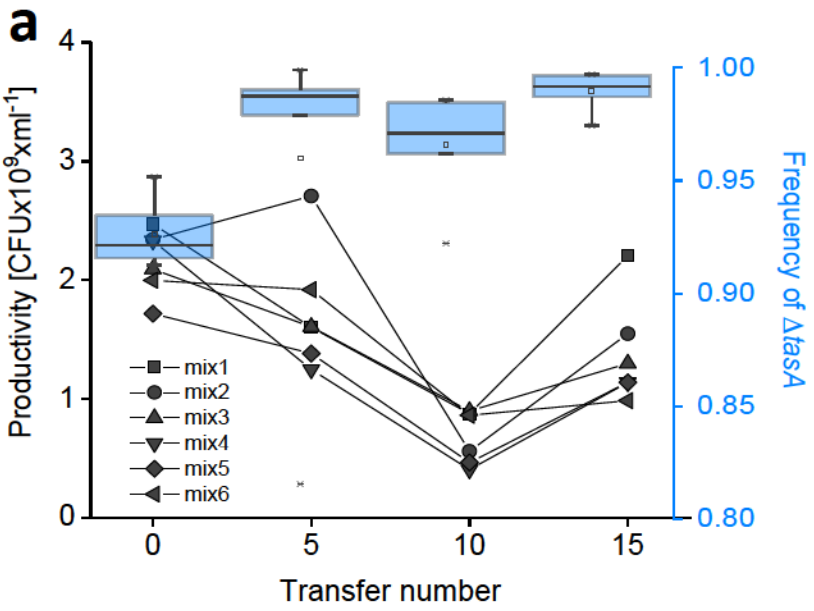

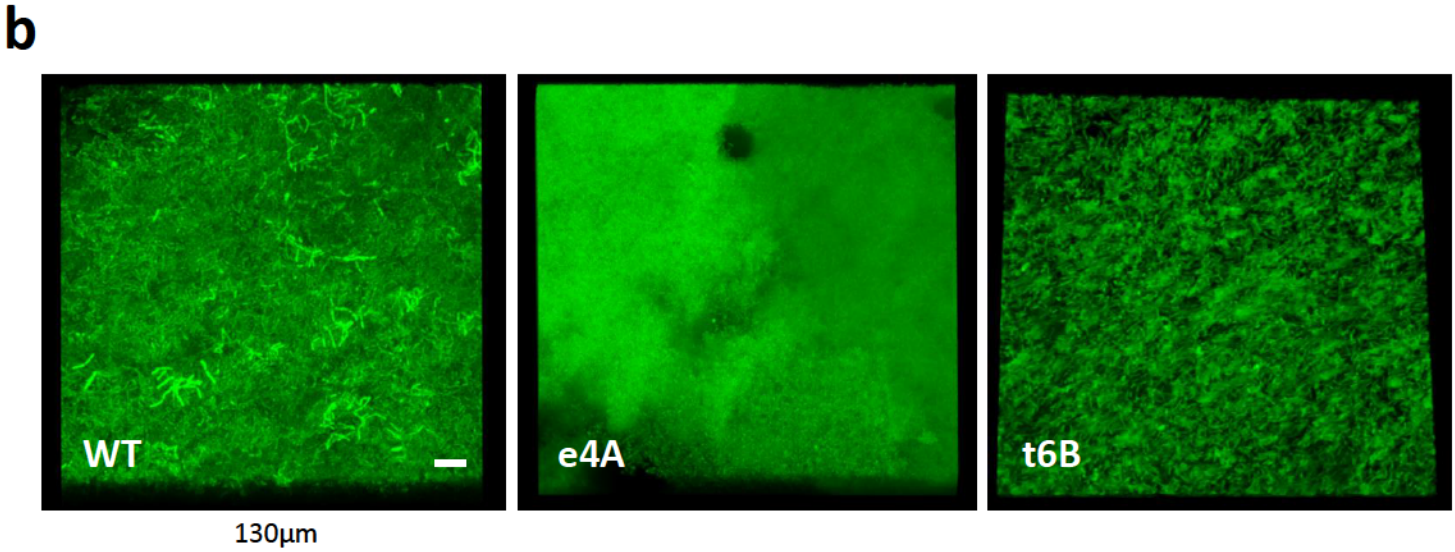

Supplementary Fig. 1 | Reproducibility of Δ*eps*+Δ*tasA* pellicle collapse and single-cell level structure of solitarily evolved pellicles of Δ*eps* and Δ*tasA* (a) Six parallel Δ*eps*+Δ*tasA* co-cultures were initiated from fresh stocks and the evolution experiment was repeated (as in Fig. 1). Pellicle productivities and relative frequencies of Δ*eps* and Δ*tasA* in the mixes were systematically monitored every 5th transfer (as CFU/ml) until the pellicle collapse scenario coupled with increased Δ*tasA* frequency were reproduced. Relative frequency of the Δ*tasA* strain at each evolutionary time point (pulled from six parallel co-cultures) is shown as a blue box plot. Boxes represent Q1–Q3, lines represent the median, and bars span from max to min (n=6). **(b)** Pellicles formed by WT (wild-type *B. subtilis* strain NCBI 3610), e4A (representative evolved Δ*eps* isolate with improved surface-colonizing properties) and t6B (representative evolved Δ*tasA* isolate with improved surface-colonizing properties) were analysed at single-cell level using a confocal microscope. All strains were labelled with constitutive fluorescent reporter GFP. Scale bar indicates 10µm. Similar result was obtained in 2 independent experiments.

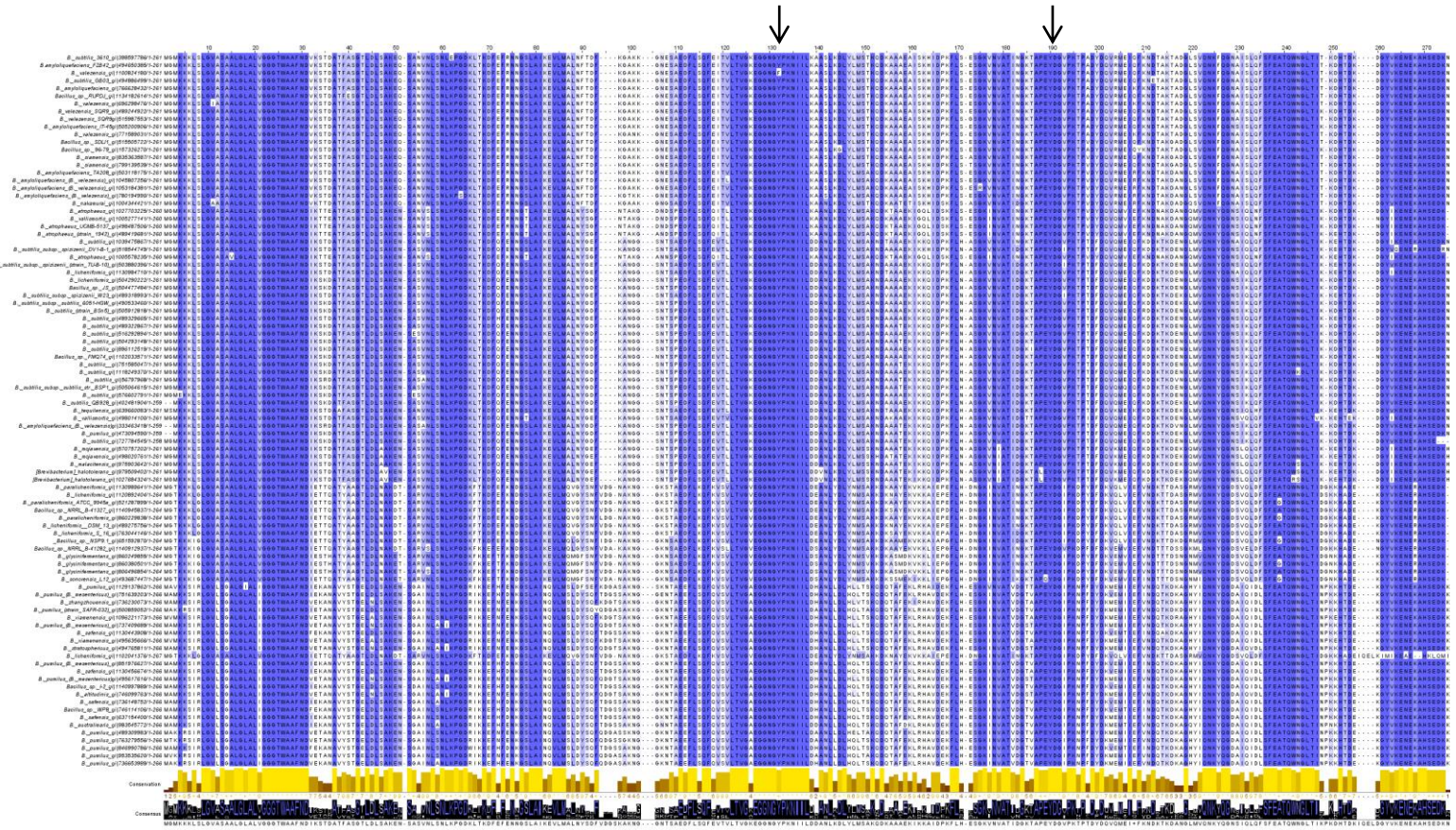

Supplementary Fig. 2 | Conservation of residues that were substituted to cysteines in evolved form of TasA. Multiple alignment of TasA homologs with min. 50% identity to TasA of *B. subtilis* NCBI 3610 (WP_004398632.1) was performed using the Constraint-based Multiple Alignment Tool (COBALT; https://www.ncbi.nlm.nih.gov/tools/cobalt/re_cobalt.cgi) and visualized using JalView software (Waterhouse et al., 2009). A colour-by-conservation tool was used to visualize conserved regions of TasA (dark purple). The conservation score and consensus (calculated by JalView) are presented below the alignment. Black arrows above the alignment indicate the positions of Tyr124 and Gly183 that were substituted to Cys in evolved Δ*eps* strains with improved surface-colonizing properties.

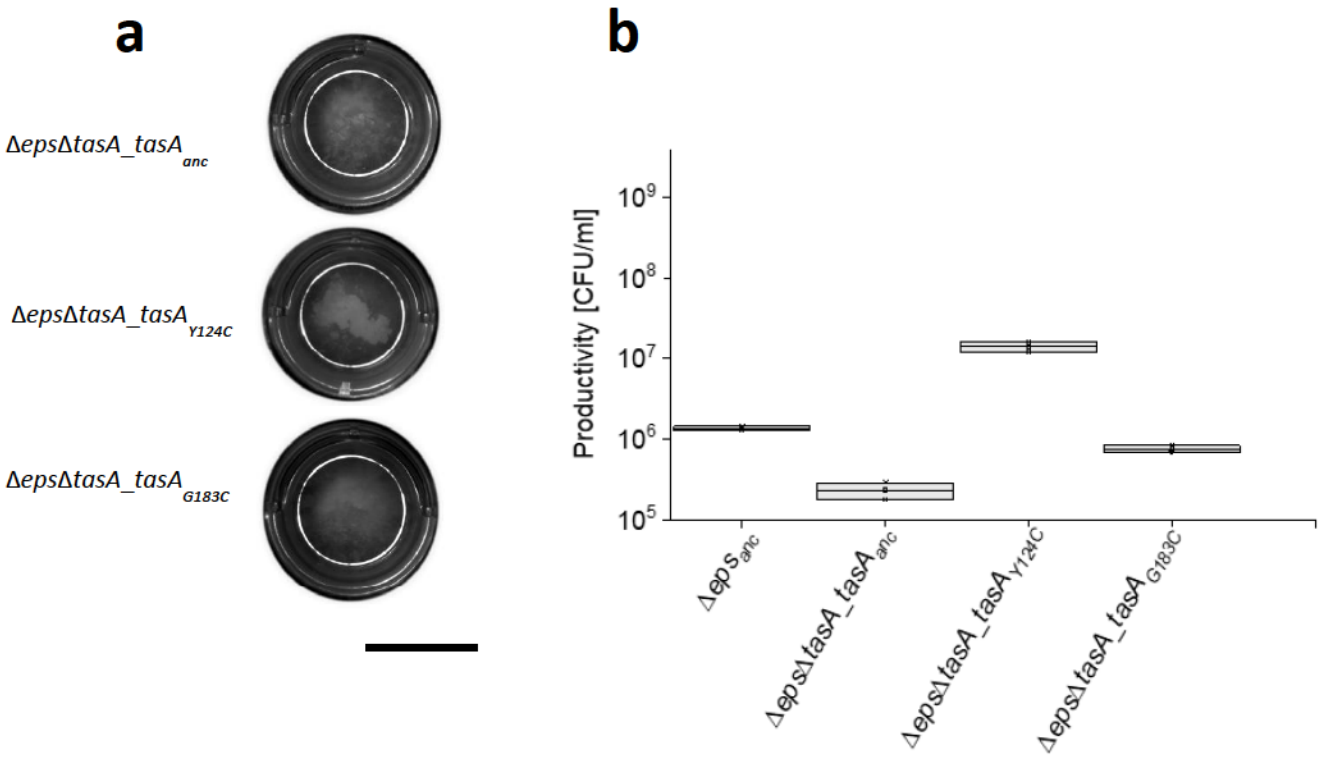

Supplementary Fig. 3 | Pellicle morphology and productivity of *tasA*-complemented strains in the absence of IPTG. (a) Pellicle morphology developed by Δ*eps*Δ*tasA*_*tasA*$_{anc}$ (Δ*eps*Δ*tasA* double-mutant complemented with the native form of the *tasA* gene in the ectopic *amyE* locus) and Δ*eps*Δ*tasA*_*tasA*$_{Y124C}$ and Δ*eps*Δ*tasA*_*tasA*$_{G183C}$ (Δ*eps*Δ*tasA* double-mutants complemented with evolved forms of *tasA*) in the absence of IPTG. Pellicles were cultivated in 24 well plate (well diameter = 15 mm). Scale bar indicates 10mm. Similar result was obtained in >5 independent experiments **(b)** Productivities of surface-colonizing Δ*eps*$_{anc}$ (ancestor Δ*eps* strain), Δ*eps*Δ*tasA*_*tasA*$_{anc}$, Δ*eps*Δ*tasA*_*tasA*$_{Y124C}$ and Δ*eps*Δ*tasA*_*tasA*$_{G183C}$ in the absence of IPTG, assessed as CFU/ml (n = 4 biologically independent replicates). Boxes represent Q1–Q3, lines represent the median, and bars span from max to min.

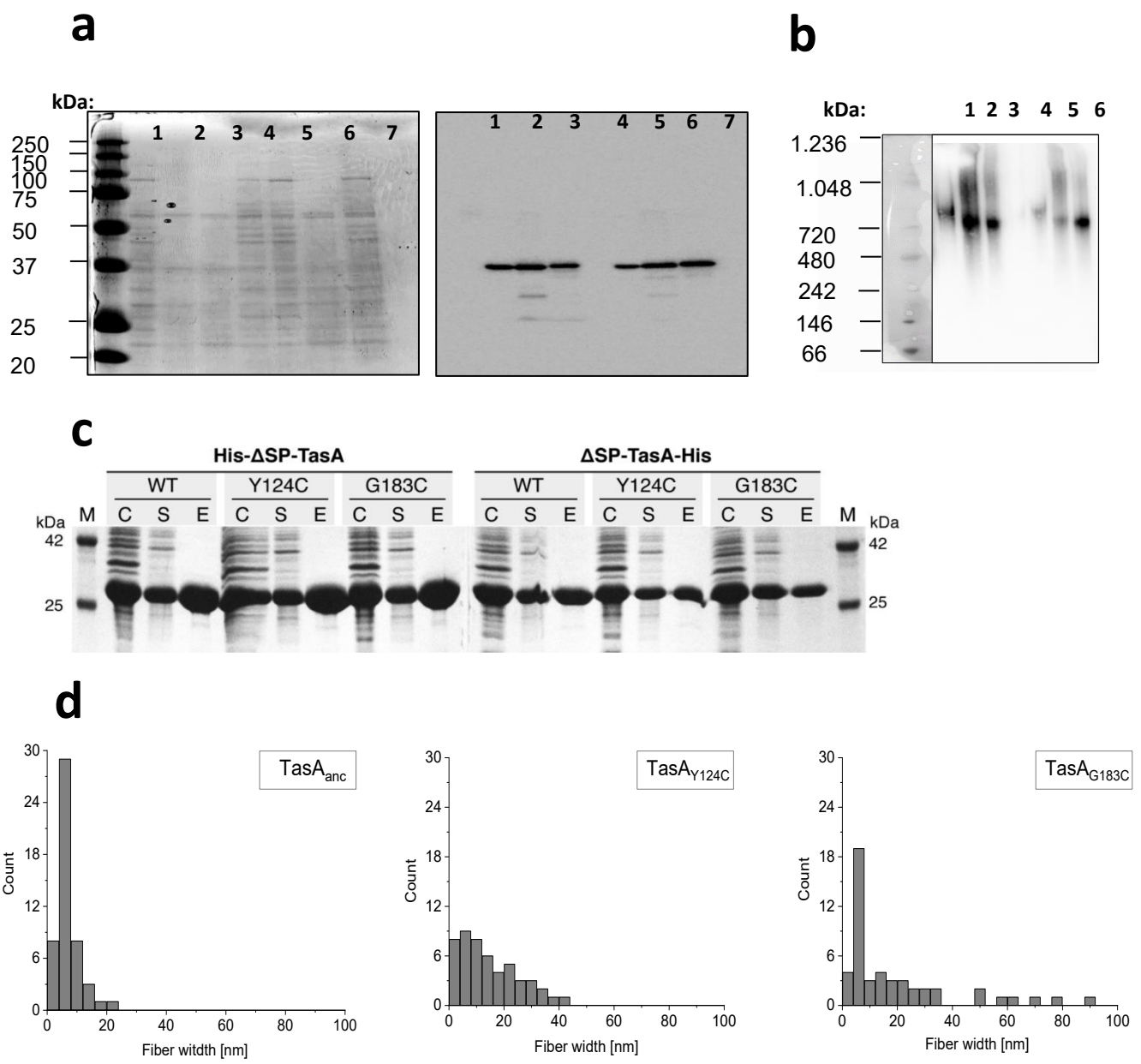

Supplementary Fig. 4 | Biochemical characterization and purification of evolved TasA variants. (a) SDS-PAGE of total protein fraction obtained from: 1, Δ*eps*$_{anc}$; 2, e4A; 3, e6A; 4, Δ*eps*Δ*tasA*; 5, Δ*eps*Δ*tasA*_*tasA*$_{anc}$; 6, Δ*eps*Δ*tasA*_*tasA*$_{Y124C}$; and 7, Δ*eps*Δ*tasA*_*tasA*$_{G183C}$ pellicles. On the right – Western blot detection of TasA in corresponding SDS-PAGE samples using TasA antibody combined with secondary goat anti-rabbit IgG. Similar result was obtained in 3 independent experiments. **(b)** Blue-native PAGE was performed with samples obtained from: 1, Δ*eps*$_{anc}$; 2, e4A; 3, e6A; 4, Δ*eps*Δ*tasA*; 5, Δ*eps*Δ*tasA*_*tasA*$_{anc}$; 6, Δ*eps*Δ*tasA*_*tasA*$_{Y124C}$; and 7, Δ*eps*Δ*tasA*_*tasA*$_{G183C}$ pellicles. Similar result was obtained in 2 independent experiments. Detection of TasA was performed as described in (b). **(c)** Ni-NTA purification of ΔSP-TasA. SDS-PAGE (12%) of N-terminally and C-terminally hexa-histidine tagged ΔSP-TasA Ni-NTA purification fractions. The lanes are labelled: M: marker; WT: wild-type ΔSP-TasA; Y124C: ΔSP-TasA_Y124C; G183C: ΔSP-TasA_G183C. C: induced total cells; S: soluble fraction; E: purified protein. Single purification round allowed to obtain sufficient material to perform comparative TEM analysis. **(d)** Distributions of fiber width formed by TasA$_{anc}$, TasA$_{Y124C}$ and TasA$_{G183C}$, obtained by measurements of 50 randomly selected regions for each micrograph.

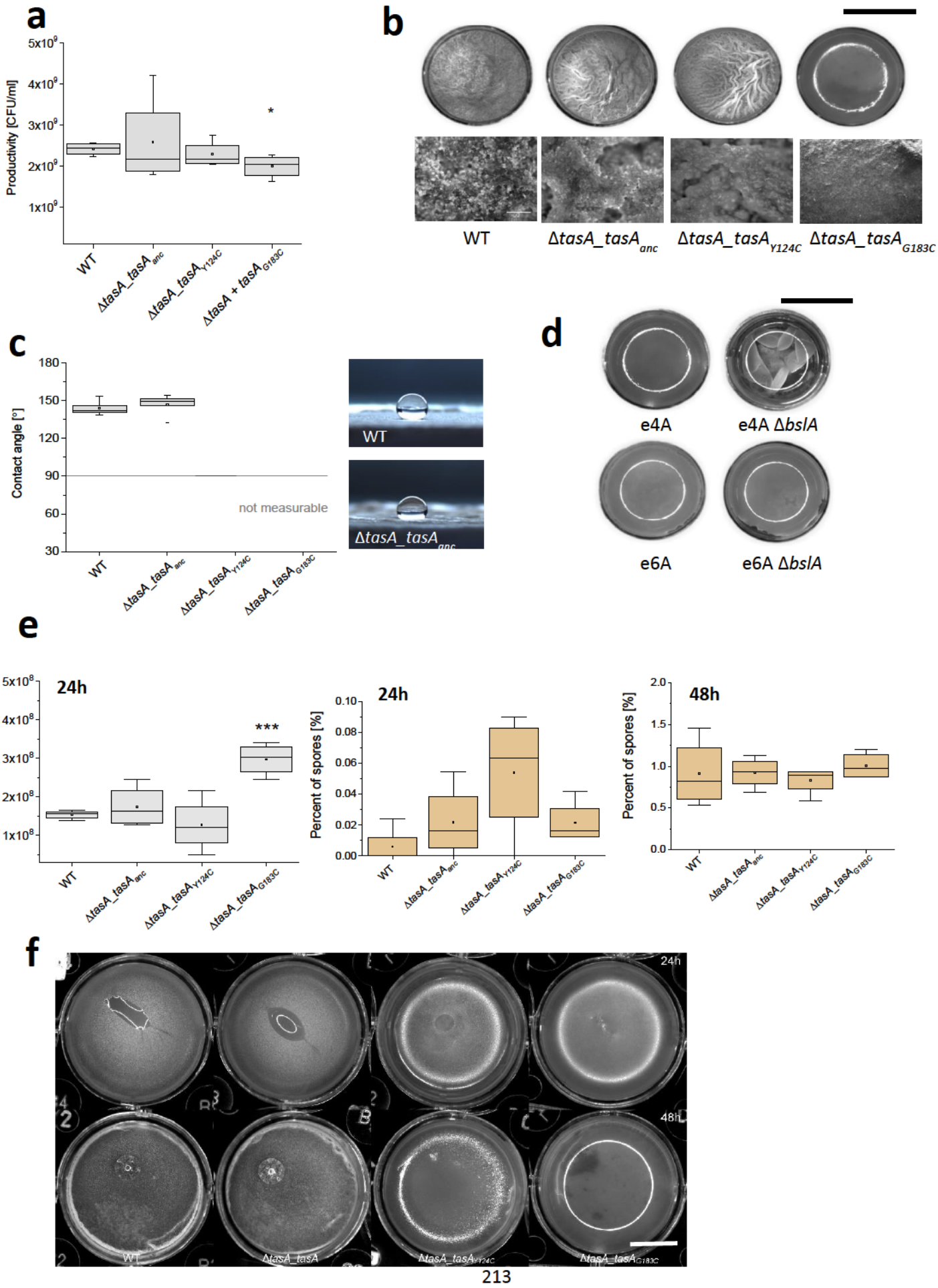
a
Productivity [CFU/ml]
5x10^9
4x10^9
3x10^9
2x10^9
1x10^9
*
WT
ΔtasA_tasA_anc
ΔtasA_tasA_Y124C
ΔtasA + tasA_G183C
b
WT
ΔtasA_tasA_anc
ΔtasA_tasA_Y124C
ΔtasA_tasA_G183C
c
Contact angle [°]
180
150
120
90
60
30
not measurable
WT
ΔtasA_tasA_anc
d
e4A
e4A ΔbslA
e6A
e6A ΔbslA
e
24h
Productivity [CFU/ml]
5x10^8
4x10^8
3x10^8
2x10^8
1x10^8
***
Percent of spores [%]
0.10
0.08
0.06
0.04
0.02
0.00
48h
2.0
1.5
1.0
0.5
0.0
f
24h
48h
WT
ΔtasA_tasA

Supplementary Fig. 5 | Effects of cysteine-containing TasA in the wild-type background and in BslA-negative background. (a) Productivities of pellicles formed by WT, Δ*tas*_Δ$tasA_{anc}$ (Δ*tasA* complemented with the native form of the *tasA* gene in the ectopic *amyE* locus), Δ*tas*_Δ$tasA_{Y124C}$ and Δ*tas*_Δ$tasA_{G183C}$ (Δ*tasA* complemented with evolved forms of the *tasA* gene in the ectopic *amyE* locus) assessed as CFU/ml (n = 4 biologically independent samples). Boxes represent Q1–Q3, lines represent the median, and bars span from max to min. An asterisk above the box indicates that the obtained productivity was significantly different from the productivity of WT ($p < 0.05$; t-test, two-tail). **(b)** Pellicle morphology developed by WT, Δ*tas*_Δ$tasA_{anc}$, Δ*tas*_Δ$tasA_{Y124C}$, and Δ*tas*_Δ$tasA_{G183C}$. Pellicles were cultivated in 24 well plates (well diameter = 15 mm). Below, magnified images of corresponding pellicles. Black scale bar equals 10 mm, white scale bar = 500 µm. Similar result was obtained in 5 independent experiments each containing 3 biologically independent samples **(c)** Contact angles were determined as described in Werb et al., 2017 (NPJ Biofilms and Microbiomes), and were calculated for water spotted onto pellicle material that was carefully placed on a glass slide. Contact angles could not be measured for Δ*tas*_Δ$tasA_{Y124C}$ and Δ*tas*_Δ$tasA_{G183C}$ pellicles as the droplet instantly sank below the pellicle surface, indicating its porosity. The line represents the contractual hydrophobicity cut-off, separating hydrophilic (below the line) from hydrophobic (above) surfaces. Boxes represent Q1–Q3, lines represent the median, and bars span from max to min (n = 5 biologically independent samples). For productivity (a), morphology (b) and wetting (c) studies, complemented strains were grown in the presence of 0.2 mM IPTG to induce the expression of introduced *tasA* variants. **(d)** Pellicle morphology developed by the evolved strains e4A and e6A (evolved Δ*eps* isolates with improved surface-colonizing properties) and their mutant derivatives carrying a *bslA* deletion. Pellicles were cultivated in 24 well plates (well diameter = 15 mm). Scale bar equals 10 mm. Similar result was obtained in 2 independent experiments each containing 3 biologically independent samples. **(e)** On the left-productivities of early pellicles (24h) formed by WT, Δ*tas*_Δ$tasA_{anc}$, Δ*tas*_Δ$tasA_{Y124C}$ and Δ*tas*_Δ$tasA_{G183C}$ assessed as CFU/ml; middle – percentage of spores in early pellicles (24h) formed by WT, Δ*tas*_Δ$tasA_{anc}$, Δ*tas*_Δ$tasA_{Y124C}$ and Δ*tas*_Δ$tasA_{G183C}$; right – percentage of spore in mature pellicles (48h) formed by WT, Δ*tas*_Δ$tasA_{anc}$, Δ*tas*_Δ$tasA_{Y124C}$ and Δ*tas*_Δ$tasA_{G183C}$ (n = 4 biologically independent samples). Boxes represent Q1–Q3, lines represent the median, and bars span from max to min. A triple asterisk above the box indicates that the obtained productivity was significantly different from the productivity of WT ($p < 0.001$; t-test, two-tail). **(f)** Water-repellent properties of early (24h) and mature (48h) pellicles formed by WT, Δ*tas*_Δ$tasA_{anc}$, Δ*tas*_Δ$tasA_{Y124C}$ and Δ*tas*_Δ$tasA_{G183C}$ were accessed by spotting a 20µl water droplet onto pellicle surface. Scale bar equals 0.5cm. Similar result was obtained in 2 independent experiments each containing 3 biologically independent samples.

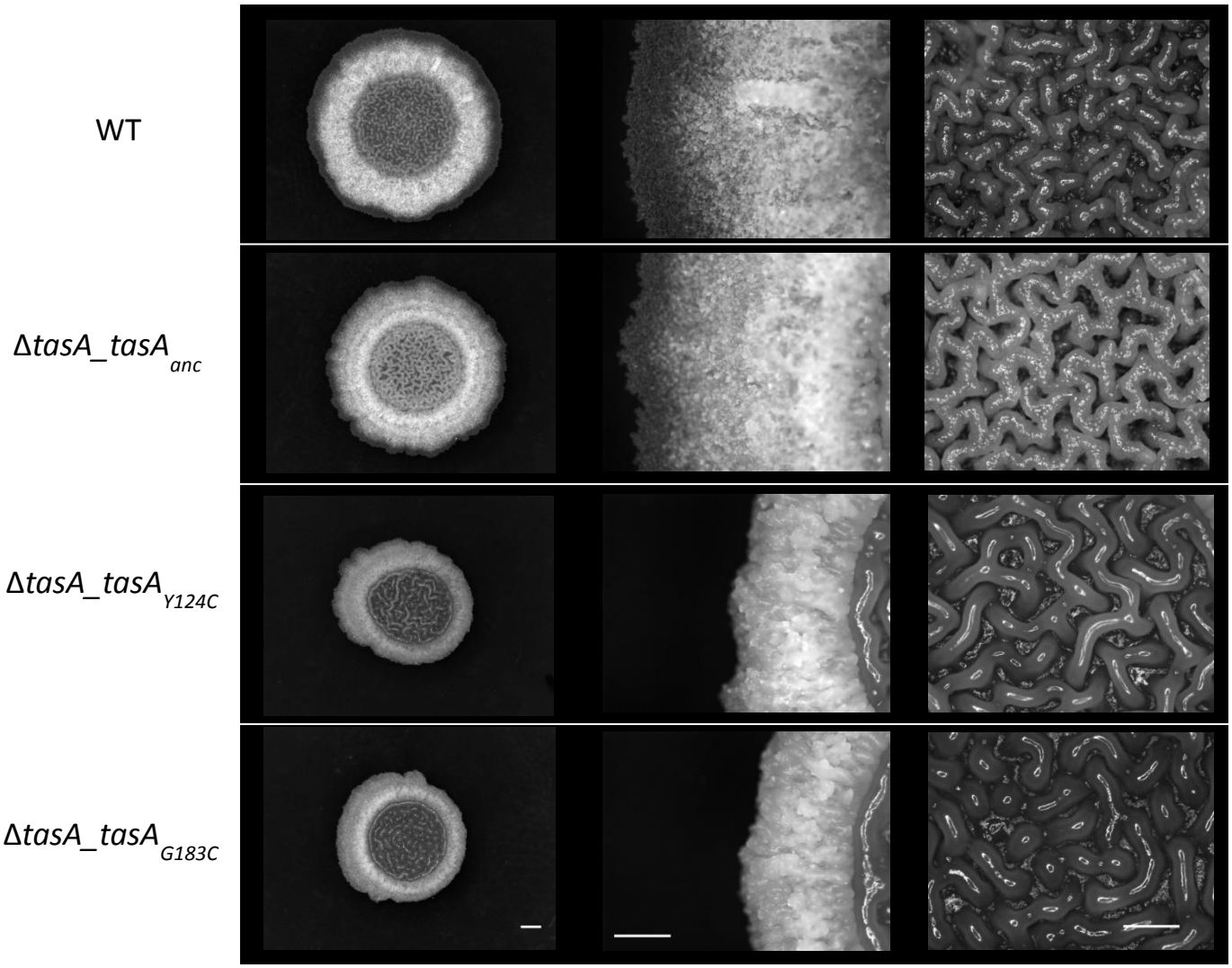

Supplementary Fig. 6 | Effects of cysteine-containing TasA on colony biofilms. Cultures of WT, Δ*tas*_Δ*tasA*$_{anc}$, Δ*tas*_Δ*tasA*$_{Y124C}$, and Δ*tas*_Δ*tasA*$_{G183C}$ were spotted on solid MSgg medium (1.5% agar) containing 0.2 mM IPTG and grown for 48 h at 30°C. Colonies were visualized using a stereomicroscope (bright field). The first column shows the entire colony (scale bar = 1000 µm); the second column shows a zoom into the colony edge (scale bar = 500 µm); the third column shows a zoom into the colony centre (scale bar = 500 µm). Similar result was obtained in 2 independent experiments each containing 3 biologically independent samples.

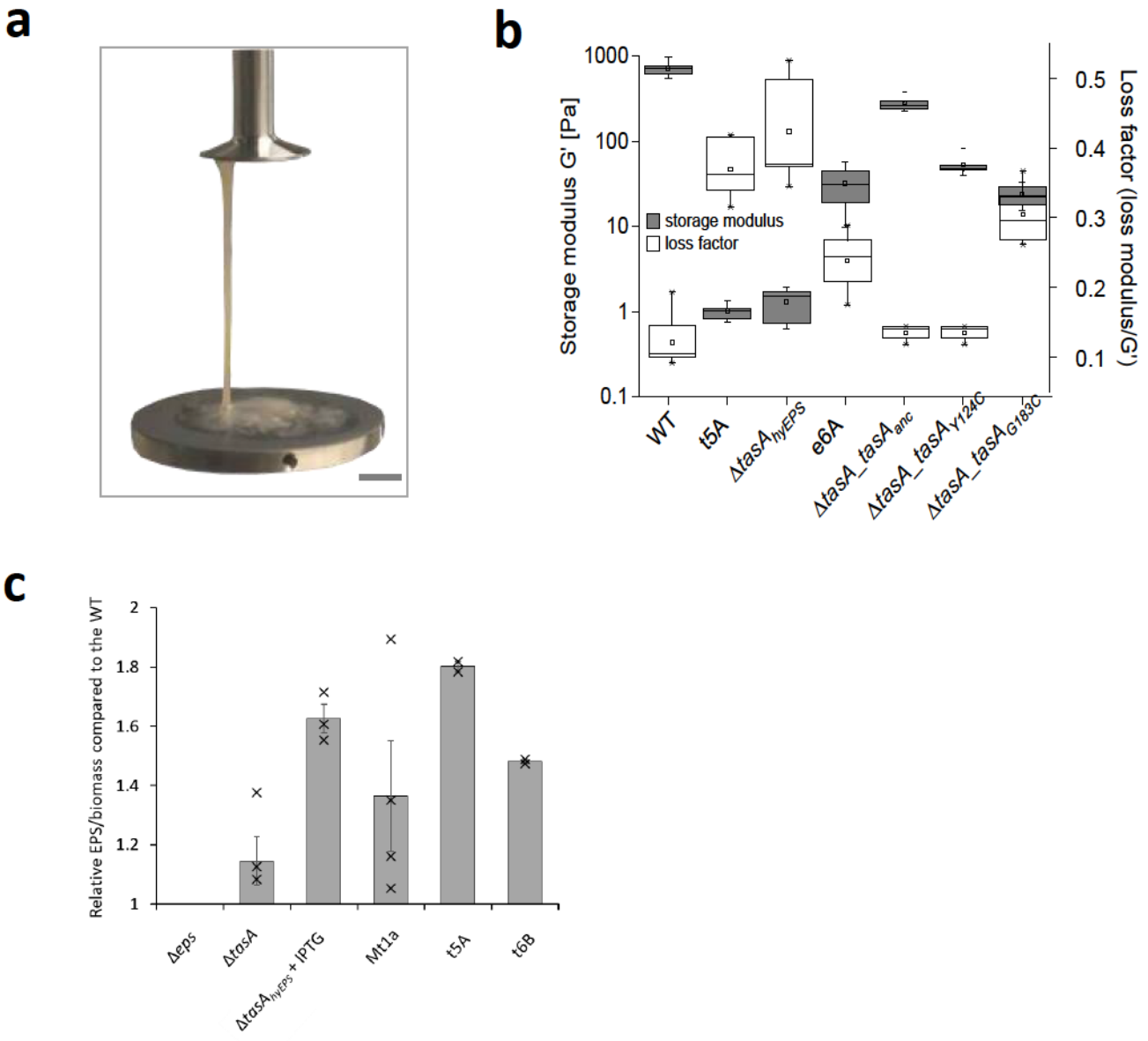

Supplementary Fig. 7 | Viscoelasticity and EPS measurements performed for the evolved and complemented strains. (a) Image of rheometer rotor captured during viscoelasticity measurement of strain t5A (a representative evolved Δ*tasA* isolate with improved surface-colonizing properties) showing distinctly slimy properties of the biofilm material (scale bar = 1cm). **(b)** Viscoelastic properties of pellicles developed by WT, t5A, Δ$tasA_{hyEPS}$ (Δ*tasA* strain with the native *eps* promoter replaced with an IPTG-inducible promoter), e6A, Δ*tas*_Δ$tasA_{anc}$, Δ*tas*_Δ$tasA_{Y124C}$, and Δ*tas*_Δ$tasA_{G183C}$. All complemented strains and Δ$tasA_{hyEPS}$ were cultivated with 0.2 mM IPTG. Boxes represent Q1–Q3, lines represent the median, and bars span from max to min (for WT n = 9; for t5A n = 6; for e6A n = 4; for the remaining samples n = 5 biologically independent samples). **(c)** EPS was extracted from the WT, Δ*eps*, Δ*tasA* and selected evolved Δ*tasA* strains. The obtained EPS/biomass values were normalized to the EPS/biomass of the WT. Bars represent the averages with standard errors indicated (for Δ*eps*, t5A and t6B n=2; for Δ*tasA,* Mt1A and Δ$tasA_{hyEPS}$ + IPTG n=4 biologically independent samples).

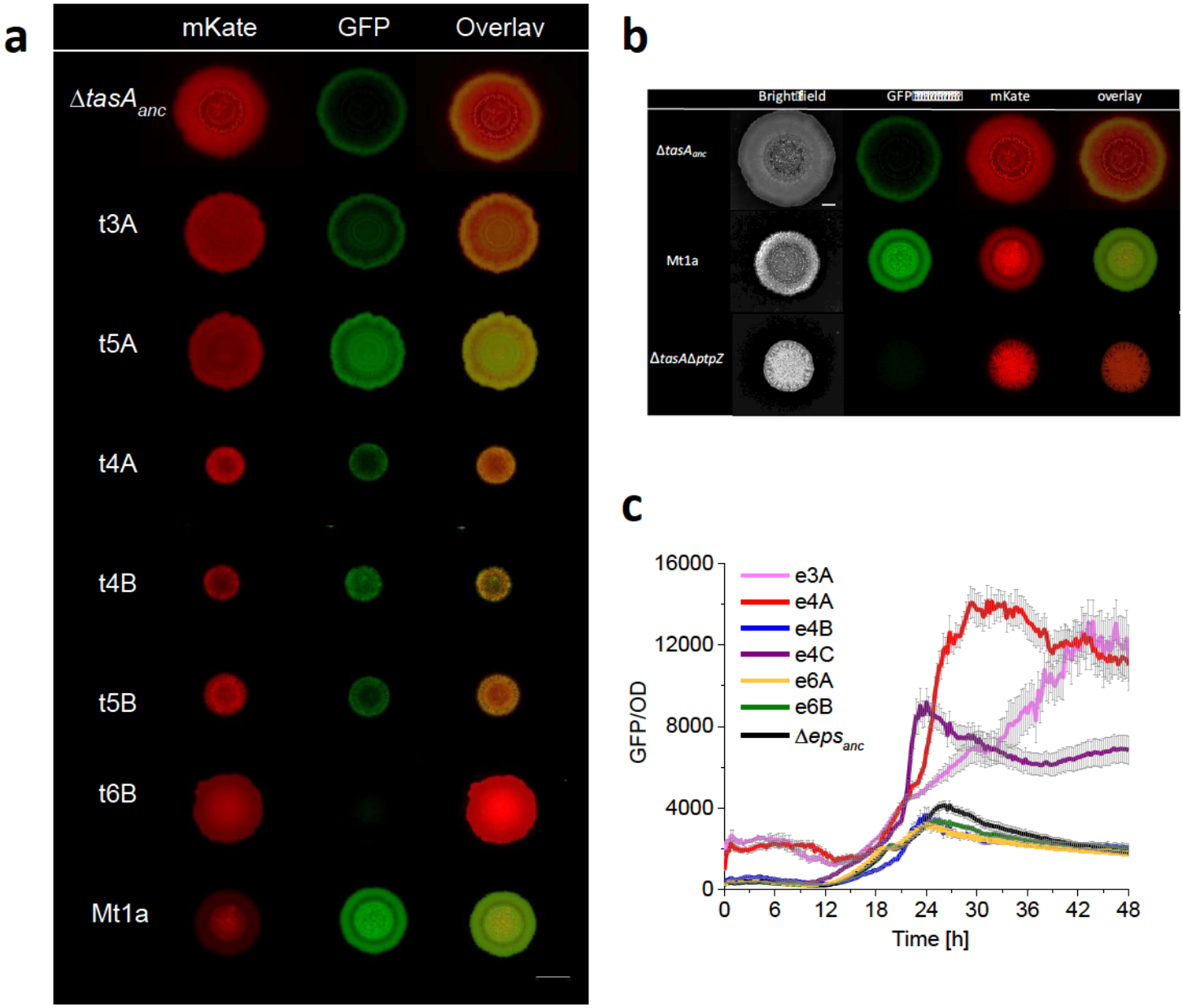

Supplementary Fig. 8 | Expression of matrix-genes in evolved Δ*tasA* and Δ*eps* strains. (a) Qualitative comparison of *eps* expression by different evolved Δ*tasA* isolates and Δ*tasA*$_{anc}$. Expression of *eps* was monitored in colonies developed on MSgg (1.5% agar) using a P$_{eps}$-*gfp* reporter fusion. In addition, all strains carried the constitutive mKate reporter. Scale bar = 5mm. Similar result was obtained in 2 independent experiments each containing 3 biologically independent samples. **(b)** Qualitative comparison of *eps* expression by strains Δ*tasA*$_{anc}$, Mt1a and Δ*tasA*Δ*ptpZ*. The experiment was performed as in (a), with all strains carrying P$_{eps}$-*gfp* and constitutive mKate reporter. Scale bar = 2 mm. Similar result was obtained in 3 independent experiments each containing 3 biologically independent samples. **(c)** Expression of *tapA-sipW-tasA* operon in Δ*eps*$_{anc}$ and six evolved isolates that showed either improved or ancestor-like surface-colonizing properties was compared using corresponding strains carrying P$_{tapA}$-*gfp* reporter fusions (n = 8 biologically independent samples). Data points represent the mean and error bars represent standard error.

a

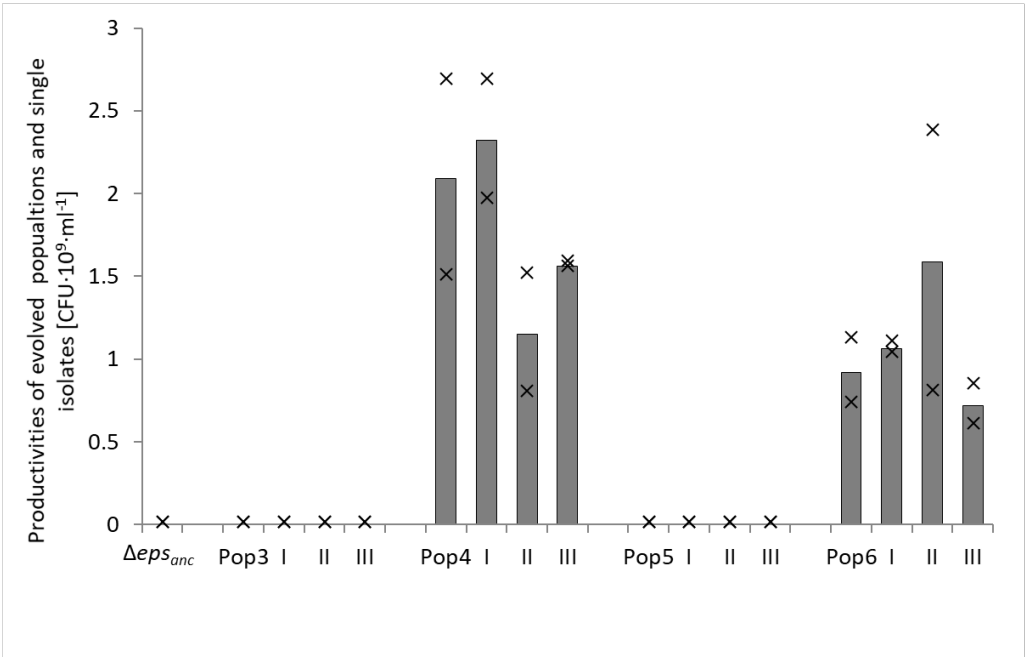

b

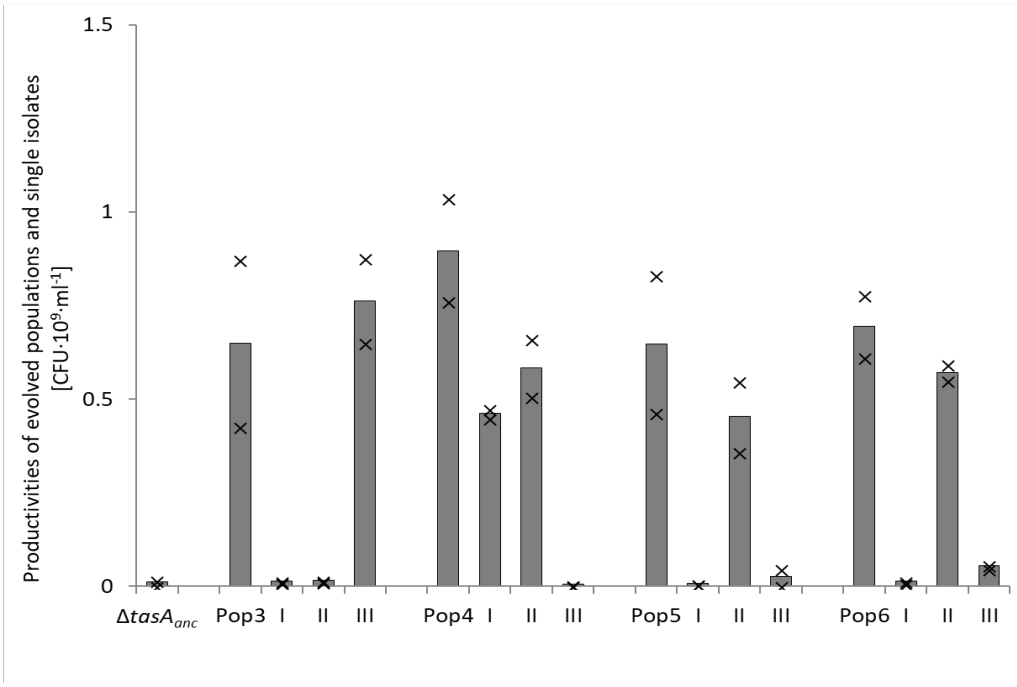

Supplementary Fig. 9 | Population structure of the evolved Δ*eps* and Δ*tasA* populations. (a) Four independently evolved Δ*eps* populations (Δ*eps*3, Δ*eps*4, Δ*eps*5, Δ*eps*6) were examined for diversity at the productivity level within the population. Specifically, three randomly selected isolates from each population were allowed to form pellicles that were examined for productivity (CFU/ml) (n = 2 biologically independent samples). **(b)** Four independently evolved Δ*tasA* populations (Δ*tasA*3, Δ*tasA*4, Δ*tasA*5, Δ*tasA*6) were examined for diversity at the productivity level within the population. Specifically, three randomly selected isolates from each population were allowed to form pellicles that were examined for productivity (CFU/ml) (n = 2 biologically independent samples).

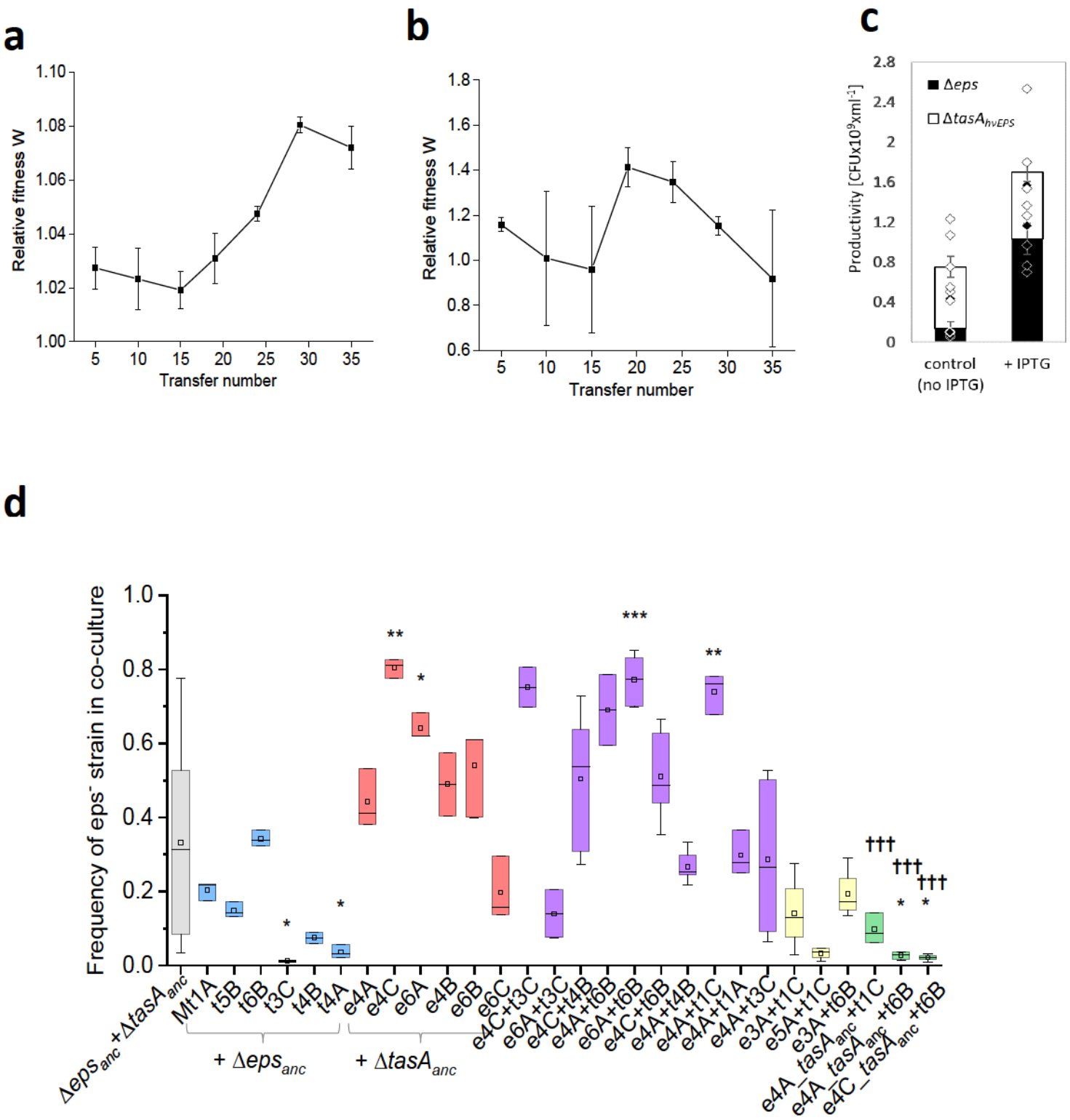
a
Relative fitness W
Transfer number
b
Relative fitness W
Transfer number
c
Δeps
ΔtasA hvEPS
Productivity [CFUx10^9xml^-1]
control (no IPTG)
+ IPTG
d
Frequency of eps- strain in co-culture
Δeps anc +ΔtasA anc
Mt1A
t5B
t6B
t3C
t4B
t4A
e4A
e4C
e6A
e4B
e6B
e6C
e4C+t3C
e6A+t3C
e4C+t4B
e4A+t6B
e6A+t6B
e4C+t6B
e4A+t4B
e4A+t1C
e4A+t1A
e4A+t3C
e3A+t1C
e5A+t1C
e3A+t6B
e4A_tasA anc +t1C
e4A_tasA anc +t6B
e4C_tasA anc +t6B
+ Δeps anc
+ ΔtasA anc

Supplementary Fig. 10 |Productivity, fitness and frequencies of the ancestral and evolved Δ*eps* and Δ*tasA* in different Δ*eps*+Δ*tasA* mixes. (a) Changes in fitness in Δ*eps*6 population thorough evolutionary time when challenged with Δeps_{anc} under pellicle biofilm forming conditions (n = 4 biologically independent samples). Data points represent the mean and error bars represent standard error. **(b)** Changes in fitness in Δ*tasA3* population thorough evolutionary time when challenged with $\Delta tasA_{anc}$ under pellicle biofilm forming conditions (n = 4 biologically independent samples). Data points represent the mean and error bars represent standard error. **(c)** Productivity of Δ*eps* and $\Delta tasA_{hyEPS}$ in mixed pellicles was accessed in presence of IPTG (EPS-overproduction by Δ*tasA* induced) and without IPTG (n=6 biologically independent samples). Data points represent the mean and error bars represent standard error. **(d)** Effects of evolutionary advantage of Δ*eps* or Δ*tasA* on final Δ*eps* frequency in the mixed pellicle. Pellicles formed by: Δeps_{anc}+$\Delta tasA_{anc}$ (grey), Δeps_{anc}+$\Delta tasA_{evolved}$ (blue), $\Delta eps_{evolved}$+$\Delta tasA_{anc}$ (red), $\Delta eps_{evolved}$+$\Delta tasA_{evolved}$ (purple), $\Delta eps_{evolved}$+$\Delta tasA_{evolved}$ where $\Delta eps_{evolved}$ did not show improve surface colonization properties and did not carry TasA_Cys variant (yellow) and $\Delta eps_{evolved}$+$\Delta tasA_{evolved}$ where TasA_Cys in $\Delta eps_{evolved}$ was replaced by native TasA variant (see methods). Boxes represent Q1–Q3, lines represent the median, and bars span from max to min (for Δeps_{anc}+$\Delta tasA_{anc}$ co-culture n = 22; for e4C:t4B, e4C:t6B, e6A:t6B, e4A:t4B and e4A:t3C, n = 6; for e4C:t3C, e6A:t3C and e4A:t6B, n = 2; for other co-cultures n = 3 biologically independent samples). Asterisks indicate statistically significant differences from the ancestral mix (*$p < 0.05$; **$p < 0.01$, ***$p < 0.001$; t-test, two-tail). Crosses indicate statistically significant differences from the corresponding mix where $\Delta eps_{evolved}$ strain still carries TasA_Cys variant (†††$p < 0.001$; t-test, two-tail).

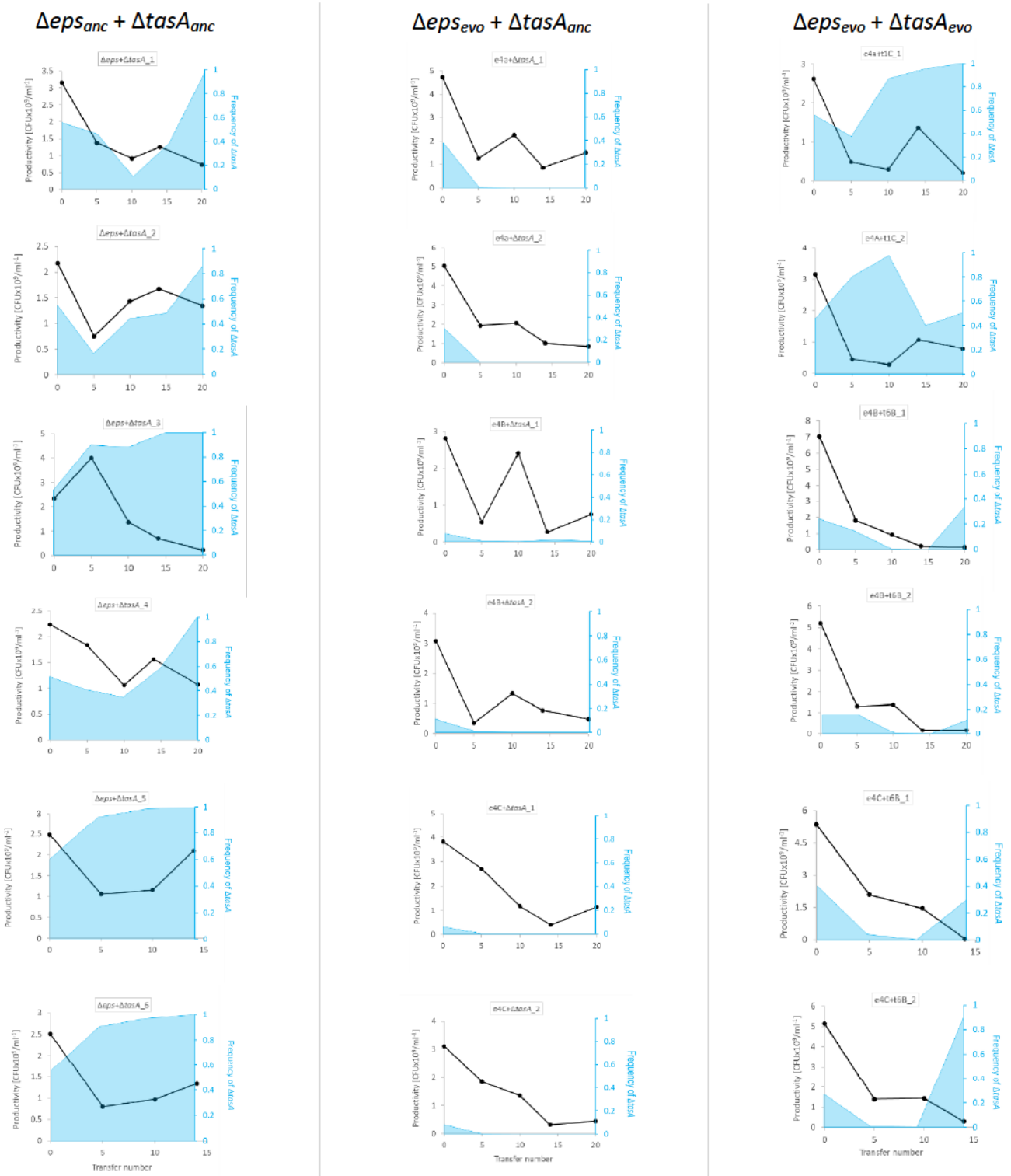

Supplementary Fig. 11 | Co-evolution in co-cultures of Δ*eps* and Δ*tasA* with similar or different evolutionary histories. Six parallel Δeps_{anc}+$\Delta tasA_{anc}$ co-cultures, six parallel $\Delta eps_{evolved}$+$\Delta tasA_{anc}$ co-cultures and six parallel $\Delta eps_{evolved}$+$\Delta tasA_{evolved}$ co-cultures were initiated from fresh stocks and subjected to co-evolution. Pellicle productivities and relative frequencies of Δ*eps* and Δ*tasA* in the mixes were systematically monitored every 5th transfer (as CFU/ml) Relative frequency of the Δ*tasA* strain at each evolutionary time point is shown as a blue area chart. Data for each biological replicate are presented on separate graph.

Supplementary Dataset 1 | List of mutations detected in evolved single isolates and populations. Mutations were divided into 4 different categories, each presented in separate datasheet: common SNPs - SNPs detected in all single isolates that were sequenced in this study; unique for Δ*eps* – mutations detected only in evolved Δ*eps* strains (SNPs resulting in substitutions to cysteine in TasA were highlighted in yellow); unique for Δ*tasA* – mutations detected only in evolved Δ*tasA* strains; randomly occurring – mutations that could be detected in both types of biofilm mutants (Δ*eps* or Δ*tasA)* but not in all sequenced isolates. Additionally, data for resequenced populations of Δ*eps* and Δ*tasA* from different evolutionary time points (5,14,24) are presented on separate sheet. Except from the mutations listed at the 'resequenced populations (mix)' sheet, all the populations contained nearly all SNPs listed in 'common SNPs' sheet.

Supplementary Movie 1 | Effects of cysteine-containing TasA on wetting behaviour of *B. subtilis* pellicles. Pellicles of WT, Δ*tasA*_$tasA_{anc}$ (strain with *tasA* knockout, complemented with native *tasA* gene in the *amyE* locus), Δ*tasA*_$tasA_{Y124C}$ (Δ*tasA* complemented with $tasA_{Y124C}$) and Δ*tasA*_$tasA_{G183C}$ (Δ*tasA* complemented with $tasA_{Y124C}$) were grown for 48h at 30°C. Next, 50 µl water droplet was gently spotted on pellicle surface to examine its wetting properties (upper panel). To minimize the potential effects of pellicle stretching under the weight of the droplet, the same assay was performed on the corresponding pellicles resting on the glass slides (bottom panel). Both assays suggest that WT and Δ*tasA*_$tasA_{anc}$ pellicles are hydrophobic, while pellicles formed by Δ*tasA*_$tasA_{Y124C}$ and Δ*tasA*_$tasA_{G183C}$ have increased porosity. Scale bar indicates 10 mm. Similar result was obtained in 2 independent experiments each containing 3 biologically independent samples.

Supplementary Results 1 |Negative effects of cysteine-containing TasA in EPS-proficient background. Morphologies and productivities of pellicles formed by the WT, and Δ*tasA* strain complemented either with native TasA variant (control) or with cysteine-containing TasA variant (Y124C or G183C) were examined. Surprisingly, in EPS-proficient background, the evolved TasA variants did not have positive effects on biofilm productivity and in the case of strain Δ*tasA*_$tasA_{G183C}$, the effects on fitness even appeared negative (Supplementary Fig. 5A). The pellicle formed by this strain showed a lack of surface complexity (Supplementary Fig. 5B). When magnified, the pellicle surfaces of Δ*tasA*_$tasA_{Y124C}$ and Δ*tasA*_$tasA_{G183C}$ appeared more "slimy" than those of the WT or Δ*tasA*_$tasA_{anc}$ (Supplementary Fig. 5B). Moreover, the pellicles formed by the strains with cysteine-containing TasA completely lost their water repellence (Supplementary Fig. 5C). We could not determine whether the biofilm material lost its hydrophobicity, because the droplet immediately penetrated through the Δ*tasA*_$tasA_{Y124}$ and Δ*tasA*_$tasA_{G183C}$ pellicles (Supplementary Movie 1) suggesting a porous microstructure. Alternatively, Δ*tasA*_$tasA_{Y124}$ and Δ*tasA*_$tasA_{G183C}$ biofilms could suffer from premature disassembly. If so, the water repellency of early pellicles (24 h) of Δ*tasA*_$tasA_{Y124}$ and Δ*tasA*_$tasA_{G183C}$ should be similar to those of the WT and Δ*tasA*_$tasA_{anc}$. Premature disassembly could also manifest in earlier entry into sporulation, resulting in an increased spore content in Δ*tasA*_$tasA_{Y124}$ and Δ*tasA*_$tasA_{G183C}$ biofilms. Both scenarios were tested, but the results contradicted the hypothesis of premature disassembly of Δ*tasA*_$tasA_{Y124}$ and Δ*tasA*_$tasA_{G183C}$ (Supplementary Fig. 5E–F). In addition, cysteine-containing TasA was disadvantageous when *B. subtilis* was cultivated in a colony biofilm setup, as surface spreading of Δ*tasA*_$tasA_{Y124C}$ and Δ*tasA*_$tasA_{G183C}$ colonies was limited (Supplementary Fig. 6).

Supplementary Results 2 | Potential role of BslA-TasA interaction in pellicle formation by evolved Δ*eps*.

Recently, it was shown that the main biofilm hydrophobin, BslA, carries a conserved CXXC motif on its C-terminal tail, which is crucial for protein oligomerization and therefore the hydrophobicity of *B. subtilis* biofilms [3]. As TasA and BslA are major extracellular proteins of the biofilm matrix, these components might interact, and the mat formed by e4A and e6A might depend on TasA-BslA contact. Indeed, deletion of *bslA* in the e4A background completely abolished pellicle formation (Supplementary Fig. 5d), suggesting that $TasA_{Y124C}$ might interact with BslA. However, the performance of e6A was unaltered in the Δ*bslA* background, suggesting that $TasA_{G183C}$ relies instead on homo-oligomerization (Supplementary Fig. 5d). Importantly, expression of *bslA* was previously reported to be influenced by Δ*epsA* mutation (up- or downregulated depending on the strain) [4,5]; therefore, the stoichiometric ratio of TasA to BslA might be also altered compared to the WT strain.

Supplementary Results 3 | Potential role of mutation in *ptpZ* in fitness increase of evolved Δ*tasA*.

A frame-shift mutation or non-synonymous substitution in *ptpZ* gene were identified in the evolved Mt1a and t5B genomes, respectively (Supplementary Table 1). This gene encodes for phosphotyrosine protein phosphatase, which is involved in biofilm regulation [6]. Indeed, deletion of the *ptpZ* gene in the $\Delta tasA_{anc}$ background could partially restore pellicle formation (Fig. 4c–d) and resulted in nearly identical, complex colony morphology to that observed for Mt1a (Supplementary Fig. 8b). However, as PtpZ affects biofilm formation via posttranslational regulation [7], strain Δ*tasA*Δ*ptpZ* did not exhibit increased *epsA–O* expression (Supplementary Fig. 8b).

References

1. Konkol, M. A., Blair, K. M. & Kearns, D. B. Plasmid-encoded ComI inhibits competence in the ancestral 3610 strain of *Bacillus subtilis*. *J. Bacteriol.* **195,** 4085–4093 (2013).
2. Murray, E. J., Kiley, T. B. & Stanley-Wall, N. R. A pivotal role for the response regulator DegU in controlling multicellular behaviour. *Microbiology* **155,** 1–8 (2009).
3. Arnaouteli, S. *et al.* Bifunctionality of a biofilm matrix protein controlled by redox state. *Proc. Natl. Acad. Sci. U. S. A.* **114,** E6184–E6191 (2017).
4. Verhamme, D. T., Murray, E. J. & Stanley-Wall, N. R. DegU and Spo0A jointly control transcription of two loci required for complex colony development by *Bacillus subtilis*. *J. Bacteriol.* **191,** 100–8 (2009).
5. Kovacs, A. T. & Kuipers, O. P. Rok regulates *yuaB* expression during architecturally complex colony development of *Bacillus subtilis* 168. *J. Bacteriol.* **193,** 998–1002 (2011).
6. Gao, T., Greenwich, J., Li, Y., Wang, Q. & Chai, Y. The bacterial tyrosine kinase activator TkmA contributes to biofilm formation largely independently of the cognate kinase PtkA in *Bacillus subtilis. J. Bacteriol.* **197,** 3421–32 (2015).
7. Kiley, T. B. & Stanley-Wall, N. R. Post-translational control of *Bacillus subtilis* biofilm formation mediated by tyrosine phosphorylation. *Mol. Microbiol.* **78,** 947–963 (2010).

Supplementary data set and video can be found at https://www.nature.com/articles/s41564-018-0263-y#Sec24

Supporting information for Chapter 6

Cheater-mediated evolution shifts phenotypic heterogeneity in *Bacillus subtilis* biofilms

Submitted to The ISME Journal (2019)

Deposited in bioRxiv (2019)

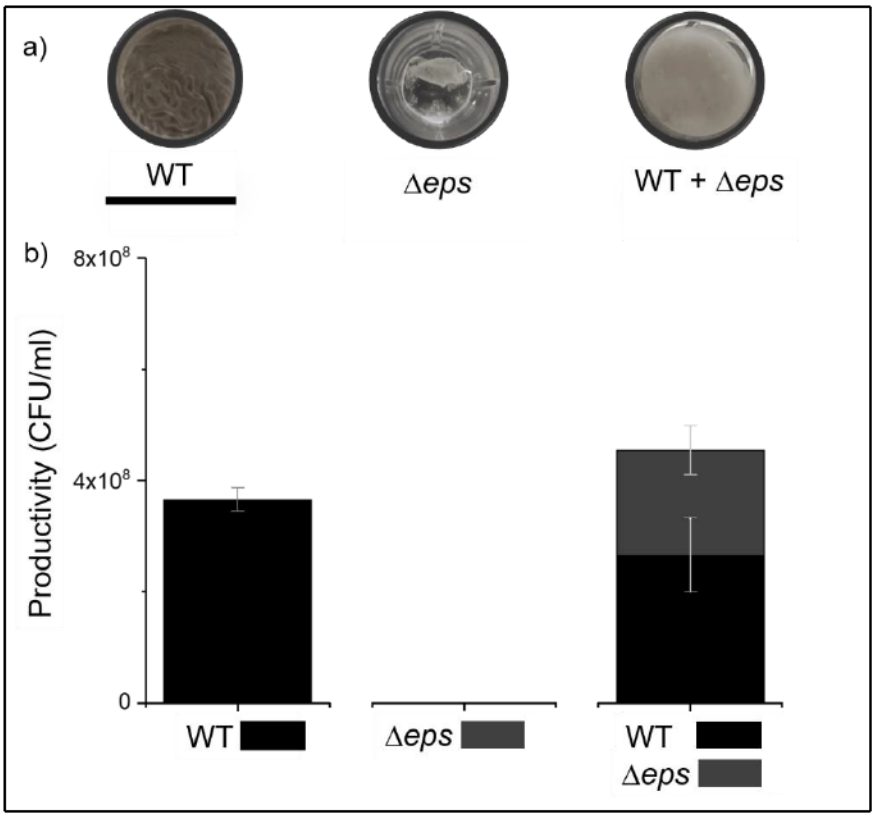

Supplementary Fig. 1. Pellicle biofilm formation and total productivity assessment. **a)** Pellicle biofilms formed by mono-cultures of WT, Δ*eps,* and co-culture of WT+ Δ*eps* in 2xSG medium incubated for 48 hours at 30°C recorded using Samsung Galaxy S6 Phone Camera. Scale bar, 1cm. **b)** Productivity assessment based on CFU/ml were performed on pellicle biofilms of WT, Δ*eps,* and WT+ Δ*eps* co-culture. Productivity of Δ*eps* dramatically increased when co-cultured with WT, while productivity of WT decreased in the presence of Δ*eps*, thus suggesting the ability of the mutants to act as cheaters. (n=3, error bar based on Standard Error)

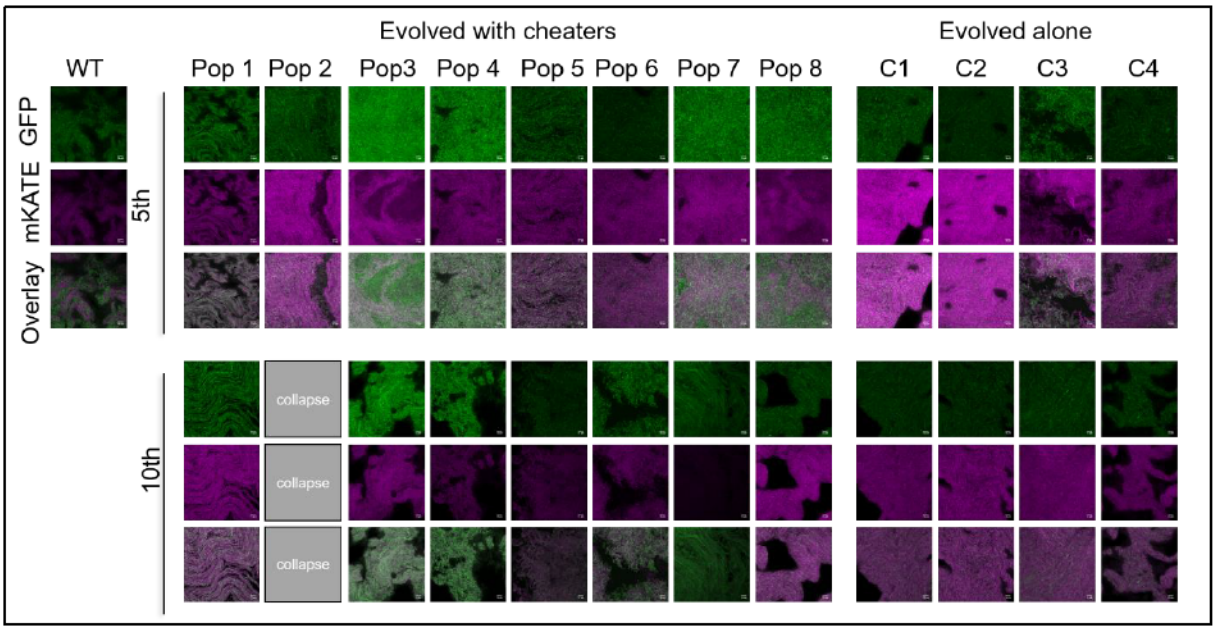

Supplementary Fig. 2. Qualitative assessment of *eps* gene expression based on confocal laser scanning microscopy. Pellicles formed by WT strain 168 mKATE P*eps*-GFP (TB869) **a)** non-evolved **b)** single clones of mono-culture of WT strains 168 mKATE P*eps*-GFP (TB869) that were evolved (Pop 1-8) in the presence of cheaters and **c)** in the absence of cheaters (Pop C1-C4) viewed under the confocal laser scanning microscope. Cells constitutively expressing mKATE are represented in magenta (OFF cells) and *eps* expressing cells (ON cells) are represented in green. Scale bar 10µm.

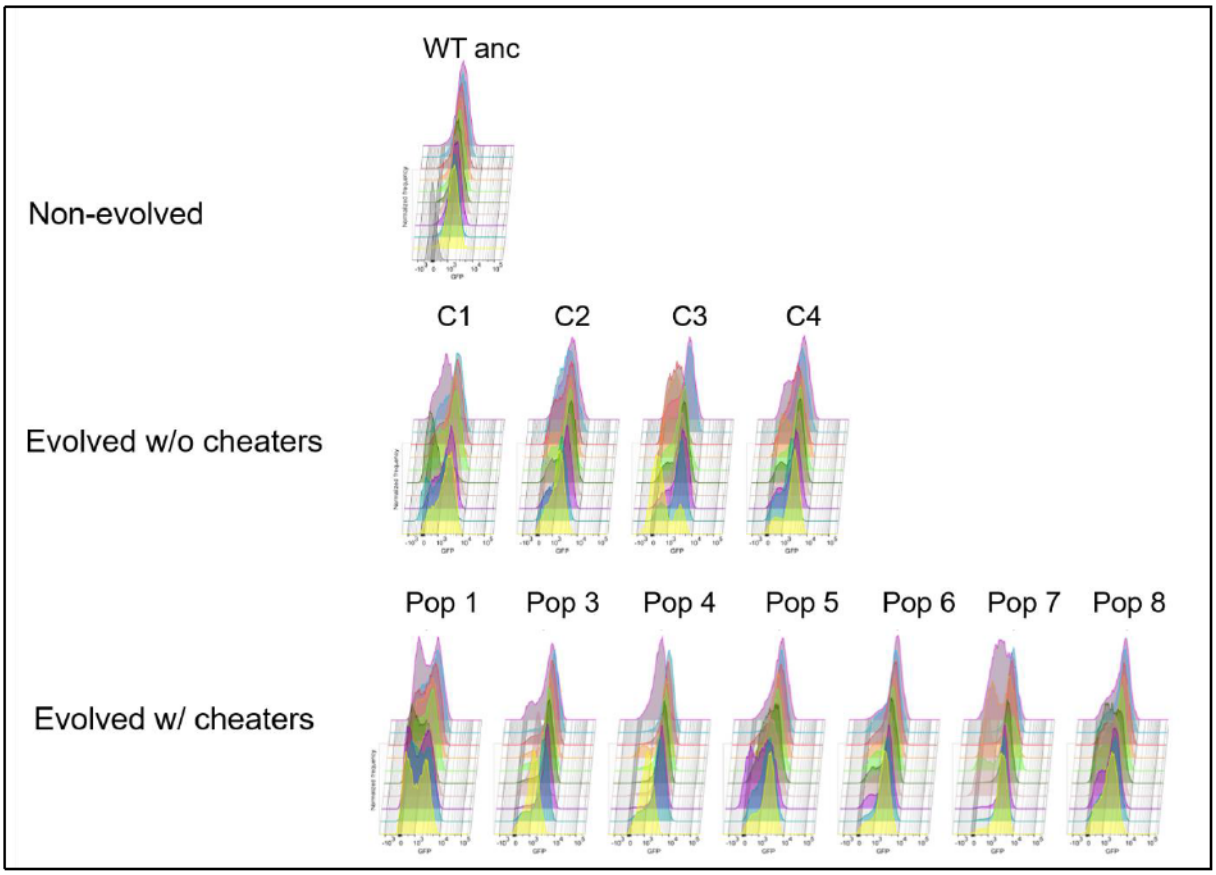

Supplementary Fig. 3. Flow cytometry data showing distributions of fluorescence intensity median of 24-hour old pellicles established by randomly selected single isolates from populations of WT evolved in the absence (4 populations) or presence of cheaters (7 populations) that were disrupted and diluted in comparison to WT non-labelled and WT ancestor as controls.

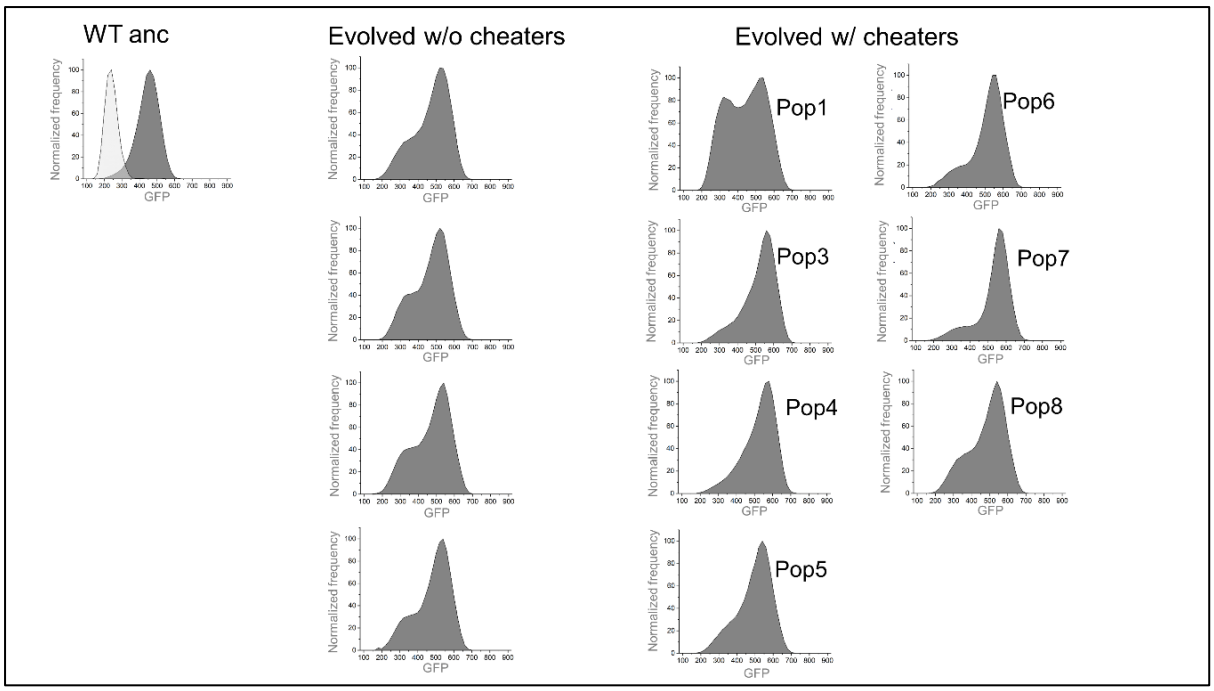

Supplementary Fig. 4. Flow cytometry data showing averaged (n=10) distributions of fluorescence intensity median of 24-hour old pellicles established by populations of WT evolved in the absence (4 populations) or presence of cheaters (7 populations) that were disrupted and diluted in comparison to WT non-labelled and WT ancestor as controls. Averaged histograms were obtained by averaging histograms obtained for different single isolates derived from the same population (specifically, by extracting the average count for each bin).

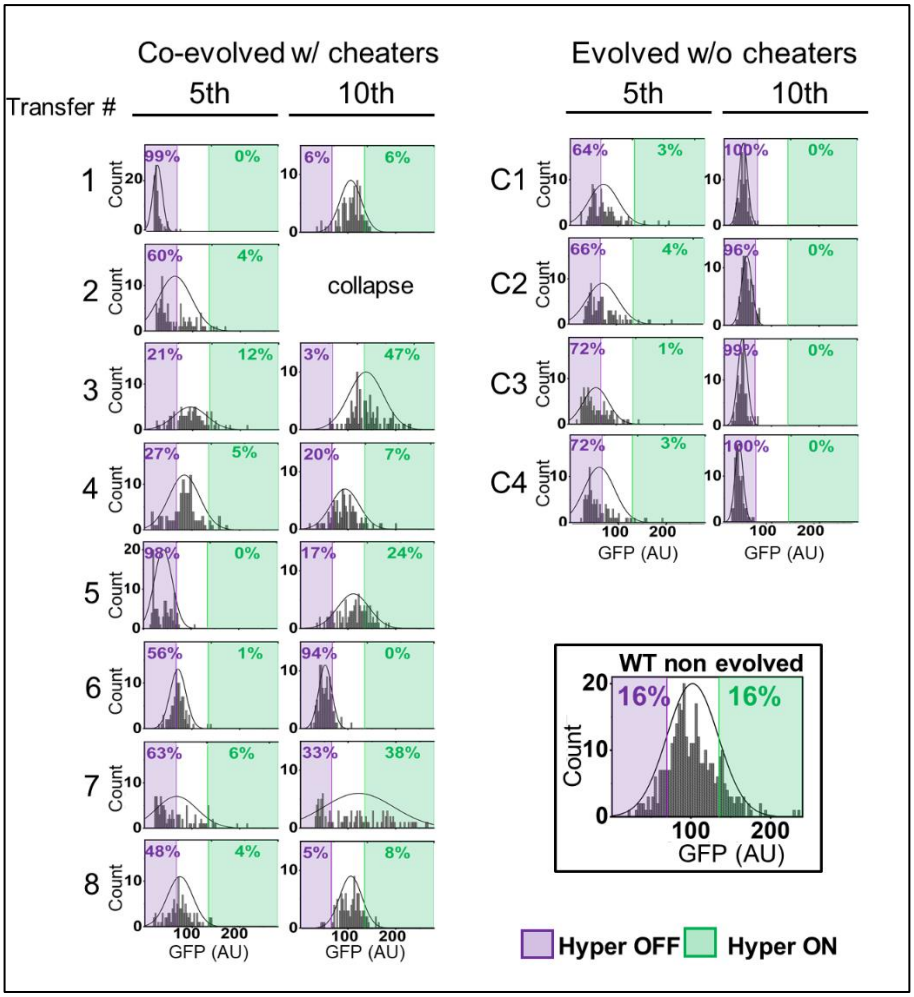

Supplementary Fig. 5. Quantitative assessment of hyper ONs and hyper OFFs present per evolved population. Ninety-five single clones from each population of mono-cultures of WT co-evolved in the presence of cheaters were allowed to form one-day-old pellicles in the absence of cheaters. Each pellicle was vortexed, bath sonicated and subjected to fluorescence measurement using TECAN Infinite F200 PRO microplate reader. Percentage of isolates >134 AU value expressing high intensity level of P_{eps}-GFP (hyper ON) and low intensity value of < 70 AU (hyper OFF) is represented in histogram for WT evolved and non-evolved strains per timepoint from 5th to 10th transfer for all 8 populations evolved in the presence cheaters and 4 populations evolved alone (n=95). Cut off based on the mean ± 1SD of WT ancestor strain taken at six different days (n=336).

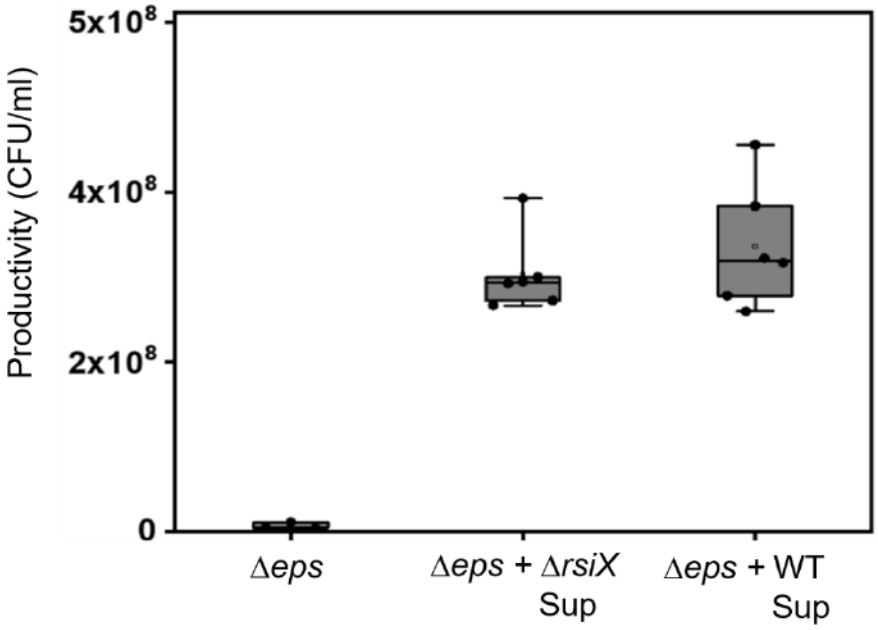

Supplementary Fig. 6. Complementation assay of Δ*eps* with supernatant from Δ*rsiX* or WT. Productivity data of pellicles produced by the complementation showed that hyper ON Δ*rsiX* mutant does not contribute to improved performance of Δ*eps*. Mean is represented in square inside the box plots; median is denoted by horizontal line within the boxes; whiskers represent the min and max; single dots symbolize the individual data points (n).

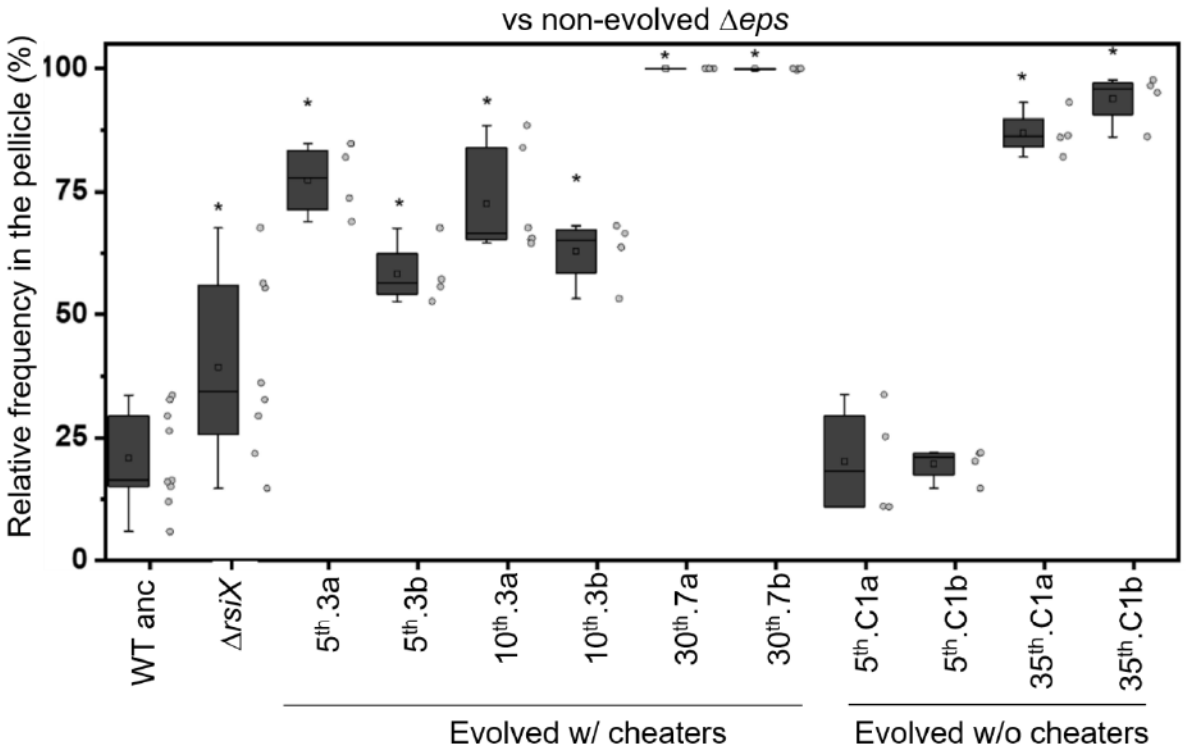

Supplementary Fig. 7. Pellicle competition assay of single clones belonging to producer populations (non-evolved (n=9), Δ*rsiX* (n=8), evolved with (n=4) and without cheaters (n=4)) against Δ*eps* ancestor. Mean is represented in square inside the box plots; median is denoted by horizontal line within the boxes; whiskers represent the min and max; single dots represent the individual data points (n); asterisk (*) represents the significant difference from the WT ancestor ANOVA (P value 0.05).

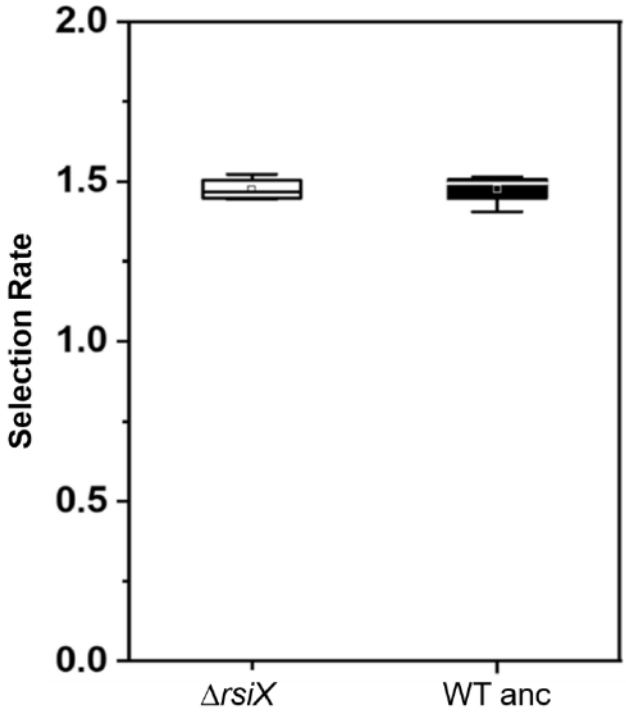

Supplementary Fig. 8. Selection rate based on fitness assay in pairwise competition of Δ*rsiX* and WT ancestor showing no significant fitness cost brought about by *rsiX* mutation. Relative fitness of Δ*rsiX* is 1.00 ± 0.024 SD. Mean is represented in square within the boxplots; median is denoted by horizontal line inside the boxes; whiskers represent the min and max.

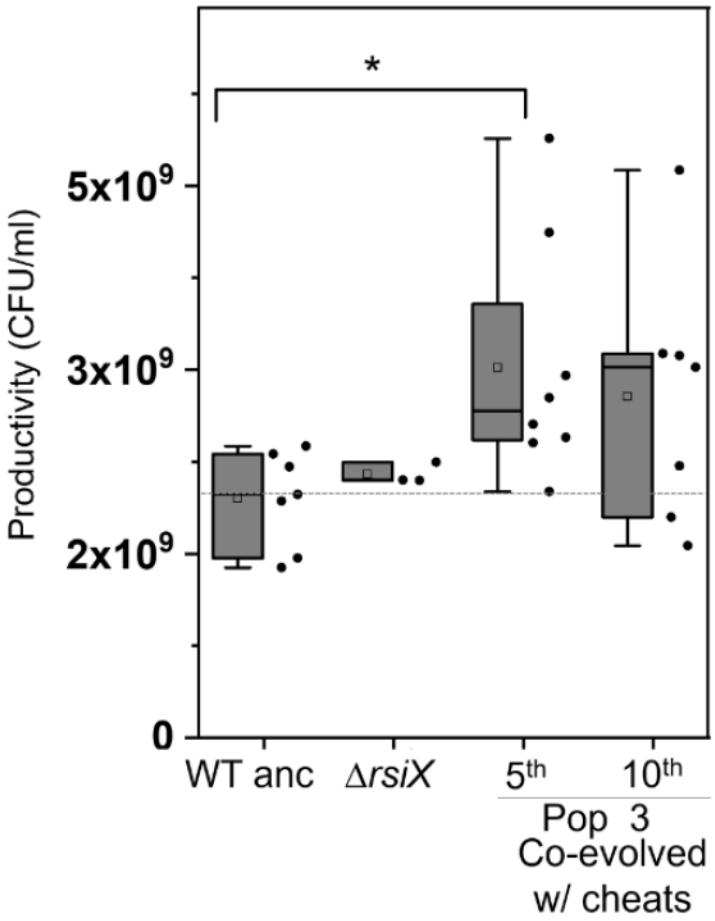

Supplementary Fig. 9. Pellicle productivity of monocultures. Total CFU/ml of pellicles produced by mono-cultures of WT ancestor (n=7), Δ*rsiX* (n=3) and evolved with cheaters (n=8) from population 3 (5^{th}, $10^{th)}$ and 7 (30^{th}) and single clones of WT evolved without cheaters (n=4). Mean is represented in square; median is denoted by horizontal line inside the box; whiskers represent the min and max; single dots represent the individual data points (n); asterisk (*) represents the significant difference based on ANOVA (P value 0.05).

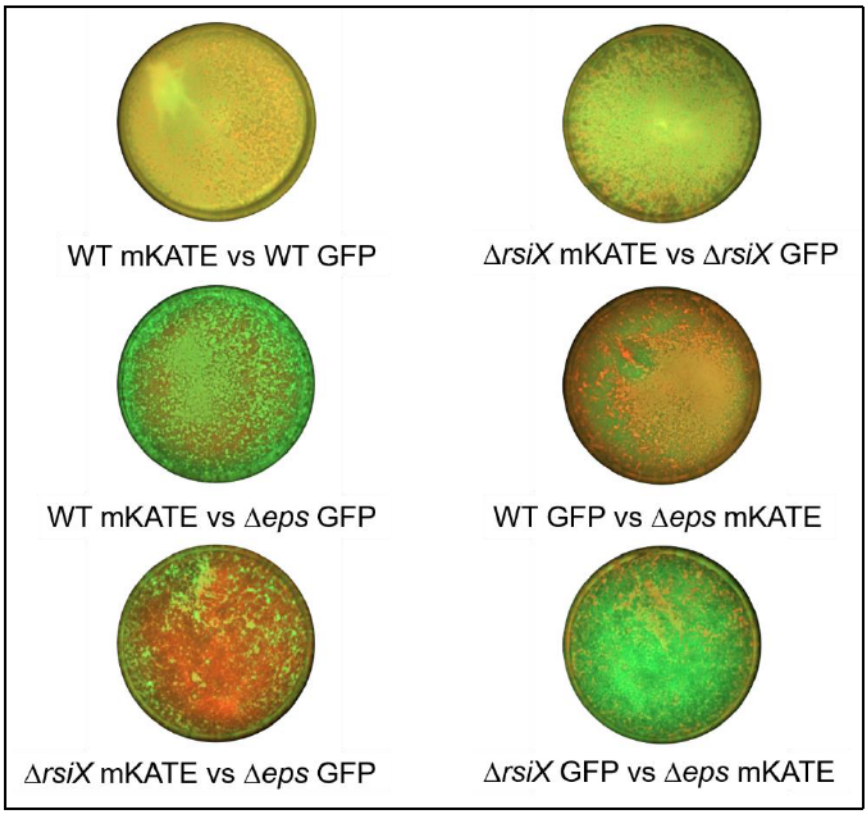

Supplementary Fig. 10. Competition assay between fluorescently WT vs Δ*eps* and Δ*rsiX* vs Δ*eps*. Strains labelled with constitutively expressed GFP and mKate proteins, were inoculated in 1:1 initial frequency, pellicles were cultivated for 48h at 30^{0}C and visualized using stereomicroscope. Upper panels represent controls (two isogenic WT or Δ*rsiX* strains labelled with different fluorescent markers), middle panel represents pellicles formed by WT vs Δ*eps* and bottom panels represent pellicles formed by Δ*rsiX* vs Δ*eps,* each in two alternative combinations of fluorescent markers. Well size = 1.5cm.

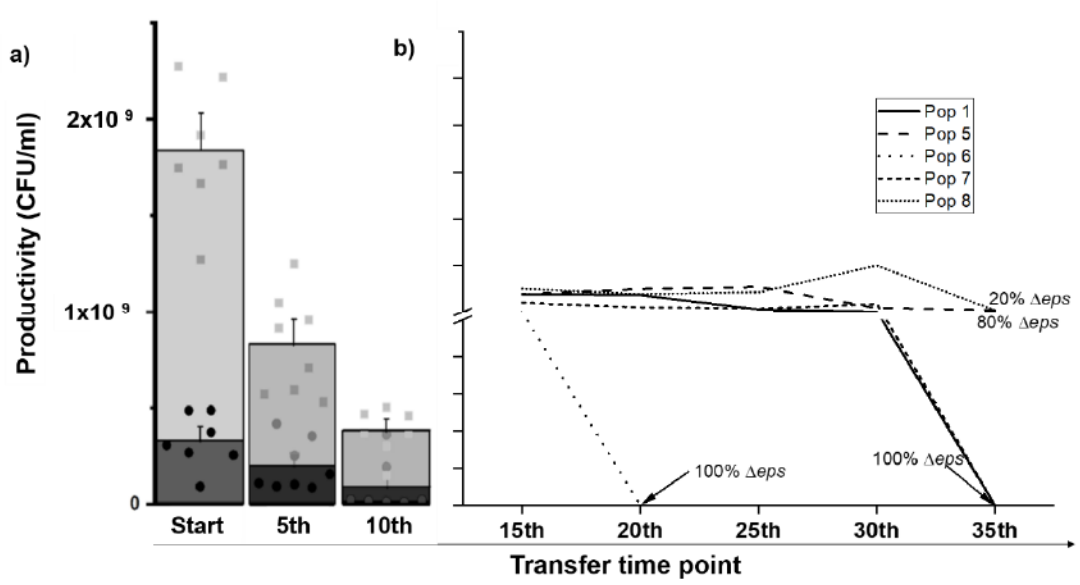

Supplementary Fig. 11. Pellicle productivity. Total colony forming unit per ml of WT and Δ*eps* in 48-hour old pellicles **a)** non-evolved (Start) (n=9), after experimental evolution at 5th (n=8 populations) and 10th transfer (n=7 populations) One population after 10th transfer was incapable to form pellicle attributed to WT being totally outnumbered by Δ*eps*. **b)** Line graph showing the fate of populations Data were obtained from plate count assay using selective antibiotic marker, Kanamycin for selecting WT strains and Tetracycline for selecting Δ*eps.*

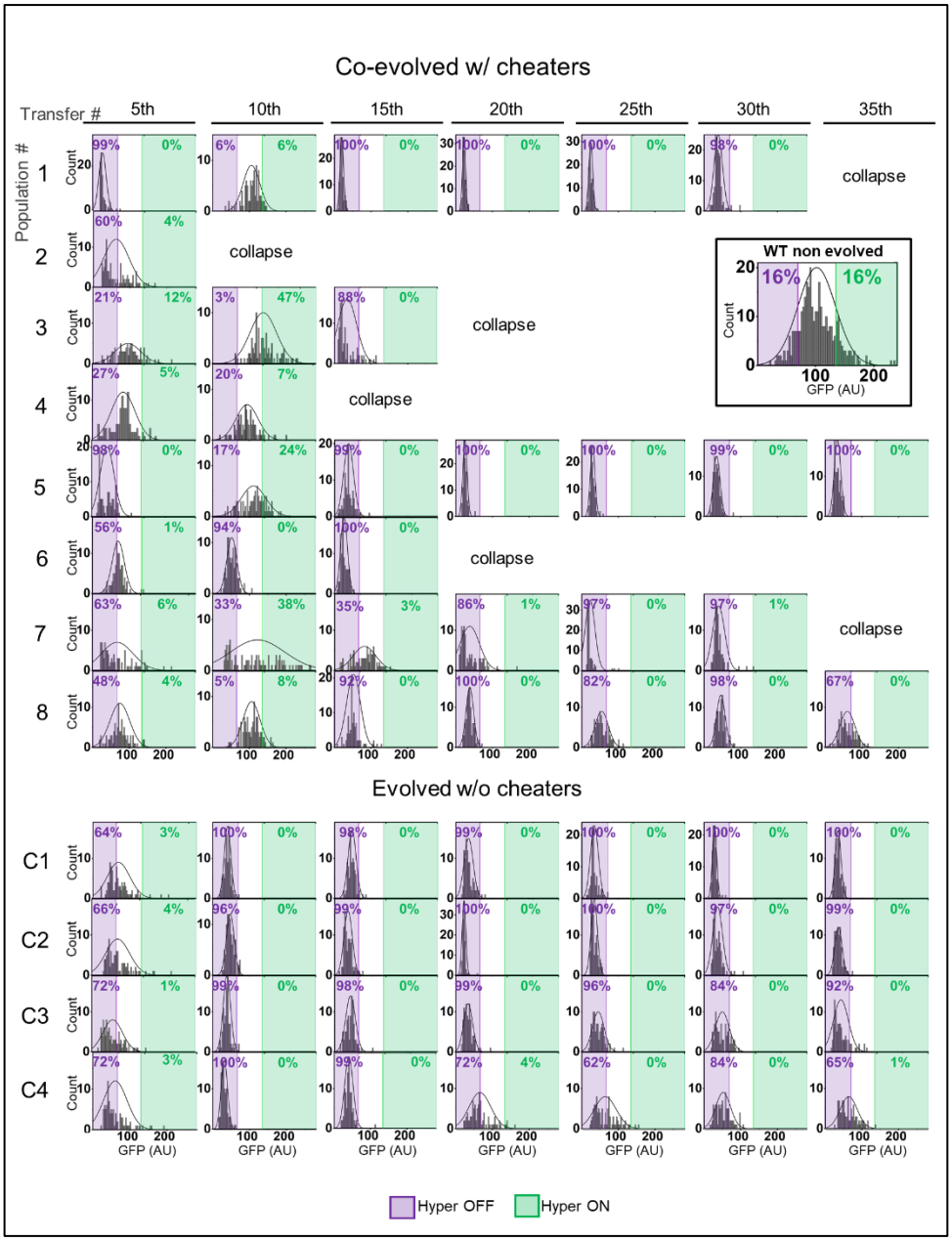

Supplementary Fig. 12. Quantitative assessment of hyper ONs and hyper OFFs present per evolved population. Percentage of isolates with hyper ON and hyper OFF represented in histogram for WT evolved and non-evolved strains per timepoint from 5th to 35th transfer for all 8 populations evolved in the presence of cheaters and 4 populations evolved alone (n=95). Cut off based on the mean ± 1SD of WT ancestor strain taken at six different days (n=336).

Supplemental Data Set 1

COMMON SNPs

Reference position	Type	Coding region	AA change	Overlapping Annotation	Function	Evolved Strain		
						Population	Transfer number	Evolution set-up
2414375	SNV	317T>C	Val106Ala	*rsiX*	control of SigX activity (cell envelope stress response)	3	5th, 10th	WT co-evolved with cheaters
2414377	SNV	315T>C	--					
2414384	Insertion	308_309insC	Ser104fs					
2413653	Deletion	1039delA	Ile347fs			7	30th	
2414092	Deletion	600delA	Lys200fs			1	30th	WT evolved alone
980633	Deletion	161delC	Ala54fs	*yhcE*	ABC transporter (membrane protein)	7	30th	WT co-evolved with cheaters
981069	SNV	597G>A	Trp199*			1	5th	WT evolved alone
981069	SNV	597G>A	Trp199*			1	30th	
1471547	SNV	1522C>T	Gln508*	*kinA*	initiation of sporulation	7	30th	WT co-evolved with cheaters
1471598	SNV	1573G>A	Gly525Arg			8	30th	
1471564	SNV	1539A>T	Leu513Phe			4	25th	WT evolved alone
1471121	SNV	1096G>A	Gly366Ser			1	30th	
1612774	SNV	254C>T	Ser85Phe	*divIVA*	septum placement	7	30th	WT co-evolved with cheaters
1612774	SNV	254C>T	Ser85Phe			1	30th	WT evolved alone
3407265	SNV	1092G>T	Leu364Phe	*yvrG*	regulation cell surface maintenance	8	30th	WT co-evolved with cheaters
3406906	SNV	1451G>T	Gly484Val			4	25th	WT evolved alone
1112663	SNV	1256T>C	Val419Ala	*hemAT*	movement towards oxygen	1	30th	WT evolved alone

Unique for WT co-evolved with cheaters

Reference position	Type	Coding region	AA change	Overlapping Annotation	Function	Evolved Strain		
						Population	Transfer number	Evolution set-up
3922789	SNV	175T>G	Phe59Val	*ywcC*	control of SlrA expression	7	30th	WT co-evolved with cheaters
123314	SNV	1396C>G	Gln466Glu	*rpoB*	transcription			
127020	SNV	1459C>A	Pro487Thr	rpoC	transcription			
1980287	SNV	2262C>T	--	*ppsC*	production of the antibacterial compound plipastatin	2	5th	
1995669	SNV	2289G>A	--	*ppsA*	production of the antibacterial compound plipastatin			
1995672	SNV	2286A>G	--					
1995696	SNV	2262A>C	--					
3666267	SNV	639C>T	--	*gtaB*	biosynthesis of teichoic acid	8	30th	
3666282	SNV	654A>G	--					
3673211	SNV	283A>G	Ile95Val	*yvzE*	unknown			
3673230	SNV	302A>G	Asp101Gly					

Unique for WT evolved alone								
Reference position	**Type**	**Coding region**	**AA change**	**Overlapping Annotation**	**Function**	**Evolved Strain**		
						Population	**Transfer number**	**Evolution set-up**
1231276	Deletion	194delA	Ala68fs	*pepF*	protein degradation	1	5th	WT evolved alone
1424253	SNV	182A>T	Lys61Ile	*mtnK*	methionine salvage			
1511746	SNV	439A>G	Lys147Glu	*sipT*	protein secretion			
1709323	SNV	1610C>T	Thr537Met	*flhA*	export of flagellum components			
2426968	SNV	102G>A	--	*ypuF*	unknown			
3101174	SNV	294T>C	--	*melA*	melibiose utilization			
300013	Insertion	490_491insA	Ile164fs	*ycdA*	swarming motility	4	25th	
1012090	SNV	1169G>A	Trp390*	*lytF*	cell separation	1	30th	
1863010	SNV	19A>G	Ile7Val	*ymzE*	unknown		30th	
2350091	SNV	2376C>T	--	*dinG*	response to DNA damage			
2636152	SNV	988G>A	Glu330Lys	*holA*	DNA replication	1	5th ; 30th	
3039917	SNV	15G>A	--	*acsA*	utilization of acetate, fatty acids	1	30th	
2417270	SNV	634G>A	Glu212Lys	*resD*	regulation of aerobic and anaerobic respiration			

Legend:

Hyper ON phenotype

Supplemental Data Set 2

Common SNPs

Reference Position	Type	Reference	Allele	Overlapping annotations	Amino acid change	Gene name	Product name
96240	SNV	G	A	non-coding			
96240	SNV	G	A	non-coding			
96260	SNV	G	A	non-coding			
165749	Deletion	C	-	non-coding			
165751	Deletion	C	-	non-coding			
165826	Insertion	-	C	non-coding			
166038	Insertion	-	T	non-coding			
166344	Deletion	G	-	non-coding			
171331	SNV	T	G	non-coding			
557866	Insertion	-	T	non-coding			
608215	Insertion	-	A	non-coding			
1317153	Insertion	-	GT	non-coding			
1317154	Insertion	-	T	non-coding			
2097081	Insertion	-	A	non-coding			
2271424	SNV	T	C	CDS: uvrX, Gene: uvrX		*uvrX*	UV-damage repair protein
2271505	SNV	C	T	CDS: uvrX, Gene: uvrX		*uvrX*	UV-damage repair protein
2271523	SNV	A	C	CDS: uvrX, Gene: uvrX	CAB14068.2:p.Asp45Glu	*uvrX*	UV-damage repair protein
2480646	MNV	TA	AT	non-coding			
2480654	Deletion	T	-	non-coding			
2480667	Deletion	T	-	non-coding			
2581727	Insertion	-	T	non-coding			
3770059	Insertion	-	A	non-coding			
3935823	Deletion	T	-	non-coding			
4155391	Insertion	-	A	non-coding			

Present in all WT population and absent in all Δ*eps* populations

Reference Position	Type	Reference	Allele	Overlapping annotations	Amino acid change	Gene name	Product name
328570	SNV	A	C	CDS: amyE, Gene: amyE	CAB12098.2:p.Glu318Ala	*amyE*	alpha-amylase
3530081	SNV	A	T	non-coding			
3679626	Insertion	-	T	CDS: tagE, Gene: tagE	CAB15590.1:p.Ser266fs	*tagE*	UDP-glucose:polyglycerol phosphate glucosyltransferase
3902306	SNV	C	A	CDS: sacA, Gene: sacA	CAB15830.2:p.Leu448Phe	*sacA*	phosphosucrase
3903814	SNV	T	A	CDS: sacP, Gene: sacP		*sacP*	sucrose-specific PTS permease, EIIBC component
3904116	MNV	GC	AA	CDS: sacP, Gene: sacP		*sacP*	sucrose-specific PTS permease, EIIBC component
3904123	SNV	G	A	CDS: sacP, Gene: sacP		*sacP*	sucrose-specific PTS permease, EIIBC component

Unique for WT populations without collapse

Reference Position	Type	Reference	Allele	Overlapping annotations	Amino acid change	Gene name	Product name	Pop5	Pop8
117039	SNV	T	G	CDS: sigH, Gene: sigH	CAB11874.1:p.Met147Arg	*sigH*	RNA polymerase sigma factor SigH		X
213822	SNV	G	A	non-coding				X	
368696	SNV	G	A	CDS: yckB, Gene: yckB	CAB12132.1:p.Leu55Phe	*yckB*	unknown		X
424357	SNV	T	G	CDS: yclH, Gene: yclH	CAB12181.1:p.Ile178Leu	*yclH*	ABC transporter ATP-binding protein	X	
1471598	SNV	G	A	CDS: kinA, Gene: kinA	CAB13272.1:p.Gly525Arg	*kinA*	two-component sensor kinase		X
1731633	SNV	G	A	Misc. RNA: surG, Gene: surG		*surG*		X	
3407265	SNV	C	A	CDS: yvrG, Gene: yvrG	CAB15311.2:p.Leu364Phe	*yvrG*	two-component sensor histidine kinase		X
3408346	SNV	C	T	CDS: yvrG, Gene: yvrG	CAB15311.2:p.Arg4Lys	*yvrG*	two-component sensor histidine kinase	X	
3646029	SNV	C	A	CDS: degS, Gene: degS	CAB15567.1:p.Gly170Cys	*degS*	two-component sensor histidine kinase	X	
3666267	SNV	C	T	CDS: gtaB, Gene: gtaB		*gtaB*	UTP-glucose-1-phosphate uridylyltransferase		X
3666282	SNV	A	G	CDS: gtaB, Gene: gtaB		*gtaB*	UTP-glucose-1-phosphate uridylyltransferase		X
3667410	SNV	A	T	CDS: ggaB, Gene: ggaB	CAB15585.1:p.Tyr834*	*ggaB*	galactosamine-containing minor teichoic acid biosynthesis		X
3673211	SNV	A	G	CDS: yvzE, Gene: yvzE	yvzE:p.Ile95Val	*yvzE*	putative UTP-glucose-1-phosphate uridylyltransferase		X
3673230	SNV	A	G	CDS: yvzE, Gene: yvzE	yvzE:p.Asp101Gly	*yvzE*	putative UTP-glucose-1-phosphate uridylyltransferase		X

Unique for WT populations with early collapse

Reference Position	Type	Reference	Allele	Overlapping annotations	Amino acid change	Gene name	Product name	Pop2	Pop4	Pop6
147575	SNV	G	C	non-coding				X		
1917461	Deletion	G	-	non-coding						X
1980287	SNV	G	A	CDS: ppsC, Gene: ppsC		*ppsC*	plipastatin synthetase	X		
1995696	SNV	T	G	CDS: ppsA, Gene: ppsA		*ppsA*	plipastatin synthetase	X		
2518342	SNV	T	C	CDS: spo0A, Gene: spo0A	CAB14353.1:p.His162Arg	*spo0A*	phosphorelay response regulator	X		
2552727	SNV	G	A	CDS: sinR, Gene: sinR		*sinR*	transcriptional regulator (Xre family) of post-exponential-phase responses genes	X		
2920854	SNV	A	T	CDS: yshE, Gene: yshE	CAB14817.1:p.Leu23His	*yshE*	unknown UPF0719 transmembrane protein			X

Unique for WT populations evolved alone											
Reference Position	Type	Reference	Allele	Overlapping annotations	Amino acid change	Gene name	Product name	Pop1	Pop2	Pop3	Pop4
116567	SNV	A	G	non-coding					X		
116946	SNV	A	G	CDS: sigH, Gene: sigH	CAB11874.1:p.Tyr116Cys	*sigH*	RNA polymerase sigma factor SigH			X	
247055	SNV	C	T	CDS: ybfK, Gene: ybfK	CAB12020.1:p.Ser133Phe	*ybfK*	carboxylesterase NP				X
300013	Insertion	-	T	CDS: ycdA, Gene: ycdA	CAB12072.1:p.Ile164fs	*ycdA*	lipoprotein, required for swarming motility				X
965908	SNV	C	T	non-coding							X
981117	SNV	G	A	CDS: yhcE, Gene: yhcE	CAB12733.1:p.Trp215*	*yhcE*	ABC transporter (membrane protein)			X	
981122	SNV	T	A	CDS: yhcE, Gene: yhcE	CAB12733.1:p.Leu217*	*yhcE*	ABC transporter (membrane protein)		X		
984338	SNV	T	G	CDS: cspB, Gene: cspB	CAB12738.1:p.Glu43Ala	*cspB*	major cold-shock protein		X		
1113473	SNV	T	C	CDS: hemAT, Gene: hemAT	CAB12878.1:p.Glu149Gly	*hemAT*	haem-based aerotactic transducer				X
1471564	SNV	A	T	CDS: kinA, Gene: kinA	CAB13272.1:p.Leu513Phe	*kinA*	two-component sensor kinase				X
1704100	SNV	G	A	CDS: cheY, Gene: cheY	CAB13506.1:p.Met89Ile	*cheY*	two-component response regulator		X		
1917467	SNV	T	C	non-coding					X		
2414092	Deletion	T	-	CDS: rsiX, Gene: rsiX	CAB14241.2:p.Lys200fs	*rsiX*	anti-SigX				X
2605441	SNV	C	T	CDS: ccpN, Gene: ccpN	CAB14454.1:p.Glu53Lys	*ccpN*	transcriptional regulator (CcpN family)	X			
2780825	SNV	C	T	CDS: yrhF, Gene: yrhF	CAB14663.1:c.69G>A	*yrhF*	unknown			X	
3210462	SNV	G	A	CDS: mcpB, Gene: mcpB	CAB15104.2:p.Gln658*	*mcpB*	methyl-accepting chemotaxis protein		X		
3406906	SNV	C	A	CDS: yvrG, Gene: yvrG	CAB15311.2:p.Gly484Val	*yvrG*	two-component sensor histidine kinase				X
3407274	SNV	A	C	CDS: yvrG, Gene: yvrG	CAB15311.2:p.Ile361Met	*yvrG*	two-component sensor histidine kinase		X		
3645818	SNV	A	T	CDS: degS, Gene: degS	CAB15567.1:p.Ile240Lys	*degS*	two-component sensor kinase for exoenzyme and competence regulation			X	

ACKNOWLEDGEMENT

This PhD journey is almost at the last phase. Honestly, it feels bitter-sweet as it has been like a roller coaster ride that I will never regret taking. I did find myself asking quite several times during this journey if I have made the right decision of taking this path. Often, I had to motivate and tell myself that "nothing worth having comes easy". It was a very different life from the career I have gotten used to for thirteen years. But just as what is implied in this dissertation, evolution is inevitable, and I am a not an exception. Those experiments that required me to work late nights, on many weekends and holidays, those late-night graph-wrestlings, all-day and night manuscript writing, nerve-wracking oral presentations in scientific meetings and conferences, the unlimited pursuit of scientific discoveries and learnings, and all the ups and downs of doing research have evolved me into a better person career-wise and personality-wise.

I am thankful to all those people who have been part of this extraordinary expedition with me. You all made this PhD path worth taking.

First and foremost to my supervisor and mentor Prof. Dr Akos T. Kovacs. It all started when you entrusted me the chance to do my M.Sc. thesis with you, which continued into a PhD study. I appreciate your trust in me, and I am grateful not only for your scientific advice and academic influence on me but also for being a very understanding and patient supervisor.

To all my colleagues in the Terrestrial Biofilms Group (TeBi - Jena) and the Bacterial Interactions and Evolution Group (BIE- Denmark) for making work fun and enjoyable through our social interactions in and out of the laboratory. For the cooperative interactions whether during a weekly task in the lab, sharing space in the biosafety hood, incubators, oven, agar media, or scientific brainstorming during group meetings. And of course, for sharing your baking and culinary talents during cake and picnic time in the kitchen, in the park or at the beach. For the competitive interactions (only) during gaming nights. I am very grateful for having met such amazing people like you.

To Dr Anna Dragos, all your helpful insights into my research and non-judgemental views and advice in life are very much appreciated. I had a great time with all those conferences and scientific events, not to mention the post-conference trips and the conference

dinner/parties we attended. You will always be my favourite roommate in conferences. Also, thank you to Matics for your encouragements and advice outside science. You guys are on the list of my favourite power couple.

To Dr Eisha Mhatre, thank you for your honest comments about my research. I enjoyed having you as my office seatmate as it was effortless to strike any conversation with you.

To Dr Ramses Gallegos-Monterossa, for being that person who made me see things from a different perspective. For making me feel not alone in the lab because you too, were also working in the lab even on weekends and holidays.

To Dr Theresa Hölscher- Jautzus, for being your wonderful self, I am very grateful with all your assistance and for being my reliable contact in Jena.

To Anne Richter, for the fun times in Jena and Denmark. For being the first one to personally welcome me in Denmark by picking me up from the airport. For being that person who understands my love-hate opinions about staying in Denmark.

To Heiko Kiessewalter, for being that dependable go-to guy in Denmark just because "Heiko knows". To you and Daniel Schäfer for being great M.Sc. students. You both made my task of being your supervisors enjoyable. Thank you for being eager learners, and for being patient with me. I wish you both the best in your career/study.

Thank you to all the previous students in TeBi, Felix, Tim, Manasa, Anand, Surabhi, Niveda, Soumyajit, Tino, Tina, Vali, Jan, Stefi, Tadeja, Sonja and in loving memory of Franzi. Also to the previous BIE members that I have worked with, to Regina, Aneta, Alex, Jonas and Priya.

Thank you also to my colleagues in DTU Bioengineering in Denmark and Microbial Communications group in Jena for being friendly and kind to me. To Christin Reichmann for the prompt replies to my emails.

To Prof. Kothe, for being that empowered woman in science that serves me as a good inspiration.

To all the collaborators that made these researches possible. To DFG and SPP 1617 for the funding. To the FEMS Research and Training Grant, for the financial support while I was in Denmark.

To my friends back in the Philippines, especially to my Mead Johnson friends for staying in touch and always telling me that even though they miss me, they are happy with where I am right now. Special mention to my long-time besties, Jane and Roselle. To Jane for always making sure to meet up with me every time I visit the Philippines. I appreciate your taking a day off from work just to be able to see me. To Roselle, for constantly and tirelessly hearing my adventures and mishaps in Germany and Denmark. For being always there for me despite the distance.

To those wonderful friends I met in Denmark who made my stay there worth remembering, especially to Monique, Ivy, Joy, Ausra, Demi and Steve, to the Companions Group and Choir Group in Sankt Knut Lyngby for being my spiritual family in Denmark. Special mention to the lovely couple Dr Robert and Sumi Olinski, for your genuine care and support for me. You are such a very blessed power couple. To Lotte Lacour and Rene Karottki, for being my wonderful landlord, you and your family made me feel very much welcomed in your home. Thank you for your genuine concern and assistance during those days that I fell terribly sick. Thank you for showing me around and for inviting me to dinners, afternoon tea and cakes.

To my Internationaler Kreis family, for being my spiritual home in Jena. To Dorothea Reeps, Dr Markus Müller, Hanna Africiska Duruck, Anthony I and Anthony II for making my Friday nights colourful and my stomach well fed. To Wiwin Winjaya, for your beautiful friendship, for your encouragements and for taking time to meet up with me. To the awesome Malaysian family, Merlinda, Ambrose and Isabelle. Thank you for your genuineness and your warm, welcoming hearts.

To my previous flatmates in Jena, thank you, lovely ladies, for making my short stay in your flat a delightful one. Thank you for the encouragements and prayers, Sarah Hummel, Sarah Schmidt, Sophia Sczesny and Dorothea Reeps.

To all the Pinoys in Jena who made my stay in Jena less homesick. For the dinner invitations filled with delicious Pinoy food and videoke sessions. To Vanessa Stärker and family, for not getting tired of inviting me for lunch/dinner even though at times, I could not make it due to my experiments. To Ate Anita, for your sunshine smile and talent, because of you, my haircut problems disappeared.

To Dr Maria Leilani Torress-Mapa and Louise Mapa, for the warm friendship and for inviting me to your home. To Louise, for your excellent cooking skills and for your sense of humour that reminds me very much of Pinas. To Lani for all the words of encouragements and advice, for that person who understands my worries in this field. I am really grateful for all of those.

A lot of thanks to my friends in Jena who were always there for me when I needed them. To Vincensius Surya Putra Oetama and Luke Donald Halder, for being awesome and reliable every time I feel helpless. For taking the time to pick me up at the cold and dark station in Lobeda whenever I feel scared of walking alone in the dark and for your impressive culinary and baking skills (especially the non-spicy ones). For all the senseless and sensible conversations and dinners. To Vini, for being that dependable big brother that you are. To my other brother Luke, for your know-how skills that helped me a lot in formatting this dissertation, for always making sure I have a place to stay in Jena every time I visit. I will forever cherish our friendship together with Kangping, Prince and Rasul.

To Dr Karen Grace Bondoc, for all the advice, for the sleepovers (mostly at my flat), for the meaningful and meaningless conversations about everything. For the encouragements, for your warm friendship, for making me feel at home in Jena, for the scientific and non-scientific chats, and for staying in contact even though we are thousands of miles apart.

To Daniel Pohle, my splendid source of Vitamin D, my personal attending physician, my best friend and love, I appreciate the support and encouragements, especially during those late nights of manuscript writings and graph-wrestlings. Thank you for always being there, and especially for giving me back massages (with special lectures on the names of the muscles that are sore) when I am too stressed. For making sure I keep up with a healthy work-life balance and not go back to a vampire lifestyle. Of course, to Emilia, Alice and Lukas, for the positive distractions that shower me with genuine warmth.

Most profound appreciation to my family who has never failed to support and encourage me all my life. To my kuya, Engr. Melvin Martin, sis-in-law Engr. Edna Martin, to my wonderful nieces Bianca and Ingrid. Thank you for welcoming me to your home in

Stuttgart and Fellbach every time I have no place to go. For making me feel the warmth of family away from home. Also, dedicating this to my family in the Philippines, Engr. Jic, Engr. Maanne, Jianne and Thirdy, Engr. Mark, Engr. JV and Victoria, for the motivation, love and prayers.

Most especially to my loving parents, Victor and Mercedes Martin, for the unwavering love and support. For teaching me the values of persistence and hard work. For setting a good example to my brothers and me. I am proud of who I have become because of how you have raised me.

Lastly, to the divine strength from my Saviour that guides me to get through anything, to You, I give back all the glory.

Thank you very much. Vielen Dank. Maraming Salamat.

Declaration of Independent Assignment

I declare in accordance with the conferral of the degree of doctor from the Faculty of Biology and Pharmacy of the Friedrich-Schiller-University of Jena that the submitted thesis was written only with the assistance of the literature cited in the text.

People who assisted in experiments, data analysis and writing of the manuscripts are listed as co-authors of the respective manuscripts.

A consultant for doctorate theses did not assist me.

The thesis has not been previously submitted elsewhere, whether to the Friedrich-Schiller- University of Jena or to any other university.

Jena, 24th June, 2019

Marivic Martin